Deriving Scattering Amplitudes from Hadron Spectra: Novel Quantization Conditions in Lattice QCD and Their Applications

Zachary T. Draper

A dissertation
submitted in partial fulfillment of the
requirements for the degree of

Doctor of Philosophy

University of Washington

2024

Reading Committee:
Stephen R. Sharpe, Chair
Masha Baryakhtar
Joaquin Turiaci

Program Authorized to Offer Degree:
Physics

University of Washington

Abstract

Deriving Scattering Amplitudes from Hadron Spectra:
Novel Quantization Conditions in Lattice QCD and Their Applications

Zachary T. Draper

Chair of the Supervisory Committee:
Stephen R. Sharpe
Department of Physics

The Standard Model of particle physics, the most precise scientific description of nature yet devised, is a comprehensive framework that encapsulates our understanding of the fundamental particles and their interactions. A keystone of this model is quantum chromodynamics (QCD), a quantum field theory describing the strong nuclear force, which binds together fundamental particles known as quarks to form composite particles such as protons and neutrons, and which binds these protons and neutrons together to form atomic nuclei. Together with electrons, which orbit these nuclei, quarks constitute the basic building blocks of all matter, forming the atoms that compose us and making up everything we have ever seen and ever touched.

One of the most powerful computational tools for understanding the dynamics of quarks is lattice QCD. By discretizing a finite volume of space and time onto a four-dimensional grid, lattice QCD enables the calculation of correlation functions that capture the behavior of quarks and the gluons that bind them together. This framework provides a bridge between the mathematical formulation of QCD and experimental results, allowing for tests of the Standard Model and offering insights into the behavior of particles and their interactions under extreme conditions that may be inaccessible to direct observation. To connect lattice calculations with experimental results and the real, infinite-volume world, one must account

for the effects of finite volume and boundary conditions through the use of quantization conditions. It is these quantization conditions, their derivation, and implementation, that form the heart of this body of work.

TABLE OF CONTENTS

Page

Part I: Introduction 1

Chapter 1: Background 2
1.1 From QED to QCD 2
1.2 QCD: The Mathematical Framework 5
1.3 Lattice QCD 11
1.4 Chiral Perturbation Theory 23
1.5 Quantization Conditions 29
1.6 Summary 36

Part II: Theoretical Advancements 38

Chapter 2: Applicability of the two-particle quantization condition to partially-quenched theories 40
2.1 Abstract 40
2.2 Introduction 40
2.3 Theoretical setup 43
2.4 PQχPT calculation of $\pi\pi$ correlators 49
2.5 Diagrammatic interpretation and alternative criteria 52
2.6 Applications and implications for previous work 56
2.7 Conclusions 57

Chapter 3: $\pi\pi$ scattering in partially-quenched twisted-mass chiral perturbation theory 60
3.1 Abstract 60
3.2 Introduction 60
3.3 Theoretical setup 63

3.4 Leading-order TMPQχPT results 68
3.5 Applicability of two-particle quantization condition 76
3.6 Implications for previous work 80
3.7 Conclusion 83

Chapter 4: Interactions of πK, $\pi\pi K$ and $KK\pi$ systems at maximal isospin from lattice QCD 85
4.1 Abstract 85
4.2 Introduction 86
4.3 Finite-volume Spectrum Extraction 89
4.4 Theoretical background 99
4.5 Extraction of scattering parameters 111
4.6 Discussion of results 139
4.7 Conclusion 150

Chapter 5: Three relativistic neutrons in a finite volume 153
5.1 Abstract 153
5.2 Introduction 153
5.3 Recap of the formalism for identical scalars 156
5.4 Formalism for three spin-half particles 160
5.5 Summary of results and implementation 191
5.6 Parametrization of $\mathcal{K}_{\text{df},3}$ 196
5.7 Conclusions 201

Chapter 6: Three-particle formalism for multiple channels: the $\eta\pi\pi + K\overline{K}\pi$ system in isosymmetric QCD 204
6.1 Abstract 204
6.2 Introduction 204
6.3 Overview 206
6.4 Derivation of quantization condition 208
6.5 Reduction to single-channel formalism for $E^* < M_{KK\pi}$ 236
6.6 Parametrizations of $\mathcal{K}_{\text{df},3}$ 241
6.7 Conclusions 246

Chapter 7: Conclusion 248

Appendix A: Appendix to Chapter 3 251
A.1 Higher-order contributions in χPT 251

Appendix B: Appendix to Chapter 4 253
B.1 Energy levels used in fits 253
B.2 ChPT result for $\mathcal{K}_{\mathrm{df},3}$ including $\mathcal{O}(a^2)$ errors 253
B.3 NLO ChPT result for the $I = 3/2$ p-wave πK scattering length 258
B.4 Tables of interpolating operators 261

Appendix C: Appendix to Chapter 5 267
C.1 Further details of the derivation 267
C.2 Antisymmetrizing the scattering amplitude 270
C.3 Operators with two derivatives 272

Appendix D: Appendix to Chapter 6 275
D.1 Isospin relations 275
D.2 Kinematic functions 276
D.3 Form of matrix $\widehat{\mathcal{K}}_{2,L}$ in charge basis 283
D.4 Isospin decompositions of two-particle K matrices 284
D.5 Conversion from charge to isospin basis for 18-d matrices 285
D.6 Quadratic terms in the threshold expansion of $\mathcal{K}_{\mathrm{df},3}$ 287
D.7 Symmetrization of the quantization condition 290

Bibliography 293

ACKNOWLEDGMENTS

I am deeply grateful to my advisor, Steve Sharpe, for his constant support and guidance throughout our time working together. It has been a privilege to learn and grow under his mentorship. I also wish to express my gratitude to my collaborators, Fernando Romero-López, Max Hansen, Drew Hanlon, Ben Hörz, and Colin Morningstar. Each has significantly contributed to the work presented here, and I am thankful for their invaluable assistance and expertise. Finally, I would like to thank my family, without whom this journey would not have been possible.

Part I

INTRODUCTION

The first part of this dissertation introduces key concepts essential to understanding the subsequent chapters. Topics covered include an introduction to quantum chromodynamics and its historical development, lattice methods, effective field theories, and quantization conditions. These concepts lay the foundation for the subsequent part of the dissertation, which comprises five distinct papers representing published research. These papers extend the principles established in the introductory chapter, exploring topics such as the applicability of two-particle quantization conditions for partially-quenched systems, the application of the formalism for three-particle finite-volume systems, and the generalization of this formalism to encompass spin and multiple channels. Each paper contributes novel insights and methodologies to the field, building upon the theoretical framework established in the introduction and showcasing their practical implementations.

Chapter 1
BACKGROUND

1.1 From QED to QCD

The historical narrative of QCD's development is intricately interwoven with the broader context of the development of quantum field theory and the Standard Model's evolution. Originating in the mid-20th century, the Standard Model gradually emerged as a synthesis of quantum mechanics, special relativity, and fundamental principles rooted in the mathematical framework of symmetry.

Quantum Electrodynamics (QED), the first quantum field theory to be formulated, describes the electromagnetic force and provided a blueprint for extending the Standard Model. Developed in the mid-20th century, QED emerged as a cornerstone of modern physics, offering a comprehensive framework for understanding the behavior of electrically charged particles and their interactions with electromagnetic fields [1]. At its core, QED postulates that electromagnetic interactions arise from the exchange of virtual photons between charged particles, leading to attraction or repulsion between them. The theory incorporates principles of quantum mechanics and special relativity to calculate precise probabilities of various particle interactions, yielding remarkably accurate predictions that have been verified through experimental observations. Its success provided a compelling impetus for extending the principles of quantum field theory to encompass other fundamental forces, culminating in the formulation of the electroweak theory, which unified electromagnetism with the weak nuclear force [2].

However, the puzzle of the strong nuclear force remained unsolved. Physicists grappled with understanding the intricate particle zoo—a plethora of seemingly elementary particles observed in high-energy collisions. Attempts to model nucleon interactions led to the proposal

of various theoretical frameworks, such as the meson theory [3] and the bootstrap model [4], yet none provided a satisfactory explanation for the underlying structure of matter.

It wasn't until the introduction of QCD in the early 1970s that a coherent picture began to emerge [5]. Quarks, initially proposed as hypothetical building blocks of nucleons by Murray Gell-Mann and independently by George Zweig in the 1960s [6, 7], played a pivotal role in resolving the mysteries of the particle zoo. Coming in six types, or "flavors"—up, down, charm, strange, top, and bottom—quarks are now thought to be among the elementary building blocks of matter. Just as electrons possess a property called electric charge, quarks possess a property called color charge. However, unlike electric charge, which exists in one form, taking either a positive or a negative value, color charge in QCD comes in three types—red, green, and blue—along with their corresponding anticolors.

These color charges interact via the exchange of gluons, the carriers of the strong force, in a manner analogous to how photons mediate electromagnetic interactions in quantum electrodynamics. This interplay of color charges and gluon exchange is responsible for the binding of quarks into composite particles, including a host of three-quark particles called baryons (like the protons and neutrons found in the atomic nucleus) and quark-antiquark pairs called mesons (such as pions and kaons), thus explaining the multitude of particles identified in the particle zoo. Additional experimental observations, such as the detection and analysis of "jets," collimated sprays of particles produced from quark-gluon interactions in particle accelerators, provided further evidence for the validity of QCD at high energies, where quarks exhibit a property known as asymptotic freedom.

Asymptotic freedom, a hallmark of QCD, refers to the phenomenon wherein the strength of the strong force diminishes as quarks are brought closer together at high energies [5, 8, 9]. This behavior allows quarks to behave almost as free particles at very short distances, facilitating perturbative calculations within QCD. In this type of calculation, one systematically expands physical quantities in terms of a small parameter, typically the strength of the interaction, such that higher-order terms contribute less to the quantity being calculated, allowing one to make progressively more accurate predictions by including more terms in the

expansion. Such computations enable the study of quark-gluon interactions under extreme conditions.

On the other hand, at low energies, the strong force exhibits the opposite behavior, becoming stronger as quarks are separated. This phenomenon, known as confinement, resolved the puzzle of why no free quarks had ever been observed: quarks are prevented from existing in isolation, instead always being found within color-neutral composite particles [10]. A color-neutral state can be achieved through various combinations, such as combining quarks with different color charges—red, green, and blue—resulting in a baryon; or pairing a quark with its corresponding antiquark, which carries the opposite (anti) color charge, to form a meson. In both cases, the combination cancels out the individual color charges, resulting in an overall neutral color state. As a result of the increased strength of the binding force in this regime, perturbative calculations, which rely on the assumption of weak coupling between particles, become impractical or impossible at low energies. Instead, lattice QCD methods provide a powerful approach for studying QCD at low energies.

By discretizing spacetime onto a four-dimensional grid, lattice QCD enables calculations of properties of hadrons and other non-perturbative phenomena, providing invaluable insights into the behavior of quarks and gluons in the regime where perturbative methods fail [10–12]. Through lattice simulations, one can investigate a wide range of QCD phenomena, including hadron spectroscopy, the structure of nucleons, and the behavior of matter under extreme conditions such as those found in neutron stars and the early universe.

One cannot simulate an unlimited expanse of spacetime, so by necessity, lattice QCD computations are performed within a finite volume. However, in physical reality, we are interested in understanding the behavior of quarks and gluons in the infinite-volume limit. To bridge this gap, quantization conditions are employed in lattice QCD calculations. These conditions establish relationships between the finite-volume energy levels of the particles in a lattice calculation and the corresponding scattering amplitudes in the infinite-volume continuum [13–17]. Scattering amplitudes characterize the probabilities of particles interacting and altering their trajectories when they collide, serving as crucial tools for comparing

the physics of the Standard Model to experimental data, exploring phenomena outside the reach of current experiments, and searching for potential new physics beyond our current understanding.

1.2 QCD: The Mathematical Framework

We now delve into the mathematical framework underlying QCD, providing the theoretical basis for understanding the strong force on a quantitative level [18]. At the heart of quantum field theories lie a set of mathematical constructs—including the action and Lagrangian density, the gauge group, and the running coupling—which encode the fundamental principles governing the dynamics of matter particles and the gauge fields that mediate their interactions. In this section, we explore these mathematical structures in detail, laying the groundwork for the introduction of lattice methods used in probing the complexities of QCD in the low-energy, non-perturbative regime.

1.2.1 The QCD Path Integral

Correlation functions in quantum field theory provide a means to study the behavior and interactions of particles by quantifying the probability amplitudes for specific processes to occur [19–21]. These functions involve the expectation values of products of field operators at different spacetime points. In the Euclidean path integral formalism of QCD, correlation functions are computed using the action, which encapsulates the dynamics of the system. We select the Euclidean metric, $(+,+,+,+)$, with foresight so that we can seamlessly transition to a discussion of lattice methods in section 1.3. To change from the Minkowski spacetime of the physical universe, characterized by a metric with signature $(-,+,+,+)$, to the Euclidean metric, we employ Wick rotation, replacing the time coordinate with a new imaginary time dimension: $t \to -i\tau$. Using the Euclidean metric, the correlation function between two field operators $\mathcal{O}_1$ and $\mathcal{O}_2$ is given by:

$$\langle \mathcal{O}_1(x_1)\mathcal{O}_2(x_2)\rangle = \frac{1}{Z}\int \mathcal{D}[\psi,\bar{\psi},A]\,\mathcal{O}_1(x_1)\mathcal{O}_2(x_2)\,e^{-S[\psi,\bar{\psi},A]} \tag{1.1}$$

where

$$Z = \int \mathcal{D}[\psi, \bar{\psi}, A]\, e^{-S[\psi,\bar{\psi},A]} \tag{1.2}$$

is the partition function, $\mathcal{D}[\psi, \bar{\psi}, A]$ represents the functional integration over fermionic quark fields and bosonic gluon fields, and $S_{QCD}[\psi, \bar{\psi}, A]$ is the Euclidean QCD action [22, 23]. By computing correlation functions for different field operators, this formalism enables the extraction of physical observables such as particle masses, scattering amplitudes, and decay rates.

The action governs the behavior of these correlation functions, providing a mathematical framework for investigating the dynamics of quarks and gluons. The action is defined as the integral of the Euclidean Lagrangian density over spacetime:

$$S_{QCD}(x) = \int d^4x\, \mathcal{L}_{QCD}(x)\,, \tag{1.3}$$

where the Euclidean QCD Lagrangian density is given by

$$\mathcal{L}_{QCD}(x) = \frac{1}{4}\mathcal{G}^k_{\mu\nu}(x)\mathcal{G}^{\mu\nu}_k(x) + \bar{\psi}(x)\gamma^\mu D_\mu \psi(x) + \bar{\psi}(x) m \psi(x)\,. \tag{1.4}$$

The first term represents the self-interactions of the gluon fields, the second accounts for the kinetic energy of quarks in the presence of gluon fields, and the third incorporates the mass of the quarks. As in much of physics, this notation is compact and hides significant complexity. One by one, we will examine the quantities appearing in the Lagrangian density, unpacking the notation as we go.

1.2.2 Quark and Gluon Fields

We start with $\psi(x)$ and $\bar{\psi}(x)$, spin-$\frac{1}{2}$ Dirac spinors, representing quark and anti-quark fields. These fermionic fields carry three discrete indices,

$$\psi(x) = \psi^{\alpha\, a\, f}(x) \tag{1.5}$$

where $\alpha = 1, 2, 3, 4$ is the Dirac index, specifying the component of the spinor; $a = 1, 2, 3$; (r, g, b) is the color index, indicating the color charge of the quark field; and $f = 1, \ldots, N_f$ is

the flavor index, denoting the flavor of the quark field. In a theory with all six quark flavors, (up, down, charm, strange, top, bottom), $N_f = 6$; however, depending on the application, the heaviest quarks (top, bottom, and sometimes charm) may be omitted from calculations. These quark fields belong to and transform under the fundamental representation of the gauge group, $SU(3)$.

The Euclidean Dirac matrices, γ^μ, labeled with spacetime indices $\mu = 1, 2, 3, 4$, are 4×4 matrices that act on the index space of Dirac spinors. The covaraint derivative, with which the Dirac matrices are contracted, includes the coupling of quarks to the gluon fields, ensuring that the QCD Lagrangian remains invariant under local gauge transformations. Expressed as

$$[D_\mu]_{ab} = \partial_\mu \delta_{ab} - ig[T_k]_{ab} A^k_\mu(x)\,, \tag{1.6}$$

it can be thought of as a matrix acting on color space (with color indices a, b made explicit in the above equation). Here, A^k_μ are the gluon fields, vectors belonging to the adjoint representation of $SU(3)$, while T_k are the generators of $SU(3)$ in the fundamental representation, and g is the coupling strength of the quark and gluon fields. Note that the gluon fields come with a spacetime index indicating the directionality of the field at each point in space and are labeled by the generators of $SU(3)$, indicating that each gluon field can be associated with a combination of color and anti-color charge. Unlike in QED, where the gauge fields (photons) are uncharged, the gluon fields in QCD carry color charge. This distinction is significant because it leads to self-interactions among gluons, as well as interactions between quarks and gluons that change the color charge of the quarks, resulting in the non-Abelian nature of the strong force.

The last quantity to define is the gluon field strength tensor, which characterizes the strength and curvature of the gluon fields. It is given by

$$\mathcal{G}^k_{\mu\nu}(x) = \partial_\mu A^k_\nu - \partial_\nu A^k_\mu + g f^{k\ell m} A^\ell_\mu A^m_\nu\,, \tag{1.7}$$

where $f^{k\ell m}$ are the structure constants of $SU(3)$, with k, l, m indices that run from 1 to 8, labeling the generators of the gauge group.

1.2.3 Gauge Symmetry

We now turn our attention to the gauge symmetry of QCD. Gauge invariance maintains the internal consistency of the theory by preventing the introduction of unphysical degrees of freedom; ensures the conservation of physical observables; and preserves the underlying symmetries of the theory. The gauge group of QCD, $SU(3)$, expressed in its defining representation is the group of unitary 3×3 matrices with determinant one. In general, one can express an element of $SU(3)$ as

$$\Omega = \exp[i\omega^k T_k] \,, \tag{1.8}$$

where T_k are the generators of the group in the chosen representation. For the fundamental, defining representation, the generators are a complete set of Hermitian traceless 3×3 matrices. The generators must satisfy the following properties:

$$[T_k, T_\ell] = i f_{k\ell m} T^m \,, \tag{1.9}$$

$$\mathrm{tr}(T_k T_\ell) = \rho \delta_{k\ell} \,, \tag{1.10}$$

where $\rho = \frac{1}{2}$ in the fundamental representation, the representation of the quark fields, and $\rho = 3$ in the adjoint representation, that of the gluon fields.

Given the constraint that QCD action is invariant under gauge transformations, we require the terms that build the Lagrangian to transform as follows:

$$\psi'(x) = \Omega(x)\psi(x) \,, \tag{1.11}$$

$$\bar{\psi}'(x) = \bar{\psi}(x)\Omega^\dagger(x) \,, \tag{1.12}$$

$$D'_\mu(x)\psi(x) = \Omega(x)D_\mu(x)\psi(x) = \Omega(x)D_\mu(x)\left(\Omega^\dagger(x)\psi'(x)\right) \,, \tag{1.13}$$

from which we find the transformation rule for the covariant derivative:

$$D'_\mu(x) = \Omega(x)D_\mu(x)\Omega^\dagger(x) \,. \tag{1.14}$$

This in turn gives us the transformation rule for the gluon fields:

$$A'_\mu = \Omega(x)A_\mu(x)\Omega^\dagger(x) + ig\Omega(x)\partial_\mu(x)\Omega^\dagger(x) \,, \tag{1.15}$$

which is consistent with the requirement that the field tensor $\mathcal{G}_{\mu\nu} = \mathcal{G}^a_{\mu\nu} T_a$ transforms as

$$\mathcal{G}'_{\mu\nu}(x) = \Omega(x)\mathcal{G}_{\mu\nu}(x)\Omega^\dagger(x)\,. \tag{1.16}$$

We can rewrite the purely gluonic contribution to the Lagrangian density as

$$\mathcal{G}^k_{\mu\nu}(x)\mathcal{G}^{\mu\nu}_k(x) = \frac{1}{\rho}\mathrm{tr}\left(\mathcal{G}_{\mu\nu}(x)\mathcal{G}^{\mu\nu}(x)\right)\,, \tag{1.17}$$

a gauge invariant quantity.

With a gauge invariant Lagrangian in hand, it is natural to wonder if there might be any more terms consistent with the symmetries of the theory that could be incorporated into the Lagrangian. In fact, there is one such term, which takes the form:

$$\mathcal{L}_\theta = \frac{\theta}{32\pi^2}\mathcal{G}^k_{\mu\nu}\tilde{\mathcal{G}}^{\mu\nu}_k\,, \tag{1.18}$$

where θ is a parameter representing the vacuum angle, $\mathcal{G}^k_{\mu\nu}$ is the gluon field strength tensor, and $\tilde{\mathcal{G}}^{\mu\nu}_k$ is its dual. While gauge invariance dictates certain symmetries and constraints on the QCD Lagrangian, it does not explicitly forbid this term, so we must take seriously its inclusion.

In fact, there is one more change to the QCD Lagrangian that we must consider. The most general quark mass term consistent with gauge symmetry has the form $me^{i\theta'\gamma_5}$. However, by redefining the quark fields with the following transformation,

$$\psi' = e^{i\alpha\gamma_5/2}\psi \qquad \bar{\psi}' = e^{i\alpha\gamma_5/2}\bar{\psi}\,, \tag{1.19}$$

we are able to shift the values of θ and θ' such that $\theta \to \theta + \alpha$ and $\theta' \to \theta' - \alpha$. By choosing α appropriately, we can eliminate θ' such that only the θ term needs to be considered.

The theta term in the QCD Lagrangian introduces a potential source of charge-parity (CP) violation, affecting the behavior of strong interactions. This phenomenon, determined by the vacuum angle, may manifest as observable differences between processes involving particles and their antiparticles. Experimental searches, such as those investigating the electric dipole moment of the neutron, aim to detect CP-violating effects related to the theta

term. Despite ongoing efforts, no definitive evidence of CP violation has been observed, placing constraints on possible values of the vacuum angle. This suggests that the phase of the vacuum angle is finely tuned, leading to minimal or no CP violation in the strong force—an intriguing puzzle known as the strong CP problem.

1.2.4 The Running Coupling

While the QCD Lagrangian provides a foundation for understanding strong interactions, the energy dependence of these interactions is not directly apparent from the Lagrangian alone. To incorporate this dynamic behavior into our description of the strong force, we turn our attention to one particular quantity in the Lagrangian, the strong coupling constant, g. In fact, calling this quantity a constant is a misnomer. The strength of the strong interaction, is not constant, but instead varies with the energy scale at which interactions occur. This phenomenon, known as the running of the coupling, is governed by renormalization group equations that describe how physical quantities evolve with changes in the energy scale μ. The running of g is described by the beta function $\beta(g)$, given by the differential equation

$$\mu \frac{dg}{d\mu} = \beta(g)\,. \tag{1.20}$$

At low energies, the strong coupling becomes large, leading to the phenomenon of confinement, where quarks and gluons are confined within bound states. The beta function itself can be computed from QCD correlation functions and is given to one loop order by the following:

$$\beta(g) = -\frac{b_0}{(4\pi)^2} g^3\,, \tag{1.21}$$

where b_0 is the first coefficient of the beta function expansion and is given by $b_0 = \frac{11}{3}N_c - \frac{2}{3}N_f$, where N_c is the number of colors (for QCD, $N_c = 3$) and N_f is the number of active quark flavors.

As the energy scale increases, the strong coupling decreases, a behavior described by the beta function. The scale at which the strong coupling becomes nonperturbative, known as

the QCD scale Λ_{QCD}, sets the energy scale where the running coupling becomes large and perturbative methods break down. It is given by:

$$\Lambda_{\mathrm{QCD}} \approx \mu \exp\left(-\frac{1}{2b_0 g^2(\mu)}\right) \tag{1.22}$$

where b_0 is the first coefficient of the beta function expansion, defined above. In the perturbative regime, where g is small, calculations can be performed using perturbation theory. However, at energies near or below Λ_{QCD}, nonperturbative methods such as lattice QCD are required.

1.3 Lattice QCD

Lattice methods serve as a powerful tool not only for addressing scenarios where perturbative methods become inadequate due to large coupling constants, but also for providing a systematic approach to understanding and interpreting quantum field theories [22–24]. The QCD path integral, encapsulated by eq. (1.1), represents the summation over all conceivable field configurations, each weighted by its associated measure. In the context of QCD, this involves integrating over all possible arrangements of gluon and quark fields across spacetime. The measure, expressed explicitly as $\mathcal{D}[\psi, \bar{\psi}, A] = [\mathcal{D}\psi][\mathcal{D}\bar{\psi}][\mathcal{D}A]$, underscores the separate integration over the quark, antiquark, and gluon fields (ψ, $\bar{\psi}$, and A) respectively, at all points in spacetime. To render this summation mathematically rigorous, it is useful to discretize spacetime, thereby introducing a lattice structure. By imposing this lattice framework, these integrals are evaluated at a discrete set of points, rather than across a continuous volume of spacetime. In doing so, the path integral assumes a well-defined form, allowing for mathematical rigor and enabling concrete calculations. To return to the continuum theory, the lattice structure needs to be removed by taking the limit that the lattice spacing becomes increasingly small, a non-trivial task.

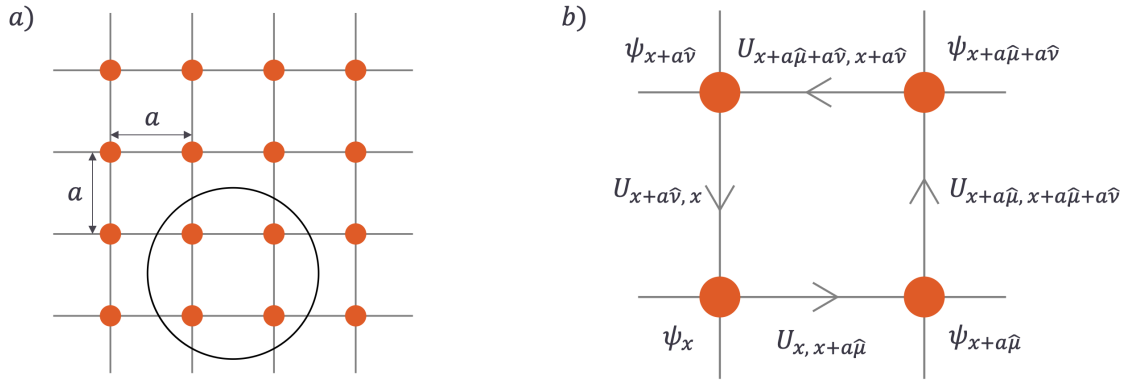

Figure 1.1: Image a) shows a 2-d lattice with lattice spacing a. Image b) shows an enlargement of the region circled in a). The quark fields ψ_x are defined on the lattice sites, while the link variables $U_{\mu x} = U_{x,x+a\hat{\mu}}$ are defined on the links between sites.

1.3.1 Constructing a Lattice

To begin, we divide four-dimensional spacetime into a discrete lattice with a spacing denoted by a. Each lattice point corresponds to a specific position in spacetime, with a determining the resolution, similar to the pixel size in a digital image. This spacing acts as the fundamental length scale in lattice QCD, regulating the theory for numerical calculations. An example of a two-dimensional lattice is provided in figure 1.1. We consider a finite spacetime volume, represented by a lattice with a finite number of sites in each direction. Let N be the number of lattice sites per direction, totaling N^4 sites, such that the physical size of the hypercubic box is $L = Na$. Each lattice site's position is specified by $x_\mu = m_\mu a$, where m_μ labels the mth site along direction μ.

In discretizing our theory, we replace integrals over the spacetime volume by sums over the lattice sites. To return to the continuum limit the reverse replacement is made,

$$\sum_x f(x) \to \int_0^L f(x)\, d^4x\,, \tag{1.23}$$

where in this limit, we want $N \to \infty$ and $a = \frac{L}{N} \to 0$ with L held fixed. In the above

equation, the sum over positions, x, is equivalent to a sum over site indices, m:

$$\sum_x = a^4 \sum_{m_1=0}^{N} \dots \sum_{m_4=0}^{N} = a^4 \sum_m . \tag{1.24}$$

1.3.2 Defining Fields on a Lattice

With our lattice constructed, we now introduce the lattice versions of the quantities that enter into the QCD Lagrangian. We begin by defining our quark fields on the discrete lattice sites. The quark field at position x, denoted by $\psi_x = \psi(x)$, changes under gauge transformations as

$$\psi'_x = \Omega_x \psi_x \, . \tag{1.25}$$

Continuum derivatives are replaced with finite differences on the lattice

$$\partial_\mu \psi_x = \frac{1}{a} \left[\psi_{x+a\hat{\mu}} - \psi_x \right] \tag{1.26}$$

and the covariant derivative is replaced by

$$D_\mu \psi_x = \frac{1}{a} \left[\psi_{x+a\hat{\mu}} - \psi_x \right] - ig \left[\tilde{C}_{\mu,x} \psi_x + C_{\mu,x} \psi_{x+a\hat{\mu}} \right] , \tag{1.27}$$

where $C_{\mu,x}$ and $\tilde{C}_{\mu,x}$ are yet-to-be-determined quantities that play the role of A_μ in the continuum theory, compensating for the lack of gauge covariance. For simplicity, we have chosen an asymmetric finite difference; however, in practice, a higher-order, symmetric finite difference may be used. To have a gauge invariant action, we require that the covariant derivative transforms as

$$D'_\mu \psi'_x = \Omega_x D_\mu \psi_x \, , \tag{1.28}$$

which leads to

$$\begin{aligned} &\frac{1}{a} \left[\psi'_{x+a\hat{\mu}} - \psi'_x \right] - ig \left[\tilde{C}'_{\mu,x} \psi'_x + C'_{\mu,x} \psi'_{x+a\hat{\mu}} \right] \\ &= \Omega_x \left[\frac{1}{a} \left[\psi_{x+a\hat{\mu}} - \psi_x \right] - ig \left[\tilde{C}_{\mu,x} \psi_x + C_{\mu,x} \psi_{x+a\hat{\mu}} \right] \right] \\ &= \Omega_x \left[\frac{1}{a} \left[\Omega^\dagger_{x+a\hat{\mu}} \psi'_{x+a\hat{\mu}} - \Omega^\dagger_x \psi'_x \right] - ig \left[\tilde{C}_{\mu,x} \Omega^\dagger_x \psi'_x + C_{\mu,x} \Omega^\dagger_{x+a\hat{\mu}} \psi'_{x+a\hat{\mu}} \right] \right] , \end{aligned} \tag{1.29}$$

where the first equality comes from evaluating the covariant derivative in left and right sides of eq. (1.28), and in the second equality we have used the inverse of the gauge transformation in eq. (1.25). Comparing coefficients between the left and right sides of the equation allows us to determine the transformation properties of $C_{\mu,x}$ and $\tilde{C}_{\mu,x}$, giving us

$$\tilde{C}'_{\mu,x} = \Omega_x \tilde{C}_{\mu,x} \Omega_x^\dagger \,, \tag{1.30}$$

$$\begin{aligned} C'_{\mu,x} &= \Omega_x C_{\mu,x} \Omega^\dagger_{x+a\hat{\mu}} + \frac{i}{ga}\left[\Omega_x \Omega^\dagger_{x+a\hat{\mu}} - 1\right] \\ &= \Omega_x C_{\mu,x} \Omega^\dagger_{x+a\hat{\mu}} + \frac{i}{ga}\left[\Omega_x \Omega^\dagger_{x+a\hat{\mu}} - \Omega_x \Omega^\dagger_x\right] \\ &= \Omega_x C_{\mu,x} \Omega^\dagger_{x+a\hat{\mu}} + \frac{i}{g}\Omega_x \partial_\mu \Omega^\dagger_x \,. \end{aligned} \tag{1.31}$$

By examining eq. (1.30), we see that we can set $\tilde{C}_{\mu,x} = 0$, since this satisfies the required transformation rule. For $C_{\mu,x}$, we find that the transformation rule is very similar to that of the continuum gauge potential. With this in mind, let us define the field strength as

$$C_{\mu\nu,x} = D_\mu C_{\nu,x} - D_\nu C_{\mu,x} \tag{1.32}$$

$$= \frac{1}{a}\left[C_{\nu,x+a\hat{\mu}} - C_{\nu,x}\right] - igC_{\mu,x}C_{\nu,x+a\hat{\mu}} - \frac{1}{a}\left[C_{\mu,x+a\hat{\nu}} + C_{\mu,x}\right] - igC_{\nu,x}C_{\mu,x+a\hat{\nu}} \,, \tag{1.33}$$

which transforms homogeneously under gauge transformations:

$$C'_{\mu\nu,x} = \Omega_x C_{\mu\nu,x} \Omega^\dagger_{x+a\hat{\mu}+a\hat{\nu}} \,. \tag{1.34}$$

To parameterize $C_{\mu,x}$, we want to select a form that is consistent with the transformation rule for $C_{\mu,x}$, so we try

$$C_{\mu,x} = \frac{i}{ga}\left(U_{\mu x} - 1\right) \,, \tag{1.35}$$

where $U_{\mu x}$ is a unitary matrix transforming as

$$U'_{\mu x} = \Omega_x U_{\mu x} \Omega^\dagger_{x+a\hat{\mu}} \,. \tag{1.36}$$

To relate the $C_{\mu,x}$ fields arising from the consideration of a lattice covariant derivative to the continuum gluon fields, we can write

$$U_{\mu x} = \exp\left(-iagA_{\mu,x}\right) \,. \tag{1.37}$$

where $A_{\mu,x} = A^k_{\mu,x} T_k$, and where we identify the lattice gauge field at site x, represented by $A^k_{\mu,x}$, with the continuous gauge field evaluated at position x, denoted $A^k_\mu(x)$. We have chosen the parameterization of C such that in the limit as $a \to 0$ and $aA_\mu(x) \to 0$,

$$C_{\mu,x} \to A_\mu(x) \tag{1.38}$$

$$C_{\mu\nu,x} \to \mathcal{G}_{\mu\nu}(x)\,. \tag{1.39}$$

By changing notation slightly such that

$$U_{x,x+a\hat{\mu}} \equiv U_{\mu x} \qquad U_{x+a\hat{\mu},x} \equiv U^\dagger_{\mu x} \tag{1.40}$$

and by reexamining eq. (1.36) in the context of this new notation,

$$U'_{x,y} = \Omega_x U_{x,y} \Omega^\dagger_y \quad \text{where} \quad y = x + a\hat{\mu}\,, \tag{1.41}$$

we can provide a physical interpretation to the gauge fields. In particular, we can think of $U_{x,x+a\hat{\mu}}$ as belonging on the link between the lattice sites at x and $x + a\mu$, as illustrated in figure 1.1. $U_{x,y}$ is the parallel transporter from y to x along the link denoted (x, y). When transporting quark and gluon fields along the lattice links, the parallel transport operation preserves the local SU(3) gauge symmetry of QCD, ensuring the color charge of quarks and gluons remains unchanged.

With the lattice versions of each term in the QCD action in hand, and recalling eq. (1.17), we can express the lattice-regulated action as

$$S_{\text{lattice}} = \sum_x \left[\frac{1}{4\rho} \text{tr}\left(C_{\mu\nu,x} C^{\mu\nu,x}\right) + \frac{1}{2}\left(\bar{\psi}_x \gamma^\mu D_\mu \psi_x - \bar{\psi}_x \gamma^\mu D^\dagger_\mu \psi_x\right) + \bar{\psi}_x m \psi_x \right] \tag{1.42}$$

$$= \sum_x \left[\frac{1}{4a^4\rho} \sum_{\mu<\nu} \text{tr}\left(2 - U_{\mu\nu,x} - U^\dagger_{\mu\nu,x}\right) \right.$$
$$\left. + \frac{1}{2a} \sum_\mu \left(\bar{\psi}_x \gamma^\mu U_{\mu x} \psi_{x+a\hat{\mu}} - \bar{\psi}_{x+a\hat{\mu}} \gamma^\mu U^\dagger_{\mu x} \psi_x\right) + \bar{\psi}_x m \psi_x \right]. \tag{1.43}$$

where in the second equation we have substituted in eqs. (1.27) and (1.35) to give us a new expression only in terms of the quark fields defined on the lattice sites and the link variables defined on the links between sites. The trace is taken over the color space, and repeated

spacetime indices are summed over in the first line, while in the second line the sum over μ and ν is made explicit. Here, we are defining

$$U_{\mu\nu,x} = U^{\dagger}_{\nu\mu,x} = U_{x,x+a\hat{\mu}}\, U_{x+a\hat{\mu},x+a\hat{\mu}+a\hat{\nu}}\, U_{x+a\hat{\mu}+a\hat{\nu},x+a\hat{\nu}}\, U_{x+a\hat{\nu},x}\,, \tag{1.44}$$

which we can interpret as the parallel transport around a closed loop of four lattice sites (with one corner at x) laying in the μ-ν plane.

Through the choice of lattice action, we can incorporate different physics of interest into our calculations. For instance, if we want to include the CP-violating theta term of eq. (1.18), one way to do so is through the gerneralized quark mass, $me^{i\theta'\gamma_5}$. By expanding the exponential to linear order, we can incorporate CP violation with the inclusion of the following term in our lattice action,

$$S_\theta = \sum_x \bar{\psi}_x \left(im\frac{\theta'}{2}\gamma_5 \right) \psi_x + \mathcal{O}(\theta'^2)\,. \tag{1.45}$$

Here, as before, θ' is a phase that quantifies the extent of CP violation. Though this alteration to the lattice action is not required unless studying strong CP violation, we now turn our attention to a problem that will require us to adapt the lattice action in new ways.

1.3.3 Fermion Doubling

In the continuum limit as $a \to 0$, the lattice action should converge to the continuum QCD action, faithfully reproducing the physics of quarks and gluons. However, a significant challenge known as the fermion doubling problem arises when this limit is taken [10, 25, 26]. In the lattice formulation of QCD expressed by the above action, the discretization of spacetime leads to the appearance of additional fermionic degrees of freedom not present in the continuum theory. Specifically, for each flavor of quark, this lattice action introduces multiple replicas or "doublers" of each quark flavor.

This doubling arises due to the discretization of the Dirac operator on the lattice, where the dispersion relation for fermions exhibits additional unwanted momentum states known as fermion doublers. These doublers contribute to the path integral over the fermion fields, and

if unaccounted for, lead to unwanted contributions that distort the physical predictions of lattice QCD calculations. Addressing this issue is crucial for achieving accurate and reliable predictions. But before we explore how the problem can be addressed, let us examine the source of the problem in more detail.

We start by examining the fermionic part of the partition function for the above lattice action,

$$Z_{\text{fermi}} = \int [D\bar{\psi}][D\psi] \exp[-\bar{\psi}_x M \psi_x] \,, \tag{1.46}$$

where the measure of integration can be defined explicitly as

$$[D\bar{\psi}][D\psi] = \prod_{x,\alpha} d\bar{\psi}_{x\alpha} d\psi_{x\alpha} \,, \tag{1.47}$$

where α is the Dirac index of the fermion field. We can read off the form of M from eq. (1.43) by setting all link variables to unity:

$$M_{xy} = \sum_x \left[\gamma^\mu \frac{1}{2a} \left(\delta_{x,z} \delta_{y,z+a\hat{\mu}} - \delta_{x,z+a\hat{\mu}} \delta_{y,z} \right) + m \delta_{x,z} \delta_{y,z} \right] \,, \tag{1.48}$$

where in the finite-difference term, the repeated μ index is summed over. Assuming infinite spacetime, we can calculate the fermion propagator $S_{xy} = M_{xy}^{-1}$ in momentum space by taking the discrete Fourier transform of M_{xy}:

$$M(k,-q) = \sum_{x,y} \exp\left(-ikx + iqy\right) M_{xy} = S(k)^{-1} \delta(k-q) \,, \tag{1.49}$$

from which we find

$$S(k)^{-1} = i\gamma^\mu s_\mu + m \quad \text{with} \quad s_\mu = \frac{\sin(k_\mu a)}{a} \,, \tag{1.50}$$

for $-\pi < a k_\mu \leq \pi$. Inverting this expression, we find the propagator

$$S(k) = \frac{m - i\gamma^\mu s_\mu}{m^2 + s^2} \,, \tag{1.51}$$

which in the continuum limit, $a \to 0$, gives

$$S(k) = \frac{m - i\gamma^\mu k_\mu}{m^2 + k^2} + \mathcal{O}(a^2) \,. \tag{1.52}$$

This expression has a pole at $k_4 = i\sqrt{\boldsymbol{k}^2 + m^2}$, corresponding to a Dirac particle. However, this isn't the only pole of the propagator. The propagator can be expanded around each of the zeros of s_μ, of which there are two for each of the four values of μ. This results in a total of $2^4 = 16$ regions in which the sine functions vanish, each of which corresponds to a Dirac particle. The fifteen unwanted particles are the doublers, which disrupt the continuum limit of the theory, preventing agreement with continuum QCD.

Wilson fermions address the fermion doubling problem by introducing a mass-like term in the lattice action, effectively suppressing unwanted fermion modes at high energies, allowing only the desired low-energy modes to contribute to physical observables [10]. This is achieved by adding the following "Wilson term" to the lattice action:

$$S_{\text{Wilson}} = \sum_x \left[\frac{r}{2a} \sum_\mu \left(\bar{\psi}_x U_{\mu x} \psi_{x+a\hat{\mu}} - \bar{\psi}_{x+a\hat{\mu}} U^\dagger_{\mu x} \psi_x \right) + \bar{\psi}_x r \psi_x \right] \tag{1.53}$$

One can show that the momentum space propagator for Wilson fermions is

$$S(k) = \frac{(m - \frac{r}{2}\hat{k}^2) - i\gamma^\mu s_\mu}{(m + \frac{r}{2}\hat{k}^2)^2 + s^2}\,, \tag{1.54}$$

where $\hat{k}_\mu = 2\sin(k_\mu/2)$. Unlike for the naive fermion propagator given in eq. (1.51), which has poles of mass m near $k_\mu = \pi$, the Wilson fermion propagator has poles of mass $m + 2rn$, where n is the number of components of k_μ close to π. If one keeps r non-zero in the limit as $m = m_{\text{physical}}$ $a \to 0$, the effective masses of the doublers becomes infinite. Thus, as we take the continuum limit, only the physical pole near $k = 0$ survives.

Although the Wilson term successfully resolves the fermion doubling problem, it does so at the expense of explicitly breaking chiral symmetry. Chiral symmetry, an (approximate) symmetry of QCD, is an essential feature of the continuum QCD Lagrangian, related to the conservation of the axial current and the existence of massless (or low-mass) Goldstone bosons (or pseudo-Goldstone bosons). In the limit as the quark masses go to zero, chiral symmetry becomes an exact symmetry, and the left- and right-handed components of the quark fields decouple.

To define the chirality or handedness of our quark fields, we require the gamma matrix

$$\gamma_5 = \gamma_1\gamma_2\gamma_3\gamma_4 = \begin{pmatrix} \mathbf{1} & 0 \\ 0 & -\mathbf{1} \end{pmatrix} \tag{1.55}$$

where $\mathbf{1}$ is the 2×2 identity matrix. The chirality operators project out the left- and right-handed components of the fermion field:

$$\psi_L = \frac{1}{2}(1-\gamma_5)\psi\,, \quad \psi_R = \frac{1}{2}(1+\gamma_5)\psi, \quad \bar{\psi}_L = \bar{\psi}\frac{1}{2}(1+\gamma_5)\,, \quad \bar{\psi}_R = \bar{\psi}\frac{1}{2}(1-\gamma_5) \tag{1.56}$$

where ψ_L and ψ_R are the left- and right-handed components of ψ respectively. Note that to project out the left (right) chrial components of the antifermion field, $\bar{\psi}_L$ ($\bar{\psi}_R$), we act on $\bar{\psi}$ from the right rather than the left. What's more, we use the same projector needed to project out the right (left) components of the fermion field, ψ_R (ψ_L). There is no conflict in defining ψ_L and $\bar{\psi}_L$ with different projectors since ψ and $\bar{\psi}$ are independent fields.

The Wilson term mixes left- and right-handed components of the fermion field, violating chiral symmetry on the lattice. One might wonder if another method of fermion discretization could remove fermion doublers while maintaining the approximate chiral symmetry of QCD; however, the Nielson-Ninomiya theorem states that it is impossible to formulate a lattice fermion action that simultaneously satisfies all of the following criteria: locality, gauge invariance, absence of species doubling, and exact chiral symmetry at finite lattice spacing [27].

To address the fermion doubling problem and mitigate the breaking of chiral symmetry, various approaches have been developed. Staggered fermions, for example, reduce the number of fermion degrees of freedom by a factor of 2^d, where d is the number of lattice dimensions [28]. This approach leads to a residual flavor symmetry, which is an approximate symmetry of the action. Other methods include domain wall fermions [26] and overlap fermions [29], which attempt to lessen the effects of chiral symmetry breaking, albeit at the cost of introducing additional computational complexity. Each approach has its advantages and limitations, depending on the specific physics being studied and the computational resources available.

1.3.4 Evaluating the Path Integral

Monte Carlo methods are indispensable in lattice QCD due to the colossal computational demands imposed by the high-dimensional integration required. In lattice QCD, we aim to simulate the behavior of quarks and gluons within the confines of four-dimensional spacetime discretized onto a lattice. This lattice comprises numerous points, with typical lattice sizes ranging from tens to hundreds of points in each direction. However, the real challenge lies in the dimensionality of the integration space.

At each lattice site, we must integrate over all possible values of the quark fields, considering multiple colors and flavors of quarks. Additionally, similar integrals must be performed over the gluon fields, which reside on the links connecting neighboring lattice sites. The dimensionality of these integrals grows with the size of the lattice, resulting in a staggeringly high-dimensional configuration space that defies exhaustive exploration using traditional numerical techniques.

To address this challenge, Monte Carlo methods offer an effective solution. Rather than attempting to evaluate the integrals analytically or through brute-force numerical techniques, Monte Carlo methods provide a probabilistic approach to sampling the high-dimensional configuration space. By generating a large number of random lattice configurations according to their probability distribution, Monte Carlo methods enable us to approximate the desired integrals by averaging over the sampled configurations. Most configurations yield a large action and thus have a very small weight in the path integral. It is the high-weight configurations that are most important to sample. Though there are many methods of sampling configurations according to their weight in the path integral, here we study one particular tool for sampling configurations, the Metropolis algorithm [11, 30].

Starting from some initial configuration of link variables, the Metropolis algorithm generates new configurations with probability proportional to their weight in the path integral. Let C be a configuration of link variables that we want to update to generate new configurations. Starting from C, the first step is to use Monte Carlo methods to suggest a new

configuration C' with probability $T_0(C \to C')$. With this new configuration selected, we have to decide whether or not to accept it. The candidate configuration is accepted with probability

$$T_A(C \to C') = \min\left[1,\ \frac{T_0(C' \to C)\exp(-S[C'])}{T_0(C \to C')\exp(-S[C])}\right] . \tag{1.57}$$

In practice, one often uses a symmetric probability distribution such that the probability of suggesting (but not necessarily accepting) the transition from C to C' is equal to the probability of suggesting the opposite transition:

$$P_0(C \to C') = P_0(C' \to C) . \tag{1.58}$$

In this case eq. (1.57) simplifies to

$$T_A(C \to C') = \min\left[1,\ \exp(-\Delta S)\right] , \tag{1.59}$$

where $\Delta S = S[C'] - S[C]$ is the change in action from the original configuration to the new configuration. In this special case, all changes that lower the action are accepted, and a new configuration that would increase the action is less likely to be accepted the greater the increase in action.

The total transition probability is then the product of the probability of the new configuration being suggested and the probability of the suggested configuration being accepted:

$$T(C \to C') = T_0(C \to C')T_A(C \to C') . \tag{1.60}$$

If the suggested change is not accepted, the original, unchanged configuration is kept.

The process of suggesting and accepting or rejecting new configurations is repeated many times, using the updated configuration as the starting point. To avoid correlations between configurations, one does not save every configuration for analysis, but repeats the process several times (perhaps 10 or so) before picking out a new configuration to be saved. One must also be careful to update the configurations many times before the first configuration is saved so that the configurations are distributed with the desired probability distribution.

An important restriction on the transition probabilities is that no configuration can have sinks or sources of probability. In other words, the probability of transitioning to a configuration C' in the nth step of the process has to be equal to the probability of transitioning out of C' at this step. The balance equation expressing this restriction can be written as

$$\sum_C T(C \to C')P(C) = \sum_C T(C' \to C)P(C')\,, \tag{1.61}$$

where $P(C)$ is the probability that the system is in configuration C. A sufficient condition for the balance equation to hold, known as the detailed balance condition,

$$T(C \to C')P(C) = T(C' \to C)P(C')\,, \tag{1.62}$$

is satisfied by the Metropolis algorithm. To see this, we evaluate the left side of the equation using the expression for $T(C \to C')$ and the fact the probability of being in a given configuration should be proportional to its weight in the path integral, $P(C) = \alpha \exp(-S[C])$, where we define α to be the constant of proportionality. Doing so yields the following result,

$$\begin{aligned}
T(C \to C')P(C) &= T(C \to C')\ \alpha \exp(-S[C]) \\
&= T_0(C \to C')\ \min\left[1,\ \frac{T_0(C' \to C)\exp(-S[C'])}{T_0(C \to C')\exp(-S[C])}\right] \alpha \exp(-S[C]) \\
&= \alpha\ \min\Big[T_0(C \to C')\exp(-S[C]),\ T_0(C' \to C)\exp(-S[C'])\Big] \\
&= T(C' \to C)\ \alpha \exp(-S[C']) \\
&= T(C' \to C)P(C')\,,
\end{aligned} \tag{1.63}$$

demonstrating that the balance equation is indeed satisfied.

The central value of Monte Carlo methods lies in their ability to generate statistically representative samples from complex probability distributions. Although we only examined the Metropolis algorithm, there are many different procedures for sampling configurations. Each provides us the means to navigate the high-dimensional configuration space efficiently, providing insights into the nonperturbative behavior of the strong interaction. Through the repeated sampling of lattice configurations, we can compute observables such as hadron

masses, correlation functions, and scattering amplitudes, shedding light on fundamental aspects of QCD that remain elusive to analytical or perturbative methods alone.

1.4 Chiral Perturbation Theory

Despite the success of lattice methods in determining properties of quark and gluon systems, lattice calculations are limited in scope by computing power. The lattice spacing, the size of the lattice, the mass of the quarks, and the number of particles in the box are all constrained by computing resources. To connect lattice results to continuum, infinite-volume quantities at physical quark masses, one needs a theoretical model for how such quantities can be extrapolated. Chiral perturbation theory (ChPT) provides a framework with which to make this connection [31–34].

1.4.1 Effective Field Theories

In many systems, including QCD under certain circumstances, the dynamics at low energies can be effectively described by a simpler theory than the underlying fundamental theory at high energies. Effective field theories like chiral perturbation theory take advantage of this fact, capturing the relevant degrees of freedom and interactions at a given energy scale, allowing for the perturbative calculation of physical observables within a limited domain of applicability. To understand effective field theories, we have to understand how high-energy degrees of freedom may become decoupled or irrelevant at low energies, thus reducing the complexity needed to describe the system.

Dependent on the momentum of the incoming and outgoing particles, correlation functions encode the observables of a quantum field theory. Nonanalytic behaviors like cuts and poles arise in these correlation functions when kinematics allow for the formation of physical intermediate states. We find that most of the complicated dynamics arise when intermediate states go on shell, resulting in singularities in their propagators, of the form $1/(p^2 + m^2)$ for a Euclidean theory.

Consider the contribution of a heavy intermediate state to a correlation function at low

energies, far from the pole in the propagator. One could Taylor expand the propagator in powers of the relevant momenta as follows:

$$\frac{1}{p^2+m^2} \approx \frac{1}{m^2} - \frac{p^2}{m^4} + \frac{p^4}{m^6} + \dots . \tag{1.64}$$

Far from the singularity, the propagator would be well approximated by the first few terms of the Taylor series. While Taylor expanding individual amplitudes may offer simplifications in specific cases, the key insight is that in scenarios where heavy particles are kinematically inaccessible, their contribution to the correlation function simplifies.

Rather than expanding the propagator, one can imagine expanding the Lagrangian in local operators involving only light degrees of freedom. This expansion, incorporating powers of external momenta divided by the scale of heavy physics, gives rise to an effective field theory (EFT). Despite its theoretical foundation as an infinite sum of local operators, EFTs are, out of practicality, truncated at the level required to give the desired accuracy.

1.4.2 Chiral Symmetry

Effective field theories like ChPT provide a bridge between the fundamental theory of the Standard Model and experimental observations, allowing for precise calculations and predictions in regimes where direct calculations from first principles are not feasible. ChPT is a systematic expansion of QCD observables in terms of small parameters associated with the quark masses and momenta. In the limit as the quarks become massless, chiral symmetry is an exact symmetry of QCD. It is in this low-energy, small-quark-mass limit—a regime in which QCD is non-perturbative and lattice calculations are particularly computationally expensive—that ChPT is most accurate. By expanding QCD observables in powers of the quark masses and momenta, ChPT provides a way to systematically incorporate the effects of finite lattice spacing and volume, as well as non-physical quark masses, into the calculations.

Let us start by considering the fermionic part of the Euclidean QCD Lagrangian:

$$\mathcal{L}_{\text{fermi}} = \bar{\psi}\gamma^\mu D_\mu \psi + \bar{\psi} M \psi \tag{1.65}$$

$$= \bar{\psi}_L \gamma^\mu D_\mu \psi_L + \bar{\psi}_R \gamma^\mu D_\mu \psi_R + \bar{\psi}_L M \psi_R + \bar{\psi}_R M^\dagger \psi_L \tag{1.66}$$

where ψ_L and ψ_R are the left- and right-handed components of the quark fields defined in eq. (1.56), and M is the quark mass matrix. Since chiral symmetry is a good approximate symmetry of QCD when the quarks are light, we are limited to including only the two or three lightest quarks flavors. To be precise, we must specify what it means for the masses to be light. One criterion is that the quark masses must be small compared to the QCD scale, $\Lambda_{QCD} \approx 300$ MeV; however, a more precise criterion arises from ChPT calculations: the meson masses should be small compared to $\Lambda_\chi \equiv 4\pi f_\pi \approx 1200$ MeV, where $f_\pi = 93$ MeV is the pion decay constant (in one particular convention). For the purposes of illustration, we will consider just the three lightest quarks: the up and down with $(m_u + m_d)/2 \approx 3$ MeV, and the strange with $m_s \approx 100$ MeV. The values of quark masses vary depending on the specific renormalization scheme and energy scale used in their determination. Here, we quote results for the $\overline{\text{MS}}$ renormalization scheme at a scale of $\mu = 2$ GeV. The choice of including the three lightest quarks leads to the mass matrix $M = \text{diag}(m_u, m_d, m_s) = M^\dagger$. By including strange quarks, the chiral symmetry is somewhat more badly broken than it would be if we just considered the lightest two quarks, since heavier mesons are formed with masses $m_K,\ m_\eta \approx \Lambda_\chi/2$.

In the massless limit, the left- and right-handed quark fields can be rotated independently so the Lagrangian has an exact $SU(3)_L \times SU(3)_R$ chiral symmetry under which the fields transform as

$$\psi_{L,R} \to U_{L,R}\ \psi_{L,R}\,, \quad \bar{\psi}_{L,R} \to \bar{\psi}_{L,R}\ U^\dagger_{L,R}\,, \quad \text{where} \quad U_{L,R} \in SU(3)_{L,R}\,. \tag{1.67}$$

One can decompose independent rotations of the left- and right-handed fields into transformations in which the left and right fields are rotated in the same way, $U_L = U_R$, corresponding to a vector symmetry; and transformations in which the left- and right-handed fields are rotated oppositely, $U_L = U_R^\dagger$, corresponding to an axial symmetry.

When the quarks have non-zero mass, the mass terms break the chiral symmetry, mixing the left- and right-handed fields. Specifically, non-zero masses break the axial symmetries, while non-degenerate masses break the vector symmetries. However, we can retain the chiral symmetry of the theory by treating the mass matrix, M, as a complex "spurion field," transforming as

$$M \to U_L M U_R^\dagger\,, \quad M^\dagger \to U_R M U_R^\dagger\,. \tag{1.68}$$

This trick allows us to keep track of the symmetry-breaking of the mass term.

1.4.3 Spontaneous Symmetry Breaking

In massless QCD, we expect chiral symmetry to be spontaneously broken by the vacuum. This expectation is based on an accumulation of experimental evidence including the lightness of the π, K, and the η, and the absence of parity-doubling in hadron spectra. We would expect to find degenerate states with opposite intrinsic parities were the symmetry unbroken. This evidence of spontaneous symmetry breaking motivates us to consider Goldstone's theorem, which states that spontaneous breaking of a continuous symmetry leads to the emergence of massless scalar particles called Goldstone bosons. These bosons arise due to the degeneracy of the vacuum manifold associated with the broken symmetry.

Goldstone's theorem can be illustrated using the wine bottle potential, which serves as an analogy for spontaneous symmetry breaking. In this potential, represented as

$$V = -\mu^2 \phi^\dagger \phi + \frac{\lambda}{2}(\phi^\dagger \phi)^2\,, \tag{1.69}$$

a $U(1)$ phase symmetry exists, denoted as $\phi \to \exp(i\alpha)\phi$. Spontaneous symmetry breaking occurs when $\mu^2 > 0$, leading to a non-zero vacuum expectation value (VEV), $|\langle\phi\rangle| = v = \sqrt{\frac{\mu^2}{\lambda}}$. The vacuum manifold, a circle of minima in the ϕ-plane, is formed by the phase of $\langle\phi\rangle$, making it $U(1)$. However, due to fluctuations or quantum effects, the system can settle into any point on this circle, breaking the $U(1)$ symmetry spontaneously. Consequently, the ground state becomes non-unique, as any point on the circle is energetically equivalent. In

non-relativistic quantum mechanics, the ground state would be spread around the vacuum manifold, but in quantum field theory, a single point on the vacuum manifold is picked out.

The Goldstone bosons emerge as excitations around the degenerate vacuum manifold. These excitations correspond to oscillations of the field along the flat circular base of the potential. Since these modes have zero energy, they give rise to massless particles, the Goldstone bosons, which are a manifestation of the broken symmetry. If we write our complex scalar field as

$$\phi(x) = ve^{\rho(x)}e^{i\theta(x)}\,, \tag{1.70}$$

we can explicitly pick out the Goldstone boson degree of freedom, θ, and "integrate out" the heavy radial degree of freedom ρ to obtain an effective Lagrangian in terms of $e^{i\theta(x)}$. When the symmetry is only approximate, such as in the presence of explicit symmetry-breaking terms in the Lagrangian, the masslessness of the Goldstone bosons is lifted, leading to the emergence of pseudo-Goldstone bosons. These pseudo-Goldstone bosons acquire small but nonzero masses due to the explicit breaking of the symmetry, resulting in them being light compared to other particles in the theory, as is the case for the π, K, and η mesons. Despite their nonzero masses, pseudo-Goldstone bosons often retain many properties of their massless counterparts, making them crucial in understanding the dynamics of broken symmetry systems.

The massless QCD analog of $\langle\phi\rangle$ is the condensate

$$\Omega_{ij} = \langle\psi_{L,i,\alpha,a}\bar{\psi}_{R,j,\alpha,a}\rangle \tag{1.71}$$

where i and j are flavor indices and α and a are the Dirac and color indices respectively. Here, we assume the conventional vacuum orientation in which $\Omega_{ij} = \omega\delta_{ij}$ with $\omega = -\langle\bar{q}q\rangle = -\langle(\bar{q}_L q_R + \bar{q}_R q_L)\rangle \neq 0$ for $q = u, d, s$. Since we are considering the massless theory, we have $\langle\bar{u}u\rangle = \langle\bar{d}d\rangle = \langle\bar{s}s\rangle$. In analogy to how we can promote $e^{i\theta(x)}$ to a field corresponding to the fluctuations in the condensate, we can promote Ω_{ij}/ω to a field $\Sigma_{ij}(x)$. Just as $e^{i\theta(x)}$ is an element of $U(1)$, the spontaneously broken symmetry of the wine bottle potential, $\Sigma_{ij}(x)$ is an element of the spontaneously broken $SU(3)$ axial symmetry:

$$\Sigma(x) \in SU(3) \quad \text{such that} \quad \Sigma(x) \to U_L\Sigma(x)U_R^\dagger \tag{1.72}$$

under chiral transformations. The fixed magnitude of Σ, such that $\Sigma\Sigma^\dagger = \Sigma^\dagger\Sigma = 1$, implies that the only degrees of freedom are the massless Goldstone bosons. If $\langle\Sigma\rangle = 1$, we can expand the field as

$$\Sigma(x) = \exp(2i\Pi(x)/f) = \exp(2i\pi^k(x)T^k/f)\,. \tag{1.73}$$

where T^k are generators of the spontaneously broken $SU(3)_A$ axial symmetry, π^k are the Goldstone boson fields, and f_π is a constant included to make the argument of the exponential unitless. Consistent with Goldstone's theorem, we see that there are 8 massless Goldstone bosons corresponding to the π, K, and η, each associated with one of the eight generators of the broken axial symmetry. For the conventional vacuum orientation, these are

$$\langle\pi^i(p)|\psi\gamma_\mu\gamma_5 T^j\bar{\psi}|0\rangle = -if p_\mu\delta^{ij}\,. \tag{1.74}$$

1.4.4 The Chiral Lagrangian

With this in hand, we have all the pieces required to construct an EFT: knowledge of the symmetries of the system we want to describe and a separation of scales. The massless Goldstone bosons (and the low-mass pseudo-Goldstone bosons) are much lighter than the heavier hadrons, like the proton, neutron, the ρ, and the η', which have masses on the order of 1 GeV. With this information, we are now able to build the ChPT Lagrangian.

The key elements of the EFT will be the fields Σ and $\Sigma^\dagger$, along with the spurion fields M and $M^\dagger$, which transform as

$$\Sigma \to U_L\Sigma U_R^\dagger\,, \quad \Sigma^\dagger \to U_R\Sigma^\dagger U_L^\dagger\,, \quad M \to U_L M U_R^\dagger\,, \quad M^\dagger \to U_R M^\dagger U_L^\dagger\,. \tag{1.75}$$

To construct our chiral Lagrangian, it is useful to work with objects that transform solely under the left-handed or right-handed subgroups. For the left-handed subgroup, we have the following objects:

$$L_\mu = \Sigma\partial_\mu\Sigma^\dagger = -\partial_\mu\Sigma\Sigma^\dagger = -L_\mu^\dagger \to U_L L_\mu U_L^\dagger\,, \tag{1.76}$$

$$M\Sigma^\dagger \to U_L(M\Sigma^\dagger)U_L^\dagger\,, \quad \Sigma M^\dagger \to U_L(\Sigma M^\dagger)U_L^\dagger\,, \tag{1.77}$$

while for the right-handed subgroup, we have:

$$R_\mu = \Sigma^\dagger \partial_\mu \Sigma = -\partial_\mu \Sigma^\dagger \Sigma = -R_\mu^\dagger \to U_R R_\mu U_R^\dagger \,, \tag{1.78}$$

$$M^\dagger \Sigma \to U_R (M^\dagger \Sigma) U_R^\dagger \,, \quad \Sigma^\dagger M \to U_R (\Sigma^\dagger M) U_R^\dagger \,. \tag{1.79}$$

Because one can cyclically permute matrices inside a trace, taking the trace of such an object results in a gauge invariant quantity. Using these building blocks, we can easily construct terms that satisfy the C, P, and T symmetries of QCD, and which are real and local. We will assume a power counting in which $p^2/\Lambda_{\rm QCD}^2 \sim m_q/\Lambda_{\rm QCD}$, treating terms with more than one factor of the mass matrix or two derivatives as higher-order in the expansion of the Lagrangian. Doing so allows us to write down the following leading-order chiral Lagrangian density:

$$\mathcal{L}_\chi^{\rm LO} = \frac{f^2}{4} {\rm tr}\left(\partial_\mu \Sigma \partial_\mu \Sigma^\dagger\right) - \frac{f^2 B_0}{4} {\rm tr}\left(M\Sigma^\dagger + \Sigma M^\dagger\right) \,, \tag{1.80}$$

where f and B_0 are unknown low-energy constants that can be determined by matching the predictions of ChPT to experimental results or lattice calculations. Higher orders in the power counting introduce new terms, each with their own low-energy constant. As we shall see in chapter 3, by treating the lattice spacing as a spurion, just as we did for the mass matrix, we can incorporate the effects of lattice discretization into our EFT, facilitating comparison between lattice QCD and ChPT, and allowing for a controlled extrapolation to the continuum.

1.5 Quantization Conditions

The strong interaction is characterized by an abundance of short-lived resonances, observed through scattering amplitudes of stable particles like pions, kaons, and nucleons. Resonances are very short-lived, non-asymptotic states that appear as distinct peaks in scattering experiments. These resonances exhibit intriguing patterns when classified by properties such as spin, charge, and strangeness, reflecting underlying quark and gluon degrees of freedom. Higher-lying resonances, like the $f_0(980)$ and $a_0(980)$, challenge the simplistic quark model

in which particles are analyzed as either baryons or mesons, suggesting more complex structures like tetraquarks or pentaquarks. Recent discoveries, such as the X, Y, and Z states, further highlight the need for a more nuanced understanding of hadron spectroscopy.

Lattice QCD offers a first-principles approach to predict hadron properties, approaching sub-percent level accuracy if one controls for statistical errors and uncertainties arising from lattice spacing, quark masses, and finite-volume effects. To understand these resonances, one can employ finite-volume quantization conditions, pioneered by Lüscher. Initially developed for two-particle scattering, these quantization conditions have been extended to three-particle systems, offering valuable insights into resonance physics. The essential observation that allows for the development of quantization conditions is that the volume dependence of the energies of multiparticle states is governed by infinite-volume scattering amplitudes. By analyzing the finite-volume spectrum, lattice QCD indirectly accesses scattering information critical for understanding resonances involving multiple particles.

1.5.1 The Two-Particle Quantization Condition

To understand how these quantization conditions arise in detail, we first turn our attention to the two-particle quantization condition [13, 14]. The derivation we sketch here assumes the system is described by a generic relativistic effective field theory (RFT) comprised of a single species of scalar field, though the derivation has been extended to more complex systems [15]. Let us use the scattering process $\pi^+\pi^+ \to \pi^+\pi^+$ as our motivation for the derivation. The goal is to find a quantitative relationship between the infinite-volume $2 \to 2$ scattering amplitude $\mathcal{M}_2 \equiv \mathcal{M}_{\pi^+\pi^+\to\pi^+\pi^+}$ and the finite-volume spectrum of the theory.

We begin by writing the Minkowski two-point finite-volume correlator:

$$C_L(E, \boldsymbol{P}) = \int_L d^4x e^{i(Ex^0 - \boldsymbol{p}\cdot\boldsymbol{x})} \langle 0|T\sigma(x)\sigma^\dagger(0)|0\rangle \,, \tag{1.81}$$

where $P^\mu = (E, \boldsymbol{P})$ is the four-momentum of the two-pion system and $\sigma^\dagger(x)$ is an interpolating operator creating a state at position x that couples to the desired $\pi^+\pi^+$ state. As we have seen in the context of the development of effective field theories, nonanalyticity arises in

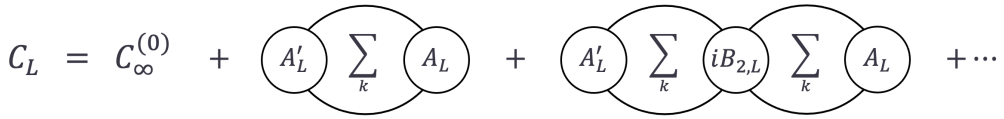

Figure 1.2: Skeleton expansion of the $2 \to 2$ finite-volume correlator, C_L

correlation functions when the intermediate states go on shell. This nonanalyticity encodes much of the interesting information about scattering processes and the finite-volume energy spectrum.

With this in mind, let us consider expressing the finite-volume correlator, C_L, as an infinite sum of Feynman diagrams in which we divide intermediate states into two classes: those with more than two internal lines, referred to as two-particle irreducible (2PI); and those with two or fewer internal states. The rationale for making this distinction is that if we restrict ourselves to the kinematic regime in which the center-of-mass frame (CMF) energy, $E^* \equiv \sqrt{E^2 - \boldsymbol{P}^2}$, is below the energy at which three-particle states can go on shell, then the two-particle irreducible segments of a Feynman diagram cannot contribute poles to the finite-volume correlator. We now repackage the two-particle irreducible sections into three types of terms: finite-volume amputated $2 \to 2$ Bethe-Salpeter kernels denoted $B_{2,L}$, encoding two-particle interactions; generalized endcaps A'_L and A_L, corresponding to the creation and annihilation of the $\pi^+\pi^+$ state; and C_L^0, which contains all diagrams that are completely 2PI. With these terms in hand, we can now express C_L in terms of a skeleton expansion, consisting of only these two-particle irreducible quantities, as depicted in figure 1.2.

We now make use of the Poisson summation formula to rewrite sums over finite-volume momenta in terms of integrals, up to exponentially suppressed corrections:

$$\frac{1}{L^3}\sum_k^{UV} f(k) = \int^{UV} \frac{d^3k}{(2\pi)^3} f(k) + \mathcal{O}(e^{-mL})\,. \tag{1.82}$$

Here, we require that $f(k)$ be a smooth function over the integration domain, for which the derivatives scale as powers of m. The UV scale is set by the lattice spacing, and for our purposes, the mass that appears will be m_π, the lightest degree of freedom in our system. We

will not keep track of exponentially suppressed volume corrections, as we will assume they are small for the mass scales and box sizes we consider. Using the Poisson summation formula, we can now equate the finite-volume Bethe-Salpeter kernel, $B_{2,L}$, with the infinite-volume quantity, $B_2 \equiv B_{2,\infty}$, up to exponentially suppressed finite-volume corrections. In fact, by neglecting these small corrections, we can make the following substitutions for each of the quantities appearing in our skeleton expansion: $B_{2,L} \to B_2$, $C_L^{(0)} \to C_\infty^{(0)}$, $A'_L \to A' \equiv A'_\infty$, $A_L \to A \equiv A_\infty$.

The next step is to project these infinite-volume kernels onto the physical shell. We begin by decomposing the kernels into spherical harmonics with angular momentum indices ℓ and m. We then rewrite the discrete finite-volume sums over the two-particle states that appear between adjacent 2PI kernels as $\Sigma = [\Sigma - \mathrm{PV}\int] + \mathrm{PV}\int$, where PV indicates that we are using a principal value prescription for the integral. We denote the first of these terms, corresponding to the sum integral difference, as

$$iF_2(\boldsymbol{P}, L) = \frac{1}{2}\left[\frac{1}{L^3}\sum_k - \mathrm{PV}\int \frac{d^3k}{(2\pi)^3}\right] \frac{i\mathcal{Y}_{\ell''m''}(\boldsymbol{k}^*)\mathcal{Y}^*_{\ell'm'}(\boldsymbol{k}^*)}{2\omega_k 2\omega_{P-k}(E - \omega_k - \omega_{P-k})} \tag{1.83}$$

which is a matrix of geometric functions that incorporate the L-dependence of the correlator. Here, $\omega_k \equiv \sqrt{m^2 + \boldsymbol{k}^2}$, while $\mathcal{Y}_{\ell m}(\boldsymbol{k}^*) = \sqrt{4\pi}(k^*/q^*)^\ell \, Y_{\ell m}(\boldsymbol{k}^*)$ is proportional to a spherical harmonic with the prefactor removing spurious singularities near $\boldsymbol{k}^* = 0$. Asterisks denote quantities evaluated in the center-of-mass frame, and $q^* = \sqrt{(E^*)^2/4 - m^2}$.

We denote the remaining part of the finite-volume sum, $\mathrm{PV}\int$, as $\mathcal{I}_{\mathrm{PV}}$, and we collect all occurrences of $\mathcal{I}_{\mathrm{PV}}$ adjacent to B_2 kernels into a new quantity

$$\mathcal{K}_2 = \sum_{m=0}^{\infty} \left[-B_2 \otimes \mathcal{I}_{\mathrm{PV}} \otimes\right]^m B_2 \,, \tag{1.84}$$

where we use $\otimes$ to indicate integration over the common momentum of adjacent quantities. $\mathcal{K}_2$ is related to the physical amplitude $\mathcal{M}_2$ via a simple algebraic relation involving the difference between the PV and $i\epsilon$ prescriptions:

$$\mathcal{M}_2 = \frac{1}{\mathcal{K}_2^{-1} - i/(8q^*E)} \,. \tag{1.85}$$

Associated with factors of iF_2, a "relevant cut" is an intermediate two-particle state that can go on shell. We now arrive at an infinite sum of terms with all possible numbers of these relevant cuts appearing:

$$C_L = \tilde{C}_\infty + \sum_{n=0}^{\infty} A' i F_2 \left[i\mathcal{K}_2 i F_2 \right]^n A \,. \tag{1.86}$$

The relevant cuts have the effect of projecting the adjacent K-matrices, as well as the other 2PI quantities, on shell such that we can replace each of the following quantities with their on-shell counterparts: $A' \to \tilde{A}'$, $A \to \tilde{A}$, and $C_\infty^{(0)} \to \tilde{C}_\infty$. Making these replacements and summing the geometric series in eq. (1.86), we arrive at an expression for the finite-volume correlator:

$$C_L = \tilde{C}_\infty + \tilde{A}' i F_2 \frac{1}{1 - i\mathcal{K}_2 i F_2} \tilde{A} \,, \tag{1.87}$$

where each quantity in the second term is an infinite-dimensional matrix with angular momentum indices ℓ and m. If the energy E lies in the finite-volume spectrum $\{E_{\boldsymbol{P},n}\}_{n=0}^{\infty}$, then C_L must have a pole arising from this second term. The implication is

$$\det[F_2^{-1}(E, \boldsymbol{P}, L) + \mathcal{K}_2(E^*)] = 0 \tag{1.88}$$

for energies in the finite-volume spectrum. This relationship between the finite-volume spectrum and $\mathcal{K}_2$, which is in turn related to $\mathcal{M}_2$, is the two-particle quantization condition. We emphasize that all power-law finite-volume dependence is contained in $F_2(E, P, L)$, a well-defined kinematic quantity that can be evaluated directly; whereas $\mathcal{K}_2(E^*)$ is an infinite-volume, on-shell, Lorentz invariant amplitude, closely related to the physical amplitude, $\mathcal{M}_2$. By parameterizing $\mathcal{K}_2(E^*)$ and attempting to match the energies that satisfy the two-particle quantization condition to the energies in the FV spectrum $\{E_{\boldsymbol{P},n}\}_{n=0}^{\infty}$, one can determine $\mathcal{K}_2$, and thus $\mathcal{M}_2$.

1.5.2 The Three-Particle Quantization Condition

Although the derivation of three-particle quantization conditions can be thought of as an extension of the derivation of the two-particle quantization condition, the introduction of a

third particle adds significant complexity absent from the two-particle case [16, 17]. Rather than include an exhaustive derivation of a three-particle quantization condition, we leave the details to chapters 5 and 6, in which we derive new three-particle quantization conditions for degenerate spin-$\frac{1}{2}$ particles, and for a multi-channel system appropriate for studying the $b_1(1235)$ and $\eta(1295)$ resonances. Here, we simply sketch the key steps in the derivation, applicable for any three-particle system, highlighting the similarities and differences to the two-particle quantization condition as we go.

The first step is to select the desired three-particle state. Consider a finite-volume correlator analogous to eq. (1.81) in the two-particle case,

$$C_{3,L}(E, \boldsymbol{P}) = \int_L d^4x e^{i(Ex^0 - \boldsymbol{p}\cdot\boldsymbol{x})} \langle 0|T\sigma_3(x)\sigma_3^\dagger(0)|0\rangle \,, \tag{1.89}$$

with σ_3 and $\sigma_3^\dagger$ operators coupling to the desired state. As was the case in the derivation of the two-particle quantization condition, we restrict the overall 4-momentum $P = (E, \boldsymbol{P})$ so that only this state is kinematically allowed to go on shell. For example, if we consider the case of a system of degenerate particles, the restriction is $m < E^* < 5m$; while for three non-degenerate particles with masses $m_1 \leq m_2 \leq m_3$ and a $\mathbb{Z}_2^3$ symmetry forbidding single-particle intermediate states, the restriction is $0 < E^* < 3m_1 + m_2 + m_3$.

As we did when deriving the two-particle quantization condition, we work in a generic relativistic effective field theory describing the interactions of the particles under consideration. However, rather than using Feynman diagrams, we will express $C_{3,L}$ as an infinite sum of diagrams in time-ordered perturbation theory (TOPT). In TOPT, one decomposes each Feynman diagram contributing to $C_{3,L}$ as a sum of all time orderings of the vertices, assigning a separate diagram to each possible ordering. The TOPT propagators are associated with an on-shell four-momentum $p^\mu = (\omega_p, \boldsymbol{p})$, giving rise to a factor of $1/(2\omega_p)$. Unlike for Feynman diagrams, spatial momentum is conserved at vertices, but energy is not. Crucially, in this expansion, we find a new type of kernel absent in the two-particle case that incorporates three-particle interactions: $B_{3,L}$. Much as $B_{2,L}$—which also enters into the three-particle correlator expansion—is the Bethe-Salpeter kernel containing two-particle

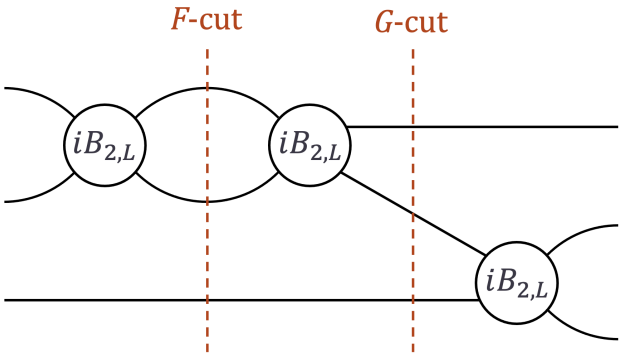

Figure 1.3: TOPT diagram of an F-cut and a G-cut between $2 \to 2$ Bethe-Salpeter kernels. The F-cut occurs between B_2 kernels in which the non-interacting particle is the same for both interactions. The G-cut occurs between kernels in which the non-interacting particle changes from one interaction to the next.

irreducible interactions, $B_{3,L}$ is the Bethe-Salpeter kernel associated with three-particle irreducible interactions.

Again, we can organize terms in the expansion by number of relevant cuts, though now the cuts correspond to sections consisting of the three-particle state of interest. What's more, in addition to the three-particle analogues of the F-cuts we saw in the two-particle quantization condition, there is a new type of cut, referred to as a G-cut. G-cuts allow for the exchange of a particle from one interacting pair to another, as can be seen in figure 1.3. By taking the infinite-volume limit of all sections involving irrelevant cuts, we arrive at a geometric series for the correlator expressed in terms of infinite-volume kernels.

By projecting the kernels on shell, we can rewrite $C_{3,L}$ in terms of on-shell two- and three-particle K-matrices, denoted $\mathcal{K}_2$ and $\widehat{\mathcal{K}}_{\text{df},3}$, along with the finite-volume kinematic quantities associated with the relevant cuts. As before, by examining the poles of a geometric series, we are able to obtain a quantization condition relating the finite-volume energy spectrum to the K-matrices:

$$\det[1 + \widehat{\mathcal{K}}_{\text{df},23,L}\widehat{F}_G] = 0\,, \tag{1.90}$$

where $\widehat{F}_G$ contains information about both the F- and G-cuts. This form of the quantization does, however, involve a K-matrix that is not Lorentz invariant and is asymmetric under particle interchange. To rewrite the quantization condition in terms of a symmetric, three-particle K matrix, denoted $\mathcal{K}_{\text{df},3}$, one must make use of symmetrization identities, discussed in more detail in chapters 5 and 6.

Whereas for the two-particle case, the relationship between $\mathcal{K}_2$ and $\mathcal{M}_2$ is given by a simple algebraic formula, the same is not true for the relationship between the K-matrices of the three-particle quantization condition and the corresponding physical scattering amplitudes, $\mathcal{M}_2$ and $\mathcal{M}_3$. Instead, they are related via nested integral equations. The solution of these equations is not a focus of this work, but the derivations of integral equations can be found in chapters 5 and 6.

Although the original RFT derivation was only applicable for identical spinless particles, subsequent works have expanded the domain of applicability to include systems of three distinct particles [35], "2+1" systems involving two species of one particle and one of another [36], and pion systems of arbitrary isospin [37]. This work goes further, and in chapter 5 we extend the formalism to incorporate spin, a non-trivial extension of the theory, while in chapter 6 the formalism is broadened to include transitions between multiple channels not simply related by isospin transformations.

It is worth noting that there are two other main approaches, in addition to the RFT approach laid out above, that have been used in the development of three-particle quantization conditions: the non-relativistic effective field theory (NREFT) approach [38, 39] and the finite volume unitarity (FVU) approach [40]. In this work, we focus on the development and application of the RFT approach and do not discuss the other methods in any detail.

1.6 Summary

This introduction has laid the groundwork for understanding the complexities of quantum chromodynamics and the challenges associated with its theoretical and numerical exploration. By introducing the fundamental concepts of QCD, such as gauge invariance and the

nonperturbative nature of the theory at low energies, we have seen the necessity of innovative methods beyond perturbation theory. Through the lens of lattice QCD, we explored how discretizing spacetime allows for the evaluation of correlation functions, shedding light on the behavior of quark and gluon fields in the low-energy regime. We have seen how chiral perturbation theory can complement lattice QCD calculations to provide reliable predictions by controlling for systematic errors, such as those arising from non-zero lattice spacing and non-physical quark masses. Lastly, our discussion of two- and three-particle quantization conditions underscores the vital role of finite-volume spectra in extracting scattering information. It is these quantization conditions that will be the focus of this body of work. Equipped with the foundational knowledge presented in this introduction, we are ready to delve into the research endeavors presented in the coming chapters.

Part II

THEORETICAL ADVANCEMENTS

The research presented in this section of the dissertation builds upon the foundational principles of quantum chromodynamics, lattice methods, effective field theories, and quantization conditions outlined in the introduction. The following five chapters comprise a compilation of the studies published during the course of this PhD.

The first study, discussed in chapter 2, explores the limitations of applying the two-particle quantization condition, introduced in section 1.5.1, to partially quenched theories in which valence quarks and sea quarks are treated differently. This chapter identifies specific conditions under which the quantization condition remains applicable despite violations of unitarity, addressing the challenges posed by partially quenched setups.

In chapter 3, the focus shifts to applying this framework to a partially quenched system with twisted-mass fermions. This chapter uses chiral perturbation theory, as detailed in section 1.4, to estimate the magnitudes of discretization errors, as well as errors arising from the application of the two-particle quantization condition in a theory that is not unitary.

The subsequent chapters concentrate on three-particle systems. Chapter 4 applies a three-particle quantization condition to study $\pi\pi K$ and $KK\pi$ scattering at maximal isospin. Utilizing extensive finite-volume energy data and fitting the spectra using the appropriate quantization condition, this chapter applies the ideas discussed in section 1.5.2 and again leverages the principles of chiral perturbation theory (section 1.4) to understand the results of the fits and put them in the context of previous work.

Chapter 5 introduces the finite-volume formalism for three identical spin-1/2 particles, relevant to systems like three neutrons or protons. This chapter addresses the complexities arising from spin interactions and provides a detailed derivation, setting the stage for future

explorations into nucleon interactions and other related systems.

The final work, detailed in chapter 6, generalizes the three-particle formalism to systems with multiple channels, focusing on $\pi\pi\eta$ and $K\overline{K}\pi$. This chapter tackles the intricacies of dealing with multiple subchannels. It provides a comprehensive approach for analyzing systems involving resonances like the $b_1(1235)$ and $\eta(1295)$, laying a foundation for future investigations into multi-channel interactions.

Chapter 2

APPLICABILITY OF THE TWO-PARTICLE QUANTIZATION CONDITION TO PARTIALLY-QUENCHED THEORIES[1]

2.1 Abstract

Partial quenching allows one to consider correlation functions and amplitudes that do not arise in the corresponding unquenched theory. For example, physical s-wave pion scattering can be decomposed into $I = 0$ and 2 amplitudes, while, in a partially-quenched extension, the larger symmetry group implies that there are more than two independent scattering amplitudes. It has been proposed that the finite-volume quantization condition of Lüscher holds for the correlation functions associated with each of the two-particle amplitudes that arise in partially-quenched theories. Using partially-quenched chiral perturbation theory, we show that this proposal fails for those correlation functions for which the corresponding one-loop amplitudes do not satisfy s-wave unitarity. For partially-quenched amplitudes that, while being unphysical, do satisfy one-loop s-wave unitarity, we argue that the proposal is plausible. Implications for previous work are discussed.

2.2 Introduction

Simulations of lattice QCD (LQCD) and related theories naturally separate into the generation of gauge fields and the calculation of quark propagators on these gauge fields. This separation allows one the freedom to "partially quench", which in broadest terms means treating valence and sea quarks differently. This can be done by using different valence- and sea-quark masses, or, as we consider here, by keeping valence- and sea-quark masses the

[1]Z. T. Draper and S. R. Sharpe, *Applicability of the two-particle quantization condition to partially-quenched theories*, *Phys. Rev. D* **104** (2021) 034510 [2107.09742]

same but considering correlation functions—combinations of quark propagators—that cannot arise in QCD. In either case, one obtains extra information about the underlying theory. The important questions are then whether that information is useful, e.g. for extracting physical quantities, and, if so, how the desired output is extracted.

There are many proposals for the extraction of additional information using partially-quenched (PQ) theories, several of which have been applied in practice. Most involve the use of partially-quenched chiral perturbation theory (PQχPT), which was developed in Ref. [42]. For reviews see Refs. [32, 43]. One usage is to aid the chiral extrapolation/interpolation to the physical point using a range of valence quark masses [44], and this has been widely applied in practice. Another example, closely related to the discussion below, is the proposal of Ref. [45] to separately calculate contributions to $\pi^+\pi^+$ correlators with and without quark exchange, so as to determine the lattice-spacing-dependent low-energy coefficients (LECs) of "WilsonχPT" (i.e. χPT applied to Wilson fermions). One can also use PQχPT to estimate quark-disconnected diagrams from more easily calculated correlators, e.g. in the hadronic vacuum polarization contribution to muonic $g-2$ [46], or in pion scattering [47]. We also note the use of partially quenched theories to study the spectral density of the Dirac operator [48–51] and its relation to random matrix theories [52].

This paper considers the proposals of Refs. [53, 54], which concern, respectively, $\pi\pi$ and $K\pi$ scattering in QCD. These works consider PQ extensions of QCD containing additional valence quarks (and corresponding ghost quarks) such that the flavor symmetry group extends from SU(2) to SU(4|2) for $\pi\pi$ scattering, and from SU(3) to SU(4|1) for $K\pi$ scattering.[2] Within these extensions the scattering amplitudes of pions and kaons (composed of either sea or valence quarks) can be decomposed into irreducible representations (irreps) of the quark flavor symmetry group, which is SU(4) in both cases. This group is larger than the symmetry group of the unquenched sea quarks, which is SU(2) and SU(3), respectively, for the two cases. This implies that the number of irreps, and associated independent ampli-

[2]The notation here is that the SU($n|m$) symmetry corresponds to $n-m$ sea quarks, m valence quarks, and m (commuting) ghost quarks. The flavor symmetry of the unquenched subsector is SU($n-m$).

tudes, is larger in the PQ theory than in the unquenched theory. For example, for s-wave $\pi\pi$ scattering, there are four independent amplitudes in the quark sector of the PQ theory, corresponding to the symmetric product of two adjoints in SU(4) [55],

$$(\mathbf{15} \times \mathbf{15})_{\text{sym}} = \mathbf{1} + \mathbf{15} + \mathbf{20} + \mathbf{84}\,, \tag{2.1}$$

whereas for unquenched pions in QCD the decomposition contains only two amplitudes, those with isospin 0 and 2. The physical $I = 2$ amplitude is equivalent to the **84**, while the $I = 0$ amplitude is equivalent to that obtained from an operator that is a linear combination of the **1** with elements of the **15**, **20** and **84**.[3] The remaining independent amplitudes, which we take to be those in the **15** and **20** irreps, are artifacts of the PQ theory, and correspond to linear combinations of Wick contractions that are not present in the unquenched theory.

We focus in this paper on nonsinglet irreps of the quark flavor group, as this simplifies the calculations and yet allows us to make our main points. We make some brief comments on the singlet irrep in the conclusions.

A central claim of Refs. [53, 54] is the following: for each of the PQ amplitudes, the corresponding PQ two-particle correlation function determines a spectrum of energies that can be related to the scattering amplitude using the two-particle quantization condition of Lüscher [13, 14]. We stress that this claim consists of two parts, the first that the correlation function can be used to extract a spectrum of states in the usual way, and the second that the resulting spectrum can be analyzed using the two-particle quantization condition. To make these statements concrete, consider the $r = \mathbf{15}$ irrep in PQ pion scattering, and let $\mathcal{O}_r$ be an operator with these quantum numbers. The first part of the claim is that

$$\langle \mathcal{O}_r(\tau) \mathcal{O}_r^\dagger(0) \rangle = \sum_{n=0}^{\infty} c_n e^{-E_n \tau} \tag{2.2}$$

where the expectation value is in the underlying PQ theory, τ is Euclidean time, the coefficients c_n are real and positive, and the energies E_n are real and bounded below. For

[3] The linear combination is $\frac{1}{5}\mathbf{1} + \frac{1}{2}\mathbf{15} + \frac{1}{4}\mathbf{20} + \frac{1}{20}\mathbf{84}$, as can be seen by considering the quark contractions. That this leads to a physical amplitude is not immediately clear from the group theory, but follows from the fact that operators living entirely in the unquenched sector are free from PQ artifacts.

convenience we order them $E_0 \leq E_1 \leq E_2$, etc. The second part of the claim is that we can insert the resulting energies E_n into Lüscher's quantization condition and correctly obtain the scattering amplitude in the corresponding irrep. We know that this procedure is valid for the **84** irrep, as it corresponds to a physical correlation function in QCD. The issue is whether it remains valid for the irreps available only in the PQ theory.

If correct, this proposal is quite powerful, as, combined with PQχPT, it allows the determination of results from types of contractions that are difficult to calculate numerically from those that are simpler to evaluate [47, 53, 54, 56]. It is, however, *prima facie* surprising, since both the existence of a normal spectral decomposition and the derivation of the two-particle quantization condition rely on unitarity, which the PQ theory violates [42, 57].

In this work we introduce a necessary (but not sufficient) criterion for whether this proposal holds in a given PQ irrep. We apply it in detail to $\pi\pi$ scattering, which allows us to develop alternative criteria for when the proposal will fail. We then apply these criteria to other systems.

The remainder of this paper is organized as follows. Section 3.3 describes the setup within PQχPT that we use to formulate our initial criterion. Section 2.4 presents the results of the application of this criterion to $\pi\pi$ scattering. Section 2.5 interprets these results using quark-line diagrams, presents two alternative versions of the criterion, and discusses the extent to which our necessary criterion is actually sufficient. Section 2.6 discusses a few applications of our criteria, and describes their implications for previous work. Finally, Sec. 6.7 presents some closing comments.

2.3 Theoretical setup

We follow closely the methodology of Ref. [45], although here we work in the continuum. We introduce two valence quarks in addition to the physical up and down quark, as well as two ghost quarks, with all quarks and ghost quarks having a common mass m. Thus the

graded flavor symmetry group is SU(4|2).[4] This is the same theoretical setup as used in Refs. [47, 53]. We label the quark fields q_i, $i = 1 - 4$, with $q_1 = u$ and $q_2 = d$ being thought of as the sea quarks, although this choice is purely conventional given the exact SU(4) quark flavor symmetry. The two ghost quarks are labeled $\widetilde{q}_5$ and $\widetilde{q}_6$. Using this collection of fields we can write down the PQQCD functional integral in Euclidean space as described in Ref. [42].

The long-distance properties of this theory are described by PQχPT. The degrees of freedom of this effective theory are the pseudo-Goldstone (PG) boson and fermion fields, which are collected into the following straceless[5] 6×6 matrix [42, 58],

$$\Pi = \frac{1}{\sqrt{2}} \begin{pmatrix} \frac{1}{\sqrt{2}}\pi_0 + \frac{1}{2}\eta_4 + \frac{1}{2}\phi_1 & \pi_{12} & \pi_{13} & \pi_{14} & \omega_{15} & \omega_{16} \\ \pi_{21} & -\frac{1}{\sqrt{2}}\pi_0 + \frac{1}{2}\eta_4 + \frac{1}{2}\phi_1 & \pi_{23} & \pi_{24} & \omega_{25} & \omega_{26} \\ \pi_{31} & \pi_{32} & \frac{1}{\sqrt{2}}\pi_0' - \frac{1}{2}\eta_4 + \frac{1}{2}\phi_1 & \pi_{34} & \omega_{35} & \omega_{36} \\ \pi_{41} & \pi_{42} & \pi_{43} & -\frac{1}{\sqrt{2}}\pi_0' - \frac{1}{2}\eta_4 + \frac{1}{2}\phi_1 & \omega_{45} & \omega_{46} \\ \omega_{51} & \omega_{52} & \omega_{53} & \omega_{54} & \frac{1}{\sqrt{2}}\phi_0 + \phi_1 & \phi_{56} \\ \omega_{61} & \omega_{62} & \omega_{63} & \omega_{64} & \phi_{65} & -\frac{1}{\sqrt{2}}\phi_0 + \phi_1 \end{pmatrix}. \tag{2.3}$$

Here π_0 is the usual neutral pion field (in isosymmetric QCD), with π_0' being the corresponding valence field, while η_4 is the four flavor generalization of the η meson in QCD. The 15 fields in the quark sector of Π fill out the SU(4) adjoint irrep of PG bosons (PGBs). The ω_{ij} are PG fermion (PGF) fields corresponding to quark-ghost combinations, while the ϕ_0, ϕ_{ij}, and ϕ_1 are PG ghost bosons (with propagators having an unphysical overall sign).

We will only need the leading order (LO) chiral Lagrangian for this theory, which is given in Euclidean space by

$$\mathcal{L}_{\text{LO}} = \frac{f^2}{4}\text{str}\Big(\partial_\mu \Sigma^\dagger \partial_\mu \Sigma\Big) - \frac{mB_0 f^2}{2}\text{str}\Big(\Sigma^\dagger + \Sigma\Big) \ , \tag{2.4}$$

where f and B_0 are the usual LO low-energy coefficients (LECs), with the former defined in

[4] Superficially, this differs from the setup in Ref. [45], where four valence quarks and corresponding ghost quarks were introduced, leading to an SU(6|4) flavor symmetry. For the purposes of our calculations, however, the difference is trivial: both calculations build the required operators out of four degenerate quark fields, leading to identical quark-level contractions and χPT results. The additional valence quarks were introduced in Ref. [45] in order to calculate a different quantity, as described in Appendix B of that work.

[5] We use "straceless" as a shorthand for having a vanishing supertrace, and refer to the latter as "strace" or "str".

the small f convention, and

$$\Sigma = \exp(2i\Pi/f)\,. \tag{2.5}$$

The masses of all the PGBs and PGFs are given, at LO, by

$$M_\pi^2 = 2B_0 m\,. \tag{2.6}$$

We note also that, because all the quarks and ghost quarks are degenerate, the PG propagators all contain only single poles, with no double-pole contributions [44, 58].

The relation of the pion fields in χPT to operators in the underlying theory can be worked out using the spurion method. The resulting correspondence is given for $j, k = 1-4$ by (see, e.g. Ref. [45]) $\bar{q}_j\gamma_5 q_k(x) = c(\Sigma - \Sigma^\dagger)_{kj}$, with c a known constant that will cancel in the ratios considered below. Choosing $j \neq k$ for simplicity, the right-hand side of this relation is proportional to π_{kj}, up to chiral corrections proportional to π^2/f^2. As discussed in Sec. C.1 of Ref. [45], these correction terms lead to subleading contributions to the correlation functions that lie beyond the accuracy that we consider. Thus we effectively have the correspondence $\pi_{kj} \sim \bar{q}_j\gamma_5 q_k$, and, similarly, $\pi^0 \sim \frac{1}{\sqrt{2}}(\bar{q}_1\gamma_5 q_1 - \bar{q}_2\gamma_5 q_2)$ and $\eta_4 \sim \frac{1}{2}(\bar{q}_1\gamma_5 q_1 + \bar{q}_2\gamma_5 q_2 - \bar{q}_3\gamma_5 q_3 - \bar{q}_4\gamma_5 q_4)$, with a common constant of proportionality. Using this correspondence, the definitions given below apply both in the underlying theory, PQQCD, and in the effective theory, PQχPT, and we will move between these two representations as needed.

The quantities that we calculate are finite-volume correlation functions involving operators coupling to pairs of PGB fields. These are built from fields having zero spatial momentum, e.g.

$$\widetilde{\pi}_{12}(\tau) = \int_L d^3x\, \pi_{12}(x,\tau)\,, \tag{2.7}$$

where the subscript L indicates that the integral is over a cubic box of side L. We assume periodic boundary conditions (PBC) in spatial directions on the PGBs and PGFs, which follow if the quark fields satisfy PBC, as it standard in LQCD simulations. We take the Euclidean time extent to be infinite. We then construct two-PGB operators by forming

linear combinations of the building blocks

$$\widetilde{\pi}_{ij}(\tau)\widetilde{\pi}_{k\ell}(\tau)\,, \tag{2.8}$$

chosen to have definite flavor quantum numbers. Explicit examples of such operators are given in the following section.

In a physical, unitary theory, we can describe the properties of these operators as follows. In the absence of interactions, such operators would simply couple to two pions at rest. In the presence of interactions, however, they couple to all states with vanishing total three-momentum, $\boldsymbol{P} = 0$, that have the same flavor as the operator. In particular, these operators couple to the lightest two-PGB state of the chosen flavor. We refer to this as the threshold state, with energy E_0. Of particular interest is the energy shift $\delta E_0 = E_0 - 2M_\pi$, for this is given by the threshold expansion of the Lüscher quantization condition [13]

$$\delta E_0 = -\frac{\mathcal{A}_{\rm thr}}{4M_\pi^2 L^3}\left[1 + c_1\frac{\mathcal{A}_{\rm thr}}{16\pi M_\pi L} + \mathcal{O}(L^{-2})\right]. \tag{2.9}$$

Here $\mathcal{A}_{\rm thr}$ is the scattering amplitude at threshold in the flavor channel under consideration, which is related to the scattering length a_0 by[6]

$$\mathcal{A}_{\rm th} = 16\pi M_\pi a_0\,, \tag{2.10}$$

while $c_1 \approx -2.84$ is a known geometric constant. We stress that both $\mathcal{A}_{\rm thr}$ and a_0 are infinite-volume quantities. Higher-order terms in $1/L$ in Eq. (2.9) are known, but will not be needed here. There are also (in general unknown) corrections to Eq. (2.9) that are exponentially suppressed in $M_\pi L$. In our theoretical calculation these can always be made arbitrarily small, compared to the power-law dependence that we control, by taking L large enough, and henceforth we ignore them.

To obtain δE_0 from finite-volume correlators, it is convenient to use ratios of the two-PGB correlator to the square of single-particle correlators. Let $\mathcal{O}_r(\tau)$ denote (as in the

[6]Here we are using the normalization appropriate for distinguishable particles.

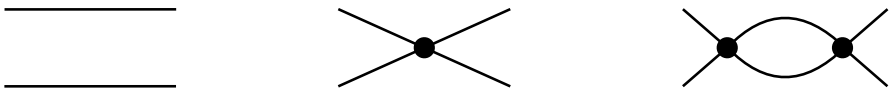

Figure 2.1: PQχPT diagrams contributing to $R_r(\tau)$, Eq. (2.11). Time runs horizontally. Solid lines are propagators of PGBs and PGFs, and filled circles represent vertices obtained from the expansion of $\mathcal{L}_{\rm LO}$, Eq. B.1. These are the diagrams needed to implement the test discussed in the text.

Introduction) a two-PGB operator transforming in the flavor irrep r. Then we consider

$$R_r(\tau) = \frac{\langle \mathcal{O}_r(\tau)\mathcal{O}_r^\dagger(0)\rangle}{\langle \widetilde{\pi}_{12}(\tau)\widetilde{\pi}_{21}(0)\rangle^2}\,. \tag{2.11}$$

where the choice of flavor of the single-PGB correlator in the denominator is arbitrary, because all such correlators fall asymptotically as $\exp(-M_\pi|\tau|)$, due to the SU(4) flavor symmetry. For a physical theory, the ratio behaves at large $|\tau|$ as

$$R_r(\tau) = Z_r e^{-\delta E_{0,r}|\tau|} + \text{excited-state contributions}\,, \tag{2.12}$$

where $\delta E_{0,r}$ is the threshold energy shift in the given flavor irrep, and Z_r is a positive real constant. In an analytic calculation, the contribution from excited states can be separated by hand, since they have a distinctive exponential falloff, with $\delta E_i \propto 1/L^2$ asymptotically. The first part of our criterion is then to check that what remains after excited-state contributions have been dropped is an exponential. More precisely, we test that the ratio contains the first three terms in the expansion,

$$R_r(\tau) = Z_r\left[1 - |\tau|\delta E_{0,r} + \frac{\tau^2}{2}(\delta E_{0,r})^2\right] + \dots\,, \tag{2.13}$$

where the ellipsis represents higher-order terms in τ as well as the excited-state contributions.

The second part of our criterion tests whether the threshold expansion, Eq. (2.9), holds to first nontrivial order in $1/L$. It turns out that one can test this, as well as Eq. (2.13), by

carrying out a next-to-leading-order (NLO) calculation of the correlator ratio in χPT. To see how this works, we need several results that follow from the similar calculation carried out in Ref. [45]. The relevant diagrams are those shown in Fig. 2.1. Diagram (a) gives the leading, τ-independent term in the exponential in Eq. (2.13), and one can choose the normalization of $\mathcal{O}_r$ such that $Z_r = 1$ at this stage. Diagram (b) leads to a term linear in $|\tau|$, in which $\delta E_{0,r} = -\mathcal{A}^{\rm LO}_{{\rm thr},r}/(4M_\pi^2 L^3)$, which is the form expected at this order from combining Eqs. (2.9) and (2.13). This result will hold for all irreps r, since the diagrams contributing to the finite-volume correlator and the scattering amplitude are essentially the same. Diagram (b) also leads to corrections to Z_r that are proportional to $1/(f^2 M_\pi L^3)$.

The key diagram for our test is that of Fig. 2.1(c). In particular, for a physical theory, it leads both to the τ^2 term in Eq. (2.13) with the LO form for the energy shift, $\delta E_{0,r} = -\mathcal{A}^{\rm LO}_{{\rm thr},r}/(4M_\pi^2 L^3)$, *and* to the first $1/L^4$ correction linear in $|\tau|$, i.e.

$$\delta E_{0,r} \supset -c_1 \frac{(\mathcal{A}^{\rm LO}_{{\rm thr},r})^2}{64\pi M_\pi^3 L^4}\,. \tag{2.14}$$

It is these contributions that will turn out to have the wrong form for some irreps in the PQ theory.

Diagram (c) also contributes to the leading $1/L^3$ part of the coefficient of $|\tau|$. Together with diagrams containing NLO vertices, as well as self-energy diagrams, this leads to the expected form of the linear term at this order [45]:

$$R_r(\tau) \supset |\tau| \frac{\mathcal{A}^{\rm NLO}_{{\rm thr},r}}{4M_\pi^2 L^3}\,, \tag{2.15}$$

where $\mathcal{A}^{\rm NLO}_{{\rm thr},r}$ is the complete threshold amplitude through NLO. As at LO, this result holds for all irreps r, because the diagrams that contribute to the $|\tau|/L^3$ term are the same as those leading to infinite-volume scattering. The only difference is that the former involve momentum sums, while the latter contain integrals, but the difference can be shown to be subleading, behaving as $|\tau|/L^4$, and leads to the c_1 term in Eq. (2.14) [45]. As stressed in Ref. [45], the result that the coefficient of $|\tau|/L^3$ gives the scattering amplitude is a finite volume version of the Lehman-Symanzik-Zimmermann reduction theorem.

Pulling all this together, we now state our criterion for whether a particular PQ channel can be treated as if it were physical.

> C1: *In order for a channel to be described by the two-particle quantization condition, one must find the following result*[7] *if one calculates the diagrams of Fig. 2.1:*
>
> $$R_r(\tau) = 1 + |\widetilde{\tau}| \left[\mathcal{A}^{\rm LO}_{{\rm th},r} + c_1 \frac{(\mathcal{A}^{\rm LO}_{{\rm th},r})^2}{16\pi M_\pi L} \right] + \frac{\widetilde{\tau}^2}{2} \left(\mathcal{A}^{\rm LO}_{{\rm th},r} \right)^2 + \dots \,, \tag{2.16}$$
>
> *where*
>
> $$\widetilde{\tau} = \frac{\tau}{4 M_\pi^2 L^3} \,, \tag{2.17}$$
>
> *and the ellipsis indicates terms of higher order in $|\widetilde{\tau}|$ and $1/L$, NLO contributions to $\mathcal{A}_{{\rm thr},r}$ in the $|\widetilde{\tau}|$ term, as well as excited state contributions.*

In other words, we can focus on the terms that lead to factors of $\mathcal{A}^{\rm LO}_{{\rm thr},r}$, with a full NLO calculation of this amplitude not required. Evaluating Fig. 2.1(b) gives the result for $\mathcal{A}^{\rm LO}_{{\rm thr},r}$, while Fig. 2.1(c) gives the c_1 and τ^2 terms, which must have the dependence on $\mathcal{A}^{\rm LO}_{{\rm thr},r}$ given in Eq. (2.16). We also note that one can check the calculation of Fig. 2.1(b) by evaluating the amplitude $\mathcal{A}^{\rm LO}_{{\rm thr},r}$ directly in infinite volume.

Passing this test is necessary in order that a channel can be treated as physical, but it is clearly not sufficient, since higher order terms in τ and in the threshold expansion of Eq. (2.9) are not checked. In addition, the test considers only the threshold state, while a complete test would also consider excited states. Possible generalizations are discussed below in Sec. 2.5.

2.4 PQχPT calculation of $\pi\pi$ correlators

We perform the test described in the previous section for the **20** and **15** irreps, which are the two that are absent in the unquenched theory. For comparison we also include the **84**

[7] Here we are assuming the above-described normalization choice for $\mathcal{O}_r$.

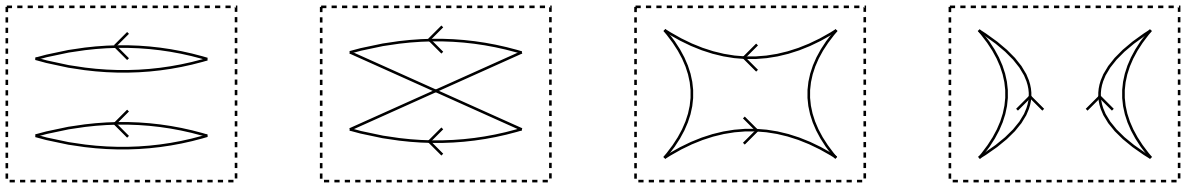

(a) D (b) S (c) R (d) V

Figure 2.2: Types of Wick contraction that contribute to the two-pion correlators, $R_r(\tau)$. Time runs horizontally. Solid lines represent quark propagators, while the dashed box is a reminder that the correlators are evaluated in finite spatial volumes.

irrep. Examples of two-pion operators transforming in these irreps are

$$\mathcal{O}_{\mathbf{84}} = \frac{1}{\sqrt{2}}\left(\widetilde{\pi}_{12}\widetilde{\pi}_{34} + \widetilde{\pi}_{14}\widetilde{\pi}_{32}\right) \tag{2.18}$$

$$\mathcal{O}_{\mathbf{20}} = \frac{1}{\sqrt{2}}\left(\widetilde{\pi}_{12}\widetilde{\pi}_{34} - \widetilde{\pi}_{14}\widetilde{\pi}_{32}\right) \tag{2.19}$$

$$\mathcal{O}_{\mathbf{15}} = \frac{1}{\sqrt{3}}\left(\widetilde{\pi}_{13}\widetilde{\pi}_{32} + \widetilde{\pi}_{14}\widetilde{\pi}_{42} + \widetilde{\pi}_{12}\widetilde{\eta}_{4}\right) . \tag{2.20}$$

The normalization factors are chosen as described in the previous section, i.e. such that the leading term in R_τ is unity. In the notation of Ref. [53] these three irreps are labeled α, β and γ, respectively. The LO threshold amplitudes for these irreps can be read off from the results for scattering lengths given in Ref. [53] (noting that the scattering length in that work is defined with opposite sign to ours), yielding

$$\mathcal{A}^{\mathrm{LO}}_{\mathrm{thr},\mathbf{84}} = -\frac{M_\pi^2}{f^2}\,, \qquad \mathcal{A}^{\mathrm{LO}}_{\mathrm{thr},\mathbf{20}} = \frac{M_\pi^2}{f^2}\,, \qquad \mathcal{A}^{\mathrm{LO}}_{\mathrm{thr},\mathbf{15}} = \frac{7}{2}\frac{M_\pi^2}{f^2}\,. \tag{2.21}$$

The implementation of the criterion C1 for the **84** and **20** irreps can be done by combining results from Ref. [45]. In the notation of that work

$$R_{\mathbf{84/20}}(\tau) = R_{\mathcal{D}}(\tau) \pm R_{\mathcal{S}}(\tau)\,, \tag{2.22}$$

where $R_{\mathcal{D}}$ involves the double-loop (or "direct" or D for short) Wick contraction in the numerator of the ratio, while $R_{\mathcal{S}}$ involves the single loop ("S") contraction, which are shown

in Figs. 2.2(a) and (b), respectively. In Refs. [47, 53], the latter contraction is labeled C for crossed. The results for $D(\tau)$ and $S(\tau)$ at NLO in PQχPT are given in Eqs. (104) and (105) of Ref. [45], including the effect of discretization errors for Wilson-like fermions. Setting all LECs associated with discretization errors to zero, and choosing $\tau > 0$ as in Ref. [45], the results read

$$R_{\mathcal{D}}(\tau) = 1 + \widetilde{\tau}\mathcal{D} + \left(\frac{M_\pi^2}{f^2}\right)^2 \left[\widetilde{\tau}\frac{c_1}{16\pi M_\pi L} + \frac{\widetilde{\tau}^2}{2}\right] + \dots\,, \tag{2.23}$$

$$R_{\mathcal{S}}(\tau) = \widetilde{\tau}\mathcal{S} + \dots\,. \tag{2.24}$$

Here $\mathcal{D}$ and $\mathcal{S}$ are the NLO PQ threshold amplitudes associated with the D and S contractions, and are given in Eqs. (106) and (107), respectively, of Ref. [45]. We only need their LO contributions, which are

$$\mathcal{D}^{\rm LO} = 0\,, \qquad \mathcal{S}^{\rm LO} = -\frac{M_\pi^2}{f^2}\,. \tag{2.25}$$

Finally, we form the combinations given in Eq. (2.22), obtaining (again for $\tau > 0$)

$$R_{\mathbf{84/20}}(\tau) = 1 + \widetilde{\tau}(\mathcal{D} \pm \mathcal{S}) + \left(\frac{M_\pi^2}{f^2}\right)^2 \left[\widetilde{\tau}\frac{c_1}{16\pi M_\pi L} + \frac{\widetilde{\tau}^2}{2}\right] + \dots\,, \tag{2.26}$$

Since $(\mathcal{D} \pm \mathcal{S})^{\rm LO} = \mp M_\pi^2/f^2$, we see that the results for both irreps satisfy the criterion C1, i.e. Eq. (2.16) with the LO amplitudes given in Eq. (2.21).[8] This is as expected for the physical $r = \mathbf{84}$ channel, while, for the $r = \mathbf{20}$ channel, it supports the proposal of Ref. [53] that one can apply the quantization condition to this unphysical channel.

Now we turn to the **15** irrep, for which a new calculation is needed. In terms of valence quark Wick contractions, one needs not only D and S contractions, but also the "rectangle" or R contraction shown in Fig. 2.2(c). We find, using $\mathcal{O}_{\mathbf{15}}$ from Eq. (2.20), that

$$R_{\mathbf{15}}(\tau) = R_{\mathcal{D}}(\tau) - \frac{1}{2}R_{\mathcal{S}}(\tau) + 3R_{\mathcal{R}}(\tau)\,, \tag{2.27}$$

[8] This result in fact holds even if we keep all contributions from the LO LECS associated with discretization errors.

in agreement with Ref. [53]. Evaluating the diagrams in Fig. 2.1, we obtain (with $\widetilde{\tau} > 0$)

$$R_{\mathbf{15}}(\tau) = 1 + \widetilde{\tau}\frac{7M_\pi^2}{2f^2} + \underbrace{\left[\frac{49}{4} - 6 - \frac{3}{4}\right]}_{11/2}\left(\frac{M_\pi^2}{f^2}\right)^2\left[\widetilde{\tau}\frac{c_1}{16\pi M_\pi L} + \frac{\widetilde{\tau}^2}{2}\right] + \dots\,, \tag{2.28}$$

where the ellipsis has the same meaning as in Eq. (2.16). The calculation leading to Eq. (2.28) is straightforward, as the $c_1\widetilde{\tau}$ and $\widetilde{\tau}^2$ terms essentially pick out contributions that are part of the square of the tree-level threshold amplitude. The only subtlety is keeping track of which two-particle intermediate states contribute, and of cancellations between contributions involving PG bosons and fermions. We have broken down the contribution to the final term in Eq. (2.28) into that from the following intermediate states: $\pi_{13}\pi_{32}$, $\pi_{14}\pi_{42}$ and $\pi_{12}\eta_4$ (leading to the unquenched result $49/4 = (7/2)^2$), $\omega_{15}\omega_{52}$ and $\omega_{16}\omega_{62}$ (leading to the -6), and $\pi_{12}\phi_1$ (leading to the $-3/4$). We have obtained these results using both the straceless form of Π given in Eq. (3.10) and an approach in which one projects out the stracefull part by introducing a Φ_0^2 term [58].

Equation (2.28) is the main new result of this paper. It is manifestly inconsistent with the form of Eq. (2.16), because the coefficient of the $\widetilde{\tau}^2$ and $c_1\widetilde{\tau}$ contributions is not the square of the LO threshold amplitude (which itself is correctly determined from the coefficient of $\widetilde{\tau}$). Thus, the $r = \mathbf{15}$ channel fails our test: $R_{\mathbf{15}}(\tau)$ cannot be given by a single exponential at long times, and the two-particle quantization condition cannot be used.

2.5 Diagrammatic interpretation and alternative criteria

To gain more understanding of why the **15** irrep does not satisfy our criterion, while the **20** does, we consider the quark-line diagrams[9] associated with the corresponding contributions to Fig. 2.1(c). These are shown for the **15** irrep in Fig. 3.1. The key observation is that, for $r = \mathbf{20}$, only diagrams of the type of Fig. 3.1(a) appear, with the four lines having different flavors. This difference arises simply because there can be no "annihilation" of quark flavors for $r = \mathbf{20}$, which is why the R-type Wick contraction, Fig. 2.2(c), is not present.

[9]For more discussion of quark-line diagrams see Ref. [32].

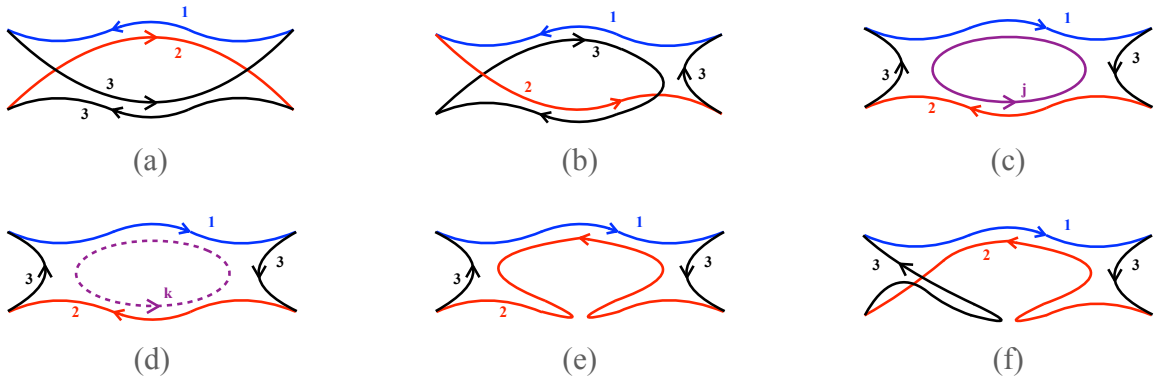

Figure 2.3: Classes of quark-line diagrams contributing to Fig. 2.1(c) for the **15** irrep. The diagrams trace the flavor indices of the quarks and antiquarks (or their ghost partners) in the PQχPT diagrams. Flavors are indicated by colors and numerical labels, with $j = 1 - 4$ in (c) and $k = 5 - 6$ in (d). Dashed lines indicate ghost-quark flavors. In diagrams (e) and (f) the hairpin vertices implicitly contain an infinite sum of intermediate loops of sea quarks (with the valence and ghost loops canceling).

This absence implies that there is no violation of unitarity in the s-channel in the one-loop diagrams, and it is this form of unitarity (which we refer to as s-channel unitarity) that the exponential time dependence and the derivation of the quantization condition depend on.

Conversely, for $r = \mathbf{15}$, the appearance of s-channel loops involving either ghost quarks [Fig. 3.1(d)] or neutral PGBs with negative norms such as ϕ_0 [Figs. 3.1(e) and (f)] suggests that s-channel unitarity is violated. We emphasize, however, that it is not sufficient to look at the diagrams alone, as the s-channel-unitarity-violating contributions can cancel. This indeed happens in the $I = 0$ channel, for which there are both R and V Wick contractions [Figs. 2.2(c) and (d)], and thus PQ diagrams involving ghost quarks and negative norm PGBs. Nevertheless, we know that these unphysical contributions must cancel, as this channel is physical.

Putting this together, the following diagrammatic version of the criterion seems highly plausible:

C2: *A channel that is not equivalent to a physical correlator will not be described by the two-particle quantization condition if intermediate ghost quarks appear in (the quark-line diagrams of) s-channel two-particle loops.*

This criterion correctly selects the **15** irrep as the single PQ nonsinglet $\pi\pi$ channel that is problematic. We have not included negative norm PGBs in the statement of C2 as it requires explicit calculations to determine whether they are present, and we are aiming here for a simplified criterion. We suspect, however, that nothing is lost by this omission, since, in our experience, diagrams with intermediate ghost quarks and negative norm PGBs come in tandem. C2 is potentially stronger than our original criterion, C1, as it applies away from threshold. We have, however, not found a general proof of C2, since this requires knowing that the total contribution from certain classes of quark-line diagrams does not cancel, and this can, in general, only be determined by an explicit calculation, leading us back to C1.

These diagrammatic considerations lead to another version of the criterion. To explain this, we need to distinguish between unitarity in the s, t and u channels. As noted above, we refer to the standard form of unitarity for an amplitude $\mathcal{T}(s,t,u)$ in the physical domain ($s \geq 4M_\pi^2$ and $t, u \leq 0$) as s-channel unitarity. One can also apply unitarity in the t channel by continuing the amplitude to the appropriate kinematic domain, $t \geq 4M_\pi^2$ and $u, s \leq 0$, and similarly for the u channel. An important point to keep in mind is that PQ amplitudes can satisfy unitarity in some channels but not in others. For example, the amplitude $\mathcal{A}_{\mathbf{20}}$ satisfies s-channel unitarity, but violates t- and u-channel unitarity. This is illustrated in Fig. 2.4, where examples of quark line diagrams contributing to t-channel loops are shown. The presence of the diagrams (b) and (c) indicates the violation of t-channel unitarity.

Using this terminology, the third version of the criterion is

C3: *A channel is not described by the two-particle quantization condition if the (infinite-volume) amplitude $\mathcal{A}_r$ violates s-channel unitarity.*[10]

[10]We stress that we are only considering energies below the first inelastic threshold, e.g. below the four pion threshold for $\pi\pi$ scattering. Above this, the two-particle quantization condition itself breaks down and the question becomes moot.

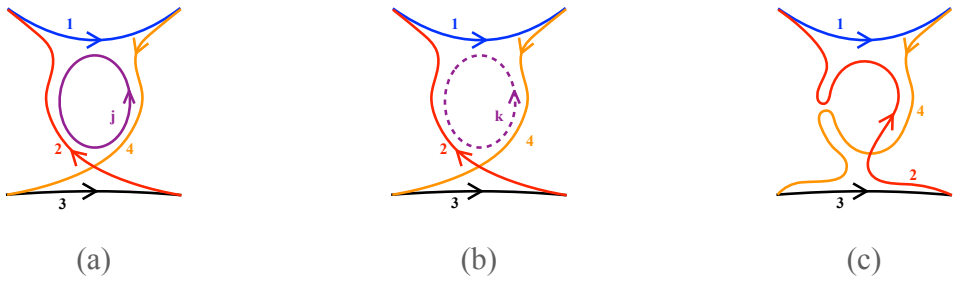

Figure 2.4: Examples of quark-line diagrams contributing to the t-channel loops for scattering in the **20** irrep. Notation as in Fig. 3.1.

Again, this correctly picks out the **15** $\pi\pi$ irrep. The simplest argument for C3 is that s-channel unitarity plays a crucial role in the derivation of the two-particle quantization condition, as is particularly clear from the derivation of Ref. [15]. C3 is stronger than the original form, C1, as the latter involves unitarity applied only infinitesimally above threshold, while C3 applies for all energies up to the first inelastic threshold.

To study C3 in χPT requires at least a NLO calculation, since loops are required for the unitarity condition to have nontrivial content. Indeed, from the NLO results for PQ $\pi\pi$ amplitudes in Ref. [47], one can see that s-channel unitarity is violated by $\mathcal{A}_{\mathbf{15}}^{\mathrm{NLO}}$. In general, C3 is harder to implement than C1, as it requires a more extensive calculation in χPT.

We end this section by discussing whether the criteria that we have introduced are actually sufficient rather than necessary. We suspect that this is the case, although to demonstrate this would require an all-orders analysis in χPT, which is beyond the scope of this work. The point is that higher order terms in the exponential in τ, and in the threshold expansion of the quantization condition, are built up by a sequence of intermediate two-particle s-channel loops, as is clear, respectively, from the calculations of Ref. [45] and the derivation of Ref. [15]. The corresponding quark-line diagrams for any irrep that passes the criteria will only involve generalizations of Fig. 3.1(a), in which quarks or antiquarks are repeatedly exchanged. In particular, there can be no annihilation diagrams at any order in χPT. The

unphysical contributions in t and u channels, such as those in Fig. 2.4, will be present, but will appear in all vertices, allowing exponentiation.

2.6 Applications and implications for previous work

We first summarize our results for the $\pi\pi$ system. In the PQ theory there are three flavor nonsinglet channels, of which one (the **84**) is equivalent to a physical channel (with $I = 2$), which thus automatically satisfies our criteria. Of the unphysical channels, one satisfies our criteria (**20**), while the other does not (**15**).

What are the implications for the application presented in Ref. [53]? In that work, the quantization condition was first applied to LQCD results in the **84** and **20** channels, and this application is thus not affected by the problem noted here. The results obtained were then used to predict the finite-volume energy spectrum in the **15** and $I = 0$ channels, while our analysis shows that there is no well-defined spectrum in the **15** channel.

We next turn to the $K\pi$ system, which has been analyzed in this context in Refs. [54,56]. Since there are now three light quarks, the isospin symmetry generalizes from SU(2) in the physical theory to SU(3) in the PQ version, which is the light quark subgroup of the graded SU(4|1) symmetry. This SU(3) is exact (assuming $m_u = m_d$), and should not be confused with the approximate SU(3) in QCD involving the strange quark. There are two physical channels, with $I = 3/2$ and $1/2$, while there are three PQ channels, corresponding to the SU(3) decomposition $\mathbf{8} \times \mathbf{3} = \mathbf{15} + \overline{\mathbf{6}} + \mathbf{3}$. These three channels are labeled α, β, and γ, respectively, in Ref. [54]. Of these, only the $\overline{\mathbf{6}}$ is unphysical, with the **15** being equivalent to the physical $I = 3/2$ channel, and the **3** to that with $I = 1/2$.

Applying the criterion C2 to the $\overline{\mathbf{6}}$ channel, we find that it passes our test, because it involves Wick contractions only of types D and S, and is thus completely analogous to the **20** irrep for $\pi\pi$ scattering. Therefore, the numerical application presented in Ref. [56], which uses the **15** and $\overline{\mathbf{6}}$ channels, does not suffer from the problem described here.

The final example we consider involves two kaons, for which the PQ extension has not been previously analyzed. For the KK system, the PQ extension involves treating the two

strange antiquarks as different, while the two light quarks can both be physical. Thus the graded symmetry group becomes $\mathrm{SU}(2) \times \mathrm{SU}(2|1)$, where the $\mathrm{SU}(2)$ is physical isospin. Thus PQ channels can be labeled by physical isospin, I, as well as "strange isospin", I_s, with both taking on the values 0 or 1. For s-wave scattering, the overall symmetry implies that there are two allowed channels, with $(I, I_s) = (1, 1)$ or $(0, 0)$, which are, respectively, symmetric and antisymmetric under quark (or antiquark) exchange . Only the former is physical. Again, the sole unphysical channel, $(0, 0)$, satisfies our criterion C2, since only contractions of type D and S are allowed as there is no annihilation in the s channel. Thus the quantization condition could be applied to both channels.

2.7 Conclusions

This paper has demonstrated that the violation of unitarity in PQ theories at best restricts the application of the two-particle quantization condition to a subset of the unphysical two-particle channels. This has been demonstrated using PQχPT, and our initial criteria C1 is stated within this effective field theory (EFT) framework. In this regard, we stress that the foundations of PQχPT as an effective theory for PQQCD are almost as strong as for QCD [57]. However, we have argued that C1 can be replaced by simpler, diagrammatic extension of the criterion, C2. This alternative version can be used irrespective of the existence of an EFT.

What is perhaps most surprising is that there may be unphysical two-particle channels in which the quantization condition *can be used*, because the derivation of the latter relies on unitarity, which is certainly violated in the PQ theory. The key observation here is that what matters for the derivation is that the corresponding scattering amplitude is unitary in the s channel, while t- and u-channel unitarity is not required. Thus for channels where the amplitude manifests its unphysicality only in the latter two channels, the problem that we raise does not occur.

We stress that, strictly speaking, we have not demonstrated this positive result, but rather only shown that one possible problem does not arise. However, we think it likely that

one could extend the argument given here to all orders in the EFT, and that, for channels that satisfy our simple criteria, the use of the quantization condition is justified.

We also note that all is not lost in the channels that do not satisfy our criteria. One can still calculate the corresponding finite-volume correlators using PQχPT, fit the results of a lattice simulation to the predicted form, and in this way determine the parameters of the EFT. This is the approach suggested in Ref. [45]. We stress, however, that our results show that one cannot bypass the problem by determining the energy shift solely from the term in the correlator ratio that is linear in τ, and inserting the result into the two-particle quantization condition, because the leading c_1/L correction in that condition does not hold in PQ channels that do not satisfy our criteria.

Applying our criteria to the $\pi\pi$ and $K\pi$ systems, we find that the two previous applications which use results from simulations of LQCD are in unphysical channels that are *not* affected by the issue that we raise. Thus, the practical impact of our observation is to limit certain future applications of the approach of Refs. [53, 54].

One way of understanding our central result is that, in a PQ theory, even if one starts with an operator that is composed of sea and valence quarks alone, in general there will be mixing with operators that include ghost quarks. In the calculation of Sec. 2.4, this mixing was with operators of the form $\omega_{1k}\omega_{k2}$ and $\pi_{12}\phi_1$, both of which transform in the same **15** irrep of the SU(4) quark flavor group. One might hope that, by taking an appropriate linear combination of these operators, one could find a channel for which one could use the quantization condition. This amounts to classifying operators under the full SU(4|2) group, a task that we have not undertaken. We do not, however, expect this approach to be fruitful, since intermediate states will inevitably involve unphysical particles. For the same reason, we expect that the SU(4) singlet channel, where there can be mixing with several unphysical channels (including ϕ_0^2), cannot be analyzed using the quantization condition.

A final comment concerns the foundational work of Bernard and Golterman [57]. They construct the transfer matrix of (latticized) PQQCD, showing that, while it is not hermitian, it has a bounded spectrum. The import is that one expects correlation functions to still

be given by a sum of exponentials as in Eq. (2.2), except the coefficients c_n need not be positive. Furthermore, the energies E_n, while having real parts that are bounded from below, could be complex, although Ref. [57] argues that this is not the case for the lightest excitations in PQχPT. Thus it could be that one can develop a generalization of the two-particle quantization condition that takes into account the possibility of negative c_n, and the concomitant cancellations. The lack of a simple exponential fall off that we have found could then be due to a cancellation between terms falling with similar exponents but opposite coefficients. The failure of the standard Lüscher threshold expansion could be due to the need to use an extension of the two-particle formalism. We do not know if such an approach will be fruitful, but it may be worth considering.

Acknowledgments

We thank Maarten Golterman, Max Hansen, Ulf Meißner and Fernando Romero-López for very helpful comments and suggestions. This work is supported in part by U.S. Department of Energy Award No. DE-SC0011637.

Chapter 3

$\pi\pi$ SCATTERING IN PARTIALLY-QUENCHED TWISTED-MASS CHIRAL PERTURBATION THEORY[1]

3.1 Abstract

We study pion-pion scattering in partially-quenched twisted-mass lattice QCD using chiral perturbation theory. The specific partially-quenched setup corresponds to that used in numerical lattice QCD calculations of the $I = 0$ scattering length. We study the discretization errors proportional to a^2, with a the lattice spacing, and the errors that arise due to the use of Lüscher's two-particle quantization condition in a theory that is not unitary. We argue that the former can be as large as $\sim 100\%$, but explain how they can be systematically subtracted using a calculation of the $I = 2$ scattering amplitude in the same partially-quenched framework. We estimate the error from the violation of unitarity to be $\sim 25\%$, and argue that this error will be difficult to reduce in practice.

3.2 Introduction

Considerable progress has been made over the last decade in studying two-particle scattering at physical, or near-physical, quark masses [60–68]. Our focus here will be on calculations using the twisted-mass (TM) formulation of lattice QCD (LQCD) [69]. In particular, the ETM collaboration has used TM fermions to determine scattering lengths in the following channels: K^+K^+ [70], $K^+\pi^+$ [71], and $\pi\pi$ scattering for $I = 2$ [62, 72] and $I = 0$ [63]. All these works are done at maximal twist, and make use of the two-particle quantization condition derived by Lüscher [13, 14].

---

[1] Z. T. Draper and S. R. Sharpe, *$\pi\pi$ scattering in partially-quenched twisted-mass chiral perturbation theory*, *Phys. Rev. D* **105** (2022) 034508 [2111.13975]

The work we consider in most detail here is the calculation of the $I = 0$ $\pi\pi$ scattering length in Ref. [63]. The $I = 0$ channel is the most challenging from a numerical point of view, due to the presence of fully disconnected quark diagrams, and is likely to have the largest systematic errors. For technical reasons described below, Ref. [63] used a partially quenched (PQ) setup, in which some of the valence quarks have differing twist angles from the corresponding sea quarks. These valence quarks are referred to as Osterwalder-Seiler (OS) quarks [73]. Using a PQ theory implies that unitarity is violated [42, 57], which introduces an additional source of systematic error. Our aim here is to use chiral perturbation theory (χPT) to shed new light on the errors due to discretization and the violation of unitarity. In this regard we note that, so far, results are only available at a single lattice spacing. The specific version of χPT that we use incorporates the effects of partial quenching and discretization errors due to the twisted-mass, and is denoted PQTMχPT.

A key feature of TMLQCD at maximal twist is that discretization errors for physical quantities are automatically $\mathcal{O}(a)$ improved [74]. Even so, when working at the physical point, generic discretization effects are comparable to those due to the nonzero values of the physical light quark masses. To see this, recall that in χPT, a measure of the former effects is $a^2\Lambda_{\rm QCD}^2$, while that of the latter is $M_\pi^2/\Lambda_{\rm QCD}^2 \approx m_q/\Lambda_{\rm QCD}$. Now, if $m_q \approx 5$ MeV, $1/a \approx 2$ GeV, and $\Lambda_{\rm QCD} \approx 300$ MeV, then $m_q/\Lambda_{\rm QCD} \approx 0.016$, while $a^2\Lambda_{\rm QCD}^2 \approx 0.022$, which is indeed of the same size. A concrete example of this result (to be discussed further below) is that a pion composed of OS quarks has, at present lattice spacings, a mass of about 250 MeV when the corresponding unquenched pions have masses close to 135 MeV. This difference is an $\mathcal{O}(a^2)$ effect, which is seen to be as large as the pion mass-squared itself. This implies that there can be large discretization errors in quantities that are proportional to M_π^2, such as the pion scattering amplitudes near threshold.

One goal of this work is to determine when such $\mathcal{O}(a^2)$ errors are present. In this regard, we note that Ref. [75] found, using TMχPT, that there are no such errors for $I = 2$ scattering with *unquenched* TM fermions. Instead, the leading discretization errors are proportional to $a^2 m_q$, and thus suppressed by $a^2\Lambda_{\rm QCD}^2$ compared to the physical result. This work also

showed, however, that studying $I = 0$ scattering with unquenched TM fermions was challenging from a theoretical point of view because of mixing with $I = 2$, $I_z = 0$ states, due to the breaking of isospin. Specifically, they found that this mixing occurred at $\mathcal{O}(a^2)$, and thus was comparable in magnitude to the scattering amplitudes themselves at the physical point. Because of this problem, Ref. [63] used pions composed of OS quarks to study $I = 0$ $\pi\pi$ scattering, since there is then an exact valence isospin symmetry, and the above-described mixing with the $I = 2$ channel does not occur. This setup has not been studied previously using χPT, and we carry out the calculation here in order to determine the form of the leading discretization errors in this approach.

The second issue we address is the use of the two-particle quantization condition in Ref. [63]. As we have stressed recently in Ref. [41], and as is discussed in Ref. [76], unitarity is needed in order to use this quantization condition. Since PQ theories are not unitary, in general one cannot use the quantization condition to determine PQ amplitudes. However, we argued in Ref. [41] that the quantization condition was likely valid if the lack of unitarity was restricted to the t and u channels, i.e. if unitarity in the s channel still held. We also proposed alternative versions of the criteria that must be satisfied for a two-particle channel in a PQ theory to be "physical enough" to allow use of the quantization condition. Here we apply these criteria to the case of OS pion scattering.

The remainder of this paper is organized as follows. Section 3.3 describes the set-up within TMPQχPT. Section 3.4 presents the results of the leading order calculation of OS pion masses and scattering amplitudes. Section 3.5 studies the unitarity of the amplitude at one-loop order [which is of next-to-next-to-leading order in our power counting]. Section 3.6 discusses the implications for the results presented in Ref. [63]. We conclude in Sec. 6.7. Some technical results concerning the NLO contributions, which we find do not give corrections to the scattering amplitudes or masses, are relegated to Appendix A.1.

3.3 Theoretical setup

In this section we construct the low-energy effective chiral theory that corresponds to the calculations carried out in Ref. [63]. We note that this work used $N_f = 2$ sea quarks.[2]

TMLQCD involves isodoublets of quarks, which have dimensionless mass terms of the form

$$m_0 + i\mu_0\gamma_5\tau_3\,, \tag{3.1}$$

as well as a standard Wilson derivative term and possibly an improvement ("clover") term [69]. We denote the doublet of unquenched (sea) quarks by (u_S, d_S). We say that u_S has a positive twist and d_S a negative twist, because of the signs in the diagonal components of τ_3. To obtain maximal twist, the "normal" bare lattice mass m_0 must be tuned to its critical value, such that the renormalized normal mass vanishes. The entire mass of the quarks is then due to the bare lattice twisted mass, μ_0. The details of this procedure and its advantages are well known [73, 74] and we do not repeat them here. We only note that the presence of the $\gamma_5\tau_3$ in the mass term leads to explicit breaking of isospin and parity, although this vanishes in the continuum limit.

As noted in the introduction, the isospin breaking introduced by the twist in the mass creates mixing between the $I = 0$ and $I = 2, I_z = 0$ states, and Ref. [63] avoids this using OS valence fermions. To describe this setup in χPT we introduce a doublet of OS valence fermions (d_V, u_V), along with a corresponding ghost-quark doublet $(\widetilde{d}_V, \widetilde{u}_V)$, with both new doublets having the same mass term as in Eq. (3.1). The ghost quarks ("ghosts" for short) cancel the determinant produced by the valence quarks [42]. We have interchanged the order of the flavors relative to the sea-quark doublet (u_S, d_S), so that the signs of the twists for the two valence flavors are opposite to those of the corresponding sea quarks. (Alternatively, this

[2]Much recent work using TM fermions uses $N_f = 2 + 1 + 1$ sea quarks, with nondegenerate strange and charm sea quarks (see, e.g. Ref. [62]). Although a calculation of $I = 0$ $\pi\pi$ scattering has not yet been attempted with $N_f = 2 + 1 + 1$ TM fermions, any future such calculation would still, at long distances, be described by the effective chiral theory that we construct. This is because, if we work at energies such that kaon-antikaon pairs cannot be created, we can integrate out the strange (and charm) quarks leaving an effective lattice theory with only up and down quarks, and having renormalized couplings.

sign flip could be achieved by replacing τ_3 with $-\tau_3$ in the mass term, while leaving the order of the flavors in the doublet unchanged.) Choosing the OS quarks to have opposite twist from the sea quarks of the same flavor allows us to pick out doublets containing one up and one down quark with the same sign of the twist. In particular, the doublet (u_S, d_V) has positive twist, while (u_V, d_S) has negative twist. There is an exact SU(2) isospin symmetry acting on each doublet with definite twist, so by constructing pions composed of quark-antiquark pairs from one of these doublets, we avoid mixing between $I = 0$ and $I = 2, I_z = 0$ states. In particular, we focus on (u_S, d_V) and refer to the isospin symmetry of this doublet as $\mathrm{SU}(2)_+$ symmetry, with the subscript denoting positive twist. In the following, we will sometimes refer to this pair as the "OS quarks", and the $SU(2)_+$ symmetry as "OS isospin."

All six fields are collected into a single spin-1/2 field,

$$Q^{\mathrm{Tr}} = (u_S, d_S, d_V, u_V, \widetilde{d}_V, \widetilde{u}_V)\,. \tag{3.2}$$

If the twisted part of the mass terms were absent, then the theory would have an SU(4|2) graded flavor symmetry, which includes a flavor SU(4) in the quark subsector. With $\mu \neq 0$, the latter group is broken down to $\mathrm{SU}(2)_+ \times \mathrm{SU}(2)_- \times U(1)$, where $SU(2)_+$ has been described above, $SU(2)_-$ is the corresponding symmetry between negative twist quarks d_S and u_V, while the U(1) acts oppositely on positive and negative twist quarks. We only make use of the $\mathrm{SU}(2)_+$ in the following.

We note in passing that one could use a formulation in which all OS quarks, both up and down, are valence quarks. This would lead to a clear separation between valence and sea quarks, whereas in the formulation described above, u_S is playing both roles. The disadvantage of this "fully valence" approach is that it would require more fields, since one would need to introduce *two* valence doublets and their corresponding ghosts, leading to the field Q having 10 components. We prefer to work with the minimal formulation given in Eq. (3.2).

The effective chiral low-energy theory describing the interactions of the pseudo-Goldstone bosons and fermions (PGBs and PGFs) in the present context has been developed in sev-

eral works. The construction of PQχPT in the continuum was worked out in Ref. [42]; see Refs. [32, 43] for reviews. The systematic extension of χPT to include the effects of discretization errors for TM fermions was made in Refs. [77–80], and applied to pion scattering in Ref. [75]. The combination of partial quenching and twisted-mass effects was described in Ref. [81] and extended in Ref. [82]. Here we simply quote the resulting form of the effective theory.

Before doing so we comment on the appropriate power counting needed to develop TMχPT. As noted in the introduction, when using near-physical quark masses, one has $m_q \sim a^2$, where here we are leaving factors of $\Lambda_{\rm QCD}$ implicit. Combined with the usual p-regime power counting of χPT, this leads to

$$\begin{aligned} \text{Leading order (LO): } & m_q \sim p^2 \sim a^2 \,, \\ \text{Next-to-leading order (NLO): } & m_q a \sim p^2 a \sim a^3 \,, \\ \text{Next-to-next-to-leading order (NNLO): } & m_q^2 \sim m_q p^2 \sim p^4 \sim m_q a^2 \sim p^2 a^2 \sim a^4 \,. \end{aligned} \tag{3.3}$$

The regime in which this power counting holds is referred to as the LCE (large cutoff effects) or "Aoki" regime.

For the most part we shall need only the LO chiral Lagrangian. This is given, in Euclidean space, by [81, 83, 84]

$$\begin{aligned} \mathcal{L}_{\rm LO} &= \frac{f^2}{4}\mathrm{str}\Big(\partial_\mu \Sigma^\dagger \partial_\mu \Sigma\Big) - \frac{f^2}{4}\mathrm{str}\Big(\chi\Sigma^\dagger + \Sigma\chi^\dagger\Big) + \mathcal{V}_{a^2} \,, \\ \mathcal{V}_{a^2} &= -\hat{a}^2 W_6' \,\mathrm{str}\Big(\Sigma + \Sigma^\dagger\Big)^2 - \hat{a}^2 W_7' \,\mathrm{str}\Big(\Sigma - \Sigma^\dagger\Big)^2 - \hat{a}^2 W_8' \,\mathrm{str}\Big(\Sigma^2 + \Sigma^{\dagger 2}\Big) \,, \end{aligned} \tag{3.4}$$

where $\Sigma \in \mathrm{SU}(4|2)$ is the field that contains PGBs and PGFs, "str" denotes supertrace (or "strace" for short), $\chi = 2B_0 M$, with M the renormalized mass matrix, and $f \approx 90$ MeV and B_0 are the usual continuum LO low-energy coefficients (LECs), while $\hat{a} = 2W_0 a$, with W_0, along with W_6', W_7', and W_8', being LECs associated with discretization errors. If we restrict ourselves to the unquenched subsector, the only combination of the latter three LECs that appears is $2W_6' + W_8'$.

The form (B.1) holds for any partially quenched, $\mathcal{O}(a)$ improved, Wilson-like LQCD

action. To obtain PQTM fermions, one uses the diagonal mass matrix

$$M = m_q e^{i\omega_m \tau_3^{VS}}, \quad \tau_3^{VS} = \mathrm{diag}(\tau_3, \tau_3, \tau_3) = \mathrm{diag}(1, -1, 1, -1, 1, -1)\,, \tag{3.5}$$

where m_q is the physical quark mass, and ω_m is the input twist angle. These are related to the bare parameters m_0 and μ_0 in the standard manner (see, e.g., Ref. [79]); all we need here is that for maximal twist, $\omega_m = \pi/2$, we have $m_q = Z_P^{-1}\mu_0/a$.

The vacuum is determined at LO by minimizing the potential, including both the mass term and $\mathcal{V}_{a^2}$. This leads to

$$\Sigma_0 \equiv \langle 0|\Sigma|0\rangle = \exp\left(i\omega_0 \tau_3^{VS}\right)\,, \tag{3.6}$$

with ω_0 the vacuum twist angle. In general ω_0 differs from ω_m by $\mathcal{O}(1)$, due to the competition between the mass and a^2 terms in the potential, but for maximal twist one has $\omega_0 = \omega_m = \pi/2$. This is the case that we study henceforth. There are corrections to this result at higher order in χPT [85], but we will not need these in the following.

This discussion has ignored the presence of the strace in the terms in the potential. Indeed, while the choice (3.6) minimizes the potential in the quark sector, it maximizes it in the ghost sector. Nevertheless, as argued in Refs. [58, 86], it is legitimate to proceed naively and develop perturbation theory by expanding about the extremum. The arguments for this also show that, for the purposes of developing perturbation theory, one can express $\mathcal{L}_{\mathrm{LO}}$ in terms of Σ and $\Sigma^\dagger$, rather than the choice Σ and Σ^{-1} that is required for a nonperturbative analysis [87, 88].

We next expand Σ about its vacuum value to define the PG fields. This is conveniently done using

$$\Sigma = \xi_0 \Sigma_{\mathrm{ph}} \xi_0\,, \quad \xi_0 = \exp\left(i\omega_0 \tau_3^{VS}/2\right)\,, \quad \Sigma_0 = \xi_0^2\,, \tag{3.7}$$

for if we then expand Σ_{ph} as

$$\Sigma_{\mathrm{ph}} = \exp(\sqrt{2} i\Pi/f)\,, \tag{3.8}$$

the fields in the PG matrix Π have their standard flavor interpretation. For example, the

upper left 2×2 block contains the unquenched pion field,

$$\pi_{\rm SS} = \begin{pmatrix} \frac{1}{\sqrt{2}}\pi^0_{\rm SS} & \pi^+_{\rm SS} \\ \pi^-_{\rm SS} = (\pi^+_{\rm SS})^\dagger & -\frac{1}{\sqrt{2}}\pi^0_{\rm SS} \end{pmatrix}, \tag{3.9}$$

as well as a singlet component. This was the basis used in Ref. [81]. We shall instead use a different basis for the neutral fields (and different nomenclature for the charged fields). Since Π is straceless, there are five linearly independent neutral fields. We choose these to be π^0_{++} and π^0_{--}, which are the neutral components of the OS pion isotriplets composed of quarks of definite twist, together with three neutral fields composed of states with differing twist: η_4, which is an SU(4) generalization of the η; ϕ_0, which is a superposition of the two ghost-antighost pairs; and ϕ_1, which spans the quark and ghost sectors.

$$\Pi = \begin{pmatrix} \frac{\pi^0_{++}}{\sqrt{2}} + \frac{\eta_4}{2} + \frac{\phi_1}{2} & \pi^+_{-+} & \pi^+_{++} & \pi^{uu}_{-+} & \omega_{15} & \omega_{16} \\ (\pi^+_{-+})^\dagger & -\frac{\pi^0_{--}}{\sqrt{2}} - \frac{\eta_4}{2} + \frac{\phi_1}{2} & (\pi^{dd}_{-+})^\dagger & (\pi^+_{--})^\dagger & \omega_{25} & \omega_{26} \\ (\pi^+_{++})^\dagger & \pi^{dd}_{-+} & -\frac{\pi^0_{++}}{\sqrt{2}} + \frac{\eta_4}{2} + \frac{\phi_1}{2} & (\pi^+_{+-})^\dagger & \omega_{35} & \omega_{36} \\ (\pi^{uu}_{-+})^\dagger & \pi^+_{--} & \pi^+_{+-} & \frac{\pi^0_{--}}{\sqrt{2}} - \frac{\eta_4}{2} + \frac{\phi_1}{2} & \omega_{45} & \omega_{46} \\ \omega_{51} & \omega_{52} & \omega_{53} & \omega_{54} & \frac{\phi_0}{\sqrt{2}} + \phi_1 & \phi_{56} \\ \omega_{61} & \omega_{62} & \omega_{63} & \omega_{64} & \phi^\dagger_{56} & -\frac{\phi_0}{\sqrt{2}} + \phi_1 \end{pmatrix}. \tag{3.10}$$

The subscripts on the various pion fields indicate the twists of the component antiquark and quark fields, respectively. This matrix is straceless and hermitian, with the ω_{jk} being PGFs, while the ϕ fields are PGBs that have propagators with an unphysical overall sign. We stress that $\pi^+_{\rm SS}$ and π^+_{-+} are different notations for the same field, as can be seen by comparing Eqs. (3.9) and (3.10). The choice of which notation we use in the following depends on which feature of the results that we wish to emphasize.

We have assumed in the above that we can treat Π as a hermitian field, so that $\Sigma^\dagger_{\rm ph} = \exp(-\sqrt{2}i\Pi/f)$. For the bosonic fields in Π this is standard, while in the fermionic sector it is a convenient convention. Specifically we are defining hermitian conjugation such that $\omega_{jk} = \omega^\dagger_{kj}$. This is a convention since ω_{jk} and ω_{kj} are treated as independent Grassman fields in Euclidean functional integrals.

The lattice simulations of Ref. [63] use the pion fields π^+_{++}, π^0_{++} and π^-_{++}, and it is on these that we mainly focus below. Due to a discrete symmetry, we could, however, have equally well used the π^a_{--} states, i.e. those composed of fields with negative twist.

Rewriting the Lagrangian in terms of $\Sigma_{\rm ph}$ leads, at maximal twist, to

$$\begin{aligned}\mathcal{L}_{\rm LO} = \frac{f^2}{4}\mathrm{str}\Big(\partial_\mu\Sigma^\dagger_{\rm ph}\partial_\mu\Sigma_{\rm ph}\Big) - \frac{f^2 B_0 m_q}{2}\mathrm{str}\Big(\Sigma^\dagger_{\rm ph}+\Sigma_{\rm ph}\Big) - \hat{a}^2 W'_6\left[\mathrm{str}\Big(\Sigma_0\Sigma_{\rm ph}+\Sigma^\dagger_{\rm ph}\Sigma^\dagger_0\Big)\right]^2 \\ - \hat{a}^2 W'_7\left[\mathrm{str}\Big(\Sigma_0\Sigma_{\rm ph}-\Sigma^\dagger_{\rm ph}\Sigma^\dagger_0\Big)\right]^2 - \hat{a}^2 W'_8\,\mathrm{str}\Big(\Sigma_0\Sigma_{\rm ph}\Sigma_0\Sigma_{\rm ph}+\Sigma^\dagger_{\rm ph}\Sigma^\dagger_0\Sigma^\dagger_{\rm ph}\Sigma^\dagger_0\Big)\ , \quad (3.11)\end{aligned}$$

Expanding in powers of Π, the quadratic term is

$$\mathcal{L}_{\rm LO} \supset \tfrac{1}{2}\mathrm{str}(\partial_\mu\Pi\partial_\mu\Pi)+B_0 m_q\mathrm{str}\Big(\Pi^2\Big)-\tfrac{1}{2}w'_6 f^2\left[\mathrm{str}\Big(\tau_3^{VS}\Pi\Big)\right]^2-\tfrac{1}{4}w'_8 f^2\left[\mathrm{str}\Big(\tau_3^{VS}\Pi\tau_3^{VS}\Pi\Big)+\mathrm{str}\left(\Pi^2\right)\right]\ , \quad (3.12)$$

while the quartic term is

$$\begin{aligned}\mathcal{L}_{\rm LO} \supset \frac{1}{6f^2}\mathrm{str}\Big[(\partial_\mu\Pi)\Pi(\partial_\mu\Pi)\Pi-(\partial_\mu\Pi)^2\Pi^2\Big] - \frac{B_0 m_q}{6f^2}\mathrm{str}\Big(\Pi^4\Big) + \frac{w'_6}{3}\mathrm{str}\Big(\tau_3^{VS}\Pi\Big)\,\mathrm{str}\Big(\tau_3^{VS}\Pi^3\Big) \\ + \frac{w'_7}{4}\mathrm{str}\Big(\tau_3^{VS}\Pi^2\Big)\,\mathrm{str}\Big(\tau_3^{VS}\Pi^2\Big) + \frac{w'_8}{24}\left[3\mathrm{str}\Big(\tau_3^{VS}\Pi^2\tau_3^{VS}\Pi^2\Big)+4\mathrm{str}\Big(\tau_3^{VS}\Pi\tau_3^{VS}\Pi^3\Big)+\mathrm{str}\Big(\Pi^4\Big)\right]\ . \quad (3.13)\end{aligned}$$

Here we have converted to the dimensionless LECs

$$w'_j = \frac{16\hat{a}^2 W'_j}{f^4} \qquad (j=6,7,8)\,. \quad (3.14)$$

The cubic term vanishes at maximal twist, a point explained in Appendix A.1.

3.4 Leading-order TMPQχPT results

In this section we use the chiral Lagrangian given in Eq. (3.11) to determine the LO results for propagators, masses and scattering amplitudes. We also briefly discuss the mixing of two OS pions having $I = 0$ with a single unquenched neutral pion, which requires working at NLO in χPT.

3.4.1 Propagators and masses

We first read off the propagators and particle masses from Eq. (3.12). For fields labeled as lower-case pions in Eq. (3.10), the propagators take the standard form $1/(p^2 + M^2)$, with the masses being

$$M(\pi^{\pm}_{-+})^2 = M(\pi^{uu}_{-+})^2 = M(\pi^{dd}_{-+})^2 = M(\pi^{\pm}_{\rm SS})^2 = 2B_0 m_q \equiv \left(M^{\pm}_{\rm SS}\right)^2 , \tag{3.15}$$

$$M(\pi^{\pm}_{++})^2 = M(\pi^{0}_{++})^2 = M(\pi^{\pm}_{--})^2 = M(\pi^{0}_{--})^2 = 2B_0 m_q - w'_8 f^2 \equiv M^2_{\rm OS} , \tag{3.16}$$

As noted in the first line, the masses of all the pions that are composed of quarks and antiquarks with opposite twists coincide, and contain no discretization errors at LO. This includes the charged sea-quark pions. These masses differ by $\mathcal{O}(a^2)$ from those of the pions in which the quarks and antiquarks have the same twist, i.e. the results in the second line. Such pions are collectively called OS pions in Ref. [63], and thus we have introduced the common nomenclature $M_{\rm OS}$ (adapted from that in Ref. [63], where $M_\pi^{\rm OS}$ is used).

As an aside, we note that $M_{\rm OS}$ is also the mass obtained from the pole in the correlator of the unquenched neutral pion, $\pi^0_{\rm SS}$, *if one keeps only the connected Wick contraction*. This mass is denoted $m_\pi^{0,{\rm conn}}$ in Ref. [81]. The separation of contractions can be formulated in a partially quenched theory, and one finds $m_\pi^{0,{\rm conn}} = M_{\rm OS}$ [81].

A prediction from Eqs. (3.15) and (3.16) is that

$$\Delta_{\rm OS} = M^2_{\rm OS} - \left(M^{\pm}_{\rm SS}\right)^2 = -w'_8 f^2 , \tag{3.17}$$

i.e. that there is a mass-independent $\mathcal{O}(a^2)$ offset between the charged sea-quark and OS pion squared masses. Since w'_8 is known to be negative [81, 87, 88], this offset is positive. To our knowledge, the accuracy of this prediction in practice has not been discussed previously. It can be tested using the results quoted in Table II of Ref. [63], and this is done in Table 3.1. Since the two masses in the difference are certainly correlated, we cannot determine the error on the difference. Nevertheless, it is clear that, to high precision, the offset is constant. This indicates that higher-order corrections to Eq. (3.17), which, among other effects, would lead to a linear dependence on μ_0, are small. The sign of the offset is as predicted, and its value

is such that the m_q and a^2 contributions to $M_{\rm OS}^2$ are comparable for physical quark masses, as already noted in the introduction. Numerically, we find $\sqrt{\Delta_{\rm OS}}/a \approx 200$ MeV, which is comparable to $\Lambda_{\rm QCD}$ and thus of the expected size.

μ_0	$aM(\pi^{\pm}_{\rm SS})$	$aM_{\rm OS}$	$a^2\Delta_{\rm OS}$
0.0009	0.06212(6)	0.11985(15)	0.0105
0.003	0.11197(7)	0.15214(11)	0.0106
0.006	0.15781(15)	0.18844(24)	0.0106

Table 3.1: Numerical results for the mass splitting defined in Eq. (3.17). These are given in the final column, and determined from the results in the second and third columns, which are taken from Ref. [63]. The first column gives the bare twisted mass, with the top row corresponding approximately to physical-mass charged pions. The lattice spacing is $a = 0.931(8)$ fm [89]

The results for the PGF masses match those of the charged pions, and, in particular, depend only on the relative sign of the twist of the component quark and ghost-quark,

$$M(\omega_{16})^2 = M(\omega_{25})^2 = M(\omega_{36})^2 = M(\omega_{45})^2 = 2B_0 m_q \,, \tag{3.18}$$

$$M(\omega_{15})^2 = M(\omega_{26})^2 = M(\omega_{35})^2 = M(\omega_{46})^2 = 2B_0 m_q - w_8' f^2 \,. \tag{3.19}$$

The propagator has the bosonic form, with the overall sign depending on the ordering of ω_{jk} and ω_{kj}. Specifically, when ordered with ω_{jk} preceding ω_{kj}, an overall minus sign arises if $j < k$.

The ghost-ghost PGBs ϕ_1 and ϕ_{56} have propagators with unphysical overall signs, $-1/(p^2+M^2)$, due to the supertrace. Their masses are

$$M(\phi_{56})^2 = 2B_0 m_q \,, \qquad M(\phi_1)^2 = 2B_0 m_q - w_8 f^2 \,, \tag{3.20}$$

again matching the pattern for the π fields.

Finally, we consider the η_4 and ϕ_0. Here there is mixing, due to the w_6' term in Eq. (3.12). In the basis $\{\eta_4, \phi_0\}$, the propagator is given by the inverse of

$$\begin{pmatrix} p^2 + 2B_0 m_q - w_8' f^2 & 0 \\ 0 & -(p^2 + 2B_0 m_q - w_8' f^2) \end{pmatrix} - w_6' f^2 \begin{pmatrix} 4 & -2\sqrt{2} \\ -2\sqrt{2} & 2 \end{pmatrix}, \tag{3.21}$$

which is

$$\frac{1}{p^2 + M(\pi^0_{\rm SS})^2} \begin{pmatrix} 1 & 0 \\ 0 & -1 \end{pmatrix} + \frac{2w_6' f^2}{[p^2 + M(\pi^0_{\rm OS})^2][p^2 + M(\pi^0_{\rm SS})^2]} \begin{pmatrix} 1 & \sqrt{2} \\ \sqrt{2} & 2 \end{pmatrix}. \tag{3.22}$$

Here

$$M(\pi^0_{\rm SS})^2 = 2B_0 m_q - (2w_6' + w_8') f^2 \equiv (M^0_{\rm SS})^2 \tag{3.23}$$

is the mass of the neutral unquenched pion. The appearance of this mass can be understood as due to hairpin diagrams with loops of sea quarks summed to all orders. We also observe that the second term in the propagator, Eq. (3.22), involves the double poles characteristic of PQχPT.

A nontrivial check on the results just presented is obtained by directly calculating the propagator of $\pi^0_{\rm SS}$, which can be done using the relation [obtained by comparing the representations of the upper left block of Π given by Eqs. (3.9) and (3.10)]

$$\pi^0_{\rm SS} = \tfrac{1}{2}\pi^0_{++} + \tfrac{1}{2}\pi^0_{--} + \tfrac{1}{\sqrt{2}}\eta_4 \,. \tag{3.24}$$

Using the results above, this propagator is given by

$$2 \times \frac{1}{4} \frac{1}{p^2 + (M^0_{\rm OS})^2} + \frac{1}{2} \left\{ \frac{1}{p^2 + (M^0_{\rm SS})^2} + \frac{2w_6' f^2}{[p^2 + (M^0_{\rm OS})^2][p^2 + (M^0_{\rm SS})^2]} \right\} = \frac{1}{p^2 + (M^0_{\rm SS})^2}, \tag{3.25}$$

which is the desired result.

We close this subsection by noting that, by using a clover term in the fermion action, the breaking of the physical isospin symmetry in the unquenched theory is greatly reduced, with $M^{\pm}_{\rm SS} \approx M^0_{\rm SS}$ (see Table II of Ref. [63]). Thus the combination $2w_6' + w_8'$, which controls isospin breaking in the physical sector, almost vanishes. We stress, however, that this does not imply that discretization errors in all quantities are similarly small, since, as we have seen from Table 3.1, w_8' itself is not small.

3.4.2 Scattering amplitudes

We next consider LO scattering amplitudes, which can be determined from the quartic term in $\mathcal{L}_{\rm LO}$, given in Eq. (3.13). Results for scattering amplitudes in the unquenched sector have already been given in Ref. [75], and we have checked that we agree with these. What we focus on here are the scattering amplitudes of OS pions, and in particular those composed of quarks with positive twist. These are the amplitudes studied numerically in Ref. [63], and we wish to determine the form of the $\mathcal{O}(a^2)$ contributions to them.

For the scattering of OS pions, the nonderivative terms in $\mathcal{L}_{\rm LO}$ collapse down to a contribution that is of the same form as that in the continuum,

$$c_{\rm OS}\left[\frac{(\pi^0_{++})^2}{2}+\pi^+_{++}\pi^-_{++}\right]^2, \tag{3.26}$$

except that the overall coefficient,

$$c_{\rm OS}=-\frac{2B_0m_q}{6f^2}+w_7'+\tfrac{2}{3}w_8'=-\frac{M^2_{\rm OS}}{6f^2}+w_7'+\tfrac{1}{2}w_8', \tag{3.27}$$

includes a^2 corrections. As expected, the form in Eq. (3.26) is invariant under the OS isospin group, $\mathrm{SU}(2)_+$, so that there is no mixing between $I=0$ and $I=2, I_z=0$ amplitudes. On the other hand, these results imply that there is an $\mathcal{O}(a^2)$ contribution to the scattering of two OS π^+ mesons, unlike for the corresponding sea pions.

Including the kinetic term, the full LO scattering amplitudes for the different choices of

OS isospin are given by

$$\mathcal{A}^{\rm LO}_{I=2} = \frac{1}{f^2}(\underbrace{-s + \tfrac{4}{3}M^2_{\rm OS}}_{\text{kinetic term}}) - 4c_{\rm OS}\,, \tag{3.28}$$

$$= \frac{1}{f^2}(-s + 2M^2_{\rm OS}) - 4w'_7 - 2w'_8\,, \tag{3.29}$$

$$= \frac{1}{f^2}\left[-s + 2M^2_{\rm OS} + 2\Delta_{\rm OS} - 4f^2 w'_7\right]\,, \tag{3.30}$$

$$\mathcal{A}^{\rm LO}_{I=1} = \frac{t-u}{f^2} = -(p_1 - p_2)\cdot(k_1 - k_2) \tag{3.31}$$

$$\mathcal{A}^{\rm LO}_{I=0} = \frac{1}{f^2}(2s - M^2_{\rm OS}) - 10w'_7 - 5w'_8\,, \tag{3.32}$$

$$= \frac{1}{f^2}\left[2s - M^2_{\rm OS} + 5\Delta_{\rm OS} - 10f^2 w'_7\right]\,. \tag{3.33}$$

The $I = 1$ result comes only from the kinetic term, since it requires momentum dependence, and thus is the same as in the continuum. The $I = 2$ and $I = 0$ results contain discretization errors from both w'_7 and w'_8, although the former can be rewritten in terms of the measured mass difference $\Delta_{\rm OS}$, as shown by the final forms for each quantity. Also useful are the s-wave scattering lengths, which are proportional to the amplitudes at threshold, where $s = 4M^2_{\rm OS}$. These are given by

$$M_{\rm OS}\; a^{\rm LO}_{0,I=2} = \frac{M^2_{\rm OS} - \Delta_{\rm OS} + 2f^2 w'_7}{16\pi f^2} \tag{3.34}$$

$$M_{\rm OS}\; a^{\rm LO}_{0,I=0} = -\frac{7M^2_{\rm OS} + 5\Delta_{\rm OS} - 10f^2 w'_7}{32\pi f^2}\,. \tag{3.35}$$

Here we are using the sign convention, standard in most of the LQCD literature (although not followed in Ref. [63]), that a positive scattering length corresponds to a repulsive interaction.

We draw two conclusions from these results. First, the $I = 0$ OS amplitude does contain $\mathcal{O}(a^2)$ terms. Since these involve both $\Delta_{\rm OS}$ (which is known) and w'_7 (which is not), we do not know *a priori* the size of these corrections. They could be comparable to the physical $M^2_{\rm OS}$ term, as for $M_{\rm OS}$ itself, or they could be smaller, as in the difference $M^{\pm}_{\rm SS} - M^0_{\rm SS}$. It is not possible to determine which option holds from the results of Ref. [63] alone, since they are available only for two quark masses, and at a single lattice spacing, and have relatively large errors.

Our second conclusion is that the size of the discretization errors for $I = 0$ scattering can be determined by calculating the $I = 2$ amplitude for OS pions. In particular, if one calculates $a_{0,I=2}$ and compares to the LO prediction (3.34), then one can determine w_7' (given the result obtained above for $\Delta_{\rm OS}$), and use this to remove the $\mathcal{O}(a^2)$ errors from $a_{0,I=0}$, Eq. (3.35). A more direct way of proceeding is to make use of the fact that the $\mathcal{O}(a^2)$ terms in the two amplitudes are proportional, so that LO discretization errors cancel in the following linear combinations:

$$\mathcal{A}^{\rm LO}_{I=0} - \tfrac{5}{2}\mathcal{A}^{\rm LO}_{I=2} = \frac{\frac{9}{2}s - 6M^2_{\rm OS}}{f^2}\,, \tag{3.36}$$

$$M_{\rm OS}\left(a^{\rm LO}_{0,I=0} - \tfrac{5}{2}a^{\rm LO}_{0,I=2}\right) = -\frac{3M^2_{\rm OS}}{8\pi f^2}\,. \tag{3.37}$$

To our knowledge a calculation of $a_{0,I=2}$ using OS pions has not been carried out; indeed, there has previously been no motivation to do so given that $I = 2$ scattering can be studied with unquenched pions. Such a calculation should, however, be straightforward, since it involves only a subset of the Wick contractions needed for the $I = 0$ calculation, and this subset involves only quark-connected diagrams.

One might be concerned that higher-order corrections in χPT could be significant. In this regard, we have two comments. First, the results in Table 3.1 provide partial evidence that the LO prediction is reliable, as there is no significant dependence on μ_0. This does not, however, rule out large a^4 corrections. Second, there are no NLO contributions to the scattering amplitudes discussed in this subsection. The reason for this is discussed in the following subsection. The first corrections occur at NNLO, an example of which is discussed in Sec. 3.5.

3.4.3 Mixing with states with vacuum quantum numbers

A significant challenge in the lattice calculation of Ref. [63] is the presence of mixing between the OS $I = 0$ state and a single neutral unquenched pion ($\pi^0_{\rm SS}$ in our notation). In the continuum, such mixing violates parity and G-parity, but with TM fermions, lattice artifacts break parity and the physical isospin symmetry in such a way that mixing is allowed. It

does not occur, however, at LO in χPT when working at maximal twist, as is evident from the absence of cubic vertices in Sec. 3.3. A natural question, therefore, is at what order does this mixing occur.

The answer is that it occurs at NLO in the expansion described in Eq. (3.3). To see this one must write down all allowed NLO terms in the Lagrangian and expand in the field Π. There are many such terms, each with a different combinations of LECs, all of which correspond to artifacts of discretization and are unknown. Thus we do not think it is useful to explicitly calculate the mixing amplitude. Instead, we determine the overall chiral scaling of the terms that contribute.

The form of the allowed NLO terms is given in Appendix A.1, Eqs. (A.1) and (A.2). If we expand these out we obtain linear terms of the form

$$(a^3 + am_q)\mathrm{str}(\Pi\tau_3^{VS}) \tag{3.38}$$

and the following cubic terms

$$\begin{aligned} &a^3\mathrm{str}(\Pi\tau_3^{VS})^3\,, \quad a^3\mathrm{str}(\Pi\tau_3^{VS}\Pi\tau_3^{VS}\Pi\tau_3^{VS})\,, \quad a^3\mathrm{str}(\Pi\tau_3^{VS}\Pi\tau_3^{VS})\mathrm{str}(\Pi\tau_3^{VS})\,, \\ &(a^3 + am_q)\mathrm{str}(\Pi^2)\mathrm{str}(\Pi\tau_3^{VS})\,, \quad (a^3 + am_q)\mathrm{str}(\Pi)\mathrm{str}(\Pi^2\tau_3^{VS})\,, \quad (a^3 + am_q)\mathrm{str}(\Pi^3\tau_3^{VS})\,, \\ &a\,\mathrm{str}(\partial\Pi\partial\Pi(\Pi\tau_3^{VS} + \tau_3^{VS}\Pi))\,, \quad a\,\mathrm{str}(\partial\Pi\partial\Pi)\mathrm{str}(\Pi\tau_3^{VS})\,. \end{aligned} \tag{3.39}$$

As is discussed in the appendix, there are no terms with even powers of Π. In these equations we are being schematic, showing simply the overall structures that appear and the form of the coefficients. Ignoring for now the linear term, we see that the three-pion vertices appear for nonzero a, and it is straightforward to see that they lead to vertices of the forms $\pi^+_{++}\pi^-_{++}\pi^0_{\mathrm{SS}}$ and $\pi^0_{++}\pi^0_{++}\pi^0_{\mathrm{SS}}$. Thus we find that the mixing discussed in Ref. [63] occurs at NLO, and that the on shell mixing amplitude is proportional to a^3 and aM^2, where M is a generic meson mass.

Now we return to the linear term, Eq. (3.38), and argue that it leads to contributions scaling in the same fashion as those from the cubic terms just discussed. This leads to a mixing of π^0_{SS} with the vacuum, and thus to a shift in the twist angle of $\mathcal{O}(a)$. This in

turn leads to additional contributions involving odd powers of Π that are fed down from the even-powered LO vertices. One way of seeing this is to take, say, a four point LO vertex and absorb one of the pions into the vacuum, leading to an additional factor of $a^3 + aM^2$ from the absorption vertex and $1/(a^2 + M^2)$ from the propagator. Combining this with the $a^2 + M^2$ from the initial vertex one ends up, crudely speaking, with the same $a^3 + aM^2$ scaling as that obtained from the cubic vertices.

3.5 Applicability of two-particle quantization condition

In this section, we discuss in which channels it is valid to use the two-particle quantization condition of Lüscher when using TM fermions with OS valence quarks.[3] To do so, we apply the criteria that we recently developed in Ref. [41]. Unitarity is an essential ingredient both in the derivation of the quantization condition, and in the justification for the standard spectral representation of correlators. The observation of Ref. [41] is that it is likely sufficient, however, for unitarity to hold in the s channel. If the unitarity violation introduced by the use of a partially quenched theory manifests itself only in the t and u channels, then this does not invalidate the use of the quantization condition. In the case at hand, this question can be studied using χPT.

The simplest criterion to implement of those proposed in Ref. [41] (which is the second of the criteria introduced in that work) uses quark line diagrams, which trace the flavor indices in χPT calculations. The criterion states that if intermediate ghost quarks appear in the quark-line diagrams for s-channel two-particle loops, then the quantization condition cannot be used. The logic here is that ghost quarks act as a proxy for the presence of intermediate states that differ from those on the external lines, indicating a breakdown of unitarity.

In Fig. 3.1 we show examples of quark-line diagrams for the one-loop s-channel scattering process for OS pions having $I = 2$, 1 and 0. For $I = 2$, we show all the distinct classes of diagrams that appear, taking account of the fact that the LO vertices, given in Eq. (3.13),

[3]The quantization condition breaks down above the first inelastic threshold, where more than two particles can go on shell, and we consider here only the kinematic regime in which this is not allowed.

can have either one or two straces. This leads to a greater number of quark-line diagrams than those appearing in the continuum theory, where only single-trace vertices occur at LO. Nevertheless, none of the diagrams involve ghost quarks, and thus using the quantization condition for $I = 2$ OS pions is not ruled out. This result extends to s-channel loops at any order in χPT.

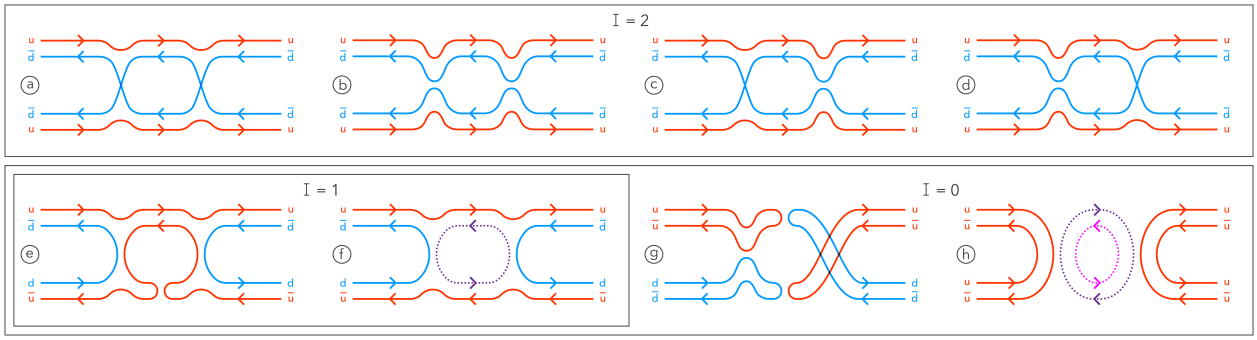

Figure 3.1: Classes of topologically distinct s-channel one-loop quark-line diagrams contributing to $I = 2 = I_z$, $I = 1, I_z = 0$, and $I = 0$ scattering. The choices of I_z are for convenience. All classes of diagram are shown for $I = 2$ (up to exchange of the quark/antiquark flavors), while only a subset are shown for $I = 1$ and $I = 0$. Labels and colors indicate quark or antiquark flavors, with lines tracing the (anti)quark flavors as they propagate through the diagram. Unlabeled dashed lines may have any flavor, and may represent sea, valence, or ghost (anti)quarks. The hairpin vertices in diagrams (e) and (g) implicitly contain an infinite sum of intermediate sea quark, valence and ghost loops.

Next, we turn to $I = 1$ and $I = 0$, for which many more classes of diagram contribute. Since the presence of a single diagram involving ghost quarks is sufficient for our criterion to invalidate the use of the quantization condition, we show in Fig. 3.1 only examples of diagrams containing ghost loops. The ghost quarks are either explicit, as in diagrams (f) and (h), or implicitly contained in the hairpin vertices, as in diagrams (e) and (g). Since we have chosen to display diagrams for $I = 1, I_z = 0$, each of the diagrams in this channel will also contribute to $I = 0$ scattering. There are many more types of diagram involving ghost

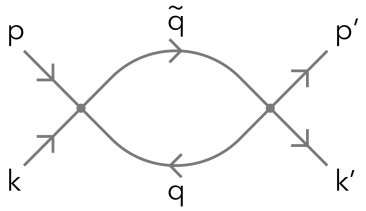

Figure 3.2: One-loop s-channel scattering diagram with p, k, p', and k' labeling the external 4-momenta, and q and $\tilde{q} = q + p + k$ labeling the internal 4-momenta.

quarks that are not shown in Fig. 3.1. However, the subset of diagrams we do include is enough to conclude that the quantization condition *cannot* be used to study OS pion $I = 1$ or $I = 0$ scattering.

As noted in Ref. [41], the diagrammatic criterion is not entirely foolproof, as the contributions corresponding to a given unphysical quark-line diagram could cancel. However, in that work we also introduced two other criteria which do not suffer from such an ambiguity. The first of these (which is the first of that work) restricts the form of the ratio of correlation functions given in Eq. (3.47), and we do make use of it here. Here we use the third criterion of Ref. [41]: the two-particle quantization condition can only be valid if the PQ scattering amplitude satisfies s-channel unitarity. We apply this criterion using one-loop results from χPT.

Since s-channel unitarity involves cutting diagrams only in the s channel, it can be tested at one-loop order simply by calculating the s-channel loop diagram, shown in Fig. 3.2. The imaginary part of this loop must be proportional to the squared magnitude of the tree-level amplitude, with the proportionality constant related to the phase space available at the chosen value of s. One way in which unitarity can fail is if the particles in the loop have different masses from those of the external particles, for then the phase space differs from that appearing in the unitarity relation.

We begin with the $I = 2$ channel, which we can pick out by studying $\pi^+_{\rm OS}\pi^+_{\rm OS}$ scattering. The key point here is that only $\pi^+_{\rm OS}\pi^+_{\rm OS}$ intermediate states can appear in the s-channel loop.

This is clear from the diagrammatic quark-line analysis given above, but can be checked by direct calculation. Specifically, we find that the contribution from the s-channel loop is

$$\begin{aligned}\mathcal{A}^{(s1)}_{\mathrm{OS},I=2} =& \frac{1}{f^4}\left(-s+2M^2_{\mathrm{OS}}+2\Delta_{\mathrm{OS}}-4f^2w'_7\right)^2 J(s,M^2_{\mathrm{OS}},M^2_{\mathrm{OS}}) \\ &+\frac{1}{9f^4}\left(5s+24w'_7f^2-12M^2_{\mathrm{OS}}-12\Delta_{\mathrm{OS}}\right) I\left(M^2_{\mathrm{OS}}\right),\end{aligned} \tag{3.40}$$

where $J(s,M^2_{\mathrm{A}},M^2_{\mathrm{B}})$ is the s-channel loop integral and $I\left(M^2_{\mathrm{A}}\right)$ is the tadpole integral that arises when derivatives act on the internal legs. These are defined as follows,

$$J(s,M^2_{\mathrm{A}},M^2_{\mathrm{B}}) \equiv \mu^{\epsilon}\int_q \frac{d^{4-\epsilon}q}{(2\pi)^{4-\epsilon}}\frac{1}{(q^2+M^2_{\mathrm{A}})(\tilde{q}^2+M^2_{\mathrm{B}})} \tag{3.41}$$

$$I\left(M^2_{\mathrm{A}}\right) \equiv \mu^{\epsilon}\int_q \frac{d^{4-\epsilon}q}{(2\pi)^{4-\epsilon}}\frac{1}{q^2+M^2_{\mathrm{A}}}. \tag{3.42}$$

Here, q and $\tilde{q}=q+p+k$ are the momenta, and M_{A} and M_{B} are the masses, that appear in the s-channel loop (see Fig. 3.2). Unitarity is studied by considering the coefficient of $J(s,M^2_{\mathrm{OS}},M^2_{\mathrm{OS}})$, since the tadpole function does not have an imaginary part. Comparing to Eq. (3.30), we see that the coefficient of J is simply the square of the LO scattering amplitude, $\mathcal{A}^{\mathrm{LO}}_{I=2}$, and that the masses in the internal propagators are the same as those of the external legs. Together this implies that $I=2$ scattering is consistent with s-channel unitarity. Although this is only based on a one-loop calculation, we argue in Ref. [41] that it will hold to all orders.

Next we turn to the $I=1$ case. We have calculated the s-channel one-loop diagram for $\pi^+_{\mathrm{OS}}\pi^0_{\mathrm{OS}}$ scattering. The intermediate states that contribute are $\pi^+_{\mathrm{OS}}\pi^0_{\mathrm{OS}}$, $\pi^+_{\mathrm{SS}}\pi^{dd}_{-+}$, $\pi^+_{\mathrm{VV}}\pi^{uu}_{+-}$, $\omega_{15}\omega_{52}$, and $\omega_{16}\omega_{62}$. A schematic form of the total result is sufficient for our purposes. Let $\mathcal{A}^{(s1)}_{\mathrm{cont}}(M_\pi)$ be the contribution from the loop in continuum QCD, which we know satisfies s-channel unitarity. Then we find

$$\mathcal{A}^{(s1)}_{\mathrm{OS},I=1} = \tfrac{1}{2}\mathcal{A}^{(s1)}_{\mathrm{cont}}(M_{\mathrm{OS}}) + \tfrac{1}{2}\mathcal{A}^{(s1)}_{\mathrm{cont}}(M^{\pm}_{\mathrm{SS}}), \tag{3.43}$$

$$\mathcal{A}^{(s1)}_{\mathrm{cont}}(M_\pi) = \frac{(t-u)}{6f^4}\left[\left(s-4M^2_\pi\right)J\left(s,M^2_\pi,M^2_\pi\right)+2I\left(M^2_\pi\right)\right]. \tag{3.44}$$

Since $M^{\pm}_{\mathrm{SS}} \neq M_{\mathrm{OS}}$, the phase-space for the second term of Eq. (3.43) does not match that required given that the external particles are OS pions, and s-channel unitarity fails. This is

consistent with the diagrammatic result from above. We do stress, however, that unitarity is recovered in the continuum limit, when $M_{\rm SS}^{\pm} = M_{\rm OS}$.

Finally, we consider the $I = 0$ channel. Here the calculation is more involved, with many intermediate states. We find that the contribution from s-channel loops is

$$\begin{aligned}\mathcal{A}_{\mathrm{OS},I=0}^{(s1)} = \frac{3s^2}{8f^4} J\left(s, (M_{\rm SS}^{\pm})^2, (M_{\rm SS}^{\pm})^2\right) + \frac{1}{8f^4} J\left(s, M_{\rm OS}^2, M_{\rm OS}^2\right) \Big(8M_{\rm OS}^2\left(8f^2 w_7' + 26M_{\rm OS}^2 + 5s\right) \\ - 8(M_{\rm SS}^{\pm})^2\left(-8f^2 w_7' + 44M_{\rm OS}^2 + 7s\right) - 112f^2 s w_7' + 256f^4 {w_7'}^2 + 160(M_{\rm SS}^{\pm})^4 + 13s^2\Big) \\ - \frac{3}{f^4}\left(-3(M_{\rm SS}^{\pm})^2 + 3M_{\rm OS}^2 + (M_{\rm SS}^0)^2\right)^2 J\left(s, M_{\rm OS}^2, (M_{\rm SS}^0)^2\right) \\ + \frac{3}{2f^4}\left(3(M_{\rm SS}^{\pm})^2 - 2\left(M_{\rm OS}^2 + (M_{\rm SS}^0)^2\right)\right)^2 J\left(s, (M_{\rm SS}^0)^2, (M_{\rm SS}^0)^2\right) \\ + \frac{5s}{12f^4} I\left((M_{\rm SS}^{\pm})^2\right) + \frac{1}{36f^4} I\left(M_{\rm OS}^2\right)\left(-336f^2 w_7' - 168(M_{\rm SS}^{\pm})^2 + 120M_{\rm OS}^2 + 65s\right) . \quad (3.45)\end{aligned}$$

It is straightforward to check that this form violates unitarity, both because the coefficients of J are not the square of the LO amplitude, Eq. (3.33), and because the masses in the arguments of J vary from term to term. Again, this is consistent with the diagrammatic analysis.

3.6 Implications for previous work

The conclusion from the previous section is that one cannot use the two-particle quantization condition for $I = 0$ OS pion scattering. This would seem to invalidate the calculation of Ref. [63], and render the χPT results of Sec. 3.4 irrelevant. In this section we argue that the situation is not quite so dire. The application of an invalid quantization condition introduces additional systematic errors into the results of Ref. [63], and these new errors can be approximately quantified.

The breakdown of s-channel unitarity leads to two distinct but related problems if one nevertheless applies Lüscher's formalism. The first concerns the fit that is used to extract the finite-volume energies. In particular, if $\mathcal{O}_I^\dagger$ is an operator that creates the pair of OS pions with OS isospin I, and $\mathcal{O}_I$ is the corresponding annihilation operator, then the energies are

extracted from

$$\langle \mathcal{O}_I(\tau)\mathcal{O}_I^\dagger(0)\rangle = \sum_{n=0}^{\infty} c_n e^{-E_n\tau}\,, \tag{3.46}$$

where $E_0 \le E_1 \le E_2 \le ...$, and the c_n's are real and positive coefficients. For physical theories, one can extract quantities of interest such as the energy shift $\delta E_0 = E_0 - 2M_\pi$ using a ratio of correlation functions

$$R(\tau) = \frac{\langle \mathcal{O}_I(\tau)\mathcal{O}_I^\dagger(0)\rangle}{\langle \pi^+_{++}\pi^-_{++}\rangle^2} = Ze^{-\delta E_0|\tau|} + \text{excited-state contributions}, \tag{3.47}$$

which may be expanded as

$$R(\tau) = Z\left[1 - |\tau|\,\delta E_0 + \frac{\tau^2}{2}(\delta E_0)^2 + \dots\right] + ... \tag{3.48}$$

where Z is some positive real constant. Here, for simplicity, we are assuming that the pions in the denominator of $R(\tau)$, and two-pion system propagating in the numerator, are at rest, as in the calculation of Ref. [63].[4]

For theories in which s-channel unitarity does not hold, the coefficient of the term quadratic in τ will not be half the square of the coefficient of $|\tau|$. Explicit examples of this failure are given in Refs. [41, 45]. For the examples of interest here, our results in Sec. 3.5 show that the expansion of the ratio $R(\tau)$ for $I = 1$ and $I = 0$ OS pions will not satisfy Eq. (3.48). If one nevertheless fits to this form, then an additional systematic error will appear in δE_0.

To estimate the size of this error, we need to know the relative contribution of the linear and quadratic terms for the values of τ that contribute to the fit. In the calculation of Ref. [63], and focusing on the lightest quark mass, the energy shift is $\delta E_0 \sim -0.01\ a^{-1}$, while the fit extends up to $\tau \sim 10\ a$. Thus $|\tau\ \delta E_0| \lesssim 0.1$ in the fit range, implying that the quadratic term is a no larger than a 5% correction to the linear term. We therefore expect the error in the extraction of the energy shifts arising from the breakdown of unitarity to be small, and in particular much smaller than the second source of error we now discuss.

[4]We note that Ref. [63] does not fit to the ratio of correlators, but rather to the numerator itself. This does not affect our argument as it is only the part of the correlator dependent on δE_0 that is impacted by partial quenching.

The second problem that arises from the breakdown of s-channel unitarity concerns the quantization condition itself. This converts energy shifts into scattering phase shifts. For our considerations it will be sufficient to use the threshold expansion, which reads [13, 14]

$$\delta E_0 = -\frac{4\pi a_0}{M_\pi L^3}\left[1 + c_1\frac{a_0}{L} + c_2\frac{a_0^2}{L^2} + \mathcal{O}(L^{-3})\right], \tag{3.49}$$

with $c_1 = -2.837$ and $c_2 = 6.375$. If s-channel unitarity is violated, then only the leading order term is correct: the c_1/L correction, and all higher-order terms, are invalid. To estimate the size of the error that arises from nevertheless applying expression (3.49), we can determine the size of the first two corrections for the parameters used in Ref. [63]. For their lightest quark mass, the OS pion mass is $aM_\pi = 0.11985$, on a lattice of size $L/a = 48$, and the scattering length obtained from solving the quantization condition for $I = 0$ OS pions is $Ma_0 = 0.73$. The $1/L$ and $1/L^2$ corrections are then of size -36% and $+10\%$, respectively, compared to the leading term. We therefore estimate the error arising from applying the quantization condition in a situation where it is not valid to be approximately 25%.

In principle, one could account for this source of error by calculating the explicit form of the $1/L$ (and possibly higher order) corrections using χPT at finite volume. One would forgo the Lüscher formalism and instead fit the finite-volume correlation functions that are calculated on the lattice directly to the predictions from χPT. This approach was first proposed for the quenched theory [90], and was worked out for Wilson fermions (without twisting) in Ref. [45]. Unlike the two-particle quantization condition, it is not model-independent, but relies on the effective theory, here PQTMχPT, to capture the violations of unitarity.

In the present case, however, this approach is likely to be very difficult to implement. This is because the one-loop contributions that lead both to the τ^2 term in Eq. (3.48) and the c_1/L term in Eq. (3.49) involve, in part, contributions with an OS π^0 and a sea-quark π^0 appearing in the loop, and also contributions with two sea-quark π^0s, as can be seen from Eq. (3.45). Both of these intermediate states are lighter than that with two OS pions, so the simple exponential fall off assumed in Eq. (3.48) is not valid, and the correct form with which to replace Eq. (3.49) is unclear.

Based on this discussion, we conclude that an additional systematic error of $\sim 25\%$ from unitarity violation should be added to the result for a_0 obtained in Ref. [63]. We view this as an essentially irreducible error, due to the difficultly in correcting for violations of unitarity. In addition, based on the analysis of Sec. 3.4.2, we expect that there is an $\mathcal{O}(a^2)$ discretization error that could be as large as 100%. The key point here is that we do not know whether the two $\mathcal{O}(a^2)$ terms in Eq. (3.35)—those proportional to $\Delta_{\rm OS}$ and w_7'—partly cancel or not. This is because we have, at present, no information on the size of w_7'. However, as noted in Sec. 3.4.2, calculations of the scattering length for $I = 2$ OS pions, which are not affected by unitarity violations, could be used to determine w_7' and thus correct for the LO discretization errors. Thus this nominally very large discretization error could be substantially reduced, very likely well below the size of the error due to the violation of unitarity.

3.7 Conclusion

Twisted-mass fermions offer many advantages for computations in LQCD, including automatic $\mathcal{O}(a)$ improvement, but these come at the price of the violation of isospin and parity symmetries away from the continuum limit. The size of unphysical effects due to the violation of these symmetries is, generically, of $\mathcal{O}(a^2)$, which is, for presently accessible values of a, of comparable size to physical contributions proportional to the light quark masses. This makes it challenging to calculate quantities that are themselves proportional to the light quark masses, an important example being the pion scattering amplitudes near threshold. While the $I = 2$ amplitude evades this concern, as all discretization errors turn out to be proportional to $a^2 m_q$ [75], the $\mathcal{O}(a^2)$ isospin breaking makes it difficult to calculate the $I = 0$ amplitude.

This problem was avoided in Ref. [63] by working in a PQ setup using OS valence quarks, such that a modified version of isospin was an exact symmetry. This allowed a result for the s-wave, $I = 0$ scattering length to be determined. In this work we have shown, however, that there are two additional source of systematic error in this result that have not previously been accounted for. The first is that OS pion scattering amplitudes do contain $\mathcal{O}(a^2)$ contributions,

and these cannot be subtracted using previously-determined quantities. Thus there is, *a priori*, a systematic error of $\mathcal{O}(100\%)$ in the resulting scattering length. We show, however, that this error can be substantially reduced if one also calculates the scattering of $I = 2$ OS pions, for a range of quark masses. Such a calculation, though not previously undertaken, is much simpler than that required for $I = 0$ OS pions.

The second, and ultimately more challenging, source of error is due to partial quenching. As we have recently emphasized, one cannot, in general, apply the two-particle quantization condition to PQ correlators [41]. What we have shown here is that this prohibition applies for systems of two OS pions with $I = 0$ (or $I = 1$), whereas the quantization condition can be used for the $I = 2$ OS pion channel. The breakdown for $I = 0$ implies that, if one nevertheless proceeds using the quantization condition, then there is an additional systematic error. We have estimated this error to be $\sim 25\%$, and argued that it is essentially irreducible.

Our work suggests that a systematically improvable calculation of the $I = 0$ scattering amplitude near threshold using twisted-mass fermions is very challenging. It appears to us that one must work in an unquenched setup, so that the two-particle quantization condition is valid, and thus deal with the isospin breaking, which in effect makes this a problem involving the $\pi^+_{\rm SS}\pi^-_{\rm SS}$ and $\pi^0_{\rm SS}\pi^0_{\rm SS}$ channels. To remove the unphysical $\mathcal{O}(a^2)$ effects from the results would likely require using the χPT results of Ref. [75], together with higher-order corrections.

Acknowledgments

We thank André Walker-Loud and Carsten Urbach for helpful comments and correspondence. This work is supported in part by U.S. Department of Energy Contract No. DE-SC0011637.

Chapter 4

INTERACTIONS OF πK, $\pi\pi K$ AND $KK\pi$ SYSTEMS AT MAXIMAL ISOSPIN FROM LATTICE QCD[1]

4.1 Abstract

We study the interactions of systems of two and three nondegenerate mesons composed of pions and kaons at maximal isospin using lattice QCD, specifically π^+K^+, $\pi^+\pi^+K^+$ and $K^+K^+\pi^+$. Utilizing the stochastic LapH method, we determine the spectrum of these systems on two CLS $N_f = 2+1$ ensembles with pion masses of 200 MeV and 340 MeV, and include many levels in different momentum frames. We constrain the K matrices describing two- and three-particle interactions by fitting the spectrum to the results predicted by the finite-volume formalism, including up to p waves. This requires also results for the $\pi^+\pi^+$ and K^+K^+ spectrum, which have been obtained previously on the same configurations. We explore different fitting strategies, comparing fits to energy shifts with fits to energies boosted to the rest frame, and also comparing simultaneous global fits to all relevant two- and three-particle channels to those where we first fit two-particle channels and then add in the three-particle information. We provide the first determination of the three-particle K matrix in $\pi^+\pi^+K^+$ and $K^+K^+\pi^+$ systems, finding statistically significant nonzero results in most cases. We include s and p waves in the K matrix for π^+K^+ scattering, finding evidence for an attractive p-wave scattering length. We compare our results to Chiral Perturbation Theory, including an investigation of the impact of discretization errors, for which we provide the leading order predictions obtained using Wilson Chiral Perturbation Theory.

---

[1] Z. T. Draper, A. D. Hanlon, B. Hörz, C. Morningstar, F. Romero-López and S. R. Sharpe, *Interactions of πK, $\pi\pi K$ and $KK\pi$ systems at maximal isospin from lattice QCD*, *JHEP* **05** (2023) 137 [2302.13587]

4.2 Introduction

Multihadron dynamics emerge nonperturbatively from the strong interactions between quarks and gluons described by Quantum Chromodynamics (QCD). Processes involving several hadrons have important implications for Nature, such as the properties of hadronic resonances and the emergence of nuclei as multi-particle systems. Thus, understanding these processes from first principles is an important goal for lattice QCD (LQCD) [92].

The study of hadron spectroscopy using LQCD has progressed rapidly in recent years; see Refs. [93–100] for recent reviews. One of the current frontiers is the systematic computation of three-hadron processes from LQCD. Indeed, there has been a concerted effort by several collaborations to understand three-particle processes in finite volume [16,17,35–39,101–122]. Using these theoretical tools in conjunction with numerical simulations of LQCD, several applications to simple systems have been carried out [40,67,91,123–134].

A class of three-particle systems that has not been extensively explored in simulations is that which involves nondegenerate particles. Two examples of resonances that decay to such three-hadron systems are (i) the doubly-charmed tetraquark, $T_{cc} \to DD\pi$ [135], and (ii) the Roper resonance $N(1440) \to N\pi\pi$ [136]. Both are exotic resonances for which there is a great deal of interest in obtaining predictions from LQCD. The formalism for such processes is rather complicated (and, indeed, has not yet been fully developed), and the LQCD computations are technically involved. Thus, for now, we leave aside the complications of resonances and spin quantum numbers, and focus on simpler systems of nondegenerate, spinless particles. Specifically, in this work we study systems of kaons and pions at maximal isospin, in particular $\pi^+\pi^+K^+$ and $K^+K^+\pi^+$, which we refer to as "2+1" systems. We use two ensembles with different values of the pion and kaon masses, which allows a rough extrapolation to the physical values.

The formalism for these systems was developed in Ref. [36], following the relativistic field theory approach (RFT). Further details of the implementation of the formalism, as well as useful theoretical results, were presented in Ref. [121]. These 2+1 systems exhibit new

features compared to three identical particles, namely the presence of interactions in odd partial waves and of multiple two-particle subchannels, e.g. both $\pi\pi$ and πK subchannels contribute to $\pi\pi K$ scattering. One of the goals of this work is to determine the three-particle K matrix, denoted $\mathcal{K}_{\text{df,3}}$, that describes short-range three-body interactions.[2] The only previous work that considers this quantity (to our knowledge) is Ref. [121], in which the leading order prediction of chiral perturbation theory (ChPT) is obtained. Compared to the corresponding quantity for three identical particles, $\mathcal{K}_{\text{df,3}}$ has reduced particle-interchange symmetry, and thus the number of independent terms in the threshold expansion of $\mathcal{K}_{\text{df,3}}$ is increased. This makes the determination of their coefficients more challenging.

A second goal of this work is to address the timely question of fitting strategies for multihadron systems. As the complexity of the system grows, the number of quantities to constrain from LQCD becomes larger. Indeed, a qualitative step can already be seen in this work compared to that for identical particles: we require more terms in $\mathcal{K}_{\text{df,3}}$, and two different two-meson amplitudes. In particular, the question arises whether it is preferable to determine the two-meson amplitudes from results for the two-particle spectrum (e.g. for $\pi^+\pi^+$ and π^+K^+), and then use the results in a fit to the three-particle spectrum (e.g. for $\pi^+\pi^+K^+$), or, instead, do a global fit to all channels at once. This is but one example of a general issue. An extreme case is provided by the determination of the $\gamma^*\gamma^* \to \pi\pi$ amplitude using finite-volume methods: the formalism requires also input from the finite-volume processes $\pi\pi \to \pi\pi$, $\pi\gamma^\star \to \pi$, $\gamma^\star \to \pi\pi$, and $\pi\pi\gamma^\star \to \pi\pi$ [137]. To determine which fitting procedures are preferable for more complex fits, we investigate and compare several fitting strategies.

Byproducts of this work are well-determined two-particle amplitudes. In particular, we compute the isospin $I = 3/2$ πK scattering amplitude in both s and p waves. By comparing

[2]We note that results for zero-momentum three-particle interactions for $2+1$ systems were obtained in Ref. [123] by fitting the ground state energy shifts of systems of multiple π^+ and K^+ mesons to the results of a $1/L$ expansion. The results used heavier pion and kaon masses than we consider. The relation of the interactions so obtained to $\mathcal{K}_{\text{df,3}}$ is not known, but we expect it to dominantly involve the leading terms in the threshold expansion, namely $\mathcal{K}_0$ and $\mathcal{K}_1$.

our results for the s-wave scattering length to ChPT, we are able to extract low energy constants (LECs) in a threshold expansion. Our results for the $I = 3/2$ p-wave scattering length are at lower pion masses than that obtained previously in Ref. [138]. We compare our result with this LQCD calculation, with the ChPT prediction, and with the results from a dispersive analysis.

This work also contains the first estimates of discretization errors in the three-particle K matrix. To achieve this, we present a new calculation of $\mathcal{K}_{\mathrm{df},3}$ using an extension of continuum chiral perturbation theory (ChPT) in which the effects of discretization errors are included, so-called Wilson ChPT (WChPT) [83, 84]. This allows us to determine the dependence of $\mathcal{K}_{\mathrm{df},3}$ on the lattice spacing in terms of low energy constants. We also calculate the corresponding dependence for two-particle amplitudes, which allows a determination of the relevant LECs by fitting to our results for these amplitudes. Thus we can estimate the magnitude of discretization effects in $\mathcal{K}_{\mathrm{df},3}$.

This paper is organized as follows. In section 4.3 we provide details of the LQCD simulation, describe our choice of interpolating operators, and discuss the fitting and results for the single and multiple-hadron spectra. Then, in section 4.4, we review the finite-volume formalism required for this work, present the parametrizations of the K matrices that we use, and collect the results from ChPT that we need. Next, in section 4.5, we describe the strategies that we use to fit to the spectra, and the results obtained, comparing different approaches. We collect our final results for infinite-volume scattering parameters in section 4.6, and compare them to ChPT, extracting several low-energy coefficients. We conclude in section 6.7. We include four appendices. Appendix B.1 displays a table with the energy levels used in fits, section B.2 provides details on the calculation of discretization effects using WChPT, section B.3 sketches the derivation of the analytical result for the p-wave πK scattering length at NLO in ChPT, and section B.4 summarizes the sets of operators used in this work.

4.3 Finite-volume Spectrum Extraction

Here we present the details regarding the extraction of the finite-volume spectrum from the two-point correlation functions computed using LQCD. The computational methods and strategies used follow those laid out in Ref. [132]. However, for convenience, we review the pertinent details.

4.3.1 Computation of Correlators

The extraction of finite-volume energies proceeds by first calculating two-point temporal correlation functions, which can be seen to contain all the information on the spectrum through their spectral decomposition

$$C_{ij}(t_{\text{sep}}) \equiv \langle \mathcal{O}_i(t_{\text{sep}} + t_0)\overline{\mathcal{O}}_j(t_0)\rangle = \sum_{n=0}^{\infty} \langle\Omega|\, \mathcal{O}_i \,|n\rangle \, \langle\Omega|\, \mathcal{O}_j \,|n\rangle^* \, e^{-E_n t_{\text{sep}}}, \tag{4.1}$$

where $\mathcal{O}_i(t)$ and $\overline{\mathcal{O}}_j(t)$ are annihilation and creation operators,[3] respectively, $|\Omega\rangle$ corresponds to the vacuum state, and E_n is the energy of the nth eigenstate $|n\rangle$ of the Hamiltonian. The indices on the operators indicate the possibility of a set of linearly independent interpolators that all share the same quantum numbers. Details on the procedure for extracting the spectrum from these correlators will be given in later sections, and we now turn to how the correlators themselves are computed.

The multi-hadron interpolating operators we consider in this work (see section 4.3.2 and section B.4) involve definite-momentum projections for the individual hadrons, which in turn necessitates quark propagators from all spatial sites at a given source time to all other lattice sites. One such method, referred to as distillation, acheives this with a smaller computational cost by utilizing a particular smearing based on the covariant Laplacian that cuts off higher-lying modes within the quark fields [139]. The smeared quark propagators can then be obtained by performing inversions within the much smaller subspace spanned by

[3]The operators $\mathcal{O}_j$ and $\overline{\mathcal{O}}_j$ are the analytic continuation to Euclidean space of the Minkowski-space operators $\mathcal{O}^{(M)}$ and $\mathcal{O}_j^{(M)\dagger}$, respectively.

the N_{ev} retained eigenvectors of the covariant Laplacian. However, the number of required eigenvectors needed to keep a constant smearing radius grows proportionally with the volume L^3 and can quickly become prohibitively expensive for large volumes. To mitigate this issue, rather than use distillation directly, we use a stochastic variant, referred to as stochastic LapH which has a better cost scaling [140]. This strategy combines stochastic sources within the distillation subspace and the method of dilution [141] to estimate the smeared quark propagators in terms of source $\varrho^{(r,d)}$ and sink $\varphi^{(r,d)}$ functions

$$\varrho^{(r,d)} = V_s P^{[d]} \varrho^{(r)}, \tag{4.2}$$

$$\varphi^{(r,d)} = \mathcal{S} D^{-1} \varrho^{(r,d)}, \tag{4.3}$$

where r labels the N_r stochastic sources, d labels the dilution partition, the columns of V_s contain the N_{ev} retained eigenvectors, $P^{[d]}$ is a dilution projector, $\mathcal{S} = V_s V_s^\dagger$ is the smearing kernel, D is the Dirac matrix, and $\varrho^{(r)}$ is a noise vector within the distillation subspace.

From the quark sinks and sources we form the meson sinks and sources, respectively, which are rank-2 tensors in the dilution indices. The final correlators are constructed from contractions of these tensors over the dilution indices. We make use of common subexpression elimination [142] to reduce the number of needed contractions and diagram consolidation to speed up the optimization. These algorithms have also been utilized for two-baryon [143] and meson-baryon [144] systems. Further details on our implementation of these contraction speedups can be found in Ref. [124], the code for which has been made publicly available [145].

4.3.2 Interpolating Operators

The single-hadron interpolators we use, which annihilate the single-hadron states, are

$$H_{\pi^+}(\mathbf{p}, t) = \sum_{\mathbf{x}} e^{-i\mathbf{p}\cdot\mathbf{x}}\, \overline{d}(x)\gamma_5 u(x), \tag{4.4}$$

$$H_{K^+}(\mathbf{p}, t) = \sum_{\mathbf{x}} e^{-i\mathbf{p}\cdot\mathbf{x}}\, \overline{s}(x)\gamma_5 u(x), \tag{4.5}$$

where u, d, s are up, down, and strange quark fields, respectively. These are then substituted into our two- and three-hadron interpolating operators, which are of the form

$$[H_{f_1}H_{f_2}]_\Lambda(\mathbf{P},t) = \sum_{\mathbf{p}_1,\mathbf{p}_2} c^{\mathbf{P},\Lambda}_{\mathbf{p}_1,f_1;\mathbf{p}_2,f_2} H_{f_1}(\mathbf{p}_1,t)H_{f_2}(\mathbf{p}_2,t), \tag{4.6}$$

$$[H_{f_1}H_{f_2}H_{f_3}]_\Lambda(\mathbf{P},t) = \sum_{\mathbf{p}_1,\mathbf{p}_2,\mathbf{p}_3} c^{\mathbf{P},\Lambda}_{\mathbf{p}_1,f_1;\mathbf{p}_2,f_2;\mathbf{p}_3,f_3} H_{f_1}(\mathbf{p}_1,t)H_{f_2}(\mathbf{p}_2,t)H_{f_3}(\mathbf{p}_3,t), \tag{4.7}$$

respectively, where $\mathbf{P} = \sum_i \mathbf{p}_i$ is the total momentum, Λ is the irrep of the little group of $\mathbf{P}$, f_i labels the flavor of the individual hadrons, and $c^{\mathbf{P},\Lambda}$ are Clebsch-Gordan coefficients. The Clebsch-Gordan coefficients are determined by requiring the overall operator transform according to the irrep Λ. The sum on the right-hand-side includes all momenta related via rotations within the little group of $\mathbf{P}$, with the constraint that $\sum_i \mathbf{p}_i = \mathbf{P}$. A table listing the multi-hadron interpolating operators used in this work is given in section B.4.

4.3.3 Lattice details

Our calculations are performed on two ensembles generated by the CLS (Coordinated Lattice Simulations) consortium [146]. The ensembles use $N_f = 2 + 1$ flavors of nonperturbatively $\mathcal{O}(a)$-improved Wilson fermions and the tree-level $\mathcal{O}(a^2)$-improved Lüscher-Weisz gauge action. The bare quark masses are tuned such that they follow a chiral trajectory in which the sum of the quark masses is held fixed. The practical effect of this choice is that the kaon mass approaches its physical value from below as the pion mass approaches its physical value from above. The two ensembles used in this study, named N203 and D200, both share a lattice spacing of $a \approx 0.06426(76)$ fm, which was determined from the linear combination $\frac{2}{3}(F_K + \frac{1}{2}F_\pi)$ of decay constants [147].[4] Other details, including the stochastic LapH setup, on these two ensembles can be found in Table 4.1.

In order to prevent topological charge freezing at fine lattice spacings, open temporal boundary conditions are employed [150]. This requires care when choosing the temporal

[4] The scale setting of Ref. [147] was recently updated, also using the pseudoscalar decay constants, giving a value of $a \approx 0.0633(4)(6)$ fm [148]. Additionally, a scale setting using baryon masses was recently reported, giving a value $a \approx 0.06379(37)$ fm [149].

	$(L/a)^3 \times (T/a)$	M_π [MeV]	M_K [MeV]	N_{cfg}	t_{src}/a	N_{ev}	dilution	$N_r(\ell/s)$
N203	$48^3 \times 128$	340	440	771	32, 52	192	(LI12,SF)	6/3
D200	$64^3 \times 128$	200	480	2000	35, 92	448	(LI16,SF)	6/3

Table 4.1: Specific details on the ensembles used in this work, including the name, geometry, approximate pseudoscalar masses, number of configurations N_{cfg}, source positions t_{src} used, number of eigenvectors N_{ev} of the covariant Laplacian retained, dilution scheme (see Ref. [140] for details), and number of noises N_{r} used for the light (l) and strange (s) quark sources. Both ensembles have the same lattice spacing $a \approx 0.063$ fm.

locations of the source and sink times used for the correlators, as we must make sure that they are sufficiently far from the temporal boundaries in order to suppress any effects from the boundary. As there was no need to produce additional quark sinks beyond what was used in our previous study [132], the arguments used there to justify the source and sink positions carry over here. Essentially, evidence for sufficient suppression of boundary effects on the D200 ensemble was given in Ref. [151], where it was found that a temporal distance of $\sim 32a$ from the boundary was enough for the exponentially decaying boundary effects to be negligible. Further, it is expected that the boundary effects are more severe on D200 than N203, as the leading contribution comes from the lowest state with quantum numbers of the vacuum, which should be a two-pion state for the quark masses considered here, and therefore has a smaller energy on D200. Thus, as the source positions considered for N203 are even further from the boundary than D200, our choices should be safe from the effects of the open boundary conditions. Note that the source position of $t_{\text{src}} = 92a$ for D200 only has sink times smaller than $92a$ associated with it (i.e. the correlators go backward in time, see Ref. [132] for more details).

Finally, autocorrelations, which lead to underestimated errors, can be checked for by observing dependence on the error estimates from averaging N_{rebin} successive configurations

across all the original measurements into $N_{\text{cfg}}/N_{\text{rebin}}$ new bins. While there is evidence that values as high as $N_{\text{rebin}} = 20$ are needed for D200 to completely remove autocorrelations [144], this is not plausible for our use-case, as the number of energies used in our fits in section 4.5.2 is too high to reliably estimate the covariance matrix with so few bins. However, we have found little to no dependence on the final results for N203 when using $N_{\text{rebin}} = 1$ or $N_{\text{rebin}} = 3$, suggesting the observables of interest here are not affected significantly by autocorrelations. We therefore use $N_{\text{rebin}} = 1$ for N203, while using $N_{\text{rebin}} = 3$ for D200 in order to still obtain reliable estimates for the covariance matrix while removing some autocorrelation. Additionally, we note that the configurations used on N203 are separated in Markov time by twice the distance used for D200, which is why we use a conservative choice for the rebinning on D200.

4.3.4 Finite-volume energies from correlators

As can be seen from the spectral decomposition in eq. (4.1), in principle one can extract any energy so long as the operators used have non-zero overlap onto the corresponding eigenstate. However, with finite statistics, reliably determining the states beyond the first few terms from fits to a single correlator is difficult. As we are only interested in the ground states for the single-hadron particles, we can obtain these from single-exponential fits to the correlators starting after all higher-lying states are exponentially suppressed. Fortunately, for the single hadron correlators, the signal-to-noise ratio is either constant or slowly decaying which allows for a good signal after all higher-lying states have decayed away. The needed single-hadron masses were determined in our previous work [132] and are reproduced in Table 4.2 for convenience, along with the decay constants needed for the chiral extrapolations performed later.

Our eventual goal is to obtain the multi-hadron interactions, which are constrained by the multi-hadron finite-volume energies. Each of these energies provides a constraint on these interactions, and, therefore, including as many energies as possible will typically improve the reliability of the extracted interactions. In general, the gaps between the multi-hadron states

	aM_π	aM_K	$M_\pi L$	$M_K L$	M_π/F_π	M_K/F_K
N203	0.11261(20)	0.14392(15)	5.4053(96)	6.9082(72)	3.4330(89)	4.1530(72)
D200	0.06562(19)	0.15616(12)	4.200(12)	9.9942(77)	2.2078(67)	4.5132(93)

Table 4.2: Pion and kaon masses and decay constants for the two ensembles considered in this work. The masses were determined in our previous work [132]. The decay constants were determined in Ref. [152].

are smaller than those of the single-hadron states, making a reliable extraction more challenging, especially coupled with the increased statistical errors of the multi-hadron fits. Thus, we need a method to reliably determine several energies from the multi-hadron correlators. We utilize a variational method [153, 154], which relies on solving a generalized-eigenvalue problem (GEVP) using a correlator matrix built from sets of interpolating operators that all transform in the same way. This is the same method used in Ref. [132], but we repeat most of the details here to make the discussion self-contained.

For each overall flavor, irrep, and total momentum squared, we construct a set of N operators and use them to calculate a correlation matrix $C_{ij}(t_{\text{sep}})$ as in eq. (4.1). We then form a GEVP as

$$C(t)\upsilon_n(t,t_0) = \lambda_n(t,t_0)C(t_0)\upsilon_n(t,t_0), \tag{4.8}$$

where t_0 is referred to as the metric time. As long as $t_0 \geq t/2$, one can show that the generalized eigenvalues behave as

$$\lambda_n(t,t_0) = |A_n|^2 e^{-E_n(t-t_0)}\Big[1 + \mathcal{O}(e^{-\Delta_n t})\Big], \tag{4.9}$$

where $n = 0, \ldots, N-1$, E_n is the nth eigenenergy, and $\Delta_n \equiv E_N - E_n$. Thus, the method provides a straightforward way of extracting the excited-state energies without having to perform a fit which includes many exponentials. In fact, the eigenvalues of $C(t)$ also share this advantage, but with a gap $\Delta_n \equiv \min_{m\neq n}|E_n - E_m|$ that is smaller than or equal to the

gaps found in the case of the GEVP. Therefore, the gap from the GEVP helps to further suppress unwanted contributions in the generalized eigenvalues.

One technical complication involves matching the eigenvectors at one time separation to another or one resampling to the next (*i.e.* eigenvector pinning), which can easily become problematic from ambiguous choices, especially at large time separations where the noise grows. Instead, we solve the GEVP on the mean and at a single time separation t_d, where $t_0 < t_d \lesssim 2t_0$, and then use the eigenvectors to rotate the original correlator matrix on all resamplings and at all other times not equal to t_d

$$\hat{C}_n(t) = (\upsilon_n(t_d, t_0), C(t)\upsilon_n(t_d, t_0)), \tag{4.10}$$

where the parentheses indicate an inner product. To avoid any systematics associated with only solving the GEVP for one time separation, we look for stability in the extracted spectrum as the diagonalization time t_d and metric time t_0 are varied.

To obtain the two- and three-hadron finite-volume energies, we use single-exponential correlated-χ^2 fits to the ratios

$$R_n(t) = \frac{\hat{C}_n(t)}{\prod_i C_{f_i}(\mathbf{p}_i^2, t)}, \tag{4.11}$$

where $C_{f_i}(\mathbf{p}_i^2, t)$ is an average of single-hadron correlators with flavor f_i over all rotationally equivalent momentum with magnitude $\mathbf{p}_i^2$. The product of single-hadron correlators in the denominator is chosen based on the expected non-interacting energy level associated with the nth eigenstate, in which case the asymptotic behavior is

$$\lim_{t\to\infty} R_n(t) \propto e^{-\Delta E^n_{\text{lab}} t}, \tag{4.12}$$

where ΔE^n_{lab} is the energy shift of the nth eigenstate from its non-interacting value in the lab frame. The use of the ratio has a few advantages over fitting directly to $\hat{C}_n(t)$: there is a strong cancellation of correlated fluctuations between the numerator and denominator, and the plateau in the effective energy of the ratio begins at earlier time separations and is more stable across several time separations. However, despite the earlier plateau seen from the ratio, in order to not introduce any further systematics, we typically make a conservative

choice for the beginning of our fit range t_{min} such that the single-hadron correlators have already attained their asymptotic behavior.

In figure 4.1, we show the dependence of several extracted energy shifts on t_{min} and the GEVP parameters t_0 and t_d. The energies shown correspond to the first excited state in an irrep with $\mathbf{P}^2 = 2(2\pi/L)^2$ and the ground state in an irrep with the largest momentum-squared used for a given flavor. We include all three mixed-flavor systems and both ensembles. As can be seen in these t_{min} plots, typically there is a wide region of t_{min} with consistent energy shifts before correlated fluctuations take over when the signal starts to be lost. The ability of the variational method to suppress contributions from unwanted nearby states is illustrated by the results with $\mathbf{P}^2 = 2(2\pi/L)^2$, for in these cases there are usually several nearby energy levels. Additionally, the dependence on the choices for (t_0, t_d) is either very mild or not visible.[5] The value of t_{min} is chosen such that it is much larger than the onset of the stability in the extracted energy, but not so large that correlated fluctuations begin to arise. Among the fits satisfying this critera, our final value is based on making a conservative choice to ensure that any systematics are smaller than the statistical errors, while also making sure the fit quality is reasonable. Examples of the choices of t_{min} are shown in the figure.

To illustrate the number of levels that we are able to determine, and the errors that we obtain, we show in figure 4.2 the energy levels for the $\pi\pi K$ system on the N203 ensemble. To better compare the levels from different momentum frames, we show the center-of-mass frame (CMF) energies $E^* = \sqrt{E^2 - \boldsymbol{P}^2}$. Also shown (as teal dots) are the result of our standard fit to these levels, to be discussed below, in which we fit only to levels that lie below the first inelastic threshold. Although the formalism is not, strictly speaking, valid above this threshold, we also display its predictions for some of the higher levels (as orange dots). Analogous plots for the other three-meson systems that we consider are shown in section B.1. Detailed discussion of these and other fits are provided below.

[5] At a late stage in the fitting of the spectrum, one level was found to have a $\sim 3\sigma$ variation in the shift away from the free level as (t_d, t_0) were varied. The specific level and the small effect it has on the final results is discussed in more detail in section 4.5.2.

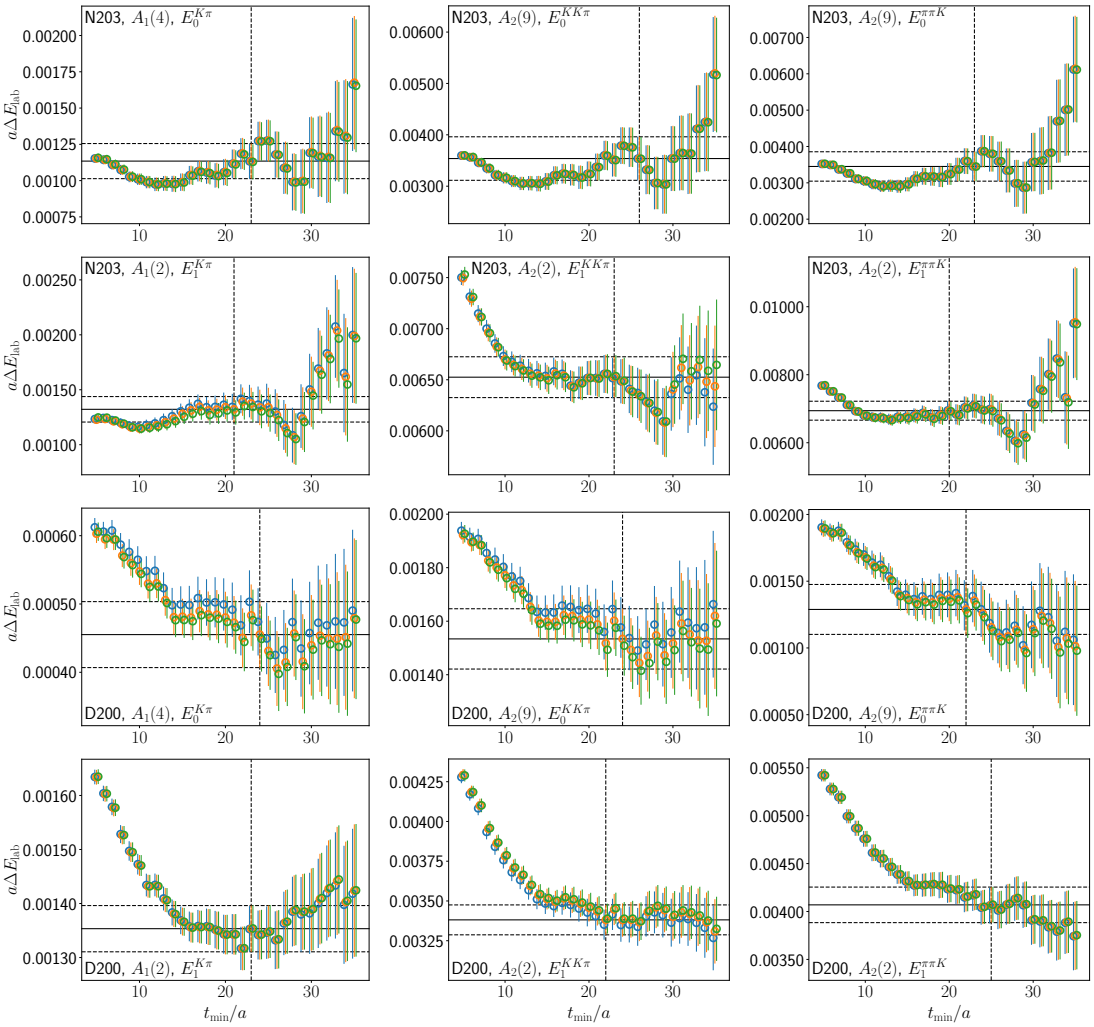

Figure 4.1: The dependence of the energy shift in the lab frame extracted from fits to the ratio $R_n(t)$ on the smallest time separation $t_{\rm min}$ included in the fit. The colors correspond to different values of the GEVP metric time t_0 and diagonalization time t_d: $t_0/a = 4, t_d/a = 8$ (blue), $t_0/a = 6, t_d/a = 12$ (orange), $t_0/a = 12, t_d/a = 24$(green). A small horizontal offset is applied to separate these three choices. Each plot indicates the ensemble, irrep, total momentum-squared (in units of $(2\pi/L)^2$, energy level, and flavor. For example, in the bottom-right plot, the notation $A_2(2)$ indicates the A_2 irrep with momentum squared being $2(2\pi/L)^2$, while $E_1^{\pi\pi K}$ indicates that this is the first excited $\pi^+\pi^+K^+$ level in this irrep. In each panel, the black horizontal solid and dashed lines indicate the mean and error, respectively, of the energy shift for the chosen fit, for which the value of $t_{\rm min}$ is indicated by the vertical dashed line.

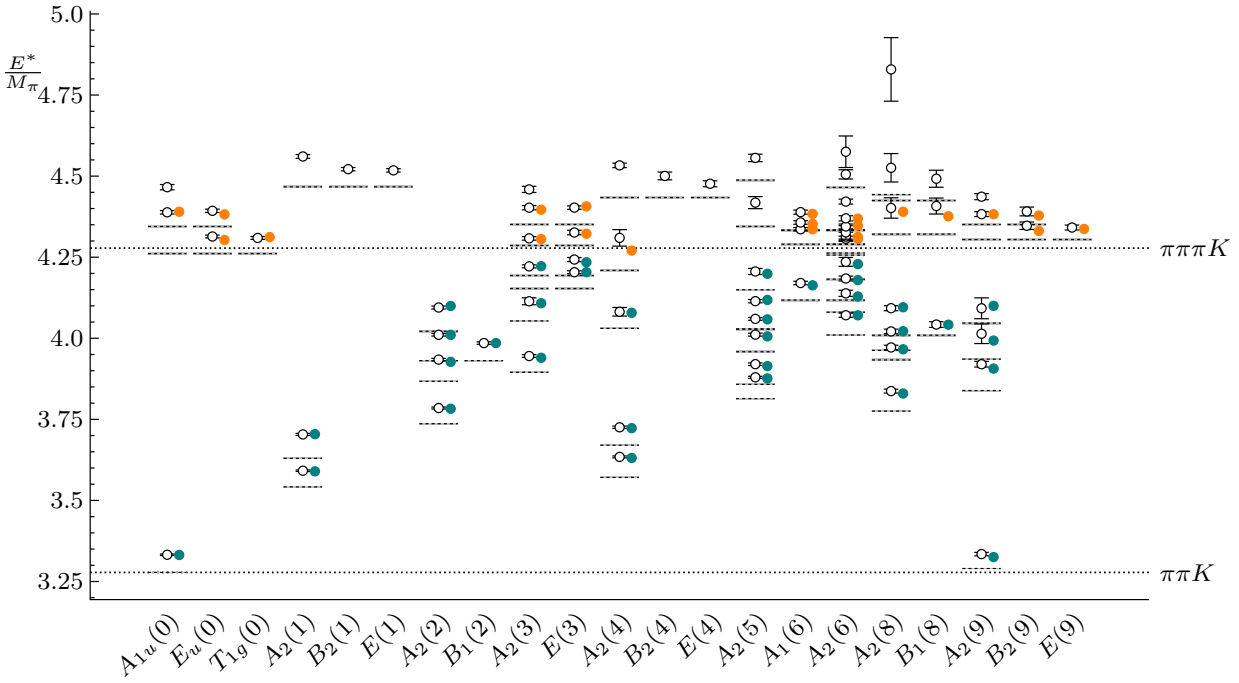

Figure 4.2: The $\pi\pi K$ center-of-mass frame energies, in units of M_π, on the N203 ensemble. The horizontal axis labels the irrep and (in parentheses) the total momentum squared in units of $(2\pi/L)^2$. The horizontal dashed lines and grey boxes (the latter barely visible) indicate the mean and error of the non-interacting energy levels, while the open circles with error bars correspond to the interacting energies. The colored symbols show the solutions of the quantization condition with the parameters found in the 82-level fit in Table 4.8. Teal colored points are associated with energy levels included in the fit, while the orange points are for levels not in the fit. The horizontal dashed lines running across the entire plot show the ground state energy ($E^* = 2M_\pi + M_K$) and the first inelastic threshold ($E^* = 3M_\pi + M_K$).

4.4 Theoretical background

In this section we collect theoretical results needed to constrain the two- and three-particle K matrices from the two- and three-particle spectra obtained using lattice QCD. As discussed in the previous section, we have results for both degenerate and nondegenerate two- and three-particle channels. The formalism for the degenerate cases has been reviewed in Ref. [132], so we focus on the formalism needed for the new channels considered here, i.e. πK for the two-particle case, and $\pi\pi K/KK\pi$ for three particles. We first provide a brief recapitulation of the quantization conditions and our fitting strategy, then describe the parametrizations of K matrices that we use, and finally collect the predictions of ChPT.

4.4.1 Quantization conditions and fitting strategy

To extract infinite-volume scattering parameters from a finite-volume energy spectra, we make use of both two- and three-particle quantization conditions. The two-particle finite-volume formalism was first developed by Lüscher [13, 14]. We will need the generalizations to moving frames and to nondegenerate particles given in Refs. [15, 155, 156].

The three-particle formalism has been developed using three approaches: the relativistic field theory (RFT) approach [16, 17], which will be the basis of this analysis, the non-relativistic effective field theory (NREFT) approach [104, 106] (subsequently relativized in Ref. [120]), and the finite-volume unitarity (FVU) approach [40]. The formal equivalence (up to technical differences) of the RFT and FVU formalisms was established in Ref. [116], and the equivalence of FVU and relativized NREFT formalisms is noted in Ref. [120]. Reviews of these approaches and comparisons between them can be found in Refs. [94, 95, 97, 99], and a direct comparison of their application is given in Ref. [134]. We will use the RFT result for three identical particles given in Refs. [16,17], and the extension given in Refs. [35,36,117] to so-called "2+1"-systems, i.e. those involving one distinct and two identical spinless particles.

We will not recap the derivations here. We only note that the RFT method is based on an all-orders diagrammatic analysis in a generic relativistic effective field theory, and applies in a

kinematic regime in which only three-particle channels can go on shell. As one might expect from the name, this approach applies for relativistic particles; and if the relativistic forms of kinematic functions are used (see Ref. [110]), the formalism leads to Lorentz-invariant scattering amplitudes.

An extensive discussion of the implementation of the quantization condition for 2+1 systems is given in Ref. [121], and thus we present only an overview here. In particular, quantities not defined here can be found in that work. We also make use of the formalism for identical particles derived in Ref. [16], and in particular the implementation presented in Ref. [110]. A general feature of the three-particle formalism is a division into a spectator particle and the remaining pair or dimer. For practical applications, one must impose a cutoff on the angular momentum, ℓ, of the pairs. In our previous work analyzing $3\pi^+$ and $3K^+$ spectra, we used $\ell_{\max} = 2$, thus including s and d waves (p wave being forbidden for identical particles) [132]. However, working up to $\ell_{\max} = 2$ is not possible here, due to the proliferation of fit parameters, as discussed in Ref. [121] and recapitulated below. Instead we use $\ell_{\max} = 1$, with s and p waves in the π^+K^+ subsystems, and only s waves for subsystems with identical particles ($2\pi^+$ and $2K^+$).

We begin by considering the two-particle quantization condition. The inputs are the total momentum, $\boldsymbol{P}$, the box size, L, a kinematic function denoted F, which contains the effects of finite-volume physics, and the two-particle K matrix, $\mathcal{K}_2$. By solving the following two-particle quantization condition,

$$\det\left[F\left(E_2, \boldsymbol{P}, L\right)^{-1} + \mathcal{K}_2(E_2^*)\right] = 0\,, \tag{4.13}$$

we can determine the two-particle energies, E_2, and, from these, the corresponding center-of-mass frame (CMF) energies, $E_2^* = \sqrt{E_2^2 - \boldsymbol{P}^2}$, up to corrections suppressed by factors of $\exp(-M_\pi L)$ and $\exp(-M_K L)$. As in the lattice simulations, we work in a cubic spatial box with side length L, which restricts the allowed total momenta to the set $\boldsymbol{P} = (2\pi/L)\boldsymbol{d}$, where $\boldsymbol{d} \in \mathbb{Z}^3$.

The three-particle quantization condition determines the energies of three-particle states

in a finite volume, and is given by

$$\det\left[F_3\left(E,\boldsymbol{P},L\right)^{-1}+\mathcal{K}_{\mathrm{df},3}(E^*)\right]=0\,. \tag{4.14}$$

Here E is the lab-frame energy of the three-particle state, $E^*=\sqrt{E^2-\boldsymbol{P}^2}$ is the corresponding CMF energy, and $\mathcal{K}_{\mathrm{df},3}$ is a three-particle K matrix discussed further below. Although, superficially, the three-particle quantization condition may look similar to that for two particles, the former hides significant complexity. In particular, we note that whereas the quantity F that appears in the two-particle quantization condition is a purely kinematic function, F_3 depends on F, on an additional kinematic function G, as well as on the two-particle K matrix, $\mathcal{K}_2$. The detailed form is given in Ref. [121]. We also note that while the three-particle quantization in several different contexts takes exactly the same form as in eq. (4.14) (see, e.g. Ref. [37] for the case of degenerate but nonidentical scalars), the indices over which the determinant is taken differ.

We now describe the meaning of the determinants in eq. (4.13) and eq. (4.14). For the two-particle quantization condition, F and $\mathcal{K}_2$ are matrices in which the indices $\{\ell,m\}$ label the angular momentum of the two-particle state, and the determinant runs over these two labels. For the three-particle quantization condition, additional indices are required. These are given by the spectator momentum $\boldsymbol{k}$, which is constrained to lie in the finite-volume set, and the angular-momentum indices for the pair, $\{\ell,m\}$. In addition, we need an index, i, to specify whether the spectator is identical to one of the other two particles ($i=1$) or whether it is distinct ($i=2$). For such a system, we therefore have a determinant which runs over the indices $\{k_i,\ell,m,i\}$, where k_i labels the momentum of a spectator of particle species i. The quantities F_3 and $\mathcal{K}_{\mathrm{df},3}$ are matrices with these indices.

The derivation of Refs. [16,36] requires a cutoff on the spectator momenta, which must be implemented by a smooth function (rather than a sharp cutoff). One way to understand the need for the cutoff is that, for a given total energy E, the pair is driven below threshold as the spectator momentum increases. Far enough below threshold the two-particle interaction has a left-hand cut, and this must be avoided as it introduces power-law volume dependence

that is not controlled in the derivation. The details of the required cutoff are discussed in Ref. [121]. It implies that only a finite number of values of $\boldsymbol{k}_i$ contribute. Combined with the cutoff on ℓ discussed above, this implies that all matrices in eq. (4.14) are of finite dimension.[6]

We now return to the K matrices appearing in the quantization conditions. Both $\mathcal{K}_2$ and $\mathcal{K}_{\text{df},3}$ are infinite-volume Lorentz-invariant quantities, but have important differences. In particular, $\mathcal{K}_2$ is algebraically related to the two-particle scattering amplitude $\mathcal{M}_2$, while $\mathcal{K}_{\text{df},3}$ is related to the three-particle scattering amplitude $\mathcal{M}_3$ through integral equations [17]. Furthermore, $\mathcal{K}_{\text{df},3}$ depends on the cutoff function, whereas $\mathcal{K}_2$ is cutoff independent above threshold. However, both $\mathcal{K}_2$ and $\mathcal{K}_{\text{df},3}$ share the property of being real and smooth functions of Lorentz invariants below the relevant inelastic thresholds.[7] We make use of these properties to parametrize the K matrices in section 4.4.2.

For given choices of $\mathcal{K}_2$ and $\mathcal{K}_{\text{df},3}$, the quantization conditions predict the two- and three-particle spectra. Details of our numerical methods are given in Ref. [121], and a basic python implementation is publicly available [157]. We first block-diagonalize the quantization conditions by projecting them onto irreducible representations of the subgroup of the cubic group that leaves the overall momentum, $\boldsymbol{P}$, invariant. This is the little group $\text{LG}(\boldsymbol{P})$. Within each block, we track the smallest eigenvalues of the matrix lying within the determinant, and find zero crossings using a root-finding algorithm. A finite-volume energy level in the given irrep is predicted to occur for each such crossing. We find that it is useful to have a good initial guess for the energy levels, and, for the most part, this is provided by either the measured energy levels or the free levels. We have implemented this methodology in three independent python codes, and all results presented below have been obtained with at least two of these codes. We find that, when running on about ~ 50 cores, the convergence for the most challenging cases (simultaneous fits to 2 two-particle and 1 three-particle channels)

[6] We note that in the NREFT approach a hard cutoff can be used, and its value is not constrained by the position of the left-hand cut [104, 106, 120].

[7] The only exceptions are that $\mathcal{K}_2$ and $\mathcal{K}_{\text{df},3}$ can have poles in the presence of two- and three-particle resonances, respectively. These exceptions do not occur in this work.

takes $2-3$ days. The use of the Python compiler `numba` [158] to speed up core routines is essential to achieve this speed.

As discussed in Refs. [108,110,114], one must ensure that the zero crossings are physical. In particular, the eigenvalue must cross from negative to positive values as the energy is increased, and no higher-order zeros are allowed. The exception to the latter restriction is that there can be higher-order zeros at noninteracting energies, but these are present only because of the truncation of the K matrices, as discussed extensively in Ref. [110]. Such solutions can be dropped. We find that all the crossings are physical.

4.4.2 Parametrizing K matrices

We now turn to the parametrizations that we use for the matrices $\mathcal{K}_2$ and $\mathcal{K}_{\text{df},3}$. The former is diagonal in angular momenta,

$$\mathcal{K}_2(E_2^*)_{\ell' m';\ell m} = \delta_{\ell'\ell}\delta_{m'm}\mathcal{K}_2^{(\ell)}(E_2^*)\,, \tag{4.15}$$

$$\left[\mathcal{K}_2^{(\ell)}(E_2^*)\right]^{-1} = \frac{\eta}{8\pi E_2^*}\left\{q\cot\delta_\ell(q) + |q|[1-H(q^2)]\right\}\,. \tag{4.16}$$

We have written the expression so that it holds for both degenerate ($\pi\pi$ and KK) and nondegenerate (πK) channels: in the former case, $\eta = 1/2$, while $\eta = 1$ in the latter. In both cases, q is the the magnitude of the three-momentum for each of the two particles in the CMF of the pair. The function $H(q^2)$ plays the role of a cutoff. It equals unity for $q^2 \geq 0$ [so that the $1-H$ term in eq. (4.16) vanishes above threshold], and smoothly drops to zero well below threshold (so that $\mathcal{K}_2^{(\ell)}$ transitions into $\mathcal{M}_2^{(\ell)}$). The form of this function depends on the particle masses, as explained in Ref. [121]. The H function does not play a role in the two-particle quantization condition, eq. (4.13), because it also appears in the quantity F, in such a way that the H dependence cancels. It is, however, essential in the three-particle quantization condition (in which $\mathcal{K}_2$ enters through F_3), as it cuts off the sum over the spectator momenta.

As in Ref. [132], we explore two choices for the parametrization of the phase shift: an "Adler zero" form, and the effective-range expansion (ERE). The former is motivated by chi-

ral perturbation theory, which predicts that the scattering amplitude vanishes below threshold at the position denoted the Adler zero. For $\ell = 0$, the Adler zero form is

$$\frac{q}{M_1}\cot\delta_0(q) = \frac{M_1 E_2^*}{E_2^{*2} - z^2(M_1^2 + M_2^2)} \sum_{n=0}^{\infty} B_n \left(\frac{q^2}{M_1^2}\right)^n , \tag{4.17}$$

where z^2 and the B_n are dimensionless parameters. Two masses appear in this parameterization: M_1, the mass which we use to set the units, e.g. of q, and M_2, the mass of the other particle. M_1 and M_2 are chosen from the set $\{M_\pi, M_K\}$ based on the particular scattering process being considered, and may or may not be distinct. At leading order in ChPT $z^2 = 1$, while B_0 and B_1 take nonzero values to be discussed in the next section, with all other parameters vanishing. In practice, we use two choices of parametrization:

1. ADLER2, in which $z^2 = 1$, B_0 and B_1 are free parameters, and $B_n = 0$ for $n \geq 2$;

2. ADLER3, in which z^2, B_0, and B_1 are free parameters, and $B_n = 0$ for $n \geq 2$.

We use superscripts and subscripts to denote the corresponding channel, e.g. $z^2_{\pi K}$ and B_0^{KK}. The relation of these parameters to the scattering length a_0 and effective range r_0 is given by

$$a_0 M_1 = -\frac{(M_1 + M_2)^2 - z^2(M_1^2 + M_2^2)}{M_1(M_1 + M_2)B_0} , \tag{4.18}$$

$$a_0 r_0 M_1^2 = \frac{M_1}{M_2}\frac{(M_1 + M_2)^2 + z^2(M_1^2 + M_2^2)}{(M_1 + M_2)^2 - z^2(M_1^2 + M_2^2)} - 2\frac{B_1}{B_0} . \tag{4.19}$$

Here we are using the convention in which a_0 is positive for repulsive interactions.

The ERE form is simply an expansion in powers of q^2,

$$\frac{q}{M}\cot\delta_0(q) = \sum_{n=0}^{\infty} B_n \left(\frac{q^2}{M^2}\right)^n , \tag{4.20}$$

where the B_n are dimensionless. We use the same names for the coefficients as in the ADLER forms, but it will always be clear from the context which fits are being used. The mass M sets the scale of q and may be chosen to be either of the masses of the particles in the scattering pair. In Ref. [132], we found that the Adler zero form was preferred for the $\pi\pi$ and $\pi\pi\pi$

channels, while for kaons the ERE form was slightly preferred. This was not unexpected, as ChPT should work better for pions than kaons. Here we only use the ERE form for KK and KKK channels, where we compare it to the ADLER forms. Specifically, we use

3. ERE3, in which B_0, B_1, and B_2 are free parameters, and $B_n = 0$ for $n \geq 3$.

The relation of the ERE3 parameters to the scattering length and effective range is

$$Ma_0 = -\frac{1}{B_0} \quad \text{and} \quad a_0 r_0 M^2 = -2\frac{B_1}{B_0}\,. \tag{4.21}$$

For $\ell = 1$, which is present only for πK scattering, we use a one-parameter form,

$$\frac{q^3}{M_1^3}\cot\delta_1(q) = \frac{E_2^*}{M_1 + M_2}\frac{1}{P_0^{\pi K}}\,. \tag{4.22}$$

Here $P_0^{\pi K}$ is the p-wave scattering length, and the same notation for masses is used as above. The factor of E_2^* is adopted from standard continuum analyses [159, 160]. We find that the signal for nonzero p-wave scattering is sufficiently weak that we cannot include higher-order terms and obtain stable fits.

We now turn to the three-particle K matrix. As noted above, $\mathcal{K}_{\text{df,3}}$ is a real, analytic function of Lorentz invariants. We use the analog of the ERE, which is an expansion about threshold, and has been worked out for $2+1$ systems in Ref. [36]. We denote M_1 as the mass of the particle that appears twice, while M_2 is the mass of the singleton. Implementing the relevant particle interchange symmetries, as well as parity and time reversal, the resulting form is

$$M_1^2 \mathcal{K}_{\text{df,3}} = \mathcal{K}_0 + \mathcal{K}_1\Delta + \mathcal{K}_B\Delta_2^S + \mathcal{K}_E\tilde{t}_{22} + \mathcal{O}(\Delta^2). \tag{4.23}$$

Here, $\mathcal{K}_0$, $\mathcal{K}_1$, $\mathcal{K}_B$, and $\mathcal{K}_E$ are real, dimensionless constants,[8] to be determined from fits to the three-particle spectrum, while Δ, Δ_2^S and $\tilde{t}_{22}$ are functions of the Mandelstam variables. The initial (incoming) momenta are $\{k_1, k_{1'}, k_2\}$, while the (outgoing) final momenta are

[8] Previously we have used a more elaborate notation for $\mathcal{K}_0$ and $\mathcal{K}_1$, namely $\mathcal{K}_{\text{df,3}}^{\text{iso}}$ and $\mathcal{K}_{\text{df,3}}^{\text{iso,1}}$, respectively [110, 121, 132]. Here we stick with the simpler notation. We also stress that the quantity $\mathcal{K}_B$ used here differs from that in Ref. [132]; the latter involves d-wave interactions for identical particles.

$\{p_1, p_{1'}, p_2\}$, where k_2 and p_2 are the momenta of the singleton. The kinematic quantities appearing in eq. (4.23) are

$$\Delta \equiv \frac{s - M_\Sigma^2}{M_\Sigma^2}, \quad \Delta_2^S \equiv \frac{(p_1 + p_{1'})^2 - 4M_1^2}{M_\Sigma^2} + \frac{(k_1 + k_{1'})^2 - 4M_1^2}{M_\Sigma^2}, \\ \tilde{t}_{22} \equiv \frac{(p_2 - k_2)^2 - (M_1 - M_2)^2}{M_\Sigma^2}, \quad (4.24)$$

where

$$s \equiv (p_1 + p_{1'} + p_2)^2 = E^{*2} \quad \text{and} \quad M_\Sigma \equiv 2M_1 + M_2\,. \quad (4.25)$$

Δ, Δ_2^S and $\tilde{t}_{22}$ are all of the same order in the threshold expansion, but only Δ_2^S and $\tilde{t}_{22}$ have to a nontrivial angular dependence and lead to contributions with both $\ell = 0$ and 1.

The expansion in eq. (4.23) can be continued to higher order, with terms of $\mathcal{O}(\Delta^2)$ including d-wave ($\ell = 2$) contributions. However, this leads to a proliferation of parameters, and so we restrict ourselves here to $\ell_{\max} = 1$. This is in contrast to Ref. [132], where the analysis used $\ell_{\max} = 2$ for the $3\pi^+$ and $3K^+$ spectra, which was possible because there are many fewer allowed forms in $\mathcal{K}_{\mathrm{df},3}$ for identical particles. Here, where needed, we have redone the identical-particle fits with $\ell_{\max} = 1$, implying that $\mathcal{K}_{\mathrm{df},3}$ contains only the $\mathcal{K}_0$ and $\mathcal{K}_1$ contributions, since the $\mathcal{K}_B$ and $\mathcal{K}_E$ terms in eq. (4.23) vanish for a fully symmetric system.

The explicit forms for the $\mathcal{K}_B$ and $\mathcal{K}_E$ terms in the $\{k\ell m\}$ basis have been worked out in Ref. [121], and we simply use the results.

4.4.3 Results from chiral perturbation theory

Analyzing the two- and three-particle spectra for two different pion masses allows us to investigate the mass dependence of the scattering parameters we derive from fits. In this subsection we collect results from ChPT that will be useful when we fit the dependence of these scattering parameters versus M_π^2/F_π^2. Since our focus is on systems including both pions and kaons, we consider results from SU(3) ChPT. We note that a criterion for the utility of these results is that $M_K^2/(4\pi F_K)^2 \ll 1$, where F_K is the kaon decay constant in the convention that $F_\pi \simeq 92$MeV. For ensembles D200 and N203 the ratio $M_K^2/(4\pi F_K)^2$ is 0.11

and 0.13 respectively.

The next-to-leading order (NLO) ChPT expressions for the $\pi\pi$ and KK scattering lengths can be found in Refs. [76, 161]. Both depend on the mass of the η meson as well as the pion and kaon, but it is consistent in the NLO contribution to use the LO result $3M_\eta^2 = 4M_K^2 - M_\pi^2$, as well as to treat F_π^2 and F_K^2 as interchangeable. In this way we can express the pion and kaon scattering lengths as functions of just M_π, M_K, F_π, and F_K:

$$M_\pi a_0^{\pi\pi} = \frac{M_\pi^2}{16\pi F_\pi^2}\left[1 + \frac{M_\pi^2}{16\pi^2 F_\pi^2}\left(\frac{3}{2}\log\frac{M_\pi^2}{16\pi^2 F_\pi^2} + \frac{1}{18}\log\frac{4M_K^2 - M_\pi^2}{48\pi^2 F_\pi^2} - \frac{4}{9} - 256\pi^2 L_{\pi\pi}\right)\right] \tag{4.26}$$

$$\begin{aligned} M_\pi a_0^{KK} = \frac{M_K^2}{16\pi F_K^2}\Bigg[1 + \frac{M_K^2}{16\pi^2 F_K^2}\Bigg(&\log\frac{M_K^2}{16\pi^2 F_K^2} - \frac{M_\pi^2}{4(M_K^2 - M_\pi^2)}\log\frac{M_\pi^2}{16\pi^2 F_\pi^2} \\ &+ \frac{20M_K^2 - 11M_\pi^2}{36(M_K^2 - M_\pi^2)}\log\frac{4M_K^2 - M_\pi^2}{48\pi^2 F_\pi^2} - \frac{7}{9} - 256\pi^2 L_{\pi\pi}\Bigg)\Bigg]. \end{aligned} \tag{4.27}$$

Here the chiral logarithms are given by

$$L_\pi = 2\log\frac{M_\pi}{4\pi F_\pi}, \quad L_K = 2\log\frac{M_K}{4\pi F_\pi}, \quad L_\eta = \log\frac{4M_K^2 - M_\pi^2}{48\pi^2 F_\pi^2}, \tag{4.28}$$

while $L_{\pi\pi}$ is an LEC, which is evaluated at the scale $4\pi F_\pi$.

We also need the expression for the s-wave πK scattering length, which may be found in Ref. [161]:

$$\begin{aligned} \mu_{\pi K} a_0^{\pi K} = \frac{\mu_{\pi K}^2}{8\pi F_\pi F_K}\Bigg[1 &- \frac{16M_\pi M_K}{F_\pi F_K}L_{\pi\pi} + \frac{4(M_K - M_\pi)^2}{F_\pi F_K}L_5 \\ &+ \frac{1}{32\pi^2 F_\pi F_K}\left(\kappa_\pi L_\pi + \kappa_K L_K + \kappa_\eta L_\eta - \frac{86}{9}M_\pi M_K + X_{K\pi}\right)\Bigg], \end{aligned} \tag{4.29}$$

where $\mu_{\pi K} = M_\pi M_K/(M_\pi + M_K)$ is the reduced mass, L_5 is another LEC, and

$$\kappa_\pi = -\frac{M_\pi^2}{4}\frac{(11M_K^2 + 22M_K M_\pi - 5M_\pi^2)}{M_K^2 - M_\pi^2}\,, \tag{4.30}$$

$$\kappa_K = \frac{M_K}{18}\frac{(-9M_K^3 + 134M_K^2 M_\pi + 55M_K M_\pi^2 - 16M_\pi^3)}{M_K^2 - M_\pi^2}\,, \tag{4.31}$$

$$\kappa_\eta = \frac{(-36M_K^3 - 12M_K^2 M_\pi + M_K M_\pi^2 + 9M_\pi^3)}{36(M_K - M_\pi)}\,, \tag{4.32}$$

$$X_{K\pi} = \frac{16M_\pi M_K}{9}\frac{\sqrt{2M_K^2+M_K M_\pi - M_\pi^2}}{M_K - M_\pi}\ \arctan\frac{2(M_K - M_\pi)\sqrt{2M_K^2+M_K M_\pi - M_\pi^2}}{(2M_K - M_\pi)(M_K + 2M_\pi)}\,. \tag{4.33}$$

For the effective ranges, we compare only to the LO prediction, since NLO results from SU(3) ChPT are not given explicitly in the literature (see Refs. [162, 163] for the full πK scattering amplitude at NLO). For identical particles, the LO predictions are $M_\pi^2 r^{\pi\pi} a_0^{\pi\pi} = M_K^2 r^{KK} a_0^{KK} = 3$, while for non-identical particles, one has

$$M_\pi^2 a_0^{\pi K} r_0^{\pi K} = 1 + \frac{M_\pi}{M_K} + \frac{M_\pi^2}{M_K^2}. \tag{4.34}$$

We turn now to the p-wave scattering length, which is nonzero only for πK scattering. The NLO ChPT prediction for the πK scattering amplitude has been worked out in Refs. [162, 163]. However, no closed form for the corresponding scattering length has been provided in the literature, and so we have worked it out and present the results in section B.3—see eq. (B.18). The expression, which is rather lengthy, depends on two different combinations of LECs.

Since we have only two data points, we opt to fit to the expected leading order chiral behavior. From eq. (B.18), one can determine that the p-wave scattering length is finite in the chiral limit (proportional to M_K/F_π^4), so that

$$P_0^{\pi K} = -M_\pi^3 a_1^{\pi K} \propto (M_\pi/F_\pi)^3\,, \tag{4.35}$$

with higher-order terms suppressed by powers of M_π/F_π. Neglecting chiral logs, this is equivalent to considering only the effect of the LECs proportional to M_K^2 in eq. (B.18).

We conclude this section by presenting the LO chiral predictions for $\mathcal{K}_{\mathrm{df},3}$ for 2+1 systems, which were derived in Ref. [121]. At LO, only $\mathcal{K}_0$ and $\mathcal{K}_1$ in the expansion shown in eq. (4.23)

are nonzero:

$$M_\pi^2 \mathcal{K}_0^{\pi\pi K} = 2x_\pi^4 + 4x_\pi^3 x_K \,, \qquad M_\pi^2 \mathcal{K}_1^{\pi\pi K} = x_\pi^2 (2x_\pi + x_K)^2 \,, \tag{4.36}$$

$$M_K^2 \mathcal{K}_0^{KK\pi} = 2x_K^4 + 4x_K^3 x_\pi \,, \qquad M_K^2 \mathcal{K}_1^{KK\pi} = x_K^2 (2x_K + x_\pi)^2 \,, \tag{4.37}$$

where

$$x_\pi = \frac{M_\pi}{F_\pi} \quad \text{and} \quad x_K = \frac{M_K}{F_K} \,. \tag{4.38}$$

To obtain these forms we have used the interchangeability of F_π and F_K in LO terms. We note that $\mathcal{K}_{\mathrm{df},3}$ is independent of the cutoff function at LO in ChPT, and is in this sense a physical quantity at this order. Cutoff dependence only enters at NLO.

Predictions are not yet available for $\mathcal{K}_B$ and $\mathcal{K}_E$, since these quantities are expected to appear first at NLO, and no calculation at this order has been done. Following Ref. [121], we choose generic forms for these quantities

$$M_\pi^2 \mathcal{K}_{\mathrm{B}}^{\pi\pi K} = c_{\mathrm{B}}^{\pi\pi K} x_\pi^4 x_K^2 \,, \qquad M_\pi^2 \mathcal{K}_{\mathrm{E}}^{\pi\pi K} = c_{\mathrm{E}}^{\pi\pi K} x_\pi^4 x_K^2 \,, \tag{4.39}$$

$$M_K^2 \mathcal{K}_{\mathrm{B}}^{KK\pi} = c_{\mathrm{B}}^{KK\pi} x_K^4 x_\pi^2 \,, \qquad M_K^2 \mathcal{K}_{\mathrm{E}}^{KK\pi} = c_{\mathrm{E}}^{KK\pi} x_K^4 x_\pi^2 \,. \tag{4.40}$$

We stress that the full dependence on x_π and x_K will likely be much more complicated, but this form satisfies the correct chiral power counting and is sufficient given that we have only two values of pion masses.

A potentially important, and so far unquantified, source of systematic errors in our results comes from working at a single lattice spacing. In this regard, it is useful to know the form of the prediction for discretization effects that is given by Wilson ChPT (WChPT), i.e. ChPT including contributions proportional to powers of the lattice spacing a [83,84]. In section B.2 we have worked out the leading, $\mathcal{O}(a^2)$, terms for the two-particle scattering amplitudes and $\mathcal{K}_{\mathrm{df},3}$, both for the degenerate and nondegenerate cases. The results for scattering lengths

are

$$M_\pi a_0^{\pi\pi} = M_\pi a_0^{\pi\pi}\Big|_{a=0} - \frac{(2w_6' + w_8')}{16\pi}\,, \tag{4.41}$$

$$M_K a_0^{KK} = M_K a_0^{KK}\Big|_{a=0} - \frac{(2w_6' + w_8')}{16\pi}\,, \tag{4.42}$$

$$M_{\pi K} a_0^{\pi K} = M_{\pi K} a_0^{\pi K}\Big|_{a=0} - \frac{(2w_6' + w_8')}{16\pi}\,, \tag{4.43}$$

where w_6' and w_8' are dimensionless LECs proportional to a^2. Note that we make $a_0^{\pi K}$ dimensionless by multiplying by the average mass $M_{\pi K} = (M_\pi + M_K)/2$, rather than the reduced mass $\mu_{\pi K}$ used in eq. (4.29). With this choice we see that all three quantities have the same offset.

The corresponding results for $\mathcal{K}_{\mathrm{df},3}$ are

$$M_\pi^2 \mathcal{K}_{\mathrm{df},3}^{\pi\pi K} = M_\pi^2 \mathcal{K}_{\mathrm{df},3}^{\pi\pi K}\Big|_{a=0} - 6x_\pi^2(2w_6' + w_8')\,, \tag{4.44}$$

$$M_K^2 \mathcal{K}_{\mathrm{df},3}^{KK\pi} = M_K^2 \mathcal{K}_{\mathrm{df},3}^{KK\pi}\Big|_{a=0} - 6x_K^2(2w_6' + w_8')\,. \tag{4.45}$$

Thus the predicted shifts are proportional to the same combination of LECs as for the scattering lengths. In section 4.6.3, we will use these results to estimate the magnitude of discretization effects contributing to $\mathcal{K}_{\mathrm{df},3}$.

We close with a comment on the appropriate power counting in WChPT. In the standard power counting one takes $a^2\Lambda_{QCD}^2 \sim M_\pi^2/(4\pi F)^2$, and, using this, it would be inconsistent to include NLO terms proportional M_π^4/F^4, while not including discretization contributions proportional to a^3, $a^2 M_\pi^2$, etc. Since such terms have not been calculated, however, we simply attempt fits using the available information, namely using eqs. (4.41) to (4.45), in which we take the continuum NLO expressions given above for the $a = 0$ part. In effect, we are assuming that $a^2\Lambda_{QCD}^2 \sim M_\pi^4/(4\pi F)^4$. We find, in section 4.6.3, that the a^2 contributions are in fact considerably smaller than the estimate from standard power counting, providing *a posteriori* justification for this approach.

4.5 Extraction of scattering parameters

In this section we discuss the extraction of scattering quantities from the energy levels obtained in lattice QCD. We start by discussing the different strategies that one can use to fit the spectrum using the quantization conditions. We then turn to the results of the fits using different methods. Finally, we compare the different approaches and discuss what seems to be the optimal one for this dataset.

4.5.1 Fitting strategies

In this work, we will use variations of the so-called spectrum method [164]. The main idea is to obtain the best fit parameters by minimizing a χ^2 function that depends only on some spectral quantity X:

$$\chi^2\left(\vec{p}\right) = \sum_{ij} \Delta X_i (C^{-1})_{ij} \Delta X_j, \quad \Delta X_i = X_i - X_i^{\mathrm{QC}}\left(\vec{p}\right), \tag{4.46}$$

where X_i is the lattice QCD result for that spectral quantity in the i-th energy level, $X_i^{\mathrm{QC}}\left(\vec{p}\right)$ represents the prediction from the finite-volume formalism assuming a certain parametrization of the K matrices with parameters $\vec{p}$, and C is the covariance matrix of all the X_i quantities, such that $C_{ij} = \mathrm{cov}(X_i, X_j)$.

Several choices for the spectral quantity X are possible. While, in the limit of infinite statistics, all should lead to the same answer, in practice some may be more advantageous. Specifically, some choices can lead to covariance matrices with larger condition numbers, such that the calculation of the inverse matrix appearing in eq. (4.46) may be more unstable. Some examples for X are listed below.

1. The original energy levels obtained from lattice QCD, which are, in general, in a moving (or "laboratory") frame. These are denoted E_{lab}.

2. The energy levels boosted to the center-of-mass frame (CMF), assuming the continuum dispersion relation, i.e. ignoring possible lattice artifacts. The resulting energies are

denoted E_{cm}.[9] This is the choice of Ref. [132].

3. The shift with respect to the non-interacting finite-volume energy, with the latter calculated assuming a continuum dispersion relation. This can be done either in the lab or cm frame, yielding ΔE_{lab} or ΔE_{cm}, respectively.

4. In the two-particle sector, it is also possible to use the CM momentum, q^2. This is the choice used, for example, in Ref. [144].

As we discuss in detail below, we use ΔE_{lab} for our preferred fits.

Once the best fit parameters have been obtained by minimizing eq. (4.46), the errors of the best fit parameters (and their covariance) need to be estimated. One possibility to do so is to perform a separate fit on each jackknife sample, and use the results to estimate the covariance of the parameters. While an option in the two-particle sector, present evaluations of the predictions of the three-particle quantization condition are too slow for this approach to be practical in general. Instead, we perform a fit only on the mean, while using the jackknife samples to estimate the covariance matrix C of the data, and then apply the derivative method. This method, discussed in Ref. [132], estimates the covariance between the fit parameters p_n and p_m as

$$V_{nm} = \left(\frac{\partial X_i^{\text{QC}}}{\partial p_n} (C^{-1})_{ij} \frac{\partial X_j^{\text{QC}}}{\partial p_m} \right)^{-1}, \tag{4.47}$$

where the derivatives are evaluated numerically at the minimum of the χ^2 function, χ^2_{min}. A very similar approach is to find the 1σ interval by finding the contour such that $\chi^2 = \chi^2_{\text{min}} + 1$, and assuming that the dependence of χ^2 on $\vec{p}$ is quadratic. In practice, we find that these two methods give essentially identical results, and we use them interchangeably to quote errors in the following.

---

[9] Above we have used the quantity E^* to refer to the CMF energy. Here we prefer the more explicit notation E_{cm}.

Another issue to address is how to combine information from the different channels, e.g. those with different numbers of particles. In particular, when analyzing three-particle energies, the two-particle interaction parameters are also needed. In previous work, e.g. in Refs. [125, 132], the approach has been to perform a combined fit to both two- and three-particle energy levels. For example, in the pion sector, one defines a χ^2 function that combines $\pi\pi$ and $\pi\pi\pi$ levels, and uses the covariance matrix of all levels, including cross-correlations between two- and three-particle energies. Fits using this approach will be referred as "fully correlated fits". In this work, we take this approach one step further by considering nondegenerate systems, where two different two-particle spectra are needed. For example, for the $\pi\pi K$ sector, we must consider also the $\pi\pi$ and πK levels. This leads to a larger number of total energy levels, and one may be concerned about the reliability of the calculation of the covariance matrix between levels. We find, in practice, that this is not an issue in the fits done here (either for the $\pi\pi K$ or $KK\pi$ cases), but it certainly will become a problem eventually, as the number of channels and levels increases further. For example, we have not attempted fully correlated simultaneous fits to the $\pi\pi$, πK, KK, $\pi\pi K$ and $KK\pi$ levels.

Because the issue of fitting to multiple channels is a generic one in multiparticle physics, it is worthwhile investigating alternative approaches. We consider two approaches in which varying amounts of information about the correlations between two- and three-particle levels is dropped. We can imagine these being relevant in situations where one has limited information on correlations, because, for example, different ensembles have been used to calculate two- and three-particle quantities, or the determination of the full covariance matrix is unstable. The underlying idea here is that two-particle spectra might be able to pin down two-particle scattering quantities sufficiently well that the three-particle spectra can be used primarily to determine three-particle scattering quantities.

Our first alternative is to use what we refer to as a "chained fit". Here, we first perform a fit to the two-particle sector. Minimizing the two-body χ^2 function will lead to the two-particle best fit parameters, $\vec{p}_{\rm 2P}^{\,\rm fit}$ and their covariance. We will use these values to construct

the chained χ^2 function as:

$$\chi^2_{\text{chain}}(\vec{p}) = \begin{pmatrix} \Delta\vec{p}_{2\text{P}} \\ \Delta\vec{X}_{3\text{P}} \end{pmatrix}^T \begin{pmatrix} \text{cov}(\vec{p}^{\,\text{fit}}_{2\text{P}}, \vec{p}^{\,\text{fit}}_{2\text{P}}) & \text{cov}(\vec{p}^{\,\text{fit}}_{2\text{P}}, \vec{X}_{3\text{P}}) \\ \text{cov}(\vec{X}_{3\text{P}}, \vec{p}^{\,\text{fit}}_{2\text{P}}) & \text{cov}(\vec{X}_{3\text{P}}, \vec{X}_{3\text{P}}) \end{pmatrix}^{-1} \begin{pmatrix} \Delta\vec{p}_{2\text{P}} \\ \Delta\vec{X}_{3\text{P}} \end{pmatrix}, \tag{4.48}$$

where $\vec{p} = (\vec{p}_{2\text{P}}, \vec{p}_{3\text{P}})$ is a vector that contains the two and three-particle parameters, $\Delta\vec{p}^{\,2\text{P}} = \vec{p}^{\,\text{fit}}_{2\text{P}} - \vec{p}_{2\text{P}}$, and $\vec{X}_{3\text{P}}$ represents a specific spectral quantity for all three-particle energy levels. Note that the method requires also covariance between the three-particle energy levels and the two-particle best-fit parameters, $\text{cov}(\vec{X}_{3\text{P}}, \vec{p}^{\,\text{fit}}_{2\text{P}})$. These can be estimated using a resampling technique, e.g., jackknife.

This approach can be further simplified by neglecting completely the off-diagonal terms in the covariance matrix of eq. (4.48). In this case, the χ^2 functions becomes:

$$\chi^2_{\text{aug}}(\vec{p}) = \Delta\vec{X}^T_{3\text{P}} \left(\text{cov}(\vec{X}_{3\text{P}}, \vec{X}_{3\text{P}})\right)^{-1} \Delta\vec{X}_{3\text{P}} + \Delta\vec{p}^{\,T}_{2\text{P}} \left(\text{cov}(\vec{p}^{\,\text{fit}}_{2\text{P}}, \vec{p}^{\,\text{fit}}_{2\text{P}})\right)^{-1} \Delta\vec{p}_{2\text{P}}. \tag{4.49}$$

This can be seen as the augmented χ^2 of a "Bayesian fit", where $\vec{p}^{\,\text{fit}}_{2\text{P}}$ is the prior of those parameters. In the context of nondegenerate spectra, a further simplification of such Bayesian fits is possible. For example, for the $\pi\pi K$ case, the Bayesian augmentation can include, or not, the correlations between the fit parameters in the $\pi\pi$ and πK channels.

4.5.2 Fit results

In this section we present results from fitting the spectra using the two- and three-particle quantization conditions. We begin with examples showing the impact of using the different fitting methods described above, and then present our core new results for the parameters describing the $\pi\pi K$ and $KK\pi$ systems. Finally, we compare the results for the two-particle scattering parameters (scattering length and effective range) obtained using different fits.

For every fit we need to choose a maximum value of E_{cm} for the levels to be included. The quantization conditions that we use formally break down above the lowest inelastic threshold, which for systems of pions occurs when two additional pions can be created (single-pion production being forbidden by G-parity), while for systems involving kaons the breakdown

occurs when only a single additional pion can be produced. The issue is discussed in detail in Ref. [132], where it is noted that, in practice, the quantization conditions are likely to remain applicable some distance above the nominal maximal $E_{\rm cm}$, a conclusion supported by the numerical results of that work. Thus, here we also work with values of $E_{\rm cm}$ that lie above the nominal maximal, making the same choices for the 2π, 3π, $2K$, and $3K$ channels as in Ref. [132], and similar choices for the πK, $\pi\pi K$ and $KK\pi$ channels.

As discussed above, we include only s- and p-wave terms in the quantization conditions, but not d-wave terms. For two identical particles, i.e. for $\pi\pi$ and KK, this implies that we must exclude from the fits levels that lie in nontrivial irreps, since such levels are only shifted by d-wave terms (p waves being absent). For three identical particles, levels in nontrivial irreps are shifted by s-wave terms because there can be relative angular momentum between the dimer pair and the spectator, but these shifts are incomplete due to the absence of d-wave terms in the dimer. Thus we also keep only $\pi\pi\pi$ and KKK levels in trivial irreps in the fits. This is different from the fits in Ref. [132], where were able to include d-wave terms, and thus also levels in nontrivial irreps.

By contrast, for the nondegenerate channels that are of central interest here, the inclusion of p waves implies that fits to levels in all available irreps are possible, and we include such levels in the fits.

Comparison of fitting strategies

We begin by showing examples of the differences between results obtained by fitting to $E_{\rm cm}$ and $\Delta E_{\rm lab}$. As discussed above, the latter fits have the advantage of being to quantities that are closer to those that are actually obtained from the lattice simulations, and are in this sense preferable. We used $E_{\rm cm}$ fits in Ref. [132], where we studied the 3π and $3K$ systems, and our aim here is to study the impact of changing to $\Delta E_{\rm lab}$ fits. We expect that the latter fits will lead, in general, to larger values of χ^2, but that this provides a more accurate reflection of the goodness of fit. We recall that our fits to correlator ratios yield $\Delta E_{\rm lab} a$. This "primary" quantity is then converted to $\Delta E_{\rm lab}/M$, where M is either M_π or M_K depending

on the quantity being studied, and we use the value of M from the rest frame fit in the corresponding jackknife sample. The "$\Delta E_{\rm lab}$ fits" are to $\Delta E_{\rm lab}/M$. When fitting to $E_{\rm cm}/M$, a further conversion is needed, first from $\Delta E_{\rm lab}$ to $E_{\rm lab}$, and then by a boost to the rest frame. The key point is that this conversion depends on ML, and that fluctuations in this quantity between jackknife samples leads to an increase in the errors in $E_{\rm cm}/M$. Thus we expect, in general, that fitting to $E_{\rm cm}/M$ will lead to a smaller χ^2, but that this reduction is not due to having a better fit, but rather due to the errors being overestimated. What we do not know *a priori* is how the results for the fit parameters will change, and that is the focus of our investigation here.

In a few cases, the difference between $E_{\rm cm}$ and $\Delta E_{\rm lab}$ fits is minimal. An example is provided by fits to the πK spectrum on the D200 ensemble, which are shown in Table 4.3. We find good fits in both cases, leading to consistent fit parameters, although there is a small decrease in the errors in the fit parameters when fitting to $\Delta E_{\rm lab}$. Most striking is the change in the condition number of the correlation matrix for the values of $E_{\rm cm}$ or $\Delta E_{\rm lab}$. The correlation matrix is closely related to the covariance matrix, differing by a normalization procedure that guarantees each element of the principal diagonal is 1, and each off-diagonal element lies in the range $[-1, 1]$:

$$\mathrm{corr}\left(\vec{X}\right) = \left(\mathrm{diag}\left[\mathrm{cov}(\vec{X},\vec{X})\right]\right)^{-\frac{1}{2}} \mathrm{cov}(\vec{X},\vec{X}) \left(\mathrm{diag}\left[\mathrm{cov}(\vec{X},\vec{X})\right]\right)^{-\frac{1}{2}}. \tag{4.50}$$

By providing a more natural normalization, the correlation matrix is better suited to estimate the condition number, as it avoids issues of significantly different errors among the extracted energies which can lead to artificially large condition numbers. The reduction in the condition number of the correlation matrix by an order of magnitude for the $\Delta E_{\rm lab}$ fits implies that the fits will be more stable. We observe a substantial reduction in the condition number in fits to all quantities.

In most cases, however, the value of χ^2 increases substantially when fitting to $\Delta E_{\rm lab}$. As a first illustration of this behavior, we show, in Table 4.4, fits to the KK spectrum on D200. First, we note that values of $\chi^2_{\rm ref} = \chi^2/\mathrm{DOF}$ are large in all cases, where DOF

Method	$E_{\rm cm}$	$\Delta E_{\rm lab}$
Cond. #	28630	68
χ^2	28.3	31.0
DOF	26-3=23	26-3=23
$B_0^{\pi\pi}$	-13.24(64)	-13.13(45)
$B_1^{\pi\pi}$	-2.51(28)	-2.41(23)
$P_0^{\pi\pi}$	0.0029(13)	0.0013(7)

Table 4.3: Comparison of fitting approaches for the πK spectrum on the D200 ensemble. All quantities are in units in which $M_\pi = 1$. The fits are to the 26 levels lying below the cutoff $E_{\rm cm} = 5M_\pi = (M_\pi + M_K) + 1.62M_\pi$, and use the fit form eq. (4.17). The position of the Adler zero is fixed to its leading order value (i.e. $z_{\pi K} = 1$).

stands for degrees of freedom. One reason for this is that we are fitting without including the d-wave interaction, a choice we make, as explained above, in order to have practical fits when we consider nondegenerate three-particle systems. As an example of the impact of this omission, we note that, were we to include a d-wave scattering length in the $E_{\rm cm}$ fit, χ^2 would be reduced by about 20 [132]. Our focus here, however, is on the differences between $E_{\rm cm}$ and $\Delta E_{\rm lab}$ fits, and we see that χ^2 increases significantly, consistent with our general expectation discussed above. However, we note that the fit parameters themselves change little (B_1^{KK} is reduced by $\sim 2\sigma$), and the errors are essentially unchanged.

Now we turn to examples involving three-particle spectra. The results from a joint fit to 2π and 3π levels are shown in Table 4.5, while those for $2K$ and $3K$ levels are presented in Table 4.6. In the former table, we also include rebinned results to be discussed below.

Both tables show the same pattern as for the KK results above: there is an increase in χ^2 when using $\Delta E_{\rm lab}$ fits, while fit parameters and errors are largely consistent. The largest change is for B_1, which decreases by more than 2σ. The conclusions drawn in Ref. [132],

Method	$E_{\rm cm}$	$\Delta E_{\rm lab}$
Cond. #	163	28
χ^2	61	84
DOF	28-2=26	28-2=26
B_0^{KK}	-2.865(49)	-2.865(46)
B_1^{KK}	-2.67(12)	-2.37(11)

Table 4.4: Comparison of fitting approaches for the KK spectrum on the D200 ensemble. All quantities are in units in which $M_K = 1$. The fits are to the 28 levels in trivial irreps lying below the cutoff $E_{\rm cm} = 2.53M_K = 2M_K + 1.26M_\pi$, using the two-parameter Adler form of eq. (4.17), with the Adler zero fixed to its leading order position ($z_{KK} = 1$).

namely that $\mathcal{K}_{\rm df,3}$ is significantly different from zero, and that $\mathcal{K}_{\rm df,3}^{\rm iso,1}$ is negative, remain valid for the $\Delta E_{\rm lab}$ fits. Since the fit parameters are highly correlated, one cannot judge the significance of a nonzero $\mathcal{K}_{\rm df,3}$ from the tables alone; using the full covariance matrices we find this to be 7.0σ and 4.4σ for the $E_{\rm cm}$ and $\Delta E_{\rm lab}$ fits to $\pi\pi + \pi\pi\pi$, while the corresponding results for the $KK + KKK$ fits are 6.4σ and 4.5σ, respectively. Thus the significance of the nonzero $\mathcal{K}_{\rm df,3}$ is somewhat reduced, but remains high.

In the remainder of this section we only consider fits to $\Delta E_{\rm lab}$. Our first task is to compare the results of fits using the different choices for χ^2 described in section 4.5.1 above. We do so only for the $\pi\pi + \pi K + \pi\pi K$ fits, on ensemble D200, as the pattern we find is the same in all other fits.

In Table 4.7 we compare the results when using (a) the standard choice of χ^2, given in eq. (4.46), (b) chained fits, using the χ^2 from eq. (4.48), and (c) Bayesian fits using the χ^2 given in eq. (4.49). (The final column will be discussed in section 4.5.2 below.) We recall that there are two types of Bayesian fits, depending on whether one keeps the correlations between the results of the parameters for the $\pi\pi$ and πK fits, or not. We find little difference

Method	E_{cm}	ΔE_{lab}	ΔE_{lab}, rebin2
Cond. #	1681	744	717
χ^2	94	130	143
DOF	27+27-4=50	27+27-4=50	27+27-4=50
$B_0^{\pi\pi}$	-4.88(9)	-4.87(9)	-4.86(8)
$B_1^{\pi\pi}$	-2.27(11)	-1.90(9)	-1.91(9)
$\mathcal{K}_0$	240(220)	500(210)	310(180)
$\mathcal{K}_1$	-1700(330)	-1400(340)	-1100(320)

Table 4.5: Fits to the $\pi\pi + \pi\pi\pi$ spectrum on ensemble N203. All quantities are in units in which $M_\pi = 1$. We use cutoffs of $E_{\text{cm}} = 3.46M_\pi$ and $4.46M_\pi$ respectively from the $\pi\pi$ and $\pi\pi\pi$ spectra, and fit only to levels in trivial irreps, leading to 27 levels for each channel. In the two-particle channel, the fit model used is the Adler zero form given in eq. (4.17), with the Adler zero fixed to its leading order position ($z_{\pi\pi} = 1$). The fit model used in the three-particle channel includes only the $\mathcal{K}_0$ and $\mathcal{K}_1$ terms of eq. (4.23).

in the results of these two approaches, and present results only for the latter.

The standard fit is to a total of 69 levels,[10] using 9 parameters. This is a challenging fit, but we see no signs of numerical instability in the calculation of χ^2. Indeed, the main challenge is finding the minimal χ^2 with a large number of parameters, and our minimizer takes $\sim 10^3$ iterations to converge. In all cases we have checked the fits by repeating them with different initial conditions, and by using three independent codes. The final χ^2 is high, but a large part of this arises from the fit to the $\pi\pi$ sector, where a fit to the 22 levels alone leads to $\chi^2 \approx 52$ due to the absence of d-wave terms (as discussed above in the context of KK fits). In addition, we have seen above that moving from E_{cm} fits to ΔE_{lab} fits leads to

[10]We note here that one level (the second level in the $A_2(8)$ irrep) shows $\sim 3\sigma$ fluctuations due to the choice of GEVP parameters. We opt to keep it in the fit, but have checked that removing this level from the fit barely impacts the best fit parameters in Table 4.7.

Method	E_{cm}	ΔE_{lab}
Cond. #	7075	4044
χ^2	92	118
DOF	28+26-4=50	28+26-4=50
B_0^{KK}	-2.89(4)	-2.91(4)
B_1^{KK}	-2.58(13)	-2.29(11)
$\mathcal{K}_0$	-880(900)	-240(920)
$\mathcal{K}_1$	-10000(3500)	-8300(3600)

Table 4.6: Fits to the $KK + KKK$ spectrum on ensemble D200. All quantities are in units in which $M_K = 1$. We use cutoffs of $E_{\text{cm}} = 2.53M_K = 2M_K + 1.26M_\pi$ and $3.53M_K = 3M_K + 1.26M_\pi$ for the KK and KKK spectra, respectively, leading to 28 and 26 levels in the trivial irreps. In the two-particle channel, the fit model used is the Adler zero form given in eq. (4.17), with the Adler zero fixed to its leading order position ($z_{KK} = 1$). The fit model used in the three-particle channel includes only the $\mathcal{K}_0$ and $\mathcal{K}_1$ terms of eq. (4.23).

increased χ^2.

The large number of levels that must be fit motivates investigating the alternatives provided by using chained and Bayesian fits. We stress that the values of χ^2 in the three fits cannot be compared. A rough comparison can be obtained by adding to the χ^2 for fits (b) and (c) the values of the χ^2 from the individual $\pi\pi$ and πK fits, which are 52 and 31, respectively, leading to total values of ~ 115 for fits (b) and (c). However, this ignores the impact on the χ^2 in fit (a) of including the full correlations between the levels.

Comparing the results, we see that the central values for all two-particle scattering parameters are very similar, and have essentially the same errors, in all three fits. By contrast, while the values of the three-particle parameters are consistent within errors, those errors are significantly larger for the chained fit than the standard fit, and larger still for the Bayesian

Fit	(a) Standard	(b) Chained	(c) Bayesian	(d) Standard*
Cond. #	2027	792	670	1881
χ^2	129	32	31	112
DOF	22+26+21-9=60	21+5-9=17	21+5-9=17	22+16+21-9=50
$B_0^{\pi\pi}$	-11.7(6)	-11.5(6)	-11.3(6)	-11.5(6)
$B_1^{\pi\pi}$	-2.4(4)	-2.5(4)	-2.4(4)	-2.5(4)
$B_0^{\pi K}$	-13.0(4)	-13.2(4)	-13.1(4)	-12.9(4)
$B_1^{\pi K}$	-2.58(20)	-2.43(21)	-2.45(23)	-2.8(3)
$P_0^{\pi K}$	0.0010(6)	0.0017(7)	0.0014(7)	0.0007(6)
$\mathcal{K}_0$	220(70)	500(200)	650(310)	190(80)
$\mathcal{K}_1$	-620(340)	-300(500)	-70(620)	-690(340)
$\mathcal{K}_B$	140(640)	-500(1100)	-500(1200)	160(650)
$\mathcal{K}_E$	290(410)	1200(800)	2200(1400)	170(420)

Table 4.7: Fits to the $\pi\pi + \pi K + \pi\pi K$ spectrum on ensemble D200, using $\Delta E_{\rm lab}$. All quantities are in units in which $M_\pi = 1$. For the first three columns, we use cutoffs $E_{\rm cm} = 3.74M_\pi$, $5M_\pi = (M_\pi + M_K) + 1.62M_\pi$, and $5.4M_\pi = (2M_\pi + M_K) + 1.02M_\pi$ for the $\pi\pi$, πK and $\pi\pi K$ channels, respectively, leading to 22, 26 and 21 levels. For fit (d), the cutoff for the πK spectra is reduced to $4.64M_\pi = (M_\pi + M_K) + 1.26M_\pi$, so that there are 16 πK levels. In the two-particle channel, the fits use the functions of eq. (4.17) and eq. (4.22), with the $\pi\pi$ and πK Adler zeros fixed to their lowest-order values. The fit model used in the three-particle channel is given by eq. (4.23). In fits (b) and (c), the number of DOF is given by the number of levels (21) plus the number of fit parameters in the $\pi\pi + \pi K$ fits (2+3), minus the number of parameters fit (9).

fit. In other words, the information on correlations between levels that is lost when using "sequential" fits makes it harder to pin down the (already challenging) three-particle parameters. It is thus no surprise that the significance of the nonzero $\mathcal{K}_{\mathrm{df},3}$ is reduced when moving from the standard fit to the chained and Bayesian fits: it is 3.4σ, 2.4σ and 2.8σ, respectively for the three fits.

A similar pattern is observed for all other channels, and thus we conclude that standard fits are clearly preferable if they are possible, as is the case here. We use only standard fits for our central results to be presented shortly.

The final issue that we address in this subsection is whether to rebin the results on the D200 ensemble. As discussed above, the results on the D200 ensemble are rebinned by $N_{\mathrm{rebin}} = 3$, leading to 771 jackknife samples. As discussed in Ref. [132], this rebinning is useful to account for autocorrelations, and indeed the errors in the energy levels increase as one increases the rebinning factor. However, for N203, where we have only 666 configurations, rebinning can lead to unstable fits when the number of samples becomes too close to the number of levels being considered. We have tested this in several cases, two examples being given in Table 4.5 above and Table 4.8 below. What we find is that the fits are stable for both $N_{\mathrm{rebin}} = 2$ or 3, that they lead to essentially the same results for all fit parameters, with no change in errors, but that χ^2 increases significantly (as do the condition numbers). We interpret these results as indicating that any autocorrelations have minimal effect on the scattering parameters, while the reduction in the number of samples leads to less well conditioned fits. Thus we choose to use no rebinning for our central fits N203. The choice of using $N_{\mathrm{rebin}} = 3$ for D200 is, therefore, conservative.

Fits to nondegenerate channels

As noted above, our central values are obtained from fits to ΔE_{lab}, using the standard, fully-correlated χ^2, and without rebinning on ensemble N203. Results for $\pi\pi + \pi K + \pi\pi K$ are shown in Table 4.7 (above) and Table 4.8, while those for $KK + \pi K + KK\pi$ are shown in Table 4.9 and Table 4.10.

Fit	72 level	82 level	82 level, rebin 2
Cond. #	612	834	985
χ^2	117	119	155
DOF	27+19+26−9 = 63	27+19+36−9 = 73	27+19+36−9 = 73
$B_0^{\pi\pi}$	-5.05(10)	-5.05(10)	-5.01(10)
$B_1^{\pi\pi}$	-1.77(9)	-1.78(9)	-1.82(9)
$B_0^{\pi K}$	-5.40(11)	-5.39(11)	-5.39(11)
$B_1^{\pi K}$	-1.88(17)	-1.89(17)	-1.80(16)
$P_0^{\pi K}$	0.005(4)	0.006(4)	0.007(4)
$\mathcal{K}_0$	-250(160)	-240(150)	-380(160)
$\mathcal{K}_1$	-1400(600)	-1300(600)	-1080(580)
$\mathcal{K}_B$	1100(800)	990(740)	1020(680)
$\mathcal{K}_E$	-3300(1000)	-3200(1000)	-3200(1000)

Table 4.8: ΔE_{lab} fits to the $\pi\pi + \pi K + \pi\pi K$ spectrum on ensemble N203. All quantities are in units in which $M_\pi = 1$. In all fits, the cutoffs for $\pi\pi$ and πK are $E_{\text{cm}} = 3.464M_\pi = 2M_\pi + 1.464M_\pi$ and $3.4M_\pi = (M_\pi + M_K) + 1.12M_\pi$, corresponding to 27 and 19 levels, respectively. For the first column, the cutoff for $\pi\pi K$ is $4.1M_\pi = (2M_\pi + M_K) + 0.82M_\pi$, while for the remaining two columns it is $4.3M_\pi = (2M_\pi + M_K) + 1.02M_\pi$, corresponding to 26 and 36 levels, respectively. In the two-particle channel, the fits are to eq. (4.17) and eq. (4.22) with $\pi\pi$ and πK Adler zeros fixed to their lowest-order values. The fit model used in the three-particle channel is given by eq. (4.23).

Fit	ADLER2	ADLER3	ERE3
Cond. #	10200	10200	10200
χ^2	163	162	161
DOF	$28+16+29-9=64$	$28+16+29-10=63$	$28+16+29-10=63$
B_0^{KK}	-2.90(4)	-3.55(78)	-2.87(4)
B_1^{KK}	-2.32(11)	-1.95(45)	1.40(25)
z_{KK}^2/B_2^{KK}	1 (fixed)	0.76(28)	-1.25(38)
$B_0^{K\pi}$	-2.44(7)	-2.42(7)	-2.41(7)
$B_1^{K\pi}$	-2.18(31)	-2.28(32)	-2.28(32)
$P_0^{K\pi}$	0.027(8)	0.027(8)	0.027(8)
$\mathcal{K}_0$	180(270)	170(270)	150(270)
$\mathcal{K}_1$	-6600(1700)	-6800(1700)	-6800(1700)
$\mathcal{K}_B$	2800(1300)	2800(1300)	2900(1200)
$\mathcal{K}_E$	-5700(3800)	-5900(3700)	-6000(3700)

Table 4.9: ΔE_{lab} fits to the $KK + \pi K + KK\pi$ spectrum on ensemble D200. All quantities are in units in which $M_K = 1$. Note that this means that $B_0^{K\pi}$ differs from $B_0^{\pi K}$ in Table 4.7 by powers of (M_π/M_K), and similarly for other parameters. Cutoffs are given by $E_{\text{cm}} = 2.53M_K$, $1.95M_K = (M_K+M_\pi)+1.26M_\pi$, and $2.832M_K = (2M_K+M_\pi)+0.98M_\pi$ for the KK, πK and $KK\pi$ channels, respectively, corresponding to 28, 16, and 29 levels, respectively. In the KK channel, the ADLER2 and ADLER3 fits use eq. (4.17), with the Adler zero fixed to its leading-order position for the former fit and allowed to vary for the latter, while the ERE3 fit uses eq. (4.20). In all three fits the πK channel is fit using the ADLER2 form for the s-wave K matrix and eq. (4.22) for the p wave, while the fit model used in the three-particle channel is given by eq. (4.23).

Fit	ADLER2	ADLER3	ERE3
Cond. #	770	770	770
χ^2	181	173	187
DOF	23+19+32−9 = 65	23+19+32−10 = 64	23+19+32−10 = 64
B_0^{KK}	-3.41(5)	-2.8(2)	-3.39(5)
B_1^{KK}	-2.08(8)	-2.39(13)	2.20(15)
z_{KK}^2/B_2^{KK}	1 (fixed)	1.19(6)	-1.53(13)
$B_0^{K\pi}$	-3.25(8)	-3.31(8)	-3.24(8)
$B_1^{K\pi}$	-2.17(19)	-2.07(19)	-2.18(19)
$P_0^{K\pi}$	0.018(8)	0.020(8)	0.021(8)
$\mathcal{K}_0$	170(300)	260(310)	90(310)
$\mathcal{K}_1$	-3900(1700)	-3900(1700)	-3400(1700)
$\mathcal{K}_B$	3500(1600)	3500(1600)	3500(1700)
$\mathcal{K}_E$	-1100(2000)	-400(2000)	-100(2100)

Table 4.10: ΔE_{lab} fits to the $KK + \pi K + KK\pi$ spectrum on ensemble N203. All quantities are in units in which $M_K = 1$. Note that this means that $B_0^{K\pi}$ differs from $B_0^{\pi K}$ in Table 4.8 by powers of (M_π/M_K), and similarly for other parameters. Cutoffs are given by $E_{\text{cm}} = 2.9M_K$, $2.66M_K = (M_K+M_\pi)+1.12M_\pi$, and $3.521M_K = (2M_K+M_\pi)+0.95M_\pi$ for the KK, πK and $KK\pi$ channels, respectively, corresponding to 23, 19, and 32 levels, respectively. For the KK channel, only the ground state in the frame with $\boldsymbol{d}^2 = 9$ is kept. In the KK channel, the ADLER2 and ADLER3 fits use eq. (4.17), with the Adler zero fixed to its leading-order position for the former fit and allowed to vary for the latter, while the ERE3 fit uses eq. (4.20). In all three fits the πK channel is fit using the ADLER2 form for the s-wave K matrix and eq. (4.22) for the p wave, while the fit model used in the three-particle channel is given by eq. (4.23).

For the $\pi\pi + \pi K + \pi\pi K$ fits we show examples of the results of fitting to different levels. Table 4.7 compares our "standard" fit, in the first column, with an alternative, in the final column, in which the cutoff on the πK levels is reduced from $0.62M_\pi$ above the inelastic threshold ($2M_\pi + M_K$) to $0.26M_\pi$ above this threshold. The fits are of similar quality and give consistent results, and errors, for all parameters, indicating that our more aggressive cutoff is acceptable. Table 4.8 compares using a cutoff below the inelastic threshold for the $\pi\pi K$ channel (72 level fit) to one slightly above this threshold (82 level fit). Here we are investigating whether fits to 82 levels are stable, and we find that they are. The results from the two fits are consistent within errors, and we use the results from the 82-level fit henceforth.

For the $KK + \pi K + KK\pi$ fits we show comparisons between different fit choices.[11] In Ref. [132] it was observed that the KK interactions were slightly better described on the D200 ensemble (for which the kaon is heavier) if, compared to our standard two-parameter Adler-zero fit, one either allowed the position of the Adler zero to float, or used a three-parameter ERE fit. Thus we have done all three fits for both ensembles and compare the results in the tables. Freeing the position of the Adler zero leads to no significant improvement in χ^2_{ref} on D200, but a mild improvement on N203. Switching to an ERE fit, leads to a slight improvement on D200, but a worse fit on N203. Results for the πK and $KK\pi$ fit parameters are essentially unchanged.

One of our major aims is to study how well three-particle interactions can be determined by using a large collection of energy levels. As can be seen from the tables, the significance of the nonzero values for individual terms in $\mathcal{K}_{\text{df},3}$ varies, with the most significant parameter being $\mathcal{K}_1$ on the D200 ensemble. The significance of the entire $\mathcal{K}_{\text{df},3}$ being nonzero, including the correlations between the parameters, is 3.4σ and 3.6σ for the $\pi\pi + \pi K + \pi\pi K$ standard fits on the D200 and N203 ensembles, respectively, and 5.0σ and 2.4σ for these ensembles in

[11] Note that in the $KK + \pi K + KK\pi$ case we fit to $\Delta E_{\text{lab}}/M_K$ rather than to $\Delta E_{\text{lab}}/M_\pi$, as in the $\pi\pi + \pi K + \pi\pi K$ fits. This makes a small difference as there are fluctuations of the single-particle masses between jackknife samples.

the $KK + \pi K + KK\pi$ fits.

Visualization of fits

We have shown several global views of the fits in figures B.1 to B.3 and 4.2, which illustrate that the fits match the spectrum well both in the fit range and also above the nominal inelastic threshold. To investigate this more carefully, we need to zoom in and show results for the quantities $\Delta E_{\rm lab}$ to which we actually fit. This is the purpose of this section.

We focus first on the $KK+\pi K+KK\pi$ fit on the D200 ensemble, as this is the fit for which both $\mathcal{K}_{\rm df,3}$ and P_0 are determined to be nonzero with the greatest significance. Specifically, we consider the ADLER3 fit to 73 levels in Table 4.9. In the upper panel of figure 4.3 we compare the results for $\Delta E_{\rm lab}$ from our simulations to those obtained using the quantization condition with the best fit parameters. The latter is shown by the red dots just above each of the data points. We see that the shifts are small (of order 1% of M_K), but are determined with errors ranging from a few percent to $10-15\%$. We note that all levels, whether in trivial or nontrivial irreps, are shifted by the same order of magnitude. This differs from the situation with the two particle spectrum, as will be seen below, and is due to the fact that the two-particle K matrix, $\mathcal{K}_2$, contributes to all irreps. Indeed, as is well known, and was clearly seen in Ref. [132], the dominant physical effect leading to these energy shifts is the two-particle interaction, and it is nontrivial to determine the subdominant contribution of $\mathcal{K}_{\rm df,3}$. To illustrate the impact of $\mathcal{K}_{\rm df,3}$, we also show, as blue squares, the results predicted by the quantization condition if we set $\mathcal{K}_{\rm df,3} = 0$ while keeping all other parameters unchanged. The shifts in the levels are small, reaching the size of the error bars in the data only for the higher energy levels. From this figure alone, it would appear that there is little chance of determining $\mathcal{K}_{\rm df,3}$, but this is misleading because all levels are correlated, and the fit includes not only these 29 levels, but also the 28 K^+K^+ and 16 $K^+\pi^+$ levels. One illustration of the claim that the nonzero value of $\mathcal{K}_{\rm df,3}$ leads to a significant improvement in the fit is that χ^2 increases from 162 to 188 when $\mathcal{K}_{\rm df,3}$ is turned off.

We also include, using orange triangles, the result of turning off the p-wave πK scattering

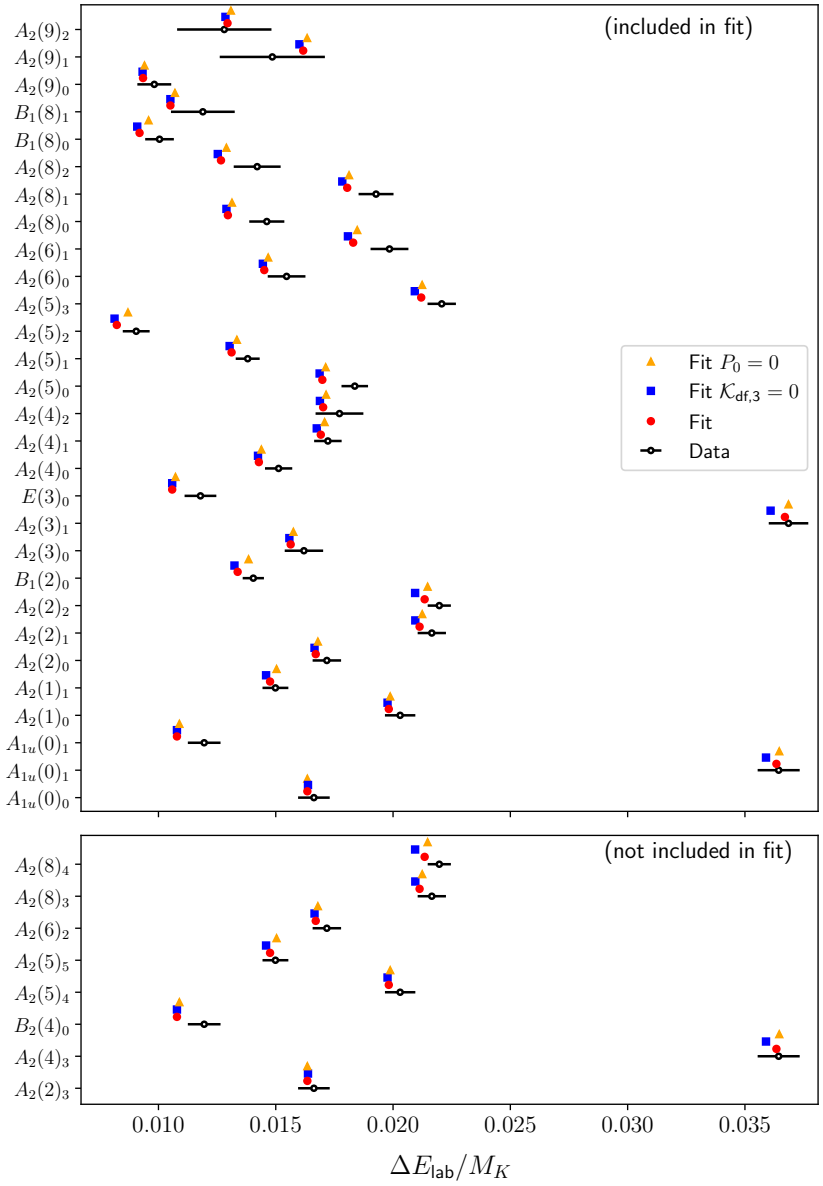

Figure 4.3: Comparison of values for $\Delta E_{\text{lab}}/M_K$ to the predictions of various fits for $K^+K^+\pi^+$ levels on D200. The upper panel shows 29 levels included in the fits, while the lower panel shows eight that lie above our maximal E_{cm} and are thus not included in the fits. Level are denoted by their irrep, followed in parenthesis by the value of total momentum-squared parametrized by $\boldsymbol{d}^2_{\text{ref}}$, with the subscript indicating the level number for the given irrep and total momentum, starting at 0. Above each data point we show, using red dots, blue squares, and orange triangles, respectively, the fit values from the ADLER3 fit of Table 4.9, the values predicted by the quantization condition if $\mathcal{K}_{\text{df},3} = 0$ but all other parameters are unchanged, and the values predicted if $P_0 = 0$ with all other parameters unchanged.

amplitude by setting $P_0 = 0$, with all other parameters unchanged from the ADLER3 fit. This changes the levels by an amount that is typically smaller than that caused by setting $\mathcal{K}_{\mathrm{df},3}$ to zero.

We next investigate how the fit works for the levels that are not included in the fit, because they lie above the maximal CMF energy, $E_{\mathrm{cm}} = (2M_K + M_\pi) + 0.98M_\pi$. These levels thus lie at or above the inelastic threshold. We have determined eight of them, and the comparison of their lab shifts to the ADLER3 fit is shown in the lower panel of figure 4.3, along with the predictions if $\mathcal{K}_{\mathrm{df},3}$ or P_0 are set to zero. The values of the shifts are comparable to those for the fitted levels, and we see that the fit continues to work at a similar level of accuracy even in the inelastic regime.

We next display the corresponding results for the $K^+\pi^+$ channel in the same fit. These are shown in figure 4.4: the upper panel shows 16 levels that are included the fit, and the lower panel shows 10 that are not. We recall from Table 4.9 that the cutoff for the fit lies at $E_{\mathrm{cm}} = (M_K + M_\pi) + 1.26M_\pi$ in this channel, and thus lies slightly above the inelastic threshold. Since two-particle levels do not depend on $\mathcal{K}_{\mathrm{df},3}$, we show only the impact of setting P_0 to zero.

For the trivial irreps, the situation is similar to that for the $KK\pi$ levels: the fit works well, and continues to do so in the inelastic regime. The shifts due to the nonzero P_0 are small, although they increase for the higher-lying levels. The levels in nontrivial irreps, however, are shifted only by the p-wave interactions (as can be seen by the fact that the yellow triangles lie at $\Delta E_{\mathrm{lab}} = 0$. This is as expected based on group-theoretical considerations. For some of these levels, there is evidence that the energy shift is negative, and it is this that leads to the result that the scattering length is slightly attractive.

The situation for the other fits and ensembles is qualitatively similar, and we do not show the corresponding plots for these other cases.

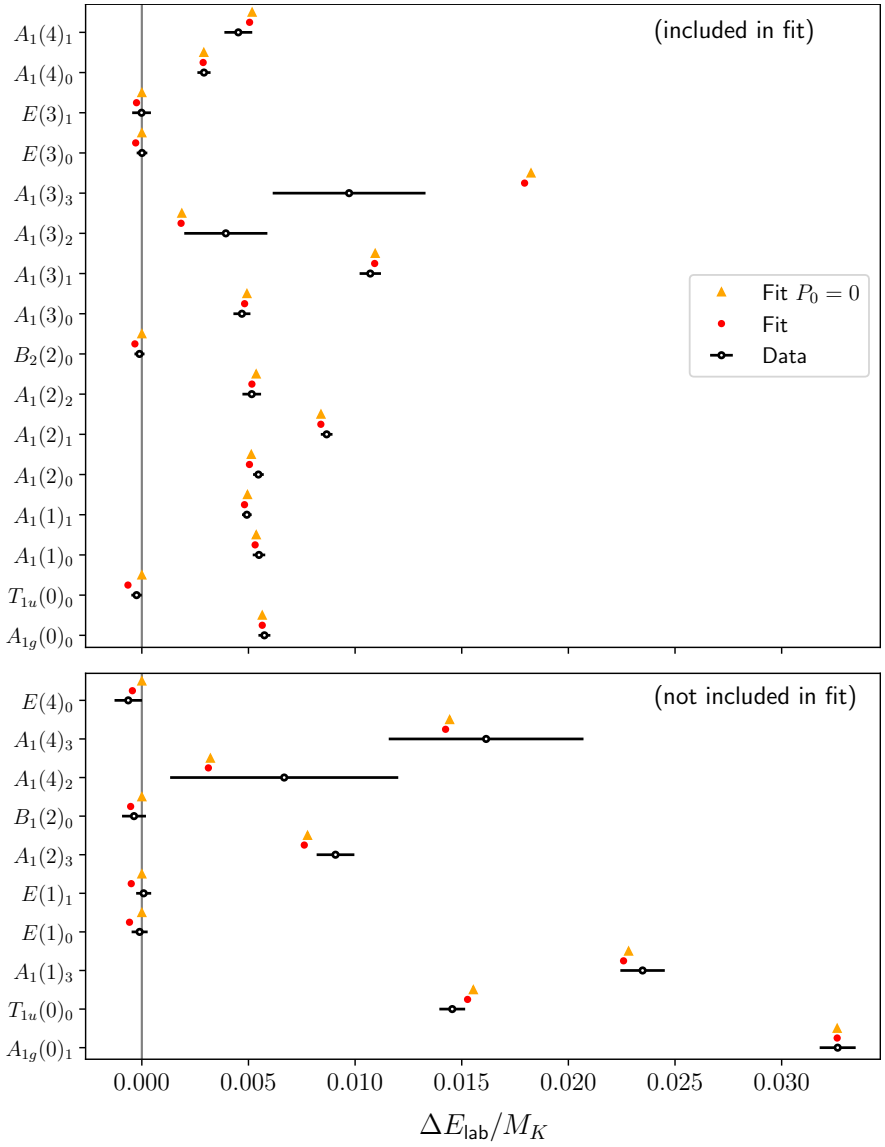

Figure 4.4: Same as for figure 4.3 except for the π^+K^+ levels in the ADLER3 $KK + \pi K + KK\pi$ fits. The upper panel shows the 16 levels included in the fit, while the lower panel shows 10 levels lying above our maximal E_{cm} and which thus are not included in the fit.

Derived results for two-particle scattering quantities

In this section we collect the results for the scattering lengths and effective ranges for $\pi\pi$, πK and KK scattering. These quantities are obtained from the fits presented above, and from additional fits to the following systems: $\pi\pi$ alone, $\pi\pi + \pi\pi\pi$, KK alone, and $KK + KKK$. We stress that these additional fits are different from those presented in Ref. [132], as here we fit to $\Delta E_{\rm lab}$, rather than $E_{\rm cm}$. Our overall aim in this section is to compare the results, and in particular the errors, obtained by using fits to different sets of levels. We discuss the chiral behavior of these results in the following section.

One of the methods used here is to determine the scattering length from the $1/L$ expansion of the energy shift of the ground state (i.e. for which the noninteracting state has all particles at rest). For two nondegenerate scalars the result is [165]

$$\Delta E^{(2)}_{\rm g.s.} = \frac{2\pi a_0}{\mu_{12} L^3}\left[1 - \mathcal{I}\frac{a_0}{\pi L} + (\mathcal{I}^2 - \mathcal{J})\left(\frac{a_0}{\pi L}\right)^2 + \mathcal{O}(1/L^3)\right], \tag{4.51}$$

where μ_{12} is the reduced mass of the pair, a_0 the corresponding scattering length, and the constants are [102]

$$\mathcal{I} = -8.91363291759\,, \qquad \mathcal{J} = 16.532315960\,. \tag{4.52}$$

For three degenerate particles of mass M the result is [102]

$$\Delta E^{(3)}_{\rm g.s.} = \frac{12\pi a_0}{M L^3}\left[1 - \mathcal{I}\frac{a_0}{\pi L} + (\mathcal{I}^2 + \mathcal{J})\left(\frac{a_0}{\pi L}\right)^2 + \mathcal{O}(1/L^3)\right]. \tag{4.53}$$

We observe that the first two orders are a factor of 3 larger for three particles than for two particles, reflecting the number of two-particle pairs. This implies an increased sensitivity to a_0 in the three-particle channel.

The above-described truncated $1/L$ expansions of the ground state energy shifts are sometimes used to determine scattering lengths from two-particle energy shifts (see, e.g., Ref. [166]). Truncation at the $1/L^5$ term is needed to have a one-to-one relation between the energy shift and a_0, since the $1/L^6$ terms include the effective range and, for three particles, also a subtracted version of the three-particle amplitude at threshold [167]. Thus, in this

approach, one must proceed by assuming the $1/L^6$ term is numerically small, and then estimate the resulting systematic error due to truncation [166]. Here our interest is less in the central value obtained in this fashion, but rather in the size of the error obtained in this method compared to those from global fits.

Fit	$B_0^{\pi\pi}$	$B_1^{\pi\pi}$	χ^2/DOF	$M_\pi a_0^{\pi\pi}$	$M_\pi^2 a_0^{\pi\pi} r_0^{\pi\pi}$
ADLER2 fits					
$\pi\pi + \pi\pi\pi$	-11.5(6)	-2.4(4)	74/37	0.0869(47)	2.587(86)
$\pi\pi + \pi K + \pi\pi K$	-11.5(6)	-2.5(4)	112/50	0.0869(45)	2.561(84)
$\pi\pi$ (22 levels)	-11.6(7)	-2.3(4)	52/20	0.0862(50)	2.604(90)
$\pi\pi$ (12 levels)	-11.5(8)	-3.0(7)	25/10	0.0873(60)	2.48(15)
Fitting ground-state energy shift to $1/L$ expansion					
$\pi\pi\pi$	N/A	N/A	N/A	0.0885(76)	N/A
$\pi\pi$	N/A	N/A	N/A	0.0816(76)	N/A
$E_{\rm cm}$ ADLER2 fit, including d waves [132]					
$\pi\pi + \pi\pi\pi$ ($E_{\rm cm}$)	N/A	N/A	N/A	0.0859(41)(28)	2.62(8)(26)

Table 4.11: Comparison of $\pi\pi$ scattering parameters from different fits to $\Delta E_{\rm lab}$ on the D200 ensemble, using units in which $M_\pi = 1$. The $\pi\pi + \pi\pi\pi$ fits are to 22 $\pi\pi$ and 19 $\pi\pi\pi$ levels, all in trivial irreps, with cutoffs at $E_{\rm cm} = 3.74$ and 4.74, respectively (the same values as used in Ref. [132]). The $\pi\pi + \pi K + \pi\pi K$ fits are from Table 4.7 (59 level fit). The next two rows give the results of fits to the $\pi\pi$ data alone, with cutoff for the two fits being $E_{\rm cm} = 3.74 M_\pi$ and $3.0 M_\pi$, respectively. The next block of two rows give the results obtained using the ground-state energy shifts alone, as described in the text. The final row gives the results from Ref. [132] from $E_{\rm cm}$ fits, with the first error being statistical and the second a systematic error due to the variation between fits.

We begin with results for $\pi\pi$ scattering, which are shown in Table 4.11 and Table 4.12, respectively, for the D200 and N203 ensembles. These include the results of the core fits

Fit	$B_0^{\pi\pi}$	$B_1^{\pi\pi}$	χ^2/DOF	$M_\pi a_0^{\pi\pi}$	$M_\pi^2 a_0^{\pi\pi} r_0^{\pi\pi}$
ADLER2 fits					
$\pi\pi + \pi\pi\pi$	-4.87(9)	-1.9(9)	130/50	0.2052(38)	2.222(46)
$\pi\pi + \pi K + \pi\pi K$	-5.05(10)	-1.78(9)	119/73	0.1981(39)	2.296(45)
$\pi\pi$ (27 level)	-4.94(11)	-1.83(9)	66/25	0.2024(44)	2.258(51)
$\pi\pi$ (16 level)	-4.87(11)	-2.00(15)	19/14	0.2055(48)	2.178(74)
Fitting ground-state energy shift to $1/L$ expansion					
$\pi\pi\pi$	N/A	N/A	N/A	0.2125(56)	N/A
$\pi\pi$	N/A	N/A	N/A	0.2095(54)	N/A
$E_{\rm cm}$ ADLER2 fit, including d waves [132]					
$\pi\pi + \pi\pi\pi$ ($E_{\rm cm}$)	N/A	N/A	N/A	0.2059(34)(21)	2.15(5)(12)

Table 4.12: Comparison of $\pi\pi$ scattering parameters from different fits to $\Delta E_{\rm lab}$ on the N203 ensemble, using units in which $M_\pi = 1$. The $\pi\pi\pi$ fits are from Table 4.5, while those for $\pi\pi K$ fits are from Table 4.8. The next two rows give results from fits to the $\pi\pi$ data alone, using cutoffs $E_{\rm cm} = 3.436 M_\pi$ (which is the same as that used in the $\pi\pi + \pi\pi\pi$ and $\pi\pi + \pi K + \pi\pi K$ fits) and $3.0 M_\pi$. The next block of two rows give the results obtained using the ground-state energy shifts alone, as described in the text. The final row gives the results from Ref. [132] from $E_{\rm cm}$ fits, with the first error being statistical and the second a systematic error due to the variation between fits.

presented above, as well as those to different numbers of $\pi\pi$ levels, and the results of fitting the truncated $1/L$ expansions to the ground-state energy shifts. We see that all central values are consistent within $1 - 2\sigma$, including results obtained from in Ref. [132] using $E_{\rm cm}$ fits. Our focus here is on a comparison of the errors. In particular, we want to know if anything is gained by increasing the number of levels in the fits, i.e. moving from a single level (in the ground-state-only fits), to the $\pi\pi$ levels alone, and finally to the fits involving two- and three-particle levels. Our results indicate that, for the scattering lengths, the errors decrease slightly as the number of levels in the fit increases. This trend is what we would have

naively expected, but the size of the change is relatively small. We attribute this smallness to the fact that the higher levels constrain the phase shift at values away from threshold, and because of the strong correlations between two- and three-particle levels. A similar pattern is observed for the errors in $a_0 r_0$.

In light of this discussion, in the chiral fits below we will take the values from the fits involving two- and three-particle levels. Specifically, we use the $\pi\pi + \pi K + \pi\pi K$ fits, since the χ^2_{ref} of this fit is significantly smaller on the N203 ensemble, while the values and errors are essentially the same as those from the $\pi\pi + \pi\pi\pi$ fits on D200.

We next turn to the results for KK scattering parameters, which are collected in Table 4.13 and Table 4.14. Here we also show results with the ADLER3 and ERE3 choices for the KK phase shift, as these can lead to improved fits, as noted above. For a given choice of fit type, the sizes of the errors follow a similar pattern to those for $\pi\pi$ scattering, with those from fits involving two and three particles being smallest. As expected, errors increase for the fits in which the KK phase shift is described with three parameters.

All fits using ΔE_{lab} lead to consistent results for a_0^{KK}. Additionally, these fits are consistent with those using E_{cm} at the $\lesssim 2\sigma$ level. There is, however, much more variation in the results for $a_0^{KK} r_0^{KK}$.

Finally, in Table 4.15 and Table 4.16, we present results for πK scattering parameters. In both cases we show results with two choices of E_{cm} cutoff for the πK fits: the 16-level fit with excellent χ^2_{ref} and the more aggressive 32-level fit with slightly poorer fit quality. The results for $P_0^{\pi K}$, $a_0^{\pi K}$ and $r_0^{\pi K}$ are consistent within $1 - 2\sigma$. The pattern of the sizes of errors is consistent with that described above.

Fit	B_0^{KK}	B_1^{KK}	z_{KK}^2/B_2^{KK}	χ^2/DOF	$M_K a_0^{KK}$	$M_K^2 a_0^{KK} r_0^{KK}$
ADLER2						
KK+KKK	-2.91(4)	-2.29(11)	N/A	118/50	0.3438(50)	1.43(9)
KK+πK+$KK\pi$	-2.90(4)	-2.32(11)	N/A	163/64	0.3444(48)	1.40(9)
KK (28)	-2.87(5)	-2.37(11)	N/A	84/26	0.3489(56)	1.34(10)
KK (15)	-2.84(5)	-2.50(18)	N/A	25/13	0.3521(62)	1.24(15)
Fitting ground-state energy shift to $1/L$ expansion						
KKK	N/A	N/A	N/A	N/A	0.3541(83)	N/A
KK	N/A	N/A	N/A	N/A	0.3531(83)	N/A
ADLER3						
KK+KKK	-3.4(8)	-2.0(5)	0.8(3)	117/49	0.3467(62)	1.20(29)
KK+πK+$KK\pi$	-3.6(8)	-2.0(5)	0.8(3)	162/63	0.3478(58)	1.14(27)
KK (28 levels)	-3.3(8)	-2.2(5)	0.9(3)	84/25	0.3512(69)	1.17(32)
KK (15 levels)	-2.6(1.2)	-2.7(8)	1.1(4)	25/12	0.3515(71)	1.31(48)
ERE3						
KK+KKK	-2.88(5)	1.47(25)	-1.32(38)	116/49	0.3472(57)	1.02(17)
KK+πK+$KK\pi$	-2.87(4)	1.40(25)	-1.25(38)	161/63	0.3486(54)	0.98(16)
KK (28 levels)	-2.84(5)	1.35(29)	-1.25(44)	84/25	0.3524(65)	0.95(19)
KK (15 levels)	-2.84(5)	1.65(41)	-2.4(1.0)	24/12	0.3518(67)	1.16(27)
$E_{\rm cm}$ fit, ADLER3, including d waves [132]						
KK+KKK	N/A	N/A	N/A	N/A	0.3648(59)(29)	0.77(24)(23)

Table 4.13: Comparison of KK scattering parameters from different fits to $\Delta E_{\rm lab}$ on the D200 ensemble, using units in which $M_K = 1$. The exception is the final line, which is a fit to $E_{\rm cm}$ from Ref. [132]. Blocks are divided according to the form of the fit function used for the KK phase shift, as discussed in the text. Note that the meaning of the entry in the z_{KK}^2/B_2^{KK} column depends on which fit function is used: it is z_{KK}^2 in the ADLER3 block and B_2^{KK} in the ERE3 block. $KK + \pi K + KK\pi$ fits are the same as those in Table 4.9. $KK + \pi K + KK\pi$ fits are the same as those in Table 4.10. The ADLER2 $KK + KKK$ fit is the same as that in Table 4.6; the ADLER3 and ERE3 $KK + KKK$ fits use the same set of energy levels.

Fit	B_0^{KK}	B_1^{KK}	z_{KK}^2/B_2^{KK}	χ^2/DOF	$M_K a_0^{KK}$	$M_K^2 a_0^{KK} r_0^{KK}$
ADLER2						
KK+KKK	-3.38(4)	-2.12(7)	N/A	153/42	0.2959(37)	1.75(5)
KK+πK+$KK\pi$	-3.41(5)	-2.08(8)	N/A	181/65	0.2931(39)	1.78(6)
KK (23 levels)	-3.36(5)	-2.14(8)	N/A	90/21	0.2973(42)	1.73(6)
Fitting ground-state energy shift to $1/L$ expansion						
KKK	N/A	N/A	N/A	N/A	0.3060(51)	N/A
KK	N/A	N/A	N/A	N/A	0.3022(54)	N/A
ADLER3						
KK+KKK	-2.72(19)	-2.45(12)	1.21(6)	144/41	0.2896(43)	2.28(20)
KK+πK+$KK\pi$	-2.81(20)	-2.39(13)	1.19(6)	173/64	0.2872(45)	2.26(20)
KK (23 levels)	-2.75(21)	-2.47(13)	1.20(7)	88/20	0.2926(49)	2.18(21)
ERE3						
KK+KKK	-3.32(4)	1.94(13)	-1.33(12)	175/41	0.3008(39)	1.17(7)
KK+πK+$KK\pi$	-3.39(5)	2.20(15)	-1.53(13)	187/64	0.2953(41)	1.30(7)
KK (23 levels)	-3.33(5)	2.04(17)	-1.40(14)	96/20	0.2999(46)	1.22(8)
$E_{\rm cm}$ fit, ADLER3, including d waves [132]						
KK+KKK	N/A	N/A	N/A	N/A	0.3012(44)(18)	1.92(19)(41)

Table 4.14: Comparison of KK scattering parameters from different fits to $\Delta E_{\rm lab}$ on the N203 ensemble, using units in which $M_K = 1$. The exception is the final line which is a fit to $E_{\rm cm}$ from Ref. [132]. Blocks are divided according to the form of the fit function used for the KK phase shift, as discussed in the text. Note that the meaning of the entry in the z_{KK}^2/B_2^{KK} column depends on which fit function is used: it is z_{KK}^2 in the ADLER3 block and B_2^{KK} in the ERE3 block. The KK and KKK fits use cutoffs of $2.9E_K$ and $3.9M_K$, respectively, keeping only levels in trivial irreps, and discarding all but the lowest $\boldsymbol{d}^2 = 9$ level in the KK channel. This leads to 23 levels in both channels.

Fit	$B_0^{\pi K}$	$B_1^{\pi K}$	$P_0^{\pi K}$	χ^2/DOF	$M_\pi a_0^{\pi K}$	$M_\pi a_0^{\pi K} r_0^{\pi K}$
$\pi\pi+\pi K+\pi\pi K$	-12.9(4)	-2.8(3)	0.0007(6)	112/50	0.110(3)	1.154 (53)
$KK+\pi K+KK\pi$	-13.7(4)	-2.3(3)	0.0020(6)	162/63	0.103(3)	1.263(54)
πK (16 level)	-13.1(5)	-2.5(3)	0.0012(7)	15/13	0.107(4)	1.217(62)
πK (26 level)	-13.1(5)	-2.4(2)	0.0013(6)	31/23	0.107(4)	1.229(45)
Fitting ground-state energy shift to $1/L$ expansion						
πK	N/A	N/A	N/A	N/A	0.106(5)	N/A

Table 4.15: Comparison of πK scattering parameters from different fits on the D200 ensemble, using units in which $M_\pi = 1$. All fits use the ADLER2 + ERE1 form for the πK phase shift. The first row gives the results from the 59-level fit in Table 4.7, while the second gives the result from the ADLER3-KK fit in Table 4.9, with the latter converted to units in which $M_\pi = 1$. The next two give the results of fits to the πK data alone, The cutoff energies for the these fits are, respectively, $E_{\rm cm} = 3.64 M_\pi$ and $5.0 M_\pi$, with the former also used for the πK channel in the $\pi\pi + \pi K + \pi\pi K$ and $KK + \pi K + KK\pi$ fits. The final row shows the result of fitting the ground-state energy shift to the $1/L$ expansion.

Fit	$B_0^{\pi K}$	$B_1^{\pi K}$	$P_0^{\pi K}$	χ^2/DOF	$M_\pi a_0^{\pi K}$	$M_\pi^2 a_0^{\pi K} r_0^{\pi K}$
$\pi\pi+\pi K+\pi\pi K$	-5.39(11)	-1.89(17)	0.006(4)	119/73	0.208(4)	1.693(74)
$KK+\pi K+KK\pi$	-5.40(13)	-2.07(19)	0.010(4)	173/64	0.208(5)	1.630(83)
πK (19 level)	-5.42(15)	-2.07(21)	0.004(4)	21.1/16	0.207(6)	1.630(94)
πK (36 level)	-5.45(15)	-2.02(21)	0.002(3)	36.1/33	0.206(6)	1.653(80)
Fitting ground-state energy shift to $1/L$ expansion						
πK	N/A	N/A	N/A	N/A	0.213(7)	N/A

Table 4.16: Comparison of πK scattering parameters from different fits on the N203 ensemble, using units in which $M_\pi = 1$. All fits use the ADLER2 + ERE1 form for the πK phase shift. The first row gives the results from the 82-level fit in Table 4.8, while the second gives the result from the ADLER3-KK fit in Table 4.10, with the latter converted to units in which $M_\pi = 1$. The next two rows give the results of fits to the πK data alone, using cutoff energies $3.4M_\pi$ and $4.3M_\pi$, respectively, with the former also used for the πK channel in the $\pi\pi + \pi K + \pi\pi K$ and $KK + \pi K + KK\pi$ fits. The final row shows the result of fitting the ground-state energy shift to the $1/L$ expansion.

4.6 Discussion of results

In this section, we present and discuss our final results for different two- and three-meson scattering quantities. First, in section 4.6.1, we provide our final numbers for these quantities by combining results from different fits. Then, in section 4.6.2, we compare these numbers to expectations and predictions from ChPT. Finally, in section 4.6.3, we discuss the size of discretization errors, based on the LO Wilson-ChPT results presented above.

4.6.1 Final results for scattering parameters

In section 4.5.2, we have presented results for the two- and three-meson scattering parameters using different fit forms and strategies. While we find overall consistency, it is useful to have a set of final results that contain both statistical uncertainties as well an estimate of the systematic spread due to different fit forms. Note that we always use lab-frame shift fits for this set of final results.

We first consider two-particle parameters. Results for scattering lengths and for the combination $M_X a_0^{XY} r_0^{XY}$ are given in Table 4.17 and Table 4.18, respectively. In each case, the central values are obtained by averaging the results from a pair of three-particle fits (which pair will be explained shortly), and include a systematic error that is obtained from the spread of the fit results (and which we call the "fit systematic"). For the $\pi\pi$ case, the central values are the average of those from fits to $\pi\pi + \pi\pi\pi$ and $\pi\pi + \pi K + \pi\pi K$—see Tables 4.11 and 4.12—while the fit systematic is the standard deviation obtained from the two results. For the πK case, the same procedure is used but now taking the $\pi\pi + \pi K + \pi\pi K$ and $KK + \pi K + KK\pi$ fit results from Tables 4.15 and 4.16. For the KK case, the central value and statistical error are obtained using the same procedure but taking the $KK + KKK$ and $KK + \pi K + KK\pi$ fits obtained using the ADLER3 parametrization for the KK phase shift from Tables 4.13 and 4.14. The fit systematic is given by the standard deviation of the results from these two fits together with those obtained with the ADLER2 and ERE3 parametrizations (six fits in total). In all cases, we take the largest of the statistical errors

when combining results.

Ensemble	$M_\pi a_0^{\pi\pi}$	$M_\pi a_0^{\pi K}$	$M_K a_0^{KK}$	$P_0^{\pi K} = -M_\pi^3 a_1^{\pi K}$
D200	0.0869(47)(0)	0.107(3)(5)	0.3473(62)(19)	0.0014(6)(9)
N203	0.2017(39)(50)	0.208(5)(0)	0.2884(45)(48)	0.008(4)(3)

Table 4.17: Final results for s- and p-wave scattering lengths obtained by combining fits in section 4.5.2, as explained in the text. The errors are respectively statistical and systematic, with the latter obtained from variations between fits.

Ensemble	$M_\pi^2 a_0^{\pi\pi} r_0^{\pi\pi}$	$M_\pi^2 a_0^{\pi K} r_0^{\pi K}$	$M_K^2 a_0^{KK} r_0^{KK}$
D200	2.574(86)(18)	1.209(54)(77)	1.17(29)(19)
N203	2.259(46)(52)	1.662(83)(45)	2.27(20)(46)

Table 4.18: Final results for products $a_0 r_0$ obtained by combining fits in section 4.5.2, as explained in the text. The errors are respectively statistical and systematic, with the latter obtained from variations between fits.

For the three-particle parameters, we quote the final values in Table 4.19. In this case we take the results from a single fit—the one we view as most reliable, based on the discussion in the previous section—and do not quote a fit systematic as any such error would be dwarfed by the statistical errors.

4.6.2 Comparison with chiral perturbation theory

We now turn to the comparison of the final results of Tables 4.17 to 4.19 to ChPT. We perform fits to ChPT expressions wherever they are available, and compare with the form of the expected dependence on M_π^2 in other cases. We also compare to previous results in the literature.

Ensemble	$\mathcal{K}_0$	$\mathcal{K}_1$	$\mathcal{K}_B$	$\mathcal{K}_E$
$\pi\pi + \pi K + KK\pi$ fits				
D200	190(80)	-690(340)	160(650)	170(420)
N203	-240(150)	-1300(600)	990(740)	-3200(1000)
$KK + \pi K + KK\pi$ fits				
D200	170(270)	-6800(1700)	2800(1300)	-5900(3700)
N203	260(310)	-3900(700)	3500(1600)	-400(2000)

Table 4.19: Final results for parameters in $\mathcal{K}_{\mathrm{df},3}$ for $2+1$ systems. Results are from the Standard* fit in Table 4.7, the 82-level fit in Table 4.8, and the ADLER3 fits in Table 4.9 and Table 4.10.

We start with the scattering lengths. Figure 4.5 shows the results for each of the dimensionless s-wave scattering lengths,[12] along with the LO chiral prediction, and a fit to the NLO expressions in eqs. (4.26), (4.27) and (4.29). We have not determined the correlations between the three quantities on a given ensemble, and thus use an uncorrelated fit. In order to plot the result as a function of $(M_\pi/F_\pi)^2$, we use an interpolating function for M_K/F_K as a function of M_π/F_π extracted from the results of Ref. [132]. We find a good fit with $\chi^2/\mathrm{DOF} = 1.5/4$ (6 data points and 2 parameters). We determine the two LECs (evaluated at a renormalization scale $\mu = 4\pi F_\pi$) to be

$$L_{\pi\pi} = -8.77(36) \times 10^{-4}, \quad L_5 = 0.0(1.5) \times 10^{-3}\,. \tag{4.54}$$

We can compare these values to previous determinations. In Ref. [132], a larger value of $L_{\pi\pi} = -1.13(3)\cdot 10^{-3}$ was found, which is many standard deviations away from our new result. However, an important difference that may explain the discrepancy is that Ref. [132] included d-wave interactions, which is not possible here. For L_5, we can compare to results from lattice QCD, which are summarized in the FLAG report [168], and based on Refs. [169, 170]), or

[12] We use $M_{\pi K} a^{\pi K} = [(M_\pi + M_K)/2] a^{\pi K}$ rather than the quantity $M_\pi a^{\pi K}$ quoted earlier so as to separate the curves, and because the a^2 dependence predicted by WChPT is simpler, as seen in eq. (4.43).

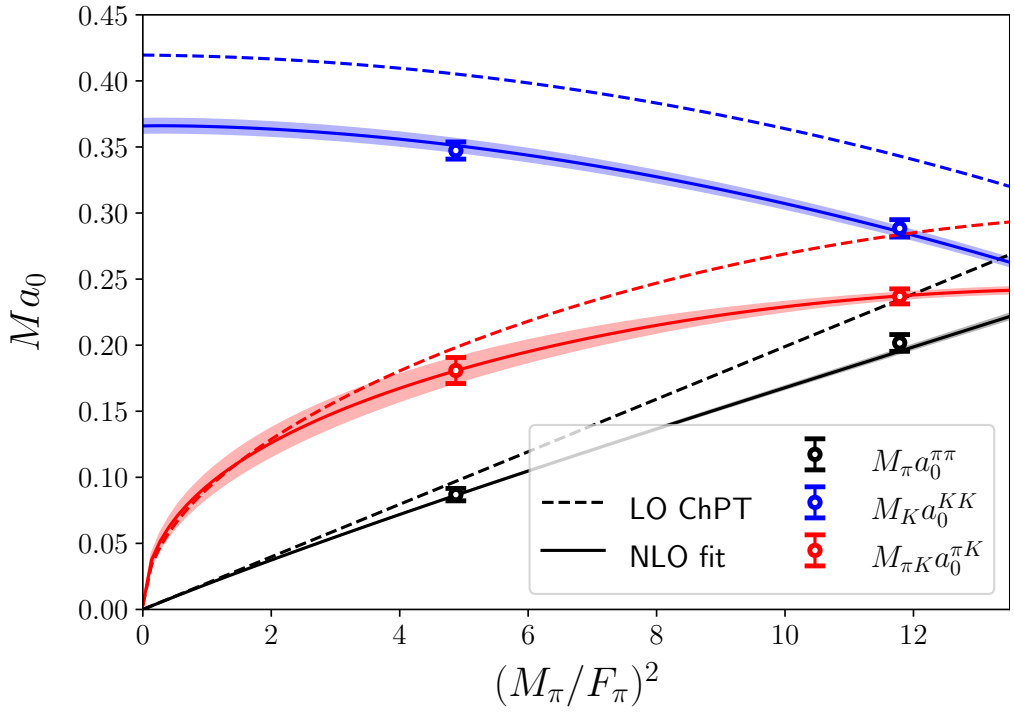

Figure 4.5: Results for $M_\pi a^{\pi\pi}$, $M_{\pi K} a^{\pi K}$ and $M_K a^{KK}$ as a function of M_π^2/F_π^2, where $M_{\pi K} = (M_\pi + M_K)/2$. The LO ChPT result is shown, along with a fit to NLO SU(3) ChPT. The shaded bands show the 1σ uncertainties in the fit.

from phenomenological determinations [171]. These are, however, quoted at a different renormalization scale, $\mu = 770$ MeV. Changing the renormalization scale using

$$L_i^r(\mu_2) = L_i^r(\mu_1) + \frac{\Gamma_i}{16\pi^2} \ln\left(\frac{\mu_1}{\mu_2}\right), \tag{4.55}$$

with $\Gamma_5 = 3/8$, we find that the result from our fit yields $L_5(770\text{ MeV}) = 1.0(1.5) \cdot 10^{-3}$. Varying the choice of $4\pi F_\pi$ to take for the initial scale (using the physical value of F_π, or the value on either of the ensembles) leads to changes in L_5 that are significantly smaller than the error. Our result for L_5 is in agreement with all values in the literature, although we note that our error is much larger than that in the other values.

Next, we discuss our results for the effective range parameters, which are presented in Table 4.18 in the combination $M_X^2 r^{XY} a_0^{XY}$. For the case of identical particles ($X = Y = \pi$

or K), the LO ChPT prediction from section 4.4.3 is that this quantity equals 3. For two pions, the results lie 15% and 25% below this prediction on the D200 and N203 ensembles, respectively, which is consistent with being due to an NLO correction. For two kaons, the results lie very far away from the LO prediction. Both findings are qualitatively similar to those obtained in Ref. [132].

For the πK channel, which is a novel result of this work, the LO ChPT prediction—given in eq. (4.34)—depends on the ensemble:

$$M_\pi^2 a_0^{\pi K} r_0^{\pi K}\Big|_{\text{D200}}^{\text{LO ChPT}} = 1.597, \quad M_\pi^2 a_0^{\pi K} r_0^{\pi K}\Big|_{\text{N203}}^{\text{LO ChPT}} = 2.395. \tag{4.56}$$

Our results in Table 4.18 lie $\sim 25\%$ and $\sim 30\%$, respectively, below the LO ChPT prediction. Again we view this as reasonable consistency, given the absence of NLO corrections.

We now turn to the p-wave π^+K^+ scattering length, reported in the rightmost column of Table 4.17 through the dimensionless combination $P_0^{\pi K} = -M_\pi^3 a_1^{\pi K}$. Note that, in contrast to all the s wave results, the value of $P_0^{\pi K}$ corresponds to slightly attractive interactions. We plot the results for the two ensembles in figure 4.6, including a fit to the leading chiral behavior given by eq. (4.35), which shows reasonable consistency.

We also plot the NLO ChPT prediction given in section B.3. To do so we use values for the requisite LECs determined in Ref. [172] from experimental data (specifically, fit 10 to $\mathcal{O}(p^4)$ from that work). As can be seen, the NLO ChPT result has the same sign as our results, but its magnitude is significantly smaller. The failure of NLO ChPT for this quantity was, in fact, expected, based on the observation of Ref. [163] that the NNLO contribution is two orders of magnitude larger than the NLO one at the physical point (see table 2 of that work).

We can also compare to the expectations and results in the literature from experiment and dispersive analyses. The current understanding is summarized in figure 10 of Ref. [173]. Experimental results [174] for the p-wave phase shift point to a negative (repulsive) value at high energies. By contrast, the dispersive analysis indicates a change of sign for the phase at around $\sqrt{s} \simeq M_K + 3M_\pi$ (physical values of the masses), resulting in an attractive scattering

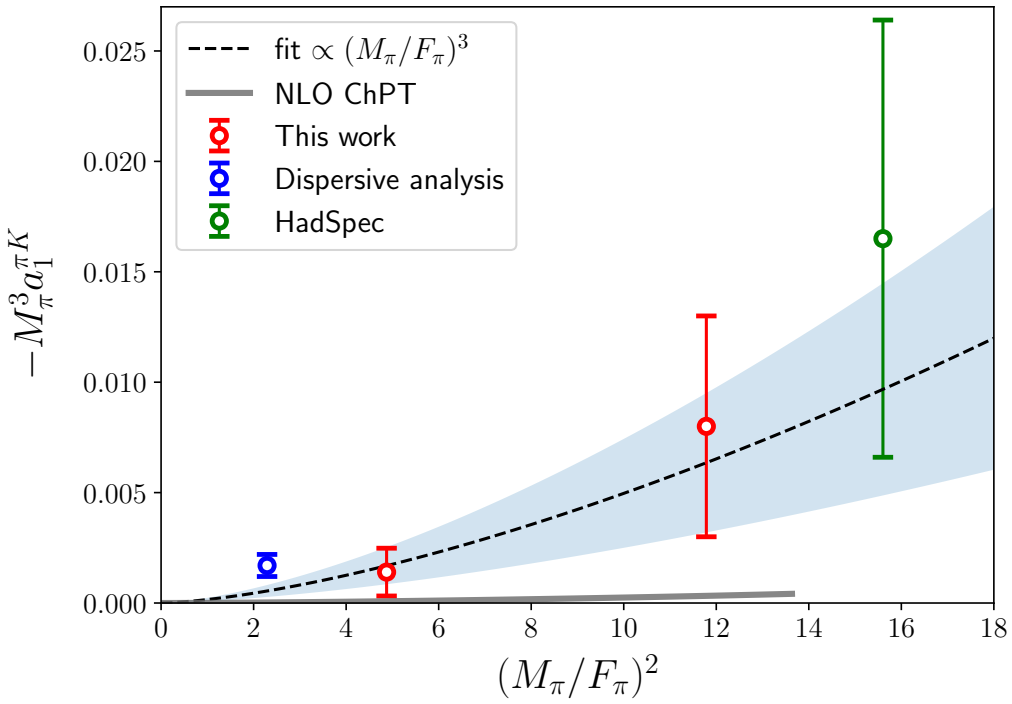

Figure 4.6: Results for the p-wave scattering parameter, $P_0^{\pi K} = -M_\pi^3 a_1^{\pi K}$, plotted as a function of M_π^2/F_π^2. A fit to the leading chiral scaling of $P_0^{\pi K} \propto (M_\pi/F_\pi)^3$ is shown with the corresponding error band, as well as the NLO ChPT prediction as described in section B.3. Also included are the result at the physical point from the dispersive analysis of Ref. [173] (see Table 29 of that work), and the lattice QCD determination of the HadSpec collaboration at a heavier pion mass [138].

length. The value from analysis of Ref. [173] is also shown in figure 4.6. As can be seen, our results for the two ensembles of this work are in qualitative agreement with the low-momentum behavior found by the dispersive analysis. We note that our fits only include levels in the region where the phase shift is expected to stay positive.

We are aware of two other LQCD results concerning p-wave π^+K^+ scattering. First, Ref. [175], reports a single energy level far from threshold (at much higher energy than our levels, and in the inelastic regime) that is dominated by p-wave interactions. There, the p-wave πK interactions seems repulsive, which is consistent with what experiments find at those high energies. This result therefore gives no information concerning the scattering

length.

Second, Ref. [176] computed the p-wave scattering length at heavy meson masses, $M_\pi \simeq 391$ MeV and $M_K \simeq 549$ MeV, and its sign and magnitude are consistent with our results at lighter pion masses. We include this result with the label "HadSpec" in the plot, although it is not strictly speaking comparable as Ref. [138] does not follow the same chiral trajectory. We conclude that, overall, the results from LQCD are in qualitative agreement with dispersive and experimental results.

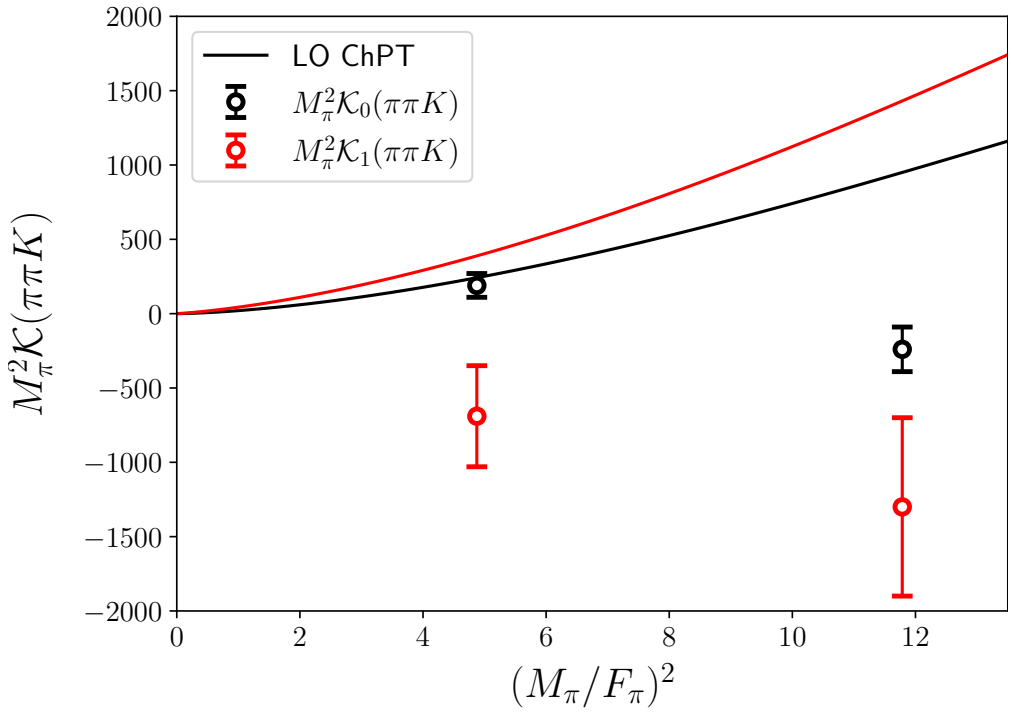

Figure 4.7: Results for $\mathcal{K}_0$ and $\mathcal{K}_1$ for $\pi\pi K$ scattering as a function of M_π^2/F_π^2. The LO SU(3) ChPT predictions given in eq. (4.37) are also shown.

Finally, we compare our results for $\mathcal{K}_{\text{df},3}$ for $2+1$ systems to ChPT. In figures 4.7 and 4.8 we plot the results for $\mathcal{K}_0$ and $\mathcal{K}_1$ for $\pi\pi K$ and $KK\pi$ scattering, respectively. We compare to the LO ChPT predictions of eqs. (4.36) and (4.37), and find substantial disagreement, most notably in the sign of $\mathcal{K}_1$, while the magnitudes are better matched. Similar disagreement has

been observed for 3π and $3K$ systems [132]. There are two possible interpretations for this disagreement. First, it may be that we have underestimated the errors in the determinations of $\mathcal{K}_0$ and $\mathcal{K}_1$. One possibility is that discretization errors might be large, although we present evidence against this option in section 4.6.3. Second, NLO terms in ChPT may be substantial, and invalidate the LO result, such as in the case of $M_K^2 a_0^{KK} r_0^{KK}$ discussed above. To address the latter possibility, a NLO ChPT calculation would be needed, but, while NLO results are available for the three-particle scattering amplitude [177,178], the relation to $\mathcal{K}_{\mathrm{df},3}$ has yet to be worked out.

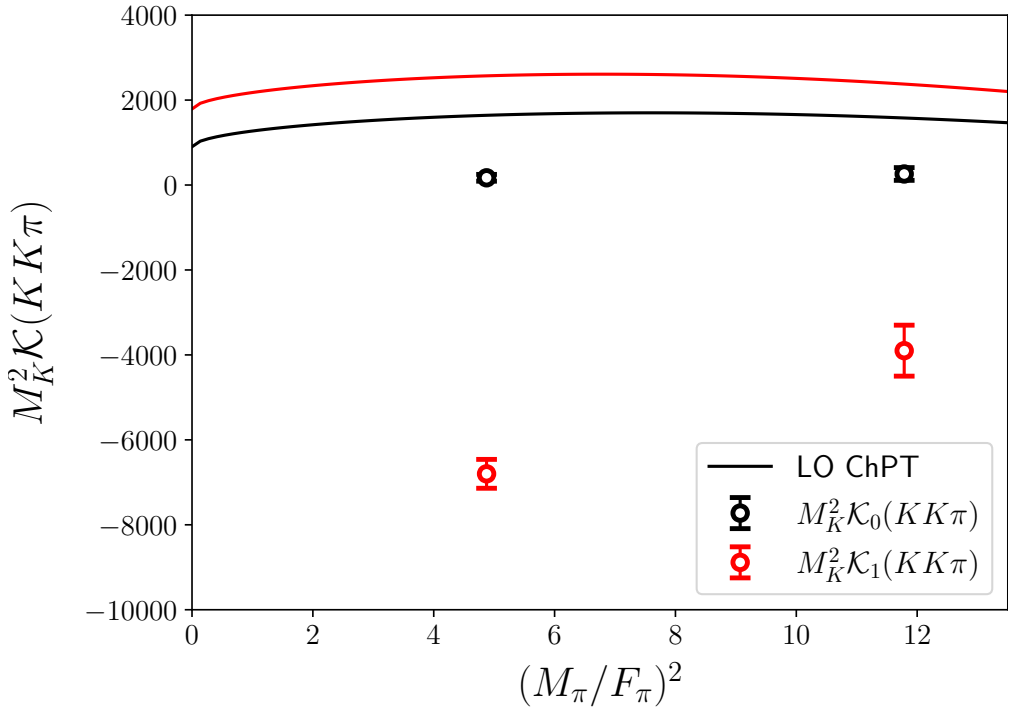

Figure 4.8: Results for $\mathcal{K}_0$ and $\mathcal{K}_1$ for $KK\pi$ scattering as a function of M_π^2/F_π^2. The LO SU(3) ChPT predictions given in eq. (4.36) are also shown.

In figures 4.9 and 4.10 we plot the results for $\mathcal{K}_{\mathrm{B}}$ and $\mathcal{K}_{\mathrm{E}}$ for $\pi\pi K$ and $KK\pi$ scattering, respectively. These quantities vanish at LO in ChPT; their first nontrivial contribution is expected to appear at NLO in ChPT. Since a NLO calculation has yet to be done, we have

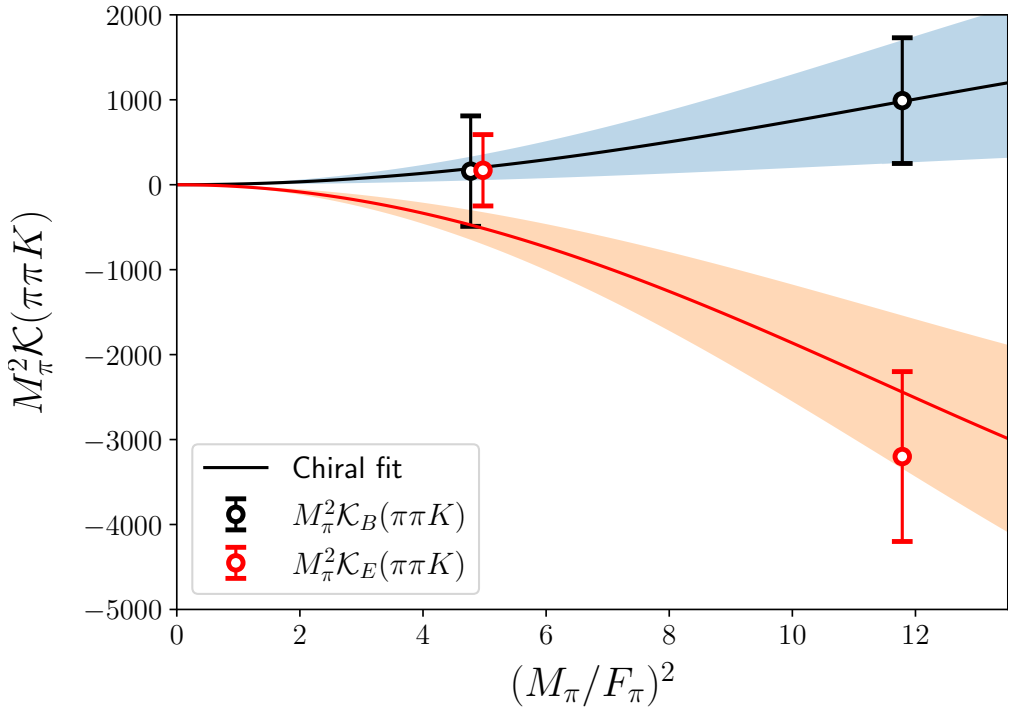

Figure 4.9: Results for $\mathcal{K}_B$ and $\mathcal{K}_E$ for $\pi\pi K$ scattering as a function of M_π^2/F_π^2. Fits to the expected leading chiral behavior given in eq. (4.39) are plotted alongside the data. For better visibility, the x-coordinates of the left-most datapoints have been shifted.

fit to the expected chiral scaling given in eqs. (4.39) and (4.40), finding parameters

$$\begin{aligned} c_B^{\pi\pi K} &= 0.41(30), \quad \chi^2/\text{DOF} = 0.0036, \qquad c_E^{\pi\pi K} = -1.02(38), \quad \chi^2/\text{DOF} = 3.1, \\ c_B^{KK\pi} &= 1.13(37), \quad \chi^2/\text{DOF} = 0.24, \qquad c_E^{KK\pi} = -0.36(54), \quad \chi^2/\text{DOF} = 2.1. \end{aligned} \tag{4.57}$$

We find a reasonable description of the data based on these fit forms.

4.6.3 Discretization errors

Up to this point we have neglected the effects of discretization errors in our two- and three-particle fits. Since the ensembles used in this work are $\mathcal{O}(a)$ improved, these errors are of $\mathcal{O}(a^2)$. Here we extend the fits by including the leading a^2 terms predicted by WChPT. As explained in section 4.4.3, this is only consistent with chiral power counting if we assume

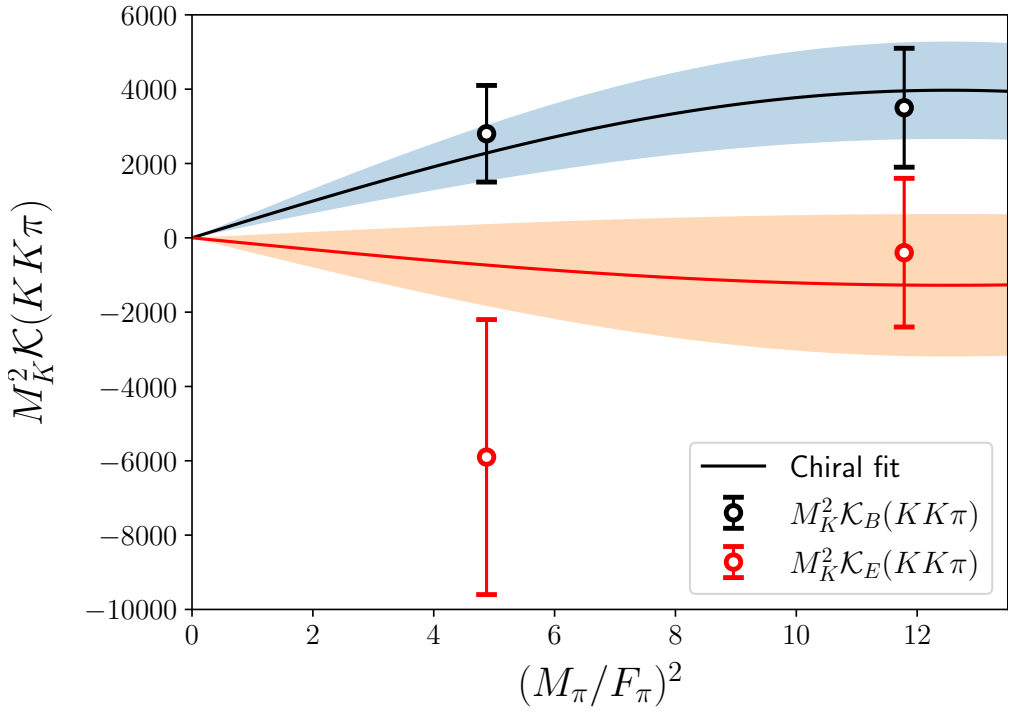

Figure 4.10: Results for $\mathcal{K}_B$ and $\mathcal{K}_E$ for $KK\pi$ scattering as a function of M_π^2/F_π^2. Fits to the expected leading chiral behavior given in eq. (4.40) are plotted alongside the data.

$a^2\Lambda_{QCD}^2 \sim M_\pi^4/(4\pi F_\pi)^4$.

We begin with the two-particle scattering lengths. The WChPT results of eqs. (4.41) to (4.43) predict that each of these quantities receive a common offset proportional to a^2. Repeating the global fit to the six s-wave scattering lengths shown in Table 4.17, allows us to find the value of this offset, which we denote as follows,

$$\delta_a(Ma_0) = \lim_{M_\pi \to 0} M_\pi a_0^{\pi\pi} = -\frac{(2w_6' + w_8')}{16\pi}\,. \tag{4.58}$$

The new fit has $\chi^2/\text{DOF} = 1.1/3$ (6 data points and 3 parameters), and yields

$$L_{\pi\pi} = -8.47(59)\times 10^{-4}, \quad L_5 = -0.3(1.6)\times 10^{-3}, \quad \delta_a(Ma_0) = 2.7(4.5)\times 10^{-3}\,. \tag{4.59}$$

The results for $L_{\pi\pi}$ and L_5 are consistent with those found in the fit without discretization errors, given in eq. (4.54), and the offset is found to be consistent with zero. The result for

$\delta_a(Ma_0)$ can be converted into a determination of the $\mathcal{O}(a^2)$ LECs,

$$2w_6' + w_8' = -0.14(23)\,. \tag{4.60}$$

As noted above, the magnitude of this effect is very small. For example, at the physical pion mass $M_\pi a_0^{\pi\pi} \sim 0.04$ in our fits, which is about an order of magnitude larger than the central value of, or error in, $\delta_a(Ma_0)$.

Using the WChPT results given in eqs. (4.44) and (4.45), we can use eq. (4.60) to predict the size of the $\mathcal{O}(a^2)$ terms in the leading isotropic contribution to $\mathcal{K}_{\mathrm{df},3}$. This is because they are proportional to the same combination of LECs. The resulting predictions are presented in Table 4.20. We observe that the size of the discretization errors is an order of magnitude smaller than the central values and errors we obtain from fits to the spectrum This indicates that, given the precision with which we are able to calculate the parameters in $\mathcal{K}_{\mathrm{df},3}$, discretization effects can be viewed as negligible. Similar results hold also for the 3π and $3K$ channels, for which the WChPT results are presented in section B.2.

Ensemble	$\mathcal{K}_0$	$\delta_a(\mathcal{K}_0)$
$\pi\pi + \pi K + \pi\pi K$ fits		
D200	190(80)	4(7)
N203	-240(150)	10(16)
$KK + \pi K + KK\pi$ fits		
D200	170(270)	17(27)
N203	260(310)	14(23)

Table 4.20: Final results for $\mathcal{K}_0$ compared to the estimated discretization effects based on WChPT, $\delta_a(\mathcal{K}_0) = -6(2w_6' + w_8')M_X^2/F_X^2$, where $X = \pi$ for the $\pi\pi + \pi K + \pi\pi K$ fits, and $X = K$ for the $KK + \pi K + KK\pi$ fits.

4.7 Conclusion

This works represents the first determination, theoretical or experimental, of quantities related to $\pi\pi K$ and $KK\pi$ scattering at maximal isospin. In particular, we have studied these systems using LQCD for two different ensembles along a trajectory of approximately constant trace of the quark mass matrix, $2m_\ell + m_s \simeq$ const.

We have extracted more than 200 finite-volume energies across the $\pi\pi K$ and $KK\pi$ systems, leading to roughly 35 – 45 and 20 – 30 levels below the inelastic thresholds on N203 and D200, respectively. As with our previous work in Ref. [132], the ability to determine such a large number of energies was enabled by advanced algorithms, like stochastic LapH and common subexpression elimination. In order to facilitate the use of our extracted spectrum by other collaborations, we have made the jackknife samplings for all energies determined in this work available in HDF5 format as ancillary files with the arXiv submission.

As explained in section 4.5.1, we have tested several strategies to extract scattering quantities from the finite-volume spectra. Our findings can be summarized as follows. First, in the systems of this work, it is better to perform fits to energy shifts with respect to the noninteracting energies, rather than to the energy levels themselves. This leads to less correlation between energy levels (better-conditioned correlation matrices), and to more constrained best-fit parameters. Second, it seems that the best approach when dealing with multiple processes is to fit all the available information at the same time (which here means a simultaneous fit to the two- and three-hadron spectra). Other fitting strategies, such as first fitting the two-particle spectra and then using the results as Bayesian priors for a fit to the three-particle levels, produce consistent results, but with significantly larger uncertainties. We expect that these conclusions will be relevant for other finite-volume systems.

The main results of this work are summarized in Tables 4.17 to 4.19. First, we are able to extract two-particle threshold parameters, including the p-wave π^+K^+ scattering length. Second, for each of the 2+1 systems, we extract the four parameters of $\mathcal{K}_{\text{df},3}$ corresponding to first and second order in the threshold expansion. We observe the expected hierarchy, that

is, interactions in the $KK\pi$ channel are stronger than in $\pi\pi K$. Moreover, the values for the different terms of the K matrix have the correct order of magnitude, at least based on chiral expectations. We are also able to determine their values to be nonzero with greater than 2σ significance in some cases, and we find the entire $\mathcal{K}_{\mathrm{df},3}$ to be nonzero with significance between 2.4 and 5.0σ in all channels on each ensemble.

Another novel feature of this work is the extraction of discretization errors in $\mathcal{K}_{\mathrm{df},3}$, which at leading order in the appropriate power counting enter only in $\mathcal{K}_0$. By comparing the two-particle scattering lengths computed on the lattice to those calculated in WChPT, we are able to determine a numerical value for the magnitude of discretization effects in a WChPT calculation of $\mathcal{K}_0$. We find the discretization errors to be small compared to both the central values and uncertainties of $\mathcal{K}_0$ for each scattering channel and on each ensemble.

Natural extensions of this work are to three pseudo-Goldstone bosons at nonmaximal isospin, for which two- and three-meson resonances are present, or to the doubly charmed tetraquark T_{cc}. While there is a long way to go to determine properties of particles coupling to both two- and three-particle channels, and involving particles with spin, such as the Roper resonance, the strategies and tools of this work bring us one step closer.

Acknowledgments

We thank A. Rodas for useful discussions.

The work of ZTD and SRS is supported in part by the U.S. Department of Energy (US-DOE) grant No. DE-SC0011637. The work of ADH is supported by The U.S. Department of Energy, Office of Science, Office of Nuclear Physics through *Contract No. DE-SC0012704*, and within the framework of Scientific Discovery through Advanced Computing (SciDAC) award *Fundamental Nuclear Physics at the Exascale and Beyond*. CJM acknowledges support from the U.S. NSF under award PHY-2209167. FRL has been supported in part by the USDOE, Office of Science, Office of Nuclear Physics, under grant Contract Numbers DE-SC0011090 and DE-SC0021006. FRL acknowledges financial support by the Mauricio and Carlota Botton Fellowship.

Calculations for this project were performed on the HPC clusters “HIMster II” at the Helmholtz-Institut Mainz and “Mogon II” at JGU Mainz. We are grateful to our colleagues in the CLS consortium for sharing ensembles.

Chapter 5

THREE RELATIVISTIC NEUTRONS IN A FINITE VOLUME[1]

5.1 Abstract

We generalize the relativistic field-theoretic (RFT) three-particle finite-volume formalism to systems of three identical, massive, spin-1/2 fermions, such as three neutrons. This allows, in principle, for the determination of the three-neutron interaction from the finite-volume spectrum of three-neutron states, which can be obtained from lattice QCD calculations.

5.2 Introduction

First-principles lattice QCD (LQCD) calculations of two-baryon scattering amplitudes, including the properties of subthreshold bound states, are rapidly progressing (see, e.g., refs. [143, 180–189]). This includes the determination of masses and other properties of certain light nuclei and hypernuclei, albeit at heavier-than-physical quark masses [190–194]. However, less progress has been made using LQCD to determine the three-nucleon interaction, which plays an important role for nuclei near the neutron driplines, for nuclear saturation, and in determining the neutron-star equation of state [195, 196]. To advance such calculations, a formalism relating finite-volume energies to infinite-volume forces must be developed.

Such relations often take the form of quantization conditions, which relate the finite-volume spectrum obtained from lattice calculations to infinite-volume scattering amplitudes. At this stage, the two-body formalism, based on the seminal work of Lüscher [13, 14], is very well understood, and its application has become a standard technique in LQCD. The development of the three-body formalism is an active area of research, with many cases un-

[1] Z. T. Draper, M. T. Hansen, F. Romero-López and S. R. Sharpe, *Three relativistic neutrons in a finite volume*, *JHEP* **07** (2023) 226 [2303.10219]

derstood [16,17,35–39,101–122], and with a rapidly growing number of applications to LQCD results [40,67,91,123–134]. For recent reviews see refs. [94,95,97,99,100]. Other finite-volume approaches, which we do not discuss, include formulating EFTs in finite volume [197–201], the finite-volume Hamiltonian method (see, e.g., ref. [202]), and the HAL-QCD method [193]. Still another approach, which does not take advantage of finite-volume effects, is to determine multi-hadron observables via smeared spectral functions, extracted from a regulated estimate of the notoriously ill-posed inverse Laplace transform [203–208].

To date, the finite-volume three-body formalism has only considered spinless (scalar or pseudoscalar) particles, including both identical and non-identical particles and, in the latter case, non-degenerate masses. To study more interesting quantities in the realm of nucleon and nuclear physics—such as the Roper resonance, the tritium nucleus, or the three-nucleon force—one must understand how to include particles with spin in the formalism. In this work we take the first step in this direction by considering three identical spin-1/2 fermions. This allows us to address the issues arising from the presence of spin in the simplest context. It also gives access to a very important three-particle system, namely that of three neutrons. Further generalizations, e.g., to generic three-nucleon systems or the $N\pi + N\pi\pi$ system needed to describe the Roper resonance, will be left for future work.

We follow the relativistic field theory (RFT) approach, pioneered in refs. [16, 17]. The main technical complication in the derivation is the description of spin in relativistic systems of three particles. This is mainly due to the fact that the projection of the spin along an axis is not Lorentz invariant. This leads to the mixing of spin-1/2 and spin-3/2 three-neutron states. The complication is absent in the finite-volume formalism for two particles with arbitrary spin [209], since all pairwise interactions occur at fixed overall two-particle momentum. In addition, in two-nucleon systems, the total spin is effectively conserved, since spin-1 or spin-0 states have opposite parities and do not mix.

The formalism is only valid for center-of-momentum frame (CMF) energies up to the first inelastic threshold, which for the three-nucleon system occurs at the pion production threshold, $3N \to 3N + \pi$. For physical quark masses, this threshold occurs at energies for

which the nucleons are in the nonrelativistic regime. Thus, one might argue that developing a relativistic formalism is overkill, as the NREFT approach of refs. [104, 106] is simpler. However, we expect LQCD studies of three nucleons to use heavier-than-physical quarks in the near term, and in this case the inelastic threshold is higher, with relativistic effects correspondingly enhanced.[2] In addition, as noted above, the complications introduced by spin must be understood in the relativistic domain to discuss higher baryon resonances such as the Roper.

As is always the case in the finite-volume three-particle relations, the formalism for three neutrons involves two steps: (1) deriving the three-neutron quantization condition, which connects the spectrum to an intermediate K-matrix, $\mathcal{K}_{\text{df},3}$; and (2) deriving an integral equation relating $\mathcal{K}_{\text{df},3}$ to the three-neutron scattering amplitude, $\mathcal{M}_3$. We find that the resulting equations can be written in essentially identical form to those for identical scalars, with the complications from spin leading to additional indices, the presence of signs resulting from Fermi statistics, and the need for momentum-dependent spin transformation operators related to Wigner rotations.

A necessary step to analyze lattice QCD data using the quantization condition is to have parametrizations of the three-particle K-matrix, $\mathcal{K}_{\text{df},3}$. As in previous work [16, 36, 108, 110], we develop an expansion about threshold for the three-neutron amplitude. The constraints from Fermi statistics significantly restrict the allowed forms that can appear through next-to-leading order in this expansion.

The remainder of this paper is organized as follows. We begin, in section 5.3, recalling the essential features of the RFT formalism for identical scalars, from which the generalization presented here is developed. This section also introduces the required kinematic notation. The core of this work is section 5.4, in which we describe the derivation of formalism for three identical spin-1/2 particles. We divide this long section into three parts. In the first,

[2]The relative magnitude of relativistic effects with respect to the leading nonrelativistic contribution can be quantified by the size of $\boldsymbol{k}^2/m_N^2$. In the vicinity of the $3m_N + m_\pi$ threshold, this quantity can take values up to 0.5 for a setting such as the one in Refs. [143, 189], with $m_\pi \simeq 700 - 800$ MeV.

section 5.4.1, we describe the kinematic modifications that arise in the presence of spin, in particular due to the need for Wigner rotations. We then, in section 5.4.2, describe how the building blocks of the RFT formalism are modified in the presence of spin. Finally, in section 5.4.3, we show how these new building blocks appear in the derivation, and discuss the generalization to all orders in the skeleton expansion. In order to make this paper more accessible, we present a separate summary of the final results in section 5.5. The parametrization of $\mathcal{K}_{\text{df},3}$ is described in section 5.6, and we conclude in section 6.7. We relegate technical details to three appendices. In section C.1 we describe the way in which the antisymmetry of three fermion fields alters the derivation, while in section C.2 we detail the specific antisymmetrization of momenta needed to define the relation between $\mathcal{K}_{\text{df},3}$ and $\mathcal{M}_3$. Finally, section C.3 provides additional technical details concerning the enumeration of operators appearing in section 5.6.

5.3 Recap of the formalism for identical scalars

In this section we review the RFT finite-volume scattering formalism for identical spin-zero particles, derived in refs. [16, 17]. The derivation assumes a $\mathbb{Z}_2$ symmetry that decouples the sectors with even and odd numbers of particles. For pions in isosymmetric QCD this symmetry is G-parity, and for nucleons in the energy range below pion production it is baryon number.

The formalism for spin-zero particles consists of two parts: the first is a quantization condition relating the finite-volume energy spectrum (in a periodic box with side-length L) to an intermediate quantity called $\mathcal{K}_{\text{df},3}$, and the second is a set of integral equations relating this quantity to the physical three-to-three scattering amplitude. Both parts can be derived using a particular finite-volume correlation function denoted $\mathcal{M}_{3,L}^{(u,u)}$, which can be shown to

satisfy the following relation:[3]

$$\mathcal{M}_{3,L}^{(u,u)}(P) \equiv \mathcal{D}^{(u,u)} + \mathcal{L}_L^{(u)} \frac{1}{1 + \mathcal{K}_{\mathrm{df},3} F_3} \mathcal{K}_{\mathrm{df},3} \mathcal{R}_L^{(u)} \,. \tag{5.1}$$

All quantities here are matrices on an index space that parametrizes three degenerate particles of mass m having fixed total energy E and spatial momentum $\boldsymbol{P} = (2\pi/L)\boldsymbol{n}_P$ in the finite-volume frame. As indicated, the value of $\boldsymbol{P}$ is constrained by the periodicity to be an integer three-vector ($\boldsymbol{n}_P \in \mathbb{Z}^3$) multiple of $2\pi/L$. The energy and three-momentum are grouped into the four-vector $P^\mu = (E, \boldsymbol{P})$ that appears in the argument of $\mathcal{M}_{3,L}^{(u,u)}$ on the left-hand side of eq. (6.76). With energy and momentum fixed, one can additionally select one of the three particles, called the spectator, and denote its on-shell four-momentum by $k^\mu = (\omega_k, \boldsymbol{k})$ where $\omega_k = \sqrt{\boldsymbol{k}^2 + m^2}$. The remaining two particles, sometimes called the interacting pair or dimer, then have four-momentum $P^\mu - k^\mu$ and their squared energy in their two-particle CMF is given by

$$(P - k)^2 \equiv E_{2,k}^{*2} = (E - \omega_k)^2 - (\boldsymbol{P} - \boldsymbol{k})^2 \,. \tag{5.2}$$

Since this energy is fixed by E, $\boldsymbol{P}$ and $\boldsymbol{k}$, the same is true for the magnitude of back-to-back momenta for the two dimer particles. As a result, the only remaining degree of freedom is directional, and can be decomposed in spherical harmonics with indices ℓm. Combining the spherical harmonic indices with the momentum $\boldsymbol{k} = (2\pi/L)\boldsymbol{n}$ gives a discrete index space abbreviated as $\{k\ell m\}$. This is the space on which all matrices in eq. (6.76) are defined.[4]

$\mathcal{M}_{3,L}^{(u,u)}$ depends on $\mathcal{K}_{\mathrm{df},3}$, as shown, together with four additional matrices (F_3, $\mathcal{D}^{(u,u)}$, $\mathcal{L}_L^{(u)}$ and $\mathcal{R}_L^{(u)}$) that can each be expressed in terms of four more fundamental building blocks. The first of these is the single-particle energy, ω_k, promoted to a matrix in a trivial way:

$$\omega_{\boldsymbol{k}'\ell'm',\boldsymbol{k}\ell m} \equiv \delta_{\boldsymbol{k}'\boldsymbol{k}} \delta_{\ell'\ell} \delta_{m'm} \sqrt{\boldsymbol{k}^2 + m^2} \,. \tag{5.3}$$

[3] In the derivation for three neutrons presented in section 5.4.3 below, we use a different, though closely related, correlator to derive the quantization condition, as it is conceptually simpler and has been used in previous work, e.g. refs. [16, 37]. The connection to the three-particle scattering amplitude is, however, made using the three-neutron generalization of $\mathcal{M}_{3,L}^{(u,u)}$.

[4] Since we are considering identical particles, only even values of ℓ contribute. This will not be the case for three neutrons, due to the spin degree of freedom.

The second building block is $\mathcal{K}_2(E, \boldsymbol{P})$, which encodes the two-to-two scattering that arises as a subprocess:

$$\mathcal{K}_{2,\boldsymbol{k}'\ell'm',\boldsymbol{k}\ell m}(E, \boldsymbol{P}) = \delta_{\boldsymbol{k}'\boldsymbol{k}}\mathcal{K}_{2,\ell'm',\ell m}(E^*_{2,k}) = \delta_{\boldsymbol{k}'\boldsymbol{k}}\delta_{\ell'\ell}\delta_{m'm}\mathcal{K}_2^{(\ell)}(E^*_{2,k})\,, \tag{5.4}$$

$$\mathcal{K}_2^{(\ell)}(E^*_{2,k})^{-1} = \frac{1}{16\pi E^*_{2,k}}\Big[p\cot\delta^{(\ell)}(p) + |p|\Big(1 - H(\boldsymbol{k})\Big)\Big]\Big|_{p=q^*_{2,k}}\,, \tag{5.5}$$

where $\delta^{(\ell)}(p)$ is the scattering phase shift and

$$q^*_{2,k} = \sqrt{E^{*2}_{2,k}/4 - m^2} \tag{5.6}$$

is the momentum of each of the particles in the dimer in their CMF. We have also introduced $H(\boldsymbol{k})$, a smooth cutoff function defined, for example, in eqs. (28)-(29) of ref. [16]. This is a non-standard part of the K-matrix definition used in this formalism, but is required to avoid inducing unwanted power-like volume effects, as explained in refs. [16, 17].

The final two building blocks are two finite-volume quantities denoted $F(E, \boldsymbol{P}, L)$ and $G(E, \boldsymbol{P}, L)$. These are defined, respectively, in eqs. (22-24) of ref. [16] and eq. (B.3) of ref. [37].[5] We give their respective extensions to spin one-half particles in eqs. (5.51) and (5.53) (for F) and eqs. (5.42) and (5.45) (for G) below. With these in hand F_3, for example, can be written as

$$F_3 \equiv \frac{1}{2\omega L^3}\left[\frac{F}{3} - F\frac{1}{1 + \mathcal{M}_{2,L}G}\mathcal{M}_{2,L}F\right], \qquad \mathcal{M}_{2,L} \equiv \frac{1}{\mathcal{K}_2^{-1} + F}\,. \tag{5.7}$$

The first application of $\mathcal{M}^{(u,u)}_{3,L}$ is that, up to neglected e^{-mL} effects, the three-particle finite-volume energies correspond to poles in the factor appearing between $\mathcal{L}^{(u)}_L$ and $\mathcal{R}^{(u)}_L$ in eq. (6.76). This leads to the quantization condition

$$\det_{k\ell m}\Big[1 + \mathcal{K}_{\mathrm{df},3}(E^*_3)F_3(E_3, \boldsymbol{P}, L)\Big] = 0\,, \tag{5.8}$$

[5] Alternatively, $F(E, \boldsymbol{P}, L)$ can be obtained from $\mathbf{F}^{\mathsf{lab}}$ in eq. (5.51) below by multiplying by $2\omega_k L^3/i$ and dropping spin indices, while $G(E, \boldsymbol{P}, L)$ can be obtained from $\mathbf{G}^{\mathsf{lab}}$ in eq. (5.42) by multiplying by $-2\omega_p L^3/i$, and dropping the spin indices.

valid for $m < E_3^* < 5m$, where we have labeled the energy coordinate by E_3 to emphasize that the result applies for finite-volume energies with three-particle quantum numbers, and $E_3^* = \sqrt{E_3^2 - \boldsymbol{P}^2}$ is the energy in the overall CMF.

Superficially, this looks very similar to the quantization condition for two-particle states, arising from poles in $\mathcal{M}_{2,L}$ with fixed values of the spectator momentum $\boldsymbol{k} = \boldsymbol{k}'$. In this case the quantization condition is defined over angular-momentum indices,

$$\det_{\ell m}\Big[1 + \mathcal{K}_2(E_2^*)F_2(E_2, \boldsymbol{P}_2, L)\Big] = 0\,, \tag{5.9}$$

and is valid for $0 < E_2^* < 4m$, where $(E_2, \boldsymbol{P}_2) = (E_3 - \omega_k, \boldsymbol{P} - \boldsymbol{k})$ is the two-particle total energy-momentum, and $E_2^* = \sqrt{E_2^2 - \boldsymbol{P}_2^2}$ is the two-particle CMF energy. In this result, $\mathcal{K}_2(E_2^*) = \mathcal{K}_{2,\ell'm',\ell m}(E_2^*)$ refers to the quantity in the middle equality of eq. (5.4), i.e. the K matrix carrying only angular momentum indices, and

$$F_{2,\ell'm',\ell m}(E_2, \boldsymbol{P}_2, L) = F_{\boldsymbol{k}\ell'm',\boldsymbol{k}\ell m}(E_2 + \omega_k, \boldsymbol{P}_2 + \boldsymbol{k}, L)\,. \tag{5.10}$$

To implement the formalism in practice, one must truncate the sum over angular momentum at some $\ell = \ell_{\mathsf{max}}$ in order that the matrices are finite. Calculations to date have used $\ell_{\mathsf{max}} = 0$, 1 or 2. For both the two- and three-particle quantization conditions, solving for the roots at fixed L and $\boldsymbol{P}$ for a given parametrization of $\mathcal{K}_2(E_2^*)$ and $\mathcal{K}_{\mathrm{df},3}(E_3^*)$ gives a prediction for the finite-volume energies. Conversely, extracting the energies from a numerical lattice calculation gives constraints on the two K-matrices and fitting to a range of parametrizations allows one to determine these infinite-volume quantities.

It now remains to relate the K matrices to the physical three-particle amplitude. This is done by using $\mathcal{M}_{3,L}^{(u,u)}$ to derive an integral equation. To do so requires explicit definitions for the remaining quantities appearing in eq. (6.76):

$$\mathcal{D}^{(u,u)} \equiv -\frac{1}{1 + \mathcal{M}_{2,L}G}\mathcal{M}_{2,L}G\mathcal{M}_{2,L}(2\omega L^3)\,, \tag{5.11}$$

$$\mathcal{L}_L^{(u)} \equiv \left[\frac{F}{2\omega L^3}\right]^{-1} F_3\,, \tag{5.12}$$

$$\mathcal{R}_L^{(u)} \equiv F_3\left[\frac{F}{2\omega L^3}\right]^{-1}. \tag{5.13}$$

With these in hand, the derivation of the integral equations follows in two steps. First one notes that in definition of $\mathcal{M}_{3,L}^{(u,u)}$ the external kinematics are treated asymmetrically, as indicated by the (u,u) superscript. As discussed in refs. [16, 17], and recalled in section C.2, this is corrected by a symmetrizing step in which one combines the matrix with appropriate spherical harmonics to obtain a function of the external momenta, and then sums over separate permutations of the initial and final momenta. We denote this combination by

$$\mathcal{M}_{3,L}(P) \equiv \mathcal{S}\Big[\mathcal{M}_{3,L}^{(u,u)}(P)\Big]\,. \tag{5.14}$$

The quantity on the left-hand side is a symmetric function of the three incoming and three outgoing momenta, and thus does not have the (u,u) superscript.

The second step is to formally take an ordered double limit in which $\mathcal{M}_{3,L}(P)$ becomes the physical scattering amplitude

$$\mathcal{M}_3(E_3^*) = \lim_{\epsilon\to 0^+}\lim_{L\to\infty} \mathcal{M}_{3,L}(E+i\epsilon, \boldsymbol{P})\,. \tag{5.15}$$

In this definition, the energy is made slightly complex so that the $L\to\infty$ limit is well-defined. The limit can be directly applied to the known functions F and G and, after sending $\epsilon\to 0$, this leads to integral equations relating $\mathcal{K}_2$ and $\mathcal{K}_{\mathrm{df},3}$ to the scattering amplitude. These integral equations are given explicitly in ref. [17], and solved in certain approximations in refs. [128, 134, 210, 211]. We give the explicit forms of the integral equations for the three-neutron system in section 6.4.7 below.

5.4 Formalism for three spin-half particles

In the following subsections, we present the extension of the formalism reviewed above to three identical spin-1/2 particles. The section is divided into four subsections. First, in section 5.4.1, we introduce the different bases of spin states required to derive and express our final result. Then, in section 5.4.2, we work through each of the building blocks mentioned for spin-0 particles above, and explain how these quantities are modified for the case of spin-1/2 particles. This allows us to efficiently summarize the new derivation, first, in section 5.4.3,

for the simplest contributing classes of diagrams, and then, in section 5.4.3, extending to all orders. The final result in then presented in the following section, section 5.5.

5.4.1 Three-body spin states in a relativistic formalism

We begin with a discussion of the construction of spin states in a relativistic framework, and the transformation properties of such states under Lorentz boosts. An extended discussion on this can be found, e.g., in ref. [212].

We start by considering the states of a particle at rest, with mass m, spin s and azimuthal component m_s. The states are denoted by $|s\, m_s\rangle$ where, as usual, we take $\hat{z}$ as the quantization axis. These states transform in the usual way under a general rotation R,

$$U(R)\,|s\, m_s\rangle = |s\, m_s'\rangle\, \mathcal{D}^{(s)}_{m_s', m_s}(R)\,, \tag{5.16}$$

where $U(R)$ is the unitary operator corresponding to R, $\mathcal{D}^{(s)}_{m_s', m_s}(R)$ is the Wigner matrix for angular momentum s, and there is an implicit sum over m_s'. We then construct states with nonzero momentum $\boldsymbol{p}$ as

$$|\boldsymbol{p}, s\, m_s\rangle = U(L(\boldsymbol{\beta}_p))\,|s\, m_s\rangle\,, \tag{5.17}$$

where $L(\boldsymbol{\beta}_p)$ is a pure boost with velocity $\boldsymbol{\beta}_p = \boldsymbol{p}/\omega_p$, with $\omega_p = \sqrt{\boldsymbol{p}^2 + m^2}$, such that the boosted state has four-momentum $p^\mu = (\omega_p, \boldsymbol{p})$. In this way, $|\boldsymbol{p}, s\, m_s\rangle$ is defined unambiguously without specifying a quantization axis in the moving frame. This is referred to as the standard basis and corresponds in the spin-1/2 case precisely to the state with the spinor $u(\boldsymbol{p}, m_s)$.

The boost in eq. (5.17) can be represented as

$$L(\boldsymbol{\beta}_p) = R(\theta_p, \hat{\boldsymbol{n}}_p) \cdot L(\beta_p \hat{\boldsymbol{z}}) \cdot R(\theta_p, \hat{\boldsymbol{n}}_p)^{-1}, \tag{5.18}$$

where $R(\theta_p, \hat{\boldsymbol{n}}_p)$ is a rotation that takes a vector in the z-direction to point along the indicated momentum, i.e. $\hat{\boldsymbol{p}} = R(\theta_p, \hat{\boldsymbol{n}}_p)\hat{\boldsymbol{z}}$. Here $\hat{\boldsymbol{n}}_p$ defines the axis about which the rotation is performed and θ_p is the rotation angle. Using this representation, it is straightforward to

determine the transformation of the states in eq. (5.17) under rotations to be

$$U(R)\,|\boldsymbol{p}, s\,m_s\rangle = |R\boldsymbol{p}, s\,m_s'\rangle\,\mathcal{D}^{(s)}_{m_s',m_s}(R)\,. \tag{5.19}$$

This is advantageous as it is equivalent to the transformations of a nonrelativistic spin state.

The transformation of the states in eq. (5.17) under boosts requires some additional discussion. This is due to the fact that the azimuthal component of the spin does not remain unchanged under a generic boost. Consider the transformation

$$U(L(\boldsymbol{\beta}_k))\,|\boldsymbol{p}, s\,m_s\rangle = U(L(\boldsymbol{\beta}_k))U(L(\boldsymbol{\beta}_p))\,|s\,m_s\rangle\,, \tag{5.20}$$

with $\boldsymbol{\beta}_k$ a generic velocity. To work this out, we can use the well-known result that the product of two boosts is equal to the combination of a single boost and a rotation,

$$L(\boldsymbol{\beta}_k)L(\boldsymbol{\beta}_p) = L(\boldsymbol{\beta}')R(\theta, \hat{\boldsymbol{n}}). \tag{5.21}$$

Here $\boldsymbol{\beta}'$ represents the velocity of the resulting boost, while $\hat{\boldsymbol{n}}$ and θ are, respectively, the axis and angle of the required rotation, whose expressions we provide below. It follows that

$$U(L(\boldsymbol{\beta}_k))\,|\boldsymbol{p}, s\,m_s\rangle = |\boldsymbol{p}_k, s\,m_s'\rangle\,\mathcal{D}^{(s)}_{m_s',m_s}(R(\theta, \hat{\boldsymbol{n}})), \tag{5.22}$$

where $\boldsymbol{p}_k$ is the spatial component of the four-momentum resulting from boosting $p^\mu = (\omega_p, \boldsymbol{p})$ with velocity $\boldsymbol{\beta}_k$. Since we only consider spin-1/2 particles in this work, we can represent the Wigner matrices as

$$\mathcal{D}(R(\theta, \hat{\boldsymbol{n}})) = \mathbb{1}\cos\frac{\theta}{2}\; - i\boldsymbol{\sigma}\cdot\boldsymbol{n}\sin\frac{\theta}{2}\,, \tag{5.23}$$

with $\boldsymbol{\sigma}$ a vector composed of the Pauli matrices. Here, and for the remainder of the main text, we suppress the $(s) = (1/2)$ superscript on the Wigner matrices.

It remains to provide the expressions for the axis and angle of the rotation $R(\theta, \hat{\boldsymbol{n}})$,

$$\hat{\boldsymbol{n}} = \frac{\boldsymbol{\beta}_k \times \boldsymbol{\beta}_p}{|\boldsymbol{\beta}_k \times \boldsymbol{\beta}_p|}, \qquad \cos\theta = \frac{(1+\gamma_p+\gamma_k+\gamma')^2}{(1+\gamma_p)(1+\gamma_k)(1+\gamma')} - 1, \tag{5.24}$$

where $\gamma_k = (1-\beta_k^2)^{-1/2}$ and similarly for γ_p, and

$$\gamma' = \gamma_k\gamma_p(1+\boldsymbol{\beta}_p\cdot\boldsymbol{\beta}_k), \tag{5.25}$$

is the Lorentz factor of the boost $L(\boldsymbol{\beta}')$. We also stress that, with these definitions, $\sin\theta \geq 0$. A result that will be useful later is that if $\boldsymbol{\beta}_p$ and $\boldsymbol{\beta}_k$ lie on the same axis, or if one or both vanish, then $\cos\theta = 1$, and the Wigner matrix is just the identity.

With these identities in hand, we are now in position to define two coordinate systems that will play an important role in the derivation that follows and in our statement of the final result for the generalized quantization condition. As noted in the previous section, on-shell three-particle variables are abbreviated by $\{k\ell m\}$, where k is shorthand for the spectator momentum $\boldsymbol{k}$, and ℓm refer to the decomposition of the remaining pair into spherical harmonics *in their CMF*. Here we have the complication of an additional spin degree of freedom for each of the particles. Two natural choices arise for the definition of the quantization axes used to define spin degrees of freedom:

1. The *lab-frame axis*: Label the on-shell four-momenta in the finite-volume frame (also called the lab frame) as k, a and b, so that $k + a + b = P$. Define the spin degree of freedom for all three particles via the boost of eq. (5.17) directly to this frame, i.e. use the states $|\boldsymbol{k}, m_s(\boldsymbol{k})\rangle \otimes |\boldsymbol{a}, m_s(\boldsymbol{a})\rangle \otimes |\boldsymbol{b}, m_s(\boldsymbol{b})\rangle$, where, for example,

$$|\boldsymbol{a}, m_s(\boldsymbol{a})\rangle \equiv U(L(\boldsymbol{\beta}_a))\,|\boldsymbol{0}, m_s\rangle\,. \tag{5.26}$$

   The notation of matching the momentum label on the state $\boldsymbol{a}$ with that inside $m_s(\boldsymbol{a})$ indicates that a single boost is applied starting in the particle's rest frame. As we will see below, this choice of quantization axis occurs most naturally for $\mathcal{K}_{\mathrm{df},3}$.

2. The *dimer-frame* axis: For k, continue to define the spin degree of freedom in the finite-volume frame, i.e. to use the state $|\boldsymbol{k}, m_s(\boldsymbol{k})\rangle$. For a and b, however, boost the four-momenta to the two-particle CMF. In this frame the four-momenta are denoted a^* and b^*, with $|\boldsymbol{a}^*| = |\boldsymbol{b}^*| = q^*_{2,k}$ fixed by the choices of k and P. Define the spin degree of freedom for the $\boldsymbol{a}^*$ state via eq. (5.17),

$$|\boldsymbol{a}^*, m_s(\boldsymbol{a}^*)\rangle = U(L(\boldsymbol{\beta}_{a^*}))|\boldsymbol{0}, m_s\rangle\,, \tag{5.27}$$

and define $|\boldsymbol{b}^*, m_s(\boldsymbol{b}^*)\rangle$ analogously. We stress that the notation matches that introduced above, in that the use of a single boost is represented by the presence of $\boldsymbol{a}^*$ both in the label of the state and as the argument of m_s. The reason for using these states is that the spin indices rotate like NR spinors in the two-particle CMF, as shown in eq. (5.19), and are thus naturally combined with the pair orbital angular momentum ℓ. Altogether, the *dimer-frame* axis convention uses spin indices $m_s(\boldsymbol{k}), m_s(\boldsymbol{a}^*), m_s(\boldsymbol{b}^*)$. This choice occurs naturally for $\mathcal{K}_2$, and for the kinematic function F.

To relate these two choices we need to boost the lab-frame axis states for the dimer to their CMF,

$$|\boldsymbol{a}^*, m_s(\boldsymbol{a})\rangle \equiv U(L(-\boldsymbol{\beta}_{P-k}))\,|\boldsymbol{a}, m_s(\boldsymbol{a})\rangle\ , \tag{5.28}$$

and similarly for $|\boldsymbol{b}^*, m_s(\boldsymbol{b})\rangle$, where $\boldsymbol{\beta}_{P-k} = (\boldsymbol{P}-\boldsymbol{k})/(E-\omega_{\boldsymbol{k}})$. Here we anticipate that the spin indices after boosting do not match those of the state $|\boldsymbol{a}^*, m_s(\boldsymbol{a}^*)\rangle$ by using $\boldsymbol{a}$, rather than $\boldsymbol{a}^*$, as the argument of m_s in $|\boldsymbol{a}^*, m_s(\boldsymbol{a})\rangle$. The relation between spin indices is obtained using

$$\begin{aligned}
|\boldsymbol{a}^*, m_s(\boldsymbol{a})\rangle &= U(L(-\boldsymbol{\beta}_{P-k}))U(L(\boldsymbol{\beta}_a))|\boldsymbol{0}, m_s\rangle\,, &(5.29)\\
&= U(L(\boldsymbol{\beta}_{a^*}))U(R_a)|\boldsymbol{0}, m_s\rangle\,, &(5.30)\\
&= |\boldsymbol{a}^*, m_s'(\boldsymbol{a}^*)\rangle\,\mathcal{D}(R_a)_{m_s' m_s}\,. &(5.31)
\end{aligned}$$

To obtain the first line we have used the definition of $|\boldsymbol{a}, m_s(\boldsymbol{a})\rangle$. We have then used the relation between boosts and rotations, eq. (5.21), to express $|\boldsymbol{a}^*, m_s(\boldsymbol{a})\rangle$ as a rotation of $|\boldsymbol{a}^*, m_s(\boldsymbol{a}^*)\rangle$. Here $R_a = R(\theta_a, \hat{\boldsymbol{n}}_a)$ is defined via eqs. (5.24) and (5.25) with the replacements

$$\boldsymbol{\beta}_p \to \boldsymbol{\beta}_a = \frac{\boldsymbol{a}}{\omega_a}\,, \quad \text{and} \quad \boldsymbol{\beta}_k \to -\boldsymbol{\beta}_{P-k} = -\frac{\boldsymbol{P}-\boldsymbol{k}}{E-\omega_k}\,. \tag{5.32}$$

Detailed expressions for R_a, and the corresponding rotation for b, are given below.

For both of the coordinate systems summarized above, the final step is to project the dimer-pair to definite orbital angular momentum, always using the quantization axis in the two-particle CMF. As a result, the orbital-angular momentum and spin axes are aligned in

the dimer-frame convention, but not in the lab-frame convention. In addition, as discussed below in sections 5.4.2 and 5.5.3, a better choice is to project onto pair total spin (0 or 1 for two spin-half particles). This, together with the antisymmetry of the three-neutron state, and parity, decouples the even and odd sectors of orbital angular momentum for infinite-volume quantities.

5.4.2 Modifications to the RFT building blocks

We now summarize the modifications to the various quantities entering the generalized RFT formalism. As we proceed, we provide some intuition regarding these changes, leaving a more complete explanation to the derivation section below, section 5.4.3.

$\mathcal{K}_{\text{df,3}}$

As we describe in section 5.6, the three-particle K-matrix is most naturally expressed using spin components defined with respect to the lab-frame axis, since the spin components correspond to those of Dirac spinors. In particular, we are led to consider

$$\left[\mathcal{K}_{\text{df,3}}^{\mathsf{lab}}\right]_{\boldsymbol{m}_s',\boldsymbol{m}_s} = \mathcal{K}_{\text{df,3}}^{\mathsf{lab}}\Big(\boldsymbol{k}', m_s(\boldsymbol{k}'); \boldsymbol{a}', m_s(\boldsymbol{a}'); \boldsymbol{b}', m_s(\boldsymbol{b}')\Big|\boldsymbol{k}, m_s(\boldsymbol{k}); \boldsymbol{a}, m_s(\boldsymbol{a}); \boldsymbol{b}, m_s(\boldsymbol{b})\ \Big)\,, \quad (5.33)$$

where, on the left-hand side, we have collected the spin labels as subscripts, using the shorthand

$$\boldsymbol{m}_s' = \Big(m_s(\boldsymbol{k}'), m_s(\boldsymbol{a}'), m_s(\boldsymbol{b}')\Big)\,, \qquad \boldsymbol{m}_s = \Big(m_s(\boldsymbol{k}), m_s(\boldsymbol{a}), m_s(\boldsymbol{b})\Big)\,. \quad (5.34)$$

For the quantization condition, however, it turns out to be most convenient to use spin components defined with the dimer-frame axis, as we discuss below. In terms of explicit coordinates, this is simply given by

$$[\mathcal{K}_{\text{df,3}}]_{\boldsymbol{m}_s'^*,\boldsymbol{m}_s^*} \;=\; \mathcal{K}_{\text{df,3}}\Big(\boldsymbol{k}', m_s(\boldsymbol{k}'); \boldsymbol{a}', m_s(\boldsymbol{a}'^*); \boldsymbol{b}', m_s(\boldsymbol{b}'^*)\Big|\boldsymbol{k}, m_s(\boldsymbol{k}); \boldsymbol{a}, m_s(\boldsymbol{a}^*); \boldsymbol{b}, m_s(\boldsymbol{b}^*)\Big)\,, \quad (5.35)$$

where we have introduced a second set of abbreviated spin indices, analogous to eq. (5.34) above, but defined in the dimer-axis frame:

$$\boldsymbol{m}_s'^{*} = \Big(m_s(\boldsymbol{k}'), m_s(\boldsymbol{a}'^{*}), m_s(\boldsymbol{b}'^{*})\Big)\,, \qquad \boldsymbol{m}_s^{*} = \Big(m_s(\boldsymbol{k}), m_s(\boldsymbol{a}^{*}), m_s(\boldsymbol{b}^{*})\Big)\,. \tag{5.36}$$

The relation between these two choices can be worked out by repeated use of eq. (5.31). It is given by a rotation in spin space for fixed values of the momenta,

$$[\mathcal{K}_{\mathrm{df},3}]_{\boldsymbol{m}_s'^{*},\boldsymbol{m}_s^{*}} \equiv \mathcal{D}^{(k',a')\dagger}_{\boldsymbol{m}_s'^{*}\boldsymbol{m}_s''} \left[\mathcal{K}^{\mathsf{lab}}_{\mathrm{df},3}\right]_{\boldsymbol{m}_s'',\boldsymbol{m}_s'''} \mathcal{D}^{(k,a)}_{\boldsymbol{m}_s'''\boldsymbol{m}_s^{*}}\,, \tag{5.37}$$

where we have used shorthand for the change-of-basis matrices. For example, the right-most matrix is given by

$$\mathcal{D}^{(k,a)}_{\boldsymbol{m}_s'''\boldsymbol{m}_s^{*}} = \delta_{m_s'''(\boldsymbol{k})m_s(\boldsymbol{k})}\mathcal{D}(R_a^{-1})_{m_s'''(\boldsymbol{a})m_s(\boldsymbol{a}^{*})}\mathcal{D}(R_b^{-1})_{m_s'''(\boldsymbol{b})m_s(\boldsymbol{b}^{*})}\,, \tag{5.38}$$

where the rotation R_a is defined using eqs. (5.24) and (5.25), with the replacements of eq. (5.32). The explicit definition is $R_a = R(\theta, \hat{\boldsymbol{n}})$ with

$$\begin{gathered}\hat{\boldsymbol{n}} = -\frac{\boldsymbol{\beta}_{P-k}\times\boldsymbol{\beta}_a}{|\boldsymbol{\beta}_{P-k}\times\boldsymbol{\beta}_a|}, \qquad \cos\theta = \frac{(1+\gamma_a+\gamma_{P-k}+\gamma')^2}{(1+\gamma_a)(1+\gamma_{P-k})(1+\gamma')} - 1\,, \\ \gamma' = \gamma_{P-k}\gamma_a(1-\boldsymbol{\beta}_{P-k}\cdot\boldsymbol{\beta}_a)\,.\end{gathered} \tag{5.39}$$

R_b is defined in the same way but with $\boldsymbol{\beta}_a \to \boldsymbol{\beta}_b$.

To convert this to the matrix entering the quantization condition, we apply the same steps that are used in the spin-zero formalism. The dimers (defined with momenta $\boldsymbol{a}$ and $\boldsymbol{b} = \boldsymbol{P} - \boldsymbol{k} - \boldsymbol{a}$ in the initial state and $\boldsymbol{a}'$ and $\boldsymbol{b}' = \boldsymbol{P} - \boldsymbol{k}' - \boldsymbol{a}'$ in the final state) are projected to definite orbital angular momentum in their two-particle CMFs. This is done via integration with a spherical harmonic and we express the action as a projection,

$$\mathcal{P}^{\hat{\boldsymbol{a}}^{*}}_{\ell m} \circ f(\boldsymbol{k},\boldsymbol{a},\boldsymbol{b}) = \frac{1}{4\pi}\int d\Omega_{\hat{\boldsymbol{a}}^{*}} Y^{*}_{\ell m}(\hat{\boldsymbol{a}}^{*}) f^{*}(\boldsymbol{k},\boldsymbol{a}^{*})\,, \tag{5.40}$$

for a generic function f. Here $\boldsymbol{a}^{*}$ is the spatial part of the four-momentum that results from boosting $a^{\mu} = (\omega_a, \boldsymbol{a})$ with boost velocity $\boldsymbol{\beta}_k = -(\boldsymbol{P}-\boldsymbol{k})/(E-\omega_k)$ and f^{*} is just f expressed

in terms of the new coordinates as shown. (The dependence on $\boldsymbol{b}^* = -\boldsymbol{a}^*$ is redundant and is thus omitted within f^*.) We then define

$$[\mathbf{K}_{\mathrm{df},3}]_{k'\ell'm'\boldsymbol{m}'^*_s;k\ell m\boldsymbol{m}^*_s} \equiv i[\mathcal{P}^{\hat{\boldsymbol{a}}'^*}_{\ell'm'}]^\dagger \circ \mathcal{P}^{\hat{\boldsymbol{a}}^*}_{\ell m} \circ \mathcal{K}_{\mathrm{df},3}(\cdots)\,, \tag{5.41}$$

where the $(\cdots)$ on the right-hand side indicates the full set of arguments shown in the first line of eq. (5.35) above. The momenta $k' = \boldsymbol{k}'$ and $k = \boldsymbol{k}$ are expressed as indices on the left-hand side, and it is understood that these are in the finite-volume set. Here we have also introduced the boldface notation $\mathbf{K}_{\mathrm{df},3}$ to represent the matrix version of $\mathcal{K}_{\mathrm{df},3}$ within the generalized spin formalism. The factor of i on the right-hand side of eq. (5.41) is for convenience.[6]

We now return to the issue of why the dimer-frame axis is the more natural for the quantization condition. The point is that we wish to be able to combine orbital and spin angular momenta of the dimer in a simple way, and this is only possible if both are defined with respect to the same frame. Since orbital angular momenta are defined in the dimer CMF, the spin variables need to be as well, and this corresponds to using the dimer-frame axis. We stress that the spin rotation in eq. (5.37) and the partial-wave projection in eq. (5.40) do not commute, so there is not a simple relation between the matrix forms of $\mathcal{K}_{\mathrm{df},3}$ in the dimer- and lab-frame axes. In particular if the three-body K-matrix is parametrized in the lab frame, then the angular momentum projection of eq. (5.41) will include an integral over the angular dependence appearing inside the Wigner-D matrices.

G

Next we consider the kinematic switch function, denoted by G. The defining property of G is that the spectator particle (and thus also the spectator momentum) differs between the left and right side of the insertion.

As illustrated in the central portion of figure 5.1(c), G is defined with an initial state

[6] The use of boldface for matrix quantities entering the quantization condition follows the conventions of ref. [37].

containing the spectator momentum k and the scattering pair (with momenta p and $b_{pk} = P - p - k$), transitioning to a final state containing spectator p and scattering pair (with momenta k and b_{pk}). Henceforth, in this subsection we will abbreviate b_{pk} by b, in order to avoid a proliferation of subscripts; this should not be confused with the momentum labeled b in figure 5.1(c). The exact definition makes use of momentum coordinates in the two-particle CMF of the scattering pair, both before and after the switch. Specifically we define $\boldsymbol{k}_p^*$ [$\boldsymbol{p}_k^*$] as the spatial part of the four-momentum arising from boosting $k^\mu = (\omega_k, \boldsymbol{k})$ [$p^\mu = (\omega_p, \boldsymbol{p})$] with boost velocity $-\boldsymbol{\beta}_{P-p}$ [$-\boldsymbol{\beta}_{P-k}$]. In addition to the momenta, we require the two-particle CMF energy $E_{2,k}^*$, defined in eq. (5.2), and the analogous quantity $E_{2,p}^*$ obtained by replacing k with p. From these one can define the on-shell two-particle CMF momentum $q_{2,k}^*$ and $q_{2,p}^*$ using eq. (5.6).

We are now ready to give the lab-frame axis version of G for three spin-half particles:

$$[\mathbf{G}^{\mathsf{lab}}]_{p\ell' m' \boldsymbol{m}'_s; k\ell m \boldsymbol{m}_s}(E, \boldsymbol{P}, L) \equiv -\delta_{m'_s(\boldsymbol{p}), m_s(\boldsymbol{p})} \delta_{m'_s(\boldsymbol{k}), m_s(\boldsymbol{k})} \delta_{m'_s(\boldsymbol{b}), m_s(\boldsymbol{b})} \times \frac{i}{4\omega_p \omega_k L^6} \frac{H(\boldsymbol{p}) H(\boldsymbol{k})}{b^2 - m^2} \frac{4\pi \mathcal{Y}_{\ell' m'}(\boldsymbol{k}_p^*) \mathcal{Y}_{\ell m}^*(\boldsymbol{p}_k^*)}{q_{2,p}^{*\ell'} \, q_{2,k}^{*\ell}}, \quad (5.42)$$

where $\mathcal{Y}_{\ell m}(\boldsymbol{x}) = |\boldsymbol{x}|^\ell Y_{\ell m}(\hat{\boldsymbol{x}})$ is a harmonic polynomial, and

$$b^2 = (E - \omega_k - \omega_p)^2 - (\boldsymbol{P} - \boldsymbol{p} - \boldsymbol{k})^2 . \quad (5.43)$$

The smooth cutoff function $H(\boldsymbol{k})$ was already introduced in eq. (5.5). In the context of three neutrons, we note that the allowed support for the H function is set by the left-hand cut arising from t-channel pion exchange in the two-neutron amplitude. A similar situation is discussed in refs. [91, 121] in the context of the RFT formalism for $K\pi\pi$ and $KK\pi$, see also ref. [213]. Relative to the spin-zero G function discussed in section 5.3 [see the explanation above eq. (5.7)], the definition (5.42) contains an extra factor of $i/(2\omega_p L^3)$, matching the conventions of ref. [37].

There are two key new features relative to the form for spin-zero particles. The first is the overall minus sign. This results from the antisymmetry of the fermionic multi-particle state

or, equivalently, from the anti-commutation of Grassmann variables in evaluating Feynman diagrams. This is discussed in more detail in section 5.4.3 below.

The second new feature is the appearance of a product of Kronecker deltas in the spin components. This encodes the fact that, for spin components defined in the lab frame, G simply acts like an identity matrix in spin space, a point that will be discussed further in section 5.4.3. Strictly speaking this only holds when all three particles are on shell, which is not the case in general: although k and p are on shell by construction, b is not. This is potentially problematic because the lab-frame state $|\boldsymbol{b}, m_s(\boldsymbol{b})\rangle$, given by eq. (5.26), is defined only for on-shell four-momenta. In particular, the boost velocity used to define the state is $\boldsymbol{\beta}_b \equiv \boldsymbol{b}/\omega_b$, even though $b^0 \neq \omega_b$ in general. The resolution to this issue is that all that matters for the derivation of the quantization condition is that the choice of state is correct on shell, i.e. at the pole where $b^2 = m^2$. Choices that differ off shell lead to finite shifts in $\mathcal{K}_{\mathrm{df},3}$, since the differences cancel the pole.

We stress that the Kronecker deltas in eq. (5.42) cannot be written as $\delta_{\boldsymbol{m}_s'\boldsymbol{m}_s}$, because the order of spin components in the compound labels does not match:

$$\boldsymbol{m}_s' = \Big(m_s(\boldsymbol{p}), m_s(\boldsymbol{k}), m_s(\boldsymbol{b})\Big)\,, \qquad \boldsymbol{m}_s = \Big(m_s(\boldsymbol{k}), m_s(\boldsymbol{p}), m_s(\boldsymbol{b})\Big)\,. \tag{5.44}$$

Non-trivial spin structure arises when we transform to the dimer-axis frame. The transformation is similar to that for $\mathcal{K}_{\mathrm{df},3}$ discussed in the previous subsection,

$$\mathbf{G}_{p\ell' m' \boldsymbol{m}_s'^*; k\ell m \boldsymbol{m}_s^*} = \mathcal{D}^{(p,k)\dagger}_{\boldsymbol{m}_s'^*\boldsymbol{m}_s''}\, \mathbf{G}^{\mathsf{lab}}_{p\ell' m' \boldsymbol{m}_s''; k\ell m \boldsymbol{m}_s'''}\, \mathcal{D}^{(k,p)}_{\boldsymbol{m}_s'''\boldsymbol{m}_s^*}\,, \tag{5.45}$$

where $\boldsymbol{m}_s''$ and $\boldsymbol{m}_s'''$ are summed.

The change of basis matrices are given explicitly by

$$\mathcal{D}^{(k,p)}_{\boldsymbol{m}_s'''\boldsymbol{m}_s^*} = \delta_{m_s'''(\boldsymbol{k})m_s(\boldsymbol{k})} \mathcal{D}(R_p^{-1})_{m_s'''(\boldsymbol{p})m_s(\boldsymbol{p}^*)} \mathcal{D}(R_{b_k}^{-1})_{m_s'''(\boldsymbol{b}_k)m_s(\boldsymbol{b}_k^*)}\,, \tag{5.46}$$

$$\mathcal{D}^{(p,k)}_{\boldsymbol{m}_s'''\boldsymbol{m}_s^*} = \delta_{m_s'''(\boldsymbol{p})m_s(\boldsymbol{p})} \mathcal{D}(R_k^{-1})_{m_s'''(\boldsymbol{k})m_s(\boldsymbol{k}^*)} \mathcal{D}(R_{b_p}^{-1})_{m_s'''(\boldsymbol{b}_p)m_s(\boldsymbol{b}_p^*)}\,. \tag{5.47}$$

These depend on a total of four rotations, denoted by R_p, R_{b_k}, R_k and R_{b_p} as shown. Each of the four is induced by relating two successive boosts to a single boost, via eq. (5.21). Thus

all rotations can be expressed according to eq. (5.24). Specifically, we define

$$R_p: \qquad \hat{\boldsymbol{n}} = -\frac{\boldsymbol{\beta}_{P-k} \times \boldsymbol{\beta}_p}{|\boldsymbol{\beta}_{P-k} \times \boldsymbol{\beta}_p|}, \qquad \cos\theta = \frac{(1+\gamma_p+\gamma_{P-k}+\gamma'_{P-k,p})^2}{(1+\gamma_p)(1+\gamma_{P-k})(1+\gamma'_{P-k,p})} - 1\,, \tag{5.48}$$

$$R_k: \qquad \hat{\boldsymbol{n}} = -\frac{\boldsymbol{\beta}_{P-p} \times \boldsymbol{\beta}_k}{|\boldsymbol{\beta}_{P-p} \times \boldsymbol{\beta}_k|}, \qquad \cos\theta = \frac{(1+\gamma_k+\gamma_{P-p}+\gamma'_{P-p,k})^2}{(1+\gamma_k)(1+\gamma_{P-p})(1+\gamma'_{P-p,k})} - 1\,, \tag{5.49}$$

where

$$\gamma'_{P-k,p} = \gamma_{P-k}\gamma_p(1-\boldsymbol{\beta}_{P-k}\cdot\boldsymbol{\beta}_p)\,, \qquad \gamma'_{P-p,k} = \gamma_{P-p}\gamma_k(1-\boldsymbol{\beta}_{P-p}\cdot\boldsymbol{\beta}_k)\,. \tag{5.50}$$

R_{b_k} is defined as for R_p, but with $\boldsymbol{\beta}_p$ replaced by $\boldsymbol{\beta}_b = \boldsymbol{b}/\omega_b$, and γ_p replaced by $\gamma_b = \sqrt{1/(1-\beta_b^2)}$. Similarly, R_{b_p} is defined as for R_k, but with $\boldsymbol{\beta}_p$ replaced by $\boldsymbol{\beta}_b$ and γ_k replaced by γ_b. As noted above, since b is off shell in general, the choice of boost velocities is only unambiguous at the on-shell point. Any off-shell extension choice that is used consistently is sufficient to perform the derivation, and our choice here is to use $\boldsymbol{\beta}_b = \boldsymbol{b}/\omega_b$ rather than, say, $\boldsymbol{b}/b^0$.

F

We next turn to the kinematic function F, which implements the sum-integral difference for a loop involving two of the three-particles. The definition in the lab-axis frame is obtained from the standard form for F for scalar particles by adding Kronecker deltas in spin space,

$$[\mathbf{F}^{\mathsf{lab}}]_{k'\ell'm'\boldsymbol{m}'_s;k\ell m\boldsymbol{m}_s}(E,\boldsymbol{P},L) \equiv \delta_{\boldsymbol{m}'_s\boldsymbol{m}_s}\delta_{k'k}\frac{iH(\boldsymbol{k})}{2\omega_k L^3}\frac{1}{2}\left[\frac{1}{L^3}\sum_{\boldsymbol{a}} - \text{p.v.}\int_{\boldsymbol{a}}\right] \times \frac{4\pi\mathcal{Y}_{\ell'm'}(\boldsymbol{a}^*_k)\mathcal{Y}^*_{\ell m}(\boldsymbol{a}^*_k)}{2\omega_a(b^2-m^2)}\frac{1}{(q^*_{2,k})^{\ell+\ell'}}\,, \tag{5.51}$$

where here the order of the compound spin indices do match, such that we can use

$$\delta_{\boldsymbol{m}'_s\boldsymbol{m}_s} = \delta_{m'_s(\boldsymbol{k})m_s(\boldsymbol{k})}\delta_{m'_s(\boldsymbol{a})m_s(\boldsymbol{a})}\delta_{m'_s(\boldsymbol{b})m_s(\boldsymbol{b})}\,. \tag{5.52}$$

This definition of F differs from that for scalar particles, given in eqs. (22-24) of ref. [16], by a factor of $i/(2\omega_k L^3)$, as well as by the addition of the spin factors, and thus follows the normalization conventions of ref. [37].

The quantities in eq. (5.51) are defined as follows. The four-momentum b is given by $b^\mu = (E - \omega_k - \omega_a, \boldsymbol{P} - \boldsymbol{k} - \boldsymbol{a})$, while the on-shell magnitude $q^*_{2,k}$ is defined in eq. (5.6). Following the usual pattern, $\boldsymbol{a}^*_k$ is the spatial part of the four-momentum resulting from boosting $a^\mu = (\omega_a, \boldsymbol{a})$ with boost velocity $-\boldsymbol{\beta}_{P-k}$. The sum runs over values of $\boldsymbol{a} = 2\pi \boldsymbol{n}_a / L$ where $\boldsymbol{n}_a$ is a three-vector of integers. The notation p.v. indicates a principal value pole prescription, including the possible extensions discussed in ref. [114]. Finally, it is understood that an ultraviolet cutoff must be included to evaluate the sum and integral separately. Any dependence on the cutoff vanishes in the difference as can be shown using the Poisson summation formula. The numerical evaluation of the sum-integral difference is discussed in more detail, e.g., in appendix B of ref. [108] and also in appendix B of ref. [110].

As with G, this quantity must reflect the exchange properties of identical fermions. One aspect of this is the symmetry factor of $1/2$ for the ab loop, which is present exactly as in the spin-zero case. To understand additional consequences, in particular of the antisymmetry, it is useful to transition from the lab-axis frame and dimer-axis frame. However, in this case there is no distinction

$$\mathbf{F} = \mathbf{F}^{\mathsf{lab}} \,. \tag{5.53}$$

This is an important simplification as the change of basis matrices would in fact depend on the summed coordinate. However, since $\mathbf{F}^{\mathsf{lab}}$ is diagonal in spectator momentum, the dimer frame is the same in the initial and final states. As a result the change of basis matrices exactly cancel.

$\mathcal{K}_2$

The final building block is the two-particle K matrix. This quantity is naturally defined in the *dimer-axis frame*, and we discuss only this version of the K matrix. It can be written in a manner analogous to that for scalars, eq. (5.4),

$$[\mathbf{K}_2]_{k'\ell' m' \boldsymbol{m}'^*_s; k\ell m \boldsymbol{m}^*_s}(E, \boldsymbol{P}) = i\delta_{k'k} 2\omega_k L^3 \mathcal{K}_2^{(\ell' m' \boldsymbol{m}'^*_s, \ell m \boldsymbol{m}^*_s)}(E^*_{2,k}) \,, \tag{5.54}$$

with $\mathcal{K}_2^{(\cdots)}(E^*_{2,k})$ on the right-hand side a generalization of the quantity $\mathcal{K}_2^{(\ell)}(E^*_2)$ in eq. (5.4) to the case of spin one-half particles, with the additional factor of $i2\omega_k L^3$ to match the convention in ref. [37]. As above, the superscripts $\boldsymbol{m}^*_s$ and $\boldsymbol{m}'^*_s$ indicate that the spin quantization axis is defined in the two-particle CMF. The role of the spectator here is trivial and the K matrix can be unpacked as

$$\mathcal{K}_2^{(\ell' m' \boldsymbol{m}'^*_s, \ell m \boldsymbol{m}^*_s)}(E^*_{2,k}) = \delta_{m'_s(\boldsymbol{k}) m_s(\boldsymbol{k})}\, \mathcal{K}_2^{[\ell' m' m'_s(\boldsymbol{a}'^*) m'_s(\boldsymbol{b}'^*)],\, [\ell m m_s(\boldsymbol{a}^*) m_s(\boldsymbol{b}^*)]}(E^*_{2,k})\,. \tag{5.55}$$

In words, the incoming state is labeled with orbital angular momentum ℓ, m together with spin components $m_s(\boldsymbol{a}^*)$ and $m_s(\boldsymbol{b}^*)$, and the outgoing state carries the same set with primes as indicated.

To parametrize $\mathcal{K}_2$, it is more common to work in the basis which diagonalizes the total spin of the dimer, s. This can take the values $s = 0$ (spin singlet) or $s = 1$ (spin triplet). Enforcing antisymmetry, the singlet can only couple to even values of ℓ, while the triplet couples only to odd values. Although not mentioned above, these constraints apply also to $\mathcal{K}_{\mathrm{df},3}$, F and G.

In general, s and ℓ are not conserved by two-particle interactions, and one should convert to the basis in which the total dimer angular momentum, j, and its azimuthal component, μ_j, are diagonal. One simplification here, however, is that there is no mixing between $s = 0$ and 1 states for two identical fermions, because their parities, given by $(-1)^\ell$, are opposite. Furthermore, if $s = 0$ then $j = \ell$ and thus ℓ is also conserved (and takes only even values). On the other hand, if $s = 1$, then $j = \ell + 1$, ℓ, $\ell - 1$, so that, given that ℓ is odd, each odd value of j arises from only a single value of ℓ, while for all even values of j except zero there are two choices of ℓ.

We now describe in detail the conversions between bases. The first step is to convert to the basis of total dimer spin s and azimuthal component m:

$$\begin{aligned}\mathcal{K}_2^{(s,\ell',m',\mu'_s,\ell,m,\mu_s)}\delta_{s's} = \sum_{m'_s(\boldsymbol{a}'^*), m'_s(\boldsymbol{b}'^*), m_s(\boldsymbol{a}^*), m_s(\boldsymbol{b}^*)} &\left\langle s', \mu'_s \middle| {}^1\!/_2\ m'_s(\boldsymbol{a}'^*),\ {}^1\!/_2\ m'_s(\boldsymbol{b}'^*) \right\rangle \\ &\times \mathcal{K}_2^{[\ell' m' m'_s(\boldsymbol{a}'^*) m'_s(\boldsymbol{b}'^*)],\, [\ell m m_s(\boldsymbol{a}^*) m_s(\boldsymbol{b}^*)]} \left\langle {}^1\!/_2\ m_s(\boldsymbol{a}^*),\ {}^1\!/_2\ m_s(\boldsymbol{b}^*) \middle| s, \mu_s \right\rangle, \end{aligned} \tag{5.56}$$

where the angle-bracketed quantities are standard Clebsch-Gordan coefficients, and the conservation of s is enforced by the Kronecker delta on the left-hand side. From here one can reach the final basis via

$$\mathcal{K}_2^{(j,s,\ell',\ell)}\ \delta_{j'j}\delta_{\mu'_j\mu_j} = \sum_{\mu_s,\mu'_s} \Big\langle j', \mu'_j | \ell' m', s\mu'_s \Big\rangle \mathcal{K}_2^{(s,\ell',m',\mu'_s,\ell,m,\mu_s)} \Big\langle \ell m, s\mu_s | j, \mu_j \Big\rangle \,. \tag{5.57}$$

Then one can write[7]

$$[\mathcal{K}_2(E^*_{2,k})^{-1}]^{(j,s,\ell',\ell)} = [\mathcal{M}_2(E^*_{2,k})^{-1}]^{(j,s,\ell',\ell)} + \delta_{\ell',\ell} \frac{|p|\Big(1 - H(\boldsymbol{k})\Big) + ip}{16\pi E^*_{2,k}}\bigg|_{p=q^*_{2,k}} , \tag{5.58}$$

with subthreshold analytic continuation following from $-ip \to |p|$ for $p^2 < 0$. Here $\mathcal{M}_2(E^*_{2,k})$ is the standard scattering amplitude.

The parametrization of the resulting scattering amplitudes depends on whether there is mixing between different values of ℓ. The simplest case is $s = 0$, which, as discussed above, always involves only a single channel with even $\ell = j$. Then we write the scattering amplitude in terms of a phase shift

$$[\mathcal{M}_2(E^*_{2,k})^{-1}]^{(j,s=0,\ell',\ell)} + \delta_{\ell',\ell} \frac{ip}{16\pi E^*_{2,k}}\bigg|_{p=q^*_{2,k}} = \delta_{\ell',\ell} \frac{q^*_{2,k} \cot \delta^{(j=\ell,s=0)}(q^*_{2,k})}{16\pi E^*_{2,k}} \,. \tag{5.59}$$

This, in turn, can be parametrized with an effective range expansion

$$p^{2\ell+1} \cot \delta^{(j=\ell,s=0)}(p) = -\frac{1}{a_0} + \sum_{n=1}^{\infty} a_n (p^2)^n \,. \tag{5.60}$$

Two-channel mixing is possible for $s = 1$, but only for $j = 2, 4, 6, \ldots$, for which both $\ell = j \pm 1$ are possible. In such cases one can parametrize the phase shift using, for example, the Blatt-Biedenharn parametrization [214, 215]. For $j = 0$ and 1, however, which arise from $\ell = 1$, there is only a single channel and one can proceed as for $s = 0$.

5.4.3 Derivation

In the previous section we have provided the generalization of the four key quantities required to develop the finite-volume formalism for three identical spin-1/2 particles. The generalized

[7] This form assumes that the generalization of the p.v. prescription to include an "$I_{\rm PV}$ term" is not being made. The generalization to this case can be easily determined from ref. [114].

version for each of the four is written in bold face, in particular $\mathbf{K}_{\text{df},3}$ [section 5.4.2], $\mathbf{G}$ [section 5.4.2], $\mathbf{F}$ [section 5.4.2] and $\mathbf{K}_2$ [section 5.4.2]. In this section, we show how, using these building blocks, the derivation of refs. [16,17] can be extended to apply to identical spin-1/2-particle systems. For simplicity, we use the language of three neutrons in the following, but emphasize that the formalism we obtain holds for any system of three spin-1/2 particles.

The derivation proceeds in several steps. First, in section 5.4.3, we define an appropriate finite-volume correlator, the poles in which give the finite-volume energies. Next, in section 5.4.3, we analyze the three classes of Feynman diagrams that enter into the skeleton expansion of the correlator. Third, in section 5.4.3, we explain how the results generalize to all orders. We also present the result for a related quantity, the finite-volume unsymmetrized scattering amplitude. These ingredients are then used in the following section, section 5.5, to determine the quantization condition and the relation between $\mathbf{K}_{\text{df},3}$ and the infinite-volume scattering amplitude. This basic workflow is analogous to the presentation of ref. [37], in which the formalism of refs. [16, 17] was generalized to describe all three-pion states with generic isospin.

Finite-volume correlator

The Minkowski-space finite-volume correlation function is defined as

$$C_L(P) \equiv \int_L d^4x \, e^{iP\cdot x} \, \langle \mathrm{T}\mathcal{O}(x)\mathcal{O}^\dagger(0)\rangle_L \,, \tag{5.61}$$

where $P \cdot x = Ex^0 - \boldsymbol{P}\cdot\boldsymbol{x}$, and

$$\int_L d^4x \equiv \int dx^0 \int_L d^3\boldsymbol{x} \,, \tag{5.62}$$

is an integral over the infinite time direction and three finite spatial directions. The operators $\mathcal{O}^\dagger(0)$ and $\mathcal{O}(x)$ respectively create and annihilate three-neutron states. They are assumed to have support for a finite range of times around the nominal position of the operator, and can either be local or delocalized in space. In eq. (6.3), T indicates time ordering, $P^\mu = (E, \boldsymbol{P})$ is a four-vector containing the total energy and momentum, and the subscript L indicates

that the quantity is evaluated in a finite cubic spatial volume (with periodicity L in each of the three spatial directions).

It will be useful for the following derivation to give explicit definitions of the operators $\mathcal{O}$ and $\mathcal{O}^\dagger$. Let $\mathcal{N}_\alpha(x)$ denote a single-nucleon spin-1/2 field with Dirac index α. We first define the momentum-space operators

$$\widetilde{\mathcal{O}}^\dagger_{r_1,r_2,r_3}(p_1,p_2,p_3) = \prod_{i=1}^{3} \left\{ u^{r_i}_{\alpha_i}(\boldsymbol{p}_{\alpha_i}) \int_L d^4x_i \, e^{-ip_i\cdot x_i} \overline{\mathcal{N}}_{\alpha_i}(x_i) \right\} , \tag{5.63}$$

$$\widetilde{\mathcal{O}}_{r_1,r_2,r_3}(p'_1,p'_2,p'_3) = \prod_{i=1}^{3} \left\{ \overline{u}^{r_i}_{\alpha_i}(\boldsymbol{p}'_{\alpha_i}) \int_L d^4x_i \, e^{ip'_i\cdot x_i} \mathcal{N}_{\alpha_i}(x_i) \right\} , \tag{5.64}$$

where each field on the right-hand side is contracted with a spinor $\overline{u}^{r_i}_{\alpha_i}(\boldsymbol{p}'_{\alpha_i})$ or $u^{r_i}_{\alpha_i}(\boldsymbol{p}_{\alpha_i})$, with r_i indicating a specific spin component. We then obtain $\mathcal{O}(x)$ by integrating over momenta, weighted with a "form factor" that depends on the precise form of the operator. In particular, the Fourier transform of $\mathcal{O}(x)$ is given by

$$\int_L d^4x \, e^{iP\cdot x} \, \mathcal{O}(x) = \int_{p'_1,\,L} \int_{p'_2,\,L} \int_{p'_3,\,L} \sum_{r_1,r_2,r_3} \widetilde{\mathcal{O}}_{r_1,r_2,r_3}(p'_1,p'_2,p'_3) \overline{f}_{r_1r_2r_3}(p'_1,p'_2,p'_3) \, , \tag{5.65}$$

where

$$\overline{f}_{r_1r_2r_3}(p'_1,p'_2,p'_3) = 2\pi\delta(E - p'^0_1 - p'^0_2 - p'^0_3)\, L^3 \delta_{\boldsymbol{p}'_1+\boldsymbol{p}'_2+\boldsymbol{p}'_3,\boldsymbol{P}}\, f_{r_1r_2r_3}(p'_1,p'_2,p'_3) \, . \tag{5.66}$$

In eq. (5.65), we are using the finite-volume version of the momentum-space integral,

$$\int_{p,\,L} = \frac{1}{L^3} \sum_{\boldsymbol{p}} \int \frac{dp^0}{2\pi} \, , \tag{5.67}$$

in which the sum runs over all values of $\boldsymbol{p} = (2\pi/L)\boldsymbol{n}$, where $\boldsymbol{n}$ is a three-vector of integers ($\boldsymbol{n} \in \mathbb{Z}^3$). We refer to this set of momenta as the "finite-volume set." In eq. (5.66), the first two factors on the right-hand side enforce four-momentum conservation, while f is a smooth function of momenta that depends on the form of $\mathcal{O}(x)$. The detailed form of f is not important. However, its p_i^0 dependence must ensure that $\mathcal{O}(x)$ is localized in time, as described above.

Two technical points deserve mention. First, in eq. (6.3), the time ordering applies to the positions of all the single-particle operators contained in the composite operators $\mathcal{O}$ and $\mathcal{O}^\dagger$,

and not just to the component x_0. In particular, all possible orderings of the $\mathcal{N}$ and $\overline{\mathcal{N}}$ fields arise in general, since these are individually integrated over all positions. The ordering of interest, in which three neutrons are first created, and then later destroyed, will be picked out by the choice of E, as discussed shortly. Second, we stress that $\mathcal{N}$ and $\overline{\mathcal{N}}$ are anticommuting Grassmann fields and that time-ordering is also subject to the usual Grassmann definition, e.g. $\mathrm{T}\{\mathcal{N}(x^0)\mathcal{N}(y^0)\} = -\mathcal{N}(y^0)\mathcal{N}(x^0)$ for $x^0 < y^0$. The anticommuting property plays an important role in the formalism, as already noted above in the result for $\mathbf{G}$, eq. (5.42).

In this work we assume that $C_L(P)$ can be represented as an all-orders Feynman diagrammatic expansion in a relativistic effective field theory (EFT) in which the degrees of freedom are neutrons, protons and pions. We make no restrictions on the form or strength of the interaction vertices, other than requiring that they respect Lorentz invariance, baryon number, and electric charge conservation. We thus expect that the resulting formalism applies nonperturbatively. Close to the three-neutron threshold, the pions could be integrated out, leading to a pionless EFT for nucleons, but we do not need to assume that we are in this regime. What we do assume is that the total CMF energy, $E_3^* = \sqrt{P^2} = \sqrt{E^2 - \boldsymbol{P}^2}$, lies in a regime such that the only on-shell states are those involving three neutrons. In particular, for isosymmetric QCD we require that

$$\sqrt{4m_N^2 - m_\pi^2} + m_N < E_3^* < 3m_N + m_\pi \,. \tag{5.68}$$

The upper limit is required to avoid $3N + \pi$ on-shell states, while the lower limit avoids the left-hand cut in two-to-two subprocesses due to single-pion exchange. The latter restriction is necessary because, as explained in the following, the non-analyticity in $\mathbf{K}_2$ from the left-hand cut leads to power-law finite-volume dependence. We stress that, although proton degrees of freedom are present in the EFT, they cannot appear in on-shell intermediate states in the three-neutron correlator for the kinematic regime of eq. (5.68). Instead, they appear in virtual intermediate states—along with pions that lead, for example, to the dressing of the neutron propagator—as well as in Bethe-Salpeter kernels.

Our aim in the following is to keep track of all power-like dependence of $C_L(P)$ on L

(typically of the form of powers of $1/L$), while neglecting dependence falling faster than any power of $1/L$. With a slight abuse of nomenclature, we will refer to the latter as "exponentially suppressed". Indeed, this category includes exponentially-suppressed scaling of the form $e^{-m_\pi L}$, where m_π is the mass of the lightest degree of freedom in the system, e.g. the pion in QCD, and generally not the mass of the spin-1/2 particle, which we denote m in the following. For large enough L, such exponentially-suppressed terms are numerically smaller than power-law effects.

The key difference between contributions to the finite- and infinite-volume correlators is that the former involve sums over finite-volume momenta, while the latter involve integrals. Local vertices are unchanged. As discussed in ref. [16], one can use the Poisson summation formula to argue that the difference between finite-volume sums and infinite-volume integrals is exponentially suppressed unless the summand/integrand is singular. This can happen either because there is an on-shell intermediate state, or because of a non-analyticity in the vertex functions such as the above-mentioned left-hand cut. Since in the following derivation we include the effects only of three-neutron intermediate states, we are led to the same requirements on E_3^* as given in eq. (5.68). We stress that the localization of $\mathcal{O}$ in time plays an important role here, for it implies that states consisting, say, of two neutrons and an antineutron, cannot propagate forward in time for an arbitrarily long extent, and thus cannot lead to on-shell singularities.

The diagrammatic expansion involves the operators $\mathcal{O}$ and $\mathcal{O}^\dagger$ as well as the above-mentioned vertices. Simple examples are shown in figure 5.1. The neutron propagators in these diagrams are given by

$$\Delta_{L,\alpha\beta}(p) = \int_L d^4x\, e^{ip\cdot x}\, \langle \mathrm{T}\mathcal{N}_\alpha(x)\overline{\mathcal{N}}_\beta(0)\rangle_L\,. \tag{5.69}$$

They are thus fully dressed, and include loop diagrams that are not shown explicitly. The subscript L on the expectation value refers to the L-dependence that arises from the spatial periodicity, which implies that $\boldsymbol{p}$ must be drawn from the finite-volume set, and that the spatial parts of loop momenta must be summed. However, in the vicinity of the single-

particle pole at $p^2 = m^2$, all loop contributions are far off shell, so that L-dependence is exponentially suppressed, and we can write [216]

$$\Delta_{L,\alpha\beta}(p) = i\frac{(\not{p} + m)_{\alpha\beta}}{p^2 - m^2 + i\epsilon} + R_{L,\alpha\beta}(p)\,. \tag{5.70}$$

Here the first term is L-independent, while the second term is analytic for p^0 below the threshold to create a multi-particle state (a nucleon+pion state in the case of isospin-symmetric QCD). We have assumed a normalization of the fields $\mathcal{N}$ and $\overline{\mathcal{N}}$ so as to give unit residue at the pole of the dressed propagator, leading to a simple factor of $\not{p} + m$ in the numerator.

One can apply a final simplification to the numerator of the L-independent part of the propagator by setting p^0 to its on-shell value: $p^0 = \omega_p = \sqrt{\boldsymbol{p}^2 + m^2}$. This is justified since the difference cancels the pole, leading to an additional analytic contribution that can be absorbed by a redefinition of $R_{L,\alpha\beta}(p)$. This step is useful as the on-shell version of the numerator is equal to a sum of spinors,

$$(\not{p} + m)_{\alpha\beta}\Big|_{p^0=\omega_p} = \sum_r u^r_\alpha(\boldsymbol{p})\overline{u}^r_\beta(\boldsymbol{p})\,. \tag{5.71}$$

As noted in the previous section, and discussed further below, it is for this reason that the finite-volume factors $\mathbf{F}$ and $\mathbf{G}$ are proportional to Kronecker deltas in spin space in the *lab-axis frame*.

Like the momentum sums in the fully-dressed propagator, loop sums in generic Feynman diagrams for C_L contribute only exponentially suppressed L-dependence, as long as the loops do not allow three-neutron cuts. Such cuts lead to poles in the summand, and induce power-like volume effects that must be included in (and indeed are the focus of) the derivation. Heuristically, the intuition is that these physical, on-shell intermediate states can travel arbitrarily far and thus maximally feel the boundary conditions.

From these considerations, it follows that a skeleton expansion in which all three-neutron states are explicitly displayed will capture the power-like L dependence in $C_L(P)$. Such an expansion is built from all diagrams with operator-dependent vertex functions on the far left and far right, with three neutrons propagating between them, interacting via Bethe-Salpeter

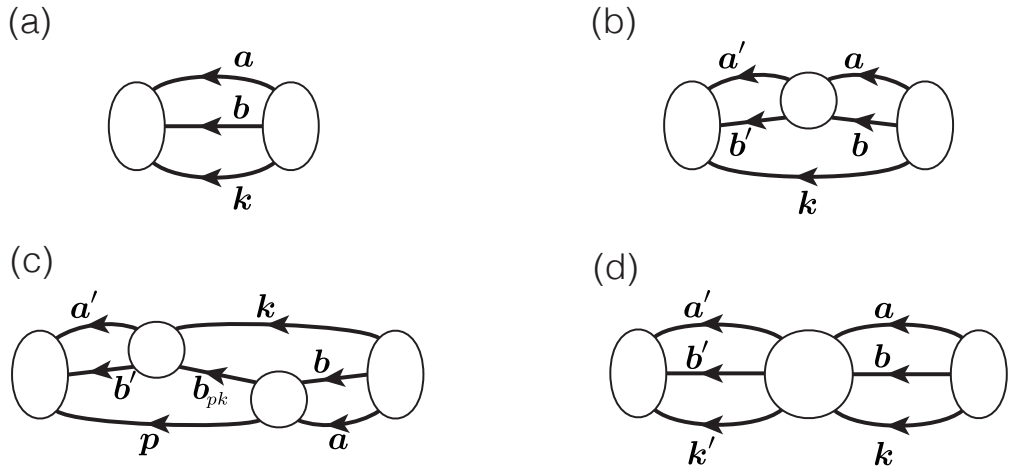

Figure 5.1: Diagrams relevant for the derivation of the quantization condition for three neutrons in a finite volume. Lines with arrows indicate fully-dressed neutron propagators. (We envision time flowing from right to left to match the ordering of incoming and outgoing states in the expressions of the main text.) The tall ellipses indicate the σ functions arising from the interpolating operators while the circles indicate two- and three-particle Bethe-Salpeter kernels.

kernels. Examples are shown in figure 5.1. The two-to-two kernels shown are defined to be two-particle irreducible in the s channel, so that there are no hidden three-particle states. There can also be three-to-three Bethe-Salpeter kernels, which are three-particle irreducible in the s channel. We discuss these kernels further in the remainder of the derivation.

Contributing diagrams

Continuing to follow the basic structure of the argument of ref. [37], we now analyze the three diagrams shown in figure 5.1 in turn, beginning with 5.1(a). Denoting the contribution of this to C_L as $C_L^{[5.1(a)]}$, we have

$$C_L^{[5.1(a)]} = \frac{1}{6} \int_{a,\,L} \int_{k,\,L} \sigma_{\alpha_1\alpha_2\alpha_3}(a,k) \Delta_{L,\alpha_1\beta_1}(a) \Delta_{L,\alpha_2\beta_2}(b) \Delta_{L,\alpha_3\beta_3}(k) \sigma^{\dagger}_{\beta_1\beta_2\beta_3}(a,k)\,, \qquad (5.72)$$

where $b = P - k - a$, and we have introduced the "endcap" $\sigma_{\alpha_1,\alpha_2,\alpha_3}(a,k)$, defined by

$$\sigma_{\alpha_1\alpha_2\alpha_3}(a,k) = \sum_{\mathsf{p}\in\mathcal{P}} \mathrm{sig}(\mathsf{p}) \times \overline{u}^{r_1}_{\alpha_1}(\boldsymbol{a})\overline{u}^{r_2}_{\alpha_2}(\boldsymbol{b})\overline{u}^{r_3}_{\alpha_3}(\boldsymbol{k}) \times \mathsf{p}[f_{r_1r_2r_3}(a,b,k)] \; . \tag{5.73}$$

Here $\mathcal{P}$ is the set of six permutations acting on the momentum and spin indices. For example if we define $\mathsf{p}_{1\leftrightarrow 2}$ as the permutation exchanging both the indices r_1 and r_2 and the corresponding momenta a and b, then

$$\mathsf{p}_{1\leftrightarrow 2}[f_{r_1r_2r_3}(a,b,k)] = f_{r_2r_1r_3}(b,a,k) \, . \tag{5.74}$$

The factor $\mathrm{sig}(\mathsf{p})$ is 1 for a cyclic permutation and -1 otherwise. As a result, only the antisymmetric part of $f_{r_1r_2r_3}(a,b,k)$ contributes in eq. (5.73).

To analyze eq. (5.72), one next uses the identity of eq. (5.70) to evaluate the k^0 and a^0 integrals within $\int_{a,\,L}$ and $\int_{k,\,L}$. This yields

$$\begin{aligned} C_L^{[5.1(a)]}(P) &= \widetilde{C}_\infty^{[5.1(a)]}(P) \\ &\quad + \frac{1}{6}\frac{1}{L^6}\sum_{\boldsymbol{a},\boldsymbol{k}} \sigma_{\alpha_1\alpha_2\alpha_3}(\boldsymbol{a},\boldsymbol{k}) \frac{i(\not{a}+m)_{\alpha_1\beta_1}\,(\not{b}+m)_{\alpha_2\beta_2}\,(\not{k}+m)_{\alpha_3\beta_3}}{2\omega_a 2\omega_k(b^2-m^2)} \sigma^\dagger_{\beta_1\beta_2\beta_3}(\boldsymbol{a},\boldsymbol{k}) \, , \end{aligned} \tag{5.75}$$

where $\widetilde{C}_\infty^{[5.1(a)]}(P)$ is a quantity with negligible (exponentially suppressed) L dependence. (The tilde is used as we will require a redefinition to reach our final quantity, $C_\infty^{[5.1(a)]}(P)$.)

To reach eq. (5.75) we have used the result that all contributions containing at least one factor of $R_{L,\alpha\beta}(p)$ lead to exponentially suppressed volume dependence. In the term proportional to $1/[(a^2-m^2)(b^2-m^2)(k^2-m^2)]$ we have evaluated the a^0 and k^0 integrals by closing the contours in the complex plane, encircling poles at $a^0 = \omega_a$ and $k^0 = \omega_k$. This also results in the numerator factors $(\not{a}+m)$ and $(\not{k}+m)$ being evaluated on-shell, allowing the subsequent use of the result eq. (5.71), as explained below. We also note that the four-momenta in the arguments of σ and $\sigma^\dagger$ are set on shell, and, with some abuse of notation, we denote this by changing the arguments to three-vectors. All other poles that contribute to the a^0 and k^0 integrals can be seen to lead to intermediate states that cannot go on shell for our range of E_3^*, and thus give nonsingular summands, for which the sums can be replaced by integrals, so that the contributions can be absorbed in $\widetilde{C}_\infty^{[5.1(a)]}(P)$.

The remaining momentum $b^\mu = (E-\omega_k-\omega_a, \boldsymbol{P}-\boldsymbol{k}-\boldsymbol{a})$ is generally not on the mass shell, but the summand can be expanded about the on-shell point, i.e. about $E = \omega_k + \omega_a + \omega_b$,. This expansion, together with a few additional manipulations explained below, yields

$$C_L^{[5.1(a)]}(P) = C_\infty^{[5.1(a)]}(P) + \frac{1}{6}\frac{1}{L^3}\sum_{\boldsymbol{k}} H(\boldsymbol{k})\left[\frac{1}{L^3}\sum_{\boldsymbol{a}} - \text{p.v.}\int_{\boldsymbol{a}}\right] \times \sigma^{\mathsf{lab}}_{r_1r_2r_3}(\boldsymbol{a},\boldsymbol{k})\frac{i\delta_{r_1r_1'}\delta_{r_2r_2'}\delta_{r_3r_3'}}{2\omega_a 2\omega_b 2\omega_k(E-\omega_a-\omega_b-\omega_k)}\sigma^{\mathsf{lab},\dagger}_{r_1'r_2'r_3'}(\boldsymbol{a},\boldsymbol{k})\,, \quad (5.76)$$

where

$$\sigma^{\mathsf{lab}}_{r_1r_2r_3}(\boldsymbol{a},\boldsymbol{k}) = \sigma_{\alpha_1\alpha_2\alpha_3}(\boldsymbol{a},\boldsymbol{k})\, u^{r_1}_{\alpha_1}(\boldsymbol{a}) u^{r_2}_{\alpha_2}(\boldsymbol{b}) u^{r_3}_{\alpha_3}(\boldsymbol{k})\,, \quad (5.77)$$

$$= (2m)^3 \sum_{\mathsf{p}\in\mathcal{P}} \text{sig}(\mathsf{p})\mathsf{p}[f_{r_1r_2r_3}(\boldsymbol{a},b,\boldsymbol{k})]\ . \quad (5.78)$$

In the second line, the middle argument of f remains a four-vector b, since this momentum is not yet on shell. The superscript lab emphasizes that the spin components are defined with respect to the lab-frame axis. The additional steps to reach eq. (5.76) include the subtraction of the integral, which is then added back in through a redefinition of $C_\infty^{[5.1(a)]}(P)$, which is allowed since the p.v. integral yields a smooth function of $\boldsymbol{k}$, allowing the sum over $\boldsymbol{k}$ to be replaced by an integral. A similar redefinition allows us to introduce the cutoff function $H(\boldsymbol{k})$, (whose form is discussed following eq. (5.5) above). These steps are explained in detail in the original derivation of the quantization condition [16]. We can now use the expansion of the summand about the on-shell point to replace $\not{b} + m$ and other factors, with their on-shell values, for the difference cancels the pole and leads to a sum-integral difference that is exponentially suppressed. We can then apply eq. (5.71) to the Dirac factors to write each as a product of spinors, leading to the expression shown for σ^{lab}.

At this stage we could directly use the sum-integral identity given in eq. (A1) of ref. [16] to rewrite $C_L^{[5.1(a)]}(P)$ in terms of the geometrical function $\mathbf{F}^{\mathsf{lab}}$ given in eq. (5.53),

$$C_L^{[5.1(a)]} = C_\infty^{[5.1(a)]} - \frac{1}{3}\boldsymbol{\sigma}^{\mathsf{lab}}\mathbf{F}^{\mathsf{lab}}\boldsymbol{\sigma}^{\mathsf{lab},\dagger}\,. \quad (5.79)$$

The overall $1/3$ arises because $\mathbf{F}^{\mathsf{lab}}$ contains a factor of $1/2$, and the product leads to the $1/6$ in eq. (5.76). The bold-faced $\boldsymbol{\sigma}^{\mathsf{lab}}$ indicates that a factor of i has been absorbed into

σ, that this quantity has been set on shell, and projected onto spherical harmonics using eq. (5.40). $\boldsymbol{\sigma}^{\mathsf{lab}}$ also includes the lab-frame axis spin indices, which, as shown in eq. (5.76), are unchanged by the three-particle cut.[8]

However, this form is not used in our analysis, which is carried out in the dimer-axis frame. Instead, we must first rotate to the dimer-axis frame using the transformation given in eqs. (5.37) and (5.38); and then apply the sum-integral identity discussed above, which involves projecting the resulting endcaps onto spherical harmonics using eq. (5.40), and then setting them on shell. These steps lead to

$$C_L^{[5.1(a)]} = C_\infty^{[5.1(a)]} - \frac{1}{3}\boldsymbol{\sigma}\mathbf{F}\boldsymbol{\sigma}^\dagger\,, \tag{5.80}$$

i.e. a result with the same form as the lab-axis frame version eq. (5.79). We stress that this identity of form hides a nontrivial difference. In particular, since the transformation connecting the lab- and dimer-axis frames depends on the momenta, it does not commute with the projection onto spherical harmonics. Thus, one cannot directly relate eqs. (5.79) and (5.80), but must instead must go back to the starting point of eq. (5.76).

We now explain these steps in more detail. The basis rotation involves one subtlety, namely that the momentum b is off shell, while the rotation described in eqs. (5.37) and (5.38) assumes that all momenta are on shell. Thus, we must extend the definition of the rotation to the off-shell case, and this we do by setting $\boldsymbol{\beta}_b = \boldsymbol{b}/\omega_b$ in the definition of R_b needed in eq. (5.38). This is the same extension already used in section 5.4.2 when describing the form of G.

The second step is to use the sum-minus-integral identity from ref. [16], leading to endcaps that are projected, using eq. (5.40), onto definite orbital angular momentum ℓm in the dimer CMF, and then set fully on shell. Since $\boldsymbol{k}$ is only sampled at discrete finite-volume values, it can also be viewed as an index, such that σ is promoted to a vector in the combined index space of $r_1, r_2, r_3, \ell, m, \boldsymbol{k}$, where $\{r_i\}$ are spin indices in the dimer-axis frame, which were

[8]Note that we use a different labelling of the spin indices here (r_i) compared to those used in the definition of $\mathbf{F}^{\mathsf{lab}}$ ($\boldsymbol{m}_s$), but this is just for notational convenience—the indices are the same.

denoted $\{m_s(\boldsymbol{k}), m_s(\boldsymbol{a}^*), m_s(\boldsymbol{b}^*)\}$ earlier. We abbreviate the quantity labelled by all these indices as $\boldsymbol{\sigma}$ (with the symbol in bold), which also includes an additional factor of i. This leads to eq. (5.80), in which the second term on the right-hand side is a matrix product built from the vector $\boldsymbol{\sigma}$ and its conjugate, together with the matrix $\mathbf{F}$ defined in eq. (5.51). This result has the same form as in the case of three pions of arbitrary isospin [37], except that here the flavor indices are replaced with (dimer-axis) spin indices.

We now turn to figure 5.1(b). In this diagram a Bethe-Salpeter kernel, denoted $\mathcal{B}$, is inserted to scatter two of the three neutrons propagating across the diagram. The functional form is given by

$$C_L^{[5.1(b)]}(P) = \frac{1}{4}\frac{1}{L^9}\sum_{\boldsymbol{k},\boldsymbol{a},\boldsymbol{a}'}\int\frac{da^0}{2\pi}\int\frac{da'^0}{2\pi}\int\frac{dk^0}{2\pi}\sigma_{\alpha_1\alpha_2\alpha_3}(a',k)\,\Delta_{\alpha_1\alpha_1'}(a')\Delta_{\alpha_2\alpha_2'}(b')\delta_{\alpha_3\alpha_3'} \\ \times i\mathcal{B}_{\alpha_1'\alpha_2',\beta_1'\beta_2'}(a',b';a,b)\,\Delta_{\alpha_3',\beta_3'}(k)\,\Delta_{\beta_1'\beta_1}(a)\Delta_{\beta_2'\beta_2}(b)\,\delta_{\beta_3'\beta_3}\,\sigma^\dagger_{\beta_1\beta_2\beta_3}(a,k)\,. \quad (5.81)$$

Now, in contrast to the analysis of figure 5.1(a), here we only aim to identify the maximally singular contribution to the diagram. The less singular parts will be absorbed into re-definitions of factors such as $\boldsymbol{\sigma}$ and $\boldsymbol{\sigma}^\dagger$ appearing in eq. (5.80).

Because figure 5.1(b) admits two distinct cuts across three-neutron states, the maximally singular contribution contains two poles. To isolate these we perform the k_0, a'^0, and a^0 contour integrals and expand the partially on-shell propagators about the physical energy points $E = \omega_{a'} + \omega_{b'} + \omega_k$ and $E = \omega_a + \omega_b + \omega_k$ to reach

$$C_L^{[5.1(b)]}(P) = \frac{1}{4}\frac{1}{L^3}\sum_{\boldsymbol{k}}\left[\frac{1}{L^3}\sum_{\boldsymbol{a}'} - \int_{\boldsymbol{a}'}\right]\left[\frac{1}{L^3}\sum_{\boldsymbol{a}} - \int_{\boldsymbol{a}}\right] \\ \times \sigma^{\mathsf{lab}}_{r_1r_2r_3}(\boldsymbol{a}',\boldsymbol{k})\frac{i\delta_{r_1r_1'}\delta_{r_2r_2'}\delta_{r_3r_3'}H(\boldsymbol{k})}{2\omega_{a'}2\omega_{b'}2\omega_k(E-\omega_{a'}-\omega_{b'}-\omega_k)}i[2\omega_k]\mathcal{B}^{\mathsf{lab}}_{r_1'r_2',s_1's_2'}(\boldsymbol{a}',b';\boldsymbol{a},b)\delta_{r_3's_3'} \\ \times\frac{i\delta_{s_1's_1}\delta_{s_2's_2}\delta_{s_3's_3}H(\boldsymbol{k})}{2\omega_a2\omega_b2\omega_k(E-\omega_a-\omega_b-\omega_k)}\sigma^{\mathsf{lab},\dagger}_{s_1,s_2,s_3}(\boldsymbol{a},\boldsymbol{k}) + \cdots\,, \quad (5.82)$$

where the ellipsis denotes less singular terms that we do not track explicitly. Here we have already mimicked the steps performed for figure 5.1(a) above including (i) replacing the sums over $\boldsymbol{a}$ and $\boldsymbol{a}'$ with integrals and sum-integral differences (and discarding the integrals as

these lead to less singular terms) (ii) inserting the identity $1 = H(\boldsymbol{k}) + [1 - H(\boldsymbol{k})]$ and again dropping the second contribution as it is less singular (iii) expanding all Dirac structures about the on-shell point to recover outer products of spinors that are then contracted with the endcaps and with the Bethe-Salpeter kernel.

The final steps, again in a direct imitation of the analysis for figure 5.1(a), are to expand the endcap factors and Bethe-Salpeter kernel about their on-shell points, to perform a momentum-dependent change of basis to the dimer-axis frame, and then to decompose all quantities in angular momentum in the dimer-axis frame. The result takes a very compact form

$$C_L^{[5.1(b)]} = -\boldsymbol{\sigma}\,\mathbf{F}\,\mathbf{B}_2\,\mathbf{F}\,\boldsymbol{\sigma}^\dagger + \cdots\,, \tag{5.83}$$

where $\mathbf{B}_2$ is analogous to $\mathbf{K}_2$, defined in eq. (5.54) above, but based on the Bethe-Salpeter kernel rather than the full K matrix.

We finally reach figure 5.1(c), which we also write out in detail to fully explain the pattern of the derivation that we are identifying. The diagram can be expressed as

$$\begin{aligned} C_L^{[5.1(c)]}(P) = (-1)\frac{1}{4}\frac{1}{L^{12}}\sum_{\boldsymbol{k},\boldsymbol{p},\boldsymbol{a},\boldsymbol{a}'}\int\frac{da^0}{2\pi}\int\frac{da'^0}{2\pi}\int\frac{dk^0}{2\pi}\int\frac{dp^0}{2\pi} \\ \times\Big[\sigma_{\alpha_1,\alpha_2,\alpha_3}(a',p)\,\Delta_{\alpha_1\alpha'_1}(a')\Delta_{\alpha_2\alpha'_2}(b')\delta_{\alpha_3\alpha'_3} \\ \times i\mathcal{B}_{\alpha'_1\alpha'_2,\beta'_1\beta'_2}(a',b';k,b_{pk})\,\Delta_{\alpha'_3\beta'_3}(p) \\ \times\Delta_{\beta'_2\gamma'_2}(b_{pk})\delta_{\beta'_1\gamma'_3}\delta_{\beta'_3\gamma'_1} \\ \times i\mathcal{B}_{\gamma'_1\gamma'_2\sigma'_1\sigma'_2}(p,b_{pk};a,b)\,\Delta_{\gamma'_3\sigma'_3}(k) \\ \times\Delta_{\sigma'_1\sigma_1}(a)\Delta_{\sigma'_2\sigma_2}(b)\,\delta_{\sigma'_3\sigma_3}\,\sigma^\dagger_{\sigma_1\sigma_2\sigma_3}(a,k)\Big]\,, \end{aligned} \tag{5.84}$$

where the initial (-1) arises from the anti-commutation of Grassmann fields in the correlation function defining the diagram.

Each line of the lengthy expression in square brackets corresponds to a specific segment of the diagram. In particular, the first and last lines correspond to the two endcap factors, each

with the two propagators that are contracted between an endcap and its adjacent Bethe-Salpeter kernel. The second and fourth lines then correspond to the two kernels themselves, each accompanied by the spectator propagator, i.e. the propagator that is not scattered by that kernel. Finally, the middle line corresponds to the distinctive feature of figure 5.1(c), namely the change in the particle that is spectating. This switch leads to the b_{pk}-dependent propagator as well as the set of Kronecker deltas, $\delta_{\beta'_1\gamma'_3}\delta_{\beta'_3\gamma'_1}$, that encode the interchange of indices with 1 and 3 subscripts.

Again identifying the most singular term in the expression, and performing steps discussed in detail in ref. [16], we reach

$$\begin{aligned} C_L^{[5.1(c)]}(P) = \frac{1}{4}\frac{1}{L^6}\sum_{\boldsymbol{p},\boldsymbol{k}}\left[\frac{1}{L^3}\sum_{\boldsymbol{a}'} - \int_{\boldsymbol{a}'}\right]\left[\frac{1}{L^3}\sum_{\boldsymbol{a}} - \int_{\boldsymbol{a}}\right] \\ \times \sigma^{\mathsf{lab}}_{r_1r_2r_3}(\boldsymbol{a}',\boldsymbol{p})\frac{i\delta_{r_1r'_1}\delta_{r_2r'_2}\delta_{r_3r'_3}H(\boldsymbol{p})}{2\omega_{a'}2\omega_{b'}2\omega_p(E-\omega_{a'}-\omega_{b'}-\omega_p)} \\ \times i[2\omega_p]\mathcal{B}^{\mathsf{lab}}_{r'_1r'_2,s'_1s'_2}(\boldsymbol{a}',b';\boldsymbol{k},b_{pk})\delta_{r'_3s'_3} \\ \times (-1)\delta_{s'_2t'_2}\delta_{s'_1t'_3}\delta_{s'_3t'_1}\frac{i}{4\omega_p\omega_k}\frac{H(\boldsymbol{p})H(\boldsymbol{k})}{b_{pk}^2-m^2} \\ \times i[2\omega_k]\mathcal{B}^{\mathsf{lab}}_{t'_1t'_2,z'_1z'_2}(\boldsymbol{p},b_{pk};\boldsymbol{a},b)\delta_{t'_3z'_3} \\ \times \frac{i\delta_{z'_1z_1}\delta_{z'_2z_2}\delta_{z'_3z_3}H(\boldsymbol{k})}{2\omega_a2\omega_b2\omega_k(E-\omega_a-\omega_b-\omega_k)}\sigma^{\mathsf{lab},\dagger}_{z_1z_2z_3}(\boldsymbol{a},\boldsymbol{k}) \\ + \cdots . \end{aligned} \tag{5.85}$$

The key observation here is that all structures appearing in this long equation have already been used above except for the line beginning with $\times(-1)\delta_{s'_2t'_2}\delta_{s'_1t'_3}\delta_{s'_3t'_1}\cdots$. Again this is the line that encodes the switch in which pair is scattering.

We once again repeat the now usual steps of expanding about the on-shell point, performing the momentum-dependent change of basis to the dimer-axis frame and decomposing all quantities in spherical harmonics. Because the two-particle momenta differ on either side of the switch factor, the change of basis matrices do not cancel. This leads to the nontrivial form of $\mathbf{G}$ given in eq. (5.45). In our notation, the final result for the most singular-part of

figure 5.1(c) takes a very compact form:

$$C_L^{[5.1(c)]} = -\boldsymbol{\sigma}\,\mathbf{F}\,\mathbf{B}_2\,\mathbf{G}\,\mathbf{B}_2\,\mathbf{F}\,\boldsymbol{\sigma}^\dagger + \cdots \tag{5.86}$$

This completes our analysis of the three key diagrams of figure 5.1. In the following section we illustrate how these lead to a generalized quantization condition for finite-volume three-nucleon systems.

All orders generalization

To reach our final form for $C_L(P)$, the correlation function introduced in eq. (6.3), we need to analyze all contributions to the skeleton expansion. We stress that in the following we are explaining the logic and structure of the full derivation, but many details are left out. For these we refer to the derivation for identical particles given in refs. [16, 17]. One feature that changes compared to that derivation is the need for amplitudes involving three identical fermions to be antisymmetric under particle exchange, rather than symmetric. The impact of this change is discussed in section C.1.

An important building block entering the expansion that we have not considered so far is the three-particle Bethe-Salpeter kernel. An example of a diagram containing this kernel is shown in figure 5.1(d). When represented as a function of momenta and spin indices, the kernel is denoted by $\mathcal{B}_3$ in analogy to the two-particle Bethe-Salpeter kernel, $\mathcal{B}$ [appearing, for example, in eq. (5.81)]. $\mathcal{B}_3$ is defined as the sum over the set of all Feynman diagrams with three incoming and three outgoing neutrons that do not contain any three-neutron cuts intersecting the flow of total energy and momentum (s-channel cuts).[9]

$\mathcal{B}_3$ depends on the same kinematical and spin variables as $\mathcal{K}_{\text{df},3}$, allowing the description in section 5.4.2 to carry over. If the outgoing spin indices and the outgoing momenta of

[9]Unlike for the case of pions, there are no diagrams with s-channel cuts containing a single neutron, due to baryon-number conservation. Thus, an additional complication in the construction of $\mathcal{B}_3$ that was addressed for pions and similar particles in ref. [16] is avoided here.

$\mathcal{B}_3$ are fixed, then the incoming degrees of freedom exactly match those of σ, the leftmost endcap function used extensively in the previous section. From this it follows that the steps leading to the on-shell projection of σ and the rotation to the dimer-frame axis can also be followed for $\mathcal{B}_3$. If these steps are applied to both the incoming and outgoing kinematics, then $\mathcal{B}_3$ can be represented as a matrix in the same space as $\mathbf{K}_2$, $\mathbf{F}$, and $\mathbf{G}$. After absorbing a factor of i this matrix is denoted by $\mathbf{B}_3$.

Returning to the main analysis, we follow the same logic as in the original RFT derivation for identical spin-zero particles [16] by noting that every diagram generates a maximally singular piece as well as contributions with fewer singularities. The latter arise when the loop momenta associated with poles are integrated using the principal value prescription rather than summed, and from finite terms that result when expanding the coefficients of poles about their on-shell values. Such nonmaximally singular terms can be incorporated through redefinitions of infinite-volume quantities $\boldsymbol{\sigma}$, $\mathbf{B}_2$, and $\mathbf{B}_3$. For example, figure 5.1(a) has a single pole in its maximally singular contribution whereas figure 5.1(b) (which has two poles in its maximally singular term) can also generate single-pole contributions when either $\boldsymbol{a}$ or else $\boldsymbol{a}'$ (but not both) is integrated. The single-pole parts of figure 5.1(a) and (b) are ultimately combined through redefinitions of $\boldsymbol{\sigma}$ and $\boldsymbol{\sigma}^\dagger$, in a step that collects an infinite set of single-pole terms into a single contribution to $C_L(P)$.

We now identify all contributions to $C_L(P)$, beginning with the rule for identifying the maximally singular piece in each diagram.[10] To explain the rule it is convenient to first introduce the notion of a *two-to-two sub-process sector*, defined as any section of skeleton-expansion diagram that appears between insertions of $\boldsymbol{\sigma}$, $\mathbf{B}_3$ or $\boldsymbol{\sigma}^\dagger$ (and does not contain any such factors). For example, the three diagrams analyzed so far each contain exactly one two-to-two subprocess sector as no $\mathbf{B}_3$ factors are included. Within each such sector, one

[10]We emphasize that the presentation here follows a different strategy for reviewing the derivation of the RFT quantization condition, as compared, e.g., to refs. [16, 37]. This difference is not related to the consideration of particles with spin; indeed an analogous approach could also have been applied in earlier works. We think that the present approach allows a straightforward understanding of the essential features of the final results, although it hides many details explained in ref. [16].

can identify the number of times that the pair of scattering nucleons changes (the number of switches, N_{switch}) or, similarly, the number of elastic two-to-two sections, $N_{\mathsf{elast}} = N_{\mathsf{switch}} + 1$, in which pairwise scattering occurs for a given nucleon pair. We also adopt the convention that $N_{\mathsf{elast}} = 0$ if no pairwise scattering occurs in a particular two-to-two subprocess sector, as in figure 5.1(a).

The maximally singular contribution of any subprocess sector, denoted by $\mathbf{S}_L^{(\boldsymbol{n})}(P)_{\mathsf{max}}$, then takes a simple form

$$\mathbf{S}_L^{(\boldsymbol{n})}(P)_{\mathsf{max}} = \begin{cases} \mathbf{F}/3 & N_{\mathsf{elast}} = 0\,, \\ \left(\prod_{k=1}^{N_{\mathsf{elast}}} \left(\left[\mathbf{F}\mathbf{B}_2\right]^{\boldsymbol{n}(k)} \mathbf{G}\mathbf{B}_2\right)\right) \mathbf{B}_2^{-1}\mathbf{G}^{-1}\mathbf{F} & N_{\mathsf{elast}} > 0\,, \end{cases} \quad \text{(maximally singular)}, \tag{5.87}$$

where $\boldsymbol{n}$ is a vector of length $N_{\mathsf{elast.}}$, populated with positive integers counting the number of $\mathbf{B}_2$ factors in each elastic two-to-two section, and $\boldsymbol{n}(k)$ is its k^{th} component. Here it is understood that the $k = 1$ factor is on the far left and the $k = N_{\mathsf{elast.}}$ on the far right. Note that $\mathbf{G}$ appears $N_{\mathsf{elast.}} - 1 = N_{\mathsf{switch}}$ times.

In eq. (5.87) we have used the subscript max to indicate that the right-hand side is only part of the contribution. This is because we intend $\mathbf{S}_L^{(\boldsymbol{n})}(P)$, with no max subscript, to contain all contributions with a set of poles described by a given $\boldsymbol{n}$. We are missing the non-maximally-singular terms that arise when some coordinates are integrated, as well as those associated with expanding the coefficients of poles. As is shown in ref. [16], including the former has the effect of promoting the Bethe-Salpeter kernel, $\mathbf{B}_2$, to the K-matrix, $\mathbf{K}_2$, defined in section 5.4.2 and in particular in eq. (5.54) above. These can thus be incorporated by making the simple adjustment

$$\mathbf{S}_L^{(\boldsymbol{n})}(P) = \begin{cases} \mathbf{F}/3 & N_{\mathsf{elast}} = 0\,, \\ \left(\prod_{k=1}^{N_{\mathsf{elast}}} \left(\left[\mathbf{F}\mathbf{K}_2\right]^{\boldsymbol{n}(k)} \mathbf{G}\mathbf{K}_2\right)\right) \mathbf{K}_2^{-1}\mathbf{G}^{-1}\mathbf{F} & N_{\mathsf{elast}} > 0\,, \end{cases} \quad \text{(all terms)}. \tag{5.88}$$

The next step is to sum over $N_{\mathsf{elast.}}$ values and over all positive integer components of the

vectors $\boldsymbol{n}$. This gives a quantity denoted by $\mathbf{F}_3$:

$$\mathbf{F}_3 = \sum_{N_{\text{elast.}}=0}^{\infty} \sum_{\boldsymbol{n}\in(\mathbb{Z}^+)^{N_{\text{elast.}}}} \mathbf{S}_L^{(\boldsymbol{n})}(P)\,. \tag{5.89}$$

Evaluating the sum explicitly, one finds

$$\mathbf{F}_3 = \frac{\mathbf{F}}{3} + \mathbf{F}\frac{1}{1-\mathbf{M}_{2,L}\mathbf{G}}\mathbf{M}_{2,L}\mathbf{F}\,, \qquad \mathbf{M}_{2,L} = \frac{1}{\mathbf{K}_2^{-1}-\mathbf{F}}\,. \tag{5.90}$$

This matches the definition in refs. [16, 37].

A more subtle issue is the impact of finite terms obtained when the coefficients of poles are expanded about their on-shell values. We have done such an expansion, for example, in the analysis of figure 5.1(c), when we replaced the pole with the factor of $\mathbf{G}$, and set adjacent quantities on shell. The terms that are dropped effectively sew the adjacent Bethe-Salpeter kernels together creating a contribution to the three-particle K matrix. It turns out that such contributions can be absorbed into changes in $\mathbf{B}_3$, although this requires the use of a symmetrization procedure that is discussed in section C.1. This allows one to proceed by ignoring this issue for now, and adding in such terms after discussing the role of $\mathbf{B}_3$.

To explain this role, we iterate the insertion of $\mathbf{F}_3$—corresponding to a two-to-two subprocess sector—with the objects that break up these sectors, namely $\boldsymbol{\sigma}$, $\mathbf{B}_3$, and $\boldsymbol{\sigma}^\dagger$. This leads to the following naive result for $C_L(P)$,

$$C_L(P) = C_\infty(P) - \sum_{n=0}^{\infty} \boldsymbol{\sigma}\mathbf{F}_3\Big[\mathbf{B}_3\mathbf{F}_3\Big]^n\boldsymbol{\sigma}^\dagger \qquad \text{(incomplete)}\,, \tag{5.91}$$

where we have stressed that this summation is still incomplete. To complete it we need to include the above-discussed finite contributions from expanding pole coefficients about the on-shell point, as well as contributions in which momentum arguments $\boldsymbol{\sigma}$, $\mathbf{B}_3$, and $\boldsymbol{\sigma}^\dagger$ are integrated. The combined effect is that one must make replacements analogous to the $\mathbf{B}_2 \to \mathbf{K}_2$ replacement discussed above. Here these are as follows: $\mathbf{B}_3 \to \mathbf{K}_{\text{df},3}$, $\boldsymbol{\sigma} \to \mathbf{A}'_3$, $\boldsymbol{\sigma}^\dagger \to \mathbf{A}_3$. The first of the new quantities, $\mathbf{K}_{\text{df},3}$, is discussed in section 5.4.2, and the full definition is given in section 6.4.7 below via the integral equations that relate this quantity to the physical scattering amplitude. Similarly, as was shown in ref. [217], $\mathbf{A}'_3$ and $\mathbf{A}_3$ satisfy

integral equations that define them in terms of matrix elements of the operators entering $C_L(P)$. These latter two quantities play no role in the quantization condition and are not discussed further in this work.

Putting everything together we find that eq. (5.91) is replaced with an equally simple series,

$$C_L(P) = C_\infty(P) - \sum_{n=0}^{\infty} \mathbf{A}_3' \mathbf{F}_3 \Big[\mathbf{K}_{\mathrm{df},3} \mathbf{F}_3 \Big]^n \mathbf{A}_3 \,, \tag{5.92}$$

that evaluates to the final form for the finite-volume correlator

$$C_L(P) = C_\infty(P) - \mathbf{A}_3' \mathbf{F}_3 \frac{1}{1 - \mathbf{K}_{\mathrm{df},3} \mathbf{F}_3} \mathbf{A}_3 \,. \tag{5.93}$$

This result is symbolically equivalent to those of previous works on different three-particle systems, differing only in the detailed meaning of $\mathbf{K}_{\mathrm{df},3}$, $\mathbf{F}_3$ and the various matrices making up the definition of the latter, in particular $\mathbf{F}$, $\mathbf{G}$ and $\mathbf{K}_2$.

Before concluding this section we consider an alternative finite-volume correlation function that is useful for deriving the relation between the two- and three-body K-matrices and the physical three-to-three scattering amplitude. This is the generalization to spin-1/2 particles of the quantity $\mathcal{M}_{3,L}^{(u,u)}$ introduced in eq. (6.76). It is a finite-volume analog of a scattering amplitude, with three incoming and three outgoing nucleons. It can be obtained from the diagrams contributing to $C_L(P)$ by removing the endcaps and amputating external propagators. One additional technicality is required in the case where the outermost interaction, adjacent to the incoming or outgoing state, is a two-to-two rather than a three-to-three Bethe-Salpeter kernel. In this case the incoming momentum $\boldsymbol{k}$ and the outgoing momentum $\boldsymbol{p}$ are always assigned to the external nucleon not connected to the outermost $\mathbf{B}_2$ factor. Thus it is an unsymmetrized quantity, on both incoming and outgoing sides, as indicated by the superscript (u, u). It can be written using the same matrix indices as for the matrices in the quantization condition. Absorbing a factor of i, the resulting matrix is denoted $\mathbf{M}_{3,L}^{(u,u)}(P)$.

A finite-volume decomposition directly analogous to that for $C_L(P)$ can then be per-

formed for this quantity and leads to the following result:

$$\mathbf{M}_{3,L}^{(u,u)}(P) \equiv \mathbf{D}^{(u,u)} + \mathbf{L}_L^{(u)} \frac{1}{1 - \mathbf{K}_{\mathrm{df},3}\mathbf{F}_3} \mathbf{K}_{\mathrm{df},3} \mathbf{R}_L^{(u)} \,, \tag{5.94}$$

where

$$\mathbf{D}^{(u,u)} \equiv \frac{1}{1 - \mathbf{M}_{2,L}\mathbf{G}} \mathbf{M}_{2,L} \mathbf{G} \mathbf{M}_{2,L} \,, \tag{5.95}$$

$$\mathbf{L}_L^{(u)} \equiv \mathbf{F}^{-1} \cdot \mathbf{F}_3 \,, \tag{5.96}$$

$$\mathbf{R}_L^{(u)} \equiv \mathbf{F}_3 \cdot \mathbf{F}^{-1} \,. \tag{5.97}$$

Note that these results have similar form as those for identical scalars, eqs. (5.11), (5.12), and (5.13) above, with the differences resulting from the factors of i, 2ω and L^3 that have been absorbed into our boldface definitions.

5.5 Summary of results and implementation

In this section we present the final results from the derivation of the previous section. We also comment briefly on the issues that will arise when implementing the formalism.

5.5.1 Relating finite-volume energies to $\mathcal{K}_{\mathrm{df},3}$

In direct analogy to previous derivations, see e.g. refs. [15, 16], the condition that $C_L(P)$ contains a pole in E (at fixed $\boldsymbol{P}$ and L) implies the following finite-volume quantization condition

$$\det_{\boldsymbol{k},\ell,m,\boldsymbol{m}_s^*} \Big[1 - \mathbf{K}_{\mathrm{df},3}\mathbf{F}_3 \Big] = 0 \,. \tag{5.98}$$

Here the subscripts on the determinant indicate that it is taken in the space on which all matrices are defined, which is a Kronecker-product space of the spectator momentum $\boldsymbol{k}$ (discretized by the finite volume as $\boldsymbol{k} \in (2\pi/L)\mathbb{Z}^3$), the orbital angular momentum of the two-particle pair, ℓ, m, as well as the azimuthal spin components in the dimer-axis frame, $\boldsymbol{m}_s^*$. This result has the by-now standard form for quantization conditions in the RFT formalism, exemplified by eq. (5.8), aside from a sign difference arising from our boldface notation. All

the complications introduced by spin are contained in the form of the building blocks $\mathbf{K}_{\mathrm{df},3}$, $\mathbf{G}$, $\mathbf{F}$, and $\mathbf{K}_2$, which are discussed, respectively, in sections 5.4.2, 5.4.2, 5.4.2, and 5.4.2.

To use the quantization condition in practice, one must truncate the sum over angular momentum. This can be achieved, following ref. [16], by setting $\mathbf{K}_2$ and $\mathbf{K}_{\mathrm{df},3}$ to zero for $\ell > \ell_{\mathsf{max}}$, since this has the effect of truncating also the contributions of $\mathbf{F}$ and $\mathbf{G}$. Such a truncation is reasonable near to threshold, where angular-momentum barriers suppress interactions for larger values of ℓ. In principle, one can envisage using a different maximum angular momentum cutoff for $\mathbf{K}_2$ and $\mathbf{K}_{\mathrm{df},3}$, although it is plausible that they should be related. In any case, since the sum over $\boldsymbol{k}$ is automatically truncated by the cutoff function, the truncation in ℓ leads to finite-dimensional matrices, and implementing the determinant condition becomes tractable.

A further practical step is to decompose the matrices into irreducible representations (irreps) of the appropriate finite-volume symmetry group, which allows the matrix in the quantization condition to be block diagonalized. The group depends on the total momentum $\boldsymbol{P}$. In the case of three neutrons, one must use fermionic irreps, and the construction of the projectors that block-diagonalize the matrices involves Wigner D matrices representing the effect of Wigner rotations. Details on irrep projection for the three-particle quantization condition for scalars have been discussed in refs. [110, 124]. Applying the same procedure for particles with spin should be straightforward.

5.5.2 Relating $\mathcal{K}_{\mathrm{df},3}$ to the scattering amplitude

The second step of the formalism provides a relation between the two- and three-particle K matrices, determined as outlined in the previous section, and the three-particle scattering amplitude, $\mathcal{M}_3$. We obtain this relation using the correlator $\mathbf{M}_{3,L}^{(u,u)}$, whose decomposition is given in eq. (5.94) above. We first antisymmetrize the correlator to yield

$$\mathbf{M}_{3,L}(P) \equiv \mathcal{A}\left[\mathbf{M}_{3,L}^{(u,u)}(P)\right] . \tag{5.99}$$

The antisymmetrization step sums over all permutations of momenta on the external legs with appropriate signs and is described in detail in section C.2.

Second, we formally perform an infinitesimal shift in the total energy into the complex plane, denoted by $i\epsilon$, and then take an ordered double limit,

$$\mathbf{M}_3(E, \boldsymbol{P}) = \lim_{\epsilon \to 0^+} \lim_{L \to \infty} \mathbf{M}_{3,L}(E + i\epsilon, \boldsymbol{P}) \,. \tag{5.100}$$

The quantity on the left-hand side is the full three-neutron scattering amplitude, defined as the sum of all diagrams in the skeleton expansion with a standard $i\epsilon$ pole prescription in propagators. The limit on the right-hand side yields a set of infinite-volume integral equations.

To spell this out in more detail, we begin with the two-to-two amplitude that appears as a subprocess of three-to-three scattering. We define this via the two-particle K-matrix but introduce a version of the latter that is rescaled relative to that in section 5.4.2. We denote this by $\mathbf{K}_2(\boldsymbol{p})$, where $\boldsymbol{p}$ is the spectator momentum, defining

$$[\mathbf{K}_2]_{\ell' m' \boldsymbol{m}_s'^*; \ell m \boldsymbol{m}_s^*}(\boldsymbol{p}) \equiv i\mathcal{K}_2^{(\ell' m' \boldsymbol{m}_s'^*, \ell m \boldsymbol{m}_s^*)}(E_{2,p}^*) \,. \tag{5.101}$$

Comparing to eq. (5.54), note that here we have dropped a factor of $2\omega_p L^3$ and the Kronecker delta. We next define the corresponding phase-space factor

$$[\boldsymbol{\rho}]_{\ell' m' \boldsymbol{m}_s'^*; \ell m \boldsymbol{m}_s^*}(\boldsymbol{p}) = \delta_{\boldsymbol{m}_s'^* \boldsymbol{m}_s^*} \delta_{\ell' \ell} \delta_{m' m} \frac{-i|q_{2,p}^*|\Big(1 - H(\boldsymbol{p})\Big) + q_{2,p}^*}{16\pi E_{2,p}^*} \,, \tag{5.102}$$

such that the two-to-two scattering amplitude is given by

$$\mathbf{M}_2(\boldsymbol{p}) = \frac{1}{\mathbf{K}_2(\boldsymbol{p})^{-1} - \boldsymbol{\rho}(\boldsymbol{p})} \,. \tag{5.103}$$

Up to the rescaling by $2\omega_p L^3$, this is the ordered double limit ($L \to \infty$ followed by $\epsilon \to 0^+$) of $\mathbf{M}_{2,L}$, defined in eq. (5.90).

The next step is to evaluate the ordered limit for $\mathbf{D}^{(u,u)}$; we denote the result of this by $\mathbf{D}_\infty^{(u,u)}(\boldsymbol{p}, \boldsymbol{k})$, where the spectator-momentum indices have been promoted to arguments of

the function. As described, for example, in eq. (85) of ref. [17], the result of the limit can be expressed via an integral equation

$$\mathbf{D}_{\infty}^{(u,u)}(\boldsymbol{p},\boldsymbol{k}) \equiv \mathbf{M}_2(\boldsymbol{p})\mathbf{G}_{\infty}(\boldsymbol{p},\boldsymbol{k})\mathbf{M}_2(\boldsymbol{k}) + \mathbf{M}_2(\boldsymbol{p}) \int_{\boldsymbol{k}'} \mathbf{G}_{\infty}(\boldsymbol{p},\boldsymbol{k}')\mathbf{D}_{\infty}^{(u,u)}(\boldsymbol{k}',\boldsymbol{k}) \,, \tag{5.104}$$

where $\int_{\boldsymbol{k}} = \int d^3\boldsymbol{k}[(2\pi)^3(2\omega_k)]^{-1}$, and $\mathbf{G}_{\infty}(\boldsymbol{p},\boldsymbol{k})$, the exchange factor appropriate for the integral equation, is given by

$$[\mathbf{G}_{\infty}]_{\ell' m' \boldsymbol{m}'^*_s;\ell m \boldsymbol{m}^*_s}(\boldsymbol{p},\boldsymbol{k}) = 4\omega_p\omega_k L^6 \, \mathbf{G}_{p\ell' m' \boldsymbol{m}'^*_s;k\ell m \boldsymbol{m}^*_s} \,, \tag{5.105}$$

which is just a rescaled version of the finite-volume analog with the spectator-momentum indices promoted to arguments of the function. Note that, although the convention for $\int_{\boldsymbol{k}}$ differs as compared to ref. [17], this is compensated by differences elsewhere such that the convention for $\mathbf{D}_{\infty}^{(u,u)}(\boldsymbol{p},\boldsymbol{k})$ is the same.

Once $\mathbf{D}_{\infty}^{(u,u)}(\boldsymbol{p},\boldsymbol{k})$ is determined via the integral equation, one can readily evaluate the left and right dressing functions via

$$\mathbf{L}_{\infty}^{(u)}(\boldsymbol{p},\boldsymbol{k}) = \left[\frac{1}{3} + \mathbf{M}_2(\boldsymbol{k})\boldsymbol{\rho}(\boldsymbol{k})\right] \tilde{\delta}(\boldsymbol{p}-\boldsymbol{k}) + \mathbf{D}_{\infty}^{(u,u)}(\boldsymbol{p},\boldsymbol{k})\boldsymbol{\rho}(\boldsymbol{k}) \tag{5.106}$$

$$\mathbf{R}_{\infty}^{(u)}(\boldsymbol{p},\boldsymbol{k}) = \left[\frac{1}{3} + \boldsymbol{\rho}(\boldsymbol{k})\mathbf{M}_2(\boldsymbol{k})\right] \tilde{\delta}(\boldsymbol{p}-\boldsymbol{k}) + \boldsymbol{\rho}(\boldsymbol{p})\mathbf{D}_{\infty}^{(u,u)}(\boldsymbol{p},\boldsymbol{k}) \,, \tag{5.107}$$

where $\tilde{\delta}(\boldsymbol{p}-\boldsymbol{k}) = 2\omega_p(2\pi)^3\delta^3(\boldsymbol{p}-\boldsymbol{k})$. [See eqs. (92) and (94) of ref. [17]. However, for these quantities our convention differs by factors of 2ω from that work.] Either of these can then be used to construct a final integral equation for a quantity denoted by $\mathbf{T}(\boldsymbol{p},\boldsymbol{k})$ that sums an infinite series of $\mathbf{K}_{\mathrm{df},3}$ insertions:

$$\mathbf{T}(\boldsymbol{p},\boldsymbol{k}) = \mathbf{K}_{\mathrm{df},3}(\boldsymbol{p},\boldsymbol{k}) + \int_{\boldsymbol{p}'}\int_{\boldsymbol{k}'} \mathbf{K}_{\mathrm{df},3}(\boldsymbol{p},\boldsymbol{p}')\boldsymbol{\rho}(\boldsymbol{p}')\mathbf{L}_{\infty}^{(u)}(\boldsymbol{p}',\boldsymbol{k}')\mathbf{T}(\boldsymbol{k}',\boldsymbol{k}) \,. \tag{5.108}$$

[See also eq. (91) of ref. [17], where the convention here matches without rescaling.] This differs from the final amplitude because it is missing contributions from pairwise scattering outside the $\mathbf{K}_{\mathrm{df},3}$ factors and in the $\mathbf{K}_{\mathrm{df},3}$-independent term. Restoring these contributions and anti-symmetrizing gives

$$\mathbf{M}_3(E,\boldsymbol{P}) = \mathcal{A}\left[\mathbf{D}_{\infty}^{(u,u)}(\boldsymbol{p},\boldsymbol{k}) + \int_{\boldsymbol{p}'}\int_{\boldsymbol{k}'} \mathbf{L}_{\infty}^{(u)}(\boldsymbol{p},\boldsymbol{p}')\mathbf{T}(\boldsymbol{p}',\boldsymbol{k}')\mathbf{R}_{\infty}^{(u)}(\boldsymbol{k}',\boldsymbol{k})\right] . \tag{5.109}$$

This is the final result for the three-neutron scattering amplitude.

Dedicated studies concerning the solution to the corresponding integral equations for scalar particles can be found in refs. [210, 211], and we expect many of the practical details to carry over to the three-neutron case.

5.5.3 Change of basis and specific truncations

In this subsection we consider additional practical aspects of implementing the quantization condition, focusing on those that are particular to the presence of spin degrees of freedom.

We first note that it will be useful, in many cases, to rotate all matrices to the basis in which the dimer has definite total spin (as defined in the dimer-axis frame). This total-spin basis is already discussed in the context of the two-particle K-matrix, $\mathbf{K}_2$, in section 5.4.2, in particular in eq. (5.56). Extending the notation introduced there, we write

$$\begin{aligned}&\left|\boldsymbol{k}, \ell, m, s^*, \mu_s^*, m_s(\boldsymbol{k})\right\rangle \\ &\quad = \sum_{m_s'(\boldsymbol{a}^*), m_s'(\boldsymbol{b}^*)} \left|\boldsymbol{k}, \ell, m, m_s'(\boldsymbol{a}^*), m_s'(\boldsymbol{b}^*), m_s(\boldsymbol{k})\right\rangle \left\langle {}^1\!/_2\; m_s'(\boldsymbol{a}^*),\; {}^1\!/_2\; m_s'(\boldsymbol{b}^*)\right| s^*, \mu_s^*\Big\rangle\,, \quad (5.110)\end{aligned}$$

where $s^* \in \{0, 1\}$ is the total dimer spin and μ_s^* is the corresponding azimuthal component. Note that we do not assign any momentum label to these spin indices as the $*$ is sufficient to denote the dimer-axis frame. The last factor in eq. (5.110) is a standard $SU(2)$ Clebsch-Gordon coefficient for the reduction ${}^1\!/_2 \otimes {}^1\!/_2 = 0 \oplus 1$.

This change of basis block diagonalizes $\mathbf{K}_2$ to a spin-zero and spin-one block and leaves $\mathbf{F}$ proportional to the identity matrix in spin-space, with index structure $\delta_{s'^*, s^*}\ \delta_{\mu_s'^*, \mu_s^*}$. By contrast, $\mathbf{G}$ and $\mathbf{K}_{\text{df},3}$ are not expected to have any simplifications from the rotation to this basis.

Similarly, it is possible to perform a change of basis to combine s^* and ℓ into a total two-particle angular momentum j. To do this in practice one needs to fix a particular value of ℓ_{max}, leading to a finite set of ℓ values that can be combined with each s^* to reach a finite set of states labelled by $\boldsymbol{k}, j, \mu_j, \ell, s^*, m_s(\boldsymbol{k})$. For the case of $\ell_{\mathsf{max}} = 0$, for example, one has

only the channel $\{j, \ell, s^*\} = \{0, 0, 0\}$, since $s^* = 1$ requires odd values of ℓ. For $\ell_{\mathsf{max}} = 1$, we add an $s^* = 1$ component, so that there are now several channels

$$\{j, \ell, s^*\} \in \Big\{\{0, 0, 0\}, \{0, 1, 1\}, \{1, 1, 1\}, \{2, 1, 1\}\Big\}. \tag{5.111}$$

In this case no mixing occurs in $\mathbf{K}_2$ (since the two $j = 0$ cases have opposite parities), but $\mathbf{K}_{\text{df},3}$ and $\mathbf{G}$ will mix the channels, since j is not a good quantum number of the three-particle state. Mixing in the two-particle K-matrix first arises for $\ell_{\mathsf{max}} = 3$, as discussed in section 5.4.2.

5.6 Parametrization of $\mathcal{K}_{\text{df},3}$

Implementing the quantization condition for three identical fermions requires a parametrization of $\mathcal{K}_{\text{df},3}$. Since $\mathcal{K}_{\text{df},3}$ is, by construction, smooth aside from three-particle resonances or bound states, we present its parametrization in an expansion about threshold. For this expansion, we work with the quantity $\mathcal{K}_{\text{df},3}^{\mathsf{lab}}$ of eq. (5.33), in which spin components are defined with respect to the lab-frame axis. When using $\mathcal{K}_{\text{df},3}$ in, e.g., the evaluation of the quantization condition, it will be necessary to rotate the spin indices to the dimer-frame axis using eq. (5.37). The key constraint is that $\mathcal{K}_{\text{df},3}^{\mathsf{lab}}$ must have the same symmetry properties as the scattering amplitude, $\mathcal{M}_3$. It must transform covariantly under Lorentz transformations and parity, and be fully antisymmetric with respect to the simultaneous exchange of the spin and momentum labels for any pair of incoming or outgoing particles.

To construct the threshold expansion, we proceed by writing down Lorentz- and parity-invariant local operators composed of three-neutron fields and three conjugate fields and their derivatives. These have the schematic form $\overline{\mathcal{N}}^3\mathcal{N}^3$ (with derivatives and Dirac indices implicit). By using quantum fields $\mathcal{N}$ and $\overline{\mathcal{N}}$, we automatically enforce the required anti-symmetry property, and by using local operators we ensure that the momentum dependence is smooth. If we enumerate all possible independent operators with up to a certain number of derivatives, each multiplied by an independent coefficient, then, by the standard assumption of effective field theories (EFTs), the corresponding matrix elements will yield the most

general amplitudes consistent with the symmetries.

To convert the local operators into explicit forms for $\mathcal{K}^{\mathsf{lab}}_{\mathrm{df},3}$, we take matrix elements of the operators between external states in the lab-frame basis. This leads to expressions involving the Dirac spinors associated with the initial and final particles, because of the relations

$$\langle \boldsymbol{k}', m_s(\boldsymbol{k}')|\overline{\mathcal{N}}(x)|0\rangle = \bar{u}_{m_s(\boldsymbol{k}')}(\boldsymbol{k}')e^{ik'\cdot x}\,, \qquad \langle 0|\mathcal{N}(x)|\boldsymbol{k}, m_s(\boldsymbol{k})\rangle = u_{m_s(\boldsymbol{k})}(\boldsymbol{k})e^{-ik\cdot x}\,. \quad (5.112)$$

In this way an operator such as

$$\mathcal{O}_{\mathrm{SSS}}(x) = [\overline{\mathcal{N}}(x)\mathcal{N}(x)]^3\,, \quad (5.113)$$

leads to an amplitude

$$\langle \boldsymbol{k}', m_s(\boldsymbol{k}'); \boldsymbol{a}', m_s(\boldsymbol{a}'); \boldsymbol{b}', m_s(\boldsymbol{b}')|\mathcal{O}_{\mathrm{SSS}}(x)|\boldsymbol{k}, m_s(\boldsymbol{k}); \boldsymbol{a}, m_s(\boldsymbol{a}); \boldsymbol{b}, m_s(\boldsymbol{b})\rangle = 6(\bar{u}_{k'}u_k)(\bar{u}_{a'}u_a)(\bar{u}_{b'}u_b) - 6(\bar{u}_{k'}u_a)(\bar{u}_{a'}u_k)(\bar{u}_{b'}u_b) + \ldots\,. \quad (5.114)$$

Here we are using the shorthand $u_k = u_{m_s(\boldsymbol{k})}(\boldsymbol{k})$, etc., and the ellipsis represents the four other possible permutations arising from Wick contractions. We are also assuming that the external states are chosen to satisfy conservation of four-momentum. A key point here is that Dirac spinors describe spin components in the lab-frame basis. The right-hand side of eq. (5.114) has the correct symmetry properties to be a contribution to $\mathcal{K}^{\mathsf{lab}}_{\mathrm{df},3}$: it is manifestly antisymmetric under initial or final particle interchanges, and it inherits the correct Lorentz and parity transformation properties from those of the free-particle states.

We now consider the complete set of operators without derivatives, that is, with dimension

of $[E]^9$. The available Lorentz- and parity-invariant choices are $\mathcal{O}_{\rm SSS}$ and

$$\begin{aligned}
\mathcal{O}_{\rm SPP} &= [\overline{\mathcal{N}}\mathcal{N}][\overline{\mathcal{N}}\gamma_5\mathcal{N}][\overline{\mathcal{N}}\gamma_5\mathcal{N}]\,,\\
\mathcal{O}_{\rm SVV} &= [\overline{\mathcal{N}}\mathcal{N}][\overline{\mathcal{N}}\gamma_\mu\mathcal{N}][\overline{\mathcal{N}}\gamma^\mu\mathcal{N}]\,,\\
\mathcal{O}_{\rm SAA} &= [\overline{\mathcal{N}}\mathcal{N}][\overline{\mathcal{N}}\gamma_\mu\gamma_5\mathcal{N}][\overline{\mathcal{N}}\gamma^\mu\gamma_5\mathcal{N}]\,,\\
\mathcal{O}_{\rm STT} &= [\overline{\mathcal{N}}\mathcal{N}][\overline{\mathcal{N}}\sigma_{\mu\nu}\mathcal{N}][\overline{\mathcal{N}}\sigma^{\mu\nu}\mathcal{N}]\,,\\
\mathcal{O}_{\rm PVA} &= [\overline{\mathcal{N}}\gamma_5\mathcal{N}][\overline{\mathcal{N}}\gamma_\mu\mathcal{N}][\overline{\mathcal{N}}\gamma^\mu\gamma_5\mathcal{N}]\,,\\
\mathcal{O}_{\rm PTT'} &= [\overline{\mathcal{N}}\gamma_5\mathcal{N}][\overline{\mathcal{N}}\sigma_{\mu\nu}\mathcal{N}][\overline{\mathcal{N}}\sigma^{\mu\nu}\gamma_5\mathcal{N}]\,,\\
\mathcal{O}_{\rm TVV} &= [\overline{\mathcal{N}}\sigma_{\mu\nu}\mathcal{N}][\overline{\mathcal{N}}\gamma^\mu\mathcal{N}][\overline{\mathcal{N}}\gamma^\nu\mathcal{N}]\,,\\
\mathcal{O}_{\rm TAA} &= [\overline{\mathcal{N}}\sigma_{\mu\nu}\mathcal{N}][\overline{\mathcal{N}}\gamma^\mu\gamma_5\mathcal{N}][\overline{\mathcal{N}}\gamma^\nu\gamma_5\mathcal{N}]\,,\\
\mathcal{O}_{\rm T'VA} &= [\overline{\mathcal{N}}\sigma_{\mu\nu}\gamma_5\mathcal{N}][\overline{\mathcal{N}}\gamma^\mu\mathcal{N}][\overline{\mathcal{N}}\gamma^\nu\gamma_5\mathcal{N}]\,,\\
\mathcal{O}_{\rm TTT} &= [\overline{\mathcal{N}}\sigma_{\mu\nu}\mathcal{N}][\overline{\mathcal{N}}\sigma^{\nu\rho}\mathcal{N}][\overline{\mathcal{N}}\sigma_\rho{}^\mu\mathcal{N}]\,,\\
\mathcal{O}_{\rm TT'T'} &= [\overline{\mathcal{N}}\sigma_{\mu\nu}\mathcal{N}][\overline{\mathcal{N}}\sigma^{\nu\rho}\gamma_5\mathcal{N}][\overline{\mathcal{N}}\sigma_\rho{}^\mu\gamma_5\mathcal{N}]\,,
\end{aligned} \tag{5.115}$$

where we have left the x arguments implicit, and used

$$\sigma_{\mu\nu} = \tfrac{i}{2}\left[\gamma_\mu,\gamma_\nu\right]\,. \tag{5.116}$$

This list can be shortened using Fierz identities, but we give a complete enumeration as this would be relevant if we were to consider nonidentical fermions. We convert these operators into forms for $\mathcal{K}^{\mathsf{lab}}_{\rm df,3}$ by taking matrix elements as in eq. (5.114). We then explicitly evaluate the momentum dependence using `Mathematica` for arbitrary choices of spinor components (not yet constrained to satisfy the Dirac equation) and find that all 12 operators lead to forms that are proportional.[11] Thus, with zero derivatives, there is a single contribution to $\mathcal{K}^{\mathsf{lab}}_{\rm df,3}$, given by the right-hand side of eq. (5.114).

[11] By contrast, there are three "four-fermion" Lorentz- and parity-operators of the form $\overline{\mathcal{N}}^2\mathcal{N}^2$. The presence of only one "six-fermion" operator is expected at quadratic order in a nonrelativistic expansion, where it is given by eq. (5.118). What is surprising is that this holds to all orders in this expansion.

We now enforce that the spinors satisfy the Dirac equation by writing

$$u_k = \sqrt{2\omega_k} \begin{pmatrix} \chi_k \\ \frac{\boldsymbol{\sigma}\cdot\boldsymbol{k}}{\omega_k + m}\chi_k \end{pmatrix}, \tag{5.117}$$

where χ_k is the non-relativistic two-spinor corresponding to the component $m_s(\boldsymbol{k})$, and $\omega_k = \sqrt{\boldsymbol{k}^2 + m^2}$. We insert this into eq. (5.114), and perform a nonrelativistic expansion, i.e. an expansion in powers of $\boldsymbol{k}/m$. The leading-order term (with no factors of $\boldsymbol{k}$) vanishes, as is expected because one cannot antisymmetrize the spin wavefunction of three identical spin-1/2 particles. The first nonvanishing term is quadratic in momenta and proportional to

$$\mathcal{K}_A = \overline{\mathcal{A}}\left[(\chi^\dagger_{k'}\,\boldsymbol{\sigma}\cdot\boldsymbol{k'}\,\boldsymbol{\sigma}\cdot\boldsymbol{k}\,\chi_k)(\chi^\dagger_{a'}\chi_a)(\chi^\dagger_{b'}\chi_b)\right]. \tag{5.118}$$

Here $\overline{\mathcal{A}}$ indicates antisymmetrization over initial and final particle labels; it differs from the operation $\mathcal{A}$ defined in eq. (C.7), and used in eq. (5.99), by not requiring an initial step of combining with spherical harmonics. Therefore, the contribution to $\mathcal{K}_{\rm df,3}$ is:

$$m^2\mathcal{K}^{\mathsf{lab}}_{\rm df,3} \supset \frac{c_0}{m^2}\mathcal{K}_A + O\left(\frac{\boldsymbol{k}^4}{m^4}\right), \tag{5.119}$$

where c_0 is a dimensionless coefficient whose value is not fixed. Here we assume that the contribution of the operators in eq. (5.115) appears in the Lagrangian as $\mathcal{L} \supset (g_0/m^5)\mathcal{O}$, where g_0 is dimensionless and proportional to c_0 in eq. (5.119). The expansion can be continued to higher orders in $\boldsymbol{k}/m$, a point that we return to below.

At quadratic order in the nonrelativistic expansion, we must also consider operators containing two derivatives,[12] i.e. of energy dimension $[E]^{11}$. In section C.3 we enumerate all such operators that are Lorentz- and parity-invariant, that are not related by Fierz identities, and that cannot be written in terms of operators without derivatives using the equations of motion. We find 22 such operators. However, if we insert the nonrelativistic expansion of the spinors into the corresponding contributions to $\mathcal{K}^{\mathsf{lab}}_{\rm df,3}$, we find only two independent

[12]Operators with one derivative can be related to operators without derivatives using the equations of motion, and thus are not independent.

terms at quadratic order,[13] which can be chosen to be $\mathcal{K}_A$, given above, and

$$\mathcal{K}_B = \overline{\mathcal{A}} \left[\boldsymbol{k'} \cdot \boldsymbol{k} (\chi^\dagger_{k'} \chi_k)(\chi^\dagger_{a'} \chi_a)(\chi^\dagger_{b'} \chi_b) \right] . \tag{5.120}$$

Since these operators have a higher energy dimension, the couplings in the Lagrangian of the EFT will contain two inverse powers of the typical energy scale of the EFT, Λ^2_{EFT}. This way, the contribution of dimension-11 operators to $\mathcal{K}_{\text{df,3}}$ at quadratic order in momenta is:

$$m^2 \mathcal{K}^{\mathsf{lab}}_{\text{df,3}} \supset \frac{c_1}{\Lambda^2_{\text{EFT}}} \mathcal{K}_A + \frac{c_2}{\Lambda^2_{\text{EFT}}} \mathcal{K}_B + O\left(\frac{\boldsymbol{k}^4}{m^2 \Lambda^2_{\text{EFT}}} \right). \tag{5.121}$$

If we consider systems of nucleons at low momentum described by pionless EFT, the energy scale is the pion mass, $\Lambda_{\text{EFT}} \simeq m_\pi$. This choice implies that (i) the contribution from eq. (5.119) is subdominant with respect to that of eq. (5.121), and (ii) eq. (5.121) is the most general form of $\mathcal{K}_{\text{df,3}}$ through $\mathcal{O}(\boldsymbol{k}^2)$. We note, however, that the range of convergence of pionless EFT is limited by the left-hand cut ($\boldsymbol{k}^2 < m_\pi^2/4$), while the relativistic finite-volume three-neutron formalism is applicable beyond that, i.e. up to the $NNN\pi$ threshold ($\boldsymbol{k}^2 \sim m_\pi m_N$). We also stress that, at this order in the nonrelativistic expansion, we would have obtained the same result simply by enforcing rotation and parity invariance and anti-symmetry.

Proceeding to higher order in the nonrelativistic expansion is straightforward in principle. There are no terms of cubic order, due to the requirement of parity invariance of $\mathcal{K}_{\text{df,3}}$. This is because momenta flip sign, while spins remain unchanged. To determine the independent terms of quartic order would require the enumeration of allowed operators with up to four derivatives, a straightforward but tedious task that we have not undertaken. We stress that an approach in which one simply writes down operators consistent with rotation and parity invariance and antisymmetry, while working at quadratic order, would not, in general, work at higher orders, because constraints due to the Lorentz covariance would be lost (just as the relative size of the $\boldsymbol{k}^2/m^2$ and $\boldsymbol{k}^4/m^4$ terms in the relativistic dispersion relation cannot be determined without enforcing Lorentz symmetry).

[13] Because the zeroth component of the derivatives yield energies, which do not vanish at threshold, there could in principle be a zeroth order term, but this vanishes due to the antisymmetry, as discussed above.

As a final comment, we note that there is a superficial difference between the nonrelativistic expansion that we have used here, and the form of the threshold expansions for mesonic systems (e.g. three pions in refs. [37, 110]). The latter are written in terms of Lorentz invariant Mandelstam variables, whereas here we explicitly expand in powers of the nucleon's three-momentum, $\boldsymbol{k}$. There is, however, no fundamental difference between the approaches, because the quantities in the mesonic case can be rewritten in terms of a nonrelativistic expansion. For example, the quantity $\Delta = (s - 9m^2)/(9m^2)$ used in ref. [110] as an expansion parameter, is proportional to the sum of $\boldsymbol{k}^2$ for the initial and final particles, plus higher order terms. It just turns out that, in the absence of the spin degrees of freedom, one can write the expansion in a manifestly Lorentz-invariant way more easily than in the present case.

5.7 Conclusions

This work presents the finite-volume formalism in the RFT approach for three identical spin-1/2 particles. The most relevant physical system to which it is applicable is three neutrons (or protons), but also, e.g., three spin-1/2 hyperons. The new features are the presence of the spin degrees of freedom and the overall antisymmetry of the states. Since the formalism is relativistic, spin components can mix via boosts, which is indeed the main technical complication of the derivation. The solution is to include the effect of Wigner rotations when relating spin degrees of freedom in the lab (finite-volume) frame and the CMF of pairs—see section 5.4.1.

Sections 5.4.2 and 5.4.3 represent the core of this work. First, the modifications of the building blocks of the three-particle formalism are discussed in section 5.4.2. Defining the spin degrees of freedom of the interacting pair in the dimer frame leads to very simple generalizations of the blocks $\mathbf{F}$ and $\mathbf{K}_2$, which are related to sum-minus integral difference of a two-neutron loop and two-neutron interactions, respectively. By contrast, in the dimer frame, the fermionic nature of the particles is explicit in $\mathbf{G}$—the builing block related to one-neutron exchange processes. As such, $\mathbf{G}$ contains the aforementioned Wigner rotations

and minus sign from antisymmetry (see eq. (5.45)). In section 5.4.3, the derivation of the finite-volume formalism using a diagrammatic expansion of the finite-volume correlator that utilizes those building blocks is presented. Simple examples of contributions to this expansion are depicted in figure 5.1.

The outcomes of section 5.4 are the finite-volume correlator in eq. (5.93) and the finite-volume analogous of the (unsymmetrized) scattering amplitude in eq. (5.94). The quantization condition and the integral equations relating the three-particle K matrix to the scattering amplitude are easily obtained from these equations. They can be found in section 5.5, where we summarize the results of the derivation. As noted, we have focused on the derivation and form of the resulting quantization in this work, providing only a sketch of many of the details of the implementation of the formalism. We will discuss these in a follow-up work.

An important ingredient in the finite-volume formalism is the parametrization of the three-neutron K matrix, which describes short-range three-neutron interactions. In section 5.6 we show, working to lowest nontrivial order in a nonrelativistic momentum expansion, that only two different types of operators contribute—see eq. (5.121). At higher orders, more independent terms appear, as discussed in section C.3.

Now that we have determined how to include spin into the RFT approach in the simplest setting of identical fermions, there are several generalizations that can be considered. These include three nucleons of arbitrary isospin (in isosymmetric QCD), which should involve a straightforward combination of the present work with the formalism developed for the generic three-pion system [37]. Other systems of interest involve two spin-1/2 particles and a (pseudo-)scalar, or one spin-1/2 particle and two (pseudo-)scalars, for which a combination of the methods presented here with those for nondegenerate systems [35, 36] will be needed. A particularly interesting example in QCD is the $N\pi\pi$ system at non-maximal isospin, which has the additional difficulty of mixing with the $N\pi$ state. In the context of the RFT approach, this will require as well the use of a generalization of the $2 \leftrightarrow 3$ formalism of ref. [39]. Such a generalization is of great interest, as it will allow access to the Roper resonance, a puzzling baryonic excitation with the same quantum numbers of the nucleon.

Acknowledgments

We thank Raúl Briceño, Vincenzo Cirigliano, Will Detmold, Dan Hackett, Andrew Jackura, and Felix Ziegler for useful discussions.

MTH is supported by UKRI Future Leader Fellowship MR/T019956/1 and in part by UK STFC grant ST/P000630/1. The work of FRL has been supported in part by the U.S. Department of Energy, Office of Science, Office of Nuclear Physics, under grant Contract Numbers DE-SC0011090 and DE-SC0021006. FRL acknowledges financial support by the Mauricio and Carlota Botton Fellowship. The work of SRS and ZTD is supported in part by the USDOE grant No. DE-SC0011637.

FRL would like to thank the Physics Department at the University of Washington for its hospitality during a visit in which this work was initiated.

Chapter 6

THREE-PARTICLE FORMALISM FOR MULTIPLE CHANNELS: THE $\eta\pi\pi + K\overline{K}\pi$ SYSTEM IN ISOSYMMETRIC QCD[1]

6.1 Abstract

We generalize previous three-particle finite-volume formalisms to allow for multiple three-particle channels. For definiteness, we focus on the two-channel $\eta\pi\pi$ and $K\overline{K}\pi$ system in isosymmetric QCD, considering the positive G parity sector of the latter channel, and neglecting the coupling to modes with four or more particles. The formalism we obtain is thus appropriate to study the $b_1(1235)$ and $\eta(1295)$ resonances. The derivation is made in the generic relativistic field theory approach using the time-ordered perturbation theory method. We study how the resulting quantization condition reduces to that for a single three-particle channel when one drops below the upper $(K\overline{K}\pi)$ threshold. We also present parametrizations of the three-particle K matrices that enter into the formalism.

6.2 Introduction

A multitude of exotic hadrons has been unearthed in the last two decades [219–226], sparking interest in providing first-principles predictions of their properties through quantum chromodynamics (QCD). Despite the theoretical suitability of lattice QCD for such endeavors, its practical application encounters limitations due to the extensive array of open decay modes associated with many of these exotic resonances.

In this work we address one particular limitation of the formalism that has been derived to

[1]Z. T. Draper and S. R. Sharpe, *Three-particle formalism for multiple channels: the $\eta\pi\pi + k\bar{k}\pi$ system in isosymmetric qcd*, 2403.20064 [To appear in JHEP]

date [16,17,35–39,103–107,109–112,114–122], namely the restriction to a single three-particle channel [16, 17, 104, 106, 107], or to several degenerate such channels [37, 227]. In particular, we consider a system with two distinct three-particle channels, although the generalization to multiple such channels is straightforward. This is a step on the way to a completely general formalism that includes channels with two, three and more particles.[2]

To have a concrete system to discuss, we consider the $b_1(1235)$ and $\eta(1295)$ resonances in isosymmetric QCD. These have quantum numbers $I^G(J^{PC}) = 1^+(1^{+-})$ and $0^+(0^{-+})$, and in particular have positive G parity and unnatural J^P. These resonances decay into two three-particle channels, namely $K\overline{K}\pi$ and $\pi\pi\eta$, as well as into 4π modes. They cannot decay to two pions (a channel having natural J^P) or to three pions (due to G parity). Thus, if we neglect the four pion modes, and also the other kinematically allowed channels that have not yet been observed in the decays of these resonances (6π, 8π, $4\pi + \eta$), this is a system that has our desired property of two different three-particle channels.[3]

In this work we make the desired generalization using the generic relativistic field-theoretic (RFT) approach to the derivation of three-particle formalism [16, 17]. In particular, we use the method of derivation based on time-ordered perturbation theory (TOPT) introduced in ref. [115]. The formalism we obtain is a synthesis of methodologies developed previously for three distinct particles [35], for 2+1 systems (comprising two identical and one distinct particle) [36], for three pions of arbitrary isospin [37], and for the doubly-charmed tetraquark [227]. We avoid repeating steps in the derivation that are presented in these works to the extent possible while retaining readability.

This paper is organized as follows. In the following section, section 6.3, we introduce the two-channel system that we study, and point out the pertinent general features. The core

---

[2]We note that the formalism that includes channels with both two and three particles has been derived in ref. [39], but this is restricted to the case in which all the particles are spinless and identical. Another approach to the "$2+3$" case has recently been proposed for the $D^*D + DD\pi$ system in ref. [227].

[3]The b_1 resonance has been studied using lattice QCD for heavier-than-physical quark masses such that $M_\pi \approx 390$ MeV, in which case it decays primarily to the two-particle channel $\pi\omega$, and thus can be analyzed using the two-particle quantization condition [228].

of this paper is section 6.4, in which we derive the multichannel three-particle quantization condition, following what are now fairly standard steps in the TOPT approach. The only new feature is the projection onto the sector of positive G parity, discussed in section 6.4.8. Since the $\pi\pi\eta$ and $K\overline{K}\pi$ channels have substantially different thresholds, one can ask how the two-channel formalism reduces to that for a single channel as one drops below the upper ($K\overline{K}\pi$) threshold. We address this in section 6.5. Practical applications require the use of parametrizations of the three-particle K matrix, and we describe in section 6.6 how symmetries constrain the allowed forms. We conclude in section 6.7. Various technical details are collected into seven appendices.

6.3 Overview

The total isospin of both $K\overline{K}\pi$ and $\pi\pi\eta$ channels can be $I = 0$, 1, or 2. Although resonances are present only for the first two of these values, we derive the formalism for all three choices. All three can be accessed by studying the sector with quantum numbers $I_3 = 0$, $U = 0, D = 0, S = 0$.[4] There are six different flavor channels with these quantum numbers,

$$\Big\{ K^+(\boldsymbol{k}_1)\overline{K}^0(\boldsymbol{k}_2)\pi^-(\boldsymbol{k}_3),\ K^+(\boldsymbol{k}_1)K^-(\boldsymbol{k}_2)\pi^0(\boldsymbol{k}_3),\ K^0(\boldsymbol{k}_1)\overline{K}^0(\boldsymbol{k}_2)\pi^0(\boldsymbol{k}_3), \\ K^0(\boldsymbol{k}_1)K^-(\boldsymbol{k}_2)\pi^+(\boldsymbol{k}_3),\ \pi^+(\boldsymbol{k}_1)\pi^-(\boldsymbol{k}_2)\eta(\boldsymbol{k}_3),\ \pi^0(\boldsymbol{k}_1)\pi^0(\boldsymbol{k}_2)\eta(\boldsymbol{k}_3) \Big\}, \tag{6.1}$$

where we include momentum labels for later use. These decompose into isospin as the $I_3 = 0$ components of the following seven channels,

$$\begin{aligned} I = 2: &\quad a)\ [[K\bar{K}]_1\pi]_2,\ b)\ [[\pi\pi]_2\eta]_2\,; \\ I = 1: &\quad a)\ [[K\bar{K}]_1\pi]_1,\ b)\ [[K\bar{K}]_0\pi]_1,\ c)\ [[\pi\pi]_1\eta]_1\,; \\ I = 0: &\quad a)\ [[K\bar{K}]_1\pi]_0,\ b)\ [[\pi\pi]_0\eta]_0\,; \end{aligned} \tag{6.2}$$

where the subscripts indicate isospin, and the momentum labels are implicitly ordered as in eq. (6.1): $\boldsymbol{k}_1$, $\boldsymbol{k}_2$, and $\boldsymbol{k}_3$. The increase from six to seven dimensions arises because, when

[4] We have also checked the final results by considering the channels with $I_3 = 1$ and 2, which contain, respectively, total isospins $I = 1, 2$ and $I = 2$.

decomposing under isospin, the symmetric and antisymmetric parts of $\pi^+\pi^-$ are treated separately. The relation between the isospin and flavor bases, which will be needed in the subsequent discussion, is given in section D.1.

In order to avoid mixing with the three-pion channel, we must restrict the states to have $G = +$. This is automatic for the $\pi\pi\eta$ channel, but not for $K\overline{K}\pi$, which can have either G parity. This restriction can be implemented by applying relations between the four $K\overline{K}\pi$ flavor channels in eq. (6.1), or equivalently upon the corresponding four channels in eq. (6.2). It is simpler to state the restrictions for the latter:[5] To have overall $G = +$, the $K\overline{K}$ pairs must have $G = -$. This implies that $[K\bar{K}]_1$ pairs must be symmetric under $\boldsymbol{k}_1 \leftrightarrow \boldsymbol{k}_2$ (and thus have only even relative angular momentum), while $[K\bar{K}]_0$ pairs must be antisymmetric (implying odd relative angular momentum). This follows because the action on kaons of $G = Ce^{-i\pi I_y}$ (where C is the charge conjugation operator and I_y the second component of isospin) is $K^+ \to \overline{K}^0$, $K^0 \to -K^-$, $\overline{K}^0 \to -K^+$, and $K^- \to K^0$. Here we have used the result that the kaon isodoublets are (K^+, K^0) and $(-\overline{K}^0, K^-)$. Thus, for example, $[K\bar{K}]_0 \propto K^+K^- + K^0\overline{K}^0$, which under G transforms to $\overline{K}^0K^0 + K^-K^+$. Since the K and $\overline{K}$ are interchanged, to obtain a negative G parity the relative spatial wavefunction must be antisymmetric. We stress that G parity is an exact symmetry of *lattice* QCD if $m_u = m_d$, so that these considerations apply without approximation to the results of simulations.

In the derivation that follows, we will implicitly assume that these restrictions have been applied, so that only $G = +$ states are present. We will not explicitly apply these restrictions until after the final form has been obtained. Having the restrictions (implicitly) in place allows us to neglect mixing with the 3π channel. We stress that it would be straightforward, though tedious, to include this channel as a third three-particle state. This would result in a separate formalism describing the 3π and odd-G-parity $K\overline{K}\pi$ system, since G parity is an exact symmetry of isosymmetric QCD. We choose not to do so in order to keep the focus on

[5]For completeness we note that the restrictions on the channels in eq. (6.1) are as follows: the first and fourth must be symmetric under $\boldsymbol{k}_1 \leftrightarrow \boldsymbol{k}_2$, as must the difference between the second and third channels, while the sum of the second and third channels must be antisymmetric under $\boldsymbol{k}_1 \leftrightarrow \boldsymbol{k}_2$.

the essential new features that arise when there are additional three-particle channels, and to avoid cumbersome expressions.

As noted in the introduction, the $b_1(1235)$ and $\eta(1295)$ do not couple to $\pi\pi$ states, because these resonances have unnatural J^P. However, coupling between $\pi\pi\eta$ or $K\overline{K}\pi$ and $\pi\pi$ states is possible for natural J^P other than 0^+. For example, two pions in a p-wave combined with an η in a relative p-wave leads to an overall $J^P = 1^-$, which can mix with two pions. In finite volume, the rotation group is broken to a finite subgroup, with parity not being a good symmetry in moving frames. Thus mixing with two-pion states is allowed in any finite-volume irreducible representations (irreps) into which natural J^P values are subduced. Therefore, in the following, we implicitly assume that we are using irreps into which only unnatural J^P values are subduced, thus avoiding the mixing with two-pion states. It is straightforward to determine which irreps these are, using, for example, the group-theoretical results presented in ref. [229]. For the rest frame, where parity is a good symmetry, we can use the A_{1u}, T_{1g}, A_{2g}, E_u, and T_{2u} irreps, with the first two, respectively, picking out the $\eta(1295)$ and $b_1(1235)$ quantum numbers. In other frames, we can only use the A_2 irrep, which couples to both the $\eta(1295)$ and $b_1(1235)$, except for the following caveat. For frames with momenta of the form $\{0, 0, n\}$, $\{0, n, n\}$, $\{n, n, n\}$, $\{n, n, m\}$, and $\{n, m, 0\}$, natural J^P values do appear in the A_2 irrep, but only starting at 4^+, 2^+, 3^-, 1^- and 1^-, respectively. Thus we can only use these frames if we assume that the mixing is small in the corresponding values of J^P. This appears most reasonable for the $\{0, 0, n\}$ and $\{n, n, n\}$ frames.

6.4 Derivation of quantization condition

We follow the TOPT approach introduced in ref. [115], a work hereafter referred to as BS1. In particular, we make extensive use of the results for three distinguishable particles (derived in ref. [35], referred to as BS3 henceforth) and for "2+1" systems (ref. [36], referred to as BS2). We use Minkowski time and confine space within a cubic box of side-length L with periodic boundary conditions. The starting point is the finite-spatial-volume Minkowski-

space correlation matrix,

$$\widehat{C}_L(P)_{jk} \equiv \int dx^0 \int_{L^3} d^3\boldsymbol{x}\, e^{-i\boldsymbol{P}\cdot\boldsymbol{x}+iEt} \langle 0|\mathrm{T}\mathcal{O}_j(x)\mathcal{O}_k^\dagger(0)|0\rangle_L \,, \tag{6.3}$$

where the indices i and j run over the six flavors given in eq. (6.1), with $\mathcal{O}_j(x)$ being any quasilocal operator possessing the appropriate quantum numbers to annihilate states with flavor j, coupling with all allowed irreducible representations of the cubic group. The overall momentum vector $\boldsymbol{P}$ is constrained by the boundary conditions to lie in the finite volume set $2\pi\boldsymbol{n}/L$, where $\boldsymbol{n} \in \mathbb{Z}^3$.

For a specified $\boldsymbol{P}$, the energies of finite-volume states are determined by the poles of C_L as a function of E. Our derivation will hold in a kinematic range where the only relevant on-shell states are $\pi\pi\eta$ and $K\overline{K}\pi$, the thresholds for which are $M_{\pi\pi\eta} \approx 820$ and $M_{KK\pi} \approx 1130$ MeV, respectively, for physical quark masses. For the heavier-than-physical quark masses often used in present lattice simulations of multiparticle states, the two channels will lie closer together, since the pion mass rises more rapidly with increasing quark mass than those of the kaon or η. Since we are restricting ourselves to positive G parity, and to irreps that do not mix with $\pi\pi$ states, the other potentially relevant channels are 4π, 6π, 8π, $4\pi+\eta$, $6\pi+\eta$ and $K\overline{K}\pi\pi$. As noted in the introduction, we will neglect the coupling to these channels, but keep in mind that, in a practical application of our formalism, this approximation will become increasingly inaccurate as the energy increases. We expect the range of approximate applicability to be

$$M_{\pi\pi\eta} - 2M_\pi = M_\eta < E^* = \sqrt{E^2 - \boldsymbol{P}^2} < M_{KK\pi} + M_\pi \,. \tag{6.4}$$

Here the lower limit is set either by the presence of the single η intermediate state (for the $I = 0$ channel), or, more generally, by the closing of the $\pi\pi$ subchannel at the left-hand cut due to two-pion exchange.

6.4.1 All orders expression obtained using TOPT

Through a straightforward extension of the work in BS2 and BS3, we can express the finite-volume-dependent part of C_L in the relevant kinematic range as a geometric series. This

series involves TOPT Bethe-Salpeter kernels $B_{2,L}$ and B_3 situated between cut factors, D, that carry the singularities associated with three-particle states:

$$\Delta C_L \equiv C_L - C_\infty^{(0)} = A' i D \frac{1}{1 - i(B_{2,L} + B_3) i D} A + \mathcal{O}(e^{-M_\pi L}), . \tag{6.5}$$

Here, A' and A represent endcaps, encompassing all diagrams connecting the operators $\mathcal{O}_j$ and $\mathcal{O}_k^\dagger$ to a three-particle intermediate state, while $C_\infty^{(0)}$ is the contribution devoid of three-particle intermediate states. All quantities in eq. (6.5) are matrices, spanning both flavor space and momentum space. Momentum indices are denoted as $\{\boldsymbol{k}\} = \{\boldsymbol{k}_1, \boldsymbol{k}_2, \boldsymbol{k}_3\}$, with the triplets of finite-volume momenta constrained by $\boldsymbol{k}_1 + \boldsymbol{k}_2 + \boldsymbol{k}_3 = \boldsymbol{P}$. The derivation of eq. (6.5) relies on the fact that finite-volume momentum sums of nonsingular summands can be replaced by the corresponding infinite-volume integrals, with corrections exponentially suppressed in $M_\pi L$ [15]. Throughout this derivation, such corrections are assumed negligible, and will be omitted from subsequent expressions. A key consequence of this assumption is that the Bethe-Salpeter kernels, the endcaps, and $C_\infty^{(0)}$ are infinite-volume quantities, aside from a trivial L dependence in $B_{2,L}$ to be described below.

We now describe the remaining quantities present in eq. (6.5), starting with the cut factors. These are diagonal in flavor and take the form

$$D = \mathrm{diag}(D_0, D_0, D_0, D_0, \overline{D}_0, \tfrac{1}{2}\overline{D}_0)\,, \tag{6.6}$$

where D_0 and $\overline{D}_0$ are standard TOPT energy denominators,

$$D_0 = \delta_{\{\boldsymbol{p}\}\{\boldsymbol{k}\}} \frac{1}{L^6} \frac{1}{8\omega_1\omega_2\omega_3} \frac{1}{E - \omega_1 - \omega_2 - \omega_3}\,, \tag{6.7}$$

$$\overline{D}_0 = \delta_{\{\boldsymbol{p}\}\{\boldsymbol{k}\}} \frac{1}{L^6} \frac{1}{8\omega_1'\omega_2'\omega_3'} \frac{1}{E - \omega_1' - \omega_2' - \omega_3'}\,. \tag{6.8}$$

Here $\omega_i \equiv \omega_{p_i} = \sqrt{\boldsymbol{p}_i^2 + M_i^2}$ and $\omega_i' \equiv \omega_{p_i} = \sqrt{\boldsymbol{p}_i^2 + M_i'^2}$ are single-particle energies, with M_i drawn from the ordered set $\{M_K, M_K, M_\pi\}$, and M_i' drawn from $\{M_\pi, M_\pi, M_\eta\}$. The momentum-space Kronecker delta $\delta_{\{\boldsymbol{p}\}\{\boldsymbol{k}\}}$ is shorthand for

$$\delta_{\{\boldsymbol{p}\}\{\boldsymbol{k}\}} = \delta_{\boldsymbol{p}_1\boldsymbol{k}_1}\delta_{\boldsymbol{p}_2\boldsymbol{k}_2}\delta_{\boldsymbol{p}_3\boldsymbol{k}_3}\,. \tag{6.9}$$

Note that in the final entry of D, which corresponds to the 2+1 system $\pi^0\pi^0\eta$, the factor of $\overline{D}_0$ is accompanied by a symmetry factor of 1/2.

The appearance of two different cut factors, i.e. D_0 and $\overline{D}_0$, which have singularities at different energies, is the first new feature due to the presence of multiple three-particle channels. This presents no obstacle to deriving the all-orders result eq. (6.5)— one simply has to keep both types of cut factor explicit.

Next we consider the matrix $B_{2,L}$, which contains two-particle Bethe-Salpeter kernels, denoted, using calligraphic font, as $\mathcal{B}_2$. These kernels are defined as sums over all TOPT diagrams contributing to two-to-two processes that lack two-particle cuts in the s channel. In these diagrams, all momentum sums are replaced by integrals, rendering them infinite-volume quantities. Extending the analysis from BS2 and BS3, we arrive at the following block form for the flavor structure,

$$B_{2,L} = \begin{pmatrix} B_{11} & B_{12} \\ B_{21} & B_{22} \end{pmatrix} \tag{6.10}$$

where

$$B_{11} = \begin{pmatrix} \begin{matrix}\mathcal{B}_{2,L}(K^+\overline{K}^0\leftarrow K^+\overline{K}^0)\\ +\mathcal{B}_{2,L}(K^+\pi^-\leftarrow K^+\pi^-)\\ +\mathcal{B}_{2,L}(\overline{K}^0\pi^-\leftarrow\overline{K}^0\pi^-)\end{matrix} & \mathcal{B}_{2,L}(\overline{K}^0\pi^-\leftarrow K^-\pi^0) & \mathcal{B}_{2,L}(K^+\pi^-\leftarrow K^0\pi^0) & 0 \\ \mathcal{B}_{2,L}(K^-\pi^0\leftarrow\overline{K}^0\pi^-) & \begin{matrix}\mathcal{B}_{2,L}(K^+K^-\leftarrow K^+K^-)\\ +\mathcal{B}_{2,L}(K^+\pi^0\leftarrow K^+\pi^0)\\ +\mathcal{B}_{2,L}(K^-\pi^0\leftarrow K^-\pi^0)\end{matrix} & \mathcal{B}_{2,L}(K^+K^-\leftarrow K^0\overline{K}^0) & \mathcal{B}_{2,L}(K^+\pi^0\leftarrow K^0\pi^+) \\ \mathcal{B}_{2,L}(K^0\pi^0\leftarrow K^+\pi^-) & \mathcal{B}_{2,L}(K^0\overline{K}^0\leftarrow K^+K^-) & \begin{matrix}\mathcal{B}_{2,L}(K^0\overline{K}^0\leftarrow K^0\overline{K}^0)\\ +\mathcal{B}_{2,L}(K^0\pi^0\leftarrow K^0\pi^0)\\ +\mathcal{B}_{2,L}(\overline{K}^0\pi^0\leftarrow\overline{K}^0\pi^0)\end{matrix} & \mathcal{B}_{2,L}(\overline{K}^0\pi^0\leftarrow K^-\pi^+) \\ 0 & \mathcal{B}_{2,L}(K^0\pi^+\leftarrow K^+\pi^0) & \mathcal{B}_{2,L}(K^-\pi^+\leftarrow\overline{K}^0\pi^0) & \begin{matrix}\mathcal{B}_{2,L}(K^0K^-\leftarrow K^0K^-)\\ +\mathcal{B}_{2,L}(K^0\pi^+\leftarrow K^0\pi^+)\\ +\mathcal{B}_{2,L}(K^-\pi^+\leftarrow K^-\pi^+)\end{matrix} \end{pmatrix}, \tag{6.11}$$

$$B_{12} = \begin{pmatrix} \mathcal{B}_{2,L}(K^+\overline{K}^0\leftarrow\pi^+\eta) & 0 \\ 0 & \mathcal{B}_{2,L}(K^+K^-\leftarrow\pi^0\eta)S^D \\ 0 & \mathcal{B}_{2,L}(K^0\overline{K}^0\leftarrow\pi^0\eta)S^D \\ \mathcal{B}_{2,L}(K^0K^-\leftarrow\pi^-\eta) & 0 \end{pmatrix}, \tag{6.12}$$

$$B_{21} = \begin{pmatrix} \mathcal{B}_{2,L}(\pi^+\eta\leftarrow K^+\overline{K}^0) & 0 & 0 & \mathcal{B}_{2,L}(\pi^-\eta\leftarrow K^0K^-) \\ 0 & S^D\mathcal{B}_{2,L}(\pi^0\eta\leftarrow K^+K^-) & S^D\mathcal{B}_{2,L}(\pi^0\eta\leftarrow K^0\overline{K}^0) & 0 \end{pmatrix}, \tag{6.13}$$

and

$$B_{22} = \begin{pmatrix} \begin{matrix} \mathcal{B}_{2,L}(\pi^+\eta\leftarrow\pi^+\eta) \\ +\mathcal{B}_{2,L}(\pi^-\eta\leftarrow\pi^-\eta) \\ +\mathcal{B}_{2,L}(\pi^+\pi^-\leftarrow\pi^+\pi^-) \end{matrix} & \mathcal{B}_{2,L}(\pi^+\pi^- \leftarrow \pi^0\pi^0) \\ \mathcal{B}_{2,L}(\pi^0\pi^0 \leftarrow \pi^+\pi^-) & \begin{matrix} S^D\mathcal{B}_{2,L}(\pi^0\eta\leftarrow\pi^0\eta)S^D \\ +\mathcal{B}_{2,L}(\pi^0\pi^0\leftarrow\pi^0\pi^0) \end{matrix} \end{pmatrix} . \tag{6.14}$$

The texture of nonzero entries is dictated by the two-particle interactions capable of inducing the necessary changes in flavor composition. For instance, the top-right entry in B_{12} vanishes because there are no two-particle interactions that connect $K^+\overline{K}^0\pi^-$ to $\pi^0\pi^0\eta$, since all three particles must change.

The form of the individual entries in $B_{2,L}$ is exemplified by

$$\mathcal{B}_{2,L}(\pi^0\eta \leftarrow K^+K^-)_{\{\boldsymbol{p}\},\{\boldsymbol{k}\}} = 2\omega_{p_2}L^3\delta_{\boldsymbol{p}_2\boldsymbol{k}_3}\mathcal{B}_2[\pi^0(\boldsymbol{p}_1)\eta(\boldsymbol{p}_3) \leftarrow K^+(\boldsymbol{k}_1)\overline{K}^0(\boldsymbol{k}_2)] , \tag{6.15}$$

which appears in the lower row of B_{21}. The explicit L dependence arises from keeping track of TOPT propagator factors. The single momentum Kronecker-delta arises because one of the particles spectates (here, one of the π^0s). Note that we have chosen the π^0 particle in the final state of the scattering to be that with momentum $\boldsymbol{p}_1$. The other possible choice, $\boldsymbol{p}_2$, is included by the factor of S^D, a symmetrization operator defined as

$$S^D = 1 + P^D , \qquad 1 = \delta_{\{\boldsymbol{p}\},\{\boldsymbol{k}\}} , \qquad P^D = \delta_{\boldsymbol{p}_1\boldsymbol{k}_2}\delta_{\boldsymbol{p}_2\boldsymbol{k}_1}\delta_{\boldsymbol{p}_3\boldsymbol{k}_3} . \tag{6.16}$$

In words, P^D interchanges the first two momenta. All other entries in $B_{2,L}$ have a similar form, with the choice of spectator momenta depending on the flavors involved in the two-particle scattering, and factors of S^D appearing when a single π^0 is involved in the scattering.

To complete the description, it remains to define B_3. The entries in this flavor matrix are the sum over all TOPT diagrams connecting initial and final flavors with no three-particle cuts. Momentum sums are replaced by integrals, rendering all entries infinite-volume quantities. The only properties of B_3 that we will need are that it conserves isospin and is symmetric under interchanges of identical particles in either the initial or final states.

6.4.2 On-shell projection

The next step is to project the kernels and endcaps on either side of each cut factor in eq. (6.5) on shell, using the approach of BS1. The new feature due to having two three-

particle channels is that the kinematic details of on-shell projection differ for the two types of cut. This is straightforward to implement.

As explained most extensively in BS2, a convenient first step is to relocate the symmetrization operators from the Bethe-Salpeter kernels into the cut factors D. This can be accomplished by following the same steps as in BS2, leveraging the symmetry under exchange of two identical particles. We first pull out the factors of S_D in $B_{2,L}$ by writing

$$B_{2,L} = \tilde{S}_D \tilde{B}_{2,L} \tilde{S}_D \,, \tag{6.17}$$

where

$$\tilde{S}_D \equiv \mathrm{diag}(1,1,1,1,1,S^D) \,. \tag{6.18}$$

$\tilde{B}_{2,L}$ contains no factors of S_D and will be given explicitly below. Next, we introduce a rescaling matrix

$$R = \mathrm{diag}(1,1,1,1,1,\tfrac{1}{2}) \,, \tag{6.19}$$

such that the following identities hold

$$A = \tilde{S}_D R A \,, \quad A' = A' R \tilde{S}_D \,, \quad B_3 = \tilde{S}_D R B_3 R \tilde{S}_D \,. \tag{6.20}$$

These follow from the invariance under the interchange of the two π^0s, with the factor of $1/2$ in the last slot of R cancelling the double counting introduced by applying S_D. Then we can rearrange the volume-dependent part of the correlator into the form

$$\Delta C_L = \tilde{A}' i D_S \frac{1}{1 - i(\tilde{B}_{2,L} + \tilde{B}_3) i D_S} \tilde{A} \,, \tag{6.21}$$

where

$$D_S = \tilde{S}_D D \tilde{S}_D = \mathrm{diag}(D_0, D_0, D_0, D_0, \overline{D}_0, \tfrac{1}{2} S^D \overline{D}_0 S^D) \,, \tag{6.22}$$

and

$$\tilde{B}_3 = R B_3 R \,, \quad \tilde{A}' = A' R \,, \quad \tilde{A} = R A \,. \tag{6.23}$$

The explicit form of $\tilde{B}_{2,L}$ is

$$\tilde{B}_{2,L} = \begin{pmatrix} B_{11} & \tilde{B}_{12} \\ \tilde{B}_{21} & \tilde{B}_{22} \end{pmatrix}, \tag{6.24}$$

where the top-left block is unchanged from $B_{2,L}$, eq. (6.11), the off-diagonal blocks $\tilde{B}_{12}$ and $\tilde{B}_{21}$ are given by eq. (6.12) and eq. (6.13), respectively, except with the factors of S_D removed, and

$$\tilde{B}_{22} = \begin{pmatrix} \begin{smallmatrix}\mathcal{B}_{2,L}(\pi^+\eta\leftarrow\pi^+\eta) \\ +\mathcal{B}_{2,L}(\pi^-\eta\leftarrow\pi^-\eta) \\ +\mathcal{B}_{2,L}(\pi^+\pi^-\leftarrow\pi^+\pi^-)\end{smallmatrix} & \frac{1}{2}\mathcal{B}_{2,L}(\pi^+\pi^- \leftarrow \pi^0\pi^0) \\ \frac{1}{2}\mathcal{B}_{2,L}(\pi^0\pi^0 \leftarrow \pi^+\pi^-) & \begin{smallmatrix}\mathcal{B}_{2,L}(\pi^0\eta\leftarrow\pi^0\eta) \\ +\frac{1}{4}\mathcal{B}_{2,L}(\pi^0\pi^0\leftarrow\pi^0\pi^0)\end{smallmatrix} \end{pmatrix}. \tag{6.25}$$

With the form eq. (6.21) in hand, we can now apply the on-shell projection and resummation methodology of BS1. The on-shell projection changes the momentum indices into the standard $\{k\ell m\}$ coordinates of the three-particle formalism. This involves picking a spectator particle, whose momentum is $\boldsymbol{k}$ (chosen from the finite-volume set), and then projecting the remaining pair onto spherical harmonics in their rest frame (with components labeled by ℓm). As detailed in BS3, for channels with three distinct particles, and in particular the $K\overline{K}\pi$ channels, this leads to an enlargement in the flavor space by a factor of three, corresponding to the three possible choices of spectator. For the $2+1$ channel $\pi^0\pi^0\eta$, the enlargement factor is two, corresponding to the two choices of spectator, as explained in BS2. The only exception to this counting is the $\pi^+\pi^-\eta$ channel, where it is preferable to enlarge by four rather than three by decomposing the $\pi^+\pi^-$ pair into parts with even and odd relative partial waves. This facilitates the decomposition into isospin channels, and borrows from the work of ref. [227] on the doubly-charmed tetraquark.

The result of these enlargements is a flavor matrix of dimension $3+3+3+3+4+2 = 18$. Each index corresponds to a choice of spectator together with a choice of "primary" member of the pair, i.e. that with respect to which the spherical harmonic decomposition is defined.

The ordering we use is

$$\Big\{[K^+\overline{K}^0]\pi^-,\ [K^+\pi^-]\overline{K}^0,\ [\overline{K}^0\pi^-]K^+,\ [K^+K^-]\pi^0,\ [K^+\pi^0]K^-,\ [K^-\pi^0]K^+,$$
$$[K^0\overline{K}^0]\pi^0,\ [K^0\pi^0]\overline{K}^0,\ [\overline{K}^0\pi^0]K^0,\ [K^0K^-]\pi^+,\ [K^0\pi^+]K^-,\ [K^-\pi^+]K^0,$$
$$[\pi^+\pi^-]_e\eta,\ [\pi^+\pi^-]_o\eta,\ [\pi^+\eta]\pi^-,\ [\pi^-\eta]\pi^+,\ [\pi^0\pi^0]\eta,\ [\pi^0\eta]\pi^0\Big\}, \tag{6.26}$$

where in each case the pair is enclosed in square brackets, with the primary member appearing first, while the third entry corresponds to the spectator. The subscripts e and o refer to even and odd partial waves, respectively. Note that we have adopted the convention that the primary member of the pair is defined with a priority order given by $\{K, \overline{K}, \pi^\pm, \pi^0, \eta\}$.

On-shell projection converts cut factors into either F or G cuts, depending on whether the spectator is unchanged or not. We adhere to the prescriptions presented in BS2 and BS3, slightly generalized to handle flavor off-diagonal terms following ref. [227], and obtain

$$\Delta C_L = \hat{A}' i\widehat{F}_G \frac{1}{1 - i(\widehat{\mathcal{K}}_{2,L} + \widehat{\mathcal{K}}^{(u,u)}_{\mathrm{df},3})i\widehat{F}_G}\widehat{A}\,. \tag{6.27}$$

We now proceed to explain the elements of this result.

The cut-factor matrix $\widehat{F}_G$ has block-diagonal form,

$$\widehat{F}_G = \mathrm{diag}\left(F_G^{1+1+1}, F_G^{1+1+1}, F_G^{1+1+1}, F_G^{1+1+1}, F_G^{4d}, F_G^{2+1}\right), \tag{6.28}$$

with entries

$$F_G^{1+1+1} = \begin{pmatrix} \tilde{F}^\pi & P_\ell\tilde{G}^{\pi K}P_\ell & \tilde{G}^{\pi K}P_\ell \\ P_\ell\tilde{G}^{K\pi}P_\ell & \tilde{F}^K & \tilde{G}^{KK} \\ P_\ell\tilde{G}^{K\pi} & \tilde{G}^{KK} & \tilde{F}^K \end{pmatrix}. \tag{6.29}$$

$$F_G^{4d} = \begin{pmatrix} P_e\tilde{F}'^\eta P_e & 0 & P_e\tilde{G}'^{\eta\pi}P_\ell & P_e\tilde{G}'^{\eta\pi}P_\ell \\ 0 & P_o\tilde{F}'^\eta P_o & -P_o\tilde{G}'^{\eta\pi}P_\ell & P_o\tilde{G}'^{\eta\pi}P_\ell \\ P_\ell\tilde{G}'^{\pi\eta}P_e & -P_\ell\tilde{G}'^{\pi\eta}P_o & \tilde{F}'^\pi & \tilde{G}'^{\pi\pi} \\ P_\ell\tilde{G}'^{\pi\eta}P_e & P_\ell\tilde{G}'^{\pi\eta}P_o & \tilde{G}'^{\pi\pi} & \tilde{F}'^\pi \end{pmatrix}, \tag{6.30}$$

$$F_G^{2+1} = \begin{pmatrix} P_e\tilde{F}'^\eta P_e & \sqrt{2}P_e\tilde{G}'^{\eta\pi}P_\ell \\ \sqrt{2}P_\ell\tilde{G}'^{\pi\eta}P_e & \tilde{F}'^\pi + \tilde{G}'^{\pi\pi} \end{pmatrix}. \tag{6.31}$$

The standard kinematic functions $\tilde{F}^i$ and $\tilde{G}^{ij}$ are defined in section D.2. Those with a prime have the $\pi\pi\eta$ cut, while those without have the $K\overline{K}\pi$ cut. The factors of

$$P^{(\ell)}_{p'\ell'm';p\ell m} = \delta_{\boldsymbol{p}'\boldsymbol{p}}\delta_{\ell'\ell}\delta_{m'm}(-1)^\ell \tag{6.32}$$

are needed to correct for mismatches in the conventions for primary spectator between $\widetilde{F}^i$ and $\widetilde{G}^{ij}$. For example, in the upper-right element of F_G^{1+1+1}, the final-state spectator is the pion, and thus in $\tilde{G}^{\pi K}$ the initial-state $K\pi$ pair is decomposed in harmonics relative to the pion direction. This conflicts with our standard convention, requiring a factor of P_ℓ to the right (initial-state) side of $\tilde{G}^{D\pi}$. The factors of $P_e = (1 + P_\ell)/2$ and $P_o = (1 - P_\ell)/2$ project, respectively, onto even and odd partial waves. Finally, we stress that neither $\tilde{F}^i$ nor $\tilde{G}^{ij}$ contain symmetry factors; the only symmetry factors here are the occurrences of $\sqrt{2}$ in F_G^{2+1}.

Next we discuss $\widehat{\mathcal{K}}_{2,L}$, which contains the two-particle K matrices, and arises from summing products of factors of $\tilde{B}_{2,L}$ sewn together with principal-value-regulated integrals over phase space. An explicit formula can be given by generalizing results in BS2 and BS3, but will not be displayed as it is not needed in the following. The structure of $\widehat{\mathcal{K}}_{2,L}$ is straightforward: there are nonzero entries whenever two channels have a shared spectator. For example, the $\{1,1\}$ entry involves $K^+\overline{K}^0 \leftarrow K^+\overline{K}^0$ scattering with a π^- spectator, and has the explicit form

$$\left[\widehat{\mathcal{K}}_{2,L}\right]_{1k'\ell'm',1k\ell m} = \delta_{\boldsymbol{k}'\boldsymbol{k}} 2\omega_{k_\pi} L^3 \delta_{\ell'\ell}\delta_{m'm}\mathcal{K}_2^\ell(K^+\overline{K}^0 \leftarrow K^+\overline{K}^0)\,. \tag{6.33}$$

The superscript on $\mathcal{K}_2^\ell$ indicates the partial wave, and this quantity has an implicit dependence on the relative momentum in the center-of-momentum frame (CMF) of the scattering pair. An example of an offdiagonal element is that in the $\{3,6\}$ slot,

$$\left[\widehat{\mathcal{K}}_{2,L}\right]_{3k'\ell'm',6k\ell m} = \delta_{\boldsymbol{k}'\boldsymbol{k}} 2\omega_{k_K} L^3 \delta_{\ell'\ell}\delta_{m'm}\mathcal{K}_2^\ell(\overline{K}^0\pi^- \leftarrow K^-\pi^0)\,. \tag{6.34}$$

The complete set of nonzero entries of $\widehat{\mathcal{K}}_{2,L}$ is provided in section D.3.

The matrix $\widehat{\mathcal{K}}_{\mathrm{df},3}^{(u,u)}$ is algebraically related to the quantities discussed above, including B_3 in particular, but again we do not display the result as it is not needed in the following.

All that is essential to know about $\widehat{\mathcal{K}}_{\mathrm{df},3}^{(u,u)}$ is that it is an infinite-volume quantity, devoid of any singularities associated with three-particle intermediate states, and with nonzero entries in all elements. The (u,u) superscript indicates that it is an unsymmetrized quantity, the precise meaning of which we will explain in section 6.4.4 below.

Finally, the relation between the new endcaps $\widehat{A}'$ and $\widehat{A}$ (which are, respectively, 6×18 and 18×6 matrices) to the earlier endcaps is known, but not needed in the following. Indeed, we will not keep detailed track of changes to the endcaps in the subsequent manipulations.

Below, we will need to convert 18-dimensional matrices in the $\{k\ell m\}$ basis (such as $\widehat{\mathcal{K}}_{\mathrm{df},3}^{(u,u)}$) into 6-dimensional matrices in the original index space given by eq. (6.1) and labeled by triplets of momenta $\{\boldsymbol{p}\}$. Thus we need to recombine the different choices of spectator flavor, and convert from the $\{k\ell m\}$ basis to the momentum basis. A convenient notation for formalizing the basis conversion was introduced in ref. [227], and we recall this notation in section D.2. It involves operators $\boldsymbol{\mathcal{X}}^{\boldsymbol{\sigma}}_{[kab]}$, defined in eq. (D.21), that act from the left on objects with $\{k\ell m\}$ indices, as well as the conjugate operators that act from the right. In term of this, the conversion from an 18-d matrix $M_{\mathrm{ch}}^{(18)}$ to a 6-d matrix $M_{\mathrm{ch}}^{(6)}$, both in the charge basis, is accomplished by conjugation

$$M_{\mathrm{ch}}^{(6)} = \boldsymbol{\mathcal{C}} \circ M_{\mathrm{ch}}^{(18)} \circ \boldsymbol{\mathcal{C}}^{\dagger}\,, \tag{6.35}$$

where $\boldsymbol{\mathcal{C}}$ is a 6×18 matrix of operators with block form

$$\boldsymbol{\mathcal{C}} = \begin{pmatrix} \boldsymbol{\mathcal{X}}^{(3)} & 0 & 0 & 0 & 0 & 0 \\ 0 & \boldsymbol{\mathcal{X}}^{(3)} & 0 & 0 & 0 & 0 \\ 0 & 0 & \boldsymbol{\mathcal{X}}^{(3)} & 0 & 0 & 0 \\ 0 & 0 & 0 & \boldsymbol{\mathcal{X}}^{(3)} & 0 & 0 \\ 0 & 0 & 0 & 0 & \boldsymbol{\mathcal{X}}^{(4)} & 0 \\ 0 & 0 & 0 & 0 & 0 & S_D\boldsymbol{\mathcal{X}}^{(2)} \end{pmatrix}, \tag{6.36}$$

where

$$\begin{aligned}
\boldsymbol{\mathcal{X}}^{(3)} &\equiv \left(\boldsymbol{\mathcal{X}}^{(312)}_{[kab]},\ \boldsymbol{\mathcal{X}}^{(213)}_{[kab]},\ \boldsymbol{\mathcal{X}}^{(123)}_{[kab]}\right) , \\
\boldsymbol{\mathcal{X}}^{(4)} &\equiv \left(\boldsymbol{\mathcal{X}}^{(312)}_{[kab]} P_e,\ \boldsymbol{\mathcal{X}}^{(312)}_{[kab]} P_o, \boldsymbol{\mathcal{X}}^{(213)}_{[kab]}, \boldsymbol{\mathcal{X}}^{(123)}_{[kab]}\right) , \\
\boldsymbol{\mathcal{X}}^{(2)} &\equiv \left(\sqrt{\tfrac{1}{2}}\boldsymbol{\mathcal{X}}^{(312)}_{[kab]}, \boldsymbol{\mathcal{X}}^{(123)}_{[kab]}\right) .
\end{aligned} \tag{6.37}$$

The choices of superscripts in these vectors determines which momentum is assigned to each particle. The fixed subscript on these objects, $[kab]$, indicates that the first superscript index corresponds to k, the spectator; the second to a, the preferred partner in the interacting pair; and the third to b, the remaining partner. This ordering follows from the choices in eq. (6.1) as well as the conventions for momentum labels in eq. (6.26). The a and b that appear here should not be confused with those appearing in eq. (6.2), which label distinct isospin channels. The symmetry factor of $\sqrt{1/2}$ is explained in BS2, and the appearance of S_D follows from eq. (6.17).

We stress, as explained in BS2 and ref. [227], that this conversion is only precise in the $L \to \infty$ limit; this, however, will be sufficient for our purposes in the following.

6.4.3 Converting to the total isospin basis

We now convert to the total isospin basis. We choose the following ordering,

$$\begin{aligned}
\Big\{&[[K\bar{K}]_1\pi]_2, [[K\pi]_{3/2}\bar{K}]_2, [[\bar{K}\pi]_{3/2}K]_2, [[\pi\pi]_2\eta]_2, [[\pi\eta]_1\pi]_2, \\
&[[K\bar{K}]_1\pi]_1, [[K\bar{K}]_0\pi]_1, [[K\pi]_{3/2}\bar{K}]_1, [[K\pi]_{1/2}\bar{K}]_1, [[\bar{K}\pi]_{3/2}K]_1, [[\bar{K}\pi]_{1/2}K]_1, \\
&[[\pi\pi]_1\eta]_1, [[\pi\eta]_1\pi]_1, \\
&[[K\bar{K}]_1\pi]_0, [[K\pi]_{1/2}\bar{K}]_0, [[\bar{K}\pi]_{1/2}K]_0, [[\pi\pi]_0\eta]_0, [[\pi\eta]_1\pi]_0\Big\}
\end{aligned} \tag{6.38}$$

where, as before, the final entry corresponds to the spectator, and the first entry to the primary particle in the pair. The first five elements have $I = 2$, the next eight have $I = 1$, and the final five have $I = 0$. Since isospin is an exact symmetry in our setup, we must find that all matrices block diagonalize according to isospin.

The unitary matrix $C^{(18)}_{\text{ch}\to\text{iso}}$ that converts between bases is given in section D.5. We insert $[C^{(18)}_{\text{ch}\to\text{iso}}]^{-1} C^{(18)}_{\text{ch}\to\text{iso}} = 1$ between all matrices in eq. (6.27), such that each of these matrices is

converted to the isospin basis by conjugation, as in eq. (D.60), while the endcaps are rotated. We simplify notation by using the same symbols for all quantities after conversion to the isospin basis, so that the result for ΔC_L maintains exactly the form of eq. (6.27).

After conjugation, the matrices $\widehat{F}_G$, eq. (6.28), and $\widehat{\mathcal{K}}_{2,L}$, given in section D.3, are indeed found to be block digaonal in isospin. The explicit forms are given below in the summary section, section 6.4.5. As for $\widehat{\mathcal{K}}_{\mathrm{df},3}^{(u,u)}$, all we know is that it must be block diagonal, but is otherwise of general form, aside from certain symmetry constraints. We postpone discussion of its form until we reach its symmetrized version below.

At this point we observe that ΔC_L has a pole, corresponding to a finite-volume energy level, whenever

$$\det\left[1 + (\widehat{\mathcal{K}}_{2,L} + \widehat{\mathcal{K}}_{\mathrm{df},3}^{(u,u)})\widehat{F}_G\right] = 0\,. \tag{6.39}$$

This is the asymmetric form of the three-particle quantization condition, and has the standard form first given in BS1. It has potential utility as a bridge to quantization conditions derived in the finite-volume unitarity approach [107], as outlined in ref. [116]. We note that the presence of two three-particle channels leads to $\widehat{F}_G$ having two types of free-particle singularities, and to the presence of additional channels in the two- and three-particle K matrices.

6.4.4 Expressing results in terms of symmetrized quantities

The drawback of the quantization condition eq. (6.39) is that it contains a three-particle K matrix, $\widehat{\mathcal{K}}_{\mathrm{df},3}^{(u,u)}$, that is asymmetric. As discussed in detail in BS1, BS2 and BS3, the elements of this matrix are defined by summing an infinite series of products of Bethe-Salpeter kernels, such that, if the external kernel is a B_2, then the noninteracting particle is always the spectator. This means that only a subset of the total number of diagrams are being included. In this section we use the method developed in BS1, and extended in BS2 and BS3, to "symmetrize" the three-particle K matrix, by which we mean combining contributions such that all diagrams are included.

The method is most straightforwardly implemented on a different finite-volume quantity than C_L, namely $\mathcal{M}_{23,L,\text{off}}$. This is a finite-volume $3 \to 3$ correlation function involving external single-particle legs at fixed momenta (drawn from the finite-volume set). External TOPT propagators are amputated, and final and initial times are sent to $\pm\infty$, respectively. The subscript "23" indicates that this quantity contains not only fully-connected contributions, but also those in which one of the three particles spectates while the others interact. (A more detailed explanation is given in fig. 2 of BS3.) The subscript "off" indicates that this is an off-shell amplitude because the energy E does not, in general, equal the sum of the external on-shell energies. Using $\mathcal{M}_{23,L,\text{off}}$ also allows the determination of the integral equations relating the three-particle K matrix to the infinite-volume three-particle scattering amplitude, $\mathcal{M}_3$.

Just as for C_L, $\mathcal{M}_{23,L,\text{off}}$ is a 6×6 matrix in flavor space, with the channels those of eq. (6.1). It also has momentum indices $\{\boldsymbol{k}\}$. Following the arguments in BS2 and BS3, it has the form

$$\mathcal{M}_{23,L,\text{off}} = (B_{2,L} + B_3)\frac{1}{1 - iDi(B_{2,L} + B_3)}\,, \tag{6.40}$$

$$= \tilde{S}_D(\tilde{B}_{2,L} + \tilde{B}_3)\frac{1}{1 - iD_S i(\tilde{B}_{2,L} + \tilde{B}_3)}\tilde{S}_D\,, \tag{6.41}$$

where the quantities are the same as those appearing in C_L. In the second step we have moved symmetrization factors onto the Ds. We observe that the correlator can be written in terms of $\mathcal{M}_{23,L,\text{off}}$ [115]

$$\Delta C_L = A' i D_S A + A' i D_S i \mathcal{M}_{23,L,\text{off}} i D_S A\,. \tag{6.42}$$

This implies that poles in $\mathcal{M}_{23,L,\text{off}}$ can also be used to determine the finite-volume energy levels.

As in the analysis of C_L, we next introduce additional matrix indices as above to convert to 18-d matrix forms, and then project on shell (so that the subscript "off" is dropped). There then follows a series of steps that are essentially exact copies of those used in BS2, BS3 and ref. [227], and which we do not reproduce here. These involve tedious algebra, plus

the use of symmetrization identities. The end result is that

$$\begin{aligned} \mathcal{M}_{23,L} &= \boldsymbol{\mathcal{C}} \circ \widehat{\mathcal{M}}_{23,L}^{(u,u)} \circ \boldsymbol{\mathcal{C}}^\dagger \,, \\ \widehat{\mathcal{M}}_{23,L}^{(u,u)} &= \widehat{\mathcal{M}}_{2,L} + \widehat{\mathcal{D}}_L^{(u,u)} + \widehat{\mathcal{M}}_{\mathrm{df},3,L}^{(u,u)\prime} \,, \end{aligned} \tag{6.43}$$

where

$$\widehat{\mathcal{M}}_{2,L} = \widehat{\mathcal{K}}_{2,L} \frac{1}{1 - i\widehat{F} i \widehat{\mathcal{K}}_{2,L}} \,. \tag{6.44}$$

$$\widehat{\mathcal{D}}_L^{(u,u)} = -\widehat{\mathcal{M}}_{2,L} \widehat{G} \widehat{\mathcal{M}}_{2,L} \frac{1}{1 + \widehat{G}\widehat{\mathcal{M}}_{2,L}} \,, \tag{6.45}$$

$$\widehat{\mathcal{M}}_{\mathrm{df},3,L}^{(u,u)\prime} = \left[\frac{1}{3} - \widehat{\mathcal{D}}_{23,L}^{(u,u)} \widehat{F}\right] \widehat{\mathcal{K}}_{\mathrm{df},3} \frac{1}{1 + \widehat{F}_3 \widehat{\mathcal{K}}_{\mathrm{df},3}} \left[\frac{1}{3} - \widehat{F}\widehat{\mathcal{D}}_{23,L}^{(u,u)}\right] \,, \tag{6.46}$$

$$\widehat{\mathcal{D}}_{23,L}^{(u,u)} = \widehat{\mathcal{M}}_{2,L} + \widehat{\mathcal{D}}_L^{(u,u)} \tag{6.47}$$

$$\widehat{F}_3 = \frac{\widehat{F}}{3} - \widehat{F} \frac{1}{(\widehat{\mathcal{K}}_{2,L})^{-1} + \widehat{F}_G} \widehat{F} \,. \tag{6.48}$$

The quantities in these expressions are the same as earlier, with $\boldsymbol{\mathcal{C}}$ given in eq. (6.36). We have also used the decomposition

$$\widehat{F}_G = \widehat{F} + \widehat{G} \,, \tag{6.49}$$

where $\widehat{F}$ and $\widehat{G}$ contain, respectively, only the $\widetilde{F}$ and $\widetilde{G}$ terms contributing to $\widehat{F}_G$, whose form is given in eqs. (6.28) to (6.31).

Various features of eq. (6.43) deserve discussion. First, it was noted earlier that $\mathcal{M}_{23,L}$ includes disconnected contributions. These lead to the $\widehat{\mathcal{M}}_{2,L}$ term, which should be subtracted to obtain the fully connected $\mathcal{M}_{3,L}$. Second, the operators $\boldsymbol{\mathcal{C}}$ and $\boldsymbol{\mathcal{C}}^\dagger$ in eq. (6.43) serve to symmetrize $\widehat{\mathcal{M}}_{23,L}^{(u,u)}$ in the sense discussed earlier in this section, namely adding together all the terms that contribute to the finite-volume amplitude. However, as noted when these operators were defined, their action leads to terms that can be added only in the infinite-volume limit. While sufficient for deriving integral equations for $\mathcal{M}_3$, as we do below, this is problematic if one wishes to use the expression eq. (6.43) in finite volume. This brings us to the third point, which is that in BS1, BS2 and BS3, building on the work of refs. [16, 17], symmetrization operators were introduced that *can* be used in finite volume. The net effect

is that an equation of similar form to eq. (6.43) can be written, with $\boldsymbol{\mathcal{C}}$ and $\boldsymbol{\mathcal{C}}^\dagger$ replaced by these new operators, and effectively inserted into eq. (6.42). This implies that this properly symmetrized $\mathcal{M}_{23,L}$ is part of a finite-volume correlator, and thus its poles determine the finite-volume energies. Only the third term in $\mathcal{M}_{23,L}$, namely $\widehat{\mathcal{M}}_{\mathrm{df},3,L}^{(u,u)\prime}$, can lead to such poles, since three-particle energies must depend on the three-particle K matrix. This allows us to read off a new form of the quantization condition, as is done in the following section.

The fourth feature of eq. (6.43) concerns the nature of $\widehat{\mathcal{K}}_{\mathrm{df},3}$. As indicated by the absence of the (u,u) superscript, this is a symmetrized quantity. This follows from the derivation given in BS1, BS2 and BS3. In particular, for a given choice of external particles, all contributions are included in its definition. Different choices of spectator flavors lead to different decompositions into $\{k\ell m\}$ indices, but the underlying quantity is the same. This is not the case for $\widehat{\mathcal{K}}_{\mathrm{df},3}^{(u,u)}$. A particularly explicit discussion of this point is given in Appendix A of BS2.

Finally, we note that we are free to rotate from the charge basis to the isospin basis, leaving the form of all equations unchanged. In the following, we assume that this rotation has been carried out.

6.4.5 Symmetric form of three-particle quantization condition

As just discussed, the poles in $\widehat{\mathcal{M}}_{\mathrm{df},3,L}^{(u,u)\prime}$ correspond to finite-volume energy levels. This implies a second form for the quantization condition,[6]

$$\det\left[1 + \widehat{F}_3 \widehat{\mathcal{K}}_{\mathrm{df},3}\right] = 0\,, \tag{6.50}$$

where $\widehat{F}_3$ is given in eq. (6.48). This result takes the standard form for all quantization conditions obtained previously in the RFT approach [16, 35–37, 39, 109, 179, 227]. We call this the symmetric form, as it contains a symmetrized three-particle K matrix. Given that this minimizes the number of independent components of $\mathcal{K}_{\mathrm{df},3}$, it is the simplest form of the

[6] As shown in section D.7, one can also derive this form directly from the asymmetric form of the quantization condition.

quantization condition to implement in practice.

Since all matrices contained in the quantization condition block diagonalize in isospin, we can solve the condition separately for each block. This leads to our final form

$$\det\left[1 + \widehat{F}_3^{[I]}\widehat{\mathcal{K}}_{\mathrm{df},3}^{[I]}\right] = 0\,, \tag{6.51}$$

for $I = 2, 1, 0$, with

$$\widehat{F}_3^{[I]} = \frac{\widehat{F}^{[I]}}{3} - \widehat{F}^{[I]}\frac{1}{(\widehat{\mathcal{K}}_{2,L}^{[I]})^{-1} + \widehat{F}_G^{[I]}}\widehat{F}^{[I]}\,. \tag{6.52}$$

We collect here the explicit forms for the isospin blocks, beginning with those for $I = 2$,

$$\widehat{F}_G^{[I=2]} = \begin{pmatrix} F_G^{1+1+1} & 0 \\ 0 & F_G^{2+1} \end{pmatrix} \tag{6.53}$$

$$\widehat{\mathcal{K}}_{2,L}^{[I=2]} = \begin{pmatrix} \overline{\mathcal{K}}_{2,L}^{K\bar{K},I=1} & 0 & 0 & 0 & \overline{\mathcal{K}}_{2,L}^{\pi\eta\leftrightarrow K\bar{K},I=1} \\ 0 & \overline{\mathcal{K}}_{2,L}^{K\pi,I=3/2} & 0 & 0 & 0 \\ 0 & 0 & \overline{\mathcal{K}}_{2,L}^{K\pi,I=3/2} & 0 & 0 \\ 0 & 0 & 0 & \frac{1}{2}\overline{\mathcal{K}}_{2,L}^{\pi\pi,I=2} & 0 \\ \overline{\mathcal{K}}_{2,L}^{\pi\eta\leftrightarrow K\bar{K},I=1} & 0 & 0 & 0 & \overline{\mathcal{K}}_{2,L}^{\pi\eta,I=1} \end{pmatrix} \tag{6.54}$$

The subblocks in F_G^{1+1+1} and F_G^{2+1} are given in eqs. (6.29) and (6.31), respectively. The elements of $\widehat{\mathcal{K}}_{2,L}^{[I=2]}$ contain the underlying two-particle K matrix along with kinematic factors, and are defined in section D.2. The structure of these matrices follows from the ordering of indices given in eq. (6.38), with the $I = 2$ part given by

$$\left\{[[K\bar{K}]_1\pi]_2,\ [[K\pi]_{3/2}\bar{K}]_2,\ [[\bar{K}\pi]_{3/2}K]_2,\ [[\pi\pi]_2\eta]_2,\ [[\pi\eta]_1\pi]_2\right\}\,. \tag{6.55}$$

In particular, the diagonal entries of $\widehat{\mathcal{K}}_{2,L}^{[I=2]}$ correspond to the scattering of the pair, with a symmetry factor of $1/2$ for the identical particle case, while the offdiagonal entry is that for which there is a common spectator particle.

The results for the $I = 0$ blocks are similar to those for $I = 2$, as expected because of the similarity of the corresponding indices,

$$\left\{[[K\bar{K}]_1\pi]_0, [[K\pi]_{1/2}\bar{K}]_0, [[\bar{K}\pi]_{1/2}K]_0, [[\pi\pi]_0\eta]_0, [[\pi\eta]_1\pi]_0\right\}\,. \tag{6.56}$$

We find

$$\widehat{F}_G^{[I=0]} = \begin{pmatrix} \overline{F}_G^{1+1+1} & 0 \\ 0 & F_G^{2+1} \end{pmatrix} \tag{6.57}$$

$$\widehat{\mathcal{K}}_{2,L}^{[I=0]} = \begin{pmatrix} \overline{\mathcal{K}}_{2,L}^{K\bar{K},I=1} & 0 & 0 & 0 & \overline{\mathcal{K}}_{2,L}^{\pi\eta\leftrightarrow K\bar{K},I=1} \\ 0 & \overline{\mathcal{K}}_{2,L}^{K\pi,I=1/2} & 0 & 0 & 0 \\ 0 & 0 & \overline{\mathcal{K}}_{2,L}^{K\pi,I=1/2} & 0 & 0 \\ 0 & 0 & 0 & \frac{1}{2}\overline{\mathcal{K}}_{2,L}^{\pi\pi,I=0} & 0 \\ \overline{\mathcal{K}}_{2,L}^{\pi\eta\leftrightarrow K\bar{K},I=1} & 0 & 0 & 0 & \overline{\mathcal{K}}_{2,L}^{\pi\eta,I=1} \end{pmatrix}, \tag{6.58}$$

where

$$\overline{F}_G^{1+1+1} = \begin{pmatrix} \tilde{F}^{\pi} & -P_\ell \tilde{G}^{\pi K} P_\ell & -\tilde{G}^{\pi K} P_\ell \\ -P_\ell \tilde{G}^{K\pi} P_\ell & \tilde{F}^{K} & \tilde{G}^{KK} \\ -P_\ell \tilde{G}^{K\pi} & \tilde{G}^{KK} & \tilde{F}^{K} \end{pmatrix} \tag{6.59}$$

differs from F_G^{1+1+1}, given in eq. (6.29), by signs in some of the offdiagonal terms.

Finally, for $I = 1$, for which the indices are

$$\Big\{[[K\bar{K}]_1\pi]_1, [[K\bar{K}]_0\pi]_1, [[K\pi]_{3/2}\bar{K}]_1, [[K\pi]_{1/2}\bar{K}]_1, [[\bar{K}\pi]_{3/2}K]_1, [[\bar{K}\pi]_{1/2}K]_1, \\ [[\pi\pi]_1\eta]_1, [[\pi\eta]_1\pi]_1\Big\}, \tag{6.60}$$

we obtain

$$\widehat{F}_G^{[I=1]} = \begin{pmatrix} F_G^{(6)} & 0 \\ 0 & \overline{F}_G^{2+1} \end{pmatrix} \tag{6.61}$$

where

$$\overline{F}_G^{2+1} = \begin{pmatrix} P_e \tilde{F}'^{\eta} P_e & -\sqrt{2} P_e \tilde{G}'^{\eta\pi} P_\ell \\ -\sqrt{2} P_\ell \tilde{G}'^{\pi\eta} P_e & \tilde{F}'^{\pi} - \tilde{G}'^{\pi\pi} \end{pmatrix}, \tag{6.62}$$

which differs from F_G^{2+1}, eq. (6.31), by several signs, and

$$F_G^{(6)} = \begin{pmatrix} \widetilde{F}^{\pi} & 0 & -\sqrt{\frac{1}{3}} P_\ell \widetilde{G}^{\pi K} P_\ell & \sqrt{\frac{2}{3}} P_\ell \widetilde{G}^{\pi K} P_\ell & -\sqrt{\frac{1}{3}} \widetilde{G}^{\pi K} P_\ell & \sqrt{\frac{2}{3}} \widetilde{G}^{\pi K} P_\ell \\ 0 & \widetilde{F}^{\pi} & \sqrt{\frac{2}{3}} P_\ell \widetilde{G}^{\pi K} P_\ell & \sqrt{\frac{1}{3}} P_\ell \widetilde{G}^{\pi K} P_\ell & -\sqrt{\frac{2}{3}} \widetilde{G}^{\pi K} P_\ell & -\sqrt{\frac{1}{3}} \widetilde{G}^{\pi K} P_\ell \\ -\sqrt{\frac{1}{3}} P_\ell \widetilde{G}^{K\pi} P_\ell & \sqrt{\frac{2}{3}} P_\ell \widetilde{G}^{K\pi} P_\ell & \widetilde{F}^{K} & 0 & -\frac{1}{3}\widetilde{G}^{KK} & -\sqrt{\frac{8}{9}}\widetilde{G}^{KK} \\ \sqrt{\frac{2}{3}} P_\ell \widetilde{G}^{K\pi} P_\ell & \sqrt{\frac{1}{3}} P_\ell \widetilde{G}^{K\pi} P_\ell & 0 & \widetilde{F}^{K} & -\sqrt{\frac{8}{9}}\widetilde{G}^{KK} & \frac{1}{3}\widetilde{G}^{KK} \\ -\sqrt{\frac{1}{3}} P_\ell \widetilde{G}^{K\pi} & -\sqrt{\frac{2}{3}} P_\ell \widetilde{G}^{K\pi} & -\frac{1}{3}\widetilde{G}^{KK} & -\sqrt{\frac{8}{9}}\widetilde{G}^{KK} & \widetilde{F}^{K} & 0 \\ \sqrt{\frac{2}{3}} P_\ell \widetilde{G}^{K\pi} & -\sqrt{\frac{1}{3}} P_\ell \widetilde{G}^{K\pi} & -\sqrt{\frac{8}{9}}\widetilde{G}^{KK} & \frac{1}{3}\widetilde{G}^{KK} & 0 & \widetilde{F}^{K} \end{pmatrix}. \tag{6.63}$$

The two-particle K matrix is

$$\widehat{\mathcal{K}}_{2,L}^{[I=1]} = \begin{pmatrix} \overline{\mathcal{K}}_{2,L}^{K\bar{K},I=1} & 0 & 0 & 0 & 0 & 0 & 0 & \overline{\mathcal{K}}_{2,L}^{\pi\eta\leftrightarrow K\bar{K},I=1} \\ 0 & \overline{\mathcal{K}}_{2,L}^{K\bar{K},I=0} & 0 & 0 & 0 & 0 & 0 & 0 \\ 0 & 0 & \overline{\mathcal{K}}_{2,L}^{K\pi,I=3/2} & 0 & 0 & 0 & 0 & 0 \\ 0 & 0 & 0 & \overline{\mathcal{K}}_{2,L}^{K\pi,I=1/2} & 0 & 0 & 0 & 0 \\ 0 & 0 & 0 & 0 & \overline{\mathcal{K}}_{2,L}^{K\pi,I=3/2} & 0 & 0 & 0 \\ 0 & 0 & 0 & 0 & 0 & \overline{\mathcal{K}}_{2,L}^{K\pi,I=1/2} & 0 & 0 \\ 0 & 0 & 0 & 0 & 0 & 0 & \frac{1}{2}\overline{\mathcal{K}}_{2,L}^{\pi\pi,I=1} & 0 \\ \overline{\mathcal{K}}_{2,L}^{\pi\eta\leftrightarrow K\bar{K},I=1} & 0 & 0 & 0 & 0 & 0 & 0 & \overline{\mathcal{K}}_{2,L}^{\pi\eta,I=1} \end{pmatrix}, \tag{6.64}$$

The form of the isospin blocks of $\widehat{\mathcal{K}}_{\mathrm{df},3}$ is more complicated to determine, and we discuss this in the following section.

With the result in hand, we can study the impact of having multiple (here two) three-particle channels. We saw above that there are two classes of the kinematic functions $\tilde{F}$ and $\tilde{G}$, one with singularities at $\pi\pi\eta$ free energies, the other with singularities at $K\overline{K}\pi$ free energies. Above the $K\overline{K}\pi$ threshold, these free energies can lie close to each other. For each total isospin, the sub-blocks of $\widehat{F}_G$ containing these two classes are connected by the two-particle $\pi\eta \leftrightarrow K\overline{K}$ scattering, and by elements of $\widehat{\mathcal{K}}_{\mathrm{df},3}$. This connection can therefore lead to finite-volume states that cannot be thought of as close to either type of free state, but are instead mixed. The situation is analogous to that for the two-particle quantization condition when there are multiple channels. From a practical point of view, the impact is simply that the matrices in the quantization condition become larger.

6.4.6 Form of $\mathcal{K}_{\mathrm{df},3}$

As already noted, the three-particle K matrix block diagonalizes according to total isospin. In this section we present the general form of these blocks, $\widehat{\mathcal{K}}_{\mathrm{df},3}^{[I]}$. The analysis follows the methodology introduced in appendix A of ref. [227].

For each choice of I, there are some number of independent channels, as shown in eq. (6.2): two each for $I = 2$ and 0, and three for $I = 1$. These are the distinct asymptotic states that can scatter into one another. Assuming PT symmetry, this implies that there are three

independent $3 \to 3$ amplitudes for $I = 2$ and 0 (two diagonal and one offdiagonal) and six for $I = 1$. Since the corresponding $\widehat{\mathcal{K}}^{[I]}_{\rm df,3}$ matrices have $5 \times 6/2 = 15$ independent entries for $I = 0, 2$, and $8 \times 9/2 = 36$ for $I = 1$, there must be many relations between entries. Determining these relations is the task of this section.

We begin by writing down the form in the charged basis based on results for nondegenerate and $2 + 1$ systems, and then rotate to the isospin basis. The block structure of the 18-d matrices is $3+3+3+3+4+2$, where 3 indicates the nondegenerate blocks, 4 the extended nondegenerate block with even and odd $\pi\pi$ waves separated, and 2 the $2 + 1$ block, We label these blocks with an index that runs from 1 to 6. Within each block the entries of $\mathcal{K}_{\rm df,3}$ are given by the same underlying function, denoted $\mathcal{K}_{jk}(\{p\}, \{k\})$ with j, k being block indices, expressed in different coordinates, i.e. with different choices of spectator and primary member of the pair. PT symmetry symmetry relates off-diagonal blocks,

$$\mathcal{K}_{jk}(\{p_i\}, \{k_i\}) = \mathcal{K}_{kj}(\{k_i\}, \{p_i\})\,, \qquad (j \neq k)\,, \tag{6.65}$$

so there are 28 independent underlying functions. These must be related in such a way that in the isospin basis $\mathcal{K}_{\rm df,3}$ is block diagonal. We will not, however, need (or display) these relations.

The structure within each block is an outer product built from the following three vectors,

$$\boldsymbol{\mathcal{Y}}^{(3)\dagger} = \left(\boldsymbol{\mathcal{Y}}^{[kab]\dagger}_{(312)},\ \ \boldsymbol{\mathcal{Y}}^{[kab]\dagger}_{(213)},\ \ \boldsymbol{\mathcal{Y}}^{[kab]\dagger}_{(123)}\right)\,, \tag{6.66}$$

$$\boldsymbol{\mathcal{Y}}^{(4)\dagger} = \left(P_e\boldsymbol{\mathcal{Y}}^{[kab]\dagger}_{(312)},\ \ P_o\boldsymbol{\mathcal{Y}}^{[kab]\dagger}_{(312)},\ \ \boldsymbol{\mathcal{Y}}^{[kab]\dagger}_{(213)},\ \ \boldsymbol{\mathcal{Y}}^{[kab]\dagger}_{(123)}\right)\,, \tag{6.67}$$

$$\boldsymbol{\mathcal{Y}}^{(2)\dagger} = \left(\sqrt{\tfrac{1}{2}}\boldsymbol{\mathcal{Y}}^{[kab]\dagger}_{(312)},\ \ \boldsymbol{\mathcal{Y}}^{[kab]\dagger}_{(123)}\right)\,, \tag{6.68}$$

and their conjugates

$$\boldsymbol{\mathcal{Y}}^{(3)} = \begin{pmatrix} \boldsymbol{\mathcal{Y}}^{[kab]}_{(312)} \\ \boldsymbol{\mathcal{Y}}^{[kab]}_{(213)} \\ \boldsymbol{\mathcal{Y}}^{[kab]}_{(123)} \end{pmatrix}\,, \quad \boldsymbol{\mathcal{Y}}^{(4)} = \begin{pmatrix} \boldsymbol{\mathcal{Y}}^{[kab]}_{(312)}P_e \\ \boldsymbol{\mathcal{Y}}^{[kab]}_{(312)}P_o \\ \boldsymbol{\mathcal{Y}}^{[kab]}_{(213)} \\ \boldsymbol{\mathcal{Y}}^{[kab]}_{(123)} \end{pmatrix}\,, \qquad \boldsymbol{\mathcal{Y}}^{(2)} = \begin{pmatrix} \sqrt{\tfrac{1}{2}}\boldsymbol{\mathcal{Y}}^{[kab]}_{(312)} \\ \boldsymbol{\mathcal{Y}}^{[kab]}_{(123)} \end{pmatrix}\,. \tag{6.69}$$

Here we are using the operators $\boldsymbol{\mathcal{Y}}$ and $\boldsymbol{\mathcal{Y}}^\dagger$, introduced in ref. [227], which are defined in section D.2. They convert functions of the triplet of on-shell momenta to the $k\ell m$ basis, and thus are essentially the inverses of the operators $\boldsymbol{\mathcal{X}}$ introduced above. The permutation associated with the $\boldsymbol{\mathcal{Y}}$ indicates, in order, the assignment of momenta to the spectator, the primary member of the pair, and the remaining member of the pair. The ordering of these permutations within each of the vectors $\boldsymbol{\mathcal{Y}}$ is determined by our choice of momentum labels in eq. (6.1) and of the ordering within blocks given in eq. (6.26). The factor of $1/\sqrt{2}$ is explained in BS2. We note that in $\boldsymbol{\mathcal{Y}}^{(2)}$ we can freely replace $\boldsymbol{\mathcal{Y}}^{[kab]}_{(123)}$ with $\boldsymbol{\mathcal{Y}}^{[kab]}_{(213)}$ because this acts on a function that is symmetric under the interchange of the two neutral pions (whose momenta are labeled 1 and 2).

The outer product form depends only on the dimensions of the block. Thus, for example, the $\{5,3\}$ block, which has dimensions 4×3, contains $\boldsymbol{\mathcal{Y}}^{(4)}\mathcal{K}_{53}\boldsymbol{\mathcal{Y}}^{(3)\dagger}$ and similarly in other cases.

After constructing the 18×18 matrix $\widehat{\mathcal{K}}_{\mathrm{df},3}$ in this fashion, we rotate to the isospin basis, and examine the three isospin blocks in turn. For the $I=2$ block we find a sum of four outer products

$$\widehat{\mathcal{K}}^{[I=2]}_{\mathrm{df},3} = \sum_{x,y\in\{a,b\}} \boldsymbol{\mathcal{Y}}^{[I=2],x} \circ \mathcal{K}^{[I=2],xy}_{\mathrm{df},3}(\{\boldsymbol{p}\},\{\boldsymbol{k}\}) \circ \boldsymbol{\mathcal{Y}}^{[I=0/2],y\dagger}\,, \tag{6.70}$$

where

$$\begin{aligned}
\boldsymbol{\mathcal{Y}}^{[I=2],a\dagger} &= \left(\boldsymbol{\mathcal{Y}}^{[kab]\dagger}_{(312)},\ \boldsymbol{\mathcal{Y}}^{[kab]\dagger}_{(213)},\ \boldsymbol{\mathcal{Y}}^{[kab]\dagger}_{(123)},\ 0,\ 0\right)\,,\\
\boldsymbol{\mathcal{Y}}^{[I=2],b\dagger} &= \left(0,\ 0,\ 0,\ \sqrt{\tfrac{1}{2}}\boldsymbol{\mathcal{Y}}^{[kab]\dagger}_{(312)},\ \boldsymbol{\mathcal{Y}}^{[kab]\dagger}_{(213)}\right)\,,
\end{aligned} \tag{6.71}$$

with the conjugate vectors given similarly. The superscripts a,b here refer to the two independent states that contribute, respectively $[[K\bar{K}]_1\pi]_2$ and $[[\pi\pi]_2\eta]_2$. Thus, for example, $\mathcal{K}^{[I=2],ba}_{\mathrm{df},3}$ corresponds to the K matrix for the process $\pi\pi\eta \leftarrow K\overline{K}\pi$. PT invariance implies that $\mathcal{K}^{[I=2],ba}_{\mathrm{df},3}(\{\boldsymbol{p}\},\{\boldsymbol{k}\}) = \mathcal{K}^{[I=2],ab}_{\mathrm{df},3}(\{\boldsymbol{k}\},\{\boldsymbol{p}\})$, so that there are only three underlying K matrices, as claimed above. Finally, we note that, to obtain these results, we have used the fact that the $I=2$ $\pi\pi\eta$ state is symmetric under the interchange of the two pions.

The choice of normalization of the $\boldsymbol{\mathcal{Y}}^{[I=2],x}$ is arbitrary, since any changes can be absorbed by a redefinition of $\mathcal{K}_{\mathrm{df},3}^{[I=0],xy}$. The normalization that we choose is explained in the following section, and in particular is such that eq. (6.91) holds.

The result for the $I = 0$ block takes the same form as for $I = 2$,

$$\widehat{\mathcal{K}}_{\mathrm{df},3}^{[I=0]} = \sum_{x,y\in\{a,b\}} \boldsymbol{\mathcal{Y}}^{[I=0],x} \circ \mathcal{K}_{\mathrm{df},3}^{[I=0],xy}(\{\boldsymbol{p}\},\{\boldsymbol{k}\}) \circ \boldsymbol{\mathcal{Y}}^{[I=0],y\dagger}\,, \tag{6.72}$$

where

$$\begin{aligned} \boldsymbol{\mathcal{Y}}^{[I=0],a\dagger} &= \left(\boldsymbol{\mathcal{Y}}_{(312)}^{[kab]\dagger},\ -\boldsymbol{\mathcal{Y}}_{(213)}^{[kab]\dagger},\ -\boldsymbol{\mathcal{Y}}_{(123)}^{[kab]\dagger},\ 0,\ 0\right)\,, \\ \boldsymbol{\mathcal{Y}}^{[I=0],b\dagger} &= \boldsymbol{\mathcal{Y}}^{[I=2],b\dagger}\,. \end{aligned} \tag{6.73}$$

In this case a, b refer to $[[K\bar{K}]_1\pi]_0$ and $[[\pi\pi]_0\eta]_0$, respectively. Again, using PT symmetry, there are three independent underlying functions.

Finally, for $I = 1$, where the block is eight dimensional and there are three underlying states, we obtain

$$\widehat{\mathcal{K}}_{\mathrm{df},3}^{[I=1]} = \sum_{x,y\in\{a,b,c\}} \boldsymbol{\mathcal{Y}}^{[I=1],x} \circ \mathcal{K}_{\mathrm{df},3}^{[I=1],xy} \circ \boldsymbol{\mathcal{Y}}^{[I=1],y\dagger}\,, \tag{6.74}$$

where a, b, c correspond to $[[K\bar{K}]_1\pi]_1$, $[[K\bar{K}]_0\pi]_1$, and $[[\pi\pi]_1\eta]_1$, respectively, and the vectors are now

$$\begin{aligned} \boldsymbol{\mathcal{Y}}^{[I=1],a\dagger} &= \left(\boldsymbol{\mathcal{Y}}_{(312)}^{[kab]\dagger},\ 0,\ -\sqrt{\tfrac{1}{3}}\boldsymbol{\mathcal{Y}}_{(213)}^{[kab]\dagger},\ \sqrt{\tfrac{2}{3}}\boldsymbol{\mathcal{Y}}_{(213)}^{[kab]\dagger},\ -\sqrt{\tfrac{1}{3}}\boldsymbol{\mathcal{Y}}_{(123)}^{[kab]\dagger},\ \sqrt{\tfrac{2}{3}}\boldsymbol{\mathcal{Y}}_{(123)}^{[kab]\dagger},\ 0\ 0\right)\,, \\ \boldsymbol{\mathcal{Y}}^{[I=1],b\dagger} &= \left(0,\ \boldsymbol{\mathcal{Y}}_{(312)}^{[kab]\dagger},\ \sqrt{\tfrac{2}{3}}\boldsymbol{\mathcal{Y}}_{(213)}^{[kab]\dagger},\ \sqrt{\tfrac{1}{3}}\boldsymbol{\mathcal{Y}}_{(213)}^{[kab]\dagger},\ -\sqrt{\tfrac{2}{3}}\boldsymbol{\mathcal{Y}}_{(123)}^{[kab]\dagger},\ -\sqrt{\tfrac{1}{3}}\boldsymbol{\mathcal{Y}}_{(123)}^{[kab]\dagger},\ 0,\ 0\right)\,, \\ \boldsymbol{\mathcal{Y}}^{[I=1],c\dagger} &= \left(0,\ 0,\ 0,\ 0,\ 0,\ 0,\ \sqrt{\tfrac{1}{2}}\boldsymbol{\mathcal{Y}}_{(312)}^{[kab]\dagger},\ \boldsymbol{\mathcal{Y}}_{(213)}^{[kab]\dagger}\right)\,. \end{aligned} \tag{6.75}$$

Using PT symmetry, there are here six underlying functions.

The form of the underlying functions in the above expressions is constrained by symmetries. This will be discussed in section 6.6 below.

6.4.7 Integral equations relating $\mathcal{K}_{\mathrm{df},3}$ to $\mathcal{M}_3$

Implementation of the three-particle formalism involves two steps: first, determine (constraints on) the three-particle K matrix, $\widehat{\mathcal{K}}_{\mathrm{df},3}$ using the quantization condition eq. (6.50) to

fit to finite-volume energies; and, second, determine the three-particle scattering amplitude $\mathcal{M}_3$ by solving the integral equations that relate it to $\widehat{\mathcal{K}}_{\text{df},3}$ [17]. In this section we describe the required integral equations.

These are obtained by taking an appropriate limit of $\mathcal{M}_{3,L}$, which, from eq. (6.43) and subsequent discussion, is given by

$$\mathcal{M}_{3,L} = \boldsymbol{\mathcal{C}} \circ \widehat{\mathcal{D}}_L^{(u,u)} \circ \boldsymbol{\mathcal{C}}^\dagger \,. + \boldsymbol{\mathcal{C}} \circ \widehat{\mathcal{M}}_{\text{df},3,L}^{(u,u)\prime} \circ \boldsymbol{\mathcal{C}}^\dagger \,. \tag{6.76}$$

The first term describes a ladder of one-particle exchanges, as can be seen from its definition in eq. (6.45), and does not involve $\widehat{\mathcal{K}}_{\text{df},3}$. It contains the divergences that are known to be present in three-particle amplitudes. The second term is the divergence-free part of $\mathcal{M}_3$, and is denoted $\mathcal{M}_{\text{df},3}$. As can be seen from eq. (6.46), it vanishes unless $\widehat{\mathcal{K}}_{\text{df},3}$ is nonzero.

The desired integral equations are obtained by reinserting $i\epsilon$ factors in the numerators of $\widetilde{F}$ and $\widetilde{G}$, taking the $L \to \infty$ limit, and then sending $\epsilon \to 0$ [17]

$$\mathcal{M}_3 = \lim_{\epsilon \to 0} \lim_{L \to \infty} \mathcal{M}_{3,L} \,. \tag{6.77}$$

We do not write out the detailed form of the integral equations, as these are essentially the same as those that have appeared in previous RFT works; see, e.g., refs. [16, 179] and BS3. What is new here are the presence of two types of singularity in the one-particle exchange terms, due to the presence of two distinct intermediate states, namely $K\overline{K}\pi$ and $\pi\pi\eta$. This simply leads to additional matrix indices that are built into the formalism.

The additional feature of the present application is the need to decompose into different total isospin channels. In particular, the "core" of the integral equations resulting from eq. (6.77) (i.e. dropping the factors of $\boldsymbol{\mathcal{C}}$ and $\boldsymbol{\mathcal{C}}^\dagger$) involves 18-d matrices in flavor space, which, as we have seen above, block-diagonalize into 5-d, 8-d, and 5-d blocks corresponding to $I = 2, 1, 0$, respectively. The final integral equations, by contrast, involve 7-d flavor matrices, and the isospin blocks are of size 2, 3, and 2, corresponding to the states listed in eq. (6.2). This is because the integral equations are given in the momentum basis, with no choice of a spectator or pair required.

Putting this together, what we require is the 7×18 matrix of operators

$$\boldsymbol{\mathcal{C}}_{\text{iso18}\to\text{iso7}} = C_{\text{ch}\to\text{iso}}\, \boldsymbol{\mathcal{C}}\, [C^{(18)}_{\text{ch}\to\text{iso}}]^{-1}\,, \tag{6.78}$$

where the three matrices on the right-hand side are given in eq. (D.9), eq. (6.36), and section D.5, respectively. An important check on the form of these matrices is that $\boldsymbol{\mathcal{C}}_{\text{iso18}\to\text{iso7}}$ should itself be block diagonal, with 2×5 blocks for both $I = 2$ and 0, and a 3×8 block for $I = 1$. We indeed find this to be the case.

The explicit form of the 2×5 block for $I = 2$ is

$$\boldsymbol{\mathcal{C}}^{[I=2]}_{\text{iso18}\to\text{iso7}} = \begin{pmatrix} \boldsymbol{\mathcal{X}}^{[I=2],a} \\ \boldsymbol{\mathcal{X}}^{[I=2],b} \end{pmatrix}\,, \tag{6.79}$$

where

$$\begin{aligned} \boldsymbol{\mathcal{X}}^{[I=2],a} &= \left(\boldsymbol{\mathcal{X}}^{(312)}_{[kab]},\ \boldsymbol{\mathcal{X}}^{(213)}_{[kab]},\ \boldsymbol{\mathcal{X}}^{(123)}_{[kab]},\ 0,\ 0\right)\,, \\ \boldsymbol{\mathcal{X}}^{[I=2],b} &= \left(0,\ 0,\ 0,\ \sqrt{2}\boldsymbol{\mathcal{X}}^{(312)}_{[kab]},\ \boldsymbol{\mathcal{X}}^{(123)}_{[kab]} + \boldsymbol{\mathcal{X}}^{(213)}_{[kab]}\right)\,. \end{aligned} \tag{6.80}$$

For the $I = 0$ block we find

$$\boldsymbol{\mathcal{C}}^{[I=0]}_{\text{iso18}\to\text{iso7}} = \begin{pmatrix} \boldsymbol{\mathcal{X}}^{[I=0],a} \\ \boldsymbol{\mathcal{X}}^{[I=0],b} \end{pmatrix}\,, \tag{6.81}$$

where

$$\begin{aligned} \boldsymbol{\mathcal{X}}^{[I=0],a} &= \left(\boldsymbol{\mathcal{X}}^{(312)}_{[kab]},\ -\boldsymbol{\mathcal{X}}^{(213)}_{[kab]},\ -\boldsymbol{\mathcal{X}}^{(123)}_{[kab]},\ 0,\ 0\right)\,, \\ \boldsymbol{\mathcal{X}}^{[I=0],b} &= \boldsymbol{\mathcal{X}}^{[I=2],b}\,. \end{aligned} \tag{6.82}$$

Finally, for $I = 1$, the 3×8 block is

$$\boldsymbol{\mathcal{C}}^{[I=1]}_{\text{iso18}\to\text{iso7}} = \begin{pmatrix} \boldsymbol{\mathcal{X}}^{[I=1],a} \\ \boldsymbol{\mathcal{X}}^{[I=1],b} \\ \boldsymbol{\mathcal{X}}^{[I=1],c} \end{pmatrix}\,, \tag{6.83}$$

where

$$\begin{aligned} \boldsymbol{\mathcal{X}}^{[I=1],a} &= \left(\boldsymbol{\mathcal{X}}^{(312)}_{[kab]},\ 0, -\sqrt{\tfrac{1}{3}}\boldsymbol{\mathcal{X}}^{(213)}_{[kab]}, \sqrt{\tfrac{2}{3}}\boldsymbol{\mathcal{X}}^{(213)}_{[kab]}, -\sqrt{\tfrac{1}{3}}\boldsymbol{\mathcal{X}}^{(123)}_{[kab]}, \sqrt{\tfrac{2}{3}}\boldsymbol{\mathcal{X}}^{(123)}_{[kab]},\ 0,\ 0\right)\,, \\ \boldsymbol{\mathcal{X}}^{[I=1],b} &= \left(0, \boldsymbol{\mathcal{X}}^{(312)}_{[kab]}, \sqrt{\tfrac{2}{3}}\boldsymbol{\mathcal{X}}^{(213)}_{[kab]}, \sqrt{\tfrac{1}{3}}\boldsymbol{\mathcal{X}}^{(213)}_{[kab]}, -\sqrt{\tfrac{2}{3}}\boldsymbol{\mathcal{X}}^{(123)}_{[kab]}, -\sqrt{\tfrac{1}{3}}\boldsymbol{\mathcal{X}}^{(123)}_{[kab]},\ 0,\ 0\right)\,, \\ \boldsymbol{\mathcal{X}}^{[I=1],c} &= \left(0,\ 0,\ 0,\ 0,\ 0,\ 0, \sqrt{2}\boldsymbol{\mathcal{X}}^{(312)}_{[kab]}, -\boldsymbol{\mathcal{X}}^{(123)}_{[kab]} + \boldsymbol{\mathcal{X}}^{(213)}_{[kab]}\right)\,. \end{aligned} \tag{6.84}$$

To be completely explicit, the final result in the isospin basis is

$$\mathcal{M}_3^{[I]} = \lim_{\epsilon\to 0}\lim_{L\to\infty} \boldsymbol{\mathcal{C}}^{[I]}_{\text{iso18}\to\text{iso7}} \circ \left(\widehat{\mathcal{D}}_L^{(u,u),[I]} + \widehat{\mathcal{M}}^{(u,u)\prime,[I]}_{\text{df},3,L}\right) \circ \boldsymbol{\mathcal{C}}^{[I]\dagger}_{\text{iso18}\to\text{iso7}}\,, \tag{6.85}$$

where the quantities inside the parentheses on the right-hand side are given by eq. (6.45) and eq. (6.46), respectively, except that all matrices in these relations are restricted to the corresponding isospin block. As above, if we drop the $\widehat{\mathcal{D}}_L^{(u,u)}$ term from the right-hand side, then we obtain the divergence-free amplitude, $\mathcal{M}^{[I]}_{\text{df},3}$. We also stress that the operators $\boldsymbol{\mathcal{C}}$ and $\boldsymbol{\mathcal{C}}^\dagger$ convert the core matrices, which are in the $\{k\ell m\}$ basis, to the momentum basis $\{k\}$, as is appropriate for a scattering amplitude.

As a final check, we note that in the formal limit in which we treat $\mathcal{M}_2$ and $\mathcal{K}_{\text{df},3}$ as small, we find from eq. (6.46) that

$$\widehat{\mathcal{M}}^{(u,u)\prime,[I]}_{\text{df},3,L} = \frac{1}{9}\widehat{\mathcal{K}}^{[I]}_{\text{df},3}\left[1 + \mathcal{O}(\mathcal{M}_2, \mathcal{K}_{\text{df},3})\right]\,. \tag{6.86}$$

Thus, in this limit,

$$\begin{aligned}
\left[\mathcal{M}^{[I]}_{\text{df},3}\right]_{xy} &\equiv \left[\boldsymbol{\mathcal{C}}^{[I]}_{\text{iso18}\to\text{iso7}} \circ \widehat{\mathcal{M}}^{(u,u)\prime,[I]}_{\text{df},3,L} \circ \boldsymbol{\mathcal{C}}^{[I]\dagger}_{\text{iso18}\to\text{iso7}}\right]_{xy} && (6.87)\\
&\to \left[\boldsymbol{\mathcal{C}}^{[I]}_{\text{iso18}\to\text{iso7}} \circ \frac{1}{9}\widehat{\mathcal{K}}^{[I]}_{\text{df},3} \circ \boldsymbol{\mathcal{C}}^{[I]\dagger}_{\text{iso18}\to\text{iso7}}\right]_{xy} && (6.88)\\
&= \sum_{x,x',y',y} \boldsymbol{\mathcal{X}}^{[I],x} \circ \boldsymbol{\mathcal{Y}}^{[I],x'} \circ \frac{1}{9}\mathcal{K}^{[I],x'y'}_{\text{df},3} \circ \boldsymbol{\mathcal{Y}}^{[I],y'\dagger} \circ \boldsymbol{\mathcal{X}}^{[I],y\dagger} && (6.89)\\
&= \mathcal{K}^{[I],xy}_{\text{df},3}\,, && (6.90)
\end{aligned}$$

where in the penultimate step we have used the outer-product form of $\mathcal{K}_{\text{df},3}$ derived in the previous section. To do so, we have combined the individual isospin results eqs. (6.70), (6.72) and (6.74) into a generic notation, where x, x', y', y are summed over $\{a, b\}$ for $I = 2, 0$ and over $\{a, b, c\}$ for $I = 1$. In the last step we have used,

$$\boldsymbol{\mathcal{X}}^{[I],x} \circ \boldsymbol{\mathcal{Y}}^{[I],x'} = 3\delta_{xx'}\,, \tag{6.91}$$

which can be shown from the results in eqs. (6.71), (6.75), (6.80), (6.108) and (6.109) given that $\boldsymbol{\mathcal{X}}^{\boldsymbol{\sigma}}_{[kab]}$, defined in eq. (D.20), is the inverse of $\boldsymbol{\mathcal{Y}}^{[kab]}_{\boldsymbol{\sigma}}$, defined in eq. (D.22). We stress

that eq. (6.91) holds only when acting on components of $\mathcal{K}_{\mathrm{df},3}^{[I]}$, for it relies on the symmetry or antisymmetry under pion exchange in the $\pi\pi\eta$ components. The normalization of the $\boldsymbol{\mathcal{Y}}$ was chosen in the previous section so that the right-hand side of eq. (6.91) contains the factor of 3. This was done so that $\mathcal{M}_{\mathrm{df},3}$ and $\mathcal{K}_{\mathrm{df},3}$ have the same normalization in the weak coupling limit, as shown by eq. (6.90).

6.4.8 Projection onto positive G parity

In this section we discuss how the above-described formalism can be projected onto states of positive G parity. As described in section 6.3, this is necessary to avoid mixing with three-pion channels, mixing that we have ignored so far in the development of the formalism.

The projection can be applied to the external operators of eq. (6.2), in a manner already described in section 6.3. The action on this 7-d space is by the projection matrix

$$P_+^{(7)} = \mathrm{diag}\left(\tfrac{1}{2}S_{12},\ 1, \tfrac{1}{2}S_{12},\ \tfrac{1}{2}A_{12},\ 1,\ \tfrac{1}{2}S_{12},\ 1\right)\,, \tag{6.92}$$

where $S_{12} = 1 + P_{12}$ and $A_{12} = 1 - P_{12}$, with P_{12} the operator that interchanges the momenta $\boldsymbol{k}_1$ and $\boldsymbol{k}_2$. The action of this projector propagates through the formalism, and leads to a reduction in the size of the matrices entering the quantization condition. We stress that this projection commutes with total isospin, so we can consider this reduction block by block.

To determine the projectors on the isospin blocks we need the G-parity transformation of the $K\overline{K}\pi$ operators in eq. (6.1),

$$\begin{aligned}
K^+(\boldsymbol{k}_1)\overline{K}^0(\boldsymbol{k}_2)\pi^-(\boldsymbol{k}_3) &\to \overline{K}^0(\boldsymbol{k}_1)K^+(\boldsymbol{k}_2)\pi^-(\boldsymbol{k}_3)\,,\\
K^+(\boldsymbol{k}_1)K^-(\boldsymbol{k}_2)\pi^0(\boldsymbol{k}_3) &\to -\overline{K}^0(\boldsymbol{k}_1)K^0(\boldsymbol{k}_2)\pi^0(\boldsymbol{k}_3)\,,\\
K^0(\boldsymbol{k}_1)\overline{K}^0(\boldsymbol{k}_2)\pi^0(\boldsymbol{k}_3) &\to -K^-(\boldsymbol{k}_1)K^+(\boldsymbol{k}_2)\pi^0(\boldsymbol{k}_3)\,,\\
K^0(\boldsymbol{k}_1)K^-(\boldsymbol{k}_2)\pi^+(\boldsymbol{k}_3) &\to K^-(\boldsymbol{k}_1)K^0(\boldsymbol{k}_2)\pi^+(\boldsymbol{k}_3)\,.
\end{aligned} \tag{6.93}$$

Here we have used the action of G described in section 6.3, as well as the negative G-parity of pions. For the first and fourth operators G parity simply leads to the interchange $\boldsymbol{k}_1 \leftrightarrow \boldsymbol{k}_2$, while the second and third operators are themselves interchanged, with an overall sign flip,

as well as $\boldsymbol{k}_1 \leftrightarrow \boldsymbol{k}_2$ interchange. Note that the $\pi\pi\eta$ operators automatically have positive G parity and thus are unchanged. We now expand out each of the twelve $K\overline{K}\pi$ operators in the isospin basis eq. (6.38) in terms of underlying operators in eq. (6.93) (with momentum assignments changed, in general), and apply the G-parity transformation. The results are

$$[[K\bar{K}]_{1e/o}\pi]_I \to \pm[[K\bar{K}]_{1e/o}\pi]_I\,, \quad [[K\bar{K}]_{0e/o}\pi]_1 \to \mp[[K\bar{K}]_{0e/o}\pi]_1\,,$$
$$[[K\pi]_{3/2}\bar{K}]_I \leftrightarrow [[\bar{K}\pi]_{3/2}K]_I\,, \quad [[K\pi]_{1/2}\bar{K}]_I \leftrightarrow [[\bar{K}\pi]_{1/2}K]_I\,, \quad (6.94)$$

where I takes all allowed values, and e and o refer, respectively, to projections onto even and odd partial waves.

Thus the projectors onto positive G parity are

$$P_G^{[I=2]} = P_G^{[I=0]} = \begin{pmatrix} P_e & 0 & 0 & 0 & 0 \\ 0 & \frac{1}{2} & \frac{1}{2} & 0 & 0 \\ 0 & \frac{1}{2} & \frac{1}{2} & 0 & 0 \\ 0 & 0 & 0 & 1 & 0 \\ 0 & 0 & 0 & 0 & 1 \end{pmatrix}, \quad (6.95)$$

$$P_G^{[I=1]} = \begin{pmatrix} P_e & 0 & 0 & 0 & 0 & 0 & 0 & \\ 0 & P_o & 0 & 0 & 0 & 0 & 0 & \\ 0 & 0 & \frac{1}{2} & 0 & \frac{1}{2} & 0 & 0 & 0 \\ 0 & 0 & 0 & \frac{1}{2} & 0 & \frac{1}{2} & 0 & 0 \\ 0 & 0 & \frac{1}{2} & 0 & \frac{1}{2} & 0 & 0 & 0 \\ 0 & 0 & 0 & \frac{1}{2} & 0 & \frac{1}{2} & 0 & 0 \\ 0 & 0 & 0 & 0 & 0 & 0 & 1 & 0 \\ 0 & 0 & 0 & 0 & 0 & 0 & 0 & 1 \end{pmatrix}. \quad (6.96)$$

These project the 5-d blocks for $I = 2, 0$ down to 4-d, and project the 8-d blocks for $I = 1$ down to 6-d.

The result is that the quantization condition for each isospin takes the same form as above, eqs. (6.51) and (6.52), but with the matrices $\widehat{F}_G^{[I]}$, $\widehat{\mathcal{K}}_{2,L}$, and $\widehat{\mathcal{K}}_{\mathrm{df},3}$ replaced by their

reduced versions. We first describe these new versions for $\widehat{F}_G^{[I]}$ and $\widehat{\mathcal{K}}_{2,L}$. For $I = 2$, we find

$$\widehat{F}_G^{[I=2]} \to \begin{pmatrix} P_e\tilde{F}^{\pi}P_e & \sqrt{2}P_e\tilde{G}^{\pi K}P_\ell & 0 & 0 \\ \sqrt{2}P_\ell\tilde{G}^{K\pi}P_e & \tilde{F}^{K}+\tilde{G}^{KK} & 0 & 0 \\ 0 & 0 & P_e\tilde{F}'^{\eta}P_e & \sqrt{2}P_e\tilde{G}'^{\eta\pi}P_\ell \\ 0 & 0 & \sqrt{2}P_\ell\tilde{G}'^{\pi\eta}P_e & \tilde{F}'^{\pi}+\tilde{G}'^{\pi\pi} \end{pmatrix}, \tag{6.97}$$

$$\widehat{\mathcal{K}}_{2,L}^{[I=2]} \to \begin{pmatrix} P_e\overline{\mathcal{K}}_{2,L}^{K\bar{K},I=1}P_e & 0 & 0 & P_e\overline{\mathcal{K}}_{2,L}^{\pi\eta\leftrightarrow K\bar{K},I=1} \\ 0 & \overline{\mathcal{K}}_{2,L}^{K\pi,I=3/2} & 0 & 0 \\ 0 & 0 & \frac{1}{2}\overline{\mathcal{K}}_{2,L}^{\pi\pi,I=2} & 0 \\ \overline{\mathcal{K}}_{2,L}^{\pi\eta\leftrightarrow K\bar{K},I=1}P_e & 0 & 0 & \overline{\mathcal{K}}_{2,L}^{\pi\eta,I=1} \end{pmatrix}. \tag{6.98}$$

Several comments are in order. First, we note that the upper 2×2 block in $\widehat{F}_G^{[I=2]}$ now has a similar structure to the lower such block, which is given by the 2+1 form F_G^{2+1}. Thus the projection onto $G = +$ in some sense treats the K and $\overline{K}$ as identical particles. Second, we could replace $P_e\widetilde{F}^{\pi}P_e$ with $P_e\widetilde{F}^{\pi}$, due to the properties of $\widetilde{F}$, as explained in appendix A of ref. [16]. Similarly we do not need a P_e on both sides of the top-left entry in $\widehat{\mathcal{K}}_{2,L}^{[I=2]}$. Finally, the factors of P_e acting on the offdiagonal $\pi\eta \leftrightarrow K\overline{K}$ entries in $\widehat{\mathcal{K}}_{2,L}^{[I=2]}$ can be dropped, since the $G = + \pi\eta$ state only couples to the $K\overline{K}$ state with even partial waves. In all cases, we keep the factors of P_e to illustrate the action of the projectors.

The results for $I = 0$ are similar

$$\widehat{F}_G^{[I=0]} \to \begin{pmatrix} P_e\tilde{F}^{\pi}P_e & -\sqrt{2}P_e\tilde{G}^{\pi K}P_\ell & 0 & 0 \\ -\sqrt{2}P_\ell\tilde{G}^{K\pi}P_e & \tilde{F}^{K}+\tilde{G}^{KK} & 0 & 0 \\ 0 & 0 & P_e\tilde{F}'^{\eta}P_e & \sqrt{2}P_e\tilde{G}'^{\eta\pi}P_\ell \\ 0 & 0 & \sqrt{2}P_\ell\tilde{G}'^{\pi\eta}P_e & \tilde{F}'^{\pi}+\tilde{G}'^{\pi\pi} \end{pmatrix}, \tag{6.99}$$

$$\widehat{\mathcal{K}}_{2,L}^{[I=0]} \to \begin{pmatrix} P_e\overline{\mathcal{K}}_{2,L}^{K\bar{K},I=1}P_e & 0 & 0 & P_e\overline{\mathcal{K}}_{2,L}^{\pi\eta\leftrightarrow K\bar{K},I=1} \\ 0 & \overline{\mathcal{K}}_{2,L}^{K\pi,I=1/2} & 0 & 0 \\ 0 & 0 & \frac{1}{2}\overline{\mathcal{K}}_{2,L}^{\pi\pi,I=0} & 0 \\ \overline{\mathcal{K}}_{2,L}^{\pi\eta\leftrightarrow K\bar{K},I=1}P_e & 0 & 0 & \overline{\mathcal{K}}_{2,L}^{\pi\eta,I=1} \end{pmatrix}, \tag{6.100}$$

and analogous comments apply.

For $I = 1$, we find

$$\widehat{F}_G^{[I=1]} \to \begin{pmatrix} F_G^{(4)} & 0 \\ 0 & \overline{F}_G^{2+1} \end{pmatrix} , \tag{6.101}$$

where $\overline{F}_G^{2+1}$ is given in eq. (6.62), and

$$F_G^{(4)} = \begin{pmatrix} P_e \widetilde{F}^\pi P_e & 0 & -\sqrt{\frac{2}{3}} P_e \widetilde{G}^{\pi K} P_\ell & \sqrt{\frac{4}{3}} P_e \widetilde{G}^{\pi K} P_\ell \\ 0 & P_o \widetilde{F}^\pi P_o & -\sqrt{\frac{4}{3}} P_o \widetilde{G}^{\pi K} P_\ell & -\sqrt{\frac{2}{3}} P_o \widetilde{G}^{\pi K} P_\ell \\ -\sqrt{\frac{2}{3}} P_\ell \widetilde{G}^{K\pi} P_e & -\sqrt{\frac{4}{3}} P_\ell \widetilde{G}^{K\pi} P_o & \widetilde{F}^K - \frac{1}{3}\widetilde{G}^{KK} & -\sqrt{\frac{8}{9}} \widetilde{G}^{KK} \\ \sqrt{\frac{4}{3}} P_\ell \widetilde{G}^{K\pi} P_e & -\sqrt{\frac{2}{3}} P_\ell \widetilde{G}^{K\pi} P_o & -\sqrt{\frac{8}{9}} \widetilde{G}^{KK} & \widetilde{F}^K + \frac{1}{3}\widetilde{G}^{KK} \end{pmatrix} , \tag{6.102}$$

while the two-particle K matrix reduces to

$$\widehat{\mathcal{K}}_{2,L}^{[I=1]} \to \begin{pmatrix} P_e \overline{\mathcal{K}}_{2,L}^{K\bar{K},I=1} P_e & 0 & 0 & 0 & 0 & P_e \overline{\mathcal{K}}_{2,L}^{\pi\eta\leftrightarrow K\bar{K},I=1} \\ 0 & P_o \overline{\mathcal{K}}_{2,L}^{K\bar{K},I=0} P_o & 0 & 0 & 0 & 0 \\ 0 & 0 & \overline{\mathcal{K}}_{2,L}^{K\pi,I=3/2} & 0 & 0 & 0 \\ 0 & 0 & 0 & \overline{\mathcal{K}}_{2,L}^{K\pi,I=1/2} & 0 & 0 \\ 0 & 0 & 0 & 0 & \frac{1}{2}\overline{\mathcal{K}}_{2,L}^{\pi\pi,I=1} & 0 \\ \overline{\mathcal{K}}_{2,L}^{\pi\eta\leftrightarrow K\bar{K},I=1} P_e & 0 & 0 & 0 & 0 & \overline{\mathcal{K}}_{2,L}^{\pi\eta,I=1} \end{pmatrix} . \tag{6.103}$$

Next we describe the reduced forms of $\mathcal{K}_{\mathrm{df},3}$. The expressions in terms of sums over outer products, eqs. (6.70), (6.72) and (6.74), remain valid, but the vectors themselves change to

$$\begin{aligned} \boldsymbol{\mathcal{Y}}^{[I=2],a\dagger} &\to \left(\tfrac{1}{2}(\boldsymbol{\mathcal{Y}}_{(312)}^{[kab]\dagger} + \boldsymbol{\mathcal{Y}}_{(321)}^{[kab]\dagger}), \sqrt{\tfrac{1}{2}}(\boldsymbol{\mathcal{Y}}_{(213)}^{[kab]\dagger} + \boldsymbol{\mathcal{Y}}_{(123)}^{[kab]\dagger}),\ 0,\ 0 \right) , \\ \boldsymbol{\mathcal{Y}}^{[I=2],b\dagger} &\to \left(0,\ 0,\ \sqrt{\tfrac{1}{2}}\boldsymbol{\mathcal{Y}}_{(312)}^{[kab]\dagger},\ \boldsymbol{\mathcal{Y}}_{(213)}^{[kab]\dagger} \right) , \end{aligned} \tag{6.104}$$

$$\begin{aligned} \boldsymbol{\mathcal{Y}}^{[I=0],a\dagger} &\to \left(\tfrac{1}{2}(\boldsymbol{\mathcal{Y}}_{(312)}^{[kab]\dagger} + \boldsymbol{\mathcal{Y}}_{(321)}^{[kab]\dagger}), -\sqrt{\tfrac{1}{2}}(\boldsymbol{\mathcal{Y}}_{(213)}^{[kab]\dagger} + \boldsymbol{\mathcal{Y}}_{(123)}^{[kab]\dagger}),\ 0,\ 0 \right) , \\ \boldsymbol{\mathcal{Y}}^{[I=0],b\dagger} &\to \left(0,\ 0,\ \sqrt{\tfrac{1}{2}}\boldsymbol{\mathcal{Y}}_{(312)}^{[kab]\dagger},\ \boldsymbol{\mathcal{Y}}_{(213)}^{[kab]\dagger} \right) , \end{aligned} \tag{6.105}$$

$$\begin{aligned} \boldsymbol{\mathcal{Y}}^{[I=1],a\dagger} &\to \left(\tfrac{1}{2}(\boldsymbol{\mathcal{Y}}_{(312)}^{[kab]\dagger} + \boldsymbol{\mathcal{Y}}_{(321)}^{[kab]\dagger}),\ 0, -\sqrt{\tfrac{1}{6}}(\boldsymbol{\mathcal{Y}}_{(213)}^{[kab]\dagger} + \boldsymbol{\mathcal{Y}}_{(123)}^{[kab]\dagger}), \sqrt{\tfrac{1}{3}}(\boldsymbol{\mathcal{Y}}_{(213)}^{[kab]\dagger} + \boldsymbol{\mathcal{Y}}_{(123)}^{[kab]\dagger}),\ 0\ \ 0 \right) , \\ \boldsymbol{\mathcal{Y}}^{[I=1],b\dagger} &\to \left(0, \tfrac{1}{2}(\boldsymbol{\mathcal{Y}}_{(312)}^{[kab]\dagger} - \boldsymbol{\mathcal{Y}}_{(321)}^{[kab]\dagger}), \sqrt{\tfrac{1}{3}}(\boldsymbol{\mathcal{Y}}_{(213)}^{[kab]\dagger} - \boldsymbol{\mathcal{Y}}_{(123)}^{[kab]\dagger}), \sqrt{\tfrac{1}{3}}(\boldsymbol{\mathcal{Y}}_{(213)}^{[kab]\dagger} - \boldsymbol{\mathcal{Y}}_{(123)}^{[kab]\dagger}),\ 0,\ 0 \right) , \\ \boldsymbol{\mathcal{Y}}^{[I=1],c\dagger} &\to \left(\ 0,\ 0,\ 0,\ 0,\ \sqrt{\tfrac{1}{2}}\boldsymbol{\mathcal{Y}}_{(312)}^{[kab]\dagger},\ \boldsymbol{\mathcal{Y}}_{(213)}^{[kab]\dagger} \right) . \end{aligned} \tag{6.106}$$

The final change is to the integral equations relating $\mathcal{K}_{\mathrm{df},3}$ to $\mathcal{M}_3$. Here again the form of the relations, eq. (6.85), remains unchanged, as does the expressions for the conversion matrices, eqs. (6.79), (6.81) and (6.83). The vector of operators entering the latter expressions, however, change to

$$\begin{aligned}
\boldsymbol{\mathcal{X}}^{[I=2],a} &\to \left(\tfrac{1}{2}(\boldsymbol{\mathcal{X}}^{(312)}_{[kab]} + \boldsymbol{\mathcal{X}}^{(321)}_{[kab]}), \sqrt{\tfrac{1}{2}}(\boldsymbol{\mathcal{X}}^{(213)}_{[kab]} + \boldsymbol{\mathcal{X}}^{(123)}_{[kab]}),\ 0,\ 0\right) , \\
\boldsymbol{\mathcal{X}}^{[I=2],b} &\to \left(0,\ 0,\ \sqrt{2}\boldsymbol{\mathcal{X}}^{(312)}_{[kab]},\ \boldsymbol{\mathcal{X}}^{(123)}_{[kab]} + \boldsymbol{\mathcal{X}}^{(213)}_{[kab]}\right) ,
\end{aligned} \tag{6.107}$$

$$\begin{aligned}
\boldsymbol{\mathcal{X}}^{[I=0],a} &\to \left(\tfrac{1}{2}(\boldsymbol{\mathcal{X}}^{(312)}_{[kab]} + \boldsymbol{\mathcal{X}}^{(321)}_{[kab]}), -\sqrt{\tfrac{1}{2}}(\boldsymbol{\mathcal{X}}^{(213)}_{[kab]} + \boldsymbol{\mathcal{X}}^{(123)}_{[kab]}),\ 0,\ 0\right) , \\
\boldsymbol{\mathcal{X}}^{[I=0],b} &\to \left(0,\ 0,\ \sqrt{2}\boldsymbol{\mathcal{X}}^{(312)}_{[kab]},\ \boldsymbol{\mathcal{X}}^{(123)}_{[kab]} + \boldsymbol{\mathcal{X}}^{(213)}_{[kab]}\right) ,
\end{aligned} \tag{6.108}$$

$$\begin{aligned}
\boldsymbol{\mathcal{X}}^{[I=1],a} &\to \left(\tfrac{1}{2}(\boldsymbol{\mathcal{X}}^{(312)}_{[kab]} + \boldsymbol{\mathcal{X}}^{(321)}_{[kab]}),\ 0, -\sqrt{\tfrac{1}{6}}(\boldsymbol{\mathcal{X}}^{(213)}_{[kab]} + \boldsymbol{\mathcal{X}}^{(123)}_{[kab]}), \sqrt{\tfrac{1}{3}}(\boldsymbol{\mathcal{X}}^{(213)}_{[kab]} + XR123),\ 0,\ 0\right) , \\
\boldsymbol{\mathcal{X}}^{[I=1],b} &\to \left(0, \tfrac{1}{2}(\boldsymbol{\mathcal{X}}^{(312)}_{[kab]} - \boldsymbol{\mathcal{X}}^{(321)}_{[kab]}), \sqrt{\tfrac{1}{3}}(\boldsymbol{\mathcal{X}}^{(213)}_{[kab]} - \boldsymbol{\mathcal{X}}^{(123)}_{[kab]}), \sqrt{\tfrac{1}{6}}(\boldsymbol{\mathcal{X}}^{(213)}_{[kab]} - XR123),\ 0,\ 0\right) , \\
\boldsymbol{\mathcal{X}}^{[I=1],c} &\to \left(0,\ 0,\ 0,\ 0, \sqrt{2}\boldsymbol{\mathcal{X}}^{(312)}_{[kab]}, -\boldsymbol{\mathcal{X}}^{(123)}_{[kab]} + \boldsymbol{\mathcal{X}}^{(213)}_{[kab]}\right) .
\end{aligned} \tag{6.109}$$

The orthogonality relation eq. (6.91) remains true with these changes.

6.5 Reduction to single-channel formalism for $E^* < M_{KK\pi}$

Up to this point, we have had in mind working above both $\pi\pi\eta$ and $K\overline{K}\pi$ thresholds, i.e. in the regime where both resonances of interest lie. In this section we consider the range between the thresholds, $M_{\pi\pi\eta} \lesssim E^* \lesssim M_{KK\pi}$. Here our formalism remains valid, but we expect that it can be reduced to that for a single three-particle channel by "integrating out" the contributions associated with the $K\overline{K}\pi$ state. Our aim is to sketch how this reduction occurs.

The first point to observe is that, due to the presence of our cutoff functions, the $K\overline{K}\pi$ channel will be automatically and smoothly turned off as the energy is reduced. As described in section D.2, this will occur in two stages, first when the $K\overline{K}$ channel closes, and second upon the closure of the $K\pi$ channel. A similar phenomenon occurs in the $DD\pi$ system, which is where the two-stage turn-off was first noted [227]. For physical masses, the two

closures occur, respectively, at the three-particle energies

$$E_1^* = M_\pi + 2\sqrt{M_K^2 - M_\pi^2} \approx 1090\text{MeV} \quad \text{and} \quad E_2^* = M_K + \sqrt{M_K^2 - M_\pi^2} \approx 970\text{MeV}\,. \quad (6.110)$$

These lie about 40 and 160 MeV below the threshold at $M_{KK\pi} \approx 1130$ MeV, and both are well above the lower threshold at $M_{\pi\pi\eta} \approx 820$ MeV.

The regime we are interested in here is thus $E_2^* < E^* \lesssim M_{KK\pi}$, so that two-channel formalism applies but only one of the channels is kinematically open. In fact, there is a further constraint on the relevance of the considerations of this section, namely that we cannot integrate out the $K\overline{K}\pi$ channel if $\Delta = M_{KK\pi} - E^*$ is too small. This is because there are finite-volume effects arising from the proximity to on-shell $K\overline{K}\pi$ states that scale roughly as $\exp(-\Delta L)$. These are captured by the full, two-channel quantization condition, but not by the reduced version. Thus we should use $\Delta \gtrsim M_\pi$, since then the errors caused by reduction to a single-channel form are comparable to the exponentially-suppressed terms $\sim \exp(-M_\pi L)$ that the formalism does not control. This leaves a very small window $E_2^* < E^* \lesssim M_{KK\pi} - M_\pi$ where the considerations of the remainder of this section apply. Nevertheless, we think the analysis is of interest both from a purely theoretical point of view, and because the window of applicability could be larger in other multichannel systems.

The strategy we follow is to represent the matrices that enter the quantization condition in block form, where the blocks correspond to the $\pi\pi\eta$ and $K\overline{K}\pi$ channels, respectively. Thus, for example, in the $I = 0$ case after G-parity projection, the 4×4 flavor matrices such as $F_G^{[I=0]}$ in eq. (6.99) have two $\pi\pi\eta$ entries (the last two) and two $K\overline{K}\pi$ entries (the first two). In general, these two blocks will have different dimensions. We write the block form as

$$M = \begin{pmatrix} M_A & M_B \\ M_C & M_D \end{pmatrix}, \quad (6.111)$$

and make repeated use of the following standard results (valid if M^{-1} exists)

$$\det M = \det(M_A - M_B M_D^{-1} M_C) \det(M_D)\,, \quad (6.112)$$

$$
\begin{aligned}
[M^{-1}]_A &= \left(M_A - M_B M_D^{-1} M_C\right)^{-1}\,, \qquad [M^{-1}]_D = \left(M_D - M_C M_A^{-1} M_B\right)^{-1}\,, \\
M_A[M^{-1}]_B &= -M_B[M^{-1}]_D\,, \qquad [M^{-1}]_C M_A = -[M^{-1}]_D M_C\,.
\end{aligned}
\tag{6.113}
$$

We first consider the case that $\mathcal{K}_{\mathrm{df},3} = 0$, so that the quantization condition can be written $\det(F_3^{-1}) = 0$. Here, and in the remainder of this section, we drop isospin superscripts, since the considerations are general. For brevity, we also drop carets. We are thus looking for energies where an eigenvalue of F_3 diverges. Given the form of F_3, eq. (6.52), and the fact that F only diverges at noninteracting energies, we can rewrite the quantization condition as [110]

$$
\det(\mathcal{K}_{2,L}^{-1} + F_G) = 0\,. \tag{6.114}
$$

This is also equiavlent to the asymmetric quantization condition, eq. (6.39), when $\widehat{\mathcal{K}}_{\mathrm{df},3}^{(u,u)} = 0$. Our aim is to rewrite this as a single-channel three particle quantization condition. It will turn out to be easier to initially aim for the asymmetric form, which can be written

$$
\det(\overline{\mathcal{K}}^{-1} + [F_G]_A) = 0\,, \qquad \overline{\mathcal{K}} = \overline{\mathcal{K}}_{2,L} + \overline{\mathcal{K}}_{\mathrm{df},3}^{(u,u)}\,, \tag{6.115}
$$

where $\overline{\mathcal{K}}$ is a reduced matrix living only in the $\pi\pi\eta$ block. Here we allow for the possibility that integrating out the $K\overline{K}\pi$ channel leads to the reappearance of $\mathcal{K}_{\mathrm{df},3}$ (here in asymmetric form).

To proceed, we note that F_G is block diagonal with no B or C components, so that, using eq. (6.112), the quantization condition eq. (6.114) becomes

$$
\det(r_A + f_A - r_B[r_D + f_D]^{-1} r_C)\det(r_D + f_D) = 0\,, \tag{6.116}
$$

where we have introduced the shorthands $r \equiv \mathcal{K}_{2,L}^{-1}$ and $f \equiv F_G$. We now make the key assumption, namely that the second determinant does not vanish. This is plausible because $f_D \equiv [F_G]_D$ contains only the $K\overline{K}\pi$ singularity, which is finite in our kinematic regime. With this assumption, the quantization condition becomes the vanishing of the first determinant in eq. (6.116). This has the desired form of the reduced quantization condition, eq. (6.115), if we take

$$
\overline{\mathcal{K}} = \frac{1}{r_A - -r_B[r_D + f_D]^{-1} r_C}\,. \tag{6.117}
$$

Using eq. (6.113), we find, after some algebraic effort, that

$$\overline{\mathcal{K}} = [\mathcal{K}_{2,L}]_A - [\mathcal{K}_{2,L}]_B [F_G]_D \frac{1}{1 + [\mathcal{K}_{2,L}]_D [F_G]_D} [\mathcal{K}_{2,L}]_C \,. \tag{6.118}$$

To achieve our aim, we must decompose this into the form of the second equality in eq. (6.115), i.e. a $\overline{\mathcal{K}}_{2,L}$ part that involves a spectator momentum Kronecker-delta plus an overall factor of $2\omega L^3$, but is otherwise an infinite-volume quantity, and a $\overline{\mathcal{K}}_{\mathrm{df},3}^{(u,u)}$ part that is purely an infinite-volume quantity. The first part is obtained by keeping only the F terms in eq. (6.118),

$$\overline{\mathcal{K}}_{2,L} = [\mathcal{K}_{2,L}]_A - [\mathcal{K}_{2,L}]_B [F]_D \frac{1}{1 + [\mathcal{K}_{2,L}]_D [F]_D} [\mathcal{K}_{2,L}]_C \,. \tag{6.119}$$

This involves the same spectator (a pion) throughout, and the $2\omega L^3$ factors cancel between adjacent factors of F and $\mathcal{K}_{2,L}$, leaving a single overall such factor. Concerning $[F]_D$, one might expect the sum-integral difference in F to vanish, up to exponentially-suppressed corrections, since the summand/integrand involves $K\overline{K}\pi$ denominators and is nonsingular [see eq. (D.10)]. In fact, because of our definition of the PV-regulated integral [16], there is an additional infinite-volume contribution, proportional to the subthreshold part of $\widetilde{\rho}$, eq. (D.27). This leads to the following interpretation of $\overline{\mathcal{K}}_{2,L}$: the second term adds back the on-shell, but subthreshold, contributions to $\pi\eta$ scattering that involve $K\overline{K}$ intermediate states. By construction, these contributions are not included in $[\mathcal{K}_{2,L}]_A$, but are needed in the full single-channel two-particle K matrix when the $K\overline{K}\pi$ state is integrated out.

The remainder of $\overline{\mathcal{K}}$ involves at least one factor of $[G]_D$, which switches the spectator from a pion to a K or $\overline{K}$. In fact, it is easy to see that, after expanding the geometric series in eq. (6.118), at least two factors of $[G]_D$ are needed to bring the spectator back to being a pion. Although an explicit all-orders expression can be given, it is not illuminating. The important properties are that all three particles are involved in the process, that the various factors of $2\omega L^3$ [including two for each G—see eq. (D.16)] cancel aside from an inverse for each internal momentum sum, and that these momentum sums can be converted to integrals up to exponentially suppressed corrections (since the summands involve $K\overline{K}\pi$ intermediate states and are thus nonsingular). The result is a contribution to $\overline{\mathcal{K}}_{\mathrm{df},3}^{(u,u)}$, an infinite-volume

quantity involving all three particles. It is asymmetric because only the external pions are spectators. The interpretation of this contribution to the reduced three-particle kernel is simply that it adds in contributions involving intermediate $K\overline{K}\pi$ states that lead to power-law volume effects above the $K\overline{K}\pi$ threshold, due to the singularities in G, but now lead only to exponentially-suppressed volume dependence.

We now repeat the argument in the general case, but starting with the asymmetric form of the quantization condition, written as

$$\det\left([\mathcal{K}_{2,L} + \mathcal{K}_{\mathrm{df},3}^{(u,u)}]^{-1} + F_G\right) = 0\,. \tag{6.120}$$

We follow exactly the same steps as above, leading to the reduced quantization condition eq. (6.115), in which $\overline{\mathcal{K}}$ (denoted with a prime to distinguish it from the earlier form) has the form

$$\overline{\mathcal{K}}' = [\mathcal{K}_{2,L} + \mathcal{K}_{\mathrm{df},3}^{(u,u)}]_A - [\mathcal{K}_{2,L} + \mathcal{K}_{\mathrm{df},3}^{(u,u)}]_B [F_G]_D \frac{1}{1 + [\mathcal{K}_{2,L} + \mathcal{K}_{\mathrm{df},3}^{(u,u)}]_D [F_G]_D} [\mathcal{K}_{2,L} + \mathcal{K}_{\mathrm{df},3}^{(u,u)}]_C\,. \tag{6.121}$$

This can be decomposed as

$$\overline{\mathcal{K}}' = \overline{\mathcal{K}}_{2,L} + \overline{\mathcal{K}}_{\mathrm{df},3}^{(u,u)} + [\mathcal{K}_{\mathrm{df},3}^{(u,u)}]_A + \overline{\mathcal{K}}_{\mathrm{df},3}^{\prime(u,u)}\,, \tag{6.122}$$

where the first two terms on the right-hand side are those discussed above in the $\mathcal{K}_{\mathrm{df},3} = 0$ case, the third term is simply the A block of the asymmetric three-particle K matrix, and the final term is the new contribution arising from integrating out $K\overline{K}\pi$ in the presence of a non-zero $\mathcal{K}_{\mathrm{df},3}$. An example of a contribution to the final term is

$$\overline{\mathcal{K}}_{\mathrm{df},3}^{\prime(u,u)} \supset -[\mathcal{K}_{\mathrm{df},3}^{(u,u)}]_B [F_G]_D [\mathcal{K}_{2,L}]_C \tag{6.123}$$

As above, it is straightforward to see that, for all contributions, the $2\omega L^3$ factors combine to convert sums into integrals up to exponentially-suppressed volume dependence. The result is that $\overline{\mathcal{K}}_{\mathrm{df},3}^{\prime(u,u)}$ is an infinite volume quantity with the correct properties to be a contribution to the asymmetric $\mathcal{K}_{\mathrm{df},3}$. Thus the last three terms in eq. (6.122) constitute the renormalized reduced three-particle K matrix.

The final step is to symmetrize the quantization condition. This can be done using the symmetrization identities given in BS2 and BS3, as already noted in section 6.4.4. However, the method used in those works is based on $\mathcal{M}_{23,L}$, rather than the quantization condition. Since here we work directly with the latter, we provide the necessary generalization in section D.7. The conclusion is that we can convert the asymmetric form of the reduced quantization condition to the desired symmetric form,

$$\det\left[1 + \overline{F}_3 \overline{\mathcal{K}}_{\mathrm{df},3}\right] = 0\,, \tag{6.124}$$

$$\overline{F}_3 = \frac{F_A}{3} - F_A \frac{1}{(\overline{\mathcal{K}}_{2,L})^{-1} + [F_G]_A} F_A\,. \tag{6.125}$$

in which $\overline{\mathcal{K}}_{\mathrm{df},3}$ is a symmetrized three-particle K matrix that is algebraically related to $\overline{\mathcal{K}}'^{(u,u)}_{\mathrm{df},3}$.

An alternative method of determining the reduced, single-channel quantization condition is to begin with the full symmetrized quantization condition, expressed as

$$\det\left[\mathcal{K}_{\mathrm{df},3} + F_3^{-1}\right] = 0\,, \tag{6.126}$$

and to apply eq. (6.112) with $M = \mathcal{K}_{\mathrm{df},3} + F_3^{-1}$. Expanding inside the first determinant of eq. (6.112), one can identify $[F_3^{-1}]_A$ and $-[F_3^{-1}]_B([F_3^{-1}]_A)^{-1}[F_3^{-1}]_C$ as the only terms with overlap of $\overline{F}_3^{-1}$, the quantity appearing in the new single-channel quantization condition. As with the method described above, these terms split into two parts: those that contribute to $\overline{\mathcal{K}}_{\mathrm{df},3}$, and those which can be folded into $\overline{F}_3^{-1}$ through the correct definition of $\overline{\mathcal{K}}_{2,L}$. Both methods arrive at the same expression for $\overline{\mathcal{K}}_{2,L}$, given in eq. (6.119), and we expect $\overline{\mathcal{K}}_{\mathrm{df},3}$ can be brought into the same form through symmetrization.

In summary, we have shown explicitly how, if one goes far enough below the $K\overline{K}\pi$ threshold, the quantization condition reduces to the expected form for a single channel system, with a renormalized $\mathcal{K}_2$ and $\mathcal{K}^{(u,u)}_{\mathrm{df},3}$.

6.6 Parametrizations of $\mathcal{K}_{\mathrm{df},3}$

In a practical application, one must parametrize the three-particle K-matrix. This should be done respecting the symmetries of the theory, in particular Lorentz, P, and T invariance, and

the exchange symmetries of the three-meson states. Of particular interest are the behavior near threshold and in the vicinity of a three-particle resonance. We discuss these two regimes in turn, generalizing the methods introduced in refs. [37, 110].

Near threshold, $\mathcal{K}_{\mathrm{df},3}$ can be expanded in terms of kinematic invariants that vanish at threshold. The procedure for doing so was laid out in ref. [110] in the case of three identical particles, and has been subsequently generalized to many systems [36, 37, 179, 227, 230]. The main new feature here is the presence of two thresholds, corresponding to the $\pi\pi\eta$ and $K\overline{K}\pi$ channels.

From section 6.4.6, we know that the underlying functions that we have to parametrize are the $\mathcal{K}_{\mathrm{df},3}^{[I],xy}$ that appear in eqs. (6.70), (6.72) and (6.74), where x, y run over the different channels. Each of these K matrices are Lorentz-invariant functions of the three incoming on-shell four-momenta, which here we denote $\{k_i\}$, and the corresponding outgoing momenta, denoted $\{k_i'\}$. For our two channels, we use the labels $i = 1, 2$ for the two particles that are degenerate, while $i = 3$ denotes the particle with a distinct mass. We denote the initial-state masses as m_i and the final-state masses as m_i'. The threshold CMF energies for the two channels are then $M = 2m_1 + m_3$ and $M' = 2m_1' + m_3'$. We call the smaller of these M_{min}, and use this to set the scale in the following.

To parameterize the three-particle amplitude $\mathcal{K}_{\mathrm{df},3}$, we use generalized Mandelstam variables,

$$s \equiv (k_1 + k_2 + k_3)^2, \quad s_{ij} \equiv (k_i + k_j)^2, \quad s_{ij}' \equiv (k_i' + k_j')^2, \quad t_{ij} \equiv (k_i' - k_j)^2 \,. \tag{6.127}$$

It is convenient to use the following seventeen dimensionless quantities,

$$\begin{aligned} \Delta &\equiv \frac{s - M^2}{M_{\mathrm{min}}^2}, \quad \Delta' \equiv \frac{s - M'^2}{M_{\mathrm{min}}^2} = \Delta + \frac{M'^2 - M^2}{M_{\mathrm{min}}^2}, \\ \Delta_i &\equiv \frac{s_{jk} - (m_j + m_k)^2}{M_{\mathrm{min}}^2}, \qquad \Delta_i' \equiv \frac{s_{jk}' - (m_j' + m_k')^2}{M_{\mathrm{min}}^2}, \quad \widetilde{t}_{ij} \equiv \frac{t_{ij} - (m_i' - m_j)^2}{M_{\mathrm{min}}^2}, \end{aligned} \tag{6.128}$$

where, in the definitions of Δ_i and Δ_i', $\{i, j, k\}$ form a cylic permutation of $\{1, 2, 3\}$. Δ and Δ_i vanish at the initial-state threshold, while Δ' and Δ_i' vanish at the final-state threshold.

The $\widetilde{t}_{ij}$ only vanish at threshold if the initial and final channels are the same; in general they vanish if the final (i) and initial particles (j) are relatively at rest. We note that these quantities are well-defined below as well as above the corresponding thresholds.

These seventeen quantities in eq. (6.128) are constrained by the relation between Δ and Δ' given in that equation, as well as the following eight relations, seven of which are independent,[7]

$$\sum_{i=1}^{3}\Delta_i = \Delta\,, \quad \sum_{i=1}^{3}\Delta'_i = \Delta'\,, \quad \sum_{i=1}^{3}\widetilde{t}_{ij} = \Delta_j - \Delta + \frac{2m_j(M'-M)}{M_{\rm min}^2}\,,$$
$$\sum_{i=1}^{3}\widetilde{t}_{ji} = \Delta'_j - \Delta' + \frac{2m'_j(M-M')}{M_{\rm min}^2}\,, \quad (6.129)$$

where $j = 1, 2, 3$. This allows us to express $\mathcal{K}_{\rm df,3}$ in terms of the following nine variables: Δ, Δ_1, Δ_2, Δ'_1, Δ'_2, $\widetilde{t}_{11}$, $\widetilde{t}_{12}$, $\widetilde{t}_{21}$, and $\widetilde{t}_{22}$. We develop the threshold expansion treating Δ, Δ_i, Δ'_i, and the $\widetilde{t}_{ij}$ as small. Since the thresholds differ, in practice some of these quantities will be larger than others, and an asymmetric power-counting is appropriate. As the relative sizes depend on the precise kinematics, which varies according to the values of the underlying quark masses, we simply ignore this point and work to quadratic order in all variables, presenting terms of up to linear order here, and collecting the quadratic terms in section D.6.

As we have seen in section 6.3, the requirement that the $K\overline{K}$ pairs have negative G parity implies $[K\bar{K}]_1$ must be symmetric under $\boldsymbol{k}_1 \leftrightarrow \boldsymbol{k}_2$, while $[K\bar{K}]_0$ must be antisymmetric under this exchange. Similarly, the $[\pi\pi]_{0,2}$ states are symmetric, while $[\pi\pi]_1$ is antisymmetric. Using these symmetry requirements allows us to write down all allowed combinations of the nine kinematic variables in our chosen basis.

To begin, we consider $I = 0$ and $I = 2$, each of which have two channels [found in eq. (6.2)], and which have the same symmetry properties. While $\mathcal{K}_{\rm df,3}^{[I=0,2],ab}$ and $\mathcal{K}_{\rm df,3}^{[I=0,2],ba}$ are symmetric under the independent exchanges $k_1 \leftrightarrow k_2$ and $k'_1 \leftrightarrow k'_2$, $\mathcal{K}_{\rm df,3}^{[I=0,2],aa}$ and $\mathcal{K}_{\rm df,3}^{[I=0,2],bb}$ are also symmetric under PT transformations. These symmetries lead to the fol-

[7] In refs. [36, 110], the fact that only seven of these relations were independent was missed. This had no impact on the threshold expansions developed in these works. The correct counting was also noted in ref. [230].

lowing result for the diagonal terms,

$$M_{\min}^2 \mathcal{K}_{\mathrm{df},3}^{[I=0,2],xx}(\{k'\},\{k\}) = \mathcal{K}_0^{[I]xx} + \mathcal{K}_1^{[I]xx}\Delta + \mathcal{K}_2^{[I]xx}(\Delta_1+\Delta_2+\Delta_1'+\Delta_2') + \mathcal{K}_3^{[I]xx}(t_{11}+t_{12}+t_{21}+t_{22}) + \mathcal{O}(\Delta^2)\,, \quad (6.130)$$

where $x = a$ or b, and the coefficients $\mathcal{K}_j^{[I]xx}$ are real and dimensionless. For the off-diagonal contributions the lack of PT symmetry leads to one additional term at linear order

$$M_{\min}^2 \mathcal{K}_{\mathrm{df},3}^{[I=0,2],ab}(\{k'\},\{k\}) = M_{\min}^2 \mathcal{K}_{\mathrm{df},3}^{[I=0,2],ba}(\{k\},\{k'\}) = \mathcal{K}_0^{[I]ab} + \mathcal{K}_1^{[I]ab}\Delta + \mathcal{K}_2^{[I]ab}(\Delta_1+\Delta_2) + \mathcal{K}_3^{[I]ab}(\Delta_1'+\Delta_2') + \mathcal{K}_4^{[I]ab}(t_{11}+t_{12}+t_{21}+t_{22}) + \mathcal{O}(\Delta^2)\,, \quad (6.131)$$

where again the coefficients are real and dimensionless. We note that, in both eqs. (6.130) and (6.131), the leading coefficients lead to a contribution that is independent of momenta and thus isotropic. Quadratic terms are given in eqs. (D.79) and (D.80).

Now we turn our attention to $I = 1$, which contains transitions between three independent states [found in eq. (6.2)]. While state a is symmetric under $k_1 \leftrightarrow k_2$, states b and c are antisymmetric under this exchange. These exchange symmetries, coupled with the PT invariance of $\mathcal{K}_{\mathrm{df},3}^{[I=1],xx}$, lead to the following results. For $\mathcal{K}_{\mathrm{df},3}^{[I=1],aa}$ the result has exactly the same form as that for $I = 0, 2$, given in eq. (6.130). For the other diagonal terms, we find

$$\mathcal{K}_{\mathrm{df},3}^{[I=1],yy}(\{k'\},\{k\}) = \mathcal{K}_1^{[1]yy}(t_{11}-t_{12}-t_{21}+t_{22}) + \mathcal{O}(\Delta^2)\,, \quad (6.132)$$

where $y = b$ or c. For the offdiagonal contributions, we obtain

$$\mathcal{K}_{\mathrm{df},3}^{[I=1],ay}(\{k'\},\{k\}) = \mathcal{K}_{\mathrm{df},3}^{[I=1],ya}(\{k\},\{k'\}) = \mathcal{K}_1^{[1]ab}(\Delta_1'-\Delta_2') + \mathcal{K}_2^{[1]ab}(t_{11}-t_{12}+t_{21}-t_{22}) + \mathcal{O}(\Delta^2)\,. \quad (6.133)$$

with $y = b$ or c, and

$$\mathcal{K}_{\mathrm{df},3}^{[I=1],bc}(\{k'\},\{k\}) = \mathcal{K}_{\mathrm{df},3}^{[I=1],cb}(\{k\},\{k'\}) = \mathcal{K}_1^{[1]bc}(t_{11}-t_{12}-t_{21}+t_{22}) + \mathcal{O}(\Delta^2)\,. \quad (6.134)$$

The antisymmetry of the b, c channels leads to the absence of the isotropic contribution and a smaller number of linear terms. Quadratic contributions for $I = 1$ K matrices are given in eqs. (D.81) to (D.83).

We next consider how the expressions given above can be augmented in the $I = 0$ and $I = 1$ channels (in which, respectively, the $\eta(1295)$ and the $b_1(1235)$ appear) to incorporate an explicit pole that satisfies the relevant symmetries and has a factorizable residue. It is plausible that such a pole will be needed to describe a resonance in $\mathcal{M}_3$ [134]. We are guided here by the work of ref. [37] addressing the same issue for the 3π system, in particular for the $J^P = 0^-$ resonance, $\pi(1300)$, and the $J^P = 1^+$ resonance, $a_1(1260)$. We stress that the pole terms we give below are to be added to the threshold expansion forms, and that we are presenting only the simplest possible expressions in both cases. By its very nature, a pole term violates the threshold expansion, and thus one does not have any power counting to restrict the form of the residues. Thus, higher order terms may be needed in practice.

The simplest case is the $I = 0$ $\eta(1295)$ resonance. This $J^P = 0^-$ state couples to both $\pi\pi\eta$ and $K\overline{K}\pi$ in s-wave states, and thus no momentum dependence is needed in the residue. Thus the simplest form to add to $\mathcal{K}_{\rm df,3}$ is

$$\mathcal{K}_{\rm df,3}^{[I=0]xy} \supset \frac{v_x v_y}{P^2 - E_{0^-}^2}\,, \qquad (x,y) \in (a,b)\,, \tag{6.135}$$

where $\boldsymbol{v} = (v_a, v_b)$ is a real vector describing the relative coupling to the two channels, with v_a and v_b being coefficients to be determined. We stress that the pole position E_{0^-} will not equal the $\eta(1295)$ mass, since to connect $\mathcal{K}_{\rm df,3}$ to $\mathcal{M}_3$ requires solving integral equations, and this will, in general, shift the pole position.

Two additional features arise for the $I = 1$, $J^P = 1^+$ channel needed for the $b_1(1235)$. The first is due to the resonance being a vector, and thus having a polarization vector. Summing over this leads to a factor of

$$\sum_\epsilon \epsilon_\mu \epsilon_\nu^* = g^P_{\mu\nu} \equiv g_{\mu\nu} - P_\mu P_\nu / P^2\,. \tag{6.136}$$

The second new feature is the need to contract the open Lorentz indices with four-vectors having the appropriate symmetries. The simplest form is

$$\mathcal{K}_{\rm df,3}^{[I=1]xy} \supset \frac{1}{P^2 - E_{1^+}^2} g^P_{\mu\nu} w_x'^\mu w_y^\nu\,, \qquad (x,y) \in (a,b,c)\,, \tag{6.137}$$

where

$$\begin{aligned} \boldsymbol{w}^{\nu} &= (w_a[k_1^{\nu} + k_2^{\nu}], w_b[k_1^{\nu} - k_2^{\nu}], w_c[k_1^{\nu} - k_2^{\nu}]) \ , \\ \boldsymbol{w}'^{\mu} &= \left(w_a[k_1'^{\mu} + k_2'^{\mu}], w_b[k_1'^{\mu} - k_2'^{\mu}], w_c[k_1'^{\mu} - k_2'^{\mu}]\right) \ , \end{aligned} \tag{6.138}$$

with w_x being real coefficients to be determined. We note that an additional allowed contribution to the w_a terms proportional to P^{ν} can be dropped since $g^P_{\mu\nu}P^{\nu} = 0$.

6.7 Conclusions

In this work, we have generalized the three-particle formalism to accommodate systems involving multiple three-particle channels. While we have focused on the two-channel $\pi\pi\eta$ and $KK\pi$ system, the generalization to additional three-particle channels will involve a simple extension of the work presented here. Indeed, just as in the two-particle case, the generalization to multiple channels is itself not the most challenging part of the derivation. Instead, the complications mainly arise from the need to account for multiple subchannels, and to determine isospin and G-parity projections. These aspects are similar to those arising in the formalism developed for the $DD\pi$ system in ref. [227]. The need for G-parity projection is a new feature here, and turns out to reduce the dimensionality of the matrices appearing in the quantization conditions.

The general structure of the quantization conditions and associated integral equations is the same as that in all previous applications of the RFT approach. The presence of two channels simply enlarges the space of spectator flavors. In our final results, given in section 6.4.8, these spaces are of dimension 4, 6, and 4, respectively, for $I = 0$, 1, and 2. As for the $DD\pi$ system studied in ref. [227], the results for $I = 0$ and $I = 2$ are nearly identical.

The specific channels on which we have focused allow the application to the $b_1(1235)$ and $\eta(1295)$ resonances, as long as one neglects the coupling to channels with four or more particles. As discussed in section 6.3, for such an application, one must use finite-volume irreps in which there are no, or minimal, contributions from $\pi\pi$ states. There are several such irreps, so we do not expect this to be a significant practical limitation. We hope that, in

the next few years, results from lattice QCD will be available that allow one to study these resonance. This will likely first be with heavier-than-physical quark masses, which will, in fact, reduce the problem with neglected channels containing four or more particles.

A three-particle formalism has now been developed that encompasses nearly all systems of interest. The remaining lacuna is exemplified by the Roper resonance, which decays to $N\pi$ and $N\pi\pi$. This involves multiple channels with both two and three particles, as well as nondegenerate particles with a variety of spins. Given the recent extension of the formalism to three spin-1/2 particles [179], and the by now complete understanding of incorporating nondegenerate particles [35,36,117,227], the main challenge concerns the combination of two- and three-particle channels. So far, two approaches have been used: one in which the two-particle channel is incorporated explicitly [39], and the other in which it is introduced by the presence of a bound state in a two-particle subchannel of the three-particle system [114, 210, 211, 227]. It remains to be seen which approach, if either, is the best choice for generalization to the Roper system.[8]

Acknowledgments

We thank Max Hansen and Fernando Romero-López for discussions and comments on the manuscript. This work is supported in part by the U.S. Department of Energy grant No. DE-SC0011637. This work contributes to the goals of the USDOE ExoHad Topical Collaboration, contract DE-SC0023598.

[8]The same comment applies to the generalization of the work presented here to irreps in which the $\pi\pi$ contribution must be included.

Chapter 7
CONCLUSION

The research presented in this dissertation enhances the understanding and application of quantization conditions in lattice quantum chromodynamics, contributing to both the theoretical framework and practical implementations of two- and three-particle finite-volume formalisms. By addressing critical limitations and proposing novel methodologies, this work pushes the boundaries of current lattice capabilities, enabling the study of new systems in quantum chromodynamics.

The first study, presented in chapter 2, highlighted the limitations of applying the two-particle quantization condition to certain unphysical channels in partially quenched theories. It identified specific channels where the quantization condition can still be valid despite the underlying unitarity violation, laying out a rigorous criteria for determining the applicability of quantization conditions in partially quenched setups. In chapter 3, this work was applied to a partially quenched system using twisted-mass fermions in which the sea quark action differed from the valence quark action.

In subsequent chapters we focused on the three-particle finite-volume formalism. Chapter 4 presented a pioneering application of the three-particle quantization condition to the determination of $\pi\pi K$ and $KK\pi$ scattering at maximal isospin. By extracting extensive finite-volume energies and fitting to the spectrum using the appropriate quantization conditions, we determined two- and three-particle scattering parameters. The findings validate the theoretical framework and provide essential data for future research, illustrating the practical implications of the formalism for studying multi-hadron interactions and setting the stage for the study of more complex systems.

Chapter 5 introduced the finite-volume formalism for three identical spin-1/2 particles,

relevant for systems of three neutrons or protons. It addressed the technical complexities arising from spin degrees of freedom, presenting a detailed derivation and establishing the groundwork for future applications, including the study of nucleon interactions and hyperons. The final work presented in this dissertation, that of chapter 6, generalized the three-particle formalism to multiple channels, focusing on $\pi\pi\eta$ and $K\overline{K}\pi$ systems. It highlighted the technical nuances of dealing with multiple subchannels, providing a framework for analyzing systems involving resonances like the $b_1(1235)$ and $\eta(1295)$. This generalization paves the way for future studies, providing a framework for understanding multi-channel interactions.

Collectively, the body of research presented in this dissertation significantly advances the toolkit available for studying multiple particles in finite volume. The methodologies developed not only extend the reach of current lattice calculations but also lay the groundwork for future explorations into more complex systems, including those of significant experimental and theoretical interest. The work extending the three-particle finite-volume formalism, both for identical spin-1/2 particles and multi-channel systems, represents a substantial step forward, offering a robust framework that can be adapted to various physical contexts. The ongoing challenge remains the unification of approaches to handle systems like the Roper resonance, which involve combinations of two- and three-particle channels and diverse particle spins.

Work on applying these frameworks to increasingly realistic lattice simulations that incorporate physical quark masses is already underway. The synergy between theoretical innovation and advanced computational techniques will drive further progress in this field, ultimately enhancing our understanding of the strong interactions that govern the subatomic world.

Appendices

Appendix 1

APPENDIX TO CHAPTER 3

A.1 Higher-order contributions in χPT

In this appendix we collect some technical comments related to the χPT calculations presented in the main text.

First, we write out the NLO terms in the PQ chiral Lagrangian, which are used in Sec. 3.4.3. These consist of ap^2, am_q and a^3 terms,

$$\begin{aligned}\mathcal{L}_{NLO} = {} & \hat{a}W_4\mathrm{str}\Big[(\partial_\mu\Sigma)(\partial_\mu\Sigma^\dagger)\Big]\,\mathrm{str}\Big[\Sigma+\Sigma^\dagger\Big] + \hat{a}W_5\mathrm{str}\Big[(\partial_\mu\Sigma)(\partial_\mu\Sigma^\dagger)(\Sigma+\Sigma^\dagger)\Big] \\ & - \hat{a}W_6\mathrm{str}\Big[\chi'^\dagger\Sigma+\Sigma^\dagger\chi'\Big]\,\mathrm{str}\Big[\Sigma+\Sigma^\dagger\Big] - \hat{a}W_7\mathrm{str}\Big[\chi'^\dagger\Sigma-\Sigma^\dagger\chi'\Big]\,\mathrm{str}\Big[\Sigma-\Sigma^\dagger\Big] \\ & - \hat{a}W_8\mathrm{str}\Big[\chi'^\dagger\Sigma^2+\Sigma^{\dagger 2}\chi'\Big] + a^3\mathcal{L}_{\mathrm{a}^3}\end{aligned} \tag{A.1}$$

where the notation is that of Ref. [45], while the a^3 terms have the schematic form

$$\mathcal{L}_{\mathrm{a}^3} \sim \mathrm{str}\Big[\Sigma+\Sigma^\dagger\Big] + \mathrm{str}\Big[\Sigma^3+\Sigma^{\dagger 3}\Big] + \mathrm{str}\Big[\Sigma^2\pm\Sigma^{\dagger 2}\Big]\,\mathrm{str}\Big[\Sigma\pm\Sigma^\dagger\Big] + \mathrm{str}\Big[\Sigma\pm\Sigma^\dagger\Big]^2\,\mathrm{str}\Big[\Sigma+\Sigma^\dagger\Big]\ , \tag{A.2}$$

where the $\pm$ signs in the third term are both positive or both negative. Here, $\sim$ indicates that there is an independent LEC multiplying each term on the right-hand side. We do not keep track of these LECs as they are not required for our analysis.

Second, we discuss why, when working at maximal twist, there are no terms involving odd powers of the field Π in the expansion of the LO Lagrangian, Eq. (B.1). For the terms that are independent of a, this follows because, at maximal twist, the condensate cancels the twist in the mass, leading to the standard kinetic and mass terms expressed in terms of Σ_{ph}, as shown by the first two terms in Eq. (3.11). These terms are symmetric under $\Pi \to -\Pi$, so that only even powers of Π can appear in their expansions. For the terms induced by the nonzero lattice spacing, the key result is that they are proportional to a^2, as the term

linear in a has been absorbed by a redefinition of χ [84]. This implies that, when expressed in terms of $\Sigma_{\rm ph}$, as in Eq. (3.11), they involve two powers of $\Sigma_0\Sigma_{\rm ph}$. These can appear in one or two straces, with each strace containing either a hermitian or anti-hermitian combination, although the total term must be hermitian. If one expands $\Sigma_{\rm ph}$, a given strace will thus have the form

$$i^{(x_1+y_1+x_2+y_2)}\mathrm{str}\Big[\Pi^{x_1}\,(\tau_3^{VS})^{y_1}\,\Pi^{x_2}\,(\tau_3^{VS})^{y_2}\Big] \pm \mathrm{h.c.}\,, \tag{A.3}$$

where the x_i are non-negative integers, while the y_i are either 0 or 1, *h.c.* indicates hermitian conjugate, and we have used the result that $\Sigma_0 = i\tau_3^{VS}$ at maximal twist. Using the hermiticity of Π and τ_3^{VS}, together with the cyclicity of the strace, we see that the hermitian conjugate term has the same (opposite) sign if $N \equiv x_1 + x_2 + y_1 + y_2$ is even (odd). Thus to avoid a cancellation N must be even (odd) if the hermitian conjugate is added (subtracted).

Now we consider the ways in which one might obtain a cubic vertex from the a^2 terms. If there is a single strace, it must contain an odd power of Π, so that $x_1 + x_2$ is odd, while we know that $y_1 + y_2 = 2$ since there are two powers of Σ_0. Thus N must be odd. However, as there is a single strace, the term must be hermitian, and so, from above, we know that terms with odd N vanish. So there is no such vertex.

If there are two straces, to obtain a cubic vertex one of them must contain an odd power of Π, and the other an even power. Since $\sum_i y_i = 1$ for both terms, we know that N is odd for one strace, and even for the other. Since the two terms are both either hermitian or anti-hermitian, this in turn implies that one of the two terms vanishes.

Similar arguments can be used to demonstrate that the quadratic and quartic terms arising from the NLO Lagrangian in Eq. (A.1), vanish.

Appendix 2

APPENDIX TO CHAPTER 4

B.1 Energy levels used in fits

In this appendix we give further details of the fits described in the main text. First, in Table B.1 we list the energy levels used in the fits. Second, in figures B.1 to B.3 we show the CMF energy levels for the N203 $KK\pi$, D200 $\pi\pi K$ and D200 $KK\pi$ spectra, respectively, along with the predictions from the quantization condition using our standard fit parameters. The corresponding result for the N203 $\pi\pi K$ spectrum is shown in the main text in figure 4.2.

B.2 ChPT result for $\mathcal{K}_{\mathrm{df},3}$ including $\mathcal{O}(a^2)$ errors

In this appendix we extend previous SU(3) ChPT results for two- and three-particle K matrices by including discretization errors. We work at LO, and use SU(3), rather than SU(2), ChPT due to the presence of both kaons and pions. The methodology for including the effects of nonzero a into ChPT was developed in Refs. [83, 84], and is generally referred to as Wilson ChPT, or WChPT for short. Previous work has considered $\pi\pi$ scattering in SU(2) WChPT [231] (working at NLO), but, to our knowledge, no previous calculations of two- or three-particle scattering using SU(3) WChPT have been performed.

For present-day lattice calculations, with light quark masses close to their physical values, and with nonperturbative $\mathcal{O}(a)$ improvement, the appropriate power counting to use is $m_q \sim p^2 \sim a^2$ (leaving factors of Λ_{QCD} implicit). In other words, discretization errors, which begin at $\mathcal{O}(a^2)$, are comparable to the squared masses of the psuedo-Goldstone bosons (PGBs), $M^2_{\mathrm{PGB}} = \mathcal{O}(m_q)$. For an example of the appropriateness of this power counting, we point to Ref. [59], where it is noted, in the related context of simulations with twisted-mass fermions, that an $\mathcal{O}(a^2)$ contribution to PGB mass-squareds ($w_8' f^2$ in the notation below) is indeed of

$\vec{d}_{\text{ref}}$	Type	N203	D200
(0,0,0)	πK	$2A_{1g} + [A_{1g}]$	$A_{1g} + T_{1u} + [A_{1g}]$
	$\pi\pi K$	A_{1u}	A_{1u}
	$KK\pi$	$A_{1u} + E_u$	$2A_{1u} + E_u$
(0,0,1)	πK	$2A_1 + [6A_1 + 2E]$	$2A_1 + [2A_1 + 2E]$
	$\pi\pi K$	$2A_2$	$2A_2$
	$KK\pi$	$2A_2$	$2A_2$
(0,1,1)	πK	$3A_1 + B_2 + [3A_1 + 3B_1 + B_2]$	$3A_1 + B_2 + [A_1 + B_1]$
	$\pi\pi K$	$4A_2 + B_1$	$3A_2 + B_1$
	$KK\pi$	$4A_2 + B_1$	$3A_2 + B_1$
(1,1,1)	πK	$4A_1 + 2E$	$4A_1 + 2E$
	$\pi\pi K$	$A_2 + [2A_2 + 2E]$	A_2
	$KK\pi$	$3A_2 + E$	$2A_2 + E$
(0,0,2)	πK	$4A_1 + E + [A_1]$	$2A_1 + [2A_1 + E]$
	$\pi\pi K$	$3A_2$	$3A_2$
	$KK\pi$	$3A_2$	$3A_2$
(0,1,2)	$\pi\pi K$	$4A_2 + [2A_2]$	$3A_2$
	$KK\pi$	$5A_2$	$4A_2$
(1,1,2)	$\pi\pi K$	$A_2 + [3A_2 + A_1]$	$2A_2$
	$KK\pi$	$4A_2 + A_1$	$2A_2$
(0,2,2)	$\pi\pi K$	$4A_2 + B_1$	$2A_2$
	$KK\pi$	$4A_2 + B_1$	$3A_2 + 2B_1$
(0,0,3)	$\pi\pi K$	$4A_2$	$3A_2$
	$KK\pi$	A_2	$3A_2$

Table B.1: Energy levels used in the fits of this work. Notation is as follows: "$A_{1u} + E_u$" means the lowest level in the A_{1u} irrep, and the lowest in the E_u irrep. When two different energy ranges have been chosen, the levels in brackets contribute only to the fit with the higher energy cutoff. For instance, in D200 a fit with 16 πK levels is shown in the last column of Table 4.7 ("(d) Standard *"), whereas another with 26 levels is shown in the first column of the same table ("(a) Standard"). In this case, "$A_{1g} + T_{1u} + [A_{1g}]$" means that the lowest A_{1g} and T_{1u} levels contribute to the fit with 16 levels, and the second A_{1g} level is additionally included in the fit with 26 levels. The energy levels included in $\pi\pi, KK, \pi\pi\pi$ and KKK systems can be read off from Table 32 of Ref. [132] by selecting only those in trivial irreps (A_1 or A_{1g} for two particles and A_2 or A_{1u} for three).

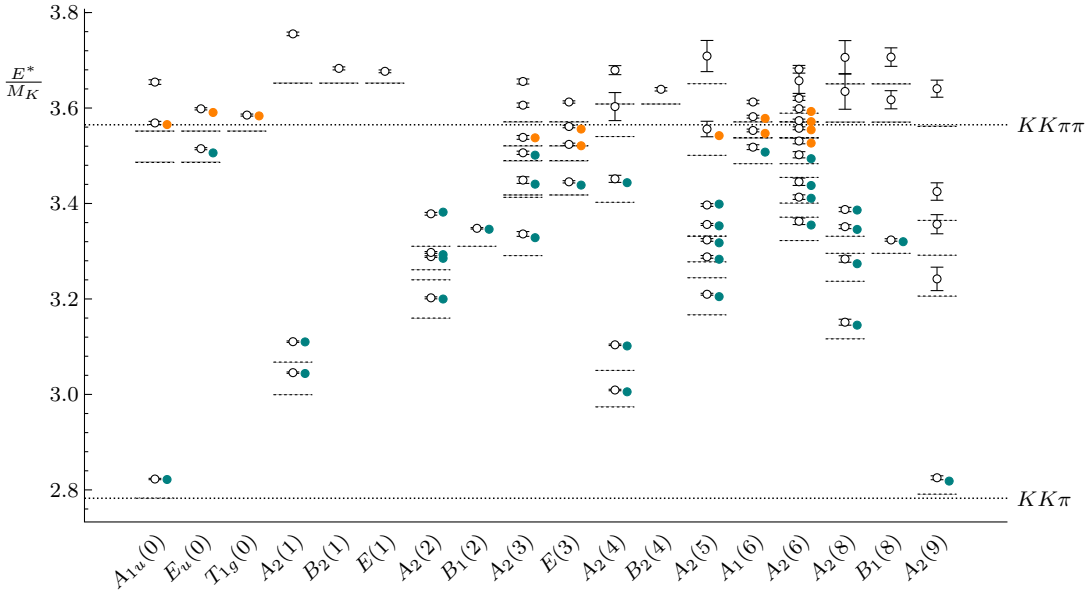

Figure B.1: $KK\pi$ CMF spectrum on ensemble N203. Notation as in figure 4.2, except energies here are in units of M_K. Colored symbols are from the ADLER3 fit in Table 4.10.

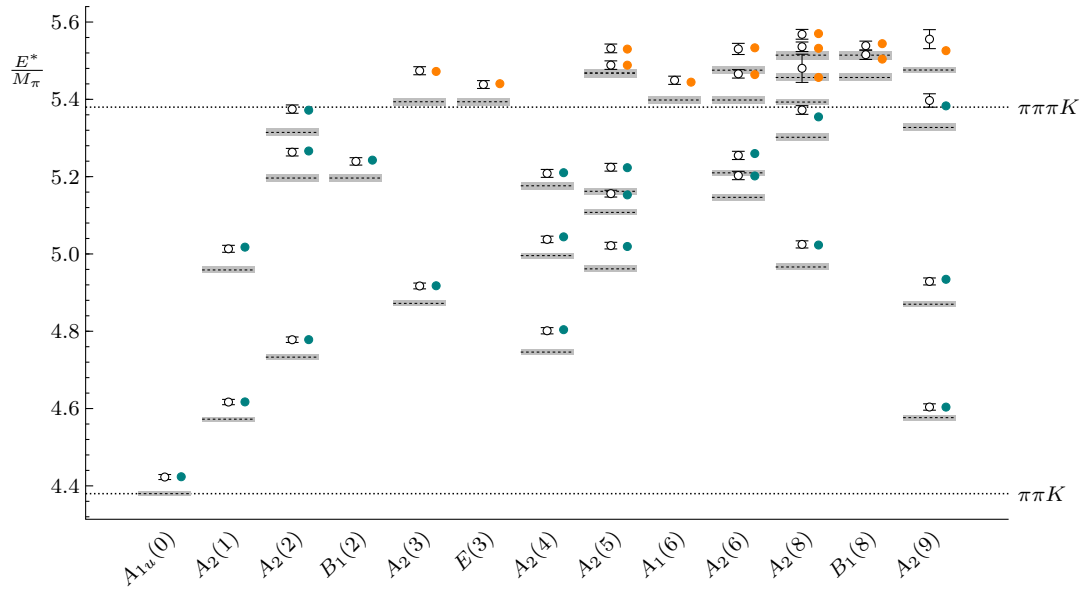

Figure B.2: $\pi\pi K$ CMF spectrum on ensemble D200. Notation as in figure 4.2. Colored symbols are from the Standard fit in Table 4.7.

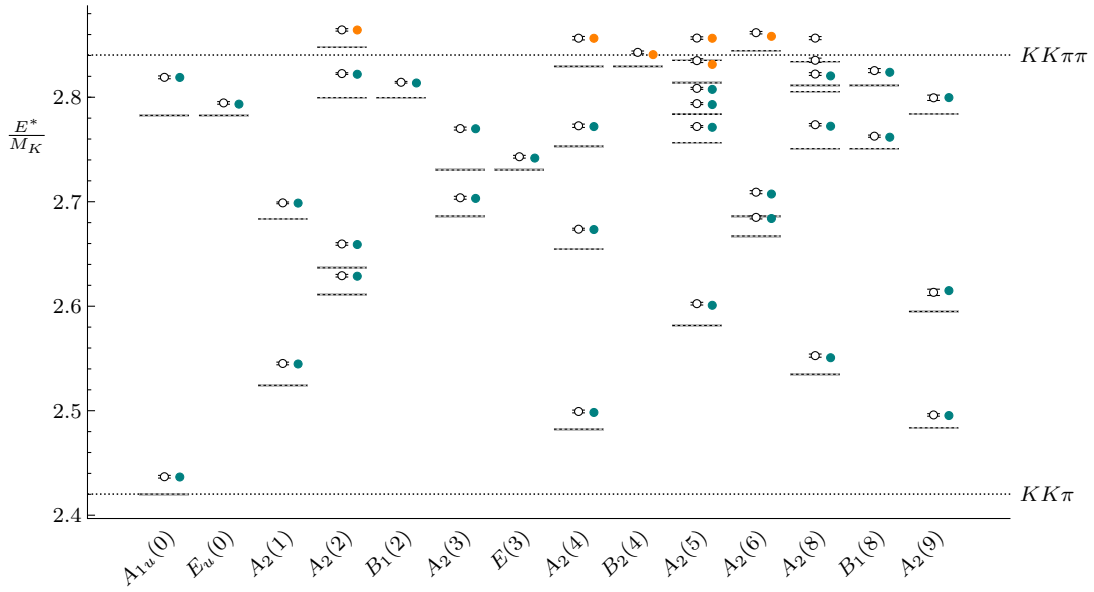

Figure B.3: $KK\pi$ CMF spectrum on ensemble D200. Notation as in figure B.1, except energies here are in units of M_K. Colored symbols are from the ADLER3 fit in Table 4.9.

the same order as the physical M_π^2.

The LO chiral Lagrangian (in Euclidean space), including discretization terms, is given by [83]

$$\begin{aligned} \mathcal{L}_{\text{LO}} &= \frac{F^2}{4}\text{Tr}\Big(\partial_\mu \Sigma^\dagger \partial_\mu \Sigma\Big) - \frac{F^2}{4}\text{Tr}\Big(\chi\Sigma^\dagger + \Sigma\chi^\dagger\Big) + \mathcal{V}_{a^2}\,, \\ \mathcal{V}_{a^2} &= -\hat{a}^2 W_6' \,\text{Tr}\Big(\Sigma + \Sigma^\dagger\Big)^2 - \hat{a}^2 W_8' \,\text{Tr}\Big(\Sigma^2 + \Sigma^{\dagger 2}\Big)\,, \end{aligned} \tag{B.1}$$

where $\Sigma \in \text{SU}(3)$ is the field that contains the PGBs, $\chi = 2B_0 M$ is proportional to M, the renormalized mass matrix, and $F \approx F_\pi \simeq 92$ MeV and B_0 are the usual continuum LO LECs. Additionally, we have $\hat{a} = 2W_0 a$, where W_0, W_6', and W_8' are LECs associated with discretization errors. We assume exact isospin symmetry, so that $M = \text{diag}(m_\ell, m_\ell, m_s)$.

With the Lagrangian in hand, we can now compute the LO pion and kaon masses,

$$M_\pi^2 = 2B_0 m_\ell + F^2(3w_6' + w_8')\,, \tag{B.2}$$

$$M_K^2 = B_0(m_\ell + m_s) + F^2(3w_6' + w_8')\,, \tag{B.3}$$

where we have converted to dimensionless quantities by defining

$$w_6' = \frac{16\hat{a}^2 W_6'}{F^4} \quad \text{and} \quad w_8' = \frac{16\hat{a}^2 W_8'}{F^4}\,. \tag{B.4}$$

We observe in eqs. (B.2) and (B.3) the violation of chiral symmetry with Wilson fermions, which here leads to an offset in the PGB masses in the (naive) chiral limit. These offsets can be effectively absorbed into shifts in the quark masses by writing subsequent expressions in terms of M_π and M_K, rather than m_ℓ and m_s.

The LO $\pi\pi$, πK, and KK scattering amplitudes are given by

$$\mathcal{M}_{\pi\pi} = \frac{1}{F^2}\left[-s + 2M_\pi^2 + 2F^2(2w_6' + w_8')\right]\,, \tag{B.5}$$

$$\mathcal{M}_{\pi K} = \frac{1}{2F^2}\left[-s + M_\pi^2 + M_K^2 + 2F^2(2w_6' + w_8')\right]\,, \tag{B.6}$$

$$\mathcal{M}_{KK} = \frac{1}{F^2}\left[-s + 2M_K^2 + 2F^2(2w_6' + w_8')\right]\,, \tag{B.7}$$

where s is the usual two-particle Mandelstam variable. We thus find that, when we express the results in terms of the PGB masses, only a single linear combination of w_6' and w_8' appears in all three expressions. Indeed, if one carries out the calculation in SU(N) WChPT, the same result is obtained, with all the N dependence absorbed into the PGB masses [3 becoming N in eq. (B.2) and eq. (B.3)]. Thus we can compare the result for $\mathcal{M}_{\pi\pi}$ with that obtained in SU(2) WChPT in Ref. [83], and find complete agreement.

The $\mathcal{O}(a^2)$ terms in eq. (B.5), eq. (B.6), and eq. (B.7) again display a violation of chiral symmetry, for the scattering amplitudes do not vanish at threshold in the chiral limit. To see this explicitly, we give the result for the scattering lengths

$$M_\pi a_0^{\pi\pi} = -\frac{1}{32\pi}\mathcal{M}_{\pi\pi}\bigg|_{s=4M_\pi^2} = \frac{M_\pi^2}{16\pi F^2} - \frac{(2w_6' + w_8')}{16\pi} + \mathcal{O}(M^4/F^4)\,, \tag{B.8}$$

$$M_{\pi K} a_0^{\pi K} = -\frac{1}{16\pi}\mathcal{M}_{\pi K}\bigg|_{s=(M_\pi+M_K)^2} = \frac{M_\pi M_K}{16\pi F^2} - \frac{(2w_6' + w_8')}{16\pi} + \mathcal{O}(M^4/F^4)\,, \tag{B.9}$$

$$M_K a_0^{KK} = -\frac{1}{32\pi}\mathcal{M}_{KK}\bigg|_{s=4M_K^2} = \frac{M_K^2}{16\pi F^2} - \frac{(2w_6' + w_8')}{16\pi} + \mathcal{O}(M^4/F^4)\,. \tag{B.10}$$

These results agree with the LO parts of eq. (4.26), eq. (4.29), and eq. (4.27), in the limit that $a^2 \to 0$. By taking appropriate linear combinations of the scattering lengths, one can

cancel the $\mathcal{O}(a^2)$ term. This prediction could be tested in simulations with several lattice spacings. We note that there are no $\mathcal{O}(a^2)$ corrections to the effective range at LO.

Finally, we turn to $\mathcal{K}_{\mathrm{df},3}$. This has previously been calculated without discretization effects for three pions in Ref. [125], three kaons in Ref. [132], and for $\pi\pi K$ and $KK\pi$ scattering in Ref. [121]. We refer to those works for the methodology, and simply quote the final results. We find that [see eq. (4.24) for notation]

$$\mathcal{K}_{\mathrm{df},3}^{\pi\pi\pi} = \frac{18}{F^4}\left[M_\pi^2 - F^2(2w_6' + w_8')\right] + \frac{27M_\pi^2}{F^4}\Delta + \mathcal{O}(M^4/F^6)\,, \tag{B.11}$$

and a nearly identical expression for $\mathcal{K}_{\mathrm{df},3}^{KKK}$ obtained by simply substituting M_K for M_π. For the nondegenerate case we obtain

$$\mathcal{K}_{\mathrm{df},3}^{\pi\pi K} = \frac{1}{F^4}\left[2M_\pi(M_\pi + 2M_K) - 6F^2(2w_6' + w_8')\right] + \frac{1}{F^4}(2M_\pi + M_K)^2\Delta + \mathcal{O}(M^4/F^6)\,, \tag{B.12}$$

with the result for $KK\pi$ obtained by switching the roles of the masses M_π and M_K. We observe that both results are isotropic. For three identical particles this is guaranteed by the fact that angular dependence only enters at relative order p^4, i.e. at NNLO in ChPT. For the nondegenerate cases, this result, first observed in Ref. [121], is not required by symmetries or power counting, as there could be terms proportional to Δ_2^S and $\tilde{t}_{22}$ [see eq. (4.23)]. Indeed, such terms enter at intermediate stages but cancel in the final result.

At LO in WChPT, the $\mathcal{O}(a^2)$ terms enter only in $\mathcal{K}_0$ (given by the above expressions with $\Delta \to 0$), since power-counting requires that at $\mathcal{O}(a^2)$ correction to $\mathcal{K}_1$ requires a NLO contribution. As with the case of the two-particle amplitudes, discretization effects lead to $\mathcal{K}_0$ having nonvanishing values in the chiral limit. What is particularly striking, however, is that this offset is given by the same combination of LECs that enters in $\mathcal{K}_{\mathrm{df},3}$ as in the two-particle amplitudes. Thus the size of the offset in $\mathcal{K}_0$ can be determined from a fit to the two-particle amplitude. We use this result in the main text, as described in section 4.6.3.

B.3 NLO ChPT result for the $I = 3/2$ p-wave πK scattering length

This Appendix discusses briefly how to obtain an analytic expression for the $I = 3/2$ πK p-wave scattering length, $a_1^{\pi K}$. We use the results from NLO ChPT presented in Ref. [163],

which refers to functions presented in Ref. [232].

The $I = 3/2$ πK amplitude is related to the s- and p-wave scattering lengths by

$$T^{3/2}(s,t,u) = -16\pi \frac{M_\pi + M_K}{2}(a_0^{\pi K} + q^2 \cos\theta\, a_1^{\pi K} + \dots)\,, \tag{B.13}$$

where we have used our convention for the sign of the scattering lengths, and have expanded about threshold showing only the terms that do not vanish at threshold for the partial-wave projected amplitudes. Here θ is the scattering angle in the CMF and q the spatial momentum of both particles in this frame. Thus we must pick out the coefficient of $q^2 \cos\theta$.

The dependence on the angle θ only enters through the two-particle Mandelstam variables t and u,

$$\begin{aligned} t &= -2q^2(1-\cos\theta) = 2q^2\cos\theta + \dots\,, \\ u &= 2M_\pi^2 + 2M_K^2 - s + 2q^2(1-\cos\theta) = u_0 - 2q^2\cos\theta + \dots\,, \\ u_0 &= (M_\pi - M_K)^2\,. \end{aligned} \tag{B.14}$$

where here and below the ellipsis consists of $\mathcal{O}(q^2)$ terms that are independent of $\cos\theta$, and $\mathcal{O}(q^4)$ terms that do depend on $\cos\theta$. We now expand $T^{3/2}$ about threshold in powers of $s - s_0$ [with $s_0 = (M_\pi + M_K)^2$], t and $u - u_0$, which are all proportional to q^2, with only t and $u - u_0$ depending on $\cos\theta$. Specifically, we write

$$T^{3/2}(s,t,u) = T^{3/2}(s_0,0,u_0) + c_t t + c_u(u-u_0) + \dots\,, \tag{B.15}$$

Then we have that

$$a_1^{3/2} = -\frac{c_t - c_u}{4\pi(M_\pi + M_K)}\,. \tag{B.16}$$

From Ref. [163], we take the result

$$T^{3/2}(s,t,u) = G_1(s) + G_2(t) + G_3(u) + (s-u)G_4(t) + (s-t)G_5(u) + G_6(s,t,u)\,, \tag{B.17}$$

where each of these functions can be expressed in terms of three one-loop functions: $\bar{A}(m_1^2)$ $\bar{B}(m_1^2, m_2^2, t)$, $\bar{B}_1(m_1^2, m_2^2, t)$, and $\bar{B}_{21}(m_1^2, m_2^2, t)$. These in turn are defined as the finite parts of the corresponding functions in $d = 4 - 2\epsilon$ dimensions presented in Ref. [232]. For $\bar{A}$, $\bar{B}$

and $\bar{B}_1$, these finite parts can be read off from the results in Ref. [232], but for $\bar{B}_{21}$ one must account for the explicit d dependence, which leads to finite "ϵ/ϵ" contributions. All these functions are given in terms of chiral logarithms and an integral $\bar{J}(m_1^2, m_2^2, t)$, which is given explicitly in Ref. [232].

Using the leading order SU(3) relation $M_\eta^2 = (4M_K^2 - M_\pi^2)/3$, and we obtain, after much algebra,

$$
\begin{aligned}
c_t - c_u = \frac{\kappa}{F_\pi^4}\frac{1}{288}\Bigg\{ & M_K M_\pi \left(16\bar{L}_2 + 8\bar{L}_3\right) - \left(M_K^2 + M_\pi^2\right)\left(16\bar{L}_1 + 4\bar{L}_3 - 8\bar{L}_4\right) \\
& + L_\pi \frac{M_\pi\left(4M_K^4 + 87M_K^3 M_\pi - 24M_K^2 M_\pi^2 + 56 M_K M_\pi^3 - 9M_\pi^4\right)}{24(M_K - M_\pi)^3} \\
& - L_K \frac{\left(M_K^5 + 279 M_K^4 M_\pi - 125 M_K^3 M_\pi^2 + 478 M_K^2 M_\pi^3 - 27 M_K M_\pi^4 - 8M_\pi^5\right)}{108(M_K - M_\pi)^3} \\
& + L_\eta \frac{\left(56M_K^5 + 36 M_K^4 M_\pi + 155 M_K^3 M_\pi^2 - 16 M_K^2 M_\pi^3 - 72 M_K M_\pi^4 + 11 M_\pi^5\right)}{216(M_K - M_\pi)^3} \\
& + \frac{-80M_K^6 + 524 M_K^5 M_\pi + 458 M_K^4 M_\pi^2 + 397 M_K^3 M_\pi^3 - 96 M_K^2 M_\pi^4 - 131 M_K M_\pi^5 - 4M_\pi^6}{36(M_K - M_\pi)^2\left(4M_K^2 - M_\pi^2\right)} \\
& + \frac{\sqrt{(2M_K - M_\pi)(M_K + M_\pi)}\left(8M_K^5 - 12 M_K^4 M_\pi - 7 M_K^3 M_\pi^2 + 2 M_K^2 M_\pi^3 - 24 M_K M_\pi^4 - 4M_\pi^5\right)}{27(M_K - M_\pi)^3(M_K + M_\pi)} \\
& \times \tan^{-1}\left[\frac{2\sqrt{(M_K - M_\pi)^2(2M_K - M_\pi)(M_K + M_\pi)}}{2M_K^2 + 3M_K M_\pi - 2M_\pi^2}\right]\Bigg\}, \qquad \text{(B.18)}
\end{aligned}
$$

where $L_\pi = \log(M_\pi^2/\mu^2)$, etc., and $\bar{L}_i^r = 16\pi^2 L_i^r$. Note that only two linearly independent combinations of LECs are accessible by varying the meson masses in this quantity.

We have performed a number of checks on this expression: (i) the expansion has been done independently by two of us, (ii) we have checked that the dependence on the scale μ cancels in $c_t - c_u$, and (iii) we have taken the chiral limit $M_\pi \to 0$ and seen that the combination $c_t - c_u$ remains finite and proportional to M_K^2/F_π^4, as expected.

For the numerical evaluation of this expression, we use values of the LECs from Ref. [172]. In particular, the ones from fit 10 to $\mathcal{O}(p^4)$ reported in that work. The results in Ref. [172] are quoted at a renormalization scale $\mu = 770$ MeV, and we convert to $\mu = 4\pi F_\pi$ using the

running as in eq. (4.55), with

$$\Gamma_1 = \frac{3}{32}, \quad \Gamma_2 = \frac{3}{16}, \quad \Gamma_3 = 0, \quad \Gamma_4 = \frac{1}{8}. \tag{B.19}$$

B.4 Tables of interpolating operators

Here we list all two- and three-hadron operators for nondegenerate channels used in this work. Our operator construction follows the procedure detailed in Ref. [233], where the notation for the irreps is given. Those for degenerate channels ($\pi\pi$, $\pi\pi\pi$, KK, KKK) are listed in Ref. [132]. π^+K^+ operators are given in Table B.2, $\pi^+\pi^+K^+$ operators in Tables B.5 and B.6, and $K^+K^+\pi^+$ operators in Tables B.3 and B.4. Note that for the π^+K^+ channel we only use operators with total momentum-squared up to $4(2\pi/L)^2$, while the three-particle operators have momentum-squared values up to $9(2\pi/L)^2$.

$\boldsymbol{d}_{\text{ref}}$	$[d_K^2, d_\pi^2]$	E^{free}/M_π		operators
		N203	D200	
(0, 0, 0)	[0, 0]	2.278	3.3798	A_{1g}
	[1, 1]	3.2609	4.6104	$A_{1g} \oplus T_{1u}^*$
	[2, 2]	4.0064	5.5243	$A_{1g}^\dagger \oplus T_{1u}^*$
	[3, 3]	4.6327		A_{1g}
(0, 0, 1)	[1, 0]	2.4675	3.505	A_1
	[0, 1]	2.5598	3.9023	A_1
	[2, 1]	3.4236	4.7539	$A_1 \oplus E$
	[1, 2]	3.4618	4.929	$A_1 \oplus E$
	[4, 1]	4.0217		A_1
	[1, 4]	4.0966		A_1
	[3, 2]	4.1491		A_1
	[2, 3]	4.1713		A_1
(0, 1, 1)	[2, 0]	2.6072	3.61	A_1
	[0, 2]	2.748	4.2192	A_1
	[1, 1]	2.8162	4.0963	$A_1 \oplus B_2$
	[3, 1]	3.5565	4.8786	$A_1 \oplus B_1$
	[1, 3]	3.6198		$A_1 \oplus B_1$
	[2, 2]	3.6536	5.1032	$A_1^\dagger \oplus B_1^\dagger \oplus B_2$
(1, 1, 1)	[3, 0]	2.7208	3.7013	A_1
	[0, 3]	2.8947	4.459	A_1
	[2, 1]	3.0032	4.2571	$A_1 \oplus E$
	[1, 2]	3.0466	4.4519	$A_1 \oplus E$
(0, 0, 2)	[1, 1]	2.2867	3.5077	A_1
	[4, 0]	2.8177	3.7828	A_1
	[0, 4]	3.0169	4.656	A_1
	[2, 2]	3.2629	4.644	$A_1 \oplus E$
	[3, 3]	4.0072		A_1

Table B.2: π^+K^+ operators used in this work. For each set of momenta that are equivalent up to allowed rotations, one representative choice of $\boldsymbol{d}_{\text{ref}}$ is given, where the total momentum is $\boldsymbol{P} = (2\pi/L)\boldsymbol{d}_{\text{ref}}$. The momentum squared (in units of $(2\pi/L)^2$) of the individual single particles in each operator is listed as d_{sh}^2, where "sh" indicates the particular single hadron. The lab-frame free energies in units of M_π are listed for those operators that are used on each ensemble together with irreps that are included. Daggered and starred irreps were only used for the N203 and D200 ensembles, respectively.

$\boldsymbol{d}_{\text{ref}}$	$[d_{K_1}^2, d_{K_2}^2, d_\pi^2]$	E^{free}/M_K		operators
		N203	D200	
(0, 0, 0)	[0, 0, 0]	2.7824	2.4202	A_{1u}
	[1, 1, 0]	3.4859	2.7826	$A_{1u} \oplus E_u$
	[1, 0, 1]	3.5515		$A_{1u} \oplus E_u \oplus T_{1g}$
(0, 0, 1)	[1, 0, 0]	2.9993	2.5243	A_2
	[0, 0, 1]	3.0678	2.6835	A_2
	[2, 1, 0]	3.6519		$A_2 \oplus B_2 \oplus E$
(0, 1, 1)	[2, 0, 0]	3.1599	2.6111	A_2
	[1, 1, 0]	3.2399	2.6367	A_2
	[0, 0, 2]	3.261	2.8478	A_2
	[1, 0, 1]	3.3104	2.7996	$A_2 \oplus B_1$
(1, 1, 1)	[3, 0, 0]	3.2907	2.6863	A_2
	[0, 0, 3]	3.4129		A_2
	[2, 1, 0]	3.4178	2.7304	$A_2 \oplus E$
	[2, 0, 1]	3.4899		$A_2 \oplus E$
	[1, 0, 2]	3.5209		$A_2 \oplus E$
	[1, 1, 1]	3.5712		$A_2 \oplus E$
(0, 0, 2)	[1, 1, 0]	2.9737	2.4823	A_2
	[1, 0, 1]	3.0503	2.6547	A_2
	[4, 0, 0]	3.4025	2.7532	A_2
	[0, 0, 4]	3.5402		A_2
	[2, 2, 0]	3.6083	2.8296	$A_2 \oplus B_2$
(0, 1, 2)	[2, 1, 0]	3.1666	2.5816	A_2
	[2, 0, 1]	3.2442	2.7565	A_2
	[1, 0, 2]	3.2776	2.8352	A_2
	[1, 1, 1]	3.3315	2.7838	$2A_2$
	[5, 0, 0]	3.5008	2.8137	A_2
	[0, 0, 5]	3.6508		A_2

Table B.3: $K^+K^+\pi^+$ operators with $d_{\text{ref}}^2 \leq 5$ used in this work, where $\boldsymbol{P} = (2\pi/L)\boldsymbol{d}_{\text{ref}}$. Notation as in Table B.2, except that free energies are in units of M_K, and if an operator irrep is multiplied by an integer (as in $2A_2$), this integer indicates the number of linearly-independent operators in that irrep that is used.

$\boldsymbol{d}_{\text{ref}}$	$[d^2_{K_1}, d^2_{K_2}, d^2_\pi]$	E^{free}/M_K		operators
		N203	D200	
(1, 1, 2)	[3, 1, 0]	3.3222	2.6672	A_2
	[2, 2, 0]	3.3713	2.6863	A_2
	[3, 0, 1]	3.4009	2.8445	A_2
	[1, 0, 3]	3.4546		A_2
	[2, 0, 2]	3.4833		$A_1 \oplus A_2$
	[2, 1, 1]	3.5377		$2A_1 \oplus 3A_2$
	[1, 1, 2]	3.5711		$A_1 \oplus 2A_2$
	[6, 0, 0]	3.5892		A_2
(0, 2, 2)	[2, 2, 0]	3.1163	2.5349	A_2
	[2, 0, 2]	3.2371	2.8054	A_2
	[2, 1, 1]	3.2956	2.7508	$A_2 \oplus B_1$
	[1, 1, 2]	3.3314	2.8342	A_2
	[5, 1, 0]	3.5702	2.8114	$A_2 \oplus B_1$
	[5, 0, 1]	3.6507		$A_2 \oplus B_1$
(0, 0, 3)	[1, 1, 1]	2.7911	2.4836	A_2
	[4, 1, 0]	3.206	2.5949	A_2
	[4, 0, 1]	3.2917	2.784	A_2
	[1, 0, 4]	3.3646		A_2
	[2, 1, 2]	3.5614		$A_2 \oplus B_2 \oplus E$

Table B.4: $K^+K^+\pi^+$ operators with $6 \leq d^2_{\text{ref}} \leq 9$ used in this work, where $\boldsymbol{P} = (2\pi/L)\boldsymbol{d}_{\text{ref}}$. Notation as in Table B.3.

$\boldsymbol{d}_{\text{ref}}$	$[d_K^2, d_{\pi_1}^2, d_{\pi_2}^2]$	E^{free}/M_π		operators
		N203	D200	
(0, 0, 0)	[0, 0, 0]	3.278	4.3798	A_{1u}
	[1, 1, 0]	4.2609		$A_{1u} \oplus E_u \oplus T_{1g}$
	[0, 1, 1]	4.3447		$A_{1u} \oplus E_u$
(0, 0, 1)	[1, 0, 0]	3.5417	4.5724	A_2
	[0, 1, 0]	3.6298	4.9585	A_2
	[2, 1, 0]	4.4668		$A_2 \oplus B_2 \oplus E$
(0, 1, 1)	[2, 0, 0]	3.7366	4.7329	A_2
	[0, 2, 0]	3.8673	5.3142	A_2
	[1, 1, 0]	3.931	5.1962	$A_2 \oplus B_1$
	[0, 1, 1]	4.0217		A_2
(1, 1, 1)	[3, 0, 0]	3.8951	4.872	A_2
	[0, 3, 0]	4.0536		A_2
	[2, 1, 0]	4.1533	5.3936	$A_2 \oplus E$
	[1, 2, 0]	4.1934		$A_2 \oplus E$
	[0, 2, 1]	4.2862		$A_2 \oplus E$
	[1, 1, 1]	4.351		$A_2 \oplus E$
(0, 0, 2)	[1, 1, 0]	3.5708	4.746	A_2
	[0, 1, 1]	3.6704	5.1762	A_2
	[4, 0, 0]	4.0305	4.9956	A_2
	[0, 4, 0]	4.2095		A_2
	[2, 2, 0]	4.4339		$A_2 \oplus B_2 \oplus E$
(0, 1, 2)	[2, 1, 0]	3.8141	4.9613	A_2
	[1, 2, 0]	3.8578	5.1619	A_2
	[0, 2, 1]	3.9584		A_2
	[1, 1, 1]	4.0286	5.4677	$2A_2$
	[5, 0, 0]	4.1496	5.1073	A_2
	[0, 5, 0]	4.3448		A_2
	[4, 1, 0]	4.488		A_2

Table B.5: $\pi^+\pi^+K^+$ operators with $d_{\text{ref}}^2 \leq 5$ used in this work, where $\boldsymbol{P} = (2\pi/L)\boldsymbol{d}_{\text{ref}}$. Notation as in Table B.3, except that free energies quoted here are in units of M_π.

$\boldsymbol{d}_{\text{ref}}$	$[d_K^2, d_{\pi_1}^2, d_{\pi_2}^2]$	E^{free}/M_π		operators
		N203	D200	
(1, 1, 2)	[3, 1, 0]	4.01	5.1463	A_2
	[1, 3, 0]	4.0804	5.4753	A_2
	[2, 2, 0]	4.1179	5.3981	$A_1 \oplus A_2$
	[0, 3, 1]	4.1821		A_2
	[6, 0, 0]	4.2564	5.2097	A_2
	[0, 2, 2]	4.2629		A_2
	[2, 1, 1]	4.2901		$A_1 \oplus 2A_2$
	[1, 2, 1]	4.3334		$2A_1 \oplus 3A_2$
	[0, 6, 0]	4.4652		A_2
(0, 2, 2)	[2, 2, 0]	3.7755	4.9662	A_2
	[0, 2, 2]	3.9331		A_2
	[2, 1, 1]	3.9626	5.3016	A_2
	[1, 2, 1]	4.0094	5.5141	$A_2 \oplus B_1$
	[5, 1, 0]	4.3212	5.4563	$A_2 \oplus B_1$
	[1, 5, 0]	4.4247		$A_2 \oplus B_1$
	[8, 0, 0]	4.4433	5.3928	A_2
(0, 0, 3)	[1, 1, 1]	3.29	4.5765	A_2
	[4, 1, 0]	3.8389	4.8698	A_2
	[1, 4, 0]	3.9356	5.3271	A_2
	[0, 4, 1]	4.0469		A_2
	[2, 2, 1]	4.3044		$A_2 \oplus B_2 \oplus E$
	[1, 2, 2]	4.3508		$A_2 \oplus B_2$
	[9, 0, 0]		5.4757	A_2

Table B.6: $\pi^+\pi^+K^+$ operators with $6 \leq d_{\text{ref}}^2 \leq 9$ used in this work, where $\boldsymbol{P} = (2\pi/L)\boldsymbol{d}_{\text{ref}}$. Notation as in Table B.5.

Appendix 3

APPENDIX TO CHAPTER 5

C.1 Further details of the derivation

In this appendix we provide additional details of the derivation sketched in the main text in section 5.4.3. In particular, we discuss the changes that must be made compared to the derivation for identical scalars, given in ref. [16] (referred to as HS throughout this appendix) due to the antisymmetric nature of the three-neutron state. In this regard, it is important to keep in mind that the antisymmetry of intermediate states is not fully manifested in the individual kinematic matrices F and G that appear in the quantization condition. Instead, these quantities can implement the antisymmetry of the nonspectator pair[1] by restrictions on allowed values of s and ℓ. Full antisymmetry is only recovered when combining F and G, and for this the overall minus sign in G is essential.

A closely related observation is that the antisymmetry is explicitly broken by the variables we choose, since we single out one of the particles to be the spectator. This leads to the presence, at intermediate stages of the derivation, of on-shell three-particle amplitudes that are not fully antisymmetric under particle interchange. The archetypical such quantity in HS is $\mathcal{K}_{\mathrm{df},3}^{(u,u)}$, the unsymmetrized form of $\mathcal{K}_{\mathrm{df},3}$. Its lack of symmetry is analogous to that for the quantity $\mathbf{M}_{3,L}^{(u,u)}$ [see eq. (5.94)]. In HS, these quantities are denoted by superscripts (u), (s) and $(\tilde{s})$, and we follow the same notation here. These labels describe the attachment of the spectator momentum to the diagrams under consideration. We denote the spectator

[1]Strictly speaking it is a choice whether to implement the antisymmetry in F and G, as these are kinematic quantities that could be defined independently of the symmetry of the particles involved. The antisymmetry then arises because F and G appear next to amplitudes, such as $\mathcal{K}_2$ and $\mathcal{K}_{\mathrm{df},3}$, that do have the requisite (anti)symmetry, and thus project out the parts of F and G with the corresponding symmetry. We choose to build this projection into F and G from the start.

momentum by k, and the pair momenta by p and b. If the final interaction before the external momenta involves two particles, then the (u), (s) and $(\tilde{s})$ quantities, respectively, are those in which the spectator particle has momentum k, p and b. (See figure 13(b) of HS—"u" stands for unscattered and "s" for scattered.) If the final interaction involves all three particles, then the contribution is divided equally into the three types of quantities.

The previous description works for identical bosons, but does not provide a complete prescription for fermions, due to the antisymmetry of the nonspectator pair. In particular, one must choose one of the pair to be "privileged", in the sense that, in some convention, it is the particle with respect to which the antisymmetry is defined. Our choice for the privileged particles are that they have momenta p, b and k, respectively, for the (u), (s), and $(\tilde{s})$ amplitudes. Another way of describing this is to list the momenta such that the first is that of the spectator, the second that of the privileged member of the pair, and third that of the other member of the pair. Then the ordering is $\{k, p, b\}$ for (u), $\{p, b, k\}$ for (s), and $\{b, k, p\}$ for $(\tilde{s})$, (i.e. the cyclic permutations of the (u) ordering). With this choice, a fully *antisymmetric* amplitude is given by *adding* the three terms

$$A = A^{(u)} + A^{(s)} + A^{(\tilde{s})}\,, \tag{C.1}$$

a result that, perhaps counterintuitively, takes the same form as that for identical bosons. This is shown explicitly in the example described in section C.2. With this choice, we can carry over most of the equations from the derivation in HS with minimal changes.

In the following, we assume that the reader has a copy of HS in front of them, and refer to equations in that work as (HS1), (HS2), etc. We do not repeat these equations here.

Among the most challenging parts of the derivation in HS is showing how asymmetric quantities such as $A^{(u)}$ end being symmetrized in the final result. Here the same issue arises, but involves antisymmetrization. (Note that for amplitudes with initial and final momenta, like $\mathbf{K}_{\mathrm{df},3}$, one must antisymmetrize separately the initial and final momenta.) Various identities are needed for this to work, and these must be generalized here from the versions applicable to identical bosons given in HS. The first example of such generalizations is in the

definitions of (u), (s) and $(\tilde{s})$ already described above, i.e. with the choice of a privileged momentum. The next example concerns the discussion between (HS140) and (HS146), which notes that the combination $A^{(u)} + 2A^{(s)}$ appears frequently in the derivation, rather than the desired combination of eq. (C.1). It is then explained that these two quantities are, in fact, equal, given the projection onto even angular momenta that occurs for identical bosons. The same conclusion holds here, although the argumentation is slightly changed, as we now describe.

In particular, a key result is that (s) amplitudes always arise in the derivation connected to (u) amplitudes by an $\mathbf{F}$ matrix, an example being $\mathbf{A}_3'^{(s)}\mathbf{F}\mathbf{A}_3^{(u)}$. Now, (u) amplitudes are antisymmetric under the interchange of the particles in the pair, leading to the constraints on ℓ and s described in the main text. This antisymmetry is preserved by $\mathbf{F}$, because it commutes with $(-1)^\ell$ (up to exponentially-suppressed corrections, a result derived in HS Appendix A), and also commutes with projectors onto definite pair spin (given the trivial nature of the spin index structure of $\mathbf{F}$). Thus, the only parts of the (s) amplitudes that contribute are those that are antisymmetric under pair exchange. These parts are, however, identical to the corresponding parts of the $(\tilde{s})$ amplitudes. This is because to go from the $\{pkb\}$ ordering for (s) to the $\{bpk\}$ ordering for $(\tilde{s})$, one must both interchange b and p, which leads to a minus sign due to the above-described antisymmetric projection, and interchange p and k, which leads to a second minus sign as these are now the momenta associated with the interacting pair, and the amplitude is antisymmetric under their exchange. Because of this identity, we can freely exchange all appearances of $2\mathbf{A}_3^{(s)}$ (for example) with $\mathbf{A}_3^{(s)} + \mathbf{A}_3^{(\tilde{s})}$.

A second place where the argumentation of HS needs to be changed concerns the results in (HS196)-(HS198), which show that combinations like $\mathbf{A}_3'\mathbf{F}(\mathbf{A}_3^{(u)} - \mathbf{A}_3^{(s)})$, which appears to be a finite-volume term, is, in fact, an infinite-volume quantity. This result is used repeatedly in HS in the steps that lead to the recasting of the quantization condition in terms of quantities symmetric under particle exchange. Here it turns out that conclusion of (HS196)-(HS198) remains valid, but this now follows because $\mathbf{A}_3'$ is *antisymmetric* under the exchange of the two on-shell momentum labels (which would be k and p in the notation above), while

$(\mathbf{A}_3^{(u)} - \mathbf{A}_3^{(s)})$ is *symmetric* [because the $k \leftrightarrow p$ interchange sends the $\{k, p, b\}$ ordering for (u) into $\{p, k, b\}$, which leads to $\mathbf{A}_3^{(u)} \to -\mathbf{A}_3^{(s)}$, since the latter is defined with the ordering $\{p, b, k\}$]. These symmetry properties are opposite to those in HS, but all that matters for the argument in HS to go through is that the symmetry properties of the quantities on the left and right of $\mathbf{F}$ are opposite, and this still holds.

With these observations, all the steps in the derivation of HS go through unchanged, except for the inclusion of spin-related factors as described in the main text. Thus, the form of the resulting quantization condition is unchanged (modulo the absorption of various factors into boldfaced quantities).

C.2 Antisymmetrizing the scattering amplitude

In this appendix we explain in detail the symmetrization and antisymmetrization procedures referred to in the main text—see, in particular, section 5.3 and section 6.4.7 and section C.1.

We first recall how *symmetrization* works in the case of identical scalars [16, 17]. This operation has been used in eq. (5.14). It acts on an unsymmetrized finite-volume quantity defined using our standard matrix indices, generically called $X^{(u,u)}_{k'\ell'm',k\ell m}$ (with the subscript L dropped for brevity), and is defined by

$$X\left(\boldsymbol{k}', \boldsymbol{a}', \boldsymbol{b}' | \boldsymbol{k}, \boldsymbol{a}, \boldsymbol{b}\right) \equiv \mathcal{S}\left[X^{(u,u)}_{k'\ell'm',k\ell m}\right] \tag{C.2}$$

$$\equiv \sum_{\{\boldsymbol{p}_3', \boldsymbol{p}_1'\} \in \mathcal{P}_3'} \sum_{\{\boldsymbol{p}_3, \boldsymbol{p}_1\} \in \mathcal{P}_3} X^{(u,u)}\left(\boldsymbol{p}_3', \boldsymbol{p}_1' | \boldsymbol{p}_3, \boldsymbol{p}_1\right) , \tag{C.3}$$

where we combine the matrix amplitude with spherical harmonics to obtain the full momentum dependence,

$$X^{(u,u)}\left(\boldsymbol{k}', \boldsymbol{a}' | \boldsymbol{k}, \boldsymbol{a}\right) \equiv 4\pi Y^*_{\ell'm'}(\hat{\boldsymbol{a}}^{\prime *}_{2,k'}) X^{(u,u)}_{k'\ell'm',k\ell m} Y_{\ell m}(\hat{\boldsymbol{a}}^*_{2,k}) , \tag{C.4}$$

and the sets of permuted momenta are

$$\mathcal{P}_3 = \{\{\boldsymbol{k}, \boldsymbol{a}\}, \{\boldsymbol{a}, \boldsymbol{b}\}, \{\boldsymbol{b}, \boldsymbol{k}\}\} \text{ and } \mathcal{P}_3' = \{\{\boldsymbol{k}', \boldsymbol{a}'\}, \{\boldsymbol{a}', \boldsymbol{b}'\}, \{\boldsymbol{b}', \boldsymbol{k}'\}\} . \tag{C.5}$$

Although we can take $\boldsymbol{k}'$ and $\boldsymbol{k}$ to lie in the finite-volume set, the constraint of having three on-shell particles will not, in general, allow the other external momenta $(\boldsymbol{a}', \ldots)$ to lie in

this set. Thus, to apply this definition, we must use the freedom to extend the definitions of finite-volume quantities to momenta lying outside the finite-volume set, which has been discussed in ref. [17]. This issue becomes irrelevant in the $L \to \infty$ limit, which is what we ultimately take in most applications of (anti-)symmetrization.

Turning now to identical fermions, a generic asymmetric finite-volume quantity has a similar form except for the additional spin labels,

$$\mathbf{X}^{(u,u)}_{k'\ell'm'\boldsymbol{m}'^{*}_{s};k\ell m\boldsymbol{m}^{*}_{s}} , \tag{C.6}$$

where we recall that the spin indices are defined using the dimer-axis convention, see eq. (5.36). We now introduce the antisymmetrizing operation

$$\mathbf{X}\left(\boldsymbol{k}', m_s(\boldsymbol{k}'); \boldsymbol{a}', m_s(\boldsymbol{a}'); \boldsymbol{b}', m_s(\boldsymbol{b}') | \boldsymbol{k}, m_s(\boldsymbol{k}); \boldsymbol{a}, m_s(\boldsymbol{a}); \boldsymbol{b}, m_s(\boldsymbol{b})\right) \equiv \mathcal{A}\left[\mathbf{X}^{(u,u)}_{k'\ell'm'\boldsymbol{m}'^{*}_{s};k\ell m\boldsymbol{m}^{*}_{s}}\right] , \tag{C.7}$$

which is defined by first combining with spherical harmonics and converting spin indices to the lab-axis frame [see eq. (5.34)],

$$\mathbf{X}^{(u,u)}\left(\boldsymbol{k}', m_s(\boldsymbol{k}'); \boldsymbol{a}', m_s(\boldsymbol{a}'); \boldsymbol{b}', m_s(\boldsymbol{b}') | \boldsymbol{k}, m_s(\boldsymbol{k}); \boldsymbol{a}, m_s(\boldsymbol{a}); \boldsymbol{b}, m_s(\boldsymbol{b})\right) \equiv 4\pi Y^{*}_{\ell'm'}(\hat{\boldsymbol{a}}'^{*}_{2,k'}) \mathcal{D}^{(k',a')}_{\boldsymbol{m}'_s\boldsymbol{m}'^{*}_s} \mathbf{X}^{(u,u)}_{k'\ell'm'\boldsymbol{m}'^{*}_{s};k\ell m\boldsymbol{m}^{*}_{s}} \mathcal{D}^{(k,a)\dagger}_{\boldsymbol{m}^{*}_s\boldsymbol{m}_s} Y_{\ell m}(\hat{\boldsymbol{a}}^{*}_{2,k}) , \tag{C.8}$$

and then antisymmetrizing by using the following sum,

$$\mathbf{X}\left(\boldsymbol{k}', m_s(\boldsymbol{k}'); \boldsymbol{a}', m_s(\boldsymbol{a}'); \boldsymbol{b}', m_s(\boldsymbol{b}') | \boldsymbol{k}, m_s(\boldsymbol{k}); \boldsymbol{a}, m_s(\boldsymbol{a}); \boldsymbol{b}, m_s(\boldsymbol{b})\right) = \sum_{\left\{\boldsymbol{p}'_i, m'_{si}\right\} \in \mathcal{P}'_3} \sum_{\{\boldsymbol{p}_i, m_{si}\} \in \mathcal{P}_3} \mathbf{X}^{(u,u)}\left(\boldsymbol{p}'_1, m'_{s1}; \boldsymbol{p}'_2, m'_{s2}; \boldsymbol{p}'_2, m'_{s3} | \boldsymbol{p}_1, m_{s1}; \boldsymbol{p}_2, m_{s2}; \boldsymbol{p}_3, m_{s3}\right) . \tag{C.9}$$

The permutations involve changing both momenta and the corresponding spin components,

$$\mathcal{P}_3 = \left\{\{\boldsymbol{k}, m_{s1}, \boldsymbol{a}, m_{s2}, \boldsymbol{b}, m_{s3}\}, \{\boldsymbol{a}, m_{s2}, \boldsymbol{b}, m_{s3}, \boldsymbol{k}, m_{s1}\}, \{\boldsymbol{b}, m_{s3}, \boldsymbol{k}, m_{s1}, \boldsymbol{a}, m_{s2}\}\right\} , \tag{C.10}$$

and similarly for $\mathcal{P}'_3$. Here we are using the shorthand

$$m_{s1} = m(\boldsymbol{k}) , \quad m_{s2} = m(\boldsymbol{a}) , \quad m_{s3} = m(\boldsymbol{b}) , \tag{C.11}$$

and similarly for the primed spin indices.

Note that antisymmetrization only requires adding terms with a positive sign, since we are using cyclic permutations. Antisymmetry under single permutations is built in to the matrix version of $\mathbf{X}^{(u,u)}$.

C.3 Operators with two derivatives

In this appendix we determine all the Lorentz- and parity-invariant operators of the form

$$\text{“}\partial^2\text{”}(\overline{\mathcal{N}}\Gamma_1\mathcal{N})(\overline{\mathcal{N}}\Gamma_2\mathcal{N})(\overline{\mathcal{N}}\Gamma_3\mathcal{N})\,. \tag{C.12}$$

Here Γ_i are Dirac matrices, and the derivatives can act on any of the fields. We allow the use of the noninteracting equations of motion to reduce the set of operators, which is equivalent to considering on-shell matrix elements. We also assume that the total momentum inserted by the operator vanishes, so that we can freely integrate by parts.

We now argue that the general operator in eq. (C.12) can be brought into a canonical form

$$([\partial\overline{\mathcal{N}}]\Gamma_1[\partial\mathcal{N}])(\overline{\mathcal{N}}\Gamma_2\mathcal{N})(\overline{\mathcal{N}}\Gamma_3\mathcal{N})\,, \tag{C.13}$$

in which both derivatives act within the same bilinear, one on $\overline{\mathcal{N}}$ and the other on $\mathcal{N}$. The two derivatives in the general operators can act in three ways: (i) both on factors of $\overline{\mathcal{N}}$, (ii) both on factors of $\mathcal{N}$, or (iii) one on each. In cases (i) and (ii), if both act on the same field, we can use the equations of motion to remove the derivatives: $\partial^2 \to -m^2$. In case (i) if both act on different factors of $\overline{\mathcal{N}}$, we can integrate by parts and move one of the derivatives onto the other fields, yielding one term that involves a ∂^2, another that has two derivatives on different $\overline{\mathcal{N}}$ fields, and three terms with one derivative each on a $\overline{\mathcal{N}}$ and a $\mathcal{N}$. The term with derivatives on two different $\overline{\mathcal{N}}$ fields can be moved to the left-hand side of the (now matrix) equation, while, using Fierz identities, we can bring terms with derivatives on $\overline{\mathcal{N}}$ and $\mathcal{N}$ fields in different bilinears to a form in which both the derivatives act within the same bilinear. Assuming that we can invert this matrix equation, each term with derivatives on different factors of $\overline{\mathcal{N}}$ can be rewritten in our canonical form together with a nonderivative term. An

essentially identical argument holds for case (ii), with the roles of $\overline{\mathcal{N}}$ and $\mathcal{N}$ interchanged. For case (iii), if needed we can use Fierz identities to reach the canonical form.

We find 30 operators of the canoncial form to be independent, 8 of which can be dropped using the equations of motion. For convenience, we divide these into those in which the Lorentz indices on the derivatives are contracted together (ten in all)[2]

$$SSS = (\partial^\mu \overline{\mathcal{N}} \partial_\mu \mathcal{N})(\overline{\mathcal{N}}\mathcal{N})(\overline{\mathcal{N}}\mathcal{N}) \,, \tag{C.14}$$

$$SPP = (\partial^\mu \overline{\mathcal{N}} \partial_\mu \mathcal{N})(\overline{\mathcal{N}}\gamma_5\mathcal{N})(\overline{\mathcal{N}}\gamma_5\mathcal{N}) \,, \tag{C.15}$$

$$PSP = (\partial^\mu \overline{\mathcal{N}} \gamma_5 \partial_\mu \mathcal{N})(\overline{\mathcal{N}}\mathcal{N})(\overline{\mathcal{N}}\gamma_5\mathcal{N}) \,, \tag{C.16}$$

$$SVV = (\partial^\mu \overline{\mathcal{N}} \partial_\mu \mathcal{N})(\overline{\mathcal{N}}\gamma_\nu\mathcal{N})(\overline{\mathcal{N}}\gamma^\nu\mathcal{N}) \,, \tag{C.17}$$

$$VSV = (\partial^\mu \overline{\mathcal{N}} \gamma_\nu \partial_\mu \mathcal{N})(\overline{\mathcal{N}}\mathcal{N})(\overline{\mathcal{N}}\gamma^\nu\mathcal{N}) \,, \tag{C.18}$$

$$ASA = (\partial^\mu \overline{\mathcal{N}} \gamma_\nu\gamma_5 \partial_\mu \mathcal{N})(\overline{\mathcal{N}}\mathcal{N})(\overline{\mathcal{N}}\gamma^\nu\gamma_5\mathcal{N}) \,, \tag{C.19}$$

$$TST = (\partial^\mu \overline{\mathcal{N}} \sigma_{\nu\rho} \partial_\mu \mathcal{N})(\overline{\mathcal{N}}\mathcal{N})(\overline{\mathcal{N}}\sigma^{\nu\rho}\mathcal{N}) \,, \tag{C.20}$$

$$PVA = (\partial^\mu \overline{\mathcal{N}} \gamma_5 \partial_\mu \mathcal{N})(\overline{\mathcal{N}}\gamma_\nu\mathcal{N})(\overline{\mathcal{N}}\gamma^\nu\gamma_5\mathcal{N}) \,, \tag{C.21}$$

$$VAP = (\partial^\mu \overline{\mathcal{N}} \gamma^\nu \partial_\mu \mathcal{N})(\overline{\mathcal{N}}\gamma_\nu\gamma_5\mathcal{N})(\overline{\mathcal{N}}\gamma_5\mathcal{N}) \,, \tag{C.22}$$

$$APV = (\partial^\mu \overline{\mathcal{N}} \gamma^\nu\gamma_5 \partial_\mu \mathcal{N})(\overline{\mathcal{N}}\gamma_5\mathcal{N})(\overline{\mathcal{N}}\gamma_\nu\mathcal{N}) \,, \tag{C.23}$$

those in which the derivatives are contracted with a Dirac matrix (12 in all),

$$SVV' = (\partial^\mu \overline{\mathcal{N}} \partial_\nu \mathcal{N})(\overline{\mathcal{N}}\gamma_\mu\mathcal{N})(\overline{\mathcal{N}}\gamma^\nu\mathcal{N}) \,, \tag{C.24}$$

$$TST' = (\partial_\nu \overline{\mathcal{N}} \sigma_{\mu\rho} \partial^\mu \mathcal{N})(\overline{\mathcal{N}}\mathcal{N})(\overline{\mathcal{N}}\sigma^{\nu\rho}\mathcal{N}) \,, \tag{C.25}$$

$$PVA' = (\partial^\mu \overline{\mathcal{N}} \gamma_5 \partial_\nu \mathcal{N})(\overline{\mathcal{N}}\gamma_\mu\mathcal{N})(\overline{\mathcal{N}}\gamma^\nu\gamma_5\mathcal{N}) \,, \tag{C.26}$$

$$VTV' = (\partial^\mu \overline{\mathcal{N}} \gamma_\rho \partial_\nu \mathcal{N})(\overline{\mathcal{N}}\sigma^{\nu\rho}\mathcal{N})(\overline{\mathcal{N}}\gamma_\mu\mathcal{N}) \,, \tag{C.27}$$

$$ATA' = (\partial^\mu \overline{\mathcal{N}} \gamma_\rho\gamma_5 \partial_\nu \mathcal{N})(\overline{\mathcal{N}}\sigma^{\nu\rho}\mathcal{N})(\overline{\mathcal{N}}\gamma_\mu\gamma_5\mathcal{N}) \,, \tag{C.28}$$

$$TTT' = (\partial^\mu \overline{\mathcal{N}} \sigma_{\mu\eta} \partial^\eta \mathcal{N})(\overline{\mathcal{N}}\sigma^{\nu\rho}\mathcal{N})(\overline{\mathcal{N}}\sigma_{\nu\rho}\mathcal{N}) \,, \tag{C.29}$$

$$TTT'' = (\partial_\mu \overline{\mathcal{N}} \sigma^{\mu\nu} \partial_\eta \mathcal{N})(\overline{\mathcal{N}}\sigma^{\eta\rho}\mathcal{N})(\overline{\mathcal{N}}\sigma_{\rho\nu}\mathcal{N}) \,, \tag{C.30}$$

[2]In all operators, derivatives act only on the object immediately to their right.

$$TTT'' = (\partial_\eta \overline{\mathcal{N}} \sigma^{\mu\nu} \partial_\mu \mathcal{N})(\overline{\mathcal{N}} \sigma^{\eta\rho} \mathcal{N})(\overline{\mathcal{N}} \sigma_{\rho\nu} \mathcal{N}) \,, \tag{C.31}$$

$$TT_5P' = (\partial^\mu \overline{\mathcal{N}} \sigma_{\mu\rho} \partial_\nu \mathcal{N})(\overline{\mathcal{N}} \sigma^{\nu\rho} \gamma_5 \mathcal{N})(\overline{\mathcal{N}} \gamma_5 \mathcal{N}) \,, \tag{C.32}$$

$$T_5VA' = (\partial^\mu \overline{\mathcal{N}} \sigma_{\mu\nu} \gamma_5 \partial^\nu \mathcal{N})(\overline{\mathcal{N}} \gamma^\rho \mathcal{N})(\overline{\mathcal{N}} \gamma_\rho \gamma_5 \mathcal{N}) \,, \tag{C.33}$$

$$T_5VA'' = (\partial^\mu \overline{\mathcal{N}} \sigma_{\rho\nu} \gamma_5 \partial^\nu \mathcal{N})(\overline{\mathcal{N}} \gamma^\mu \mathcal{N})(\overline{\mathcal{N}} \gamma^\rho \gamma_5 \mathcal{N}) \,, \tag{C.34}$$

$$T_5TT_5' = (\partial^\mu \overline{\mathcal{N}} \sigma_{\mu\nu} \gamma_5 \partial^\nu \mathcal{N})(\overline{\mathcal{N}} \sigma^{\eta\rho} \mathcal{N})(\overline{\mathcal{N}} \sigma_{\eta\rho} \gamma_5 \mathcal{N}) \tag{C.35}$$

and those that can be dropped using the equations of motion (8 in all)

$$VSV' = (\partial^\mu \overline{\mathcal{N}} \gamma_\mu \partial^\nu \mathcal{N})(\overline{\mathcal{N}} \mathcal{N})(\overline{\mathcal{N}} \gamma_\nu \mathcal{N}) \,, \tag{C.36}$$

$$VSV'' = (\partial^\nu \overline{\mathcal{N}} \gamma_\mu \partial^\mu \mathcal{N})(\overline{\mathcal{N}} \mathcal{N})(\overline{\mathcal{N}} \gamma_\nu \mathcal{N}) \,, \tag{C.37}$$

$$ASA' = (\partial^\mu \overline{\mathcal{N}} \gamma_\mu \gamma_5 \partial^\nu \mathcal{N})(\overline{\mathcal{N}} \mathcal{N})(\overline{\mathcal{N}} \gamma_\nu \gamma_5 \mathcal{N}) \,, \tag{C.38}$$

$$ASA'' = (\partial^\nu \overline{\mathcal{N}} \gamma_\mu \gamma_5 \partial^\mu \mathcal{N})(\overline{\mathcal{N}} \mathcal{N})(\overline{\mathcal{N}} \gamma_\nu \gamma_5 \mathcal{N}) \,, \tag{C.39}$$

$$VAP' = (\partial^\mu \overline{\mathcal{N}} \gamma_\mu \partial^\nu \mathcal{N})(\overline{\mathcal{N}} \gamma_\nu \gamma_5 \mathcal{N})(\overline{\mathcal{N}} \gamma_5 \mathcal{N}) \,, \tag{C.40}$$

$$VAP'' = (\partial^\nu \overline{\mathcal{N}} \gamma_\mu \partial^\mu \mathcal{N})(\overline{\mathcal{N}} \gamma_\nu \gamma_5 \mathcal{N})(\overline{\mathcal{N}} \gamma_5 \mathcal{N}) \,, \tag{C.41}$$

$$APV' = (\partial^\mu \overline{\mathcal{N}} \gamma_\mu \gamma_5 \partial^\nu \mathcal{N})(\overline{\mathcal{N}} \gamma_5 \mathcal{N})(\overline{\mathcal{N}} \gamma_\nu \mathcal{N}) \,, \tag{C.42}$$

$$APV'' = (\partial^\nu \overline{\mathcal{N}} \gamma_\mu \gamma_5 \partial^\mu \mathcal{N})(\overline{\mathcal{N}} \gamma_5 \mathcal{N})(\overline{\mathcal{N}} \gamma_\nu \mathcal{N}) \,. \tag{C.43}$$

We have checked this result using an alternative method in which we explicitly include every possible position of the action of the two derivatives, and all possible contractions with Dirac matrices, without using the analytic simplifications of this appendix. We again find that only two operators appear at quadratic order.

Appendix 4

APPENDIX TO CHAPTER 6

D.1 Isospin relations

Here we give the relations between the isospin-basis states of eq. (6.2) and the flavor-basis states of eq. (6.1). Doing so, it is important to keep in mind that, while the kaon doublet is (K^+, K^0), the antikaon doublet contains a sign: $(-\overline{K}^0, K^-)$. For $I = 2$, the results are

$$\begin{aligned} I=2,a:[[K\overline{K}^0]_1\pi]_2 \to \sqrt{\tfrac{1}{6}}\Big(&- K^+(k_1)\overline{K}^0(k_2)\pi^-(k_3) + \sqrt{2}K^+(k_1)K^-(k_2)\pi^0(k_3) \\ &- \sqrt{2}K^0(k_1)\overline{K}^0(k_2)\pi^0(k_3) + K^0(k_1)K^-(k_2)\pi^+(k_3)\Big)\,, \end{aligned} \tag{D.1}$$

$$I=2,b:[[\pi\pi]_2\eta]_2 \to \sqrt{\tfrac{1}{6}}\left(\pi^+(k_1)\pi^-(k_2) + 2\pi^0(k_1)\pi^0(k_2) + \pi^-(k_1)\pi^+(k_2)\right)\eta(k_3)\,. \tag{D.2}$$

For $I = 1$ we have

$$I=1,a:[[K\overline{K}^0]_1\pi]_1 \to \sqrt{\frac{1}{2}}\Big(- K^+(k_1)\overline{K}^0(k_2)\pi^-(k_3) - K^0(k_1)K^-(k_2)\pi^+(k_3)\Big)\,, \tag{D.3}$$

$$I=1,b:[[K\overline{K}^0]_0\pi]_1 \to \sqrt{\frac{1}{2}}\Big(K^+(k_1)K^-(k_2)\pi^0(k_3) + K^0(k_1)\overline{K}^0(k_2)\pi^0(k_3)\Big)\,, \tag{D.4}$$

$$I=1,c:[[\pi\pi]_1\eta]_1 \to \sqrt{\frac{1}{2}}\left(\pi^+(k_1)\pi^-(k_2) - \pi^-(k_1)\pi^+(k_2)\right)\eta(k_3)\,. \tag{D.5}$$

Finally, for $I = 0$ we have

$$\begin{aligned} I=0,a:[[K\overline{K}^0]_1\pi]_0 \to \sqrt{\frac{1}{6}}\Big(&-\sqrt{2}K^+(k_1)\overline{K}^0(k_2)\pi^-(k_3) - K^+(k_1)K^-(k_2)\pi^0(k_3) \\ &+ K^0(k_1)\overline{K}^0(k_2)\pi^0(k_3) + \sqrt{2}K^0(k_1)K^-(k_2)\pi^+(k_3)\Big) \end{aligned} \tag{D.6}$$

$$I=0,b:[[\pi\pi]_0\eta]_0 \to \sqrt{\frac{1}{3}}\left(\pi^+(k_1)\pi^-(k_2) - \pi^0(k_1)\pi^0(k_2) + \pi^-(k_1)\pi^+(k_2)\right)\eta(k_3)\,, \tag{D.7}$$

Thus the conversion from the charged to the isospin basis is accomplished by a 7×6 matrix

$$\boldsymbol{v}_{\text{iso}} = C_{\text{ch}\to\text{iso}} \boldsymbol{v}_{\text{ch}} \,, \tag{D.8}$$

$$C_{\text{ch}\to\text{iso}} = \sqrt{\frac{1}{6}} \begin{pmatrix} -1 & \sqrt{2} & -\sqrt{2} & 1 & 0 & 0 \\ 0 & 0 & 0 & 0 & S_{12} & 2 \\ -\sqrt{3} & 0 & 0 & -\sqrt{3} & 0 & 0 \\ 0 & \sqrt{3} & \sqrt{3} & 0 & 0 & 0 \\ 0 & 0 & 0 & 0 & \sqrt{3}A_{12} & 0 \\ -\sqrt{2} & -1 & 1 & \sqrt{2} & 0 & 0 \\ 0 & 0 & 0 & 0 & \sqrt{2}S_{12} & -\sqrt{2} \end{pmatrix} , \tag{D.9}$$

where $S_{12} = 1 + P_{12}$ is the symmetrization operator acting on the $\boldsymbol{k}_1$ and $\boldsymbol{k}_2$ arguments, with P_{12} permuting these labels, while $A_{12} = 1 - P_{12}$ is the corresponding antisymmetrization operator.

D.2 Kinematic functions

In this appendix we provide definitions of kinematic quantities and auxiliary operators that enter the three-particle formalism. These are taken from previous works in the RFT formalism, with the exception of the discussion of $\widehat{\mathcal{K}}_{2,L}$ in the case of channel mixing.

We begin with the F function for nondegenerate particles, which appears in the main text starting in eq. (6.29). There are both primed and unprimed versions, corresponding to $\pi\pi\eta$ and $K\overline{K}\pi$ triplets. The latter are given, in the notation of ref. [36], by

$$\begin{aligned} \left[\widetilde{F}^{(i)}\right]_{p'\ell'm';p\ell m} = \delta_{\boldsymbol{p}'\boldsymbol{p}} \frac{H^{(i)}(\boldsymbol{p})}{2\omega_p^{(i)} L^3} \left[\frac{1}{L^3} \sum_{\boldsymbol{a}}^{\text{UV}} - \text{PV} \int^{\text{UV}} \frac{d^3a}{(2\pi)^3}\right] \\ \times \left[\frac{\mathcal{Y}^*_{\ell'm'}(\boldsymbol{a}^{*(i,j,p)})}{\left(q^{*(i)}_{2,p'}\right)^{\ell'}} \frac{1}{4\omega_a^{(j)}\omega_b^{(k)}\left(E - \omega_p^{(i)} - \omega_a^{(j)} - \omega_b^{(k)}\right)} \frac{\mathcal{Y}_{\ell m}(\boldsymbol{a}^{*(i,j,p)})}{\left(q^{*(i)}_{2,p}\right)^{\ell}}\right] . \end{aligned} \tag{D.10}$$

Here $\{i, j, k\}$ are a permutation of $\{K, \overline{K}, \pi\}$. The superscript on $\widetilde{F}^{(i)}$ indicates the spectator particle, while the label j refers to the primary particle of the nonspectator pair, with k is

the flavor of the third particle. The ordering conventions are given in eq. (6.26).

Other quantities appearing in eq. (D.10) are the on-shell energies, exemplified by

$$\omega_p^{(i)} = \sqrt{M_i^2 + \boldsymbol{p}^2}\,; \tag{D.11}$$

the "third" momentum $\boldsymbol{b} = \boldsymbol{P} - \boldsymbol{p} - \boldsymbol{a}$; and the magnitude of the (jk) pair momentum, assuming three on-shell particles,

$$\left[q_{2,p}^{*(i)}\right]^2 = \frac{\lambda(\sigma_p^{(i)}, M_j^2, M_k^2)}{4\sigma_p^{(i)}}\,, \tag{D.12}$$

$$\sigma_p^{(i)} = (E - \omega_p^{(i)})^2 - (\boldsymbol{P} - \boldsymbol{p})^2\,, \tag{D.13}$$

$$\lambda(a, b, c) = a^2 + b^2 + c^2 - 2ab - 2ac - 2bc\,. \tag{D.14}$$

The sum over $\boldsymbol{a}$ runs over the finite-volume set, $\boldsymbol{a} = (2\pi/L)\mathbb{Z}^3$, and the integral over the pole is regulated by the principal value (PV) prescription, possibly augmented by the I_{PV} function introduced in ref. [114]. Both sum and integral are regulated in the same manner in the ultraviolet, with the particular choice only changing F by exponentially-suppressed effects. The momentum $\boldsymbol{a}^{*(i,j,p)}$ is the spatial part of the four-momentum resulting from boosting $(\omega_a^{(j)}, \boldsymbol{a})$ to the center of momentum frame (CMF) of the nonspectator pair, and thus depends on the spectator momentum $\boldsymbol{p}$, the spectator flavor i, the mass of the primary member of the pair, M_j, as well as (implicitly) the total four-momentum $(E, \boldsymbol{P})$. Note that we use * both to indicate a quantity boosted to a pair CMF, and complex conjugation. Which usage applies should be clear from the context. The cutoff function $H^{(i)}(\boldsymbol{p})$ will be defined below. Finally,

$$\mathcal{Y}_{\ell m}(\boldsymbol{r}) = \sqrt{4\pi} r^\ell Y_{\ell m}(\hat{r}) \tag{D.15}$$

are harmonic polynomials.

The G function for nondegenerate particles is given by [36]

$$\left[\widetilde{G}^{(ij)}\right]_{p\ell' m';r\ell m} = \frac{1}{2\omega_p^{(i)} L^3} \frac{\mathcal{Y}^*_{\ell' m'}(\boldsymbol{r}^{*(i,j,p)})}{\left(q_{2,p}^{*(i)}\right)^{\ell'}} \frac{H^{(i)}(\boldsymbol{p}) H^{(j)}(\boldsymbol{r})}{b_{ij}^2 - m_k^2} \frac{\mathcal{Y}_{\ell m}(\boldsymbol{p}^{*(j,i,r)})}{\left(q_{2,r}^{*(j)}\right)^{\ell}} \frac{1}{2\omega_r^{(j)} L^3}\,, \tag{D.16}$$

where i and j indicate the flavor of the final and initial spectators, respectively. The only new notation here is that $b_{ij} = (E - \omega_p^{(i)} - \omega_r^{(j)}, \boldsymbol{P} - \boldsymbol{p} - \boldsymbol{r})$.

We now return to the cutoff function. This is defined, following Refs. [16, 121, 227], as

$$H^{(i)}(\boldsymbol{p}) = J(z^{(i)}(\boldsymbol{p}))\,, \quad z^{(i)}(\boldsymbol{p}) = (1+\epsilon_H)\frac{\sigma_p^{(i)} - \sigma_{\text{min}}^{(i)}}{\sigma_{\text{th}}^{(i)} - \sigma_{\text{min}}^{(i)}}\,, \tag{D.17}$$

$$J(z) = \begin{cases} 0 & z \leq 0 \\ \exp(-\frac{1}{z}\exp[-1/(1-z)]) & 0 < z < 1 \\ 1 & 1 \leq z \end{cases} . \tag{D.18}$$

Here $\sigma_{\text{th}}^{(i)} = (M_j + M_k)^2$ is the value of $\sigma_p^{(i)}$ at the pair's threshold, while ϵ_H is a small positive constant introduced to avoid additional power-law finite-volume effects [121]. $J(z)$ is any function that smoothly interpolates between 0 and 1, and we have shown one possible form. The quantity $\sigma_{\text{min}}^{(i)}$ is the minimum allowed value of $\sigma_p^{(i)}$, and should be chosen to avoid any singularities in the two-particle K matrix for the pair. As discussed in detail in ref. [227], this singularity is typically due to the nearest left-hand cut associated with exchange of one or more particles. Here, for diagonal scattering in all the two-particle channels ($K\overline{K}$, $K\pi$, and $\overline{K}\pi$) the nearest left-hand cut is due to t-channel exchange of two pions. Avoiding this requires that

$$\sigma_{\text{min}}^{(i)} \geq \left(\sqrt{M_j^2 - M_\pi^2} + \sqrt{M_k^2 - M_\pi^2}\right)^2 . \tag{D.19}$$

We also enforce that $\sigma_{\text{th}}^{(i)} > \sigma_{\text{min}}^{(i)}$, so that the cutoff function has nonvanishing subthreshold support. Numerically, the minimum values for $\sqrt{\sigma_{\text{min}}^{(i)}}$ are ≈ 950 and ≈ 475 MeV, respectively, for $i = \pi$, and $i = \overline{K}/K$. These should be compared to the values of $\sqrt{\sigma_{\text{th}}}$, which are ≈ 990 and 630 MeV, respectively. Thus we learn that the cutoff in the $K\overline{K}$ channel ($i = \pi$) is much closer to threshold than that in the $\pi K/\pi\overline{K}$ channels ($i = \overline{K}/K$). This observation will play a role in the discussion of section 6.5.

The primed quantities $\widetilde{F}'^{(i)}$ and $\widetilde{G}'^{(ij)}$ are defined in exactly the same manner, except that $\{i, j, k\}$ is now a permutation of $\{\pi, \pi, \eta\}$. Strictly speaking, the cutoff functions should be primed, i.e. $H'^{(i)}(\boldsymbol{p})$, to indicate that a new triplet of particles is being used. The nearest left-hand cut in both $\pi\pi$ and $\pi\eta$ scattering is due to two-pion exchange so that the result for

$\sigma_{\min}^{(i)}$, eq. (D.19), still holds. Numerically, the minimum values for $\sqrt{\sigma_{\min}^{(i)}}$ are 0 and ≈ 535 MeV for $i = \eta$ and π, respectively, while those for $\sqrt{\sigma_{\text{th}}^{(i)}}$ are ≈ 270 and 685 MeV.

We now turn to the $\boldsymbol{\mathcal{X}}$ operators, introduced in ref. [227], and appearing in the main text starting in eq. (6.37). These convert from the $\{k\ell m\}$ to the momentum basis. The operator $\boldsymbol{\mathcal{X}}^{\boldsymbol{\sigma}}_{[kab]}$ acts on a vector $f_{k\ell m}$ as

$$\left[\boldsymbol{\mathcal{X}}^{\boldsymbol{\sigma}}_{[kab]} \circ f\right](\{\boldsymbol{p}\}) = \left[\sum_{\ell m} Y^*_{\ell m}(\hat{a}^*) f_{k\ell m}\right]_{\boldsymbol{k}\to\boldsymbol{p}_{\sigma_1},\boldsymbol{a}\to\boldsymbol{p}_{\sigma_2},\boldsymbol{b}\to\boldsymbol{p}_{\sigma_3}}, \tag{D.20}$$

where $\boldsymbol{\sigma}$ is a permutation of $\{1,2,3\}$. In words, the sum over ℓm yields a function of $\boldsymbol{k}$ and $\hat{a}^*$. The former is then equated to $\boldsymbol{p}_{\sigma_1}$ (the spectator momentum), while the latter, when boosted to the CMF of the nonspectator pair, is set to the direction of p_{σ_2}. For three on-shell momenta, this completely determines p_{σ_2} and also the final momentum $b = P - k - a$, which is equated with p_{σ_3}. The result is a function of the three on-shell momenta p_1, p_2, p_3. The left-acting version $\boldsymbol{\mathcal{X}}^{\boldsymbol{\sigma}\dagger}_{[kab]}$ is defined analogously,

$$\left[f \circ \boldsymbol{\mathcal{X}}^{\boldsymbol{\sigma}\dagger}_{[kab]}\right](\{k_i\}) = \left[\sum_{\ell m} f_{k\ell m} Y_{\ell m}(\hat{a}^*)\right]_{\boldsymbol{k}\to\boldsymbol{k}_{\sigma_1},\boldsymbol{a}\to\boldsymbol{k}_{\sigma_2},\boldsymbol{b}\to\boldsymbol{k}_{\sigma_3}}. \tag{D.21}$$

Next we introduce operators $\boldsymbol{\mathcal{Y}}^{[kab]}_{\boldsymbol{\sigma}}$ that have the inverse action of the $\boldsymbol{\mathcal{X}}^{\boldsymbol{\sigma}}_{[kab]}$, again borrowing notation from ref. [227]. These appear first in the main text in section 6.4.6. The $\boldsymbol{\mathcal{Y}}^{[kab]}_{\boldsymbol{\sigma}}$ act on functions $g(\{p_i\})$ of three on-shell momenta, yielding objects that have $\{k\ell m\}$ indices:

$$\left[\boldsymbol{\mathcal{Y}}^{[kab]}_{\boldsymbol{\sigma}} \circ g\right]_{k\ell m} = \frac{1}{4\pi}\int d\Omega_{a^*} Y_{\ell m}(\hat{a}^*) g(\{p_i\})\Big|_{p_{\sigma(1)}\to k,\ p_{\sigma(2)}\to a,\ p_{\sigma(3)}\to b}, \tag{D.22}$$

where $\boldsymbol{\sigma}$ is again a permutation of $\{1,2,3\}$. In words, we choose p_{σ_1} to be the spectator momentum, leaving p_{σ_2} and p_{σ_3} to be the remaining pair. We boost to the CMF of this pair, and decompose into spherical harmonics, defining $\hat{a}^*$ as the direction of $\boldsymbol{p}_{\sigma_2}$ in this frame. An analogous definition holds for the conjugate operator $\boldsymbol{\mathcal{Y}}^{[kab]\dagger}_{\boldsymbol{\sigma}}$, which acts from the right and includes the complex-conjugated spherical harmonics.

Finally, we give the explicit form for the two-particle K matrices, or, more precisely, for the inverse of these matrices, since it is the latter that enter the quantization condition [see

eqs. (6.51) and (6.52)]. We focus on channels having definite isospin, rather than using the charge basis, since the former enter the final form of the quantization condition, both before (section 6.4.5) and after (section 6.4.8) G-parity projection.

As can be seen from the form of the isospin blocks $\widehat{\mathcal{K}}_{2,L}^{[I]}$, given in eqs. (6.54), (6.58) and (6.64) before G-parity projection and eqs. (6.98), (6.100) and (6.103) after, the only mixing occurs between the $[K\bar{K}]_1$ and $[\pi\eta]_1$ channels. For the other channels, taking the inverse is straightforward as the matrix is diagonal in all indices, and we discuss these cases first. The general form of the inverse is exemplified by

$$\left[\frac{1}{\overline{\mathcal{K}}_{2,L}^{K\pi,I=3/2}}\right]_{k'\ell'm',k\ell m} = \delta_{\boldsymbol{k}'\boldsymbol{k}}\frac{1}{2\omega_k^{\bar{K}}L^3}\delta_{\ell'\ell}\delta_{m'm}\frac{1}{\mathcal{K}_2^{K\pi,I=3/2,(\ell)}(q_{2,k}^{*\bar{K}})}\,, \tag{D.23}$$

where we recall that the superscript $\bar{K}$ indicates the spectator flavor, and

$$\frac{1}{\mathcal{K}_2^{K\pi,I=3/2,(\ell)}(q_{2,k}^{*\bar{K}})} = \frac{\eta_{\bar{K}}}{8\pi\sigma_k^{\bar{K}}}\left\{q_{2,k}^{*\bar{K}}\cot\delta_\ell^{K\pi,I=3/2}(q_{2,k}^{*\bar{K}}) + \left|q_{2,k}^{*\bar{K}}\right|\left[1-H'^{\bar{K}}(\boldsymbol{k})\right]\right\}. \tag{D.24}$$

$\eta_{\bar{K}}$ is a symmetry factor that is unity here and in all other channels except for $\pi\pi$, where it is 1/2. Note that we are abusing notation slightly as the right-hand side depends on the spectator momentum $\boldsymbol{k}$ and flavor (here $i = \overline{K}$), but we do not show this explicitly on the left-hand side. The result eq. (D.24) can be generalized to deal with poles in $\mathcal{K}_2$ by introducing an I_{PV} function, matching the corresponding addition to F noted earlier. The details of this function and its role are described in ref. [114].

It will be helpful for the generalization to the case involving channel mixing to recall the argument leading to the form of the right hand side in eq. (D.24). To do so we rewrite eq. (6.44) as

$$[\widehat{\mathcal{M}}_{2,L}]^{-1} = [\widehat{\mathcal{K}}_{2,L}]^{-1} + \widehat{F}\,. \tag{D.25}$$

We first apply this to channels that only have diagonal scattering, where the inverses are trivial. We take the $L\to\infty$ limit in the fashion described in ref. [17], i.e. first introducing the standard $i\epsilon$ into the poles. A detailed description of this limit using the present notation

is given in sec. VII of ref. [35]. Removing common factors, one then finds

$$[\mathcal{M}_2^{(i)(\ell)}(q_{2,k}^{*(i)})]^{-1} = [\mathcal{K}_2^{(i)(\ell)}(q_{2,k}^{*(i)})]^{-1} + H(\boldsymbol{k})\widetilde{\rho}(q_{2,k}^{*(i)})\,, \tag{D.26}$$

$$\widetilde{\rho}(q_{2,k}^{*(i)}) = \frac{\eta_i}{8\pi\sigma_k^{(i)}} \begin{cases} -iq_{2,k}^{*(i)} & q_{2,k}^{*(i)2} \geq 0 \\ \left|q_{2,k}^{*(i)}\right| & q_{2,k}^{*(i)2} < 0 \end{cases}. \tag{D.27}$$

Here we are denoting the channel generically by the spectator index i, and we stress that $\mathcal{M}_2^{(i)(\ell)}$ is the physical infinite-volume two-particle scattering amplitude. The $H\widetilde{\rho}$ term in eq. (D.26) comes from the $L \to \infty$ limit of $\widetilde{F}$, eq. (D.10), in which limit the sum-integral difference vanishes aside from the difference between the PV and $i\epsilon$ pole prescriptions. This leads to the phase-space factor $\widetilde{\rho}$, including its analytic continuation below threshold, as well as the overall factor of H that comes with $\widetilde{F}$. The unitarity constraint on $\mathcal{M}_2$ can be resolved by writing

$$[\mathcal{M}_2^{(i)(\ell)}(q_{2,k}^{*(i)})]^{-1} = \frac{\eta_i}{8\pi\sigma_k^{(i)}} q_{2,k}^{*(i)} \cot\delta_\ell^{(i)}(q_{2,k}^{*(i)}) + \widetilde{\rho}(q_{2,k}^{*(i)})\,, \tag{D.28}$$

where the first term is the standard continuum definition of $\mathcal{K}_2^{-1}$. Equating the results in eq. (D.26) and eq. (D.28) leads to the form given above in eq. (D.24). We note that the modified $\mathcal{K}_2$ that appears in the RFT formalism agrees with the standard one above threshold (where $H = 1$) and smoothly interpolates to $\mathcal{M}_2$ below threshold, with equality holding once $H = 0$.

We now extend this discussion to the case of two channel mixing. We label the two channels $i = 1, 2$ for $[K\bar{K}]_1, [\pi\eta]_1$, respectively. We use the Blatt-Biedenharn (BB) parametrization of the S matrix [214],

$$S_2 = \begin{pmatrix} c_\epsilon & -s_\epsilon \\ s_\epsilon & c_\epsilon \end{pmatrix} \begin{pmatrix} e^{2i\delta_1} & 0 \\ 0 & e^{2i\delta_2} \end{pmatrix} \begin{pmatrix} c_\epsilon & s_\epsilon \\ -s_\epsilon & c_\epsilon \end{pmatrix}, \tag{D.29}$$

where $c_\epsilon \equiv \cos(\epsilon)$, $s_\epsilon \equiv \sin(\epsilon)$, with ϵ the mixing angle, and all quantities have an implicit label (ℓ). The relation to the scattering amplitude is [234]

$$S_2 = 1 + 2iP\mathcal{M}_2P\,, \qquad P = \mathrm{diag}\left(\sqrt{\frac{\eta_1 q_1^*}{8\pi E^*}},\ \sqrt{\frac{\eta_2 q_2^*}{8\pi E^*}}\right), \tag{D.30}$$

where we are using E^* in place of $\sqrt{\sigma_k}$ for the total energy in the CMF, which is common to both channels, and q_i^* are the channel-dependent CMF particle momenta. We include symmetry factors to keep the discussion general, although for the channels of interest $\eta_1 = \eta_2 = 1$. The unitarity of S is ensured if $\mathcal{M}$ satisfies

$$\mathcal{M}_2^{-1} = K^{-1} - iP^2\,, \tag{D.31}$$

with K a real, symmetric matrix. Inserting the BB form of S_2 into eq. (D.30) and comparing to eq. (D.31), one finds

$$K^{-1} = P \begin{pmatrix} c_\epsilon^2 \cot\delta_1 + s_\epsilon^2 \cot\delta_2 & s_\epsilon c_\epsilon(\cot\delta_1 - \cot\delta_2) \\ s_\epsilon c_\epsilon(\cot\delta_1 - \cot\delta_2) & c_\epsilon^2 \cot\delta_2 + s_\epsilon^2 \cot\delta_1 \end{pmatrix} P\,, \tag{D.32}$$

which has the expected decoupled limit when $\epsilon \to 0$.

To relate K to the matrix in the quantization condition $\widehat{\mathcal{K}}_{2,L}$, we follow the same steps as above. The result eq. (D.25) remains valid, though now as a 2-d matrix equation. Taking the $L \to \infty$ limit one now obtains

$$\mathcal{M}_2^{-1} = \mathcal{K}_2^{-1} - iHP^2\,, \quad H = \mathrm{diag}\left(H_1(\boldsymbol{k}),\ H_2(\boldsymbol{k})\right)\,, \tag{D.33}$$

where H_i are the appropriate cutoff functions for the two channels, as discussed above. Comparing to eq. (D.31) one finds

$$\mathcal{K}_2^{-1} = K^{-1} - i(1-H)P^2\,, \tag{D.34}$$

which is the generalization of eq. (D.24).

This discussion has assumed that both channels are above threshold. The analytic continuation below threshold is done as shown in the definition of $\widetilde{\rho}$, eq. (D.27): $q^* \to i|q^*|$. This suffices to define the P^2 term in eq. (D.34). As for K^{-1}, if one uses the expression eq. (D.32), it would appear that we would need to choose a branch of the square root in P. However, we know that the elements of K are smooth functions of momenta, since it involves PV-regulated integrals. Thus, in practice, it may be simplest to parametrize its three independent elements as analytic functions of the q_i^2.

D.3 Form of matrix $\widehat{\mathcal{K}}_{2,L}$ in charge basis

Here we list the nonzero entries of $\widehat{\mathcal{K}}_{2,L}$. We use the shorthand notation

$$[K_{2,L}^{(ij\leftarrow mn;p)}]_{k'\ell'm',k\ell m} = \delta_{\boldsymbol{k}'\boldsymbol{k}} 2\omega_{k_p} L^3 \delta_{\ell'\ell}\delta_{m'm}\mathcal{K}_2^{\ell}(ij\leftarrow mn)\,, \tag{D.35}$$

such that the right-hand side of eq. (6.34) is $K_{2,L}^{(\overline{K}^0\pi^0\leftarrow K^-\pi^0;K^+)}$, as well as the abbreviation

$$K_{2,L}^{(ij;p)} \equiv K_{2,L}^{(ij\leftarrow ij;p)} \tag{D.36}$$

for diagonal scattering.

The diagonal entries are

$$\begin{Bmatrix} K_{2,L}^{(K^+\overline{K}^0;\pi^-)}, K_{2,L}^{(K^+\pi^-;\overline{K}^0)}, K_{2,L}^{(\overline{K}^0\pi^-;K^+)}, K_{2,L}^{(K^+K^-;\pi^0)}, K_{2,L}^{(K^+\pi^0;K^-)}, K_{2,L}^{(K^-\pi^0;K^+)}, \\ K_{2,L}^{(K^0\overline{K}^0;\pi^0)}, K_{2,L}^{(K^0\pi^0;\overline{K}^0)}, K_{2,L}^{(\overline{K}^0\pi^0;K^0)}, K_{2,L}^{(K^0K^-;\pi^+)}, K_{2,L}^{(K^0\pi^+;K^-)}, K_{2,L}^{(K^-\pi^+;K^0)}, \\ K_{2,L}^{([\pi^+\pi^-]_e;\eta)}, K_{2,L}^{([\pi^+\pi^-]_o;\eta)}, K_{2,L}^{(\pi^+\eta;\pi^-)}, K_{2,L}^{(\pi^-\eta;\pi^+)}, \tfrac{1}{2}K_{2,L}^{(\pi^0\pi^0;\eta)}, K_{2,L}^{(\pi^0\eta;\pi^0)} \end{Bmatrix} \tag{D.37}$$

We have augmented the notation with the subscripts e and o to indicated even and odd partial waves.

The nonzero offdiagonal entries lying above the diagonal are

$$\left[\widehat{\mathcal{K}}_{2,L}\right]_{1,15} = K_{2,L}^{(K^+\overline{K}^0\leftarrow\pi^+\eta;\pi^-)}, \qquad \left[\widehat{\mathcal{K}}_{2,L}\right]_{2,8} = K_{2,L}^{(K^+\pi^-\leftarrow K^0\pi^0;\overline{K}^0)}, \tag{D.38}$$

$$\left[\widehat{\mathcal{K}}_{2,L}\right]_{3,6} = K_{2,L}^{(\overline{K}^0\pi^-\leftarrow K^-\pi^0;K^+)}, \qquad \left[\widehat{\mathcal{K}}_{2,L}\right]_{4,7} = K_{2,L}^{(K^+K^-\leftarrow K^0\overline{K}^0;\pi^0)}, \tag{D.39}$$

$$\left[\widehat{\mathcal{K}}_{2,L}\right]_{4,18} = K_{2,L}^{(K^+K^-\leftarrow\pi^0\eta;\pi^0)}, \qquad \left[\widehat{\mathcal{K}}_{2,L}\right]_{5,11} = K_{2,L}^{(K^+\pi^0\leftarrow K^0\pi^+;K^-)}, \tag{D.40}$$

$$\left[\widehat{\mathcal{K}}_{2,L}\right]_{7,18} = K_{2,L}^{(K^0\overline{K}^0\leftarrow\pi^0\eta;\pi^0)}, \qquad \left[\widehat{\mathcal{K}}_{2,L}\right]_{9,12} = K_{2,L}^{(\overline{K}^0\pi^0\leftarrow K^-\pi^+;K^0)}, \tag{D.41}$$

$$\left[\widehat{\mathcal{K}}_{2,L}\right]_{10,16} = K_{2,L}^{(K^0K^-\leftarrow\pi^-\eta;\pi^+)}, \qquad \left[\widehat{\mathcal{K}}_{2,L}\right]_{13,17} = \sqrt{\tfrac{1}{2}}K_{2,L}^{([\pi^+\pi^-]_e\leftarrow\pi^0\pi^0;\eta)}, \tag{D.42}$$

while those below the diagonal are determined by the result that the matrix is symmetric. Symmetry follows from PT symmetry, which implies that the K matrices for $ij\leftarrow mn$ and $mn\leftarrow ij$ are equal.

The factors of $1/2$ and $\sqrt{1/2}$ in the expressions above are symmetry factors that follow from the considerations of BS2.

D.4 Isospin decompositions of two-particle K matrices

In the following, the superscript ℓ is dropped, and we make use of the form of the triplet and singlet $K\overline{K}$ pairs,

$$[K\bar{K}]_1 = \left\{-K^+\overline{K}^0, \sqrt{\tfrac{1}{2}}(K^+K^- - K^0\overline{K}^0), K^0K^-\right\}, \tag{D.43}$$

$$[K\bar{K}]_0 = \sqrt{\tfrac{1}{2}}(K^+K^- + K^0\overline{K}^0)\,. \tag{D.44}$$

For $\pi\pi$ scattering we have

$$\mathcal{K}_2([\pi^+\pi^-]_e \leftarrow [\pi^+\pi^-]_e) = \frac{1}{6}\left(\mathcal{K}_2^{\pi\pi,I=2} + 2\mathcal{K}_2^{\pi\pi,I=0}\right). \tag{D.45}$$

$$\mathcal{K}_2(\pi^0\pi^0 \leftarrow \pi^0\pi^0) = \frac{1}{3}\left(2\mathcal{K}_2^{\pi\pi,I=2} + \mathcal{K}_2^{\pi\pi,I=0}\right), \tag{D.46}$$

$$\mathcal{K}_2(\pi^0\pi^0 \leftrightarrow [\pi^+\pi^-]_e) = \frac{1}{3}\left(\mathcal{K}_2^{\pi\pi,I=2} - \mathcal{K}_2^{\pi\pi,I=0}\right), \tag{D.47}$$

$$\mathcal{K}_2([\pi^+\pi^-]_o \leftrightarrow [\pi^+\pi^-]_o) = \frac{1}{2}\mathcal{K}_2^{\pi\pi,I=1}\,. \tag{D.48}$$

To obtain these results, care must be taken with the meaning of the subscripts e and o. For example, to obtain the last line, we use the fact that the $I = 1, I_3 = 0$ state is $(\pi^+\pi^0 - \pi^-\pi^+)/\sqrt{2}$, and determine the contribution of all contractions. Even partial waves cancel, while odd waves come with a factor of $(1/\sqrt{2})^2 \times 4 = 2$. Since $[\pi^+\pi^-]_o \leftarrow [\pi^+\pi^-]_o$ means "take the odd partial waves of the amplitude for $\pi^+\pi^- \leftarrow \pi^+\pi^-$", this leads to the factor of $1/2$ on the right-hand side of eq. (D.48).

For $\pi\eta$ scattering we have

$$\mathcal{K}_2(\pi^+\eta \leftarrow \pi^+\eta) = \mathcal{K}_2(\pi^0\eta \leftarrow \pi^0\eta) = \mathcal{K}_2(\pi^-\eta \leftarrow \pi^-\eta) = \mathcal{K}_2^{\pi\eta,I=1}\,, \tag{D.49}$$

while for $\pi\eta \leftrightarrow K\overline{K}$ we find

$$\begin{aligned} -\mathcal{K}_{2,L}(\pi^+\eta \leftrightarrow K^+\overline{K}^0) &= \mathcal{K}_{2,L}(\pi^-\eta \leftrightarrow K^0K^-) = \\ &= -\sqrt{2}\mathcal{K}_{2,L}(\pi^0\eta \leftrightarrow K^0\overline{K}^0) = \sqrt{2}\mathcal{K}_{2,L}(\pi^0\eta \leftrightarrow K^+K^-) = \mathcal{K}_{2,L}^{\pi\eta\leftrightarrow K\bar{K},I=1}\,. \end{aligned} \tag{D.50}$$

For $K\pi$ scattering, the results are

$$\mathcal{K}_2(K^+\pi^- \leftarrow K^+\pi^-) = \mathcal{K}_2(K^0\pi^+ \leftarrow K^0\pi^+) \ = \frac{1}{3}\left(\mathcal{K}_2^{K\pi,I=3/2} + 2\mathcal{K}_2^{K\pi,I=1/2}\right), \tag{D.51}$$

$$\mathcal{K}_2(K^0\pi^0 \leftarrow K^0\pi^0) = \mathcal{K}_2(K^+\pi^0 \leftarrow K^+\pi^0) = \frac{1}{3}\left(2\mathcal{K}_2^{K\pi,I=3/2} + \mathcal{K}_2^{K\pi,I=1/2}\right), \tag{D.52}$$

$$\mathcal{K}_2(K^+\pi^- \leftrightarrow K^0\pi^0) = \mathcal{K}_2(K^0\pi^+ \leftrightarrow K^+\pi^0) = \frac{\sqrt{2}}{3}\left(\mathcal{K}_2^{K\pi,I=3/2} - \mathcal{K}_2^{K\pi,I=1/2}\right). \tag{D.53}$$

Those for $\overline{K}\pi$ scattering can then be obtained using charge conjugation, keeping in mind that, for standard conventions, $C\pi^+ = -\pi^-$, $CK^+ = K^-$, and $CK^0 = \overline{K}^0$. We find

$$\mathcal{K}_2(K^-\pi^+ \leftarrow K^-\pi^+) = \mathcal{K}_2(\overline{K}^0\pi^- \leftarrow \overline{K}^0\pi^-) = \frac{1}{3}\left(\mathcal{K}_2^{K\pi,I=3/2} + 2\mathcal{K}_2^{K\pi,I=1/2}\right), \tag{D.54}$$

$$\mathcal{K}_2(\overline{K}^0\pi^0 \leftarrow \overline{K}^0\pi^0) = \mathcal{K}_2(K^-\pi^0 \leftarrow K^-\pi^0) = \frac{1}{3}\left(2\mathcal{K}_2^{K\pi,I=3/2} + \mathcal{K}_2^{K\pi,I=1/2}\right), \tag{D.55}$$

$$\mathcal{K}_2(K^-\pi^+ \leftrightarrow \overline{K}^0\pi^0) = \mathcal{K}_2(\overline{K}^0\pi^- \leftrightarrow K^-\pi^0) = \frac{\sqrt{2}}{3}\left(-\mathcal{K}_2^{K\pi,I=3/2} + \mathcal{K}_2^{K\pi,I=1/2}\right). \tag{D.56}$$

Finally, for $K\overline{K}$ scattering, we have

$$\mathcal{K}_2(K^+\overline{K}^0 \leftarrow K^+\overline{K}^0) = \mathcal{K}_2(K^0K^- \leftarrow K^0K^-) = \mathcal{K}_2^{K\bar{K},I=1}, \tag{D.57}$$

$$\mathcal{K}_2(K^+K^- \leftarrow K^+K^-) = \mathcal{K}_2(K^0\overline{K}^0 \leftarrow K^0\overline{K}^0) = \frac{1}{2}\left(\mathcal{K}_2^{K\bar{K},I=0} + \mathcal{K}_2^{K\bar{K},I=1}\right), \tag{D.58}$$

$$\mathcal{K}_2(K^+K^- \leftrightarrow K^0\overline{K}^0) = \frac{1}{2}\left(\mathcal{K}_2^{K\bar{K},I=0} - \mathcal{K}_2^{K\bar{K},I=1}\right). \tag{D.59}$$

D.5 Conversion from charge to isospin basis for 18-d matrices

We can convert the 18-d matrices to the isospin basis eq. (6.38) by means of conjugating by the 18×18 orthogonal matrix $C^{(18)}_{\text{ch}\to\text{iso}}$:

$$M^{(18)}_{\text{iso}} = C^{(18)}_{\text{ch}\to\text{iso}} M^{(18)}_{\text{ch}} \left[C^{(18)}_{\text{ch}\to\text{iso}}\right]^{-1}. \tag{D.60}$$

To obtain this matrix we simply expand the entries of eq. (6.38) using isospin Clebsch-Gordon coefficients, and then express in terms of the charge basis, eq. (6.26). The only subtlety is the treatment of $[\pi^+\pi^-]_{e/o}$. In order for $C^{(18)}_{\text{ch}\to\text{iso}}$ to correspond to a change of basis, it must be unitary, and this requires maintaining normalizations. Thus we must consider $[\pi^+\pi^-]_{e/o}$ as corresponding to $[\pi^+\pi^- \pm \pi^-\pi^+]/\sqrt{2}$.

The conversion matrix is too large to present in normal format, so we present it row by row in a compact notation. We begin with the first five rows, which are those corresponding to $I = 2$, and are given by

$$[[K\bar{K}]_1\pi]_2 : \sqrt{\tfrac{1}{6}}\left(-1,0,0,\sqrt{2},0,0,-\sqrt{2},0,0,1,|0\rangle_6\right) , \tag{D.61}$$

$$[[K\pi]_{3/2}\bar{K}]_2 : \sqrt{\tfrac{1}{6}}\left(0,-1,0,0,\sqrt{2},0,0,-\sqrt{2},0,0,1,0,|0\rangle_6\right) , \tag{D.62}$$

$$[[\bar{K}\pi]_{3/2}K]_2 : \sqrt{\tfrac{1}{6}}\left(0,0,-1,0,0,\sqrt{2},0,0,-\sqrt{2},0,0,1,|0\rangle_6\right) , \tag{D.63}$$

$$[[\pi\pi]_2\eta]_2 : \sqrt{\tfrac{1}{3}}\left(|0\rangle_{12},1,0,0,0,\sqrt{2},0\right) \tag{D.64}$$

$$[[\pi\eta]_1\pi]_2 : \sqrt{\tfrac{1}{6}}\left(|0\rangle_{12},0,0,1,1,0,2\right) , \tag{D.65}$$

where $|0\rangle_n$ is the vector consisting of n zeros.

The middle eight rows, corresponding to $I = 1$, are

$$[[K\bar{K}]_1\pi]_1 : \sqrt{\tfrac{1}{2}}\left(-1,0,0,0,0,0,0,0,-1,0,0,|0\rangle_6\right) , \tag{D.66}$$

$$[[K\bar{K}]_0\pi]_1 : \sqrt{\tfrac{1}{2}}\left(0,0,0,1,0,0,1,0,0,0,0,0,|0\rangle_6\right) , \tag{D.67}$$

$$[[K\pi]_{3/2}\bar{K}]_1 : \sqrt{\tfrac{1}{6}}\left(0,1,0,0,\sqrt{2},0,0,\sqrt{2},0,0,1,0,|0\rangle_6\right) , \tag{D.68}$$

$$[[K\pi]_{1/2}\bar{K}]_1 : \sqrt{\tfrac{1}{6}}\left(0,-\sqrt{2},0,0,1,0,0,1,0,0,-\sqrt{2},0,|0\rangle_6\right) , \tag{D.69}$$

$$[[\bar{K}\pi]_{3/2}K]_1 : \sqrt{\tfrac{1}{6}}\left(0,0,1,0,0,-\sqrt{2},0,0,-\sqrt{2},0,0,1,|0\rangle_6\right) , \tag{D.70}$$

$$[[\bar{K}\pi]_{1/2}K]_1 : \sqrt{\tfrac{1}{6}}\left(0,0,-\sqrt{2},0,0,-1,0,0,-1,0,0,-\sqrt{2},|0\rangle_6\right) , \tag{D.71}$$

$$[[\pi\pi]_1\eta]_1 : \left(|0\rangle_{12},0,1,0,0,0,0\right) , \tag{D.72}$$

$$[[\pi\eta]_1\pi]_1 : \sqrt{\tfrac{1}{2}}\left(|0\rangle_{12},0,0,1,-1,0,0\right) . \tag{D.73}$$

The last five rows, corresponding to $I = 0$, are

$$[[K\bar{K}]_1\pi]_0 : \sqrt{\tfrac{1}{6}}\left(-\sqrt{2},0,0,-1,0,0,1,0,0,\sqrt{2},0,0,|0\rangle_6\right) , \tag{D.74}$$

$$[[K\pi]_{1/2}\bar{K}]_0 : \sqrt{\tfrac{1}{6}}\left(0,\sqrt{2},0,0,1,0,0,-1,0,0,-\sqrt{2},0,|0\rangle_6\right) , \tag{D.75}$$

$$[[\bar{K}\pi]_{1/2}K]_0 : \sqrt{\tfrac{1}{6}}\left(0,0,\sqrt{2},0,0,1,0,0,-1,0,0,-\sqrt{2},|0\rangle_6\right) , \tag{D.76}$$

$$[[\pi\pi]_0\eta]_0 : \sqrt{\tfrac{1}{3}}\left(|0\rangle_{12},\sqrt{2},0,0,0,-1,0\right) \tag{D.77}$$

$$[[\pi\eta]_1\pi]_0 : \sqrt{\tfrac{1}{3}}\left(|0\rangle_{12},0,0,1,1,0,-1\right) , \tag{D.78}$$

D.6 Quadratic terms in the threshold expansion of $\mathcal{K}_{\rm df,3}$

Here we collect the quadratic terms in the threshold expansion developed in section 6.6, and sketch the group-theoretic analysis that allows one to determine the number of terms with given symmetry properties. Rather than give names to the coefficients we simply list the independent terms, each of which will be multiplied by an independent real coefficient.

For the $I = 0, 2$ diagonal K matrices we find 11 terms, one choice of basis for which is,

$$\begin{aligned}\mathcal{K}^{[I],xx}_{\rm df,3} : &\Delta^2,\ (\Delta_1\Delta_2 + \Delta'_1\Delta'_2),\ (\tilde{t}_{11}\tilde{t}_{22} + \tilde{t}_{12}\tilde{t}_{21}),\ (\Delta_1 + \Delta_2)(\Delta'_1 + \Delta'_2),\\ &(\tilde{t}_{11} + \tilde{t}_{22})(\tilde{t}_{12} + \tilde{t}_{21}),\ (\Delta_1^2 + \Delta_1'^2 + \Delta_2^2 + \Delta_2'^2),\\ &\Delta(\Delta_1 + \Delta'_1 + \Delta_2 + \Delta'_2),\ (\tilde{t}_{11}^2 + \tilde{t}_{12}^2 + \tilde{t}_{21}^2 + \tilde{t}_{22}^2),\ \Delta(\tilde{t}_{11} + \tilde{t}_{12} + \tilde{t}_{21} + \tilde{t}_{22}),\\ &(\tilde{t}_{11}(\Delta'_2 + \Delta_2) + \tilde{t}_{12}(\Delta'_2 + \Delta_1) + \tilde{t}_{21}(\Delta'_1 + \Delta_2) + \tilde{t}_{22}(\Delta'_1 + \Delta_1))\\ &(\tilde{t}_{11}(\Delta'_1 + \Delta_1) + \tilde{t}_{12}(\Delta'_1 + \Delta_2) + \tilde{t}_{21}(\Delta'_2 + \Delta_1) + \tilde{t}_{22}(\Delta'_2 + \Delta_2))\,,\end{aligned} \tag{D.79}$$

while for the offdiagonal case we find 17 terms,

$$\begin{aligned}\mathcal{K}^{[I],ab}_{\rm df,3} : &\Delta^2,\ \Delta_1\Delta_2,\ \Delta'_1\Delta'_2,\ (\Delta_1^2 + \Delta_2^2),\ (\Delta_1'^2 + \Delta_2'^2),\ \Delta(\Delta_1 + \Delta_2),\\ &\Delta(\Delta'_1 + \Delta'_2),\ (\tilde{t}_{11}\tilde{t}_{12} + \tilde{t}_{21}\tilde{t}_{22}),\ (\tilde{t}_{11}\tilde{t}_{21} + \tilde{t}_{12}\tilde{t}_{22}),\ (\tilde{t}_{11}\tilde{t}_{22} + \tilde{t}_{12}\tilde{t}_{21}),\\ &(\Delta_1 + \Delta_2)(\Delta'_1 + \Delta'_2),\ (\tilde{t}_{11}^2 + \tilde{t}_{12}^2 + \tilde{t}_{21}^2 + \tilde{t}_{22}^2),\ \Delta(\tilde{t}_{11} + \tilde{t}_{12} + \tilde{t}_{21} + \tilde{t}_{22}),\\ &((\tilde{t}_{11} + \tilde{t}_{21})\Delta_1 + (\tilde{t}_{12} + \tilde{t}_{22})\Delta_2),\ ((\tilde{t}_{11} + \tilde{t}_{21})\Delta_2 + (\tilde{t}_{12} + \tilde{t}_{22})\Delta_1),\\ &(\Delta'_1(\tilde{t}_{11} + \tilde{t}_{12}) + \Delta'_2(\tilde{t}_{21} + \tilde{t}_{22})),\ (\Delta'_2(\tilde{t}_{11} + \tilde{t}_{12}) + \Delta'_1(\tilde{t}_{21} + \tilde{t}_{22}))\,.\end{aligned} \tag{D.80}$$

For $I = 1$, the aa quadratic terms are as in eq. (D.79), while those for bb and cc involve the following 6 terms

$$\begin{aligned}\mathcal{K}^{[I=1],yy}_{\rm df,3} : &(\tilde{t}_{12}\tilde{t}_{21} - \tilde{t}_{11}\tilde{t}_{22}),\ (\Delta_1 - \Delta_2)(\Delta'_1 - \Delta'_2),\\ &(\tilde{t}_{11}^2 - \tilde{t}_{12}^2 - \tilde{t}_{21}^2 + \tilde{t}_{22}^2),\ \Delta(\tilde{t}_{11} - \tilde{t}_{12} - \tilde{t}_{21} + \tilde{t}_{22}),\\ &(\Delta'_1(\tilde{t}_{11} - \tilde{t}_{12}) + \Delta'_2(\tilde{t}_{22} - \tilde{t}_{21}) + (\tilde{t}_{11} - \tilde{t}_{21})\Delta_1 + (\tilde{t}_{22} - \tilde{t}_{12})\Delta_2),\\ &(\Delta'_1(\tilde{t}_{22} - \tilde{t}_{21}) + \Delta'_2(\tilde{t}_{11} - \tilde{t}_{12}) + (\tilde{t}_{22} - \tilde{t}_{12})\Delta_1 + (\tilde{t}_{11} - \tilde{t}_{21})\Delta_2).\end{aligned} \tag{D.81}$$

As for the offdiagonal $I=1$ contributions, we find 10 quadratic terms for ay, with $y=b$ or c

$$\begin{aligned}\mathcal{K}_{\mathrm{df},3}^{[I=1],ay}(\{k'\},\{k\}) : &(\tilde{t}_{11}\tilde{t}_{21}-\tilde{t}_{12}\tilde{t}_{22}),\ (\Delta'_1+\Delta'_2)(\Delta_1-\Delta_2),\ (\Delta'^2_1+\Delta'^2_2),\ (\Delta_1^2-\Delta_2^2),\\ &(\tilde{t}_{11}^2-\tilde{t}_{12}^2+\tilde{t}_{21}^2-\tilde{t}_{22}^2),\ \Delta(\tilde{t}_{11}-\tilde{t}_{12}+\tilde{t}_{21}-\tilde{t}_{22}),\\ &((\tilde{t}_{12}+\tilde{t}_{22})\Delta_1-(\tilde{t}_{11}+\tilde{t}_{21})\Delta_2),\ ((\tilde{t}_{11}+\tilde{t}_{21})\Delta_1-(\tilde{t}_{12}+\tilde{t}_{22})\Delta_1),\\ &(\Delta'_1(\tilde{t}_{11}-\tilde{t}_{12})+\Delta'_2(\tilde{t}_{21}-\tilde{t}_{22})),\ (\Delta'_2(\tilde{t}_{11}-\tilde{t}_{12})+\Delta_1(\tilde{t}_{21}-\tilde{t}_{22}))\,,\end{aligned} \tag{D.82}$$

and 8 terms for bc

$$\begin{aligned}\mathcal{K}_{\mathrm{df},3}^{[I=1],bc} : &(\tilde{t}_{12}\tilde{t}_{21}-\tilde{t}_{11}\tilde{t}_{22}),\ (\Delta_1-\Delta_2)(\Delta'_1-\Delta'_2),\\ &(\tilde{t}_{11}^2-\tilde{t}_{12}^2-\tilde{t}_{21}^2+\tilde{t}_{22}^2),\ \Delta(\tilde{t}_{11}-\tilde{t}_{12}-\tilde{t}_{21}+\tilde{t}_{22}),\\ &(\Delta'_1(\tilde{t}_{11}-\tilde{t}_{12})+\Delta'_2(\tilde{t}_{22}-\tilde{t}_{21})),\ ((\tilde{t}_{11}-\tilde{t}_{21})\Delta_1+(\tilde{t}_{22}-\tilde{t}_{12})\Delta_2),\\ &(\Delta'_1(\tilde{t}_{22}-\tilde{t}_{21})+\Delta'_2(\tilde{t}_{11}-\tilde{t}_{12})),\ ((\tilde{t}_{22}-\tilde{t}_{12})\Delta_1+(\tilde{t}_{11}-\tilde{t}_{21})\Delta_2).\end{aligned} \tag{D.83}$$

The counting of terms can be done using a group theoretic method introduced in appendix B of Ref. [230]. This has the advantage over direct enumeration of avoiding the possibility of missing terms. The method is based on the observation that all terms can be built from products of the $\widetilde{t}_{ij}$, as can be seen from the relations eq. (6.129). These 9 objects transform under the symmetry group $S_2\times S_2'$, where S_2 is the permutation group of two elements, here generated by the interchange initial momenta $k_1\leftrightarrow k_2$, while S_2' is the corresponding group for final state interchange. This is the symmetry group that is applicable for the off-diagonal elements of $\mathcal{K}_{\mathrm{df},3}$. For the diagonal elements, PT symmetry enlarges the group to $(S_2\times S_2')\rtimes Z_2$, with the Z_2 interchanging initial and final states. The Z_2 acts nontrivially—interchanging the two S_2s—so the combination involves a semidirect product.

The method is now to decompose the 9 objects $\widetilde{t}_{ij}$ and the 45 objects $\widetilde{t}_{ij}\widetilde{t}_{k\ell}$ into irreducible representations (irreps) of the appropriate group. We begin with the simpler $S_2\times S_2'$ case. Here there are four 1-d irreps, labeled $(1,1)$, $(1,-1)$, $(-1,1)$ and $(-1,-1)$ according to symmetry/antisymmetry under the two subgroups. Determining the characters of $\widetilde{t}_{ij}$, we find that these 9 objects decompose as

$$4\times(1,1)\oplus 2\times(1,-1)\oplus 2\times(-1,1)\oplus(-1,-1)\,. \tag{D.84}$$

The 4 singlets lead to the four linear terms in $\mathcal{K}_{\rm df,3}^{[I=0,2]ab}$, eq. (6.131), the two $(-1,1)$ irreps lead to the two linear terms in $\mathcal{K}_{\rm df,3}^{[1]ab}$, eq. (6.133), and the single $(-1,-1)$ irrep leads to the single linear term in $\mathcal{K}_{\rm df,3}^{[1]bc}$, eq. (6.134). A similar exercise for the $\widetilde{t}_{ij}\widetilde{t}_{k\ell}$ finds

$$17\times(1,1)\oplus 10\times(1,-1)\oplus 10\times(-1,1)\oplus 8(-1,-1)\,. \tag{D.85}$$

This determines the number of independent quadratic terms, and is consistent with the results quoted earlier in this section.

Now we turn to the diagonal cases, which have the larger $(S_2\times S_2')\rtimes Z_2$ symmetry. The group can be represented by $4-d$ matrices that act on the momentum vector $\{k_1,k_2,k_1',k_2'\}$, and is generated by the block matrices

$$s_2=\begin{pmatrix}\sigma_1 & 0\\ 0 & 1\end{pmatrix},\quad s_2'=\begin{pmatrix}1 & 0\\ 0 & \sigma_1\end{pmatrix},\quad\text{and}\quad z_2=\begin{pmatrix}0 & 1\\ 1 & 0\end{pmatrix}, \tag{D.86}$$

with σ_1 the usual Pauli matrix. There are 5 conjugacy classes, with elements $\{1\}$, $\{s_2,s_2'\}$, $\{s_2s_2'\}$, $\{z_2,s_2z_2s_2\}$, and $\{z_2s_2,z_2s_2'\}$. There are correspondingly 5 irreps, four with $d=1$ and one with $d=2$. The character table is shown in Table D.1, with rather arbitrary names chosen for the irreps.

The character vector of the $\widetilde{t}_{ij}$ is $\chi_t=\{9,3,1,3,1\}$, from which one finds the decomposition

$$3\times\mathbf{1}\oplus\mathbf{1a}\oplus\mathbf{1b}\oplus 2\times\mathbf{2}\,. \tag{D.87}$$

The three singlets correspond to the three linear terms in $\mathcal{K}_{\rm df,3}^{[I=0,2],xx}$, eq. (6.130), while the **1a** irrep is that which is fully antisymmetric, and thus leads to the single term in $\mathcal{K}_{\rm df,3}^{[I=1],yy}$, eq. (6.132).

For $\widetilde{t}_{ij}\widetilde{t}_{k\ell}$, the character vector is $\chi_{t^2}=\{45,9,5,9,1\}$, leading to the decomposition

$$11\times\mathbf{1}\oplus 6\times\mathbf{1a}\oplus 6\times\mathbf{1b}\oplus 2\times\mathbf{1c}\oplus 10\times\mathbf{2}\,. \tag{D.88}$$

This leads to the 11 fully symmetric quadratic terms in eq. (D.79) above, and the 6 fully antisymmetric terms in eq. (D.81)

Table D.1: Character table of $(S_2 \times S_2') \rtimes Z_2$.

Class	1	s_2	$s_2 s_2'$	z_2	$z_2 s_2$
Dim	1	2	1	2	2
1	1	1	1	1	1
1a	1	-1	1	1	-1
1b	1	1	1	-1	-1
1c	1	-1	1	-1	1
2	2	0	-2	0	0

D.7 Symmetrization of the quantization condition

In this appendix we sketch how the asymmetric form of the three-particle quantization condition, eq. (6.39), can be manipulated into the symmetric form, eq. (6.50). This is done using symmetrization identities, which are valid only up to exponentially-suppressed corrections. This is sufficient for our purposes, however, since the derivation of all forms of the quantization condition discards such corrections.

For simplicity, we consider a single three-particle channel with distinguishable particles, allowing us to use several results from ref. [35] (BS3). The generalization to identical particles, $2 + 1$ systems, or multiple three-particle channels, is straightforward, since the symmetrization identities take the same form in all cases. For brevity, we also drop carets in this appendix.

The asymmetric form of the quantization condition can be rewritten as

$$\det M = 0\,, \quad M = 1 + F_G(\mathcal{K}_{2,L} + \mathcal{K}_{\mathrm{df},3}^{(u,u)})\,. \tag{D.89}$$

Noting that $\mathcal{D}_{23,L}^{(u,u)}$, eq. (6.47), can be written as

$$\mathcal{D}_{23,L}^{(u,u)} = \frac{1}{\mathcal{K}_{2,L}^{-1} + F_G}\,, \tag{D.90}$$

we find

$$M = \frac{1}{1 - F_G \mathcal{D}_{23,L}^{(u,u)}} M' \,, \quad M' = \left[1 + (1 - F_G \mathcal{D}_{23,L}^{(u,u)}) F_G \mathcal{K}_{\mathrm{df},3}^{(u,u)}\right] . \tag{D.91}$$

Since energy levels must depend on the three-particle K matrix, assuming that it has a general form, we can rewrite the quantization condition as $\det M' = 0$. We note that M' has the same form as the denominator in eq. (79) of BS3.

The next step is to use the algebraic result given in eq. (D9) of BS3,

$$\mathcal{K}_{\mathrm{df},3}^{(u,u)} M'^{-1} = (1 + \mathcal{K}_{2,L} \overrightarrow{I_G}) \mathcal{T}_L (1 + \overleftarrow{I_G} \mathcal{K}_{2,L}) \,, \tag{D.92}$$

$$\mathcal{T}_L = \mathcal{K}' \frac{1}{1 + \left[F_G - I_{FG} - (F_G - \overleftarrow{I_G}) \mathcal{D}_{23,L}^{(u,u)} (F_G - \overrightarrow{I_G})\right] \mathcal{K}'} \,, \tag{D.93}$$

$$\mathcal{K}' = Z \frac{1}{1 + (I_{FG} + \overleftarrow{I_G} \mathcal{K}_{2,L} \overrightarrow{I_G}) Z} \,, \tag{D.94}$$

$$Z = \frac{1}{1 + \mathcal{K}_{2,L} \overrightarrow{I_G}} \mathcal{K}_{\mathrm{df},3}^{(u,u)} \frac{1}{1 + \overleftarrow{I_G} \mathcal{K}_{2,L}} \,. \tag{D.95}$$

where I_{FG}, $\overrightarrow{I_G}$ and $\overleftarrow{I_G}$ are integral operators that enter the symmetrization identities given in eqs. (100-102) of BS3, which, in shorthand form, are

$$F_G - I_{FG} = \frac{1}{3} \overleftarrow{\mathcal{S}} F \overrightarrow{\mathcal{S}} \,, \quad F_G - \overrightarrow{I_G} = F \overrightarrow{\mathcal{S}} \,, \quad F_G - \overleftarrow{I_G} = \overleftarrow{\mathcal{S}} F \,. \tag{D.96}$$

Here $\overrightarrow{\mathcal{S}}$ and $\overleftarrow{\mathcal{S}}$ are symmetrization operators, defined in eq. (98) of BS3.

Using these identities we find

$$\mathcal{T}_L = \mathcal{K}' - \mathcal{K}' \overleftarrow{\mathcal{S}} F_3 \frac{1}{1 + \mathcal{K}_{\mathrm{df},3} F_3} \overrightarrow{\mathcal{S}} \mathcal{K}' \,, \tag{D.97}$$

$$F_3 = \frac{F}{3} - F \mathcal{D}_{23,L}^{(u,u)} F = \frac{F}{3} - F \frac{1}{\mathcal{K}_{2,L}^{-1} + F_G} F \,, \tag{D.98}$$

$$\mathcal{K}_{\mathrm{df},3} = \overrightarrow{\mathcal{S}} \mathcal{K}' \overleftarrow{\mathcal{S}} \,. \tag{D.99}$$

This leads to the desired symmetric form of the quantization condition in the following manner. As noted above, the quantization condition can be written $\det M' = 0$, which implies that the left-hand side of eq. (D.92) must satisfy $\det(\mathcal{K}_{\mathrm{df},3}^{(u,u)} M'^{-1}) = \infty$. Now, in the right-hand side, the integral operators sew the external factors of $\mathcal{K}_{2,L}$ to the central $\mathcal{T}_L$ and

do not lead to divergences. These can only arise from $\mathcal{T}_L$ itself, so that the quantization condition can be rewritten as $\det \mathcal{T}_L = \infty$. Using eq. (D.97), we then observe that this divergence can arise only in the second term on the right-hand side, leading to the standard symmetric form of the quantization condition,

$$\det(1 + \mathcal{K}_{\mathrm{df},3} F_3) = 0 \,. \tag{D.100}$$

The symmetrization operators on both sides of $\mathcal{K}'$ ensure that $\mathcal{K}_{\mathrm{df},3}$ is symmetric. Tracing back through eqs. (D.94) and (D.95) we see that $\mathcal{K}'$ is obtained from the K matrix that enters the asymmetric form of the quantization condition, $\mathcal{K}_{\mathrm{df},3}^{(u,u)}$, by an infinite series involving attaching factors of $\mathcal{K}_{2,L}$ with the integral operators. An important point is that these attachments convert one infinite-volume quantity into another.

BIBLIOGRAPHY

[1] R. P. Feynman, *The theory of positrons*, *Phys. Rev.* **76** (1949) 749.

[2] S. Weinberg, *A model of leptons*, *Phys. Rev. Lett.* **19** (1967) 1264.

[3] H. Yukawa, *On the Interaction of Elementary Particles I*, *Proc. Phys. Math. Soc. Jap.* **17** (1935) 48.

[4] G. F. Chew and S. C. Frautschi, *Principle of equivalence for all strongly interacting particles within the s-matrix framework*, *Phys. Rev. Lett.* **7** (1961) 394.

[5] D. J. Gross and F. Wilczek, *Ultraviolet behavior of non-abelian gauge theories*, *Phys. Rev. Lett.* **30** (1973) 1343.

[6] M. Gell-Mann, *Symmetries of baryons and mesons*, *Phys. Rev.* **125** (1962) 1067.

[7] G. Zweig, *An SU(3) model for strong interaction symmetry and its breaking. Version 2*, pp. 22–101. 2, 1964. 10.17181/CERN-TH-412.

[8] D. J. Gross and F. Wilczek, *Asymptotically free gauge theories. i*, *Phys. Rev. D* **8** (1973) 3633.

[9] H. D. Politzer, *Asymptotic Freedom: An Approach to Strong Interactions*, *Phys. Rept.* **14** (1974) 129.

[10] K. G. Wilson, *Confinement of quarks*, *Phys. Rev. D* **10** (1974) 2445.

[11] M. Creutz, *Monte carlo study of quantized su(2) gauge theory*, *Phys. Rev. D* **21** (1980) 2308.

[12] M. Creutz, *Quarks, Gluons and Lattices*. Oxford University Press, 1983, 10.1017/9781009290395.

[13] M. Lüscher, *Volume Dependence of the Energy Spectrum in Massive Quantum Field Theories. 2. Scattering States*, *Commun.Math.Phys.* **105** (1986) 153.

[14] M. Lüscher, *Two particle states on a torus and their relation to the scattering matrix*, *Nucl.Phys.* **B354** (1991) 531.

[15] C. h. Kim, C. T. Sachrajda and S. R. Sharpe, *Finite-volume effects for two-hadron states in moving frames*, *Nucl. Phys.* **B727** (2005) 218 [hep-lat/0507006].

[16] M. T. Hansen and S. R. Sharpe, *Relativistic, model-independent, three-particle quantization condition*, *Phys. Rev.* **D90** (2014) 116003 [1408.5933].

[17] M. T. Hansen and S. R. Sharpe, *Expressing the three-particle finite-volume spectrum in terms of the three-to-three scattering amplitude*, *Phys. Rev.* **D92** (2015) 114509 [1504.04248].

[18] C. Ferrie, *Quantum Physics for Babies*. Sourcebooks Jabberwocky, Naperville, Illinois, 2017.

[19] M. E. Peskin and D. V. Schroeder, *An Introduction to quantum field theory*. Addison-Wesley, Reading, USA, 1995.

[20] S. Weinberg, *The Quantum theory of fields. Vol. 1: Foundations*. Cambridge University Press, 6, 2005, 10.1017/CBO9781139644167.

[21] M. Srednicki, *Quantum field theory*. Cambridge University Press, 1, 2007, 10.1017/CBO9780511813917.

[22] C. Gattringer and C. B. Lang, *Quantum chromodynamics on the lattice*, vol. 788. Springer, Berlin, 2010, 10.1007/978-3-642-01850-3.

[23] C. Ratti and R. Bellwied, *The Deconfinement Transition of QCD: Theory Meets Experiment*, vol. 981 of *Lecture Notes in Physics*. 6, 2021, 10.1007/978-3-030-67235-5.

[24] H. J. Rothe, *Lattice Gauge Theories : An Introduction (Fourth Edition)*, vol. 43. World Scientific Publishing Company, 2012, 10.1142/8229.

[25] P. H. Ginsparg and K. G. Wilson, *A remnant of chiral symmetry on the lattice*, *Phys. Rev. D* **25** (1982) 2649.

[26] D. B. Kaplan, *A Method for simulating chiral fermions on the lattice*, *Phys. Lett. B* **288** (1992) 342 [hep-lat/9206013].

[27] H. B. Nielsen and M. Ninomiya, *No Go Theorem for Regularizing Chiral Fermions*, *Phys. Lett. B* **105** (1981) 219.

[28] J. B. Kogut and L. Susskind, *Hamiltonian Formulation of Wilson's Lattice Gauge Theories*, *Phys. Rev. D* **11** (1975) 395.

[29] H. Neuberger, *Exactly massless quarks on the lattice*, *Phys. Lett. B* **417** (1998) 141 [hep-lat/9707022].

[30] N. Metropolis, A. W. Rosenbluth, M. N. Rosenbluth, A. H. Teller and E. Teller, *Equation of state calculations by fast computing machines*, *J. Chem. Phys.* **21** (1953) 1087.

[31] S. Weinberg, *Effective chiral Lagrangians for nucleon - pion interactions and nuclear forces*, *Nucl. Phys. B* **363** (1991) 3.

[32] S. R. Sharpe, *Applications of Chiral Perturbation theory to lattice QCD*, in *Workshop on Perspectives in Lattice QCD*, 7, 2006, hep-lat/0607016.

[33] G. Ecker, *Chiral perturbation theory*, *Progress in Particle and Nuclear Physics* **35** (1995) 1–80.

[34] S. Scherer and M. R. Schindler, *A chiral perturbation theory primer*, hep-ph/0505265.

[35] T. D. Blanton and S. R. Sharpe, *Relativistic three-particle quantization condition for nondegenerate scalars*, *Phys. Rev. D* **103** (2021) 054503 [2011.05520].

[36] T. D. Blanton and S. R. Sharpe, *Three-particle finite-volume formalism for $\pi^+\pi^+K^+$ and related systems*, *Phys. Rev. D* **104** (2021) 034509 [2105.12094].

[37] M. T. Hansen, F. Romero-López and S. R. Sharpe, *Generalizing the relativistic quantization condition to include all three-pion isospin channels*, *JHEP* **07** (2020) 047 [2003.10974].

[38] R. A. Briceño and Z. Davoudi, *Three-particle scattering amplitudes from a finite volume formalism*, *Phys. Rev.* **D87** (2013) 094507 [1212.3398].

[39] R. A. Briceño, M. T. Hansen and S. R. Sharpe, *Relating the finite-volume spectrum and the two-and-three-particle S matrix for relativistic systems of identical scalar particles*, *Phys. Rev.* **D95** (2017) 074510 [1701.07465].

[40] M. Mai and M. Döring, *Finite-Volume Spectrum of $\pi^+\pi^+$ and $\pi^+\pi^+\pi^+$ Systems*, *Phys. Rev. Lett.* **122** (2019) 062503 [1807.04746].

[41] Z. T. Draper and S. R. Sharpe, *Applicability of the two-particle quantization condition to partially-quenched theories*, *Phys. Rev. D* **104** (2021) 034510 [2107.09742].

[42] C. W. Bernard and M. F. L. Golterman, *Partially quenched gauge theories and an application to staggered fermions*, *Phys. Rev. D* **49** (1994) 486 [hep-lat/9306005].

[43] M. Golterman, *Applications of chiral perturbation theory to lattice QCD*, in *Les Houches Summer School: Session 93: Modern perspectives in lattice QCD: Quantum field theory and high performance computing*, 12, 2009, 0912.4042.

[44] S. R. Sharpe and N. Shoresh, *Physical results from unphysical simulations*, *Phys. Rev. D* **62** (2000) 094503 [hep-lat/0006017].

[45] M. T. Hansen and S. R. Sharpe, *Determining low-energy constants in partially quenched Wilson chiral perturbation theory*, *Phys. Rev. D* **85** (2012) 054504 [1112.3998].

[46] M. Della Morte and A. Juttner, *Quark disconnected diagrams in chiral perturbation theory*, *JHEP* **11** (2010) 154 [1009.3783].

[47] N. R. Acharya, F.-K. Guo, U.-G. Meißner and C.-Y. Seng, *Connected and disconnected contractions in pion–pion scattering*, *Nucl. Phys. B* **922** (2017) 480 [1704.06754].

[48] J. C. Osborn, D. Toublan and J. J. M. Verbaarschot, *From chiral random matrix theory to chiral perturbation theory*, *Nucl. Phys. B* **540** (1999) 317 [hep-th/9806110].

[49] L. Del Debbio, L. Giusti, M. Lüscher, R. Petronzio and N. Tantalo, *Stability of lattice QCD simulations and the thermodynamic limit*, *JHEP* **02** (2006) 011 [hep-lat/0512021].

[50] S. R. Sharpe, *Discretization errors in the spectrum of the Hermitian Wilson-Dirac operator*, *Phys. Rev. D* **74** (2006) 014512 [hep-lat/0606002].

[51] P. H. Damgaard, J. C. Osborn, D. Toublan and J. J. M. Verbaarschot, *The microscopic spectral density of the QCD Dirac operator*, *Nucl. Phys. B* **547** (1999) 305 [hep-th/9811212].

[52] P. H. Damgaard, K. Splittorff and J. J. M. Verbaarschot, *Microscopic Spectrum of the Wilson Dirac Operator*, *Phys. Rev. Lett.* **105** (2010) 162002 [1001.2937].

[53] N. R. Acharya, F.-K. Guo, U.-G. Meißner and C.-Y. Seng, *Constraints on disconnected contributions in $\pi\pi$ scattering*, *JHEP* **04** (2019) 165 [1902.10290].

[54] C. Kalmahalli Guruswamy, U.-G. Meißner and C.-Y. Seng, *Contraction diagram analysis in pion-kaon scattering*, *Nucl. Phys. B* **957** (2020) 115091 [2002.01763].

[55] S. R. Sharpe, R. Gupta and G. W. Kilcup, *Lattice calculation of I = 2 pion scattering length*, *Nucl. Phys. B* **383** (1992) 309.

[56] C. K. Guruswamy, U.-G. Meißner and C.-Y. Seng, *Extracting the low-energy constant L_0^r at three flavors from pion-kaon scattering*, 2102.03059.

[57] C. Bernard and M. Golterman, *On the foundations of partially quenched chiral perturbation theory*, *Phys. Rev. D* **88** (2013) 014004 [1304.1948].

[58] S. R. Sharpe and N. Shoresh, *Partially quenched chiral perturbation theory without Phi0*, *Phys. Rev. D* **64** (2001) 114510 [hep-lat/0108003].

[59] Z. T. Draper and S. R. Sharpe, *$\pi\pi$ scattering in partially-quenched twisted-mass chiral perturbation theory*, *Phys. Rev. D* **105** (2022) 034508 [2111.13975].

[60] Z. Fu, *Lattice QCD study of the s-wave $\pi\pi$ scattering lengths in the I=0 and 2 channels*, *Phys. Rev. D* **87** (2013) 074501 [1303.0517].

[61] PACS-CS collaboration, K. Sasaki, N. Ishizuka, M. Oka and T. Yamazaki, *Scattering lengths for two pseudoscalar meson systems*, *Phys. Rev. D* **89** (2014) 054502 [1311.7226].

[62] ETM collaboration, C. Helmes, C. Jost, B. Knippschild, C. Liu, J. Liu, L. Liu et al., *Hadron-hadron interactions from N_f = 2 + 1 + 1 lattice QCD: isospin-2 $\pi\pi$ scattering length*, *JHEP* **09** (2015) 109 [1506.00408].

[63] L. Liu et al., *Isospin-0 $\pi\pi$ s-wave scattering length from twisted mass lattice QCD*, *Phys. Rev. D* **96** (2017) 054516 [1612.02061].

[64] Z. Fu and X. Chen, *$I = 0$ $\pi\pi$ s-wave scattering length from lattice QCD*, *Phys. Rev. D* **98** (2018) 014514 [1712.02219].

[65] C. Culver, M. Mai, A. Alexandru, M. Döring and F. X. Lee, *Pion scattering in the isospin $I = 2$ channel from elongated lattices*, *Phys. Rev.* **D100** (2019) 034509 [1905.10202].

[66] M. Mai, C. Culver, A. Alexandru, M. Döring and F. X. Lee, *Cross-channel study of pion scattering from lattice qcd*, *Phys.Rev.D* **100** (2019) 114514 [1908.01847].

[67] M. Fischer, B. Kostrzewa, L. Liu, F. Romero-López, M. Ueding and C. Urbach, *Scattering of two and three physical pions at maximal isospin from lattice QCD*, *Eur. Phys. J. C* **81** (2021) 436 [2008.03035].

[68] Extended Twisted Mass, ETM collaboration, M. Fischer, B. Kostrzewa, M. Mai, M. Petschlies, F. Pittler, M. Ueding et al., *The ρ-resonance from $N_f = 2$ lattice QCD including the physical pion mass*, *Phys. Lett. B* **819** (2021) 136449 [2006.13805].

[69] Alpha collaboration, R. Frezzotti, P. A. Grassi, S. Sint and P. Weisz, *Lattice QCD with a chirally twisted mass term*, *JHEP* **08** (2001) 058 [hep-lat/0101001].

[70] C. Helmes, C. Jost, B. Knippschild, B. Kostrzewa, L. Liu, C. Urbach et al., *Hadron-Hadron Interactions from $N_f = 2 + 1 + 1$ lattice QCD: Isospin-1 KK scattering length*, *Phys. Rev. D* **96** (2017) 034510 [1703.04737].

[71] ETM collaboration, C. Helmes, C. Jost, B. Knippschild, B. Kostrzewa, L. Liu, F. Pittler et al., *Hadron-Hadron Interactions from $N_f = 2 + 1 + 1$ Lattice QCD: $I = 3/2$ πK Scattering Length*, *Phys. Rev. D* **98** (2018) 114511 [1809.08886].

[72] X. Feng, K. Jansen and D. B. Renner, *The pi+ pi+ scattering length from maximally twisted mass lattice QCD*, *Phys. Lett.* **B684** (2010) 268 [0909.3255].

[73] R. Frezzotti and G. C. Rossi, *Chirally improving Wilson fermions. II. Four-quark operators*, *JHEP* **10** (2004) 070 [hep-lat/0407002].

[74] R. Frezzotti and G. C. Rossi, *Chirally improving Wilson fermions. 1. O(a) improvement*, *JHEP* **08** (2004) 007 [hep-lat/0306014].

[75] M. I. Buchoff, J.-W. Chen and A. Walker-Loud, *pi-pi Scattering in Twisted Mass Chiral Perturbation Theory*, *Phys. Rev. D* **79** (2009) 074503 [0810.2464].

[76] J.-W. Chen, D. O'Connell, R. S. Van de Water and A. Walker-Loud, *Ginsparg-Wilson pions scattering on a staggered sea*, *Phys. Rev. D* **73** (2006) 074510 [hep-lat/0510024].

[77] G. Munster and C. Schmidt, *Chiral perturbation theory for lattice QCD with a twisted mass term*, *Europhys. Lett.* **66** (2004) 652 [hep-lat/0311032].

[78] L. Scorzato, *Pion mass splitting and phase structure in twisted mass QCD*, *Eur. Phys. J. C* **37** (2004) 445 [hep-lat/0407023].

[79] S. R. Sharpe and J. M. S. Wu, *The Phase diagram of twisted mass lattice QCD*, *Phys. Rev. D* **70** (2004) 094029 [hep-lat/0407025].

[80] A. Walker-Loud and J. M. S. Wu, *Nucleon and Delta masses in twisted mass chiral perturbation theory*, *Phys. Rev. D* **72** (2005) 014506 [hep-lat/0504001].

[81] M. T. Hansen and S. R. Sharpe, *Constraint on the Low Energy Constants of Wilson Chiral Perturbation Theory*, *Phys. Rev. D* **85** (2012) 014503 [1111.2404].

[82] A. Walker-Loud, *Strong isospin breaking with twisted mass lattice QCD*, 0904.2404.

[83] O. Bär, G. Rupak and N. Shoresh, *Chiral perturbation theory at O(a**2) for lattice QCD*, *Phys. Rev.* **D70** (2004) 034508 [hep-lat/0306021].

[84] S. R. Sharpe and R. L. Singleton, Jr, *Spontaneous flavor and parity breaking with Wilson fermions*, *Phys.Rev.* **D58** (1998) 074501 [hep-lat/9804028].

[85] S. R. Sharpe and J. M. S. Wu, *Twisted mass chiral perturbation theory at next-to-leading order*, *Phys. Rev. D* **71** (2005) 074501 [hep-lat/0411021].

[86] M. Golterman, S. R. Sharpe and R. L. Singleton, Jr., *Effective theory for quenched lattice QCD and the Aaoki phase*, *Phys. Rev. D* **71** (2005) 094503 [hep-lat/0501015].

[87] P. Damgaard, K. Splittorff and J. Verbaarschot, *Microscopic Spectrum of the Wilson Dirac Operator*, *Phys.Rev.Lett.* **105** (2010) 162002 [1001.2937].

[88] G. Akemann, P. Damgaard, K. Splittorff and J. Verbaarschot, *Spectrum of the Wilson Dirac Operator at Finite Lattice Spacings*, *Phys.Rev.* **D83** (2011) 085014 [1012.0752].

[89] ETM collaboration, A. Abdel-Rehim et al., *First physics results at the physical pion mass from $N_f = 2$ Wilson twisted mass fermions at maximal twist*, *Phys. Rev. D* **95** (2017) 094515 [1507.05068].

[90] C. W. Bernard and M. F. L. Golterman, *Finite volume two pion energies and scattering in the quenched approximation*, *Phys. Rev. D* **53** (1996) 476 [hep-lat/9507004].

[91] Z. T. Draper, A. D. Hanlon, B. Hörz, C. Morningstar, F. Romero-López and S. R. Sharpe, *Interactions of πK, $\pi\pi K$ and $KK\pi$ systems at maximal isospin from lattice QCD*, *JHEP* **05** (2023) 137 [2302.13587].

[92] J. Bulava et al., *Hadron Spectroscopy with Lattice QCD*, in *2022 Snowmass Summer Study*, 3, 2022, 2203.03230.

[93] R. A. Briceño, J. J. Dudek and R. D. Young, *Scattering processes and resonances from lattice QCD*, *Rev. Mod. Phys.* **90** (2018) 025001 [1706.06223].

[94] M. T. Hansen and S. R. Sharpe, *Lattice QCD and Three-particle Decays of Resonances*, *Ann. Rev. Nucl. Part. Sci.* **69** (2019) 65 [1901.00483].

[95] A. Rusetsky, *Three particles on the lattice*, *PoS* **LATTICE2019** (2019) 281 [1911.01253].

[96] B. Hörz, *Spectroscopy and Hadron Interactions*, *PoS* **LATTICE2021** (2022) 006.

[97] M. Mai, M. Döring and A. Rusetsky, *Multi-particle systems on the lattice and chiral extrapolations: a brief review*, 2103.00577.

[98] M. Mai, U.-G. Meißner and C. Urbach, *Towards a theory of hadron resonances*, *Phys. Rept.* **1001** (2023) 1 [2206.01477].

[99] F. Romero-López, *Three-particle scattering amplitudes from lattice QCD*, in *19th International Conference on Hadron Spectroscopy and Structure*, 12, 2021, 2112.05170.

[100] F. Romero-López, *Multi-hadron interactions from lattice QCD*, in *39th International Symposium on Lattice Field Theory*, 12, 2022, 2212.13793.

[101] W. Detmold and M. J. Savage, *The Energy of n Identical Bosons in a Finite Volume at O(L**-7)*, *Phys. Rev.* **D77** (2008) 057502 [0801.0763].

[102] S. R. Beane, W. Detmold and M. J. Savage, *n-Boson Energies at Finite Volume and Three-Boson Interactions*, *Phys. Rev.* **D76** (2007) 074507 [0707.1670].

[103] K. Polejaeva and A. Rusetsky, *Three particles in a finite volume*, *Eur. Phys. J. A* **48** (2012) 67 [1203.1241].

[104] H.-W. Hammer, J.-Y. Pang and A. Rusetsky, *Three-particle quantization condition in a finite volume: 1. The role of the three-particle force*, *JHEP* **09** (2017) 109 [1706.07700].

[105] S. Koenig and D. Lee, *Volume Dependence of N-Body Bound States*, *Phys. Lett.* **B779** (2018) 9 [1701.00279].

[106] H. W. Hammer, J. Y. Pang and A. Rusetsky, *Three particle quantization condition in a finite volume: 2. general formalism and the analysis of data*, *JHEP* **10** (2017) 115 [1707.02176].

[107] M. Mai and M. Döring, *Three-body Unitarity in the Finite Volume*, *Eur. Phys. J.* **A53** (2017) 240 [1709.08222].

[108] R. A. Briceño, M. T. Hansen and S. R. Sharpe, *Numerical study of the relativistic three-body quantization condition in the isotropic approximation*, *Phys. Rev.* **D98** (2018) 014506 [1803.04169].

[109] R. A. Briceño, M. T. Hansen and S. R. Sharpe, *Three-particle systems with resonant subprocesses in a finite volume*, *Phys. Rev.* **D99** (2019) 014516 [1810.01429].

[110] T. D. Blanton, F. Romero-López and S. R. Sharpe, *Implementing the three-particle quantization condition including higher partial waves*, *JHEP* **03** (2019) 106 [1901.07095].

[111] J.-Y. Pang, J.-J. Wu, H. W. Hammer, U.-G. Meißner and A. Rusetsky, *Energy shift of the three-particle system in a finite volume*, *Phys. Rev.* **D99** (2019) 074513 [1902.01111].

[112] A. W. Jackura, S. M. Dawid, C. Fernández-Ramírez, V. Mathieu, M. Mikhasenko, A. Pilloni et al., *Equivalence of three-particle scattering formalisms*, *Phys. Rev.* **D100** (2019) 034508 [1905.12007].

[113] R. A. Briceño, M. T. Hansen, S. R. Sharpe and A. P. Szczepaniak, *Unitarity of the infinite-volume three-particle scattering amplitude arising from a finite-volume formalism*, *Phys. Rev.* **D100** (2019) 054508 [1905.11188].

[114] F. Romero-López, S. R. Sharpe, T. D. Blanton, R. A. Briceño and M. T. Hansen, *Numerical exploration of three relativistic particles in a finite volume including two-particle resonances and bound states*, *JHEP* **10** (2019) 007 [1908.02411].

[115] T. D. Blanton and S. R. Sharpe, *Alternative derivation of the relativistic three-particle quantization condition*, *Phys. Rev. D* **102** (2020) 054520 [2007.16188].

[116] T. D. Blanton and S. R. Sharpe, *Equivalence of relativistic three-particle quantization conditions*, *Phys. Rev. D* **102** (2020) 054515 [2007.16190].

[117] J.-Y. Pang, J.-J. Wu and L.-S. Geng, *DDK system in finite volume*, *Phys. Rev. D* **102** (2020) 114515 [2008.13014].

[118] F. Romero-López, A. Rusetsky, N. Schlage and C. Urbach, *Relativistic N-particle energy shift in finite volume*, *JHEP* **02** (2021) 060 [2010.11715].

[119] F. Müller, A. Rusetsky and T. Yu, *Finite-volume energy shift of the three-pion ground state*, *Phys. Rev. D* **103** (2021) 054506 [2011.14178].

[120] F. Müller, J.-Y. Pang, A. Rusetsky and J.-J. Wu, *Relativistic-invariant formulation of the NREFT three-particle quantization condition*, *JHEP* **02** (2022) 158 [2110.09351].

[121] T. D. Blanton, F. Romero-López and S. R. Sharpe, *Implementing the three-particle quantization condition for $\pi^+\pi^+K^+$ and related systems*, *JHEP* **02** (2022) 098 [2111.12734].

[122] A. W. Jackura, *Three-body scattering and quantization conditions from S-matrix unitarity*, *Phys. Rev. D* **108** (2023) 034505 [2208.10587].

[123] W. Detmold and B. Smigielski, *Lattice QCD study of mixed systems of pions and kaons*, *Phys. Rev. D* **84** (2011) 014508 [1103.4362].

[124] B. Hörz and A. Hanlon, *Two- and three-pion finite-volume spectra at maximal isospin from lattice QCD*, *Phys. Rev. Lett.* **123** (2019) 142002 [1905.04277].

[125] T. D. Blanton, F. Romero-López and S. R. Sharpe, *$I = 3$ three-pion scattering amplitude from lattice QCD*, *Phys. Rev. Lett.* **124** (2020) 032001 [1909.02973].

[126] M. Mai, M. Döring, C. Culver and A. Alexandru, *Three-body unitarity versus finite-volume $\pi^+\pi^+\pi^+$ spectrum from lattice QCD*, *Phys. Rev. D* **101** (2020) 054510 [1909.05749].

[127] C. Culver, M. Mai, R. Brett, A. Alexandru and M. Döring, *Three body spectrum from lattice QCD*, *Phys. Rev. D* **101** (2020) 114507 [1911.09047].

[128] Hadron Spectrum collaboration, M. T. Hansen, R. A. Briceño, R. G. Edwards, C. E. Thomas and D. J. Wilson, *Energy-Dependent $\pi^+\pi^+\pi^+$ Scattering Amplitude from QCD*, *Phys. Rev. Lett.* **126** (2021) 012001 [2009.04931].

[129] NPLQCD, QCDSF collaboration, S. R. Beane et al., *Charged multihadron systems in lattice QCD+QED*, *Phys. Rev. D* **103** (2021) 054504 [2003.12130].

[130] A. Alexandru, R. Brett, C. Culver, M. Döring, D. Guo, F. X. Lee et al., *Finite-volume energy spectrum of the $K^-K^-K^-$ system*, *Phys. Rev. D* **102** (2020) 114523 [2009.12358].

[131] R. Brett, C. Culver, M. Mai, A. Alexandru, M. Döring and F. X. Lee, *Three-body interactions from the finite-volume QCD spectrum*, *Phys. Rev. D* **104** (2021) 014501 [2101.06144].

[132] T. D. Blanton, A. D. Hanlon, B. Hörz, C. Morningstar, F. Romero-López and S. R. Sharpe, *Interactions of two and three mesons including higher partial waves from lattice QCD*, *JHEP* **10** (2021) 023 [2106.05590].

[133] GWQCD collaboration, M. Mai, A. Alexandru, R. Brett, C. Culver, M. Döring, F. X. Lee et al., *Three-Body Dynamics of the a1(1260) Resonance from Lattice QCD*, *Phys. Rev. Lett.* **127** (2021) 222001 [2107.03973].

[134] M. Garofalo, M. Mai, F. Romero-López, A. Rusetsky and C. Urbach, *Three-body resonances in the φ^4 theory*, *JHEP* **02** (2023) 252 [2211.05605].

[135] LHCb collaboration, R. Aaij et al., *Observation of an exotic narrow doubly charmed tetraquark*, *Nature Phys.* **18** (2022) 751 [2109.01038].

[136] L. D. Roper, *Evidence for a P-11 Pion-Nucleon Resonance at 556 MeV*, *Phys. Rev. Lett.* **12** (1964) 340.

[137] R. A. Briceño, A. W. Jackura, A. Rodas and J. V. Guerrero, *Prospects for $\gamma^\star\gamma^\star \to \pi\pi$ via lattice QCD*, 2210.08051.

[138] D. J. Wilson, J. J. Dudek, R. G. Edwards and C. E. Thomas, *Resonances in coupled $\pi K, \eta K$ scattering from lattice QCD*, *Phys. Rev. D* **91** (2015) 054008 [1411.2004].

[139] Hadron Spectrum collaboration, M. Peardon, J. Bulava, J. Foley, C. Morningstar, J. Dudek, R. G. Edwards et al., *A Novel quark-field creation operator construction for hadronic physics in lattice QCD*, *Phys. Rev. D* **80** (2009) 054506 [0905.2160].

[140] C. Morningstar, J. Bulava, J. Foley, K. J. Juge, D. Lenkner, M. Peardon et al., *Improved stochastic estimation of quark propagation with Laplacian Heaviside smearing in lattice QCD*, *Phys. Rev. D* **83** (2011) 114505 [1104.3870].

[141] J. Foley, K. Jimmy Juge, A. O'Cais, M. Peardon, S. M. Ryan and J.-I. Skullerud, *Practical all-to-all propagators for lattice QCD*, *Comput. Phys. Commun.* **172** (2005) 145 [hep-lat/0505023].

[142] A. Hartono, Q. Lu, X. Gao, S. Krishnamoorthy, M. Nooijen, G. Baumgartner et al., *Identifying cost-effective common subexpressions to reduce operation count in tensor contraction evaluations*, in *Computational Science – ICCS 2006* (V. N. Alexandrov,

G. D. van Albada, P. M. A. Sloot and J. Dongarra, eds.), (Berlin, Heidelberg), pp. 267–275, Springer Berlin Heidelberg, 2006.

[143] B. Hörz et al., *Two-nucleon S-wave interactions at the $SU(3)$ flavor-symmetric point with $m_{ud} \simeq m_s^{\rm phys}$: A first lattice QCD calculation with the stochastic Laplacian Heaviside method*, *Phys. Rev. C* **103** (2021) 014003 [2009.11825].

[144] J. Bulava, A. D. Hanlon, B. Hörz, C. Morningstar, A. Nicholson, F. Romero-López et al., *Elastic nucleon-pion scattering at $m_\pi = 200$ MeV from lattice QCD*, 2208.03867.

[145] B. Hörz, "Contraction optimizer." https://github.com/laphnn/contraction_optimizer, 2019.

[146] M. Bruno et al., *Simulation of QCD with $N_f = 2 + 1$ flavors of non-perturbatively improved Wilson fermions*, *JHEP* **02** (2015) 043 [1411.3982].

[147] M. Bruno, T. Korzec and S. Schaefer, *Setting the scale for the CLS $2 + 1$ flavor ensembles*, *Phys. Rev.* **D95** (2017) 074504 [1608.08900].

[148] B. Strassberger et al., *Scale setting for CLS 2+1 simulations*, *PoS* **LATTICE2021** (2022) 135 [2112.06696].

[149] RQCD collaboration, G. S. Bali, S. Collins, P. Georg, D. Jenkins, P. Korcyl, A. Schäfer et al., *Scale setting and the light baryon spectrum in $N_f = 2 + 1$ QCD with Wilson fermions*, 2211.03744.

[150] M. Lüscher and S. Schaefer, *Lattice QCD with open boundary conditions and twisted-mass reweighting*, *Comput. Phys. Commun.* **184** (2013) 519 [1206.2809].

[151] C. Andersen, J. Bulava, B. Hörz and C. Morningstar, *The $I = 1$ pion-pion scattering amplitude and timelike pion form factor from $N_{\rm f} = 2 + 1$ lattice QCD*, *Nucl. Phys.* **B939** (2019) 145 [1808.05007].

[152] M. Cè, A. Gérardin, G. von Hippel, H. B. Meyer, K. Miura, K. Ottnad et al., *The hadronic running of the electromagnetic coupling and the electroweak mixing angle from lattice QCD*, *JHEP* **08** (2022) 220 [2203.08676].

[153] M. Lüscher and U. Wolff, *How to Calculate the Elastic Scattering Matrix in Two-dimensional Quantum Field Theories by Numerical Simulation*, *Nucl. Phys. B* **339** (1990) 222.

[154] B. Blossier, M. Della Morte, G. von Hippel, T. Mendes and R. Sommer, *On the generalized eigenvalue method for energies and matrix elements in lattice field theory*, *JHEP* **04** (2009) 094 [0902.1265].

[155] K. Rummukainen and S. A. Gottlieb, *Resonance scattering phase shifts on a nonrest frame lattice*, *Nucl. Phys.* **B450** (1995) 397 [hep-lat/9503028].

[156] M. Gockeler, R. Horsley, M. Lage, U.-G. Meissner, P. Rakow, A. Rusetsky et al., *Scattering phases for meson and baryon resonances on general moving-frame lattices*, *Phys. Rev. D* **86** (2012) 094513 [1206.4141].

[157] T. Blanton, F. Romero-López and S. R. Sharpe, "Implementation of the qc3." https://github.com/ferolo2/QC3_release, 2021.

[158] S. K. Lam, A. Pitrou and S. Seibert, *Numba: A llvm-based python jit compiler*, in *Proceedings of the Second Workshop on the LLVM Compiler Infrastructure in HPC*, pp. 1–6, 2015.

[159] F. J. Yndurain, R. Garcia-Martin and J. R. Pelaez, *Experimental status of the $\pi\pi$ isoscalar S wave at low energy: $f_0(600)$ pole and scattering length*, *Phys. Rev. D* **76** (2007) 074034 [hep-ph/0701025].

[160] R. Kaminski, J. R. Pelaez and F. J. Yndurain, *The Pion-pion scattering amplitude. III. Improving the analysis with forward dispersion relations and Roy equations*, *Phys. Rev. D* **77** (2008) 054015 [0710.1150].

[161] J.-W. Chen, D. O'Connell and A. Walker-Loud, *Two Meson Systems with Ginsparg-Wilson Valence Quarks*, *Phys. Rev. D* **75** (2007) 054501 [hep-lat/0611003].

[162] V. Bernard, N. Kaiser and U. G. Meissner, *pi K scattering in chiral perturbation theory to one loop*, *Nucl. Phys. B* **357** (1991) 129.

[163] J. Bijnens, P. Dhonte and P. Talavera, *πK scattering in three flavor ChPT*, *JHEP* **05** (2004) 036 [hep-ph/0404150].

[164] P. Guo, J. Dudek, R. Edwards and A. P. Szczepaniak, *Coupled-channel scattering on a torus*, *Phys. Rev. D* **88** (2013) 014501 [1211.0929].

[165] S. R. Beane, P. F. Bedaque, A. Parreno and M. J. Savage, *Exploring hyperons and hypernuclei with lattice QCD*, *Nucl. Phys.* **A747** (2005) 55 [nucl-th/0311027].

[166] ETM collaboration, L. Liu, S. Bacchio, P. Dimopoulos, J. Finkenrath, R. Frezzotti, C. Helmes et al., *Isospin-0 $\pi\pi$ s-wave scattering length from twisted mass lattice QCD*, *Phys. Rev. D* **96** (2017) 054516.

[167] M. T. Hansen and S. R. Sharpe, *Threshold expansion of the three-particle quantization condition*, *Phys. Rev.* **D93** (2016) 096006 [1602.00324].

[168] Flavour Lattice Averaging Group (FLAG) collaboration, Y. Aoki et al., *FLAG Review 2021*, *Eur. Phys. J. C* **82** (2022) 869 [2111.09849].

[169] MILC collaboration, A. Bazavov et al., *Results for light pseudoscalar mesons*, *PoS* **LATTICE2010** (2010) 074 [1012.0868].

[170] R. J. Dowdall, C. T. H. Davies, G. P. Lepage and C. McNeile, *V_{us} from π and K decay constants in full lattice QCD with physical u, d, s and c quarks*, *Phys. Rev. D* **88** (2013) 074504 [1303.1670].

[171] J. Bijnens and I. Jemos, *A new global fit of the L_i^r at next-to-next-to-leading order in Chiral Perturbation Theory*, *Nucl. Phys. B* **854** (2012) 631 [1103.5945].

[172] G. Amoros, J. Bijnens and P. Talavera, *QCD isospin breaking in meson masses, decay constants and quark mass ratios*, *Nucl. Phys. B* **602** (2001) 87 [hep-ph/0101127].

[173] J. R. Peláez and A. Rodas, *Dispersive $\pi K \to \pi K$ and $\pi\pi \to K\bar{K}$ amplitudes from scattering data, threshold parameters, and the lightest strange resonance κ or $K_0^*(700)$*, *Phys. Rept.* **969** (2022) 1 [2010.11222].

[174] P. Estabrooks, R. K. Carnegie, A. D. Martin, W. M. Dunwoodie, T. A. Lasinski and D. W. G. S. Leith, *Study of $K\pi$ Scattering Using the Reactions $K^+p \to K^+\pi^+n$ and $K^+p \to K^+\pi^-\Delta^{++}$ at 13-GeV/c*, *Nucl. Phys. B* **133** (1978) 490.

[175] C. B. Lang, L. Leskovec, D. Mohler and S. Prelovsek, *$K\pi$ scattering for isospin 1/2 and 3/2 in lattice QCD*, *Phys. Rev. D* **86** (2012) 054508 [1207.3204].

[176] D. J. Wilson, R. A. Briceño, J. J. Dudek, R. G. Edwards and C. E. Thomas, *Coupled $\pi\pi, K\bar{K}$ scattering in P-wave and the ρ resonance from lattice QCD*, *Phys. Rev.* **D92** (2015) 094502 [1507.02599].

[177] J. Bijnens and T. Husek, *Six-pion amplitude*, *Phys. Rev. D* **104** (2021) 054046 [2107.06291].

[178] J. Bijnens, T. Husek and M. Sjö, *Six-meson amplitude in QCD-like theories*, *Phys. Rev. D* **106** (2022) 054021 [2206.14212].

[179] Z. T. Draper, M. T. Hansen, F. Romero-López and S. R. Sharpe, *Three relativistic neutrons in a finite volume*, *JHEP* **07** (2023) 226 [2303.10219].

[180] S. R. Beane, P. F. Bedaque, K. Orginos and M. J. Savage, *Nucleon-nucleon scattering from fully-dynamical lattice QCD*, *Phys. Rev. Lett.* **97** (2006) 012001 [hep-lat/0602010].

[181] HAL QCD collaboration, T. Inoue, S. Aoki, T. Doi, T. Hatsuda, Y. Ikeda, N. Ishii et al., *Two-Baryon Potentials and H-Dibaryon from 3-flavor Lattice QCD Simulations*, *Nucl. Phys. A* **881** (2012) 28 [1112.5926].

[182] K. Orginos, A. Parreno, M. J. Savage, S. R. Beane, E. Chang and W. Detmold, *Two nucleon systems at $m_\pi \sim 450$ MeV from lattice QCD*, *Phys. Rev. D* **92** (2015) 114512 [1508.07583].

[183] E. Berkowitz, T. Kurth, A. Nicholson, B. Joo, E. Rinaldi, M. Strother et al., *Two-Nucleon Higher Partial-Wave Scattering from Lattice QCD*, *Phys. Lett. B* **765** (2017) 285 [1508.00886].

[184] T. Yamazaki, K.-i. Ishikawa, Y. Kuramashi and A. Ukawa, *Study of quark mass dependence of binding energy for light nuclei in 2+1 flavor lattice QCD*, *Phys. Rev. D* **92** (2015) 014501 [1502.04182].

[185] M. L. Wagman, F. Winter, E. Chang, Z. Davoudi, W. Detmold, K. Orginos et al., *Baryon-Baryon Interactions and Spin-Flavor Symmetry from Lattice Quantum Chromodynamics*, *Phys. Rev. D* **96** (2017) 114510 [1706.06550].

[186] A. Francis, J. R. Green, P. M. Junnarkar, C. Miao, T. D. Rae and H. Wittig, *Lattice QCD study of the H dibaryon using hexaquark and two-baryon interpolators*, *Phys. Rev. D* **99** (2019) 074505 [1805.03966].

[187] NPLQCD collaboration, M. Illa et al., *Low-energy scattering and effective interactions of two baryons at $m_\pi \sim 450$ MeV from lattice quantum chromodynamics*, *Phys. Rev. D* **103** (2021) 054508 [2009.12357].

[188] J. R. Green, A. D. Hanlon, P. M. Junnarkar and H. Wittig, *Weakly bound H dibaryon from SU(3)-flavor-symmetric QCD*, *Phys. Rev. Lett.* **127** (2021) 242003 [2103.01054].

[189] S. Amarasinghe, R. Baghdadi, Z. Davoudi, W. Detmold, M. Illa, A. Parreno et al., *A variational study of two-nucleon systems with lattice QCD*, 2108.10835.

[190] S. R. Beane, W. Detmold, T. C. Luu, K. Orginos, A. Parreno, M. J. Savage et al., *High Statistics Analysis using Anisotropic Clover Lattices. II. Three-Baryon Systems*, *Phys. Rev. D* **80** (2009) 074501 [0905.0466].

[191] NPLQCD collaboration, S. R. Beane, E. Chang, W. Detmold, H. W. Lin, T. C. Luu, K. Orginos et al., *The Deuteron and Exotic Two-Body Bound States from Lattice QCD*, *Phys. Rev. D* **85** (2012) 054511 [1109.2889].

[192] NPLQCD collaboration, S. R. Beane, E. Chang, S. D. Cohen, W. Detmold, H. W. Lin, T. C. Luu et al., *Light Nuclei and Hypernuclei from Quantum Chromodynamics in the Limit of SU(3) Flavor Symmetry*, *Phys. Rev. D* **87** (2013) 034506 [1206.5219].

[193] HAL QCD collaboration, T. Doi, S. Aoki, T. Hatsuda, Y. Ikeda, T. Inoue, N. Ishii et al., *Exploring Three-Nucleon Forces in Lattice QCD*, *Prog. Theor. Phys.* **127** (2012) 723 [1106.2276].

[194] T. Yamazaki, K.-i. Ishikawa, Y. Kuramashi and A. Ukawa, *Helium nuclei, deuteron and dineutron in 2+1 flavor lattice QCD*, *Phys. Rev. D* **86** (2012) 074514 [1207.4277].

[195] H.-W. Hammer, A. Nogga and A. Schwenk, *Three-body forces: From cold atoms to nuclei*, *Rev. Mod. Phys.* **85** (2013) 197 [1210.4273].

[196] K. Hebeler, J. D. Holt, J. Menendez and A. Schwenk, *Nuclear forces and their impact on neutron-rich nuclei and neutron-rich matter*, *Ann. Rev. Nucl. Part. Sci.* **65** (2015) 457 [1508.06893].

[197] M. Eliyahu, B. Bazak and N. Barnea, *Extrapolating Lattice QCD Results using Effective Field Theory*, *Phys. Rev. C* **102** (2020) 044003 [1912.07017].

[198] W. Detmold and P. E. Shanahan, *Few-nucleon matrix elements in pionless effective field theory in a finite volume*, *Phys. Rev. D* **103** (2021) 074503 [2102.04329].

[199] L. Meng and E. Epelbaum, *Two-particle scattering from finite-volume quantization conditions using the plane wave basis*, *JHEP* **10** (2021) 051 [2108.02709].

[200] X. Sun, W. Detmold, D. Luo and P. E. Shanahan, *Finite-volume pionless effective field theory for few-nucleon systems with differentiable programming*, *Phys. Rev. D* **105** (2022) 074508 [2202.03530].

[201] B. Bazak, M. Schäfer, R. Yaron and N. Barnea, *Spectrum of few-body systems in a finite volume*, *EPJ Web Conf.* **271** (2022) 01011 [2206.04497].

[202] J.-J. Wu, T. S. H. Lee, A. W. Thomas and R. D. Young, *Finite-volume Hamiltonian method for coupled-channels interactions in lattice QCD*, *Phys. Rev. C* **90** (2014) 055206 [1402.4868].

[203] M. T. Hansen, H. B. Meyer and D. Robaina, *From deep inelastic scattering to heavy-flavor semileptonic decays: Total rates into multihadron final states from lattice QCD*, *Phys. Rev. D* **96** (2017) 094513 [1704.08993].

[204] M. Hansen, A. Lupo and N. Tantalo, *Extraction of spectral densities from lattice correlators*, *Phys. Rev. D* **99** (2019) 094508 [1903.06476].

[205] J. Bulava, M. T. Hansen, M. W. Hansen, A. Patella and N. Tantalo, *Inclusive rates from smeared spectral densities in the two-dimensional O(3) non-linear σ-model*, *JHEP* **07** (2022) 034 [2111.12774].

[206] P. Gambino, S. Hashimoto, S. Mächler, M. Panero, F. Sanfilippo, S. Simula et al., *Lattice QCD study of inclusive semileptonic decays of heavy mesons*, *JHEP* **07** (2022) 083 [2203.11762].

[207] L. Del Debbio, A. Lupo, M. Panero and N. Tantalo, *Multi-Representation Dynamics of SU(4) Composite Higgs Models: Chiral Limit and Spectral Reconstructions*, 2211.09581.

[208] C. Alexandrou et al., *Probing the R-ratio on the lattice*, 2212.08467.

[209] R. A. Briceño, *Two-particle multichannel systems in a finite volume with arbitrary spin*, *Phys. Rev.* **D89** (2014) 074507 [1401.3312].

[210] A. W. Jackura, R. A. Briceño, S. M. Dawid, M. H. E. Islam and C. McCarty, *Solving relativistic three-body integral equations in the presence of bound states*, *Phys. Rev. D* **104** (2021) 014507 [2010.09820].

[211] S. M. Dawid, M. H. E. Islam and R. A. Briceño, *Analytic continuation of the relativistic three-particle scattering amplitudes*, *Phys. Rev. D* **108** (2023) 034016 [2303.04394].

[212] S. U. Chung, *SPIN FORMALISMS*, .

[213] A. B. a. Raposo and M. T. Hansen, *The Lüscher scattering formalism on the t-channel cut*, *PoS* **LATTICE2022** (2023) 051 [2301.03981].

[214] J. M. Blatt and L. C. Biedenharn, *Neutron-proton scattering with spin-orbit coupling. i. general expressions*, *Phys. Rev.* **86** (1952) 399.

[215] J. J. de Swart, C. P. F. Terheggen and V. G. J. Stoks, *The Low-energy n p scattering parameters and the deuteron*, in *3rd International Symposium on Dubna Deuteron 95*, 9, 1995, nucl-th/9509032.

[216] M. Lüscher, *Volume Dependence of the Energy Spectrum in Massive Quantum Field Theories. 1. Stable Particle States*, *Commun.Math.Phys.* **104** (1986) 177.

[217] M. T. Hansen, F. Romero-López and S. R. Sharpe, *Decay amplitudes to three hadrons from finite-volume matrix elements*, 2101.10246.

[218] Z. T. Draper and S. R. Sharpe, *Three-particle formalism for multiple channels: the $\eta\pi\pi + k\bar{k}\pi$ system in isosymmetric qcd*, 2403.20064.

[219] A. Ali, J. S. Lange and S. Stone, *Exotics: Heavy Pentaquarks and Tetraquarks*, *Prog. Part. Nucl. Phys.* **97** (2017) 123 [1706.00610].

[220] S. L. Olsen, T. Skwarnicki and D. Zieminska, *Nonstandard heavy mesons and baryons: Experimental evidence*, *Rev. Mod. Phys.* **90** (2018) 015003 [1708.04012].

[221] M. Karliner, J. L. Rosner and T. Skwarnicki, *Multiquark States*, *Ann. Rev. Nucl. Part. Sci.* **68** (2018) 17 [1711.10626].

[222] F.-K. Guo, C. Hanhart, U.-G. Meißner, Q. Wang, Q. Zhao and B.-S. Zou, *Hadronic molecules*, *Rev. Mod. Phys.* **90** (2018) 015004 [1705.00141].

[223] Y.-R. Liu, H.-X. Chen, W. Chen, X. Liu and S.-L. Zhu, *Pentaquark and Tetraquark states*, *Prog. Part. Nucl. Phys.* **107** (2019) 237 [1903.11976].

[224] N. Brambilla, S. Eidelman, C. Hanhart, A. Nefediev, C.-P. Shen, C. E. Thomas et al., *The XYZ states: experimental and theoretical status and perspectives*, *Phys. Rept.* **873** (2020) 1 [1907.07583].

[225] LHCb collaboration, T. Gershon, *Exotic hadron naming convention*, 2206.15233.

[226] R. F. Lebed et al., *Summary of Topical Group on Hadron Spectroscopy (RF07) Rare Processes and Precision Frontier of Snowmass 2021*, in *Snowmass 2021* (R. F. Lebed and T. Skwarnicki, eds.), 7, 2022, 2207.14594.

[227] M. T. Hansen, F. Romero-López and S. R. Sharpe, *Incorporating $DD\pi$ effects and left-hand cuts in lattice QCD studies of the $T_{cc}(3875)^+$*, 2401.06609.

[228] A. J. Woss, C. E. Thomas, J. J. Dudek, R. G. Edwards and D. J. Wilson, *b_1 resonance in coupled $\pi\omega$, $\pi\phi$ scattering from lattice QCD*, *Phys. Rev. D* **100** (2019) 054506 [1904.04136].

[229] J. J. Dudek, R. G. Edwards and C. E. Thomas, *S and D-wave phase shifts in isospin-2 pi pi scattering from lattice QCD*, *Phys. Rev.* **D86** (2012) 034031 [1203.6041].

[230] J. Baeza-Ballesteros, J. Bijnens, T. Husek, F. Romero-López, S. R. Sharpe and M. Sjö, *The three-pion K-matrix at NLO in ChPT*, *JHEP* **03** (2024) 048 [2401.14293].

[231] S. Aoki, O. Bär and B. Biedermann, *Pion scattering in Wilson chiral perturbation theory*, *Phys. Rev.* **D78** (2008) 114501 [0804.0473???].

[232] G. Amoros, J. Bijnens and P. Talavera, *Two point functions at two loops in three flavor chiral perturbation theory*, *Nucl. Phys. B* **568** (2000) 319 [hep-ph/9907264].

[233] C. Morningstar, J. Bulava, B. Fahy, J. Foley, Y. Jhang, K. Juge et al., *Extended hadron and two-hadron operators of definite momentum for spectrum calculations in lattice QCD*, *Phys. Rev. D* **88** (2013) 014511 [1303.6816].

[234] M. T. Hansen and S. R. Sharpe, *Multiple-channel generalization of Lellouch-Lüscher formula*, *Phys.Rev.* **D86** (2012) 016007 [1204.0826].